Procollagen C-Proteinase Enhancers in skin wound healing : expression, functions and therapeutic potential

Agnès Tessier

▶ **To cite this version:**

Agnès Tessier. Procollagen C-Proteinase Enhancers in skin wound healing : expression, functions and therapeutic potential. Cellular Biology. Université de Lyon; Albert-Ludwigs-Universität (Freiburg im Breisgau, Allemagne), 2018. English. NNT : 2018LYSE1105 . tel-02884581

HAL Id: tel-02884581

https://theses.hal.science/tel-02884581

Submitted on 30 Jun 2020

HAL is a multi-disciplinary open access archive for the deposit and dissemination of scientific research documents, whether they are published or not. The documents may come from teaching and research institutions in France or abroad, or from public or private research centers.

L'archive ouverte pluridisciplinaire **HAL**, est destinée au dépôt et à la diffusion de documents scientifiques de niveau recherche, publiés ou non, émanant des établissements d'enseignement et de recherche français ou étrangers, des laboratoires publics ou privés.

N° d'ordre NNT : 2018LYSE1105

THESE de DOCTORAT DE L'UNIVERSITE DE LYON ET DE L'UNIVERSITE DE FREIBURG

opérée au sein de **l'Université Claude Bernard Lyon 1** et de **l'Université Albert-Ludwigs Freiburg**

Ecole Doctorale Interdisciplinaire Sciences-Santé (205)

Spécialité de doctorat : Biologie, médecine et santé

Soutenue publiquement le 29/06/2018, par :

Agnès Tessier

Procollagen C-Proteinase Enhancers in skin wound healing: expression, functions and therapeutic potential

---

Devant le jury composé de :

Alain Colige, PhD, Université de Lièges, Belgique	Rapporteur
Pascale Jeannin, Professeur-Praticien hospitalier, CHU-Angers, France	Rapporteur
Efrat Kessler, Professeur Emérite, Université de Tel-Aviv, Israël	Rapporteur
Jérôme Lamartine, Professeur, Université Claude Bernard Lyon 1, France	Examinateur
Oliver Schilling, PhD, Université de Freiburg, Allemagne	Examinateur
Nicole Thielens, Directeur de recherche, Université Grenoble Alpes, France	Examinatrice
Catherine Moali, Directeur de recherche, CNRS, France	Directrice de thèse
Leena Bruckner-Tuderman, Professeur, Université de Freiburg, Allemagne	Co-directrice de thèse

---

UNIVERSITE CLAUDE BERNARD - LYON 1

Président de l'Université	**M. le Professeur Frédéric FLEURY**
Président du Conseil Académique	M. le Professeur Hamda BEN HADID
Vice-président du Conseil d'Administration	M. le Professeur Didier REVEL
Vice-président du Conseil Formation et Vie Universitaire	M. le Professeur Philippe CHEVALIER
Vice-président de la Commission Recherche	M. Fabrice VALLÉE
Directrice Générale des Services	Mme Dominique MARCHAND

COMPOSANTES SANTE

Faculté de Médecine Lyon Est – Claude Bernard	Directeur : M. le Professeur G.RODE
Faculté de Médecine et de Maïeutique Lyon Sud – Charles Mérieux	Directeur : Mme la Professeure C. BURILLON
Faculté d'Odontologie	Directeur : M. le Professeur D. BOURGEOIS
Institut des Sciences Pharmaceutiques et Biologiques	Directeur : Mme la Professeure C. VINCIGUERRA
Institut des Sciences et Techniques de la Réadaptation	Directeur : M. X. PERROT
Département de formation et Centre de Recherche en Biologie Humaine	Directeur : Mme la Professeure A-M. SCHOTT

COMPOSANTES ET DEPARTEMENTS DE SCIENCES ET TECHNOLOGIE

Faculté des Sciences et Technologies	Directeur : M. F. DE MARCHI
Département Biologie	Directeur : M. le Professeur F. THEVENARD
Département Chimie Biochimie	Directeur : Mme C. FELIX
Département GEP	Directeur : M. Hassan HAMMOURI
Département Informatique	Directeur : M. le Professeur S. AKKOUCHE
Département Mathématiques	Directeur : M. le Professeur G. TOMANOV
Département Mécanique	Directeur : M. le Professeur H. BEN HADID
Département Physique	Directeur : M. le Professeur J-C PLENET
UFR Sciences et Techniques des Activités Physiques et Sportives	Directeur : M. Y.VANPOULLE
Observatoire des Sciences de l'Univers de Lyon	Directeur : M. B. GUIDERDONI
Polytech Lyon	Directeur : M. le Professeur E.PERRIN
Ecole Supérieure de Chimie Physique Electronique	Directeur : M. G. PIGNAULT
Institut Universitaire de Technologie de Lyon 1	Directeur : M. le Professeur C. VITON
Ecole Supérieure du Professorat et de l'Education	Directeur : M. le Professeur A. MOUGNIOTTE
Institut de Science Financière et d'Assurances	Directeur : M. N. LEBOISNE

Acknowledgements

I would like to thank all the members of my jury and especially **Alain Colige**, **Efrat Kessler** and **Pascalle Jeannin** for evaluating my PhD thesis. I also thank **Jérôme Lamartine**, **Oliver Schilling** and **Nicole Thielens** for being active members of my jury. Thank all of you for coming so far to attend my PhD defence, it is really an honor to have such a diversified and international jury.

Je voudrais à présent remercier tout particulièrement mon encadrante de thèse, **Catherine Moali** pour avoir cru en moi depuis le début, avant même que ma thèse n'ait commencé. Je te remercie pour ton encadrement très pédagogique, ta rigueur et tes précieux conseils. Tu m'as donné l'opportunité de faire une thèse riche et diversifiée, que ce soit en termes de techniques, de connaissances et d'expériences à l'étranger. Bien que tout ne fut pas toujours très simple, j'ai beaucoup appris au cours de ces quatre années de thèse et c'est avec un solide background que je pars affronter le monde professionnel, merci ! I would also like to thank my co-supervisor, **Leena Bruckner-Tuderman** for giving me the great opportunity to come to Freiburg twice and to work in such an international group. It was a chance for me to do my PhD in two different countries, learning a lot from two laboratories with diverse expertise and knowledge. Thanks to both of you for supervising my work during almost four years.

Many thanks to **Sandrine Vadon-Le Goff** and **Alexander Nyström** for helping me so much during my PhD and being such good supervisors as well. Sandrine, ce fut un vrai plaisir de travailler à tes côtés (au sens propre comme au sens figuré). Mes connaissances et compétences en biochimie, c'est en grande partie à toi que je les dois (et à Catherine) ! Je m'excuse d'ailleurs pour toutes les questions que j'ai pu te poser encore et encore pendant ces quatre ans. Je te remercie pour ton encadrement et ton soutien jour après jour, tu as su être présente et trouver les bons mots pour me remotiver quand le moral n'y était pas (même à distance) et ça, ça compte beaucoup pour un doctorant en fin de thèse ! Alex, I thank you for your good mood, your optimism and your interest in my project. You were always available to answer my questions, help and teach me. Even if the results were bad, you were so optimistic and it helped me to get over it and stay motivated. Thanks also for your efficiency at correcting my thesis and for all your relevant remarks and suggestions.

I would like to thank **David Hulmes** for your advices and corrections in English, your explanations about collagen, fibrillogenesis and protein interactions. I would like to thank you for trusting me and giving me the opportunity to work on the complement/BTPs project, it was a chance to work and publish with you, an expert in the collagen field.

Un grand merci à **Frédéric Delolme** pour m'avoir initiée à la protéomique et la spectrométrie de masse, tu as pu remarquer que je ne suis pas une très bonne élève dans ce domaine mais tu as su être patient et me ré-expliquer les choses autant de fois que nécessaire. Toujours de bonne humeur, ce fut un plaisir de discuter et travailler avec toi (et de se faire offrir un café Nespresso au 2ème étage !).

Je remercie vivement toutes les personnes qui ont contribué à ma formation de futur chercheur pendant ces quatre ans de thèse. Merci notamment à **Naïma El Kholti** pour m'avoir transmis ton savoir-faire en immunofluorescence et à **Caroline Grangeasse** pour l'analyse d'images et l'utilisation d'ImageJ. Je remercie aussi toute l'**équipe Mallein-Gerin** pour toutes nos échanges de réactifs, de matériels et de connaissances et tout particulièrement, **Marielle Pasdeloup** pour ton enseignement très minutieux sur les qPCR et tes précieux conseils en culture cellulaire et **Emeline Goult** pour ton aide et ta disponibilité dès que j'en ai eu besoin (et ce, toujours avec le sourire). Merci aussi à **Patricia Rousselle** pour nos échanges sur la culture des kératinocytes et les tests d'adhésion, ainsi que sur ma future carrière professionnelle. Puis, je remercie **Audrey Nosbaum** pour avoir pris le temps de discuter et de me conseiller sur les aspects immunologiques de mon projet de recherche et **Suzana Salcedo** pour m'avoir initié à la culture de monocytes. Et enfin, je remercie vivement **Bérengère Fromy** and **Peter Bruckner** d'avoir accepté d'être membres de mes comités de thèse et d'évaluer l'évolution de mon projet. Je voudrais aussi remercier **Basma Zamit** pour ton aide dans l'organisation de ma thèse et ton grande efficacité pour tous les aspects administratifs.

I would like to thank all my french and german colleagues for their help, theirs advices and their kindness: **Cyril Anastasi**, **Maya Talantikite**, **Aurore Berthier**, **Dimitra Kiritsi**, **Daniel Kruppa**, **Christine Gretzmeier**, **Ioannis Anasthasiou**, **Juna Leppert**, **Gabi Grueninger** and **Irina Condrat**. Un remerciement tout particulier à mes deux acolytes « français », **Olivier Bornert** et **Rocco Bernasconi** pour ces six derniers mois en Allemagne. Vos blagues salaces, vos conversations insolites à table et votre humour (plus ou moins drôle…) ont bien égayé mes journées, à m'en faire oublier les difficultés et la déprime de la fin de thèse (je pourrais presque verser une larme là !). Merci aussi à tous les stagiaires de l'équipe que j'ai eu la chance d'encadrer ou avec qui j'ai travaillé : **Numa**, **Alexis**, **Laëtitia**, **Paulin** et **Manon**.

Je voudrais aussi remercier toutes les personnes du laboratoire que j'ai eu la chance de croiser au détour d'un couloir et de côtoyer régulièrement grâce nos dîners et afterworks sur les péniches ou ailleurs, à nos sorties (laser game, randonnée, Ardèche, pétanque, etc.), et aux Happy Hours: **Alexandre Dufour**, **Jérôme Sohier** (un grand merci pour l'organisation !), **Noëlle Remoué**, **Cécile Guillon**, **Choua Ya**, **Marine Montmasson**, **Stéphanie Gagné**, **Jean-Baptiste Luizet**, **Rachad Nasr**, **Guillaume David**, **Alexis Moreno**, **Christelle Folio** et tous les autres. Merci pour tous ces bons moments partagés ! Et parce que la thèse, c'est aussi participer à des congrès et faire de belles rencontres (même à l'autre bout du monde), je remercie **Myriam Lamrayah**, **Mariana Carranca** et **Bruna Gioia** que j'ai eu la chance de rencontrer au CoBIP 2015 à mon retour d'Allemagne, et **Mélanie Salamito** avec qui j'ai le plaisir de partager (des conseils de recherche, mais aussi des verres de vin ou une planche de charcuterie) depuis la Collagen Gordon Conference (2016).

Mais bien sûr, cette thèse n'aurait pas été possible sans ma team Bichoux, **Anne-Laure Durand**, **Maxime Ducret**, **Auriane Chrétien** et ma coloc, **Charlotte Muther** qui ont fait de ces quatre ans à Lyon une étape inoubliable. Je remercie Anne-Laure qui a croisé ma route en ce premier jour de thèse, le 2 octobre 2014 et qui ne l'a plus quittée après. Merci d'avoir été là du début à la fin de ma thèse, de Lyon à Freiburg, entre larmes et (fous) rires, merci pour tous ces bons moments, de nos longues conversations en culture cell à nos aventures à l'autre bout du monde. Un grand merci aussi à Max et Auriane, mes chéridoux préférés pour leur accueil chaleureux à chaque fois que l'envie me prenait de revenir sur Lyon (et ce n'est pas fini !), pour les incalculables apéros dinatoires chez vous, et tous nos voyages et week-ends ensemble. Et évidemment, merci à ma super coloc, Charlotte avec qui je partage toutes mes galères depuis PF (recherche de thèse, recherche d'appart, chômage et recherche de boulot…) ! C'est à mon tour de te remercier pour notre super année en coloc, nos (trop nombreux) apéros sur la terrasse et restaus, tes conseils professionnels (et personnels), et surtout tes généreuses attentions envers moi (pour n'en citer qu'une, merci de m'envoyer toutes ces offres d'emploi !). Et merci aussi à **Marine** et **Laurent**, **Eliane** et **Alex**, **Capucine** et tous les gens que j'ai eu la chance de rencontrer à Lyon !

Je voudrais remercier **Marine**, **Lauriane**, **Margot** et **Sylvain** pour vos encouragements et mots réconfortants tout au long de ma thèse. Je vous remercie d'être aussi présents (même si on est loin les uns des autres) et de me soutenir dans tous mes projets professionnels et personnels. Un petit mot tout particulier pour Marine qui m'a transmis sa passion pour la recherche et a contribué à ma décision de faire une thèse.

Un grand merci à mes amies d'enfance, **Emma**, **Clémence**, **Marina** et **Manon** qui sont à mes côtés depuis toutes ces années. Merci pour vos grains de folie, vos fous rires et votre joie de vivre ! Merci aussi à mes colocs de Lille, **Lucile**, **Anne-Chloé** et **Laurane** pour votre amitié depuis presque 9 ans et même si les moments ensemble se font plus rares ces derniers temps, on rit toujours autant.

J'aimerais aussi remercier ma famille pour leur soutien et leur présence, mes petites sœurs, **Aude** et **Domitille**, mes oncles et tantes, **Sylvie** (qui a notamment géré avec brio l'approvisionnement de champagne pour mon pot de thèse), **Philippe**, **Véro** et **Pascal** et mes grands-parents, **Daddy** et **Mamilie**, qui sont si fiers de mon parcours. Mes remerciements les plus sincères vont bien sûr à mes parents qui m'ont accompagnée tout au long de mes études et ce, jusqu'à la fin de ma thèse. **Papa**, je te remercie pour les innombrables déménagements que tu as faits avec moi, pour ton aide dans tous les aspects administratifs et pour les impressions de cette longue thèse. **Maman**, je te remercie de t'être rendue toujours si disponible pour moi, de montrer toujours un grand intérêt pour ma thèse et mes « petites cellules » (même si tu ne comprends pas toujours tout ce que je fais) et enfin, de m'avoir aidée dans mes choix difficiles. Et surtout merci à vous deux de m'accueillir de nouveau dans le cocon familial !

Et pour finir cette longue liste de remerciements, je voudrais remercier celui qui me fait m'évader du quotidien, celui qui me fait voyager chaque jour un peu plus et qui me fait rêver avec des projets toujours plus fous, **Skander**. Je te remercie de partager ma vie tout simplement.

Abstract

The imbalance between collagen assembly and degradation during skin wound healing is a major factor contributing to wound healing pathologies. Fibrillar collagen precursors are synthesized by fibroblasts and processed in the extracellular space by specific metalloproteases (e.g. BMP-1/Tolloid-like Proteinases, or BTPs) to form collagen fibrils. These proteolytic maturations are stimulated by Procollagen C-Proteinase Enhancer-1 (PCPE-1), a glycoprotein known to be involved in several tissue repair processes. Another PCPE isoform (PCPE-2) has been described more recently but less characterized. The main goal of our study was to analyze the possible redundant and specific roles of the two PCPE proteins during wound healing.

Using molecular biology and biochemistry approaches, expression of PCPEs and BTPs was comprehensively analyzed in mouse skin, human pathological wounds and various skin cells. Also, the *in vitro* functions of PCPE-1 and -2 in skin were compared using purified proteins and cellular models. Finally, the *in vivo* role of PCPE-2 in the skin was investigated using a *Pcolce2* knockout mouse model, deficient in PCPE-2.

BTPs (mainly the BMP-1 and mTLD isoforms) are expressed by both keratinocytes and fibroblasts, and their expression increases in mouse skin during the first week after injury. More surprisingly, PCPE-1 is highly expressed by dermal fibroblasts (not by keratinocytes), both before and after injury, whereas PCPE-2 is detected at a much lower level in fibroblasts and mainly found in basal keratinocytes. Moreover, PCPE-2 appears to be expressed by macrophage-like cells, together with BTPs suggesting that PCPE-2 might rather play a role during the inflammatory phase of the healing process. In addition, our results indicate that recombinant PCPE-2 strongly binds to fibrillar procollagens but does not act as an efficient enhancer of their proteolytic maturation, both *in vitro* and in cellular models. In contrast, the recombinant protein directly inhibits the action of BMP-1 on non-collagenous substrates, suggesting a differential and unexpected role of PCPE-2. Finally, the loss of PCPE-2 in *Pcolce2* KO mice does not strongly affect the morphology of the skin and the wound healing process, indicating that PCPE-1 is the main enhancer involved in collagen deposition during wound healing.

This work suggests that PCPE-1 and -2 play distinct roles during wound healing. PCPE-1 is involved during the granulation phase of wound healing, probably through its enhancer function. In contrast, PCPE-2 might play another role in the skin, as illustrated by a different expression pattern and by its weak enhancing effect on procollagen processing and its ability to inhibit BMP-1 *in vitro*.

Résumé

Au cours de la cicatrisation cutanée, la balance entre synthèse et dégradation des collagènes joue un rôle crucial dans la restauration et le maintien de l'intégrité structurale et mécanique de la peau. De fait, diverses pathologies de cicatrisation (plaies chroniques, cicatrices hypertrophiques et chéloïdes) affectant la santé et la qualité de vie des patients sont associées à des défauts dans la composition ou l'organisation des fibres de collagène. Les collagènes fibrillaires sont synthétisés et sécrétés sous forme de précurseurs solubles, principalement par les fibroblastes. Après sécrétion dans l'espace extracellulaire, leurs extrémités N- et C-terminales sont alors clivées par des protéases, appartenant notamment à la famille « BMP-1/Tolloid-like » (BTPs), ce qui permet la formation de fibres de collagène. Ce clivage protéolytique est stimulé de façon spécifique et efficace par une glycoprotéine, appelée « Procollagen C-Proteinase Enhancer-1 » ou PCPE-1 connue pour être impliquée dans différents processus de réparation tissulaire. Plus récemment, une deuxième isoforme de PCPE a été décrite : PCPE-2 serait également capable de stimuler la maturation des procollagènes *in vitro* et jouerait un rôle essentiel dans la synthèse du collagène chez la souris dans un modèle d'hypertrophie cardiaque. Ainsi, l'objectif de mon travail de recherche a été d'étudier les rôles de PCPE-1 et -2 dans la cicatrisation de la peau et d'évaluer leur potentiel thérapeutique pour améliorer la qualité des plaies.

Pour cela, l'expression et la distribution des BTPs et des PCPEs ont été étudiées dans différents modèles cellulaires et tissulaires par des approches de biologie moléculaire et de biochimie (qRT-PCR, Western blot, immunofluorescence et cytométrie en flux). En parallèle, un système d'expression de PCPE-2 a été mis en place afin de produire la protéine humaine recombinante dans le but d'évaluer son activité sur les procollagènes fibrillaires et de la comparer à celle de PCPE-1 déjà disponible dans l'équipe de C. Moali. Enfin, un modèle de souris déficientes en PCPE-2 a été utilisé afin d'étudier le rôle de PCPE-2 *in vivo* dans la peau et pendant la cicatrisation cutanée.

Nos résultats ont démontré que les BTPs sont exprimées à la fois par les fibroblastes et les kératinocytes dans la peau murine et humaine. Nous avons aussi étudié leur expression dans un modèle murin de cicatrisation. L'expression augmente de façon significative dans la peau de souris lésée, et plus particulièrement 7 jours après lésion, ce qui correspond à la phase de granulation, au cours de laquelle le nouveau tissu est formé. De façon intéressante, PCPE-1 et PCPE-2 ne sont pas exprimées par le même type cellulaire dans la peau. PCPE-1 est fortement

exprimée par les fibroblastes situés au niveau du derme et son expression augmente de façon significative après une lésion cutanée. L'expression de PCPE-1 est fortement corrélée à celle des BTPs avec une forte augmentation 7 jours après lésion, ce qui suggère que PCPE-1 et les BTPs jouent un rôle important dans la formation du nouveau tissu au cours de la cicatrisation. A l'inverse, PCPE-2 est faiblement exprimée par les fibroblastes du derme mais semble plus abondante dans les kératinocytes au niveau de la couche superficielle de la peau, l'épiderme. Le manque de spécificité des anticorps dirigés contre PCPE-2 a rendu difficile l'étude de l'expression et la distribution de PCPE-2 dans la peau pendant la cicatrisation et n'a pas donné de conclusion claire. Cependant, nous avons montré que PCPE-2, tout comme les BTPs, est fortement exprimée dans des lignées humaines de monocytes, THP-1 et U937 et que son expression augmente après différentiation des monocytes en macrophages.

Par différentes stratégies, nous avons pu inhiber de façon efficace l'action de PCPE-1 dans des fibroblastes de peau humaine. L'inhibition de PCPE-1 ne semble pas avoir d'effets majeurs sur la morphologie et la prolifération des cellules, ainsi que sur la synthèse protéique. Par une approche protéomique, nous avons mis en évidence que l'abondance des collagènes et d'autres protéines de la matrice extracellulaire n'était pas affectée par l'absence de PCPE-1, suggèrent que le rôle de PCPE-1 est spécifique de la maturation des collagènes et pourrait être envisagée comme une cible thérapeutique.

En parallèle, la protéine humaine recombinante de PCPE-2 a été exprimée et produite en cellules eucaryotes et plusieurs étapes de purification ont été nécessaires pour obtenir une protéine pure. Cette dernière a alors été testée *in vitro* dans le but d'évaluer son activité sur les procollagènes fibrillaires. De façon surprenante, nos résultats suggèrent que la protéine PCPE-2 purifiée a beaucoup moins d'effet que PCPE-1 sur la maturation des collagènes. Alors que PCPE-1 stimule d'un factor 5 à 10 la maturation des procollagènes I et III, collagènes majoritaires dans la peau, PCPE-2 a un effet très faible voire nul sur leur maturation (facteur de 3 maximum), qui semble dépendant de la concentration en PCPE-2 et disparaît à forte concentration. Ces résultats sont d'autant plus surprenants que PCPE-2 recombinante peut interagir avec les procollagènes, et ce avec une affinité similaire à PCPE-1 et prévenir l'action activatrice de PCPE-1. De plus, PCPE-2 recombinante semble inhiber de façon directe l'activité de BMP-1 sur d'autres substrats non collagéniques tels que la thrombospondine 1, la chordine et le bétaglycan. Ces résultats suggèrent un nouveau mode d'action de PCPE-2 : une fonction d'activateur de la maturation des procollagènes fibrillaires, combinée à une fonction d'inhibiteur de BMP-1.

Enfin, des travaux préliminaires ont été réalisés sur des souris C57BL/6 déficientes en PCPE-2 afin de comprendre le rôle de PCPE-2 *in vivo*. Bien que réalisés sur un faible nombre de souris, nos premiers résultats permettent déjà de conclure qu'il n'y a pas défauts majeurs au niveau de la fermeture de la plaie, de l'infiltration des cellules inflammatoires et de la formation du nouveau tissu en l'absence de PCPE-2. Des échantillons de peau ont également été prélevés afin de réaliser des analyses structurales des fibres de collagène par microscopie électronique à transmission.

L'ensemble de ces résultats suggère que PCPE-1 et -2 auraient des rôles distincts dans la cicatrisation cutanée. Alors que nos résultats concernant PCPE-1 sont en accord avec son rôle dans la fibrillogenèse au niveau de la peau et pendant la cicatrisation, l'expression de PCPE-2 par les kératinocytes et les cellules immunitaires ainsi que nos résultats *in vitro* indiquent une fonction alternative de cette protéine. Ainsi, ce travail nous a permis de confirmer que PCPE-1 était la cible thérapeutique la plus adaptée pour réguler la formation des fibres de collagène dans le contexte de la cicatrisation cutanée et ouvre un nouveau champs d'investigation sur le rôle de PCPE-2. Des études plus approfondies permettront de mieux comprendre l'importance de PCPE-2 dans la peau et de déterminer si, comme PCPE-1, cette protéine pourrait être une cible thérapeutique pour les pathologies cutanées en contrôlant d'autres voies importantes.

Table of contents

Abstract 9
Résumé substantiel 10
Table of contents 13
List of figures 19
List of tables 22
Abbreviations 23
Chapter 1: Introduction 29
I. Skin: structure and functions 31
1) General description 31
2) Epidermis 32
3) Dermal-epidermal junction 34
4) Dermis 35
a. Dermal extracellular matrix 36
b. Resident cells of the dermis 37
5) Hypodermis 38
6) Differences between mouse and human skin 40
a. Structure and general characteristics 40
b. Immunology 40
II. Skin wound healing 42
1) Haemostasis and inflammatory phase (0-3 days) 42
2) Proliferative phase (4-21 days) 44
3) Remodelling phase (21 days-1 year) 44
4) Pathological wound healing 45
a. Chronic wounds 45
b. Hypertrophic scars and keloids 46
III. Collagen fibrillogenesis 48
1) The collagen family 48
2) Fibrillar collagen biosynthesis 49
3) BMP-1/Tolloid-like Proteinases 52
a. Identification and structure 52

b. Direct roles in collagen fibril formation and assembly 54
c. Basement membrane assembly 57
d. Activation of growth factors 58
e. Regulators 59
f. Patho-physiological roles of BTPs 60
IV. Procollagen C-Proteinase Enhancers (PCPEs) 62
1) Identification of PCPEs 62
2) Function and specificity 62
3) Structure of PCPEs 65
a. CUB domains 66
b. NTR domain 66
c. Differences between PCPE-1 and -2 protein structures 67
4) Mechanism of action 68
a. Direct interaction between PCPE and procollagen 68
b. Superstimulation by HSPGs 70
5) Differential expression, distribution and *in vivo* roles 71
a. Expression among species 71
b. Expression and distribution in tissues 72
c. *In vivo* functions 73
i. Bone development and homeostasis 73
ii. Lipid metabolism 74
iii. Fibrosis 74
iv. Wound healing 76
Objectives 78
Chapter 2: Materials and methods 79
I. Production and purification of recombinant proteins 81
1) Vector cloning 81
a. PCPE-2 in pCEP4 expression vector 81
i. pOTB7-PCPE-2 amplification 81
ii. PCPE-2 sequence mutagenesis and cloning into pCEP4 vector 81
b. PCPE-2-8His in pCEP4 expression vector 82
c. 6His-PCPE2 in pHLSec vector 83
2) Culture and transfection of eukaryotic cell lines 83
a. Culture of HEK 293-EBNA and HEK 293-T cells 83

b. Stable transfection and production of PCPE-1, PCPE-1-8His, PCPE-2 and PCPE-2-8His 84
c. Transient transfection and production of 6His-PCPE-2 85
3) Protein purification 85
a. Affi-Blue 85
b. Ni-NTA 86
c. Heparin 87
d. Dialysis 89
e. Superdex 200 89
4) Protein analysis 90
II. Cell culture 90
1) Culture of primary keratinocytes and dermal fibroblasts 90
a. Primary cells isolated from mouse skin 90
b. Primary cells isolated from human skin 90
c. Subculture of primary cells 91
d. Freezing 91
2) Differentiation into myofibroblasts by TGFβ treatment 92
3) Inhibition of PCPE-1 in fibroblasts by RNA interference 92
a. Transfection with siRNA 92
b. Infection with shRNA-lentivirus 92
4) Keratinocyte differentiation 93
5) Culture of monocyte and macrophages cell lines 94
a. Subculture of THP-1 and U937 cells 94
b. Differentiation and polarization of macrophages 94
i. Differentiation of monocytes into M0 macrophages 94
ii. M1 or M2 macrophage polarization 94
III. *In vitro* cleavage assays 95
1) Cleavage assays with recombinant substrates 95
a. Procollagen III 95
b. Procollagen V 95
c. Chordin 95
d. Betaglycan 96
e. Thrombospondin-1 96
2) Cleavage assays with cell conditioned media 96
IV. Murine wound healing model 97

1) Mouse models 97
2) Assessment of wound healing 97
V. Transcriptional analyses 98
1) RNA extraction 98
2) PCR 98
3) qRT-PCR 99
VI. Protein analyses 101
1) Immunoblotting 101
a. Sample preparation 101
i. Cell conditioned medium 101
ii. ECM extraction 101
iii. Cell lysates 101
iv. Skin lysates 102
b. Western Blotting 102
2) Immunofluorescence 104
a. Cell cultures 104
b. Tissues 104
3) Flow cytometry 105
a. Cells 105
b. Mouse skin 105
4) Mass spectrometry 106
a. Protein sample preparation 106
b. TMT™ labelling for relative quantitation by mass spectrometry 106
c. MS/MS data analysis 107

Chapter 3: Expression of BMP-1/Tolloid-like Proteinases (BTPs) and Procollagen C-Proteinase Enhancers (PCPEs) in skin 109
I. Mouse skin wound healing model 111
1) Expression of BTPs during skin wound healing 112
2) PCPE expression patterns during skin wound healing 113
II. Pathological human wounds 119
1) BMP-1/mTLD expression in pathological wounds 119
2) Expression of PCPE-2 in human pathological wounds 121
III. Expression of BTPs and PCPEs in skin cells 124
1) Keratinocytes and fibroblasts 124
a. BTPs 124

b. PCPE-1 125
c. PCPE-2 127
2) Immune cells 131
a. PCPE-2 expression in mouse skin 131
b. PCPE-2 expression in human skin 133
c. PCPE-2 expression in cultured monocytes and macrophages 133
IV. Discussion 137
1) BTPs and PCPE-1 are upregulated in the proliferation phase of wound healing 137
2) PCPE-2 might play a different role during the inflammatory phase 137
Chapter 4: Role of PCPE-1 in fibroblasts 143
I. Introduction 145
II. Effect of TGFβ on PCPE-1 expression 146
III. Effects of PCPE-1 inhibition in fibroblasts 147
1) Inhibition of PCPE-1 and cell growth 147
a. Small interfering RNA (siRNA) 147
b. Short hairpin RNA (shRNA) 148
c. DARPins 149
2) C-terminal processing of type I procollagen 150
3) Protein synthesis 154
a. Sample preparation and TMT labelling 154
b. Protein identification and annotation 156
c. Protein quantification 157
IV. Discussion 159
1) Effect of TGFβ on PCPE-1 expression 159
2) Specificity of PCPE-1 for procollagen processing 159
Chapter 5: Functional characterization of the PCPE-2 protein 163
I. Introduction 165
II. Purification of recombinant proteins 166
1) PCPE-1 protein and its tagged-form, PCPE-1-8His 166
a. PCPE-1 166
b. PCPE-1-8His 167
2) PCPE-2 proteins: PCPE-2, PCPE-2-8His and 6-His-PCPE-2 168
a. PCPE-2 168
b. PCPE-2-8His 170

c. 6His-PCPE-2 171
III. *In vitro* cleavage assays 174
1) Fibrillar procollagens 174
a. Effect of PCPE-2 on type I procollagen 175
b. Effect of PCPE-2 on type II procollagen 176
c. Effect of PCPE-2 on type III procollagen 177
d. Effect of PCPE-2 on type V procollagen 179
2) Non collagenous substrates of BMP-1 181
3) Direct effect of PCPE-2 on BMP-1 activity 184
IV. Discussion 185
Chapter 6: *Pcolce2* knockout mice 189
I. Validation of the *Pcolce2* knockout 191
II. Characterization of the *Pcolce2* KO skin 194
1) Structure of the skin 194
2) Molecular changes 194
a. Expression of PCPE-1 and BTPs 194
b. Expression of other markers 195
III. Wound healing assay 196
1) Wound closure 197
2) Re-epithelialization 198
3) Infiltration of immune cells 199
4) α-SMA expression 200
IV. Discussion 202
1) Technical issues encountered 202
2) Consequences of the absence of PCPE-2 in skin 202
General discussion and conclusion 207
Bibliography 215
Appendixes 229
Communication & Training 239
List of publications 241
Oral communications 288
Posters 305
Funding and grants 310
Training 310

List of figures

Figure 1: Human skin overview (adapted from Ventrelli et al.[1]) 31
Figure 2: Epidermal structure based on keratinocyte differentiation[8] 33
Figure 3: Structure of the dermal-epidermal junction (adapted from Schmidt et al.[10]) 34
Figure 4: Human skin structure (adapted from Limbert et al.[14]) 35
Figure 5: Structure and cellular components of murine and human skin[25] 41
Figure 6: The three stages of skin wound healing (adapted from Gurtner et al.[45]) 42
Figure 7: Hypertrophic scar (A) and keloid (B) over time[62] 47
Figure 8: Supramolecular assemblies of the collagen family[69] 48
Figure 9: Major steps of collagen fibrillogenesis from synthesis to assembly[72] 49
Figure 10: Proteases of the metzincin family 50
Figure 11: Abnormal collagen fibrils in BTP-, ADAMTS- or meprin-deficient mice[76,78,79] ... 51
Figure 12: N- and C-terminal processing of the fibrillar procollagens (I, II III, V and XI) 55
Figure 13: BTPs play a key role in all the steps of fibrillogenesis 56
Figure 14: Procollagen VII processing and assembly into anchoring fibrils (adapted from Bruckner-Tuderman et al.[106]) 57
Figure 15: Laminin-332 (A) and perlecan (B) structures and cleavage sites by BTPs 58
Figure 16: Processing of fibrillar procollagens (type I, II and III) mediated by BMP-1 is enhanced by PCPE-1 and PCPE-2 63
Figure 17: Effect of PCPE-1 on type V procollagen processing 63
Figure 18: Processing of other BTP substrates is not enhanced by PCPE-1[150] 64
Figure 19: Human PCPE-1 and PCPE-2 protein sequences 65
Figure 20: Structure of the complex formed by the C-propeptide of procollagen III (CPIII) and the CUB1-CUB2 domains of PCPE-1 (adapted from Bourhis et al.[167]) 68
Figure 21: Multi-molecular complex formed by PCPE-1, BMP-1, procollagen and HSPGs .. 70
Figure 22: Abnormalities in collagen fibril morphology in bones from PCPE-1-null mice.[151]73
Figure 23: PCPE-2 abundance in a mouse model of myocardial infarction[179] 75
Figure 24: BTP and PCPE-1 expression during mouse corneal scarring[135] 77
Figure 25: Summary of the different purification steps used to purify each protein 86
Figure 26: Immunofluorescence negative controls 111
Figure 27: BTP mRNA expression during skin wound healing in mice 112
Figure 28: BMP-1/mTLD expression in mouse skin during wound healing 113

Figure 29: Pcolce and Pcolce2 mRNA expression during skin wound healing in mice 114
Figure 30: PCPE-1 expression during skin wound healing in mice 115
Figure 31: PCPE-2 pattern of expression using three different antibodies 116
Figure 32: PCPE-2 expression during skin wound healing in mice 117
Figure 33: PCPE-2 expression during wound healing in WT and RDEB mouse skin 118
Figure 34: BMP-1/mTLD expression in normal and RDEB human skin 119
Figure 35: BMP-1/mTLD expression in normal human skin, hypertrophic scars and keloids 120
Figure 36: PCPE-2 expression in normal and RDEB human skin 121
Figure 37: PCPE-2 expression in normal human skin and abnormal scars (HTS and keloids) 122
Figure 38: PCPE-2 expression in the keloid mass and at the keloid edges. 123
Figure 39: BTP expression in murine and human keratinocytes and fibroblasts 124
Figure 40: PCPE-1 expression in mouse keratinocytes and fibroblasts 125
Figure 41: PCPE-1 expression in human keratinocytes and fibroblasts 126
Figure 42: PCPE-1 distribution in human skin fibroblasts 126
Figure 43: PCPE-2 expression in mouse primary keratinocytes and fibroblasts. 127
Figure 44: PCPE-2 expression in human primary keratinocytes and fibroblasts 128
Figure 45: PCPE-2 is mainly expressed in basal keratinocytes 130
Figure 46: Co-localization of PCPE-2 with inflammatory markers in mouse skin 132
Figure 47: Co-localization of PCPE-2 with inflammatory markers in human skin 133
Figure 48: PCPE-2 mRNA and protein expression in THP-1 and U937 monocyte cell lines 134
Figure 49: mRNA expression of M1 and M2 markers in polarized THP-1 cells 135
Figure 50: Expression of PCPEs and BTPs in M1 and M2 polarized THP-1 macrophages.. 136
Figure 51: PCPE-1 expression in human dermal fibroblasts and myofibroblasts 146
Figure 52: PCPE-1 knockdown in primary fibroblasts using PCPE-1 siRNAs 147
Figure 53: PCPE-1 knockdown in primary human fibroblasts using PCOLCE shRNA lentivirus 149
Figure 54: Inhibition of PCPE-1 binding and enhancing effect on procollagen III processing by DARPins (DP40 and DP56) 150
Figure 55: Procollagen I processing in PCOLCE knockdown fibroblasts 151
Figure 56: Procollagen I processing in fibroblasts treated with DARPins 152
Figure 57: Mini III processing in 293-EBNA cells transfected with BMP-1 and PCPE-1 and treated with DARPins (40 and control) 153
Figure 58: Workflow for TMT™ labeling experiments and LC-/MS-MS analysis 155

Figure 59: Matrisome annotation (129 proteins out of 358 secreted and membrane proteins) 156
Figure 60: Gaussian distribution of the normalized log_2 (129/127) values 157
Figure 61: Electrophoresis analysis of each step of PCPE-1 purification (1) Affi-Blue, (2) heparin and (3) gel filtration..... 167
Figure 62: SDS-PAGE analysis of the His-tagged PCPE-1 purification steps (1) Ni-NTA and (2) gel filtration 168
Figure 63: Heparin purification of PCPE-2..... 169
Figure 64 : Nickel-agarose (Ni-NTA) and heparin purification of PCPE-2-8His 170
Figure 65 : Heparin purification of 6His-PCPE-2..... 171
Figure 66 : Nickel-agarose (Ni-NTA) purification of 6His-PCPE-2 172
Figure 67: Analysis by SDS-PAGE of the purified 6His-PCPE-2 protein in reducing or non-reducing conditions (+/-DTT) 172
Figure 68: Immunodetection of PCPE-1 in the PCPE-2 recombinant proteins 173
Figure 69: Procollagen I processing by BMP-1 with PCPE-1 or PCPE-2..... 175
Figure 70: Procollagen II processing by BMP-1 in the presence or absence of PCPE-1 or -2 177
Figure 71: CPIII-long processing by BMP-1 in the presence or absence of PCPE-1 or -2 ... 178
Figure 72: CPIII-long processing by mTLL-1 with PCPE-1 and -2 179
Figure 73: Procollagen V processing by BMP-1 in the presence or absence of PCPEs 180
Figure 74: Processing of thrombospondin-1 chordin and betaglycan by BMP-1 183
Figure 75: BMP-1 activity on a fluorogenic peptide in the presence or absence of 6His-PCPE-2 184
Figure 76: Validation of the absence of the exon 3 of Pcolce2 by PCR 191
Figure 77: Detection of the PCPE-2 protein in Pcolce2 KO mice 193
Figure 78: Structure of the Pcolce2 KO skin by H&E staining 194
Figure 79: Expression of PCPE-1 and BTPs in Pcolce2 KO mouse skin 195
Figure 80: Expression of tenascin C, TSP-1 and α-SMA in Pcolce2 KO mice 196
Figure 81: Wound closure in Pcolce2 KO mice..... 197
Figure 82: Re-epithelialization of the wounds days 3 and 7 post-injury 198
Figure 83: Recruitment of immune cells in the absence of PCPE-2..... 199
Figure 84: α-SMA expression in wounds of Pcolce2 KO mice 7 days post-injury 201
Figure 85: Possible model to explain in vitro functions of PCPE-2 on BMP-1 activity..... 211
Figure 86: Superposition of CUB domains of PCPE-2 and the CPIII-PCPE-1 structure 212

List of tables

Table 1: Comparison of PCPE-1 and -2 protein sequences in mouse and human 71
Table 2: PCR primer sequences designed to correct the mutations in PCPE-2 sequence 82
Table 3: PCR primers designed to insert a 6-histidine tag 83
Table 4: Buffers used for the Affi-Blue purification of PCPE-1 86
Table 5: Buffers used for the NiN-TA purification of PCPE-1-8His and PCPE-2-8His 87
Table 6: Buffers used for the Ni-NTA purification of 6His-PCPE-2 87
Table 7: Buffers used for the heparin purification of PCPE-1 88
Table 8: Buffers used for the heparin purification of PCPE-2-8His 88
Table 9: Buffers used for the heparin purification of PCPE-2 and 6His-PCPE-2 89
Table 10: Buffers used for the S200 purification of PCPE-1 and PCPE-1-8His 90
Table 11: *PCOLCE* and control siRNA sequences 92
Table 12: *PCOLCE* shRNA sequences 93
Table 13: Thermal cycling protocol for genotyping 98
Table 14: Description of PCR sequences 98
Table 15: Thermal cycling protocol for qRT-PCR 99
Table 16: Primer sequences used to amplify BTP and PCPE transcripts by qPCR 100
Table 17: qPCR primer sequences selected to monitor the differentiation markers of keratinocytes and macrophages 100
Table 18: Composition of sample buffers used in Freiburg (A) and Lyon (B) 101
Table 19: Antibodies used for Western blotting and immunofluorescence experiments 104
Table 20: Antibodies used for flow cytometry experiment 106
Table 21: Name of the studied proteins and their coding gene 111
Table 22: List of the anti-PCPE-2 antibodies used and their immunogenic sequence 116
Table 23: Dysregulated proteins in fibroblast secretome in the absence of PCPE-1 157
Table 24: Log_2 (129/127) ratio of collagens detected in the secretome of fibroblasts 158
Table 25: Summary of the observed effects of PCPE-1 and PCPE-2 on the tested substrates 186

Abbreviations

3D	Three-dimensional
α-SMA	α-smooth muscle actin
AAS	Antibiotic antimycotic solution
ADAM	A disintegrin and a metalloproteinase
ADAMTS	A disintegrin and a metalloproteinase with thrombospondin motifs
AEBSF	4-(2-aminoethyl)benzenesulfonyl fluoride hydrochloride
Ala	Alanine
Apo-AI	Apolipoprotein AI
Arg	Arginine
ARG28	Rho guanine nucleotide exchange factor 28
AR-OI	Autosomal recessive form of osteogenesis imperfecta
Asn	Asparagine
Asp	Aspartate
bFGF	Basic fibroblast growth factor
BMP-1	Bone morphogenetic protein 1
BP	Bullous pemphigoid
CAPS	N-cyclohexyl-3-aminopropanesulfonic acid
CD	Cluster of differentiation
CPIII	C-propeptide of procollagen III
CUB	Complement C1r/C1s – Uegf – Bmp1
Da	Dalton
DAMP	Damage associated molecular pattern molecule
DAPI	4′,6-diamidino-2-phenylindole
DETC	Dendritic epidermal T-cells
DKK-3	Dickkopf-related protein 3
DLS	Dynamic Light Scattering
DMEM	Dulbecco’s modified Eagle’s medium
DMP-1	Dentin matrix protein-1
DMSO	Dimethylsulphoxide
DNA	Deoxyribonucleic acid
D-PBS	Dulbecco's phosphate-buffered saline

DSPP	Dentin sialophosphoprotein
DTT	Dithiothreitol
EBNA	Epstein-Barr nuclear antigen
EC	Endothelial cells
ECM	Extracellular matrix
E. coli	*Escherichia coli*
EDTA	Ethylenediaminetetraacetic acid
EMILIN-2	Elastin microfibril interface-located protein
FBS	Foetal bovine serum
FGF	Fibroblast growth factor
GAG	Glycosaminoglycan
GDF	Growth differentiation factor
Gln	Glutamine
GLT25D1	Glycosyltransferase 25 domain containing 1
GLT25D2	Glycosyltransferase 25 domain containing 2
Glu	Glutamate
Gly	Glycine
GO	Gene ontology
HDL	High density lipoprotein
HEK	Human embryonic kidney
HF	Heart failure
HSPG	Heparan sulfate proteoglycans
IFN	Interferon
IGF-1	Insulin-like growth factor 1
IGFBP3	IGF-like binding protein-3
IL	Interleukin
ILC	Innate lymphoid cell
iTRAQ	Isobaric tags for relative and absolute quantification
KGM	Keratinocyte growth medium
LB	Luria Bertani
LAP	Latency-associated peptide
LC	Liquid chromatography
LLC	Large latent complex
LOX	Lysyl oxidase
LOXL	Lysyl oxidase like

LSC	Liver stellate cell
LTBP	Latent TGFβ binding protein
MASP	MBL-serine protease
MBL	Mannose-binding lectin
MCL	Medial collateral ligament
MMP	Matrix metalloproteinase
MOI	Multiplicity of infection
mRNA	Messenger RNA
MS	Mass spectrometry
MT-MMP	Membrane-type matrix metalloproteinase
mTLD	Mammalian tolloid
NEAA	Non-essential amino acids
NHF	Normal human fibroblast
NHK	Normal human keratinocyte
Ni-NTA	Nickel-nitrilotriacetic acid
NMF	Normal mouse fibroblast
NMK	Normal mouse keratinocyte
NTR	Netrin
N-TAILS	N-terminal amine isotopic labeling of substrates
OI	Osteogenesis imperfecta
ONT1	Olfactomedin noelin tiarin factor-1
OPMD	Oculopharyngeal muscular dystrophy
PEI	Polyethylenimine
P3H	Prolyl 3-hydroxylase
P4H	Prolyl 4-hydroxylase
PBS	Phosphate buffered saline
PCOLCE	Gene encoding Procollagen C-proteinase enhancer
PCPE	Procollagen C-proteinase enhancer
PDGF	Platelet-derived growth factor
PLOD	Procollagen-lysine 1, 2-oxoglutarate 5-dioxygenase
PMA	Phorbol 12-myristate 13-acetate
RDEB	Recessive dystrophic epidermolysis bullosa
RIPA	Radioimmunoprecipitation assay
RNA	Ribonucleic acid
RPMI	Roswell Park Memorial Institute

SDS-PAGE	Sodium dodecyl sulphate polyacrylamide gel electrophoresis
Ser	Serine
sFRP	Secreted frizzled-related protein
shRNA	Short hairpin RNA
siRNA	Small interfering RNA
SOC	Super optimal broth with catabolite repression
SPC	Subtilisin-like proprotein convertase
SPR	Surface plasmon resonance
SV40	Simian virus 40
TAC	Transverse aortic compression
TAM	Tumor-associated macrophage
TCA	Trichloroacetic acid
TCEP	Tris(2-carboxyethyl)phosphine
TCR	T-cell receptor
TEAB	Triethyl ammonium bicarbonate
TGFβ	Transforming growth factor β
TIMP	Tissue inhibitor of metalloproteinase
TLL-1	Tolloid-like 1
TLL-2	Tolloid-like 2
TLR9	Toll-like receptor 9
TMT	Tandem mass tag
TNFα	Tumor necrosis factor α
Tsg	Twisted gastrulation
TSP-1	Thrombospondin-type 1
VEGF	Vascular endothelial growth factor
WT	Wild-type

“Many small people, in small places, doing small things can change the world.”

Eduardo Galeano

Chapter 1: Introduction

I. Skin: structure and functions

The skin is one of the largest organs of the human body, with a surface area of 1.5 to 2 m^2 accounting for approximately 16% of total body weight[1]. By entirely covering the body, this organ provides a life-sustaining interface between an individual and its environment and protects it against a wide range of external (physical, chemical or microbial) aggressions. The skin plays a vital role in preventing water loss and regulating body temperature. Rich in blood vessels and nerves, it also has immune and sensory functions. The multiple roles of the skin rely on the simultaneous and coordinated action of its various layers, providing strength, flexibility and protection to the human body[2,3].

1) General description

The skin is a multi-layered structure made of three different tissues (***Figure 1***). The epidermis is the upper and external layer of the skin and is responsible for its barrier function. The dermis is rich in extracellular matrix (ECM) and provides mechanical resistance, tensile strength and elasticity[4]. The lowermost layer is the hypodermis, which is made of adipose tissue and protects the underlying structures. The skin is a major sensor organ and its three layers – epidermis, dermis and hypodermis – are highly innervated, sensory nerve fibres enabling the reception and the response to external stimuli (pain, touch, temperature, etc.). Moreover, skin is a dynamic organ in a constant state of change, as cells of the outer layer, the epidermis, are continuously renewed.

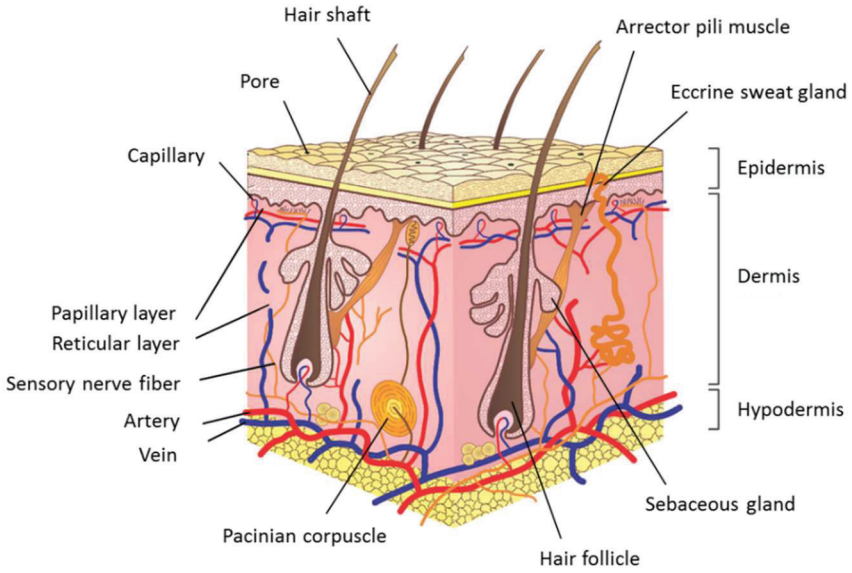

Figure 1: Human skin overview (adapted from Ventrelli et *al.*[1])
The main layers of the skin are the epidermis, which is a multilayer epithelium, the dermis consisting of papillary and reticular layers and the hypodermis, which is made of adipose tissue. The skin is rich in blood vessels, sensory nerve endings and mechanoreceptors (Pacinian corpuscles); it also contains sweat and sebaceous glands, hair follicles and arrector pili muscles.

2) Epidermis

The epidermis, an epithelial tissue derived from the ectoderm, is the outermost layer of the skin which forms a protective covering of the body[5]. It is not vascularized, but contains nerves. In humans, its thickness varies from 70 to 150 µm depending to body site[6]. The main function of the epidermis is to prevent water loss and microbial infections, through the production of a hydrolipidic film at the surface of the skin.

The epidermis is a stratified squamous keratinized epithelium in constant renewal. This multi-stratified tissue is organized in five different layers and consists of different cell types: keratinocytes, melanocytes, Langerhans cells and Merkel cells[3]. The predominant cells are by far the keratinocytes (80-85% of the cells in the epidermis), which are specialized epithelial cells responsible for synthesis of the major structural components of the epidermal barrier (keratin microfibrils, lipids, natural moisturizing factors). Basal keratinocytes migrate and differentiate following a differentiation program which occurs during transit from the deepest layer of the epidermis to the surface[7]. The five layers of the epidermis are distinguished by morphological hallmarks and specific expression markers depending on the state of keratinocyte differentiation (***Figure 2***)[8]:

- The *stratum basale* (or basal cell layer) is the deepest layer and is in contact with the dermis, allowing the passage of nutrients from the blood capillaries located in the dermis to the different layers of the epidermis. The *stratum basale* is mainly composed of basal keratinocytes that are attached to the basement membrane via hemidesmosomes and have the ability to proliferate extensively. These proliferating keratinocytes can stop dividing and start differentiating in the upper layers of the epidermis. Other cell types are found in this layer: melanocytes (5% of the cells in the epidermis) are dendritic cells producing melanin, the pigment responsible for skin colour and photoprotection against ultraviolet radiation; Merkel cells (6-10% of the cells in the epidermis), which are in contact with nerve endings, serve as mechanoreceptors and are involved in the function of touch.
- The *stratum spinosum* contains eight to ten layers of cells resulting from the migration and differentiation of basal keratinocytes. These spinous cells are polyhedral with a round nucleus; they contain filamentous structures, tonofilaments and are connected to each other through protein bridges called desmosomes. The *stratum basale* and the *stratum spinosum* together form the Malpighian layer where the Langerhans cells are found (2-5% of the cells in the epidermis). These dendritic cells play an important role in the defence of the organism by detecting foreign bodies which they carry through lymph vessels from the dermis to lymph nodes where they present them to lymphocytes[9].

- The *stratum granulosum* (granular layer) is made of keratinocytes containing granules, the keratohyalin granules. The nuclei of the keratinocytes start disintegrating and the fibrous protein keratin is deposited in the cytoplasm: this is the first stage of keratinisation.
- The *stratum lucidum* is a thin and clear layer consisting of "dead" cells, i.e. devoid of nucleus and organelles, filled with keratin. It represents a transition between the *stratum granulosum* and the *stratum corneum* and is not usually seen in thin epidermis.
- The *stratum corneum* is the most superficial layer of the skin. The corneal layer consists of corneocytes, which result from the terminal differentiation of keratinocytes. These cells are also considered as dead, but biologically active: they secrete extracellular lipids (e.g. ceramides, cholesterol, fatty acids) which function as a barrier against the entry of chemicals and microbes from the environment and protect the body from dehydration.

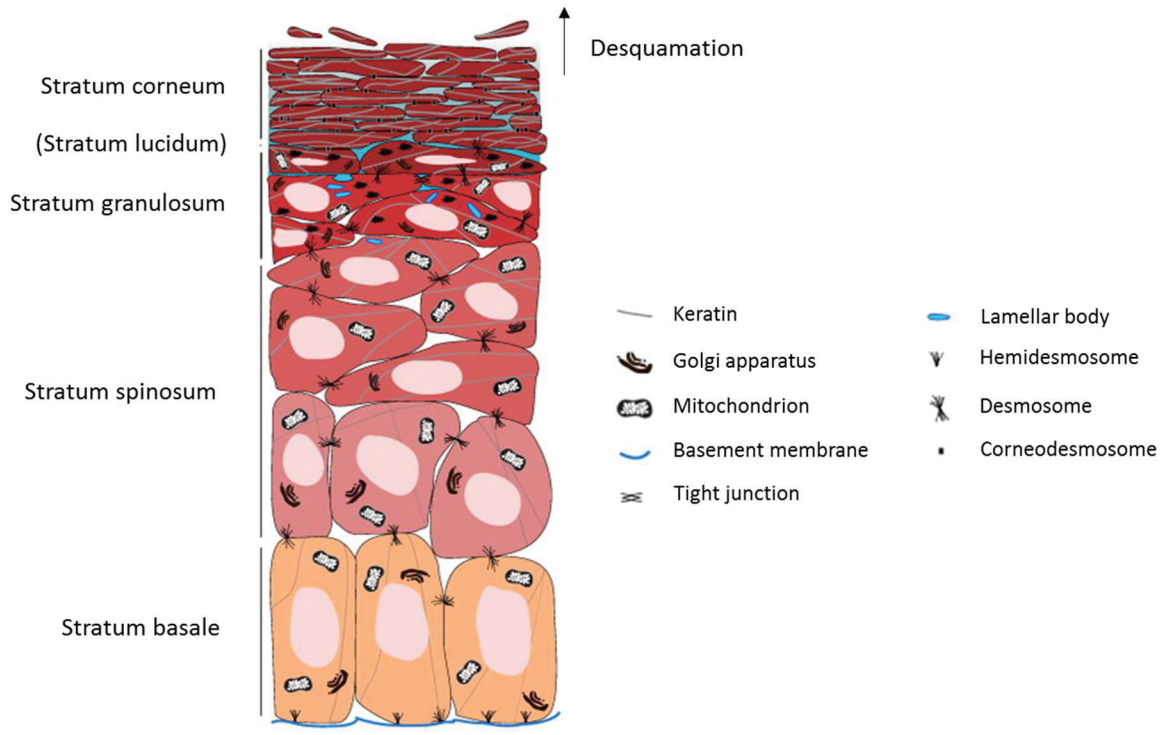

Figure 2: Epidermal structure based on keratinocyte differentiation[8]
The epidermis consists of layers at different stages of keratinocyte differentiation (the stratum lucidum is not visible here as it is only found in the very thick epidermis). Keratinocyte stem cells located in the basal cell layer and attached to the basement membrane via hemidesmosomes have the capacity to proliferate and provide new cells. Some of these cells stop proliferating, migrate and differentiate in the upper layers of the epidermis. In the superficial layer of the skin, differentiated keratinocytes, called corneocytes, express keratins that form a cornified envelope and secrete lipids. Both keratins and lipids assure cohesion between corneocytes and skin impermeability.

3) Dermal-epidermal junction

Tight interactions exist between the epidermis and the underlying layer, the dermis, through a highly specialized ECM structure called the dermal-epidermal junction (DEJ) or the epidermal basement membrane zone. Both the epidermis and the dermis cooperate to produce the different components of the basement membrane, which separates the two compartments. A main function of the DEJ is to provide adhesion between epidermis and dermis by linking the keratin filaments of the basal keratinocytes to dermal collagen fibres[3,4]. The DEJ can be divided into three different regions (***Figure 3***)[10]:

- The *lamina lucida* (20 to 40 nm) is crossed by **anchoring filaments** rich in laminin-332 that interacts with basal keratinocytes through specialized adhesion complexes, the hemidesmosomes. In more detail, the transmembrane constituents including α6β4 integrins and type XVII collagen (also called Bullous pemphigoid (BP) 180) bind, on one hand, to the anchoring filaments and the other hand, to the keratin filaments through the hemidesmosomal plaque proteins, plectin and BP230 (also known as dystonin)[11].
- The *lamina densa* (30 to 60 nm) is composed of type IV collagen, nidogen and the proteoglycan perlecan (not shown on the figure). This is the region where the anchoring filaments of the *lamina lucida* bind to the anchoring fibrils of the *subluminal densa*.
- The *sublumina densa* (20 to 60 nm) is made of type VII collagens that associate into dimers and form **anchoring fibrils**, which bind to dermal collagen fibres.

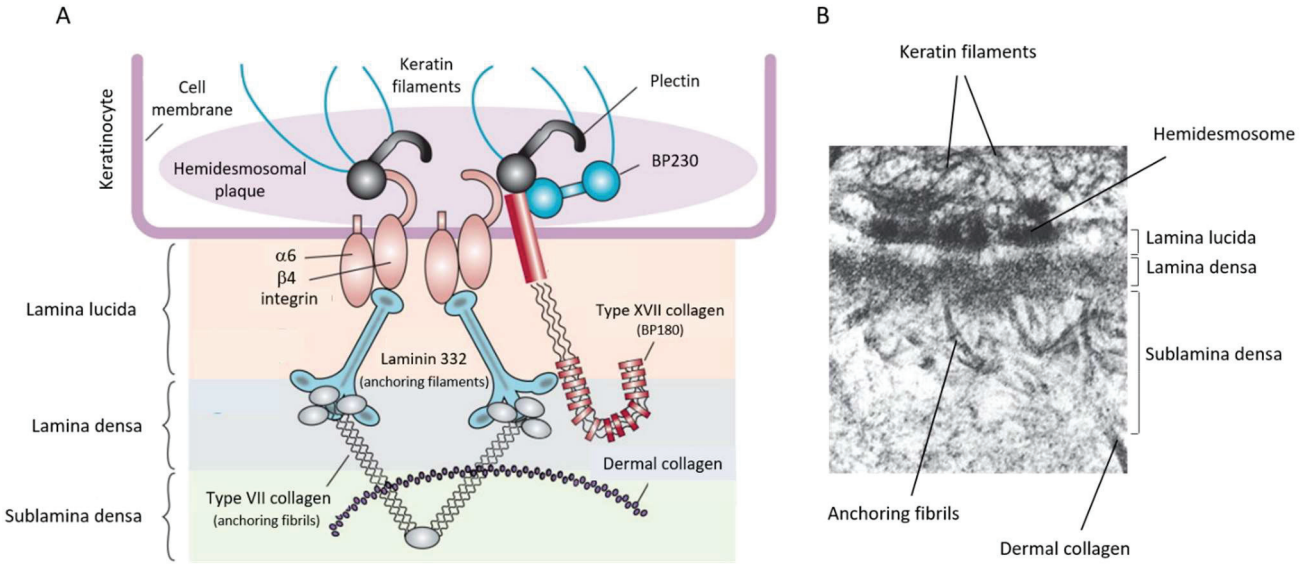

Figure 3: Structure of the dermal-epidermal junction (adapted from Schmidt et *al.*[10])
(A) The main molecular components of the dermal-epidermal junction (DEJ) are represented on the figure. Keratin filaments of basal keratinocytes are connected to the *lamina lucida* through hemidesmosomes. In the *lamina lucida*, laminin-332 forms anchoring filaments and interacts with anchoring fibrils made of collagen VII dimers. These anchoring fibrils bind to dermal collagens. **(B)** Transmission electron microscopy image of a DEJ.

These adhesion complexes are crucial for the structural and functional integrity of the skin. Alterations in one of the components of the DEJ can lead to skin-blistering diseases such as epidermolysis bullosa[12,13].

The DEJ also serves as a selective barrier by controlling the exchanges between the two layers and promotes the supply of nutrients from the blood vessels of the dermis towards the epidermis.

4) Dermis

The dermis is a thick layer of connective tissue located between the epidermis and the underlying hypodermis that provides strength and flexibility to the skin. It is mainly composed of ECM and cells; its thickness is variable, ranging from 0.6 mm on the eyelids to 3 mm on the back, palms and soles. The dermis is highly vascularized, blood vessels allowing the supply of nutrients and the infiltration of immune cells in case of infection, and innervated. As shown in Figure 1, the dermis also contains appendages such as hair follicles associated with sebaceous glands (for the secretion of sebum in the hair shaft) and sweat glands (production of sweat in response to heat and stress)[3].

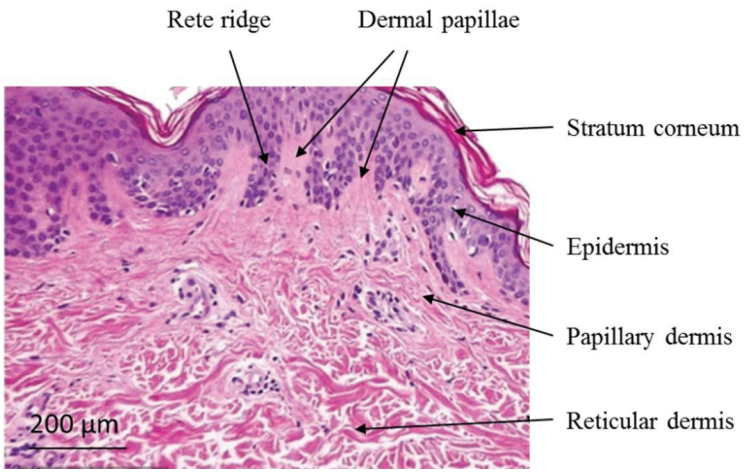

Figure 4: Human skin structure (adapted from Limbert et *al.*[14])
Histological section of H&E (haematoxylin and eosin) stained human skin showing the general structure of the skin composed of two main layers. The epidermis and the dermis are connected and communicate through the presence of rete ridges and dermal papillae, extensions of each layer found in human skin. The dermis comprises two layers: the papillary and the reticular dermis.

The dermis comprises two layers (***Figure 4***):

- The **papillary dermis**, the upper and thinnest layer, directly connected to the epidermis and consisting of loose and cell-rich connective tissue. The papillary dermis contains thin and loosely arranged collagen fibres that are sparsely distributed. Dermal papillae are the protrusions of the papillary dermis into the epidermis that interdigitate with epithelial extensions called rete ridges[14,15]. These projections increase the surface area between epidermis and dermis and enhance the adhesion between the two layers, providing mechanical strength to the skin. They are also rich in capillaries to provide nutrients to the avascular epidermis.

- The **reticular dermis**, a denser and thicker layer, contains fewer cells than the papillary dermis. Thick collagen fibres, mainly composed of types I, III and V collagens, aggregate into bundles and run parallel to the skin surface.

The papillary and reticular dermis differ in organization, as well as composition of their respective ECM. An important difference is that the papillary dermis contains more type III collagen than the reticular dermis. Another major difference is the differential expression of minor components regulating the assembly of collagens such as fibril-associated collagens with interrupted triple-helices (FACITs) and small leucine-rich proteoglycans (SLRPs)[16].

a. Dermal extracellular matrix

The ECM is the acellular component present within all tissues and organs (including the skin) which surrounds the cells. It is a complex mixture of extracellular molecules secreted by dermal cells that support the structure of the skin, but also play important roles in various biological processes. The major structural proteins of the ECM are the **fibrillar collagens**, the most abundant proteins in animal tissues. Collagen supports the integrity and strength of skin through the formation of a three-dimensional (3D) network. They will be fully described in the next part of this chapter (see §III). **Elastic fibres** are essential components of the ECM for the elastic properties of the skin. Elastin results from the assembly and cross-linking of tropoelastin monomers that accumulate on a microfibrillar skeleton[17]. Elastin fibres behave like a rubber band, stretching under tension and then snapping back when the tension is released[18].

The fibrous structural proteins collagen and elastin are embedded in gels constituted by a complex mixture of proteoglycans, glycosaminoglycans, glycoproteins and water. **Proteoglycans** are glycosylated proteins, covalently bound to **glycosaminoglycans** (GAGs), of which many forms are found in the ECM. Their biological functions depend on the physico-chemical properties of the GAG chains[19]. Heparan sulphate, dermatan sulphate, chondroitin sulphate and keratan sulphate are the most common GAGs[20]. Proteoglycans can be intracellular (serglycin), located at the cell surface (e.g. syndecan, betaglycan, glypican), pericellular (perlecan, agrin, type XVIII collagen) or extracellular (e.g. aggrecan, versican, biglycan, decorin, osteoglycin). The major proteoglycans found in the skin are versican, which is important for the structural integrity of the skin, as well as cell functions (adhesion, migration and proliferation) and perlecan, which is one of the main components of the basement membrane[21]. Moreover, decorin, a member of the SLRP family, is widely distributed in many connective tissues including the skin. It has functions in regulating the assembly of collagen fibrils (diameter, shape) and in modifying the activity of growth factors such as transforming

growth factor-beta (TGFβ) and multiple receptor tyrosine kinases[22]. Closely related to decorin, biglycan is a SLRP found in the epidermis, the basement membrane and hair follicles. It can bind to many ECM components (e.g. types I, II, III and VI collagens, elastin) and has emerging roles as a structural and signalling molecule in inflammation, bone formation and muscle integrity for example[21,23].

Other major components of the dermal ECM are **glycoproteins** such as fibronectin, tenascins, thrombospondins, vitronectin and matrilins; these are very important for cell adhesion, migration and cell-cell communication.

b. Resident cells of the dermis

The dermis has greater cell diversity than the epidermis. Whereas the epidermis mainly hosts keratinocytes and some specialized cells such as melanocytes and Langerhans cells, the dermis contains many specialized cell types and is drained by lymphatic and vascular conduits, facilitating the migration of cells within the tissue.

Fibroblasts represent the main cells of the dermis and more generally, the most common cell types found in animal connective tissues. These cells are derived from primitive mesenchyme and their main function is to maintain the structural integrity of connective tissues by secreting and/or degrading ECM components. Especially, they secrete collagens, elastin, proteoglycans, glycoproteins, growth factors, remodelling enzymes, etc. Types I and III collagens are the major collagens secreted by skin fibroblasts and are fundamental for providing the skin with strength and for the maintenance of tissue architecture. Other collagens (types V, VI, XIV, XII, etc.) are also secreted by fibroblasts in the skin and will be described later (see §III.1). Elastin, an extensible protein produced by fibroblasts, as well as smooth muscle cells, forms the elastic fibres in the dermis, and is responsible for the elastic and retractile properties of the skin and the absorption of mechanical overload[24]. Finally, fibroblasts also cooperate with the keratinocytes of the epidermis to organize the DEJ and secrete types IV and VII collagens, which are, respectively, the major components of the *lamina densa* and anchoring fibrils.

To assure a first line of defence against pathogens and physical and chemical insults, the skin and especially the dermis host resident multifunctional cells from the immune system: macrophages, dermal dendritic cells, T-cells and mast cells. **Skin-resident macrophages** originate from the yolk sac and can self-renew within the tissue[25] whereas circulating macrophages are derived from the bone marrow during inflammation. Circulating monocytes come through the blood circulation into the dermis and differentiate into macrophages; they become resident for 60-90 days before dying[26]. Resident macrophages are classified as M2-

macrophages and play roles in tissue homeostasis, angiogenesis and immune surveillance[27,28]. They perform phagocytosis of cellular debris and pathogens and can drive the recruitment of leukocytes and monocytes. Upon activation, monocyte derived-macrophages, known as M1-macrophages, are responsible for the inflammatory response through the secretion of pro-inflammatory cytokines. Then M2-macrophages have an important role in the resolution of inflammation and the return to homeostasis (secretion of anti-inflammatory cytokines and removal of apoptotic cells)[27].

As Langerhans cells in the epidermis, **dermal dendritic cells** (dermal DCs) are antigen-presenting cells that are able to initiate immune responses in the dermis. They can take up antigens and migrate into the lymph nodes to present them to B- or T-cells, promoting the clonal expansion of these cells. Plasmacytoid dendritic cells (pDCs) are rare in healthy skin but are important mediators of antiviral immunity that secrete interferon α (IFNα) in response to viral infection[25].

Resident T-cells are also found in normal healthy skin, preferentially around post-capillary venules and often beneath the DEJ or adjacent to appendages in the dermis[29]. Both $CD4^+$ and $CD8^+$ cells are present and most of them are memory T-cells. They are strategically positioned as the first line of defence in the dermis and have a major role in skin immune homeostasis, adaptive immunity and pathologies. $CD8^+$ T-cells can also be found in the basal and suprabasal layers of the epidermis.

Finally, **mast cells** are bone marrow-derived haematopoetic cells playing a crucial role in inflammatory and allergic reactions[30]. Indeed, they store a wide spectrum of biologically active mediators (histamine, cytokines, chemokines, growth factors, etc.) in granules. The content of these secretory granules is released upon activation (by specific antigens or cytokine-dependent events) leading to vasodilation, dermal oedema and activation of the immune system[31].

5) Hypodermis

Derived from the mesoderm, the hypodermis is the deepest layer of the skin and is made of loose connective tissue, large amounts of adipose tissue, subcutaneous vasculature and many specialized cells. Adipose tissue is a critical regulator of energy homeostasis; it acts as a caloric reservoir[32]. It is composed of fat-storing cells called adipocytes, which are grouped together in lobules separated by connective tissue. These specialized cells accumulate and store triglycerides; they contain large fat droplets, a flattened nucleus and a small cytoplasm. Upon activation (effort or lack of energy), fatty acids and glycerol are released from adipocyte containing-triglycerides and are used by the organism to provide energy. By covering the entire

body, the hypodermis is a major source of energy. Moreover, this thick layer of adipose tissue contributes to the thermal regulation of the body, it also absorbs shocks from impacts to the skin and protects the underlying structures.

Furthermore, the hypodermis also hosts immune cells such as macrophages, T-cells, eosinophils and neutrophils that secrete pro- and anti-inflammatory cytokines. The balance between the immune pro- and anti-inflammatory responses plays an important role in regulating adipose tissue function and energy homeostasis. For example, in obese subjects, the pro-inflammatory response becomes more important than the anti-inflammatory response and is thought to contribute to the pathogenesis of becoming overweight.

The dermis and the hypodermis are highly vascularized and contain blood and lymph vessels, the epidermis being avascular. The **blood vessels** penetrate the hypodermis, enter the deep dermis and ascend vertically to the epidermis in a large network. They also connect the hair follicles, the sebaceous and sweat glands. Blood vessels provide vital nutrients and oxygen to the skin, regulate body temperature and participate in wound healing and immune responses. The **lymphatic system** acts in concert with the blood vascular system to maintain tissue homeostasis. It controls the pressure of interstitial fluids, clears the tissue of cells, proteins and degraded substances and participates in immune reactions[9]. The skin is also highly innervated and is considered as a sensory tissue. **Nerve fibres** from the peripheral nervous system cross the dermis and penetrate the basement membrane to directly innervate epidermal cells or remain as free nerve endings[33]. They allow the perception of pain, temperature, pressure, chemical attacks, etc. from the external environment. The sensory function of the skin is mediated by sensory nerves as well as tactile corpuscles (Meissner, Pacinian and Ruffini corpuscles), which are specific receptors for touch, pressure and mechanical stimuli. Finally, **hair follicles** are present in various amounts depending on the area and the gender in human skin. Hair shafts are made by the hair follicle, considered as a complex and dynamic organ of the skin[34]. The hair follicle constitutes the pilosebaceous unit together with its associated structures, the sebaceous gland secreting sebum and the arrector pili muscle, a tiny smooth muscle that, when contracted, causes the raising of the hair (***Figure 1***). Importantly, as sebaceous and sweat glands, hair follicles cannot be restored in skin wounds and it is a challenge to regenerate skin appendages after skin injuries[35].

6) Differences between mouse and human skin

Mouse is the most common experimental model in skin research and has been used in this project. However, there are some important differences between mice and humans that must be taken into account. Here, I will describe the general characteristics of both human and murine skins, as well as the differences between human and mouse immune systems, which might have consequences for skin homeostasis and wound healing.

a. Structure and general characteristics

Numerous and significant similarities but also differences have been described so far between mouse and human skins. Both are composed of the same distinct three layers (epidermis, dermis and hypodermis) but a major difference observed between mouse and human is the thickness of the skin (***Figure 5***): human skin is much thicker than mouse skin. Indeed, human epidermis is composed of six to ten layers of keratinocytes (>100 µm), whereas mouse epidermis counts only two or three layers of cells (< 25 µm). Human skin is characterized by rete ridges which are epithelial projections that penetrate between dermal papillae into the dermis and are absent in mouse skin[15]. Because of differences in structure and organization, the function of the epithelium is also different: mouse skin shows a decreased barrier function and a greater percutaneous absorption. In addition, epidermal keratinocyte turnover is faster in mouse skin, and this is one of the reasons why mouse skin regenerate much more effectively, without scarring[25,36,37].

A further difference is that human skin contains few sparse hair follicles (only 25/mm^2), whereas mouse skin has densely distributed hair follicles (1000/mm^2 in rodents)[36]. Furthermore, mouse skin contains a cutaneous muscle layer, the *panniculus carnosus* that is non-existent in human skin. This thin layer of skeletal muscle sits below the dermal adipose layer and on the top of the subcutaneous adipose tissue; it serves to produce local movement of the skin[38]. During development, this dermal adipose layer is formed from pre-existing cells of the lower dermis and is distinct from subcutaneous adipose tissue[39]. Finally, human skin melanin-producing cells, melanocytes, are located at the basal layer of the epidermis and mostly reside in the interfollicular epidermis, whereas mouse melanocytes exhibit an almost exclusive follicular location[36].

b. Immunology

The overall organization of the immune system in mice and humans is quite similar[40] but some differences should also be mentioned. In the peripheral circulation, the balance of lymphocytes and neutrophils in adult animals is quite different: human blood is neutrophil rich

(50-70% neutrophils, 30-50% lymphocytes) whereas mouse blood has a strong preponderance of lymphocytes (75-90% lymphocytes, 10-25% neutrophils).

Human and mouse dermis are both populated by macrophages, mast cells, conventional αβ T-cells and a small population of innate lymphoid cells (ILCs). However, some differences are found in the T-cell population[25]. The most prevalent immune cell types in human epidermis are Langerhans cells and $CD8^+$ T-cells. In mice, a subset of γδ T-cells is predominant in the epidermis known as **dendritic epidermal T-cells** (DETCs), which are absent from human epidermis (***Figure 5***). In contrast to traditional T-cells that express αβ T-cell receptor (TCR), DETCs express an invariant γδ TCR (Vγ5 subset according to the Heilig and Tonegawa's nomenclature); these represent the only resident T-cell population in the mouse epidermis. In mice, there is an important contribution of these cells to skin immune surveillance, epidermal barrier function and wound closure through the production of growth factors and cytokines (e.g. interleukin IL-17A)[41,42]. DETCs also secrete FGF-9, promoting additional FGF-9 secretion by dermal fibroblasts and improving hair follicle regeneration in mouse scars[43].

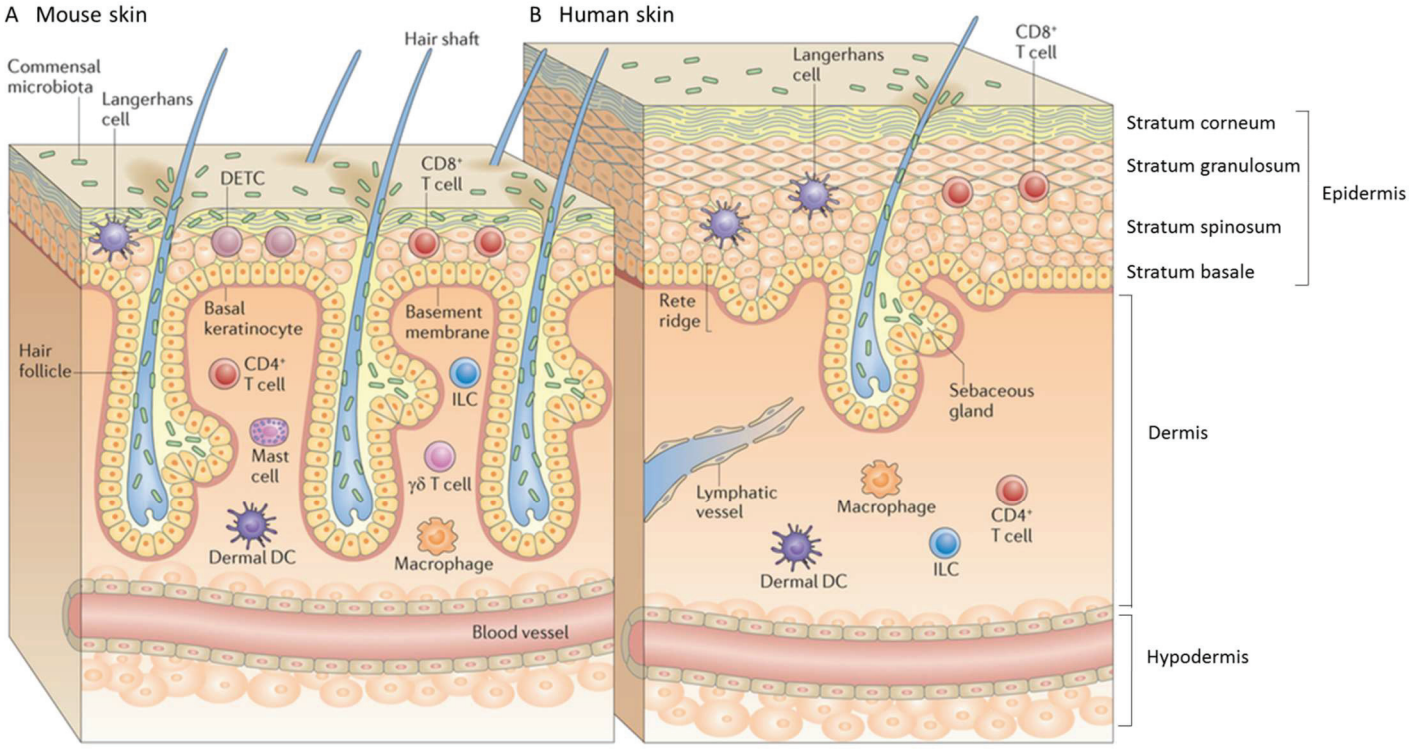

Figure 5: Structure and cellular components of murine and human skin[25]

Mouse **(A)** and human **(B)** skin exhibit differences in general organization and cell composition, especially immune cells. One major difference is the thinner epidermis in mouse skin compared to human skin. While human skin only contains Langerhans cells and CD8+ cells in the epidermis, mouse epidermis contains dendritic epidermal T-cells (DETCs) that participate in immune surveillance, barrier function and wound healing. *DC, dendritic cells; ILC, innate lymphoid cells.*

II. Skin wound healing

Wound repair is one of the most complex biological processes that occur during human life. After skin injury, multiple biological pathways become activated and numerous cell types synchronize and work together to repair the damaged tissue. Wound healing is a dynamic and very organized process that can be divided into three overlapping but distinct stages: haemostasis and inflammation (few hours after injury), proliferation (from a few hours to few weeks after injury) and remodelling (from a few weeks to a year after injury). The events in each phase must happen in a precise and regulated manner in order to restore skin tissue properly[44,45] (***Figure 6***).

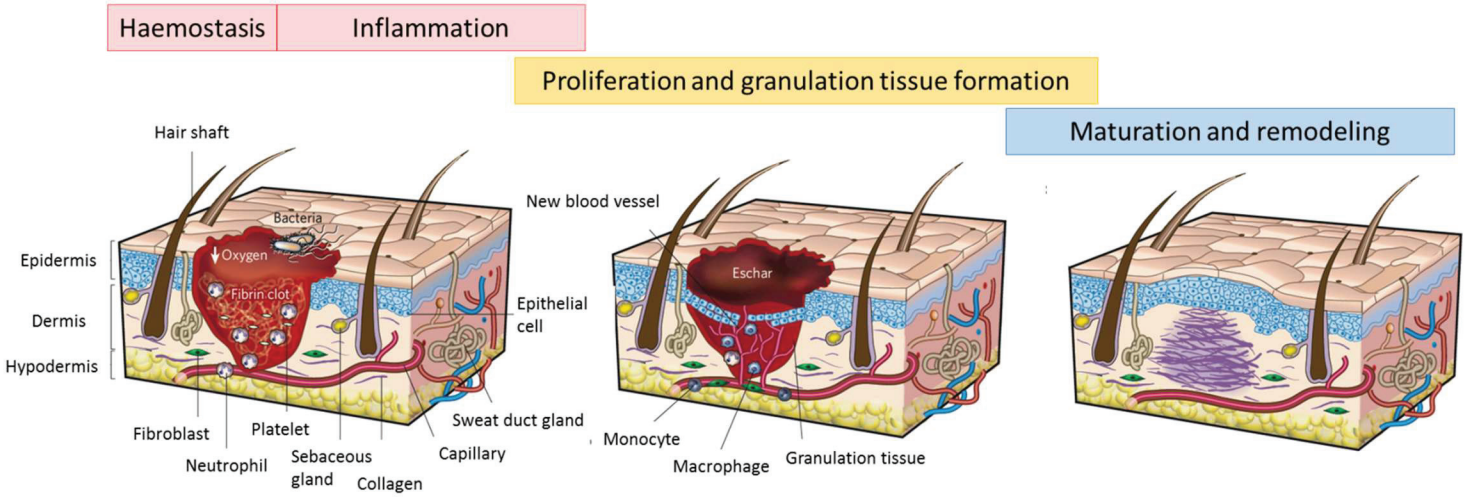

Figure 6: The three stages of skin wound healing (adapted from Gurtner et *al.*[45])
After a skin injury, a cascade of events occurs which can be divided into 3 stages: (1) Haemostasis and inflammation. Thrombocytes aggregate and trigger vasoconstriction to reduce blood loss, resulting in the formation of a fibrin clot to fill up the wound. Neutrophils are recruited through the degranulation of platelets to kill bacteria. Then, monocytes infiltrate the wound and differentiate into macrophages: M1 macrophages clean the wound and secrete pro-inflammatory mediators whereas M2 macrophages play major roles in the inflammation-proliferation transition. (2) Proliferation. Keratinocytes migrate to rebuild the epithelium, new blood vessels are formed and a granulation tissue made of a provisional ECM is produced by fibroblasts. (3) Remodelling. Newly produced ECM is remodelled to increase the tensile strength of the healed tissue.

1) Haemostasis and inflammatory phase (0-3 days)

The first stage of wound healing is the inflammatory phase that occurs directly after skin injury with the haemostasis. To prevent ongoing blood and fluid losses, injured vessels constrict, platelets become activated and aggregate to form a blood clot at the site of injury; these events result in hypoxia, increased glycolysis and pH changes. Furthermore, the blood clot contains fibrin, fibronectin, vitronectin and thrombospondin, forming a scaffold structure

for the migration of immune cells, keratinocytes, fibroblasts, etc. The fibrin clot also acts as a reservoir of growth factors and cytokines (e.g. platelet-derived growth factor, PDGF; basic fibroblast growth factor, bFGF and TGFβ) that are secreted to attract neutrophils and then macrophages to the wounded site[46]. In response to chemotactic mediators released by platelets and microorganisms, neutrophils transmigrate from the peripheral blood to skin lesions within 12 hours after injury. These are the first cells to be recruited at the wound site and are the major source of inflammatory mediators during the initial phase of wound healing. They cleanse the wounded tissue of microbes, bacteria and cellular debris by secreting antimicrobial reagents (including proteases, cytokines and chemokines) and reactive oxygen species (ROS)[47]. The release of soluble mediators is essential for the recruitment of additional neutrophils and monocytes into the wound bed. In addition, neutrophils are an important source of key regulators of wound healing (such as nitric oxide and TGFβ). Neutrophils remain for 2-5 days if the wound does not get infected and then, they undergo apoptosis or are phagocytosed by macrophages.

About 3 days after injury, circulating monocytes infiltrate the wound through capillaries in response to specific chemo-attractants. Infiltrating monocytes and resident macrophages acquire a pro-inflammatory M1 phenotype upon exposure to pro-inflammatory cytokines, interferons (IFNs), microbial products or Damage Associated Molecular Pattern molecules (DAMPs)[48,49]. M1 macrophages ensure the removal of apoptotic cells (including neutrophils), microbes and cellular debris by phagocytosis. They produce a large number of mediators and cytokines (interleukin, IL-1, -6 and -12; tumor necrosis factor α, TNFα and inducible nitric oxide synthase, iNOS), thus promoting the inflammatory response by recruiting and activating additional leukocytes. Later during healing, macrophages transit from M1 to a reparative M2 phenotype and secrete anti-inflammatory mediators (e.g. IL-10) to antagonize the pro-inflammatory M1 response. They also secrete growth factors such as TGFβ, vascular endothelial growth factor (VEGF) and insulin-like growth factor-1 (IGF-1) promoting keratinocyte and fibroblast proliferation, ECM synthesis and angiogenesis. Thereby, they play a major role in resolving inflammation and facilitating the transition from the inflammatory to the proliferative phase.

During normal wound healing, inflammation usually lasts for 2 to 5 days, even though the immune response continues during the whole process of healing through a delayed and specific response from the adaptive immune system (secretion of cytokines and growth factors by T-cells and production of antigens by B-cells)[50].

2) Proliferative phase (4-21 days)

During the proliferative phase, granulation tissue is produced and deposited to provide a wound bed for re-epithelialization. This phase can start between two and ten days after wounding and is characterized by the migration and proliferation of cells, the restoration of the vascular network and wound closure[45]. The first event is the migration of epidermal keratinocytes over the injured dermis to epithelialize the wound gap[51]. Migration stops when keratinocytes get in contact and new adhesion structures are formed; at this point, keratinocytes secrete proteins to rebuild the basement membrane. Then, reticular fibroblasts are attracted from the wound edges by macrophages. Cross-talk between keratinocytes and fibroblasts promote the migration and proliferation of both cell types.

In response to mechanical stress and TGFβ, many of the fibroblasts differentiate into myofibroblasts, α-smooth muscle actin (α-SMA)-positive cells responsible for the contraction of the wound edges[52]. These cells are characterized by enhanced features of cell contraction, migration, proliferation, cytokine production and ECM secretion and/or degradation. Fibroblasts and myofibroblasts produce large amounts of ECM, especially collagens, to form a granulation tissue that will replace the fibrin clot[24]. TGFβ is a key mediator of wound healing, mainly during the proliferative phase, since it drives fibroblast-myofibroblast differentiation[53,54], promotes wound edge contraction and stimulates collagen synthesis. To sustain the newly formed granulation tissue, formation of new blood vessels from pre-existing vasculature, known as angiogenesis, is necessary during the proliferation phase. In response to angiogenic mediators (e.g. VEGF, PDGF and FGF) secreted by a variety of cell types (keratinocytes, fibroblasts, macrophages, mast cells), endothelial cells (ECs) which form the lining of a blood vessel become activated. Activated ECs are able to disrupt junctions of the basement membrane of the vessel. Then, they can migrate, invade the surrounding ECM and form new angiogenic sprouts, leading to the formation of new capillaries[55]. Taken together, complex interactions and cross-talk between all the described cell types promote the restoration of the barrier function and the formation of new skin tissue.

3) Remodelling phase (21 days-1 year)

Following ECM synthesis and granulation tissue formation starts the final remodelling phase which can last for years[45,46]. At this stage, newly formed vessels regress and the vascular density returns to normal; most of the ECs, macrophages and myofibroblasts undergo apoptosis or exit the wound. The new ECM deposited is remodelled in order to strengthen the repaired tissue and to obtain an architecture close to that of normal skin. Under the action of metalloproteinases (see §III.2), the type III collagen produced during the proliferation phase is

replaced by type I collagen, which has a higher tensile strength. A mature avascular and acellular environment is formed. However, the new tissue never regains the properties of uninjured skin, only 80% of the original tensile strength being recovered[49].

4) Pathological wound healing

Dysregulation of any of the steps described above results in impaired healing: chronic wounds or excessive scarring leading to hypertrophic scars or keloids. These wound healing pathologies affect millions of people in the world and represent a major and increasing health and economic burden for our society. On the world scale, the economic cost of wounds is measured in billions of dollars, euros and pounds[56,57].

a. Chronic wounds

A chronic wound is defined as a full-thickness skin defect that fails to heal within a predicted time, usually three months. Chronic wounds can be generally assigned to one of the three following clinical categories: vascular ulcers (e.g. venous and arterial ulcers), diabetic foot ulcers or pressure ulcers (also known as bed sores)[58,59]. Common features shared by these wounds include persistent infections by bacteria and formation of polymicrobial communities called biofilms, and excessive inflammation. Infiltration and retention of inflammatory cells, and especially neutrophils are likely to inhibit many repair processes.

Chronic wounds are characterized by the inability of epidermal and dermal cells to respond to stimuli. Keratinocytes appear to be in a hyper-proliferative state with the upregulation of cell cycle-associated genes (e.g. cyclins, Ki67) and inhibition of cell-cycle-checkpoint regulators and p53. They also exhibit impaired migratory potential resulting in impaired re-epithelialization, which could be due to a decrease in laminin-332 or collagen VII production. In contrast, fibroblasts are senescent and also lose their capacity to migrate, impeding the formation of granulation tissue and ECM deposition. Downregulation of several genes encoding growth factors (TGFβ, VEGF, bFGF, etc.) and associated receptors could explain these phenotypic abnormalities of epidermal and dermal cells.

Furthermore, perturbations in the ECM microenvironment are likely to contribute to sustaining wound chronicity[58]. Matrix glycation (a non enzymatic reaction between reducing sugars and proteins, lipids or nucleic acids) has been observed in diabetic patients and could be responsible for, or at least linked to, premature cell senescence, apoptosis and inhibition of cell proliferation, migration and angiogenic sprout formation. Increased levels of MMPs have also been shown in chronic wounds, leading to excessive ECM degradation. All these pathologic phenomena result in the failure of these wounds to heal.

b. Hypertrophic scars and keloids

Hypertrophic scars (HTS) and keloids are both fibro-proliferative scars resulting from pathological wound healing and are characterized by chronic inflammation of the reticular dermis and excessive ECM deposition. They are caused by dermal injury (trauma, burn, surgery, vaccination, skin piercing, etc.) in patients with a susceptible background. Clinical differences between HTS and keloids reflect differences in the intensity, frequency and duration of dermal inflammation, depending on local, systemic and genetic factors[60]. Various local factors can prolong dermal inflammation; mechanical forces are the most important factor involved in the development of keloids (which occur to be mainly located on body areas frequently subjected to tensions, e.g. ears, anterior chest, arms). Systemic factors also appear to be associated with pathological scars: adolescence and pregnancy suggesting a role of sex hormones, inflammation and hypertension. Finally, it seems that HTS and keloids can be driven by genetic factors as some patients have a familial history of pathological scarring. Moreover, keloids are more likely to develop in individuals with dark skin (with an incidence of 4.5 to 16% in black and Hispanic population); they occur in parts of the body with high concentrations of melanocytes. However, whether HTS and keloids are different stages of the same wound healing defects or whether they are different pathologic forms driven by a unique mechanism is still very controversial.

Although HTS and keloids differ by clinical and histological features, the first challenge to scar therapy is to clearly distinguish these two kinds of lesions; therefore it remains crucial to establish criteria to differentiate HTS from keloids. HTS are described as visible and raised scars (< 4 mm above the skin), red or pink in colour, sometimes pruritic[61–63]. These scars do not exceed the original edges of the wound and can regress spontaneously (***Figure 7A***). HTS are characterized by a flattened epidermis and an expanded dermis made of flatter and less clearly demarcated type III collagen-rich bundles, still oriented parallel to the epithelial surface as in normal skin. They also present nodular structures, containing myofibroblasts, small vessels and fine collagen fibres. Keloids are painful, bosselated and elevated scars, with a shiny surface; the colour is pink to purple and may be accompanied by hyperpigmentation. They extend beyond the borders of the wound to spread into surrounding normal tissues, rarely regress and continue to evolve over time ***(Figure 7B***). Keloid tissues are composed of thickened, hyalinized and disorganized type I and III ("keloidal") collagen bundles without nodules. In keloids, the downregulation of type I collagen seems to be inefficient and the ratio type I/III collagen is very high (17.28 vs 6.28 in normal skin and 7.73 in HTS)[64]. Moreover, an excess of myofibroblasts and an overproduction of multiple fibroblast proteins (e.g. TGFβ, PDGF) are observed,

indicating a persistent wound healing process in keloids. In contrast to HTS, keloids never enter the final stage of wound healing, the remodelling phase.

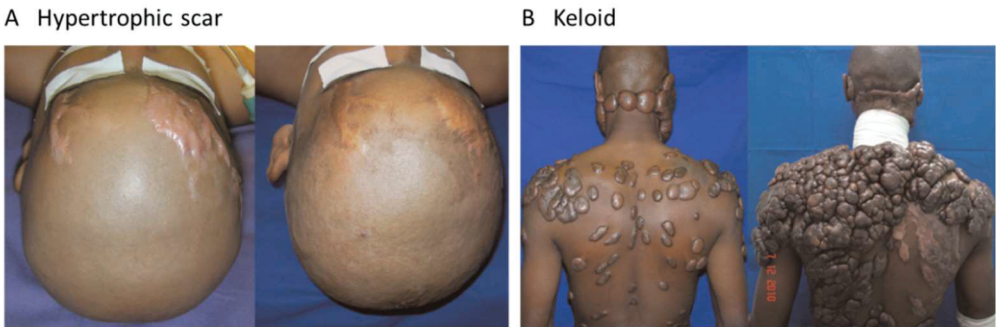

Figure 7: Hypertrophic scar (A) and keloid (B) over time[62]
(A) In a burned child, hypertrophic scars regress after 4 years. **(B)** Keloid continues to evolve after 7 years and infiltrate surrounding tissue.

Although clinical and histological features have been (partially) elucidated, the mechanisms by which these pathological scars occur remain unclear. During the transition between the inflammatory and proliferation stages, abundant macrophages inappropriately secrete cytokines that delay the healing reponse[64]. Then, cross-talk between the epidermis and the underlying dermis seems to play an important role in cutaneous scar pathology. Indeed, HTS show an increased number of epidermal Langerhans cells, whereas keloids do not, but the latter have increased numbers of lymphocytes (B- and T-cells) and macrophages. These cells, together with keratinocytes, intercommunicate with dermal cells, participating in excessive fibroblast activity and collagen deposition. In pathological scars, the balance between fibroblast proliferation and apoptosis seems to be altered. Compared to normal skin, dermal fibroblasts are found in higher density and are more proliferative and more resistant to apoptosis, especially in keloids. Moreover, mast cells are activated in keloids and release degranulation mediators such as histamine that stimulate collagen synthesis and chymase that induces a pro-fibrotic response through the TGFβ/Smad pathway in keloid fibroblasts[65].

Taken together, numerous factors contribute to the development of wound healing pathologies. The healing process is dysregulated at multiple levels from inflammation to collagen deposition and the transition from the provisional ECM to mature ECM does not happen. However, the molecular mechanisms by which chronic wounds or excessive scarring occur remain unclear because of their high complexity and the need to be further investigated. Importantly, abnormal collagen is deposited in these wounds suggesting that the imbalance between collagen assembly and degradation might be a major factor in the development of these diseases. Thus, it seems crucial to study in more detail collagen fibrillogenesis and its mechanisms of regulation.

III. Collagen fibrillogenesis

Collagen, in all its forms, represents the most abundant protein in animals[66] and is the major constituent of the ECM[67]. Collagens have versatile functions but are mainly involved in tissue architecture providing scaffolding, strength and flexibility.

1) The collagen family

So far, 28 different collagens have been described in humans (***Appendix 1***); they are all homo- or hetero-trimers formed by three identical or distinct polypeptide chains (named α chains). Collagens are characterized by the presence of at least one triple-helical domain and by the ability to form supramolecular assemblies (***Figure 8***). This domain is a tight region made of glycine-X-Y amino acid repeats where X and Y can be any amino acid (X is often a proline and Y a hydroxyproline residue) that stabilize the triple helix.

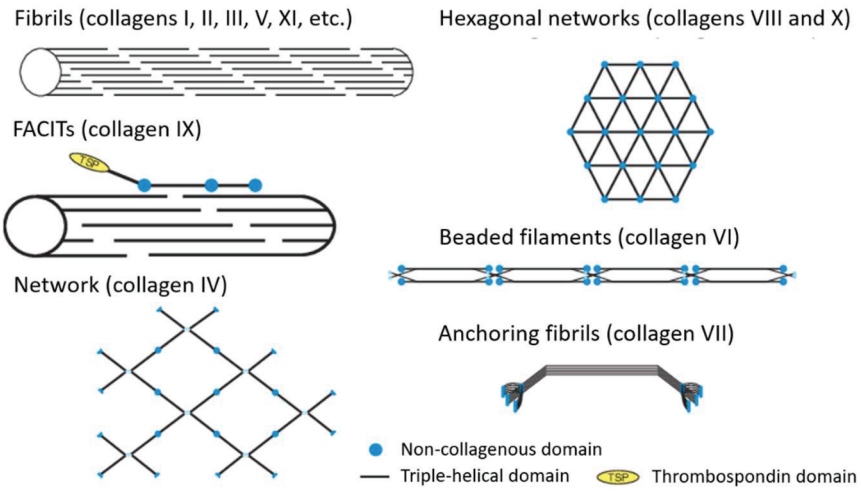

Figure 8: Supramolecular assemblies of the collagen family[69]
In humans, the large collagen family comprises 28 different collagens, which all share a common feature, the presence of a triple-helical domain, and can form supramolecular assemblies. They differ in their structural organization: domain composition and type of supramolecular assemblies (fibril-associated or network-forming collagens).

Among the large family of collagens, fibrillar collagens are able to form fibrils, which are capable of withstanding tensile forces. The fibrillar collagens include types I, II, III, V and XI collagens, and two new members types XXIV and XXVII[66]. The most abundant collagens in skin are type I (80%) and type III (10%) collagens, representing more than 90% of the total bulk of collagen[68]. They are also the main structural components of blood vessels, tendon and bones. Type II collagen is specific to cartilage and type V collagen is present in most connective tissues, including the dermis where it represents less than 5% of total collagen. Types I, III, and V collagens self-assemble into larger collagen fibres that form a 3D structural network

throughout the dermis, providing tensile strength and skin tissue integrity. Type IV collagen, in contrast, forms a relatively thin interlacing network within the basement membranes and is present at the DEJ of skin. Type VI collagen forms beaded filaments found in most connective tissues whereas type VII collagen, characterized by an extended collagenous domain, assembles into anchoring fibrils at the DEJ. Finally, the FACITs, such as types IX, XII, XIV and XVI collagens, do not form fibrils by themselves but are associated with the surface of collagen fibrils[69]. Type XII collagen is expressed in the dermis, while types XIV and XVI collagens are found both in the DEJ and the dermis[70,71].

Since fibrillar collagens are the major constituents of the skin and are essential for skin architecture and integrity, collagen fibrillogenesis has been extensively studied and will be the focus of the next sections.

2) Fibrillar collagen biosynthesis

Four different stages define fibrillar collagen assembly (***Figure 9***). Firstly, procollagen α-chains are synthesized on membrane-bound ribosomes by fibroblasts and then modified in the rough endoplasmic reticulum (ER) before being secreted extracellularly[72].

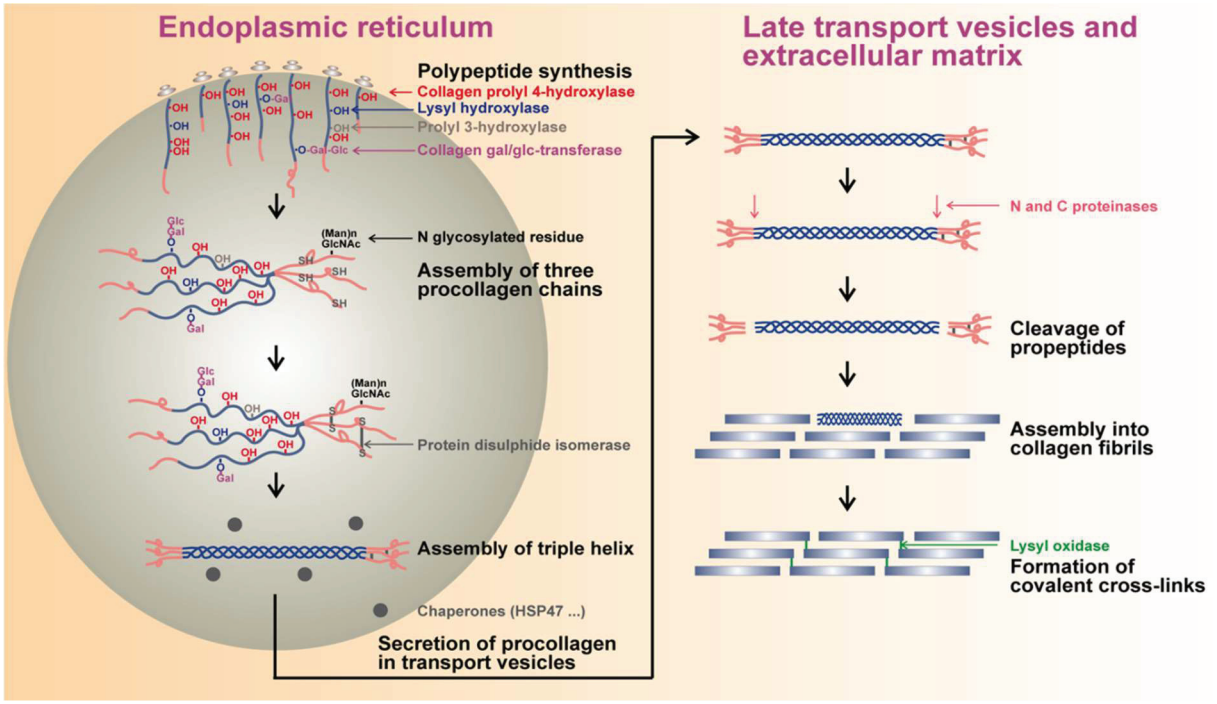

Figure 9: Major steps of collagen fibrillogenesis from synthesis to assembly[72]
Collagens are synthesized as polypeptide chains on membrane-bound ribosomes by cells. Specific lysine and proline residues are modified (hydroxylation and glycosylation) by the action of several enzymes and then the three chains assemble into a triple-helix starting at their C-terminal region. Procollagens are secreted into the extracellular space and processed by N- and C-proteinases. Mature collagens can assemble into fibrils, a network that is strengthened by the formation of cross-links.

An important collagen modification is the 4-hydroxylation of prolines to obtain 4-hydroxyproline residues that are essential for the formation of the collagen triple helix. This reaction is achieved by key enzymes in collagen biosynthesis, the prolyl 4-hydroxylases (P4HA)[73]. Several lysine residues can also be hydroxylated by lysyl hydroxylases (procollagen-lysine 1, 2-oxoglutarate 5-dioxygenase (PLOD) 1, 2, and 3). Finally, some of these hydroxylysine residues become glycosylated by the action of glycosyltransferases (GLT25D1 and GLT25D2). After hydroxylation of proline and lysine residues and glycosylation, the three procollagen α-chains can spontaneously assemble to form triple-helical procollagens made of a triple helix flanked by amino- and carboxy-terminal extensions, the N- and C-propeptides that confer solubility[74]. Trimerization of the three chains occurs within the ER and is initiated by the interaction of the C-propeptide sequences in each α-chain.

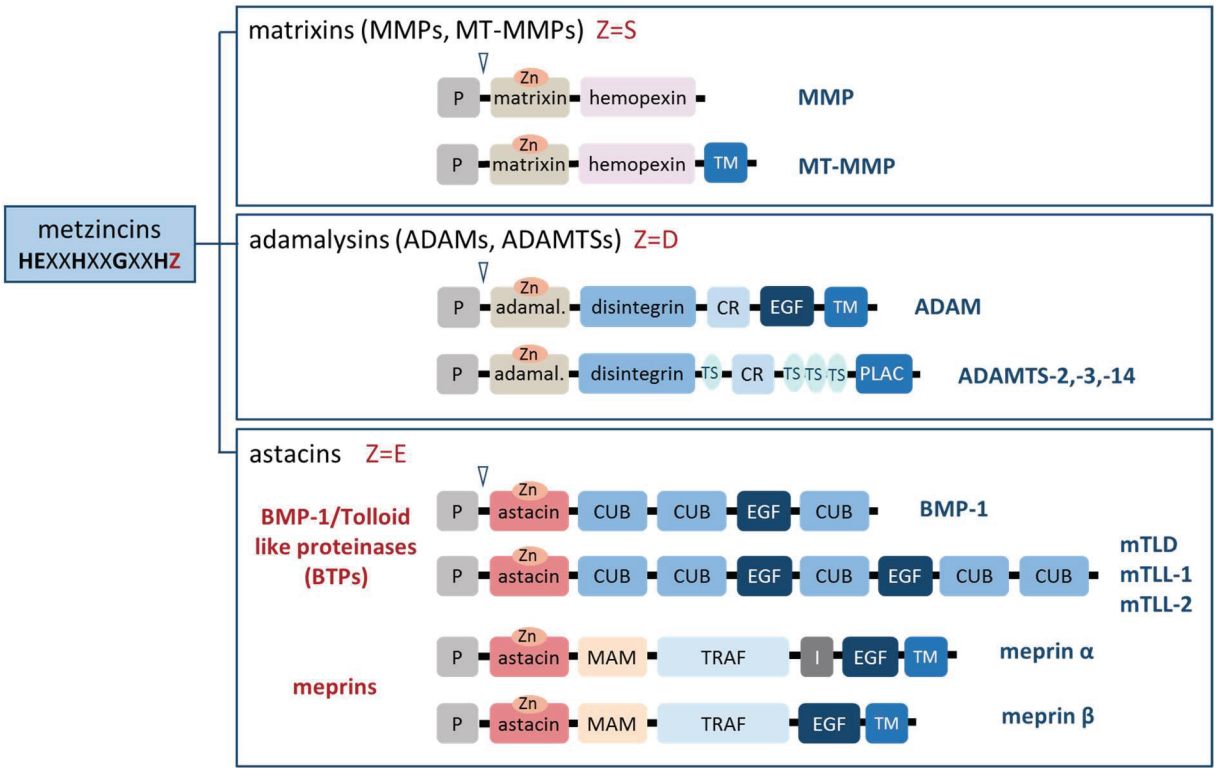

Figure 10: Proteases of the metzincin family
The metzincin family is composed of five zinc-proteinase subfamilies which include (1) the matrixins which comprise the matrix metalloproteinases (MMPs) and the membrane-type MMPs (MT-MMPs), (2) the adamalysins represented by the ADAM and the ADAMTS proteases, and (3) the astacins which regroup BMP-1/Tolloid like proteases (BTPs) and meprins. Among the BTP family, four members are found: BMP-1, mTLD, mTLL-1 and -2. The two other subfamilies that are not represented here are the serralysins and the pappalysins. *P, prodomain; Zn, zinc; CR, cysteine rich; EGF, epidermal growth factor; TM, transmembrane domain; TS, thrombospondin repeat; PLAC, protease and lacunin; CUB, Complement-Uegf-BMP-1.*

Then, this soluble precursor form of collagen is packed into secretory vesicles and secreted into the extracellular space before being converted into the mature form by proteolytic cleavage. Procollagen processing is carried out by zinc-dependent proteases, belonging to the BMP-1/Tolloid-like (BTP), A Disintegrin and Metalloproteinase with Thrombospondin motifs (ADAMTS-2, -3 and -14) or meprin families, which assure the proteolytic cleavage of the N- and C-propeptides. These three classes of metalloproteases belong to the metzincin family (***Figure 10***), which is defined by a conserved zinc-binding motif (Zn) and a methionine-containing turn near the active site[75]. They are all involved in procollagen processing and in several remodelling processes. While ADAMTS-2, -3 and -14 are responsible for the removal of the N-propeptides of types I, II, III and V procollagens, BTPs are rather involved in the C-proteinase activity in fibrillar procollagens. Meprins α and β have the ability to cleave both the N- and C-propeptides[76]. Deletion in the genes encoding the BTP[77,78], ADAMTS[79] or meprin[76] proteases leads to aberrant collagen fibrils containing unprocessed forms of collagens (***Figure 11***).

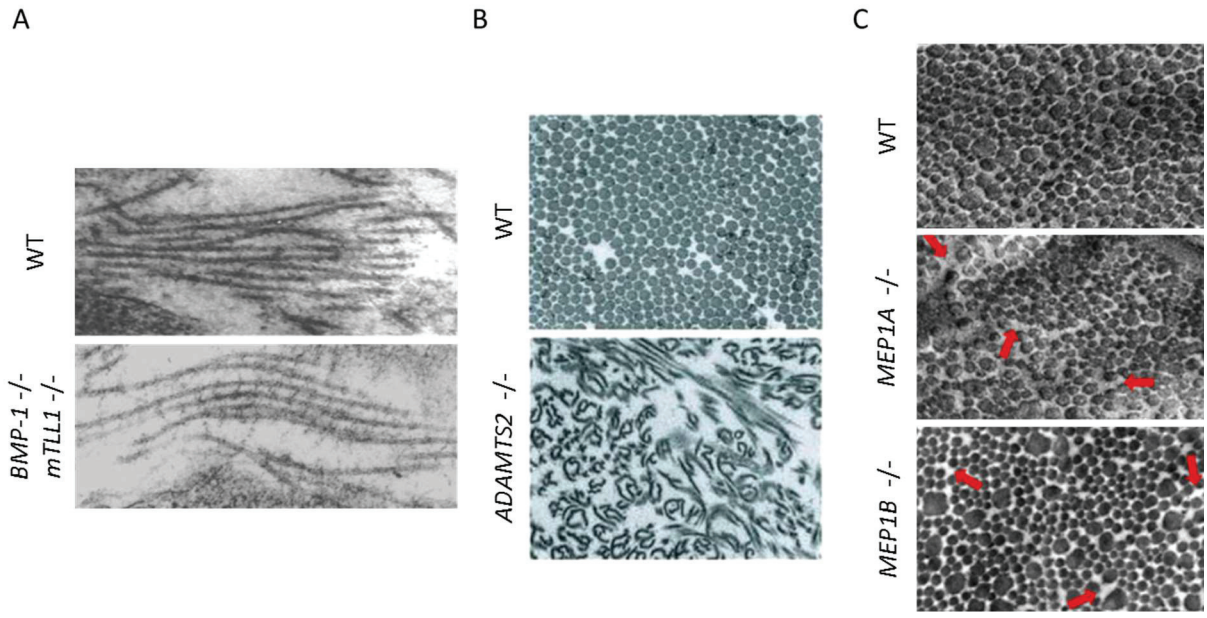

Figure 11: Abnormal collagen fibrils in BTP-, ADAMTS- or meprin-deficient mice[76,78,79]
(A) Abnormal collagens fibrils in *BMP1* -/- *mTLL1* -/- embryos are observed by transmission electron microscopy (TEM). Collagen fibrils have a "barbed wire" appearance, probably because the C-propeptide remains attached. **(B)** The absence of ADAMTS-2 leads to the formation of abnormal collagen fibrils with ribbon-like structures in *ADAMTS2* -/- mouse skin, as observed by TEM. **(C)** Fibrils in the skin of meprin α- and meprin β-deficient mice (*MEP1A* -/- and *MEP1B* -/- respectively) exhibit a less tightly packed organization (red arrows) compared to WT skin.

Thus, removal of the N- and C-propeptides, which confer solubility to the procollagen molecules, is crucial for the proper assembly and deposition of fibrils. Once these extremities are cleaved, mature and insoluble collagens can spontaneously assemble into fibrils that are

enzymatically cross-linked (***Figure 9***). Lysyl oxidase (LOX) and lysyl oxidase like (LOXL) catalyse the reaction of oxidative deamination of (hydroxy)lysine residues, leading to the formation of cross-links between collagen fibrils (and elastin fibres); this reaction provides stability and enhances tissue mechanical properties[67,80]. Collagen fibril assembly is further regulated by interactions with SLRPs, such as decorin and biglycan, which control the width and lateral growth of fibres (diameter can range from 20 to 500 nM depending on tissues)[81]; they may also influence collagen fibril cross-linking[82].

To fully understand collagen fibrillogenesis, it is important to note that intracellularly, collagen monomers can self-assemble in homo- or hetero-trimers, which makes the collagen processing much more complicated. Among the fibrillar collagens, the most abundant collagens are types I, II and III collagens and are thus considered as major collagens, while the minor collagens are types V and XI (and recently, XXIV and XXVII) collagens. Types II and III collagens are homotrimeric and made up of three identical α1 chains, $[\alpha1(II)]_3$ and $[\alpha1(III)]_3$ respectively, whereas type I can be found as a homotrimer of three α1 chains, $[\alpha1(I)]_3$ or a heterotrimer containing two α1 chains and one α2 chain, $[\alpha1(I)]_2[\alpha2(I)]$[69]. The most abundant and ubiquitous molecular form of type V collagen is the $[\alpha1(V)]_2[\alpha2(V)]$ heterotrimer[83]. For collagen XI, the [α1(XI)][α2(XI)][α3(XI)] heterotrimer isoform is found in tissues. Another factor that influences fibril assembly and increases the diversity of the collagen family is the formation of heterotypic fibrils. In most connective tissues, several types of collagens copolymerize and form hybrid collagen fibrils: I/III/V collagens in skin (type V collagen regulates the diameter of fibrils through the retention of the α1 N-propeptide)[84]; I/V in cornea[83]; II/IX/XI, II/III[85] and V/XI[86] in cartilage. In general, minor collagens V and XI assemble with major fibrillar collagens I, II and III, and then with other associated collagen or non-collagen proteins (such as FACITs and SLRPs).

This high diversity complicates procollagen processing, especially because every single α chain of each collagen type can be processed by different proteases at the N- and C-terminal extremity; this will be further described below with a particular focus on BTPs.

3) BMP-1/Tolloid-like Proteinases

a. Identification and structure

BMP-1/Tolloid-like Proteinases (BTPs) were first described for their role in procollagen processing. The BTP family belongs to the astacin subgroup of the metzincin family and is composed of four different proteases: BMP-1 (bone morphogenetic protein 1), mTLD (mammalian tolloid), mTLL-1 and -2 (mammalian tolloid-like 1 and 2). The founder member

of the family, BMP-1, was discovered in the 1980s in demineralized bone extracts for its ability to promote ectopic bone formation[87]. Its name has been confusing because BMP-1 is the only proteinase among the BMPs and is not a member of the TGFβ family like other BMPs. Because of their strong sequence homology, BMP-1 was then linked to the Tolloid protein involved in the formation of the dorso-ventral axis during early embryonic development in *Drosophila*[88]. Later, the homologous human protein (mTLD) was discovered and found to be the splicing variant of *BMP1*[89]. Two other members of the family, mTLL-1 and -2 are encoded by distinct genes, *mTLL1* and *mTLL2*[90]. The four BTP metalloproteases show similar structural organization. All of them consist of a propeptide followed by an astacin-like catalytic domain, several complement-Uegf-BMP1 (CUB) domains and epidermal growth factors (EGF) domains (***Figure 10***). They are synthesized as latent forms and become active after the cleavage of their propeptides by subtilisin-like proprotein convertases (SPCs) in the Golgi apparatus. Thus, after secretion into the extracellular space, they are expected to be mainly processed and active.

Despite strong sequence and structure similarities, BTPs have differential enzymatic activities and expression patterns, especially during embryo development[90,91]. BMP-1 is usually found to be the most efficient protease. BMP-1 and mTLD are widely distributed during and after development and are found in many adult tissues, and especially in heart, smooth and skeletal muscle, bone, liver, kidney, skin, adipose tissue, pancreas, thyroid, as well as in reproductive organs (uterus, prostate, etc.). In contrast to BMP-1, mTLD is also expressed in the developing central nervous system[89]. During development, mTLL-1 expression is more limited to the heart and the cardiovascular system whereas mTLL-2 is not detected in the developing heart[92], neither in cartilage and bone. Expression of mTLL-2 seems to be limited to skeletal muscles and the central nervous system[90]. The restricted expression pattern of mTLL-2 suggests that the function of this protease may be more limited and differs from the other BTPs, especially as a number of substrates cleaved by BMP-1, mTLD and mTLL-1 are poorly or not cleaved by mTLL-2 (e.g procollagens[90]).

Altogether, the wide distribution of BTPs in embryonic and adult tissues suggests a key role of these proteases in developmental processes and tissue homeostasis. Originally, BTPs were discovered for their exclusive role in procollagen C-terminal processing and previously named procollagen C-proteinases (PCP). More recently, many other substrates have been identified and BTPs appear to play roles in various biological functions ranging from embryogenesis and morphogenesis to ECM biosynthesis and remodelling.

b. Direct roles in collagen fibril formation and assembly

As mentioned previously, the main role of BTPs is to cleave the C-terminal propeptide domains of procollagen precursors to produce mature monomers able to form fibrillar collagens. Procollagen processing is complex; it relies on the activity of several metalloproteases and involves different cleavage sites depending on the type of collagen and the α chain (***Figure 12***). While the N-terminal processing of major fibrillar collagens is carried out by ADAMTSs (-2, -3 and -14) and meprins, BTPs are mostly responsible for their C-terminal processing[90,93,94]. They cleave the C-propeptides of the α1 and α2 chains of type I procollagen, as well as the α1 chain of types II and III homotrimeric procollagens. The cleavage sites have been identified by N-terminal amino-acid sequencing and always involve an aspartate (Asp) residue at the P1' position: Ala^{1218}/Asp^{1219} and Ala^{1119}/Asp^{1120} for the α1(I) and α2(I) chains respectively; Ala^{1241}/Asp^{1242} for the α1(II) chain and Gly^{1221}/Asp^{1222} for α1(III) chain[93,95].

BTPs are also able to cleave the minor fibrillar collagens (types V and XI), but with some important differences compared to the major fibrillar collagens. Three α chains have been reported for both type V and XI collagens. In tissues, the most common forms are $[\alpha1(V)]_2[\alpha2(V)]$ and [α1(XI)][α2(XI)][α3(XI)] hetero-trimers but other isoforms exist including [α1(V)][α2(V)][α3(V)] and $[\alpha1(V)]_3$[83]. BTPs can cleave the N-propeptides of the α1(V), α3(V)[96–98] and α1(XI) chains[99], but not the N-propeptide of the α2(V) chain which remains intact in the mature molecule[100]. It is important to note that in these cases, the cleavage sites within the N-terminal sequence lack the canonical aspartate (D) residue at the P1' position but contain instead a glutamine (Q; ***Figure 12***). Furthermore, BTPs can cleave the C-propeptides of the α1(V) and α2(V) chains. However, it seems that an upstream cleavage site in the α1 chain is used first by SPCs (such as furin) in the Golgi apparatus[98]. This is not the case in the α2 chain for which BTPs remain the only known C-proteinases. Because of high conservation between sequences, the N-propeptide of the α2(XI) is also probably processed by BTPs and the C-propeptides of the α3(V), α1(XI) and α2(XI) chains are likely to be processed by SPCs. However, these cleavage sites are only putative and need to be clearly identified.

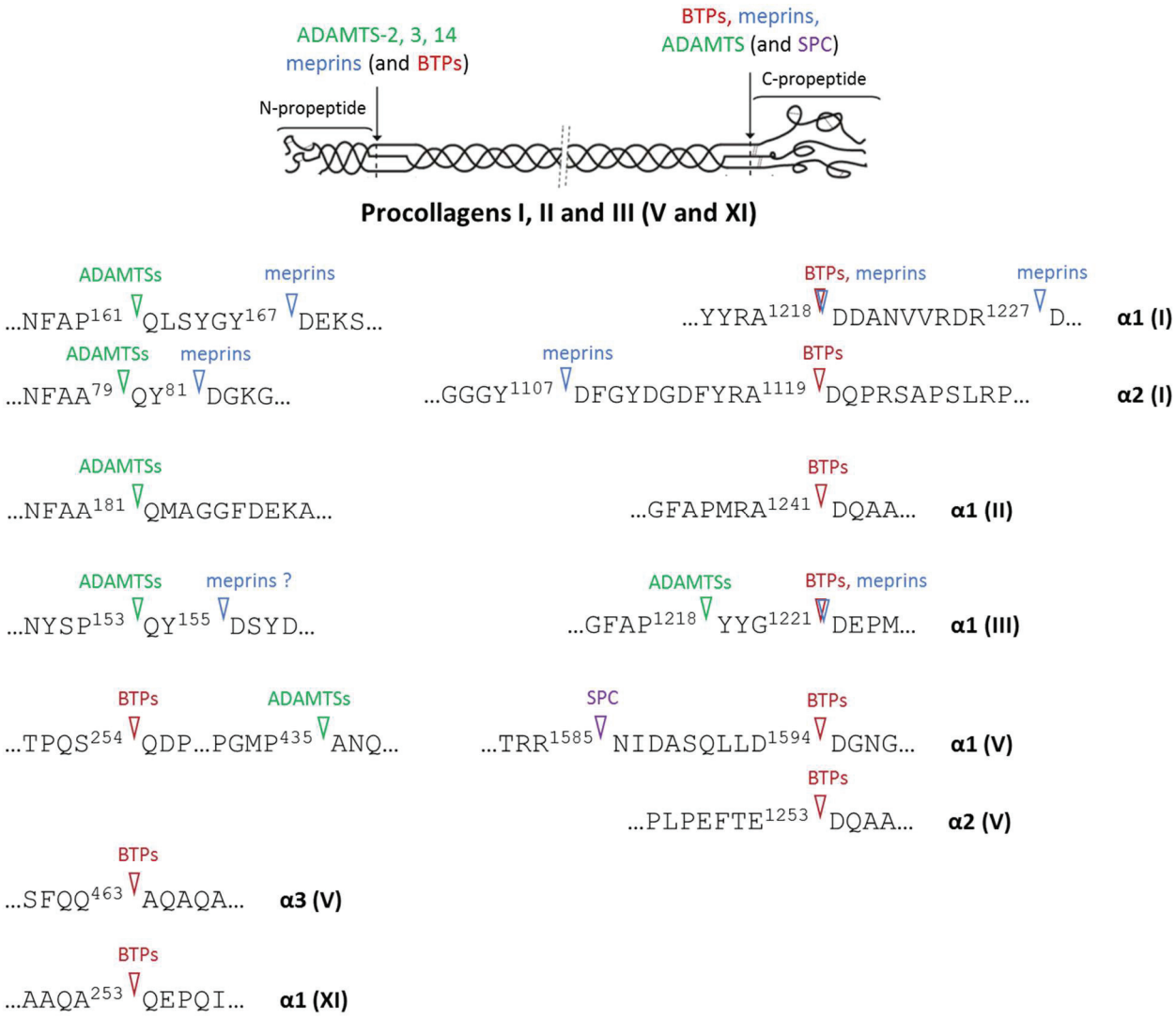

Figure 12: N- and C-terminal processing of the fibrillar procollagens (I, II III, V and XI)
Schematic representation of the cleavage sites within the N- and C-terminal sequences of procollagens and the proteases involved (BTPs, ADAMTSs, meprins and subtilisin-like convertases, SPC). BTPs are mostly responsible for the C-terminal processing of major fibrillar collagens (I, II and III) while the N-propeptide is removed by ADAMTSs and meprins. Minor fibrillar collagens (V and XI) are rather processed by BTPs in the N-terminal region and by SPCs and BTPs in the C-terminal region.

In addition to their direct role in procollagen processing, BTPs also control the maturation and activity of other proteins related to ECM assembly, e.g. the SLRPs regulating fibre width and spacing and the cross-linking enzymes (pro-forms of LOX and LOXL; ***Figure 13***). SLRPs, such as biglycan, osteoglycin and decorin are secreted as precursor forms with a conserved propeptide in the N-terminal region. BTPs cleave the N-propeptide of those SLRPs[101–103] that can then interact directly with collagen fibrils and control their diameter and spacing and the kinetics of fibril formation. Finally, BTPs convert pro-LOX[104] and pro-LOXL[105] into mature enzymes. Once matured, these enzymes initiate cross-link formation through the oxidative deamination of specific lysines in collagen trimers thereby strengthening the 3D network of collagens.

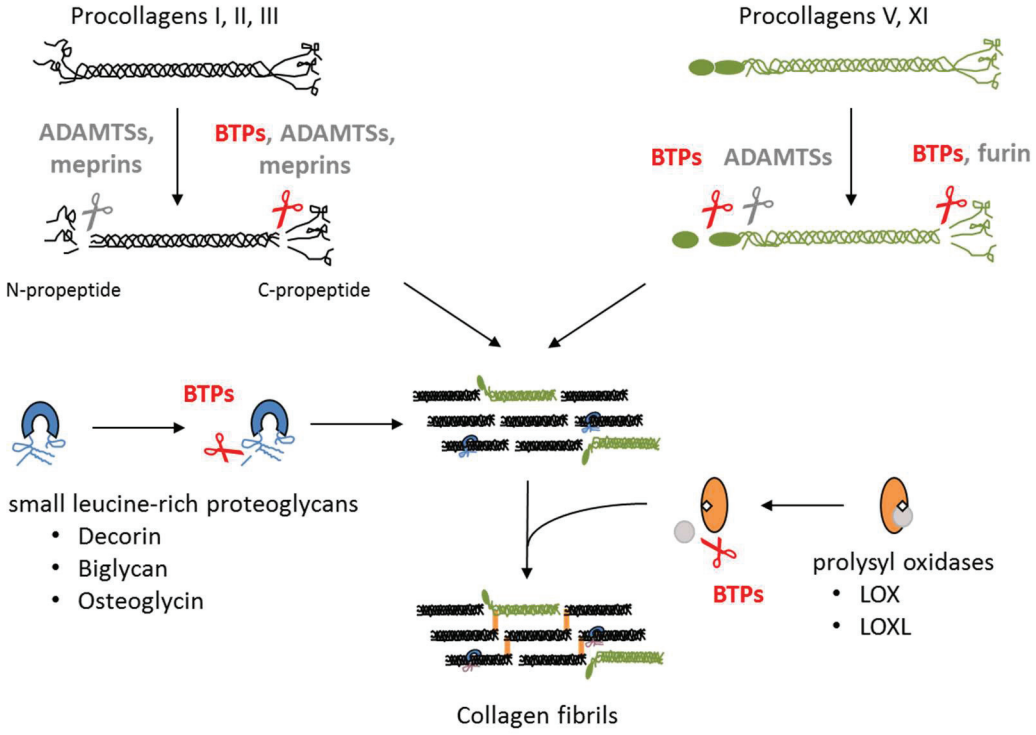

Figure 13: BTPs play a key role in all the steps of fibrillogenesis

Schematic representation of the fibrillogenesis of procollagens I, II and III (left) and procollagens V and XI (right). BTPs ensure the C-terminal processing of fibrillar procollagen, allowing the spontaneous assembly of collagen monomers into fibrils. They are also involved in the proteolytic maturation of SLRPs and LOXs, proteins controlling respectively the diameter of fibrils and the formation of crosslinks.

c. Basement membrane assembly

BTPs are also capable of processing basement membrane associated components: type VII procollagen (α1 chain), laminin-332 (γ2 and α3 chains) and perlecan, which is consistent with *in vivo* observations that BMP-1 is localized at the DEJ in the skin[106].

Type VII procollagen is synthesized by keratinocytes and fibroblasts in precursor form. The procollagen monomer consists of three α1(VII) chains folded into a triple helix which is flanked by two non-collagenous domains, NC-1 (made of 9 consecutive fibronectin III domains) and NC-2[107]. After secretion into the extracellular space, two monomers of type VII collagen form an antiparallel dimer through their NC-2 domains[108] (***Figure 14***). Then, the C-terminal NC-2 propeptides are proteolytically removed by BTPs (at the position Ala[2821]/Asp[2822])[109]. Finally, the mature dimers can assemble into anchoring fibrils at the DEJ.

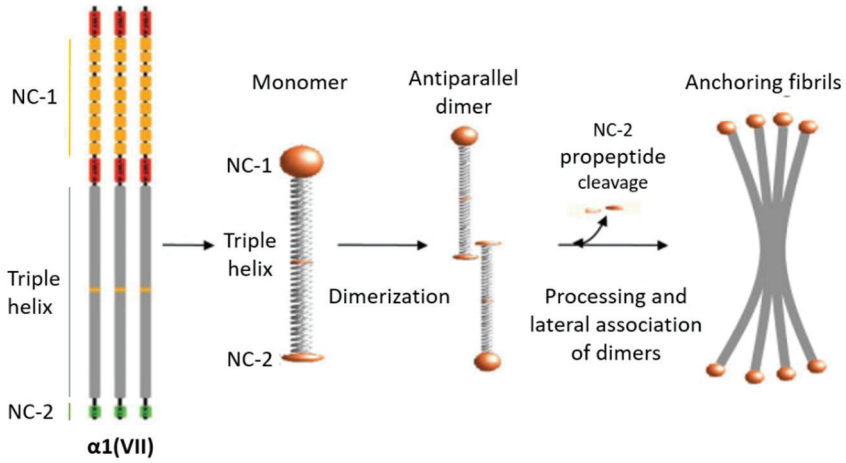

Figure 14: Procollagen VII processing and assembly into anchoring fibrils (adapted from Bruckner-Tuderman et *al.*[107])

Type VII procollagen monomers, made of three α1(VII) chains, form antiparallel dimers from which the C-terminal NC-2 domain is proteolytically removed by BTPs. Mature dimers then aggregate into anchoring fibrils.

Laminin-332 is also secreted by keratinocytes in precursor form, composed of three chains (α3, β3 and γ2; ***Figure 15A***). Laminin-332 can be processed by various proteases. The cleavage of the γ2 chain in the N-terminal region is done by BTPs (at the position Gly[434]/Asp[435])[106]. For the α3 chain, N-terminal processing is assured by BTPs whereas C-terminal processing can be carried out by several proteases of the MMP family (e.g. MMP-2), plasmin, thrombin and BTPs[106,110]. All these maturation events are essential for the structural integrity of the basement membrane and thus the cohesion between the epidermis and the dermis. In the context of wound healing, mature laminin-332 plays a major role in re-epithelialization as it appears to be the first basement membrane component to be expressed and mediates the migration of keratinocytes onto the wound bed[111].

Perlecan is a basement membrane-type heparan sulfate proteoglycan that interacts with type IV collagen and laminin-332[112]. Whereas the full-length protein has an angiogenic function, proteolytic cleavage of the C-terminal domain generates a fragment named endorepellin (corresponding to domain V) or its LG3 domain (***Figure 15B***) with anti-angiogenic activity[113]. Indeed, this fragment is able to inhibit endothelial cell migration and capillary growth. BTPs can perform the cleavage of the LG3 domain[114].

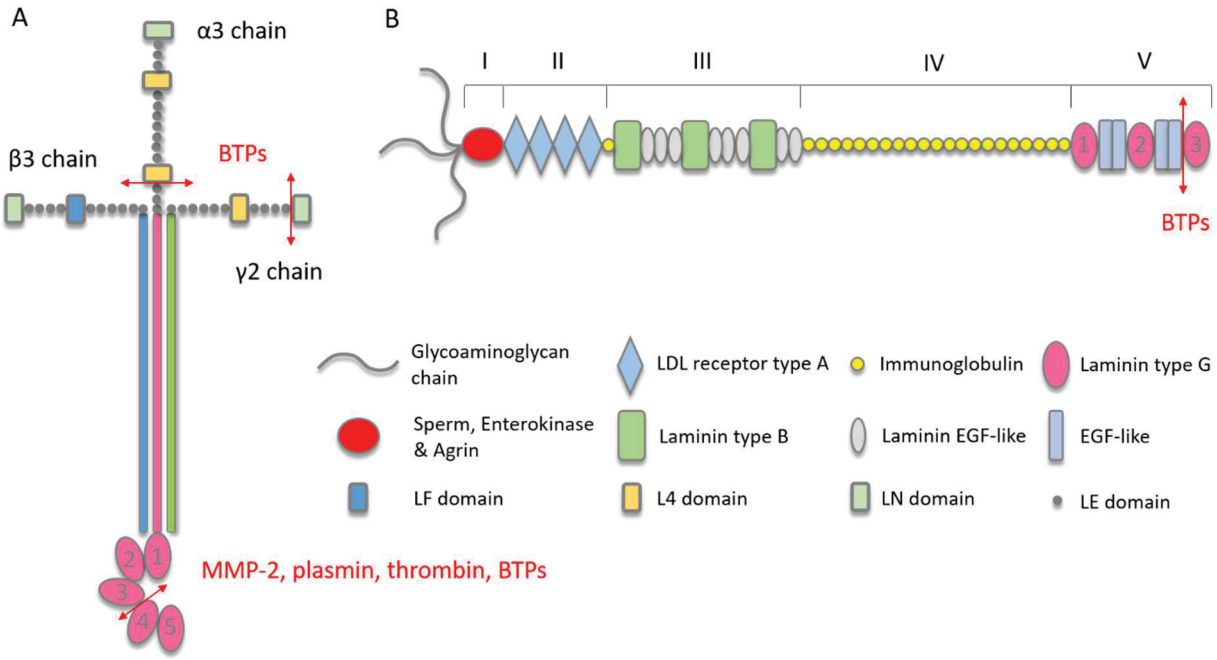

Figure 15: Laminin-332 (A) and perlecan (B) structures and cleavage sites by BTPs

(A) Structure of laminin-332, basement membrane component made of 3 chains: α3, β3 and γ2 chains, the α3 and γ2 chains being cleaved exclusively or partially by BTPs, allowing the integration of mature laminin into the basement membrane. **(B)** Structure of perlecan, a basement membrane proteoglycan which can be processed by BTPs in the C-terminal region releasing the laminin type G3 domain (LG3).

d. Activation of growth factors

Another role attributed to BTPs is the activation of growth factors[115]. Among these, BTPs have been associated with the potentiation of BMP signalling during embryogenesis. Chordin binds to BMP-2 and -4 growth factors to form a latent complex that diffuses from the ventral to the dorsal part of embryos. BTPs allow the release of the BMP factors by cleaving their chordin antagonist and thereby potentiating BMP signalling during dorso-ventral axis formation and development. Similarly, BTPs are involved in the release and activation of insulin-like growth factor-1 (IGF-1) through the cleavage of IGF-like binding protein-3. IGF-1 is also an important factor in development, growth and metabolism.

All the growth factors from the TGFβ superfamily (including BMP-2 and -4 but also TGFβ1-3, GDF, etc.) are synthesized as precursor forms containing a prodomain which is removed by SPCs. However, for some factors, such as GDF-8 (known as myostatin), GDF-11 and TGFβ itself, the prodomain remains attached to the protein by a non-covalent link and keeps the complex in latent form. BTPs are able to cleave the propeptide and release the active growth factor. In the case of TGFβ1, which is of special interest in the context of ECM deposition and wound healing, the activation process is even more complicated. TGFβ1 is secreted in latent form, in association with its propeptide called latency associated peptide (LAP). In addition, latent TGFβ forms a large latent complex (LLC) attached to the matrix through the covalent association of LAP with latent TGFβ-binding proteins (LTBPs). BTPs participate in TGFβ activation by the proteolytic cleavage of LTBPs, which releases the LLC complex from the ECM[116]; TGFβ can then be dissociated by the proteolytic cleavage of LAP by MMPs and plasmin-type proteases. Moreover, TGFβ can also be found associated with soluble co-receptor, such as betaglycan (or TGFβ type III receptor) which is also a substrate of BTPs[117]. By cleaving betaglycan, BTPs release active TGFβ. Finally, another non-proteolytic mechanism has been identified for TGFβ activation. At the cell surface, integrins can bind to LAP (through an RGD sequence). If the tissue is stiff enough, TGFβ can be released by the traction of the cell on the resistant ECM[118]. Thus, by playing a role in cross-linking formation, LOX and LOXL participate in the stiffness of the ECM and indirectly in the TGFβ activation.

Many substrates of BTPs have been identified in the last decade and not all of these will be described in this thesis, but it is important to highlight the wide repertoire of BTP substrates and their involvement in a wide range of biological processes: matrix assembly (procollagens, SLRPs, LOX, laminin), dorso-ventral patterning, organogenesis and muscle growth (chordin, GDF-8 and -11), angiogenesis (perlecan, prolactin, angiopoietin-like protein 2), mineralization (dentin matrix protein-1, DMP-1; dentin sialophosphoprotein, DSPP), peripheral nervous system (gliomedin), lipid metabolism (apolipoprotein AI), etc[75]. This list is not exhaustive and many unknown substrates remain to be identified[117].

e. Regulators

Only a few naturally occurring inhibitors of BTPs have been identified, e.g. α2-macroglobulin[119], which is a broad-spectrum protease inhibitor, BMP-4[120] and secreted frizzled-related proteins (sFRPs) which are putative inhibitors of BMP-1 as their inhibitory function is still controversial[121–123].

Several proteins act as activators of BTPs: procollagen-C proteinase enhancers (PCPEs) which are the focus of this thesis and will be extensively described in the next section, periostin, fibronectin, twisted gastrulation and olfactomedin noelin tiarin factor-1 (ONT-1)[75,115]. All these activators are able to enhance the activity of BTPs in a substrate-specific manner (except for fibronectin, which enhances the cleavage of several substrates of BTPs). While PCPEs specifically enhance the activity of BTPs in fibrillar procollagen (I-III and V) processing, periostin is a matricellular protein expressed during development and matrix remodelling which increases the proteolytic activation of LOX by BTPs[124]. Twisted gastrulation is a small cysteine-rich glycoprotein which forms a complex with BTPs and chordin, promoting the cleavage of chordin by BTPs and thus the activation of BMP growth factors (as described above; see §III.3.d)[125]. A similar activator effect has been described for ONT1 in *Xenopus* but has not yet been confirmed in mammals[126].

Finally, fibronectin favours the conversion of pro-LOX into LOX by BTPs, but also enhances the cleavage of chordin, biglycan and type I procollagen[127]. This reveals that fibronectin seems to play a role at different levels in BTP signalling and could be important in several biological processes.

f. Patho-physiological roles of BTPs

In recent years, the *BMP1* gene has been associated with an autosomal recessive form of osteogenesis imperfecta (AR-OI), a genetic disorder primarily characterized by bone fragility, causing susceptibility to fractures. The severity of the disease varies from bone deformities to lethality. In siblings diagnosed with AR-OI, a homozygous missense mutation has been identified in the catalytic protease domain of the *BMP1* gene, causing deficient procollagen I processing[128]. Moreover, because of the position of the mutation in the catalytic domain, it is highly probable that the processing of other BTP substrates is affected in these young patients, which could explain this strong phenotype. Different mutations of *BMP1* have been identified so far in patients and associated with severe OI[129–132]. All these clinical observations were confirmed in a mutant mouse model generated by Greenspan's group. While constitutive deletion of *Bmp1* and m*Tll1* causes perinatal or embryonic lethality in mice (death from failure of ventral body wall closure and heart defects)[77,133], the double *Bmp1*- and *mTll1*-conditional knockout is viable. These mice are characterized by defined features of OI, especially weak and brittle bones, with spontaneous fractures[134]. Moreover, these mice exhibit thin and fragile skin, with abnormally dense packing of collagen fibrils and aberrant wound healing[135]. Delays in wound closure and re-epithelialization are observed, as well as a reduction in ECM deposition in the healed wounds, suggesting an important role of BMP-1 during skin repair. These results

are in concordance with the upregulation of BMP-1/mTLD during corneal healing and scarring[136]. Furthermore, a conditional knockout of *Bmp1* and *mTll1* causes dental and periodontal defects in mice, accompanied with altered collagen fibres. Unprocessed procollagen I accumulates and levels of DMP-1, a critical marker of mature osteocytes, and also DSPP, the second more prominent protein in dentin are reduced[137–139]. Consistent with the identified BTP substrates[115] (including type I procollagen, DMP-1 and DSPP), these results evidence the key role of BTPs in tooth and periodontal tissue formation and homeostasis, through the processing of these proteins.

In recent years, BTPs have been of special interest in the context of fibrosis, a disease characterized by excessive collagen deposition, resulting in organ dysfunctions. Indeed, dysregulation of collagen processing involving BTP activity might be partially involved in the development of fibrosis within tissues. Several studies have supported this hypothesis in renal and cardiac fibrosis. In rats and patients with chronic kidney disease, increased circulating amounts of mTLD in the plasma were found to exacerbate renal fibrosis[140]. Moreover, following coronary artery ligation, BMP-1 expression was shown to be up-regulated in a mouse myocardial infarction model[122]. Finally, increased levels of BTPs have been found in patients with chronic heart failure[141] or with aortic stenosis, the most common valve disease in developed countries[142]. All these results clearly suggest the key role of BTPs in excessive collagen deposition leading to fibrosis.

Thus, BTPs could be interesting targets to prevent excessive collagen deposition in fibrotic diseases or to promote tissue repair during wound healing or bone disease. However, the substrate repertoire of BTPs extends far beyond collagen processing and includes proteins involved in many biological processes (see §III.3.d). As targeting BTPs would likely induce undesired side effects on various pathways, a more accurate strategy should be developed to specifically target procollagen processing and fibril deposition. In this context, PCPEs, which are specific enhancers of BTPs on procollagen processing could be considered as valuable targets to prevent or control ECM deposition.

IV. Procollagen C-Proteinase Enhancers (PCPEs)

1) Identification of PCPEs

Procollagen C-proteinase enhancers -1 and -2 (PCPE-1 and PCPE-2) are 55-kDa extracellular glycoproteins encoded by the *PCOLCE* and *PCOLCE2* genes respectively. They were discovered for their role in the enhancement of BMP-1 activity on procollagen processing. The first protein to be described in the 1980s by Kessler and colleagues[143,144] was PCPE-1. While the authors were purifying procollagen C-proteinase, i.e. BMP-1 from mouse fibroblasts, they identified a glycoprotein able to enhance the C-proteinase activity, which was co-purified. Several forms of the protein were found: a 55-kDa procollagen C-proteinase enhancer and smaller 34- and 36-kDa proteolytically processed forms of the same protein, all of which were glycosylated. In this study, they noted that in mouse, both the 55-kDa PCPE-1 protein and the proteolytic forms were able to bind to the C-propeptide of type I procollagen and to enhance C-proteinase activity. In 1994, Takahara et *al.*[145] purified for the first time this enhancer protein, PCPE-1 from mouse fibroblasts and found it to be a 468-amino acid protein based on sequence homology with a previously reported cDNA. They then cloned the human *PCOLCE* gene, which encodes a 449-amino acid protein from a placenta cDNA library and found high sequence homology between human and mouse proteins. Finally, they localized the *PCOLCE* gene to the 7q21.3-q22 chromosome.

More recently, in 2000, Xu et *al.*[146] identified a novel human procollagen C-proteinase enhancer protein-like gene, *PCOLCE2*, by sequencing an expressed sequenced tag (EST) in the primary open-angle glaucoma (most common form of glaucoma) region on chromosome 3q21. This second and homologous form of PCPE was named PCPE-2. They found 46% identity between the PCPE-1 and PCPE-2 human proteins.

2) Function and specificity

PCPE-1 and PCPE-2 are ECM glycoproteins and potent stimulators of BTP-mediated procollagen processing[147,148]. PCPE-1 is the most well-described enhancer, and its role and structure have been extensively studied over the last 20 years. PCPE-1 lacks intrinsic enzymatic activity[144] but stimulates between 2 and 20-fold the release of the C-propeptides from fibrillar procollagens mediated by BMP-1. While BTPs have multiple substrates (as described above; see §III.3), PCPE-1 seems to be highly specific for fibrillar procollagens, through a strong and direct interaction with the substrate. PCPE-1 can bind the C-propeptides of types I, II or III procollagens, thereby enhancing BMP-1 mediated-processing (***Figure 16***)[149]. It also appears to enhance the release of the N-propeptides from type V procollagen by BMP-1[150], but using a

different molecular mechanism (Vadon-Le Goff et *al.*, unpublished results). While the enhancement of major fibrillar procollagen (I, II and III) C-terminal processing by PCPE-1 has been confirmed several times[143–145,147–149,151,152], the effect of PCPE-1 on procollagen V has been described more recently. In tissues, type V collagen is widely distributed as a heterotrimer composed of two α1(V) and one α2(V) chains. Steiglitz et *al.*[152] showed that in the absence of PCPE-1, the C-terminal processing of the α2(V) chain mediated by BMP-1 was diminished (***Figure 17A***). This suggests that PCPE-1 can enhance the C-terminal processing of the α2 chain of type V procollagen. Recently, Symoens et *al.*[150] showed that PCPE-1 acts as an enhancer of the N-terminal processing of the α1 chain of type V procollagen *in vitro* (***Figure 17B***), even though its enhancing effect is weak and can be challenging to observe. This is the first report of an enhancing effect of PCPE-1 on substrates other than the major fibrillar collagens.

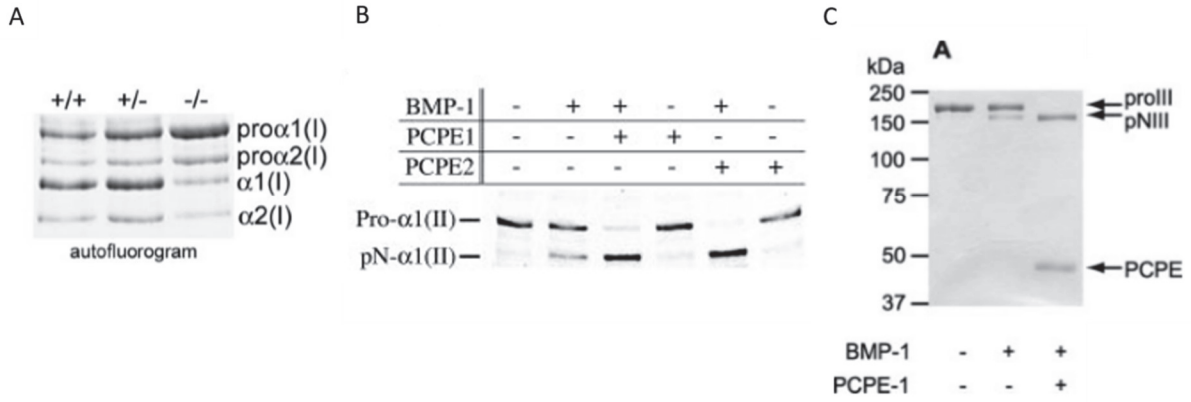

Figure 16: Processing of fibrillar procollagens (type I, II and III) mediated by BMP-1 is enhanced by PCPE-1 and PCPE-2

(A) Autofluorogram of mouse embryonic fibroblast (MEF) media. The processing of procollagen I (proα1 and proα2(I) chains) is reduced in conditioned-medium of MEFs isolated from PCPE-1-deficient mice (-/-) compared to wild-type mice (+/+)[152]. **(B)** Autofluorogram of recombinant procollagen II protein incubated with BMP-1, PCPE-1 and/or PCPE-2. Both PCPE-1 and -2 stimulate the processing of the α1 chain of procollagen II[148]. **(C)** SDS-PAGE analysis of recombinant procollagen III (ProIII) incubated with recombinant BMP-1 and PCPE-1 proteins. Procollagen III processing mediated by BMP-1 is stimulated *in vitro* in the presence of PCPE-1[151].

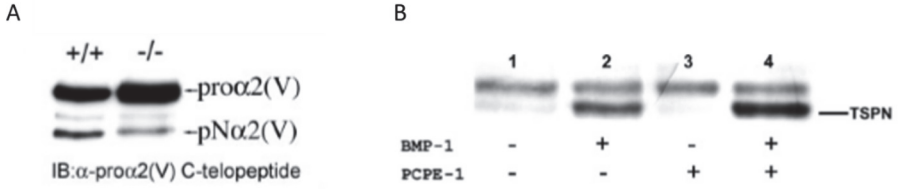

Figure 17: Effect of PCPE-1 on type V procollagen processing

(A) Western blotting showing that in the absence of PCPE-1 (-/-), the C-terminal processing of the α2 chain of procollagen V is decreased *in vivo*[152]. **(B)** Western blotting analysis of recombinant pNα1(V) protein incubated with or without BMP-1 and PCPE-1. As shown by the increase in the N-terminal fragment (TSPN), PCPE-1 enhances the N-terminal processing of the α1 chain of procollagen V[150].

Indeed, the processing of other BMP-1 substrates (for example, type VII procollagen, chordin, osteoglycin, laminin-332) is not affected by PCPE-1 (***Figure 18***)[151,153]. This substrate specific-enhancing activity is an unusual mechanism of action and suggests that PCPE-1 needs specific recognition motifs to be active.

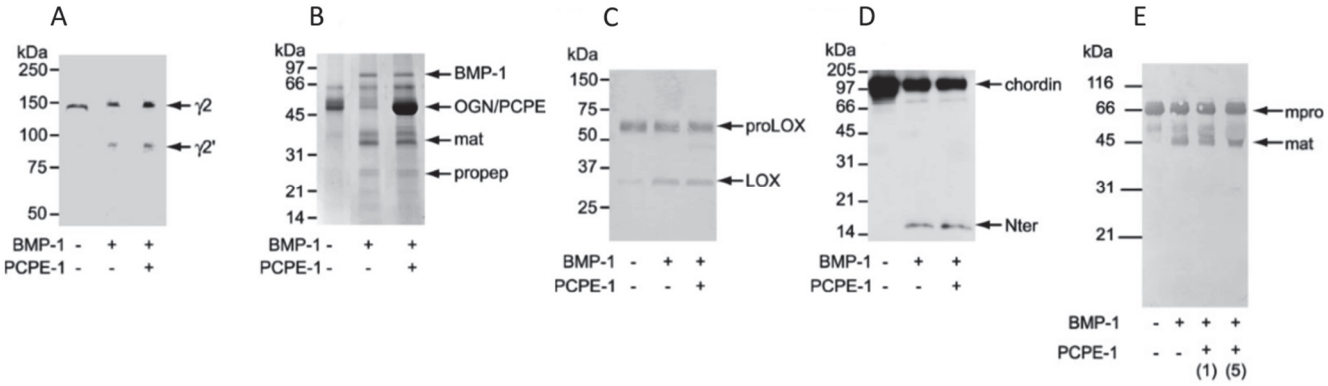

Figure 18: Processing of other BTP substrates is not enhanced by PCPE-1[151]
SDS-PAGE analyses of recombinant BTP substrates incubated with BMP-1 and PCPE-1 proteins: **(A)** γ2 chain of laminin-332, **(B)** osteoglycin (OGN), **(C)** pro-lysyl oxidase (proLOX), **(D)** chordin, **(E)** procollagen VII (mpro). *mat, mature; propep, propeptide; Nter, N-terminal fragment.*

On the contrary, PCPE-2 has been much less studied and only few studies describe its activity. The first evidence of PCPE-2 activity on procollagen processing was reported by the Greenspan's group 15 years ago[148]. They showed that *PCOLCE2* gene encodes a functional procollagen C-proteinase enhancer able to stimulate the C-terminal processing of type II procollagen by BMP-1, with activity levels similar to that of PCPE-1 (***Figure 16C***). The intrinsic enhancer activity of PCPE-2 was then confirmed on type I procollagen from fibroblast-conditioned medium[154]. The authors showed that BMP-1-mediated processing of type I procollagen was enhanced in the presence of PCPE-2. These results suggested that both PCPE-1 and PCPE-2 stimulated in a similar way the processing of fibrillar collagens by BTPs.

Understanding the mechanism by which PCPEs enhance BMP-1 activity has been the subject of intense studies. The first hypothesis was that PCPEs bind specifically to the substrate, on both sides of the BMP-1 cleavage site in order to facilitate substrate bending and the accessibility of the substrate to the protease. This would involve specific recognition and interaction sites between the protease (BMP-1), the enhancer (PCPE) and the substrate (procollagen). To unravel the mechanism of action of PCPEs, it was necessary to go further in the understanding of the protein structure, as we will see in the following paragraphs.

3) Structure of PCPEs

Human PCPE-1 (UniProt #Q15113) and PCPE-2 (UniProt #Q9UKZ9) consist of two N-terminal CUB (Complement C1r/C1s – Uegf – Bmp1) domains that bind to the C-propeptides of procollagen molecules and a C-terminal netrin (NTR)-like domain involved in the interaction with heparin and heparan sulfates (***Figure 19***). The two proteins share 46% sequence identity with a high conservation in the CUB domains (the first CUB domain of PCPE-2 shares 54% identity with PCPE-1 and the second CUB domain has 61% identity with the one of PCPE-1). In contrast, the homology in the NTR region is not as high, with only 38% identity. The lowest level of homology between PCPE-1 and -2 is found in the linker between the CUB domains and the NTR domain[145] with differences in sequence content and length.

Figure 19: Human PCPE-1 and PCPE-2 protein sequences

(A) Structure and domain composition of human PCPE-1 (PCOC1_HUMAN) and PCPE-2 (PCOC2_HUMAN). The two proteins consist of three domains, each beginning with a cysteine residue: in the N-terminal region, two CUB domains (CUB1 and CUB2) and in the C-terminal region, a NTR domain, separated from the CUB2 domain by a linker, variable in length (44 or 28 amino acids). **(B)** Alignment of PCPE-1 (Q15113) and PCPE-2 (Q9UKZ9) sequences using the Clustal Omega tool. The asterisk symbol (*) indicates fully conserved residues, the colons (:) correspond to amino acids with strongly similar properties and the period (.) indicates that the two residues have weak similar properties. The highlighted amino acids are the residues involved in the interaction with procollagen (see below).

a. CUB domains

The CUB domains are structural motifs of approximately 110 residues found almost exclusively in extracellular and plasma membrane-associated proteins, including proteases of the **C**omplement system (C1r and C1s), the embryonic sea **U**rchin protein Uegf and **B**MP-1[155]. They exhibit β-sheet folds, the second most abundant secondary structure, i.e. segments of the polypeptide chain called β-strands overlap and interact through a network of hydrogen bonds. The CUB domains mediate protein-protein interactions and some of these are calcium-binding domains, as is the case for the CUB domains found in BTPs, PCPE-1 and PCPE-2. The two CUB domains of PCPEs, CUB1 and CUB2, are separated by a short linker (9 amino acids in the human forms of PCPE-1 and -2), while the CUB2 and NTR domains are separated by a longer and flexible linker (44 and 28 residues respectively in PCPE-1 and PCPE-2) which is more sensitive to proteolysis (***Figure 19***). While the full-length protein is active, the natural processing of PCPE-1 leads to the release of the NTR domain and results in two other active forms of PCPE-1 consisting solely of the CUB domains (34- and 36-kDa proteins). Since both the full-length protein and its proteolytic forms retain the capacity to enhance procollagen processing, the CUB1-CUB2 domain is sufficient to support the PCPE-1 activity[156,157]. It is important to note that the short linker between the two CUB domains is necessary for the enhancing activity[157]. CUB1 and CUB2 act cooperatively and need to be linked to bind the substrate and enhance BMP-1 mediated-processing.

b. NTR domain

The C-terminal domain of PCPE, also found in netrins, complement proteins and secreted frizzled-related proteins (SFRPs), is homologous to the N-terminal domains of tissue inhibitors of metalloproteases (TIMPs)[158,159]. It encodes a unique basic domain, known as the netrin domain (NTR) characterized by a pattern of six conserved cysteines (only four in SFRPs) and several blocks of hydrophobic residues (including an YLLLG-like motif). In PCPEs, the NTR module does not have any direct effect on enhancing activity since the CUB1-CUB2 domain alone is sufficient for PCPE-1 activity[144,156]. The NTR domain of PCPE-1 was identified in the medium of human brain tumor cells as a metalloproteinase inhibitor[160]. However, this TIMP-like inhibitory effect remains controversial as it has not been confirmed[161].

Thus, the function of the NTR domain of PCPEs has remained mysterious for a long time until interaction with heparan sulfates was demonstrated[147]. Indeed, the NTR domains of PCPEs have a strong affinity for heparin and heparan sulfate proteoglycans (HSPGs). PCPE-1 can bind to HSPGs found at the cell surface in a calcium-dependent manner and with high affinity

(nanomolar range)[162]. However, the PCPE-1 protein is mainly secreted into the cell medium. In contrast, PCPE-2 is found to be associated with cell layers[146,148,152], presumably because of its stronger affinity for HSPGs. Thus, the NTR domain of PCPEs can mediate their binding to the cell surface through a direct interaction with HSPGs which can be inhibited by heparin, the NTR fragment itself or a NTR-specific antibody[162]. Importantly, cell-bound PCPE-1 retains its ability to enhance procollagen processing by BMP-1. Through its NTR domain, PCPE-1 was also shown to interact with syndecans (-1, -2 and -4) and fibronectin[163].

In addition to its heparin-binding affinity, the NTR domain of PCPE-1 can mediate the interaction of PCPE with other ECM proteins. For instance, the anti-angiogenic endostatin fragment can bind the NTR domain of PCPE-1 with high affinity and prevent its interaction with heparin[164]. Moreover, β2-microglobulin (β2-m), the main component of β-amyloid fibrils that accumulate in tendons, synovium and bone tissues in dialysis-related amyloidosis patients, appeared as a new partner of PCPE-1[165]. β2-m interacts with the NTR domain of PCPE-1 without affecting its enhancing activity and conversely, PCPE-1 does not promote nor stabilize β-amyloid fibrils. Finally, fibulin-4, a critical protein for elastic fibre assembly, was shown to interact with PCPE-1[80]. Whether the NTR domain is involved in this interaction has not been elucidated, but as fibulin-4 does not affect the enhancing effect of PCPE-1 on procollagen processing, we can hypothesize that the CUB1-CUB2 domain is free to bind the substrate and consequently, that the NTR domain is responsible for fibulin-4 binding. Taken together, the NTR domain seems to play a wide role in ligand binding (and/or tissue deposition of PCPEs).

c. Differences between PCPE-1 and -2 protein structures

While PCPE-1 and PCPE-2 share a high conservation of sequence and similarities in protein length and domain composition, they exhibit differences in post-translational modifications and especially glycosylation patterns. Indeed, both proteins are glycosylated but they differ from each other by the nature of their carbohydrate side chain. PCPE-2 is solely modified by *O*-glycosylation, despite the presence of a potential *N*-glycosylation site[146,148]. PCPE-1 differs from PCPE-2 in that it contains two *N*-glycosylated sites (one in the CUB1 domain, the other one in the NTR domain) and is found to have both *N*- and *O*-linked glycosylation decorated with sialic acid residues[148,166]. These differences in *N*-glycosylation suggest that they are not necessary for correct folding and activity of the proteins. Moreover, both PCPE-1 and PCPE-2 contain cysteines able to form disulfide bonds (seven bonds for each protein, with eight cysteines located in the CUB domains and six in the NTR domain), the intact disulfide bonding being necessary to maintain an active conformation of the proteins[147].

Another major difference between the two proteins is the presence of an Arg-Gly-Asp (RGD) motif in the PCPE-2 human sequence, which is absent in PCPE-1 and in mouse PCPE-2[146]. The RGD sequence is mainly an integrin-binding domain and mediates attachment to cells. Depending on its location, not all the RDG motifs are functional. However, as the RGD domain of PCPE-2 is located within the linker between the two CUB domains, it is likely to be accessible and functional. Moreover, PCPE-2 is a secreted protein mainly found associated to the cell layer[146,148,152], suggesting that its RGD motif could contribute to its interaction with the cells.

4) Mechanism of action

a. Direct interaction between PCPE and procollagen

As previously mentioned, the CUB1-CUB2 domains are solely responsible and necessary for the interaction of PCPE-1 with procollagen and thus its enhancing activity. In addition, the NTR domain has been shown to bind the BMP-1 protease, with micromolar affinity[161]. However, as the CUB1-CUB2 domain alone accounts for the enhancing activity of PCPE-1 without binding BMP-1, the NTR/BMP-1 interaction is unlikely to play a major role in the reaction.

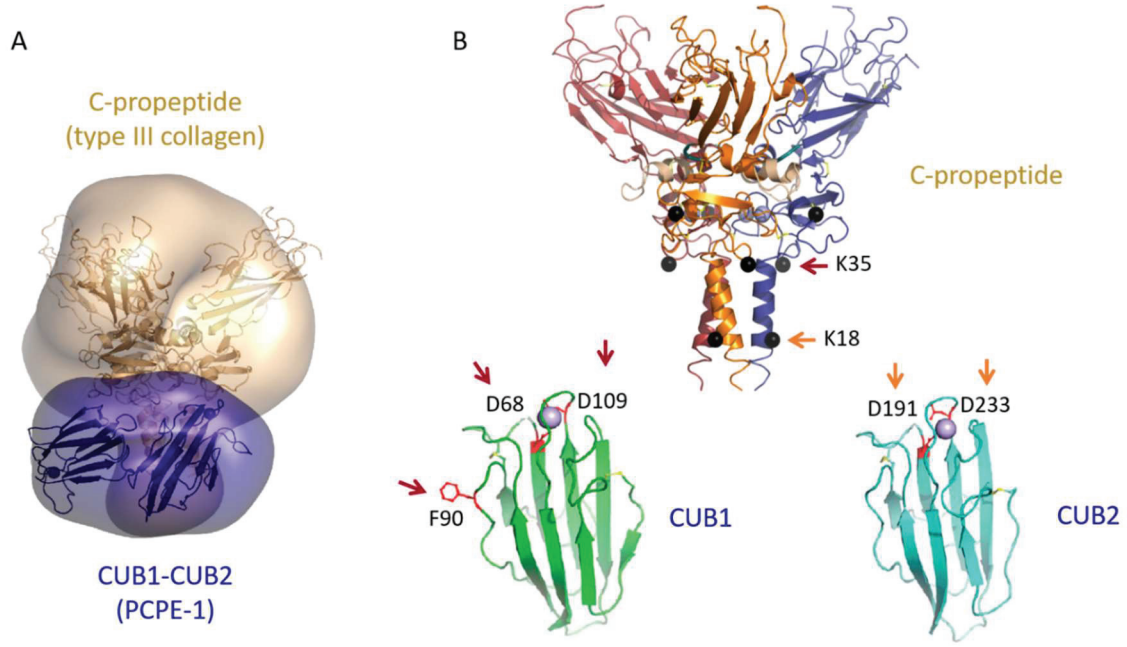

Figure 20: Structure of the complex formed by the C-propeptide of procollagen III (CPIII) and the CUB1-CUB2 domains of PCPE-1 (adapted from Bourhis et *al.*[167])
(A) Low resolution structure (SAXS) of the complex CPIII/CUB1-CUB2 made with the X-ray structure of CPIII and the predictive model of CUB1-CUB2. **(B)** Positions of the conserved amino acids critical for the interaction: lysines 18 and 35 (K18 and K35) in the procollagen chains, the aspartate residues (D68, D109, D191 and D233) involved in calcium binding in both CUB domains and a phenylalanine residue (F90) in CUB1.

The structures of the CUB1 and CUB2 domains were modeled based on the 3D structures of CUB-containing proteins (BTPs and serine proteases of the complement system; ***Figure 20***). Alignment of the CUB sequences of PCPEs and other proteins revealed that several residues were conserved within the surface-exposed loops connecting the β-sheets[167]. Among these conserved residues, several aspartate amino acids (D68 and D109 in CUB1; D191 and D233 in CUB2) were identified as critical for the binding of PCPE-1 to the procollagen molecule and its enhancing activity. As calcium is necessary to maintain the structural integrity of PCPE-1, mutations in one of these residues, which are involved in the calcium-binding site, abolished PCPE-1 enhancing activity. Recently, Bourhis et *al.*[168] obtained the low-resolution structure of the procollagen III C-propeptide (CPIII) and the PCPE-1 CUB domains complex (***Figure 20***). Based on this low-resolution structure, they found that PCPE-1 binds to the stalk region of the C-propeptide trimer and identified critical lysine residues within the α chain of procollagen[168]. Thus, binding of PCPE-1 require aspartates involved in calcium coordination in the CUB1-CUB2 domain, as well as two conserved lysines found in the substrate. The aspartates of CUB1 (D68 and D109) interact with lysine 35 (K35) of one of the procollagen α chain whereas the aspartates found in CUB2 (D191 and D233) interact with the lysine 18 (K18) of another α chain, the third α chain remaining free. Based on these interactions, only one molecule of PCPE-1 could interact with a trimer of procollagen. In addition, a surface exposed phenylalanine residue (F90), unique to the CUB1 domain of PCPE, was shown to be a major determinant of PCPE-1 activity and PCPE-1/procollagen interaction[167]. This specific amino acid could account for the specificity of PCPE-1 for fibrillar procollagen but the role of this residue in the interaction is not known yet.

Thus, in this model (***Figure 21***), the CUB1-CUB2 domains of PCPE tightly bind to the stalk region of the procollagen C-propeptide in very close proximity with the BMP-1 cleavage site. PCPE-1 forms a 1:1 complex with the substrate, only one molecule of PCPE-1 can bind to the trimeric procollagen because the C-propeptide cannot accommodate more than one molecule of PCPE-1. This strong and direct interaction would induce a conformational change in the procollagen, facilitating the accessibility of BMP-1 to the cleavage site.

As human PCPE-2 shares 46% amino acid identity with human PCPE-1 and has many structural features in common with PCPE-1, it is likely that PCPE-2 can similarly bind to procollagen. Indeed, alignment of the PCPE-1 and PCPE-2 amino acid sequences reveals that the critical residues identified for PCPE-1/procollagen interaction (D68, F90 and D109 in CUB1; D191 and D233 in CUB2) are conserved in the PCPE-2 sequence, suggesting that the mechanism by which PCPE-1 binds to the C-propeptide is also true for PCPE-2 (***Figure 19B***).

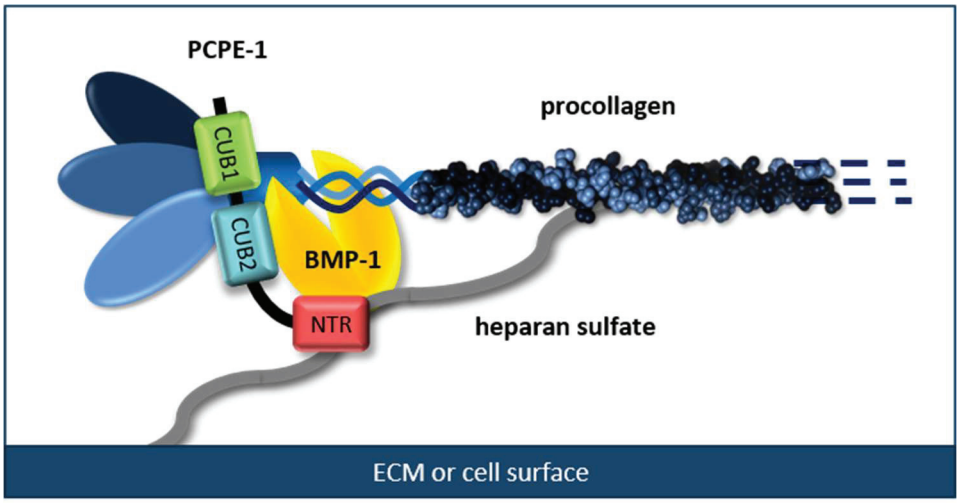

Figure 21: Multi-molecular complex formed by PCPE-1, BMP-1, procollagen and HSPGs
The BMP-1 protease cleaves the C-terminal domain of fibrillar procollagen, the C-propeptide. PCPE-1 can interact with the "stalk" region of the C-propeptide through its CUB domains and with BMP-1 via its NTR domain. By specifically binding the substrate, PCPE-1 is likely to induce a conformational change and facilitate the access by the protease, enhancing the cleavage of the C-propeptide by up to 10-fold. This enhancement is even more important (up to 2-fold) at the cell surface when HSPGs interact with both PCPE, BTP and procollagen, probably because of an increase in the concentration of each partner and/or a conformational change of the complex.

b. Superstimulation by HSPGs

As described above, PCPE-1 interacts via its CUB1-CUB2 domain with the C-propeptide of procollagen with a strong affinity (nanomolar range)[157]. Besides, the NTR domain of PCPE-1 is involved in the binding of PCPE to the cell layers, through a strong interaction with HSPGs[162]. Interestingly, the binding of the NTR domain to heparin and HSPGs can further increase by up to 2-fold the enhancing effect of PCPE-1 on type III procollagen, an effect described as a "superstimulation" of PCPE-1[161]. In addition to PCPE-1, the group of C. Moali showed that HSPGs also bind tightly to the triple-helical domains of procollagen and with a weaker affinity to BMP-1. As HSPGs can interact with PCPE-1, procollagen and BMP-1, they may act as a guiding scaffold to bring together these three partners at the cell surface, forming a large multi-molecular complex. These interactions might increase the local concentration of the reactants and/or change the conformation of the complex, thereby facilitating the action of BMP-1 and resulting in this "superstimulation". PCPE-2 was shown to have stronger affinity for heparin and HSPGs than PCPE-1[148,152]; however, whether a "superstimulation" of procollagen processing can occur in the presence of PCPE-2 and HSPGs remains unknown.

5) Differential expression, distribution and *in vivo* roles

a. Expression among species

PCPE-1 and PCPE-2 have a ubiquitous tissue expression in mammals. They are expressed in other species of vertebrates such as fish (including zebrafish), reptiles and birds, according to the Gene Tree of Ensembl genome browser (Ensembl release 91, December 2017). Finally, PCPEs have been found in frog (*Xenopus*) where BMP-1 is also expressed.

Because the role of PCPEs will be studied in human and murine skin, mouse and human PCPE-1 and -2 amino acid sequences were compared to assess similarities and differences between the two species[148] (***Table 1***). The mouse and human sequences of PCPE-1 are strongly homologous with 80% of conserved residues (92% within the CUB domains). The less conserved region is the linker between the CUB2 and NTR domains where there are 20 additional amino acids in the mouse protein sequence (68 residues in mouse and 44 residues in human). The PCPE-2 protein is also highly conserved between mouse and human with 87% amino acid identity (91% in the CUB1-CUB2 domains). The lengths of the murine and human PCPE-2 proteins are very similar, with only a single additional amino acid in the signal peptide in mouse; once the peptide signal is cleaved, the identity of the two proteins reaches 89%. However, an important difference between the two species is the lack of the RGD domain in mouse PCPE-2, which could be involved in the cell binding properties of PCPE-2 (as previously described; see §IV.3.c). If this is true, mouse PCPE-2 is more likely to be found in the extracellular medium than associated with the cells.

Protein	UniProt accession number	Protein sequence length (amino acids)	Molecular weight (kDa)	Full-length protein identity (%)	CUB1-CUB2 identity (%)
Human PCPE-1	Q15113	449	47,972	80	92
Mouse PCPE-1	Q61398	468	50,168		
Human PCPE-2	Q9UKZ9	415	45,717	87	91
Mouse PCPE-2	Q8R4W6	414	45,408		

Table 1: Comparison of PCPE-1 and -2 protein sequences in mouse and human

Because of the strong sequence conservation between mouse and human proteins, they are likely to have similar structures and functions. Besides some differences between the two species (as described in §I.6), the general organization of connective tissues is quite similar and rodent models are commonly used to study collagen fibrillogenesis. Moreover, as discussed in

the two next sections, the tissue distributions and functions of BTPs and PCPEs seem to be well conserved between mice and humans, confirming that a mouse model could be used to study the *in vivo* functions of PCPE-1 and PCPE-2.

b. Expression and distribution in tissues

To gain insights into the roles of PCPE-1 and PCPE-2, it is important to compare their expression profile and distribution in mammalian tissues.

In humans, PCPE-1 is widely distributed in the organism and seems to be highly expressed in collagen-rich tissues, such as tendon, skin, cartilage and bones[145,148,152]. PCPE-1 is also found in a wide range of other organs: heart, kidney, lung, digestive track, lymph nodes, skeletal muscles, uterus, etc. but it is barely detectable in the brain[145,148,152]. Interestingly, PCPE-1 is highly expressed in various foetal tissues (e.g. heart, kidney, liver, spleen and lung). This distribution of PCPE-1 in human foetal tissues, together with its expression at various time points during mouse development, suggest a specific role of PCPE-1 during development, which is in agreement with the strong detection of BMP-1/mTLD in mouse embryos and its role during embryogenesis[89]. In rodents, the distribution pattern of PCPE-1 is quite similar to humans with a strong expression in collagen-rich connective tissues (including tendons, skin, cornea and sterna) and a very low expression in organs containing negligible amounts of interstitial connective tissues (such as liver and brain)[145,169].

In contrast to PCPE-1, PCPE-2 has a much more limited distribution and is mainly found in the heart[148]. PCPE-2 expression seems to be quite limited in foetal tissues and is found at low levels in foetal heart, while it is highly expressed in adult heart[148,170]. This suggests that PCPE-2 rather plays a role in adult processes than embryonic development. PCPE-2 is also clearly detected in the pituitary gland, bladder, mammary gland and trachea and was also found among 5000 ESTs in cDNA libraries prepared from human cartilage by the group of Lark[171]. They identified *PCOLCE2* as a novel gene expressed in articular cartilage (in normal and osteoarthritic conditions) and also found significant levels of PCPE-2 in heart, kidney, placenta and osteosarcoma cells. Finally, PCPE-2 is present in the plasma of healthy volunteers where it is associated with high density lipoproteins (HDL)[154].

Because of the wide distribution of PCPEs in mammalian tissues and their key role in procollagen processing enhancement, PCPEs are likely to play critical roles *in vivo* and defects in PCPE expression may have important consequences for collagen-rich tissue development, repair and function in physiological and pathological conditions.

c. *In vivo* functions

i. Bone development and homeostasis

To ascertain the *in vivo* role of PCPE-1 and PCPE-2, homozygous knockout mice for each gene, *Pcolce* or *Pcolce2* have been generated. PCPE-1 and PCPE-2-deficient mice are viable and fertile and do not show gross developmental abnormalities[152,172]. In mesenchymal embryonic fibroblasts (MEFs) isolated from PCPE-1-deficient mice, the absence of PCPE-1 was not compensated by an increase in PCPE-2 expression[152] (no upregulation of PCPE-1 has been detected either in PCPE-2-deficient mice[173]). In the absence of PCPE-1, a decrease in procollagen processing was observed, accompanied by aberrant collagen fibrils in femora (***Figure 22***) and tendons. PCPE-1-deficient fibrils showed fluted and scalloped cross-sections in both tissues. These aberrant and irregular fibrils (visible in panels B and D, ***Figure 22***) affect the mechanical properties and geometry of tissues, as observed in the bones of PCPE-1-deficient mice (bone volume changes, altered morphology, reduced material properties). However, the mechanism by which the absence of PCPE-1 alters the morphology and the structure of bones and tendons remains unknown as no unprocessed collagens (retaining the C-propeptide) are incorporated into fibrils. Importantly, it should be noted that the absence of PCPE-1 did not lead to a strongly altered phenotype, as the mice did not show developmental abnormalities. In contrast to the *BMP1* mutations that lead to osteogenesis imperfecta (see §III.3.f), no patients with mutated PCPE have been reported so far.

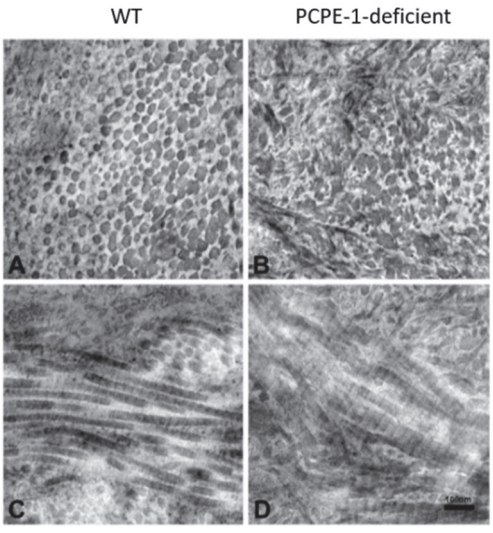

Figure 22: Abnormalities in collagen fibril morphology in bones from PCPE-1-null mice.[152]
Cross-sections (**A** and **B**) and longitudinal sections (**C** and **D**) of collagen fibrils from left femoral bones of four weeks-postnatal wild-type (**A** and **C**) and PCPE-1-deficient mice (**B** and **C**) observed by electron microscopy.

Later, PCPE-1 was detected and identified as a bone- and cartilage-related protein in the plasma of patients with acute bone fractures, suggesting a role in bone synthesis and repair[174]. As PCPE-1 could serve as a marker of bone complications, Mesilaty-Gross et *al.*[166] developed a sensitive method to detect PCPE-1 and identify its glycosylation pattern in the serum. Interestingly, the pattern of PCPE-1 glycosylation differed in women with breast cancer from

women with breast cancer associated with bone metastasis (which is the main skeletal complication of breast cancers). Moreover, a unique glycosylation pattern was detected in infants, which was not observed in preterm babies. Indeed, bone metabolism between preterm and term babies is known to be very different as the most prominent bone changes occur during foetal development. Taken together, these data confirmed the crucial role of PCPE-1 during **development** to regulate bone properties, as well as its involvement in bone metastasis.

ii. Lipid metabolism

Pcolce2 knockout mice have not been extensively characterized, especially in terms of collagen processing and fibril deposition. Initially, they were generated to investigate the *in vivo* role of PCPE-2 in the thymus[172]. Because of a differential expression of the *Pcolce2* transcript in the embryonic thymic anlage (from which the thymic stroma develops during embryogenesis) of wild-type and T-cell-deficient mice, it was hypothesized that PCPE-2 was important for T-cell development. However, these results were not confirmed as PCPE-2-deficient mice exhibit normal thymus and T-cell development. Subsequently, this model was used to investigate the role of PCPE-2 in **lipid metabolism**. Indeed, genetic studies suggest PCPE-2 levels to be associated with plasma HDL-cholesterol levels[154,175]. HDL protects against cardiovascular pathologies by regulating cholesterol efflux. Levels of HDL-cholesterol are inversely correlated to atherosclerosis and the risk of developing cardiovascular diseases.

Firstly, BMP-1 was identified as a key enzyme in the N-terminal processing of the pro-apolipoprotein AI (pro-ApoAI), the major protein component of HDL[154]. Supporting the genetic studies, PCPE-2 was shown to form a trimeric complex with BMP-1 and pro-ApoAI and to enhance its processing by up to 2-fold[154]. Then, a detailed characterization of plasma lipid profiles, ApoAI maturation and HDL metabolism in PCPE-2-deficient mice confirmed the role of PCPE-2 in this pathway[176]. Indeed, PCPE-2-deficient mice contained increased plasma levels of ApoAI as a pro-form. These mice also showed increased levels of enlarged HDL-cholesterol particles, accompanied by an elevation in ApoAI concentration in plasma. Despite a higher plasma concentration, HDL of PCPE-2-deficient mice has a reduced capacity to promote cholesterol efflux. Taken together, these studies revealed a new and unexpected role of PCPE-2 in HDL biogenesis and cholesterol efflux, through the maturation of pro-ApoAI.

iii. Fibrosis

As previously described for BMP-1, the expression of PCPE-1 and -2 has been tightly associated with excessive collagen deposition in many fibrotic disorders. Among them, abnormal collagen accumulation in the heart has been shown to impair myocardial stiffness and function and leads to heart failure. *In vivo* data support the idea that PCPE-1 and -2 are both

involved in the development of **cardiac fibrosis**. For example, patients with aortic stenosis showed a significant increase in PCPE-1 protein abundance (11.3-fold), associated with higher levels of the active form of BMP-1[142]. Moreover, the 36-kDa proteolytic form of PCPE-1 (and not the full-length protein) is upregulated in patients with chronic heart failure and this overexpression could be reversed by treating patients with an anti-fibrotic molecule[141]. Similarly, an important increase in PCPE-1 expression was detected in rat and mouse models of myocardial infarction and correlated with increased myocardial collagen deposition[177–179]. PCPE-2, which is mainly expressed in the heart, also seems to play a role in cardiac fibrosis but no data have been reported so far in patients. In mice, PCPE-2 was found to be at least twice as highly expressed in a model of chronic pressure overload induced by transverse aortic constriction (WT TAC; ***Figure 23***), compared to control mice (WT)[180]. However, myocardial collagen accumulation was significantly reduced in PCPE-2-deficient mice with chronic pressure overload, suggesting that PCPE-2 is necessary for collagen accumulation.

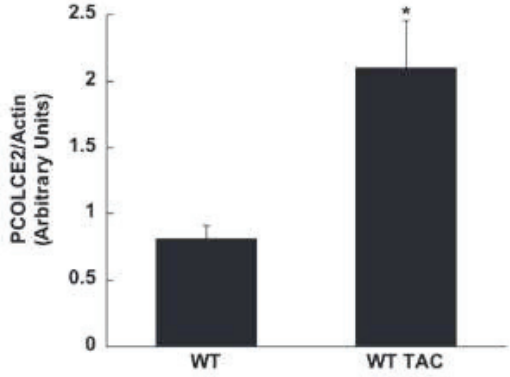

Figure 23: PCPE-2 abundance in a mouse model of myocardial infarction[180]

Quantification of PCPE-2 expression detected by Western blotting. PCPE-2 is twice as highly expressed in mice with chronic pressure overload, induced by transverse aortic constriction (TAC), compared to non-treated mice (WT).

Finally, PCPE-1 has been associated with **oculopharyngeal muscular dystrophy** (OPMD), a late-onset myopathy characterized by muscle degeneration and fibrosis[181]. As the ECM organization is essential for muscle structure and properties, excessive accumulation of collagen and other ECM components leads to aberrant muscle function and degeneration. Surprisingly, in contrast to other fibrotic diseases where PCPE-1 is overexpressed, levels of PCPE-1 in the ECM of OPMD patients and in a muscle cell system model are reduced. PCPE-1 remains entrapped in the nucleus and is not secreted extracellularly. This is the first evidence of PCPE-1 down-regulation in fibrotic organs, suggesting a novel molecular mechanism in the development of late-onset muscle fibrosis, involving an ECM dysregulation.

iv. Wound healing

Several reports support the importance of PCPEs during tissue repair and healing. Firstly, PCPE-1 has been linked to the maturation and healing of the medial collateral ligament (MCL), one of the major ligaments of the knee connecting the tibia to the femur[182]. The authors of this study compared the maturation of the MCL, a tissue mainly composed of fibrillar collagens, in physiological (development) and pathological conditions (MCL injury) in rabbits. Levels of *Pcolce* and *Bmp1* mRNA were upregulated during the normal development of the MCL, supporting their crucial role during collagen processing and fibril assembly. After a MCL injury, while the mRNA level of *Bmp1* expression remained very low during the whole healing process, *Pcolce* was significantly upregulated. These results could explain the abnormal collagen fibrils seen in MCL-injury healed tissue (e.g. disorganized and small fibrils). The strong expression of PCPE-1 during MCL healing supports its crucial role during the healing process, even if the lack of BMP-1 prevents the formation of a proper healed ligament.

Upregulation of BMP-1 and PCPE-1 has also been reported in human and mouse corneal scars, suggesting that these proteins contribute to the process of corneal repair[136]. Cornea is a specialized connective tissue mainly composed of types I and V collagens, and transiently of type III collagen during the healing process. In cornea, this collagen fibril network is highly organized and dysregulation of the ECM causes corneal opacity, loss of visual acuity and in the worse cases, blindness. In several patients with corneal opacity, BMP-1 and PCPE-1 were found to be upregulated compared to unwounded corneas, suggesting that these proteins could be involved in the disorganization of collagen fibrils. In a mouse model of corneal scarring, the levels of BMP-1 and PCPE-1 were also increased between 7 and 28 days after wounding (***Figure 24***) while the expression of PCPE-2 was diminished at the same time points, both at the RNA and protein levels. These results confirm the role of BTPs and PCPEs during **corneal scarring** in mice and humans but the mechanism remains to be elucidated.

All these findings clearly evidence the major roles played by PCPEs in collagen deposition during tissue development and repair. PCPEs are also found to be involved in pathologies associated with excessive collagen deposition such as fibrosis and scarring. Thus, they are likely to be valuable and efficient therapeutic targets to improve or prevent collagen deposition in tissues, especially in the context of skin wound healing.

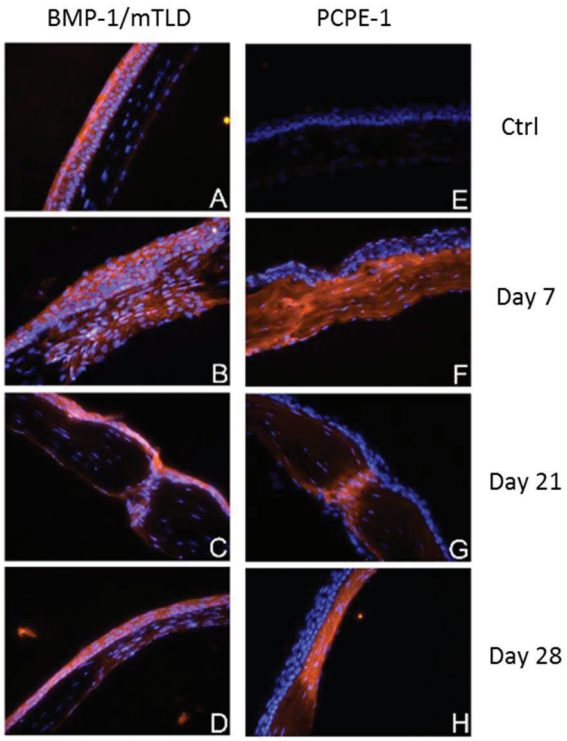

Figure 24: BTP and PCPE-1 expression during mouse corneal scarring[136]
Immunostaining of murine corneas reveals that BMP-1/mTLD expression is restricted to the epithelium in unwounded cornea **(A)** whereas PCPE-1 expression is very weak **(E)**. After corneal surgery, BMP-1/mTLD and PCPE-1 are both overexpressed, with a strong expression in the stroma 7 days after wounding **(B** and **F)**. This strong expression is maintained 21 **(C** and **G)** and 28 days after surgery **(D** and **H)**, even if it is weaker than the expression observed at day 7.

Objectives

The objectives of my thesis were to explore the function(s) of PCPE-1 and PCPE-2 in the skin and to investigate their therapeutic potential during wound healing, using cellular and animal models, human skin biopsies and proteomic approaches. As PCPEs enhance the processing of fibrillar procollagens mediated by BTPs, we hypothesized that PCPE-1 and PCPE-2 could play significant roles during wound healing and represent valuable targets to control collagen deposition in skin.

The first objective was to assess the expression patterns of PCPE-1 and PCPE-2 in wounded mouse and human skin, in correlation with their main partners (BTPs) to determine if these proteins were dysregulated in wounds or scars. This was correlated to *in vitro* studies aiming at describing their main cellular sources.

The second objective of this project was to better characterize these two proteins and obtain new information about their potential other roles (e.g. their reported function in the control of cell growth and protein synthesis) in fibroblasts. By modulating the expression of PCPE-1, the effects of its expression and activity on the phenotype and functions of human dermal fibroblasts were analysed by biochemical approaches (Western blotting, proteomics). The final part of our study was focused on PCPE-2, on which little information is currently available, to get more insight into the *in vitro* and *in vivo* role of PCPE-2 and its function on procollagen processing, using recombinant proteins and a *Pcolce2* knockout mouse model.

Chapter 2: Materials and methods

I. Production and purification of recombinant proteins

For this project, untagged PCPE-1 and -2 recombinant proteins were produced and purified, as well as histidine-tagged PCPE-1 and -2 proteins. Whereas PCPE-1 and PCPE-1-8His plasmids were already available in the group of Catherine Moali (Lyon), the production of PCPE-2 and histidine-tagged proteins had to be established entirely from the cloning into an expression vector to the production by eukaryotic cells. In the next section, the different steps of the production of the plasmids encoding the PCPE-2 protein, the PCPE-2 protein with an 8-histidine-tag at the C-terminal end (PCPE-2-8His) and the PCPE-2 protein with a 6-histidine-tag at the N-terminal end (6His-PCPE-2) will be described.

1) Vector cloning

PCPE-2 and PCPE-2-8His sequences were cloned in the pCEP4 mammalian expression vector, designed for high-level and stable expression, whereas 6His-PCPE-2 sequence was cloned into the pHLSec vector for transient transfection.

a. PCPE-2 in pCEP4 expression vector

i. pOTB7-PCPE-2 amplification

Human PCPE-2 sequence was obtained from a pOTB7-PCPE-2 plasmid purchased from Source BioScience (clone ID 3951739). This sequence contained two mutations: 829G>T, leading to a stop codon in the middle of the protein and 874C>A. Firstly, the pOTB7-PCPE-2 plasmid was amplified by culturing pOTB7-PCPE-2 bacteria (supplied by Source BioSciences) in LB growth medium containing 20 µg/mL of chloramphenicol (Euromedex, ref. 3886A) overnight. Then, plasmid DNA purification was performed with the Plasmid DNA Purification Nucleobond Xtra Midi kit (Macherey-Nagel, ref. 740.410.10) according to the manufacturer's protocol.

ii. PCPE-2 sequence mutagenesis and cloning into pCEP4 vector

PCR primers were designed and purchased from Sigma-Aldrich to correct the two mutations (***Table 2***; highlighted letters) and add two restriction sites (Acc65i and BamHI; bold and underlined characters) at the N- and C-terminal ends of the PCPE-2 sequence by PCR.

Mutation	Forward PCR primer (5' → 3')	Reverse PCR primer (5' → 3')
T829G	CTAGAAGCTG**GGTACC**ATGAG GGGCGCGAAC	GTTACAGGGAATGTG GTGGTGACAGGCTGTTCTGTAGTTG
A874C	CACATTCCCTGTAACCACGGGT TTAAAACCCACCGTGGCCTTGT	TATCATGTCT**GGATCC**TCATTAACATTG CTTATTTTTTAAGGCATCCAGGAGCTT

Table 2: PCR primer sequences designed to correct the mutations in PCPE-2 sequence
Bold and underlined characters are the Acc65i and BamHI restriction sites; highlighted letters correspond to mutated amino acids in the primer sequences designed to correct the two mutations.

The PCPE-2 sequence was amplified in two overlapping fragments using the Phusion® High-Fidelity PCR enzyme (New England Biolabs, ref. E0553S) and each fragment containing one of the bases mutated was purified by spin column-based purification (Nucleospin® Gel and PCR Clean Up, Macherey-Nagel, ref. 740609.50). Then, the entire sequence containing the correct nucleotides was re-amplified by PCR using the primers T829_for and A874C_rev and purified as described previously. The PCPE-2 sequence was cloned into a pJET1.2/blunt vector using the CloneJET PCR Cloning strategy (ThermoFisher Scientific, ref. K1231). *E. Coli* XL1 blue competent bacteria were transformed with the ligation mixture and grown onto a LB-agar plate at 37°C overnight. Individual colonies of bacteria were isolated and inoculated in LB growth medium with 100 µg/mL of ampicillin at 37°C in a shaking incubator. Then, pJET-PCPE-2 plasmid was isolated from bacterial culture using a plasmid DNA minipreparation kit (NucleoSpin® Plasmid, Macherey-Nagel, ref. 740588.250) and sequenced by Sanger sequencing (GATC, Germany). The pJET vector containing PCPE-2 sequence flanked by two restrictions sites was digested with Acc65i and BamHI enzymes (Promega). The sequence of interest was cloned into the pCEP4 vector linearized by digestion (Acc65i and BamHI as well) using the NxGen™ T4 DNA ligase low concentration (Lucigen, ref. 30241). Sanger sequencing confirmed the correct sequence of the obtained vector.

b. PCPE-2-8His in pCEP4 expression vector

The pJET-PCPE-2 vector described previously was also used to insert the 8-His tag at the C-terminal end of the PCPE-2 sequence (between the end of the coding sequence and the BamHI restriction site) by Q5® Site-Directed Mutagenesis (New England Biolabs, ref. E0554S) according to the manufacturer's protocol. As previously described, the pJET-PCPE-2-8His plasmid was amplified in *E. Coli* XL1 blue competent bacteria and isolated from bacterial culture using the same plasmid DNA minipreparation kit. After sequencing and digestion with Acc65i and BamHI, the PCPE-2-8His sequence was introduced into the pCEP4 vector, as previously done for the PCPE-2 sequence.

c. 6His-PCPE2 in pHLSec vector

To avoid a potential (negative) effect of the C-terminal tag on the protein stability and/or conformation, another tagged PCPE-2 construct was designed with a 6-His tag at the N-terminal end of the sequence. Similarly to the PCPE-2-8His protein, the pJET-PCPE-2 vector was used to produce this new construct using the In-Fusion® cloning strategy. This technology is based on the ability of an In-Fusion enzyme (Ozyme, ref. 638909) to fuse two or more PCR fragments simultaneously in a vector by recognizing a 15 bp overlap at their ends. To perform the In-Fusion experiment, specific primers were designed to add, in two successive PCR reactions, the 6-His tag in N-terminal and the 15 bp overlap at each end of the PCPE-2 sequence (***Table 3***). The PCR reactions were performed with the FideliO DNA polymerase (Ozyme, ref. OZYA005-100) and the PCR products were checked by Sanger sequencing.

Insertion	Forward PCR primer (5' → 3')	Reverse PCR primer (5' → 3')
6His-tag	CATCATCATCACCACCACCAGT CCCCAGAGAGACCTGTT	GATACTAGTCTCGAGTTAACATTGCTTA TTTTTTAAGGCATCCAGGAG
15 bp overlap	GGTTGCGTAGCTGAAACCGGTC ATCATCATCACCACCACCAGT	GATACTAGTCTCGAGTTAACATTGCTTA TTTTTTAAGGCATCCAGGAG

Table 3: PCR primers designed to insert a 6-histidine tag and 15 bases at each end of PCPE-2 sequence

For the In-Fusion strategy, the final PCR fragment was fused with the pHLSec vector, linearized previously with AgeI and XhoI restriction enzymes. Stellar competent bacteria were transformed with the In-Fusion mix by heat shock (30 minutes at 4°C, followed by 45 seconds at 42°C and then 2 minutes at 4°C) and incubated in SOC medium in 37°C shaking incubator for 1 hour. The bacterial mix was then plated onto a LB agar plate containing 100 µg/mL of ampicillin overnight. Single colonies were picked and cultured in LB medium containing 100 µg/mL of ampicillin. Plasmid DNA was isolated as described in the paragraph I.1.b. Larger amounts of DNA (1.9 µg) were then isolated with the NucleoBond Xtra Midi kit (Macherey-Nagel, ref. 740410.10). Plasmid DNA was checked by Sanger sequencing.

The three PCPE-2 constructs (PCPE-2-pCEP4, PCPE-2-8His-pCEP4 and 6His-PCPE-2-pHLSec) were then respectively used for stable or transient cell transfection.

2) Culture and transfection of eukaryotic cell lines

a. Culture of HEK 293-EBNA and HEK 293-T cells

For the production of recombinant proteins, HEK 293-EBNA (Human Embryonic Kidney – Epstein-Barr Nuclear Antigen) and HEK 293-T (Human Embryonic Kidney – T-Antigen) cell

lines were used. The HEK 293-EBNA cell line is stably transfected with the EBNA-1 gene, which drives episomal replication of OriP containing vectors. This cell line is commonly used to generate for stable expression of a gene of interest (PCPE-1 and PCPE-2 in this work). The HEK 293-T cell line is a highly transfectable cell line containing the SV40 T-antigen, it has been widely used for transient retroviral production, gene expression and protein production. Both 293-EBNA and 293-T cell lines were cultured in high glucose Dulbecco's Modified Eagle's Medium (DMEM) AQ™ media (Sigma-Aldrich, ref. D0822) with 10% of fetal bovine serum (FBS; Gibco, ref. 10270106) and 1% of Antibiotic Antimycotic Solution (AAS; Sigma-Aldrich, ref. A5955). Cells were grown in 10 cm tissue cell culture dishes or T75 cm^2 flasks at 37°C with 5% CO_2 until 90% confluence was reached. Culture medium was then removed and cells were washed with phosphate-buffered saline (PBS) twice. To harvest cells, a trypsin-EDTA solution (Sigma-Aldrich, ref. T3924) was added and cells were incubated at 37°C with 5% CO_2 for 5 minutes. When all the cells had detached, 2 volumes of complete medium were added to inhibit the action of trypsin. Released cells were collected and spun down at 200 g for 5 minutes. The cell pellet was resuspended into the appropriate volume of complete medium and transferred into a new culture cell dish or flask.

b. Stable transfection and production of PCPE-1, PCPE-1-8His, PCPE-2 and PCPE-2-8His

The HEK 293-EBNA cell line was used for semi-stable transfection of PCPE-1 and PCPE-2 recombinant proteins and the corresponding histidine-tagged proteins (PCPE-1-8His and PCPE-2-8His). Stable 293-EBNA cell lines expressing PCPE-1 (PCPE-1 293-EBNA) and PCPE-1-8His (PCPE-1-8His 293-EBNA) have been generated previously by Catherine Moali and kept in liquid nitrogen. They were thawed at 37°C for 5 minutes, centrifuged at 1500 rpm for 5 minutes to remove the freezing medium and cultured in cell culture plate in DMEM AQ™ medium containing 10% FBS and G418 sulfate (250 µg/mL; GE Healthcare Life Sciences, ref. P11-012). Stable cell lines expressing PCPE-2 and PCPE-2-8His were generated by transfecting the 293-EBNA cell line with the pCEP4-PCPE-2 and pCEP4-PCPE-2-8His plasmids. Cells were transfected using Nanofectin (PAA, ref. Q051-005) as a transfection reagent. 16 µL of transfection reagent were used for 5 µg of pCEP4-PCPE-2 plasmid (ratio 1:3) and 5 µL of transfection reagent were used for 5 µg of pCEP4-PCPE-2-8His plasmid (ratio 1:1). The pCEP4 plasmid contains a hygromycin B resistance cassette for mammalian selection. Therefore, all the transfected HEK 293-EBNA cell lines were maintained in complete medium containing DMEM AQ™ medium, 10% FBS and hygromycin B (300 µg/mL, PAA, ref. P02-015) and amplified in T225 cm^2 flasks. Confluent cells were then transferred into a double

CellSTACK® cell culture chamber (Corning, ref. CLS3310). When cells reached 80% confluence, they were washed with PBS and switched to serum-free medium containing DMEM AQ™ medium and gentamycin (50 µg/mL; GE Healthcare Life Sciences, ref. P11-004). Culture media containing PCPE-2 and PCPE-2-8His were collected every 48 hours during two and four weeks respectively and centrifuged at 1000 g to remove the dead cells. A mixture of protease inhibitors (cOmplete™ Mini, Roche, ref. 11 836 153 001) was added and the media were kept at -80°C until purification.

c. Transient transfection and production of 6His-PCPE-2

The 6His-PCPE-2 protein was transiently produced in HEK 293-T cell line. These cells were seeded in a HYPERflask® cell culture vessel (Corning, ref. 10030) in DMEM AQ™ medium containing 10% of FBS and 1% AAS. At 80-90% of confluence, cells were transfected with the pHLSec-6His-PCPE-2 plasmid using polyethylenimine (PEI; Sigma-Aldrich, ref. 408727) as transfection reagent (1 mg of PEI for 0.5 mg of DNA) in DMEM medium with only 2% of FBS and 1% of Non-Essential Amino Acids (NEAA; Sigma-Aldrich, ref. M7145). Culture medium containing the 6His-PCPE-2 protein was collected 3 and 5 days after transfection, centrifuged at 1000 g, mixed with protease inhibitors and kept at -80°C. Aliquots of medium were conserved at -20°C for Western blotting analyses.

3) Protein purification

Cell culture media were collected as described above (see §I.2.b and c) and kept at -80°C until use. For purification, they were thawed and centrifuged at 10000 g for 15 min at 4°C. The protocol for the purification and the buffers used have been adapted and optimized for each protein produced, the different steps of purification will be described in the following paragraphs (***Figure 25***).

a. Affi-Blue

The Affi-Blue purification step relies on affinity chromatography. The Affi-Gel® Blue resin, purchased from BioRad (ref. 153-7301) is a beaded, crosslinked agarose gel with covalently attached Cibacron Blue F3GA dye. This resin is used to separate and purify a large range of plasma and serum proteins and is ideally suited as a first step of purification for albumin removal (albumin capacity greater than 11 mg/mL). The binding of albumin is so strong that a high concentration of salt is required. In contrast, other proteins do not bind the resin or can be eluted with relatively low concentration of salt or a competitive eluent.

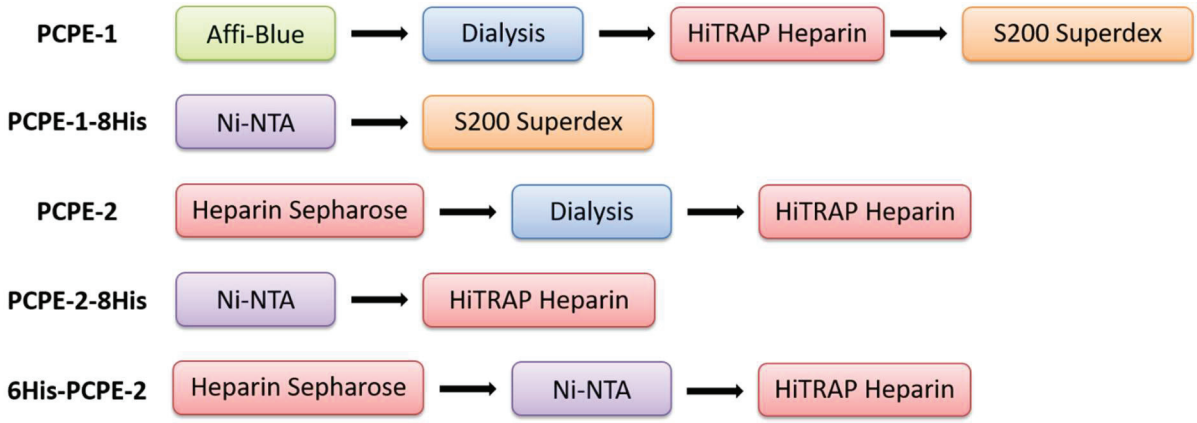

Figure 25: Summary of the different purification steps used to purify each protein

The Affi-Blue purification was used as a first purification step for the PCPE-1 recombinant protein only. Twenty mL of Affi-Gel® Blue resin (Bio-Rad, ref. 1537301) were incubated with 1L of PCPE-1 containing-medium for 3 hours at 4°C under agitation. Then, a column was packed with the Affi-Gel® Blue resin using buffer A (***Table 4***). The sample was then loaded and the column washed with buffer A. After further washing with a mixture of buffers A and B (73% of A and 27% of B, i.e. 0.6 M NaCl), proteins were eluted with buffer C containing 50% of ethylene glycol. Ethylene glycol competes with the proteins for binding to the resin and is responsible for the elution of PCPE-1 protein.

Buffer	Composition (for PCPE-1)
A	50 mM Tris, 0.15 M NaCl, pH 7.4
B	50 mM Tris, 2 M NaCl, pH 7.4
C	50 mM Tris, 2 M NaCl, pH 7.4, with 50% of ethylene glycol

Table 4: Buffers used for the Affi-Blue purification of PCPE-1

b. Ni-NTA

Ni-NTA Agarose (QIAGEN, ref. 30210) is a nickel-charged resin used to purify proteins containing a polyhistidine sequence; this was used to purify PCPE-1-8His, PCPE-2-8His and 6His-PCPE-2. Histidine residues bind with high affinity and specificity the vacant positions in the coordination sphere of the immobilized nickel ions and are eluted under native or denaturing conditions. Nickel-charged resin was batch purified with histidine-tagged protein containing medium under agitation for 3 hours at 4°C. After protein binding, the resin was loaded onto a column and washed successively with a mixture of A and B buffers (***Table 5***) in order to have a final concentration of 10 mM and then, 20 mM of imidazole. Finally, histidine-tagged proteins were then eluted with a linear gradient of imidazole (from 20 to 250 mM). Both PCPE-1-8His and PCPE-2-8His were mainly eluted with 250 mM of imidazole.

Buffer	Composition (for PCPE-1-8His and PCPE-2-8His)
A	50 mM NaH_2PO_4, 0.5 M NaCl, pH 8
B	50 mM NaH_2PO_4, 0.5 M NaCl 0.5M, 250 mM imidazole, pH 8

Table 5: Buffers used for the NiN-TA purification of PCPE-1-8His and PCPE-2-8His

For the 6His-PCPE-2 protein purification, some changes were made in the composition of buffers in order to increase the total amount of proteins eluted (***Table 6***). Specifically, imidazole was added to a final concentration of 5 mM before binding to the Ni-NTA resin to improve the binding specificity. Binding to the resin was done directly in the column with 5 mM of imidazole (99% of buffer A and 1% of buffer B). Then, the resin was washed successively with slightly higher imidazole concentrations (20 and then, 55 mM) and the protein was eluted with two successive gradients of imidazole (from 55 to 150 mM and then, from 150 to 500 mM). The majority of the 6His-PCPE-2 protein was eluted with 150 mM of imidazole.

Buffer	Composition (for 6His-PCPE-2)
A	20 mM HEPES, 0.6 M NaCl, pH 8
B	20 mM HEPES, 0.6 M NaCl, 500 mM imidazole, pH 8

Table 6: Buffers used for the Ni-NTA purification of 6His-PCPE-2

After the Ni-NTA purification step, PCPE-1-8His was pure enough to be directly injected on a gel filtration column (see §I.3.e). This was not the case for PCPE-2-8His; another purification step was needed: purification on heparin column. For 6His-PCPE-2, another strategy was tested, the heparin purification was performed before the Ni-NTA step (***Figure 25***); this protocol was definitely better to purify the histidine-tagged PCPE-2 protein.

c. Heparin

Heparin-sepharose chromatography is a common purification step extensively used to purify proteins with high affinity for heparin. Indeed, heparin binds to a wide range of biomolecules via both affinity and ion exchange mechanisms. It has been largely demonstrated that both PCPE-1 and -2 have a high affinity for heparin and heparan sulfates, so heparin-sepharose purification is a suitable technique to purify these proteins.

To further purify PCPE-1 and PCPE-2-8His recombinant proteins, a HiTRAP™ Heparin HP column (Amersham Biosciences, ref. 17-0407-01) was used. Heparin is coupled to the Sepharose High Performance matrix to give high capacity and performance and prepacked in a column, which is easier to use. Proteins were loaded directly onto the column. For PCPE-1, the column was washed with 100% of buffer A (containing 0.15 M NaCl; ***Table 7***) and proteins

were then eluted with a linear gradient of NaCl (from 0.5 to 1 M). Between 0.35 and 0.66 M of NaCl was necessary to elute completely PCPE-1 proteins. For PCPE-2-8His, the protein solution, which contained 0.6 M NaCl after Ni-NTA elution (see §I.3.b), was diluted to reach 0.25 M NaCl and loaded onto the heparin column. The column was washed with a mixture of A and B buffers (0.25 M NaCl; ***Table 8***). The PCPE-2-8His protein was eluted with a linear gradient of NaCl (from 0.25 to 1 M) and elution was efficient with 0.5 to 1 M of NaCl. No additional purification step was done for PCPE-2-8His to prevent protein loss.

Buffer	Composition (for PCPE-1)
A	50 mM HEPES, 0.15 M NaCl, pH 7.4
B	50 mM HEPES, 1 M NaCl, pH 7.4

Table 7: Buffers used for the heparin purification of PCPE-1

Buffer	Composition (for PCPE-2-8His)
A	20 mM HEPES, pH 8
B	20 mM HEPES, 2 M NaCl, pH 8

Table 8: Buffers used for the heparin purification of PCPE-2-8His

To purify PCPE-2 and 6His-PCPE-2, Heparin Sepharose® 6 Fast Flow (GE Healthcare, ref. 17-0998-01) resin, composed of cross-linked 6% agarose beads modified sodium heparin, was used. Binding of the PCPE-2 protein to heparin-sepharose resin was performed in batch mode during 3 hours at 4°C. The resin was then loaded into a column and washed with buffer A (0.15 M NaCl; ***Table 9***). The PCPE-2 protein was eluted with a linear gradient of NaCl (from 0.15 to 0.6 M NaCl); two products were obtained: the PCPE-2 protein (50 kDa) and a proteolytic fragment of PCPE-2 (31 kDa). The protein solution was then dialyzed (see §I.3.d) and then, purified on a HiTRAP™ Heparin HP column to improve the purification of PCPE-2. The same buffers were used for both heparin purification steps and the protein was stored at -80°C.

For 6His-PCPE-2, the heparin-sepharose resin was prepacked into a column before adding protein-containing medium and then, washed with buffer A (***Table 9***). A linear gradient of NaCl was performed to elute the protein (from 0.15 to 1 M NaCl) and the 6His-PCPE-2 protein was obtained after adding 0.5 to 0.8M of NaCl. This purification step was followed by a Ni-NTA purification, as previously described (see §I.3.b) and then by another heparin step (HiTRAP™ Heparin HP column) in order to remove imidazole used for the elution. The same buffers were used for both heparin purification steps. The final protein was stored in low bind Eppendorf tubes at -80°C after snap-freezing in buffer B supplemented with 5 mM $CaCl_2$ and

0.1% of n-octyl-β-D-glucopyranoside (Roth, ref. CN23.2) to improve protein storage and prevent precipitation.

Buffer	Composition (for PCPE-2 and 6His-PCPE-2)
A	20 mM HEPES, 0.15 M NaCl, pH 7.4
B	20 mM HEPES, 2 M NaCl, pH 7.4

Table 9: Buffers used for the heparin purification of PCPE-2 and 6His-PCPE-2

d. Dialysis

Between the different steps of purification, it was necessary to remove molecules that could have interfered with the next purification step. For instance, for heparin purification, it is very important that the protein solution does not contain high amounts of NaCl to bind the resin, as the NaCl inhibits the interaction of the proteins with heparin. Thus, for two of the purified proteins (PCPE-1 and PCPE-2), it was necessary to add a dialysis step before the heparin purification. PCPE-1 was first purified on a Affi-Blue resin and eluted with a buffer containing 50% ethylene glycol and 2 M NaCl (see §I.3.a). The protein was then dialyzed in dialysis tubing (pore size 12.4 kD; Sigma, ref. D0655) in three successive baths of 50 mM Tris, 0.15 M NaCl (4 hours – overnight – 8 hours; at 4°C, with stirring) before the heparin step. For PCPE-2 purification, two heparin purification steps were performed successively (***Figure 25***) and it was necessary to decrease the total amount of NaCl in the sample after the first step. PCPE-2 protein was also dialyzed in three successive baths of 20 mM HEPES, 0.15 M NaCl (3h30 min – 3h30 min – overnight; at 4°C, with stirring).

e. Superdex 200

For PCPE-1 and PCPE-1-8His, the final purification step was a gel filtration column on Superdex 200 (GE Healthcare Life Sciences, ref. 16/60). The principle of gel filtration is to use a column containing an ordered matrix of beads that have small pockets and holes. As the proteins run through the column, small proteins get caught which delays their migration, whereas larger proteins move faster through the column. Before injection on the Superdex column, proteins were concentrated by ultrafiltration on a Vivaspin® 20 concentrator (20 mL, 10 kDa, Sartorius) to reach a volume of less than 5 mL. This is the maximum volume that can be used to have a good resolution. The Superdex column was equilibrated with the corresponding buffer (***Table 10***) and the protein sample was injected. The protein of interest, PCPE-1 or PCPE-1-8His was separated from other contaminants based on its molecular weight and stored at -80°C for months.

Protein	Composition
PCPE-1	20 mM HEPES, 0.15 M NaCl, 5 mM $CaCl_2$, pH 7.4
PCPE-1-8His	20 mM HEPES, 0.3 M NaCl, pH 7.4

Table 10: Buffers used for the S200 purification of PCPE-1 and PCPE-1-8His

4) Protein analysis

After each step of purification, the elution fractions were analysed by SDS-PAGE to ensure that the protein was properly eluted and determine if contaminants were present or not. If the protein was not concentrated enough, the elution fractions were precipitated using the trichloroacetic acid/acetone protocol described below (see §VI.1.b). Otherwise, small aliquots of the elution fractions (from 5 to 50 µL) were loaded directly onto a 10% acrylamide gel. Following electrophoresis, proteins were stained using a 0.1% Coomassie Brilliant Blue (R250; Sigma, ref. 27816) solution for 30 minutes. Then, the gel was destained in a 10% acetic acid, 10% ethanol and 80% water solution for at least 2 hours in order to visualize the bands corresponding to the purified proteins.

II. Cell culture

1) Culture of primary keratinocytes and dermal fibroblasts

a. Primary cells isolated from mouse skin

Murine keratinocytes and dermal fibroblasts isolated from the back skin of wild-type (WT) mice were cultured in T75 cm^2 flasks at 37°C with 5% CO_2. Murine keratinocytes were cultured in complete CnT-07.S medium (CELLnTEC) supplemented with additives, which does not contain serum and antibiotics/antimycotics. Murine fibroblasts were grown in complete medium containing DMEM/Nutrient Mixture F12 (ThermoFisher Scientific, ref. 21331020), 10% FBS (Merck, ref. S0115), 2 mM L-glutamine, 1% penicillin-streptomycin (Gibco, ref. 15070-063) and 1% AAS.

b. Primary cells isolated from human skin

Primary keratinocytes and dermal fibroblasts were isolated from the skin of healthy donors (from the Edouard Herriot Hospital, Lyon and the Department of Dermatology, Medical Center – Freiburg University). Normal human keratinocytes (NHK) originated from the foreskin of 3-6 year old boys, while normal human fibroblasts (NHF) were isolated from breast or abdominal skin of women between 25 and 35 years old.

Human keratinocytes were cultured in supplemented Keratinocyte-SFM medium (Gibco, ref. 17005-034) containing keratinocyte supplements (Gibco, ref. 37000-015). Human fibroblasts were cultured in complete DMEM/F12 medium (in Freiburg) or in DMEM AQ™ media (in Lyon) with 10% of FBS and 1% of AAS.

c. Subculture of primary cells

Murine and human primary cells were cultured in cell culture dishes or T75 cm^2 flasks at 37°C with 5% CO_2 until 90% confluence. Cell culture medium was then removed and primary cells were washed with Dulbecco's phosphate-buffered saline (D-PBS) twice. Mouse and human fibroblasts and human keratinocytes were detached using trypsin-EDTA solution (PAN Biotech, P10-023100 in Freiburg; Sigma-Aldrich, ref. T3924 in Lyon) for 5 minutes at 37°C and 2 volumes of complete medium were added to inhibit the action of trypsin. Mouse keratinocytes were detached using a less aggressive enzyme, the TrypLE™ Select Enzyme (Gibco, ref. 12563-011) for 10-20 minutes at 37°C. Complete CnT-07S medium was added to stop the action of the TrypLE™ reagent. Released cells were collected and spun down at 200 g for 5 minutes. The cell pellet was resuspended into the appropriate volume of complete medium and transferred into a new culture cell dish or flask.

d. Freezing

To maintain a continuous source of primary cells, keratinocytes and fibroblasts were frozen and preserved for long-term storage in liquid nitrogen according to the following protocol. Confluent cells were detached from the cell culture plate following the procedure previously described (see §II.1.c). The total number of cells was determined using a Thoma cell counting chamber. Cells were centrifuged at 200 g for 5 minutes and the cell pellet was resuspended into the appropriate volume of freezing medium containing 45% DMEM medium, 45% FBS and 10% dimethylsulfoxyde (DMSO; Sigma-Aldrich, ref. D8418); 1 mL of freezing medium was usually used to freeze 1 million cells. The cell suspension was transferred into cryogenic vials (1 mL per vial) placed immediately in an isopropanol cooling chamber and stored at -80°C overnight. The day after, vials were transferred to liquid nitrogen for long-term storage.

2) Differentiation into myofibroblasts by TGFβ treatment

Human primary fibroblasts were seeded into a 6-well plate (80 000 cells per well) and incubated in complete DMEM AQ™ medium for 24 hours. At 60% confluence, cells were switched to serum-free medium containing DMEM without phenol red (Sigma-Aldrich, ref. D1145), 2 mM L-glutamine (Gibco, ref. 25030-024), 1 mM sodium pyruvate (Sigma-Aldrich, ref. S8636) and 1% AAS. They were treated with 10 ng/mL of TGFβ1 (Peprotech, ref. 100-21) for 72 hours. Supernatants and cells (RNA and protein lysates) were collected for qRT-PCR and immunoblotting experiments.

3) Inhibition of PCPE-1 in fibroblasts by RNA interference

a. Transfection with siRNA

Human primary fibroblasts were transfected with small interfering RNA (siRNA) directed against *PCOLCE* mRNA sequence and purchased from QIAGEN (***Table 11***). Fibroblasts were seeded in a 6-well plate in order to reach 60-70% confluence 24 hours later. Two µL siRNA solution (stock solution: 10 µM) were diluted in 88 µL DMEM AQ™ medium and 12 µL HiPerfect transfection reagent (QIAGEN, ref. 301704) in order to have a final concentration of siRNA of 10 nM in a volume of 102 µL. After 10 minutes of incubation allowing the formation of transfection complexes, the mix was added dropwise onto the cells.

16 hours later, fibroblast medium was removed and cells were incubated for 48 hours in serum-free DMEM medium (without phenol red) with 2 mM L-glutamine and 1 mM sodium pyruvate. After 48 hours, the medium was collected for Western Blotting and RNA was extracted from cells for qRT-PCR analysis (see §V and §VI.1).

No	Product name	Catalog No	Target sequence	Concentration
1	Hs_PCOLCE_2	SI00680750	CTC CAT CTC CTC CGA AGG GAA	10 µM
2	Hs_PCOLCE_3	SI00680757	CAG TCT TAT TGG TGC TTA TAA	10 µM
3	Hs_PCOLCE_6	SI04214686	ACG AGG CTT CCT GCT CTG GTA	10 µM
4	Hs_PCOLCE_7	SI04370520	CAC CAA CCT AAG CAA GAG GAA	10 µM
Ctrl	Control siRNA	1022076	AAT TCT CCG AAC GTG TCA CGT	10 µM

Table 11: *PCOLCE* and control siRNA sequences

b. Infection with shRNA-lentivirus

Short hairpin RNA (shRNA) oligonucleotides targeting the mRNA sequence of the human *PCOLCE* gene were purchased from Origene (ref. TL310571; ***Table 12***). shRNA sequences were cloned into a pGFP-C-shLenti expression vector (Origene, ref. TR30023)

containing a U6 polymerase III promoter for shRNA expression and a puromycin resistance gene for selection of transduced cells. After DNA amplification in stellar competent bacteria, plasmids were inserted into lentiviral particles by Caroline Costa and Didier Nègre from the AniRA Vectorology Platform of the SFR Bioscience (UMS3444, Lyon) and lentiviruses were titrated. Four different shRNA sequences directed against *PCOLCE* mRNA were compared in order to select the most efficient tool; a non-effective shRNA scrambled sequence (Origene, ref. TR30021) that does not align with any published NCBI sequence was used as a negative control for specific lentiviral products.

No	shRNA product name	Target sequence
A	TL310571A	GGACGAGGCTTCCTGCTCTGGTACAGCGG
B	TL310571B	CGCTGATGGCTTCTCAGCCTCCTACAAGA
C	TL310571C	TTGCCGTGACTGTCAGTCTTATTGGTGCT
D	TL310571D	GAAGAAAGGAGTCAGTTATCTGCTGATGG

Table 12: *PCOLCE* shRNA sequences

Human primary fibroblasts (from three different donors) were seeded in T225 cm^2 flasks (2.4 million cells per flask) in order to reach 70-80% confluence the day after. After 24 hours, the appropriate volume of shRNA lentivirus preparation was calculated to obtain a multiplicity of infection (MOI) of 50 and added dropwise onto cells. After 24 hours of infection, the virus-containing medium was removed and cells were incubated for 48 hours in serum-free DMEM medium (without phenol red) supplemented with 2 mM L-glutamine, 1 mM sodium pyruvate, 1% AAS and 50 µg/mL of ascorbic acid (Sigma-Aldrich, ref. A0278). shRNA efficiency was controlled at the mRNA level by qRT-PCR and at the protein level by Western Blotting and the medium was treated for mass spectrometry analysis (see §VI.4).

4) Keratinocyte differentiation

Proliferative normal human keratinocytes (NHK) were maintained in KSFM medium as previously described (see §II.1.b). Once keratinocytes were 90-100% confluent, they were treated with 1.8 mM calcium chloride dihydrate ($CaCl_2$; Riedel de Haën, ref. 12022) for 5 days to become terminally differentiated. Total RNA of proliferative and differentiated keratinocytes was isolated according to the manufacturer's protocol (see §V.1) and specific markers of keratinocyte differentiation (keratin 1, loricrin and involucrin) were used to control the cell differentiation at the mRNA level (***Table 17***).

5) Culture of monocyte and macrophages cell lines

a. Subculture of THP-1 and U937 cells

The human THP-1 monocyte cell line (ATCC® TIB-202™) was a gift from Alessia Landi (BIOSS, Freiburg University) and human U-937 (ATCC® CRL-1593.2™) cell line was obtained from Dr. Suzana Salcedo (MMSB, Lyon). THP-1 cells are human monocytes isolated from the peripheral blood of a one-year male patient with acute monocytic leukemia. These were cultured in suspension in RPMI medium 1640 (Gibco, ref. 31870-025) supplemented with 10% FBS, 2 mM L-glutamine and 1% penicillin-streptomycin. U-937 cells are human monocytes isolated from pleura of a 37 year-old male patient with histiocytic lymphoma. These cells were cultured in RPMI medium with 10% FBS and 1% AAS.

b. Differentiation and polarization of macrophages

i. Differentiation of monocytes into M0 macrophages

THP-1 and U-937 cells were seeded at 200,000 cells/mL in 6-well plates and maintained in the appropriate medium (see above). After 24 hours, cells were differentiated in the presence of 100 ng/mL (160 nM) phorbol 12-myristate 13-acetate (PMA; Sigma-Aldrich, ref. P1585). After 24 hours of treatment, the PMA-containing medium was replaced by fresh medium. At this point, M0 macrophages were either used for qRT-PCR or flow cytometry analyses, or polarized into M1 or M2 macrophages.

ii. M1 or M2 macrophage polarization

PMA-induced THP-1 macrophages (M0 macrophages) were polarized into M1 macrophages by incubation with 10 pg/mL of *E. Coli* lipopolysaccharides (LPS; Sigma-Aldrich, ref. L6529) and 20 ng/mL of interferon γ (IFN-γ; Peprotech, ref. 300-02) for 24 hours, according to a validated protocol[183]. M2 macrophages were obtained by treating M0 macrophages with 20 ng/mL of interleukin-4 (IL-4; Peprotech, ref. 200-04) and interleukin-13 (IL-13; Peprotech, ref. 200-13) for 72 hours. M1- (TNFα and IL1β) and M2- (MRC1 and fibronectin) specific markers were used to validate the cell polarization (***Table 17***).

III. *In vitro* cleavage assays

1) Cleavage assays with recombinant substrates

a. Procollagen III

To further characterize PCPE-1 or PCPE-2 activity, recombinant proteins were tested on different substrates available in the laboratory to identify their role *in vitro*. Firstly, the effects of PCPE-1 and -2 proteins were assayed on a well described substrate of BMP-1: type III procollagen. For this purpose, a truncated protein containing the C-propeptide, the C-telopeptide and three triplet amino acids of the triple helix, commonly used in the laboratory of C. Moali (Lyon) and previously described[168], was used as a substrate (***Figure 71A***). The procollagen III truncated protein, named CPIII-long (345 nM) was incubated with 2.4 nM of BMP-1 and various concentrations of PCPE proteins in 50 mM HEPES, 0.15 M NaCl, 5 mM $CaCl_2$, 0.02% n-octyl-β-D-glucopyranoside buffer (pH 7.4) at 37°C for 1 hour. The same buffer was used for all the cleavage assays and will be named "assay buffer" in the following paragraphs. Reaction samples were analysed by SDS-PAGE and Coomassie Brilliant Blue staining (0.1% solution). The intact protein and proteolytic fragments were quantified by densitometry using the ImageJ software. CPIII-long processing was also analysed in the presence of PCPE-1 antagonists, DARPins. Three different DARPin molecules (DP40, DP56 and control DP, the latter being a negative control) were tested at a 1.6 µM concentration with 2.5 nM of BMP-1 and 80 nM of PCPE-1 for 1 hour at 37°C.

b. Procollagen V

A truncated form of human procollagen V was given by the group of Florence Ruggiero (IGFL, Lyon) and used for the activity assay. As previously described[150], the pNα1(V)-protein is a construct derived from the N-terminal part of the procollagen V α1 chain containing a TSPN-1 domain, a variable domain and a collagenous domain (COL2; ***Figure 73***). 800 nM of the pNα1(V) protein were incubated with various concentrations of PCPE-1-8His or 6His-PCPE-2 recombinant proteins and 30 nM of BMP-1 for 2 hours at 37°C in the assay buffer.

c. Chordin

Recombinant mouse chordin was purchased from R&D (ref. 758-CN/CF). Chordin (370 nM) was incubated with 20 or 40 nM of BMP-1 and different concentrations of PCPE-1-8His or 6His-PCPE-2 for 4 hours at 37°C in the assay buffer.

d. Betaglycan

Rat betaglycan, provided by Fernando Lopez-Casillas (Universidad Nacional Autonoma de Mexico, Mexico City) was used for activity assays of BMP-1 with PCPEs. 1 µM of betaglycan was incubated with 100 nM of BMP-1 and increasing concentrations of PCPE-1-8His or 6His-PCPE-2 in the assay buffer for 4 hours at 37°C.

e. Thrombospondin-1

Human thrombospondin-1 (TSP-1) protein was purified from blood platelets in the laboratory of Catherine Moali (Anastasi et *al.*, submitted). Conditions for the cleavage of TSP-1 by BMP-1 were previously optimized in the C. Moali's laboratory and similar conditions were used for this *in vitro* assay. 200 nM of TSP-1 was incubated with various concentrations of PCPE-1-8His or 6His-PCPE-2 recombinant proteins and 70 nM of BMP-1 for 4 hours at 37°C in the assay buffer.

2) Cleavage assays with cell conditioned media

Type I and II procollagens from cell extracts were also used as substrates to evaluate the effects of PCPEs. Primary human skin fibroblasts and articular chondrocytes, respectively known for their high production of procollagens I and II, were cultured for 48 hours in the appropriate serum-free medium. The conditioned medium of fibroblasts was collected, while the conditioned medium of chondrocytes was given by the group of Frédéric Mallein-Gerin (LBTI, Lyon) and both were submitted to BMP-1 cleavage. 20 µL of medium were incubated with 10 nM of BMP-1 and 750 nM of PCPE in the assay buffer for 3 hours at 37°C. Samples were analysed by SDS-PAGE and Western blotting using antibodies specific for the C-propeptide of procollagen I (LF41, obtained from Larry Fisher, USA) or II (provided by Jean-Baptiste Vincourt, UMR 7365, Nancy).

IV. Murine wound healing model

1) Mouse models

A mouse model of recessive dystrophic epidermolysis bullosa (RDEB) was developed and previously described by the group of Pr. Bruckner-Tuderman[184]. These RDEB mice are hypomorphic for *Col7a1* gene and only express 10% of type VII collagen. Wild-type (WT) and RDEB mice were housed in the pathogen-free facility of the Freiburg University in a 12-hour light/12-hour dark environment with access to food and water at all times.

Pcolce2 knockout (KO) mice were generated by the group of C. Bleul by replacing a large part of the exon 3 of the gene (corresponding to nucleotides 258 to 431 of the mRNA sequence) by a IRES-lacZ/neomycin resistance cassette[172]. *Pcolce2* KO embryos were given as a gift by C. Happe and were injected into C57BL/6 females. Offspring was mated with C57BL/6 mice to generate both WT and *Pcolce2* KO mice. Mice were also housed in the pathogen-free facility of the Freiburg University.

2) Assessment of wound healing

The wound healing experiments were performed following the protocol described by Nyström et *al*[185]. The experiments were conducted according to the ethical approvals (G-09/80 and G13/68) obtained by the regional ethics review board. Five to seven-week-old mice were shaved, their skin was disinfected and the mice were anesthetized with isoflurane. Two full-thickness wounds per mouse were created on the back of the mice using a 6-mm punch biopsy tool (Pfm medical) through a skin fold on the mid-back. A specific position of the wounds was chosen to avoid the mice scratching or biting and inducing a secondary traumatization of the healing wounds. Mice were kept in individual cages after wounding and monitored every day for rewounding. Wounds were photographed with a Sony Cyber-shot camera (ref. DSC-RX100M3); for *Pcolce2* KO mice, wound closure was quantified using ImageJ and expressed as a percentage, of the original wound area (considered as 100%).

At different time points (1, 2, 3, 7 and 15 days after injury), mice were sacrificed and the wound tissue was carefully dissected and frozen at -80°C for RNA and protein extraction, or fixed in formalin and embedded in paraffin or directly embedded in Tissue-Tek OCT (optimum cutting temperature) compound (Sakura) and snap frozen for immunostaining.

V. Transcriptional analyses

1) RNA extraction

Total RNA from primary cells or cell lines was isolated using the RNeasy Plus Mini kit (QIAGEN, ref. 74134; Freiburg) or the Nucleospin RNA kit (Macherey-Nagel, ref. 740955.50; Lyon) according to the manufacturer's instructions. RNA from mouse skin tissue was extracted using the RNeasy Fibrous Tissue Mini kit (QIAGEN, ref. 74704). Quality and quantity of isolated RNA was determined using a Nanodrop. Then, RNA (500 ng) was reverse-transcribed to cDNA using the First Strand cDNA Synthesis Kit (ThermoFisher Scientific, ref. K1612; Freiburg) or the PrimeScript RT-PCR kit (Takara, RR037A; Lyon).

2) PCR

Polymerase chain reaction (PCR) was performed with a Mastercycler® gradient (Eppendorf) using the Taq DNA polymerase kit (Invitrogen, ref. 10342-020) according to the manufacturer's recommendations. PCR reactions were performed on cDNA or genomic DNA (gDNA) isolated from tails for the genotyping. Biopsies of mouse tails were incubated at 98°C in 200 µL of NaOH for 20 min and then, 35 µL of Tris 1 M were added. Once, the tails were crushed, the mixture was centrifuged at 15 000 g for 10 min and 5 µL of the supernatant was used for the PCR. Conditions of PCR are described in the following table (***Table 13***):

Step	**Temperature**	**Time**	
Polymerase activation and DNA denaturation	95°C	5 min	
Denaturation Annealing Extension	95°C See below 72°C	30 sec 30 sec 45 sec	40 cycles

Table 13: Thermal cycling protocol for genotyping

Sequences used to amplify *PCOLCE2* transcripts by PCR were as follows (***Table 14***):

Primers	**Sequence (5'-3')**	**Annealing temperature**	**Product lenght**
Intron 2_For	CCATCTAATGAGATTAGTCC	60°C	709 bp
Exon 3_Rev	TGTACCGTCATCTTGTTGCC		
Neocassette_Rev	CCCGGGATCAACTACC	58.5°C	584 bp
CB648	ATTCTTACCGGAGAGTCTGG	60°C	526 bp
CB650	CGTATCTGCAGTAGTTATCGC		
Exon 2_For 6	ATGTGGCGGCATTCTTACCG	60°C	391 bp
Exon 4_For 6	GGAAGGTTTTTCAAGGCGTCC		
Exon 2_For 7	CCTGGAATGTACCCTCCGAA	60°C	383 bp
Exon 4_For 7	ACGGGGTAATCTCGGTCTGG		

Table 14: Description of PCR sequences

3) qRT-PCR

Quantitative real-time PCR (qRT-PCR) analyses were performed with a CFX96 Real-Time system (BioRad) in Freiburg or the Rotor-Gene Q system (QIAGEN) in Lyon. qRT-PCR reactions were made using the iQ™ SYBR® Green Supermix (Bio-Rad, ref. 1708880; Freiburg) or the FastStart Universal SYBR® Master mix (Roche Applied Science, ref. 04913850001; Lyon) according to the manufacturer's recommendations. Conditions of transcript amplification are described in the following table (***Table 15***):

Step	**Temperature**	**Time**	
Polymerase activation and DNA denaturation	95°C	10 min	
Denaturation Annealing/extension	95°C 60°C	10 sec 20 sec	50 cycles
Melt curve analysis	72-94°C	5 sec/step	

Table 15: Thermal cycling protocol for qRT-PCR

Specific primer sequences were used to amplify the transcripts. They were carefully designed using the Primer-BLAST tool (NCBI) to satisfy essential criteria and obtain reliable qPCR results. Among these criteria, a primer length ranging from 15 to 25 nucleotides was chosen, the percentage of GC residues was around 40-60% and the melting temperature of the primers was comprised between 57 and 63°C (with a temperature difference of 3°C maximum between the forward and the reverse primers). Moreover, the primers spanned an exon-exon junction and amplified a qPCR product of 70-200 base pairs. Then, they were blasted against a mRNA RefSeq database to check amplification specificity. Finally, the primers were validated using three-fold serial dilutions of the targeted cDNA template. A standard curve was generated for each pair of primers, with the validation criterion that the amplification efficiency should be more than 90%.

Sequences used to amplify transcripts of mouse and human *BMP1, mTLD, TLL1* and *TLL2* genes, as well as *PCOLCE* and *PCOLCE2* genes were as follows (***Table 16***):

Gene	Specie	Forward primer sequence (5'-3')	Reverse primer sequence (5'-3')
GAPDH	Human	GGCCTCCAAGGAGTAAGACC	AGGGTCTACATGGCAACTG
Gapdh	Mouse	TTGATGGCAACAATCTCCAC	CGTCCCGTAGACAAAATGGT
BMP1	Human	GTTCAAGTCCGACAACACCG	CATTCCGTCCAAGGTGAGGT
Bmp1	Mouse	TGCGTGTGGAGTTCAAGTCT	CCGAGGTGAGCTTCCTGAGT
mTLD	Human	ATGACAACAAGCACGACTGC	GTCCATCTCCATGAAGGTCAGC
mTld	Mouse	GTACGTGGGCTATCTCCAGC	GCTCAGGCTTCTTACTGCCA
mTLL1	Human	Not validated	Not validated
mTll1	Mouse	GGCTGGAGTTCTTACATCTACG	CTTATCTCCCCTCCACAAATCG
mTLL2	Human	CCAGAGACTGGACCAAGCAG	ATTCTCCCGGCCATCCTTTC
mTll2	Mouse	Not validated	Not validated
PCOLCE	Human	AACTACACCAGACCCGTGTTC	CGGAATGAGAGGGACACAGT
Pcolce	Mouse	CTTCGGGCACTGAGCACCA	ACCTGGTTTGAGGGTGCAAT
PCOLCE2	Human	ATAGTCCACCTGCGCCAAT	ACCCGTGGTTACAGGGAATG
Pcolce2	Mouse	CATGTGGCGGCATTCTTACC	TGCCCTCAGGAACTGTGATT

Table 16: Primer sequences used to amplify BTP and PCPE transcripts by qPCR

Specific primers were used for human keratinocyte differentiation and macrophage polarization (M1/M2); sequences are listed below (***Table 17***):

	Gene	Forward primer sequence (5'-3')	Reverse primer sequence (5'-3')
Keratinocyte differentiation	Keratin 1	GATGAAATCAACAAGCGGACAA	TGGTAGAGTGCTGTAAGGAAATCAATT
	Loricrin	TCATGATGCTACCCGAGGTTTG	CAGAACTAGATGCAGCCGGAGA
	Involucrin	TCCTCCAGTCAATACCCATCAG	GCAGTCATGTGCTTTTCCTCTTG
M1 polarization	TNFα	CCCATGTTGTAGCAAACCCTCA	TCTCTCAGCTCCACGCATT
	IL1β	TCGCCAGTGAAATGATGGCT	TGGAAGGAGCACTTCATCTGTT
M2 polarization	CD163	AGCGGCTTGCAGTTTCCTCA	AGACACAGAAATTAGTTCAGCAGCA
	MRC1	ACGATCCGACCCTTCCTTGA	GCTTGCAGTATGTCTCCGCT
	Fibronectin	ATTCACCTACAATGGCAGGACG	ATGACGCTTGTGGAATGTGTCG

Table 17: qPCR primer sequences selected to monitor the differentiation markers of keratinocytes and macrophages

VI. Protein analyses

1) Immunoblotting

a. Sample preparation

i. Cell conditioned medium

Cells were grown until confluence and switched into serum-free medium in the presence of 50 µg/mL of ascorbic acid for 48 hours. Conditioned medium was collected and protein precipitation was performed using ammonium sulfate (Freiburg) or trichloroacetic acid/acetone (Lyon). Ammonium sulfate (Roth, ref. 3746.1) or trichloroacetic acid (TCA; Sigma-Aldrich, ref. T0699) was added to a final concentration of 30 and 10% respectively. The medium was precipitated for 1 hour at 4°C (under slow rotation for ammonium sulfate precipitation) and then, the proteins were pelleted by centrifugation (15000 g, 15 minutes at 4°C). For ammonium sulfate precipitation, the pellet was directly dissolved in 40 µL of sample buffer A (***Table 18***). For TCA/acetone precipitation, the pellet was washed with 200 µL of cold acetone and pelleted one more time by centrifugation (15000 g, 8 minutes at 4°C). Finally, it was resuspended in 15 µL of sample buffer A or B and used for Western blotting analysis.

Buffer	Sample buffer composition
A	4 M urea, 0.5 M Tris, 10% SDS, 50% glycerol, 0.05% bromophenol blue + 0.25 M DTT (dithithreitol; pH 6.8)
B	0.5 M Tris, 4% SDS, 12.5% glycerol and 0.01% bromophenol blue +/- 50 mM DTT (pH 6.8)

Table 18: Composition of sample buffers used in Freiburg (A) and Lyon (B)

ii. ECM extraction

After 48 hours of culture in serum-free medium, cells were washed twice with PBS. Once the culture plate was dry, an ammonium hydroxide solution (20 mM NH_4OH) was added onto the cells for 5 min at 4°C under agitation to detach the cells. After removing the NH_4OH solution, plates were washed with water several times and dried. Extracellular matrix attached to the plate was collected using 200 µL of Laemmli buffer (0.325M Tris, 25% glycerol, 10% SDS, pH 6.8) containing 5% of β-mercaptoethanol (>98%, Sigma, ref. M3178). The ECM lysate was mixed with sample buffer B (***Table 18***) and boiled at 100°C for 5 min.

iii. Cell lysates

As for ECM extraction, cells were washed twice with PBS and proteins from the cell layer were extracted with one of the following lysis buffers:

- **NP-40 lysis buffer** (25 mM Tris, 0.1M NaCl, 1% Np-40, 10 mM EDTA, 8M urea, pH 7.4 with protease inhibitors) incubated at 4°C for 1h (in Freiburg)
- **Laemmli buffer** (described above) containing 3% of β-merceptoethanol incubated at room temperature for 30 min (in Lyon)
- **RIPA buffer** (50 mM Tris, 0.15M NaCl, 1% Np-40, 1% SDS, 0.5% sodium deoxycholate, pH 8 with protease inhibitors) incubated at 4°C for 30 min under agitation (in Lyon).

Protein lysates were then collected, diluted into sample buffer (***Table 18***) and boiled at 100°C for 5 minutes. Amounts of samples loaded on acrylamide gels were normalized to have similar amounts of loading control protein GAPDH.

iv. Skin lysates

Wounds were removed from the back of the mice and frozen. Then, tissues were crushed with a hammer, mixed with 300 µL of sample buffer A (***Table 18***) and boiled at 100°C for 20 minutes (vortex every 3 min). After centrifugation (15000 g for 15 min), the supernatant was collected, diluted into TBS and used for Western blotting. As previously described, amounts of samples loaded on polyacrylamide gel were normalized with the GAPDH protein.

b. Western Blotting

Proteins were separated by SDS-polyacrylamide gel electrophoresis in 25 mM Tris – 0.2M Glycine – 0.1% SDS buffer. Then, proteins were electroblotted for 2 hours onto nitrocellulose membranes (BioRad) in Tris – Boric acid buffer in Freiburg or PVDF membranes (Millipore, ref. 831.1) in CAPS (N-cyclohexyl-3-aminopropanesulfonic acid) 1X – EtOH 10% buffer in Lyon. The membranes were blocked in 5% milk (AppliChem Panreac, ref. A0830) diluted into PBS – 0.05% Tween 20 (Sigma, ref. P1379) for 2 hours and then, were incubated overnight with primary antibodies diluted into the blocking buffer solution (5% milk in PBS – 0.05% Tween 20). Primary antibodies used for Western blotting are detailed in ***Table 19***. Then, membranes were washed three times with PBS – 0.05% Tween 20 and incubated with goat anti-rabbit (KPL, ref. 474-15-06), goat anti-rat (Jackson ImmunoResearch, ref. 112-035-167), goat anti-mouse (Calbiochem, ref. 401253) or donkey anti-goat (SantaCruz, ref. sc-2020) IgG HRP secondary antibodies for 2 hours. Proteins of interest were detected by chemiluminescence with the Amersham™ ECL™ Select Western blotting detection reagent (GE Healthcare, ref. RPN2235) using the Fusion FX camera system (Vilber Lourmat).

Antibody	Host	Reference	Western Blotting	Immunofluorescence	
				Material	Dilution
Human PCPE-1	Rabbit	Moali et *al.* 2005	1 :10000	Cryosections (PFA)	1 :100
Mouse PCPE-1	Goat	R&D System, AF2239	1 :1000	-	-
Human PCPE-2	Rabbit	GeneTex, GTX103410	1 :1000	Paraffin sections (pronase) and cryosections (PFA)	1 :100
Human PCPE-2	Rabbit	Xu et *al.* 2000	1 :1000	Paraffin sections (pronase) and cryosections (PFA)	1 :100
Human PCPE-2	Rabbit	Abcam, ab28345	1 :1000	Paraffin sections (pronase) and cryosections (PFA)	1 :100
Human and mouse BMP-1	Rabbit	Arnold et *al.* 2016	-	Paraffin sections (pepsin)	1:100
Human BMP-1	Rat	R&D System, MAB1927	1:1000	-	-
Mouse F4/80	Rat	A3-1, Thermo Scientific, MA1-91124	-	Paraffin sections (pronase)	1:50
Mouse GR1	Rat	RB6-8C5, Pharmingen, 550291	-	Paraffin sections (pronase)	1:20
Mouse Ly6G	Rat	RB6-8C5, eBioscience, 14-5931	-	Paraffin sections (pronase)	1:50
Human CD68	Mouse	KP1, Abcam, ab955	-	Paraffin sections (pronase)	1:200
Human elastase	Mouse	NP57, GeneTex, GTX72042	-	Paraffin sections (pronase)	1:50
C-propeptide I	Rabbit	LF41, gift from Larry Fisher	1:5000	-	-
C-propeptide II	Mouse	Gift from Jean-Baptiste Vincourt	1:4000	-	-
C-propeptide III	Mouse	48B14, gift from Elmar R. Burchardt	1:1000		
αSMA	Rabbit	Abcam, ab5694	1:1000	Cultured cells	1:500
αSMA	Mouse	Sigma, A5528	1:1000	-	-
αSMA	Mouse	Sigma, C6198	-	Paraffin sections (citrate)	1:200
TSP-1	Mouse	A6.1, Invitrogen, MA5-13398	1:1000	-	-
Tenascin C	Rat	R&D System, MAB2138	1:1000	-	-
pSTAT3	Rabbit	Cell Signaling, 9145S	1:1000	-	-

Table 19: Antibodies used for Western blotting and immunofluorescence experiments
Specie reactivity, host and reference of the antibodies are listed. For immunofluorescence experiments, the skin material used (cryosections or paraffin sections) and the appropriate dilution of the antibody are detailed. Finally, cryosections were usually fixed using paraformaldehyde (PFA); for paraffin sections, antigen retrieval was made using pronase or pepsin solutions.

2) Immunofluorescence

a. Cell cultures

Primary fibroblasts treated with TGFβ1 (10 ng/mL) were grown to subconfluence on coverslips for 5 days and fixed with methanol (Fluka Analytica, ref. 34966). Fibroblasts were permeabilized with Triton X-100 0.1% (Sigma-Aldrich, ref. T8787) and blocked in 5% Bovine Serum Albumin (BSA; Sigma, ref. A3059) for 30 minutes. Fibroblasts were stained with rabbit polyclonal anti-α-SMA antibody (1:500) and AlexaFluor 594-conjugated goat anti-rabbit IgG secondary antibody (Invitrogen, ref. A11037; 1:1500). Finally, cells were counterstained with DAPI (1 µg/mL; Euromedex, ref. 10-50A) and analysed with an Axioplan2 fluorescence microscope (Zeiss).

b. Tissues

Human skin biopsies were obtained using experimental protocols approved by the Ethics Committee of the Freiburg University (approval number 45/03-110631) in accordance with the declaration of Helsinki and with written informed consent from all participants and/or their legal guardians. Samples were obtained from patients following melanoma excision (clinically non-inflamed regions adjacent to the sites of excision, to at least ensure safety margins) and patients with RDEB, hypertrophic scars or keloids (between 20 and 70 years old). Mouse skin biopsies were collected from the back skin of WT or RDEB mice.

For immunofluorescence analysis, samples were either fixed in formalin and embedded in paraffin, or embedded in OCT and frozen. Sample preparation was different depending on the embedding. Paraffin-embedded skin biopsies were cut in 4 µm thick sections. Paraffin sections were deparaffinized and rehydrated into xylene and (100% to 60%) ethanol solutions. Then, antigens were retrieved with pepsin (Pepsin Solution Digest All™, Life Technologies, ref. 003009) or pronase (0.05% solution in PBS; Roche, ref. 10-165-921-001) digestion, depending on the primary antibody, at 37°C for 20 min; antigen retrieval is detailed for each antibody in ***Table 19***. Sections were blocked in 3% BSA (Chem Cruz, ref. sc-2323) diluted in TBS – 0.05% Tween 20 for 30 min. OCT-embedded sections were maintained frozen in liquid nitrogen until they were sectioned using a cryostat. Cryosections were thawed and dried at room

temperature, washed with PBS – 0.05% Tween 20 and fixed with 4% paraformaldehyde diluted in PBS for 20 minutes. Then, sections were permeabilized with 0.1% Triton X-100 for 5 min, blocked in 3% BSA diluted in PBS – 0.05% Tween 20 for 30 minutes.

Both paraffin- and OCT-embedded sections were stained with primary antibodies diluted in the blocking solution (3% BSA in PBS or TBS – 0.05% Tween 20) overnight. Then, sections were stained with secondary antibodies for one hour at room temperature: AlexaFluor 594-conjugated goat anti-rabbit IgG (Invitrogen, ref. A11037), AlexaFluor 488-conjugated goat anti-rat IgG (Invitrogen, ref. A11055) and -mouse IgG (Invitrogen, ref. A11029) antibodies. Finally, sections were counterstained with DAPI and mounted in Fluorescence Mounting Medium (Dako, ref. S3023). Stained sections were analysed with an Axioplan2 fluorescence microscope and images captured with a black and white camera.

3) Flow cytometry

a. Cells

PCPE-1 and PCPE-2 protein expression was analysed in cultured monocytes by flow cytometry. THP-1 cells were cultured in suspension until confluence, as previously described (see §II.9.e) and washed twice with PBS. Then, sample preparation and flow cytometry analyses were performed by Sophia Djebali from the AniRA – ImmOs Phenotyping platform of the SFR Bioscience (UMS3444, Lyon). Briefly, cells were washed with PBS containing 2% FBS and 0.01% azide and incubated with primary antibodies for 45 min at 4°C: rabbit polyclonal anti-human PCPE-1 (Moali et *al.* 2005; 1:100), rabbit polyclonal anti-human PCPE-2 (GeneTex, GTX103410; 1:100) or rabbit polyclonal anti-human PCPE-2 (Xu et *al.* 2000, 1:100). Cells were then centrifuged at 1200 rpm for 5 min and washed in the same buffer containing PBS, 2% FBS and 0.01% azide. Finally, they were incubated with BV421 goat anti-rabbit IgG antibody (BD Biosciences, ref. 565014; 1:500) for 45 min at 4°C. After several washes, expression of PCPE-1 or PCPE-2 proteins was analysed at the cell surface by using a LSRFortessa™ cytometer (BD Biosciences).

b. Mouse skin

Normal skin and wounds (days 3 and 7) were collected from WT and *Pcolce2* KO mice and kept in PBS. Tissue samples were then cut in small pieces and incubated with Liberase™ TM (Roche, ref. 05-401-127-001) under agitation for 1 hour at 37°C. The skin lysates were filtered (filter pore of 40 µm), washed with PBS and centrifuge at room temperature for 10 min at 300 g. The pellet was resuspended in 100 µL of FACS buffer (3% FBS in PBS) and spread

in several wells of a 96-well plate (depending on the number of antibodies). 20 µL of each condition were used for the fluorescence compensation. The 96-well plate was spin down at 300 g for 3 min and the supernatant was removed by reversing the place. Cells were incubated with the blocking solution (FB Block, clone 2.4G2, from the Max-Planck-Institute for Immunology and Epigenetics, Freiburg) for 10 min at 4°C. Then, the conjugated antibody solutions (***Table 20***) were added for 30 min at 4°C. Cells were washed twice with FACS buffer and analysed using the BD FACSCanto™ II cytometer. Flow cytometry experiments were performed with the help of Mareike Maler (Medical Center, Freiburg University).

Inflammatory marker	Flurochrome	References	Dilution
CD45	APC/Cya7	BioLegend, clone 30-F11, ref. 103116	1:100
CD11b	V450	BDHorizon, clone M1/70, ref. 560455	1:100
Ly6G	Pe/Cya7	BioLegend, clone 1A8, ref. 127618	1:100
F4/80	PerCP/Cya55	BioLegend, clone BM8, ref. 123128	1:100

Table 20: Antibodies used for flow cytometry experiment
List of the antibodies and the dilution used for the flow cytometry experiment performed on mouse skin. All the antibodies were conjugated.

4) Mass spectrometry

a. Protein sample preparation

Quantitative proteomic experiments were performed on the conditioned-media of primary human skin fibroblasts to analyse the extracellular proteins in the presence (control shRNA) or absence of PCPE-1 (*PCOLCE* shRNA). After 48 hours of culture, protease inhibitors were added to the collected media: 10 mM of EDTA (Sigma-Aldrich, ref. E5134), 10 µM of E-64 (EnzoLife Sciences, ref. ALX260-007-M00) and 0.25 mM of AEBSF chlorohydrate (Roth, ref. 2931.3).

The total amount of secreted proteins in the conditioned media was evaluated using a Bradford assay. Then, media were concentrated by ultracentrifugation (3500 g, 4°C) in 100 mM HEPES (pH8) using a Centricon® 70-Plus (Millipore, ref. UFC701008) with a 10 kDa cut-off in order to reach a final protein concentration around 1 mg/mL.

b. TMT™ labelling for relative quantitation by mass spectrometry

100 µg of proteins per condition were prepared and labeled using the TMT™ Isobaric Mass Tagging kit and reagents (ThermoFisher Scientific, ref. 90063), according to the

manufacturer protocol. Briefly, proteins were dissolved in triethyl ammonium bicarbonate (TEAB) and then reduced by 200 mM tris(2-carboxyethyl)phosphine (TCEP) at 55°C for an hour. Then, proteins were alkylated using iodoacetamide (375 nM) for 30 min at room temperature. After denaturation, reduction and alkylation, proteins were digested in peptides by the action of trypsin (2.5 µg per 100 µg of protein) at 37°C overnight. Peptides of each condition were labeled with a TMT Label Reagent for an hour at room temperature. The samples were then combined and stored at -80°C before analysis by mass spectrometry (MS).

The TMT-labelled samples were analysed by liquid chromatography, followed by tandem mass spectrometry (LC-MS/MS) on a Q Exactive™ HF Hybrid Quadrupole-Orbitrap™ Mass Spectrometer (ThermoScientific) by Fréderic Delolme, from the Protein Science Facility of the SFR Bioscience (UMS3444, Lyon).

c. MS/MS data analysis

Raw MS/MS datasets were converted to an open format file (e.g. mzXML) and searched against the human Swiss-Prot database (version 09-2017) with the search engine, MASCOT (v2.4.1). Cysteine carboxymethylation was set as a fixed modification; methionine oxidation, N-terminal acetylation, hydroxylation of proline and TMT labeling of the N-terminus and lysines were set as variable modifications. Two missed cleavages were allowed and trypsin cleavage was selected. The MASCOT result is a list of peptides and proteins including true and false positives. A secondary validation was then performed using the Trans-Proteomic Pipeline (TPP). Identified peptides and proteins were statistically validated using the XInteract, PeptideProphet and ProteinProphet tools of the TPP with an error rate set to 2%.

Quantitation of the TMT labelled peptides and proteins was achieved using the LIBRA tool. For each protein, $\log_2$ (*PCOLCE* shRNA/control shRNA ratio) was calculated, normalized and the standard deviation of the corresponding normal distribution of ratios was used for the determination of cut-offs. We considered as upregulated (or downregulated) the proteins with a $\log_2$ ratio superior (or inferior) to the calculated cut-off, (which corresponds to +/- 2σ of ratio distribution, σ being the standard deviation).

Chapter 3: Expression of BMP-1/Tolloid-like Proteinases (BTPs) and Procollagen C-Proteinase Enhancers (PCPEs) in skin

I. Mouse skin wound healing model

To study the expression of BTPs and PCPEs during dermal repair, a murine wound healing model, established in the laboratory of Pr. Bruckner-Tuderman in Freiburg, was used. Full-thickness wounds were created on the back skin of C57BL/6 mice and skin and wound samples collected at different time points: before wounding (control skin), 3 days post-wounding (day 3) and 7 days post-wounding (day 7). RNA was extracted from the wounds to perform qRT-PCR analyses, as described in the "Material and methods" chapter. Expression of the following transcripts was evaluated by qRT-PCR (***Table 21***).

Protein	Gene	Mouse transcript	Human transcript
BMP-1	*BMP1-1*	*Bmp1*	*BMP1*
mTLD	*BMP1-3*	*mTld*	*mTLD*
mTLL-1	*mTLL1*	*mTll1*	*mTLL1*
mTLL-2	*mTLL2*	*mTll2*	*mTLL2*
PCPE-1	*PCOLCE*	*Pcolce*	*PCOLCE*
PCPE-2	*PCOLCE2*	*Pcolce2*	*PCOLCE2*

Table 21: Name of the studied proteins and their coding gene

In addition, protein expression of BTPs and PCPEs was analysed and detected by Western blotting and/or tissue immunostaining. For all the immunostaining experiments, negative controls were performed to test for a potential binding of secondary antibodies. Mouse and human skin sections incubated without primary antibodies served as negative controls and no signal was obtained under these conditions (***Figure 26***).

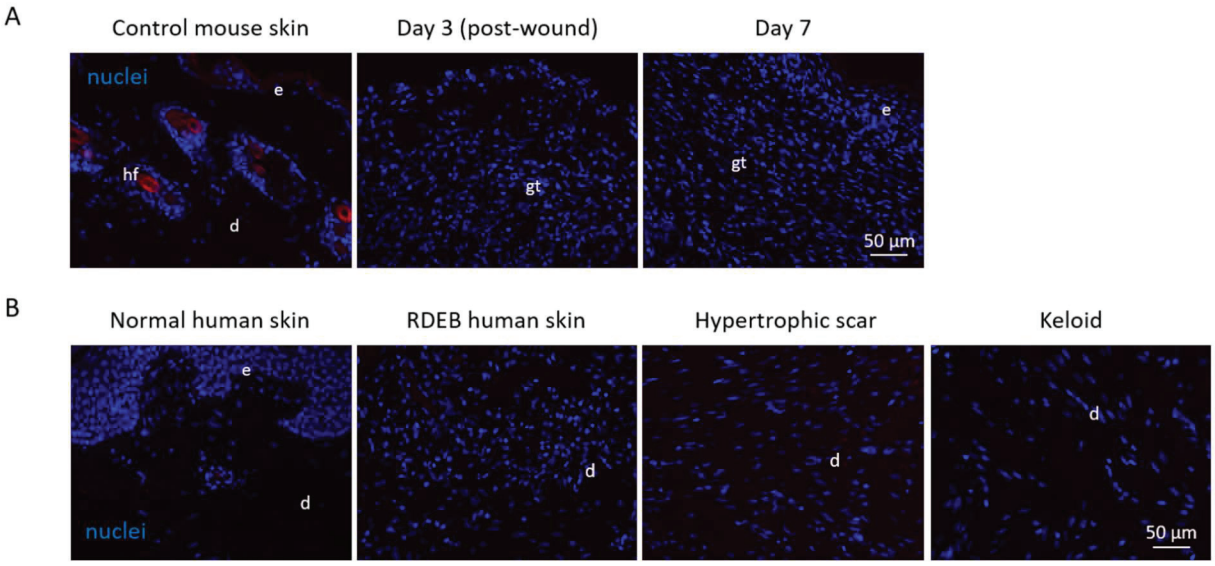

Figure 26: Immunofluorescence negative controls

Immunostaining of mouse **(A)** and human **(B)** skin sections without primary antibodies. Sections were incubated with anti-rabbit AlexaFluor-594 (red) antibody alone and nuclei were stained using DAPI (blue). Representative images of negative controls. *e, epidermis; d, dermis; hf, hair follicle; gt, granulation tissue.*

1) Expression of BTPs during skin wound healing

As BTPs are important actors in collagen fibrillogenesis, their mRNA levels were measured by qRT-PCR. The expression was normalized to the expression of a housekeeping gene (*Gapdh*) and the $2^{-\Delta Ct}$ of the two genes was calculated after applying a threshold. The $2^{-\Delta Ct}$ values for the control skin were assigned a value of 100% and all other time points (days 3 and 7) were calculated as a percentage of this value. Efficiency of the designed primers was tested and validated using serial cDNA dilutions; specific *Bmp1, mTld, mTll1* and *mTll2* primers were considered as similarly efficient, with a reaction efficiency of at least 90% over 8 dilutions (based on the slope of the amplification curves). Thus, the basal expression levels of *Bmp1, mTld* and *mTll1* were similar in mouse skin, whereas the *mTll2* transcript was not detected. During skin wound healing, no significant changes were observed in the expression of *mTll1* (***Figure 27***), whereas *mTld* showed a tendency, although not significant, to be gradually increased during the first 7 days of healing. In contrast, *Bmp1* appeared to be significantly upregulated 7 days after wounding. These results suggest that BMP-1 is the main protease of the BTP family involved during the proliferative phase of wound healing in mouse skin.

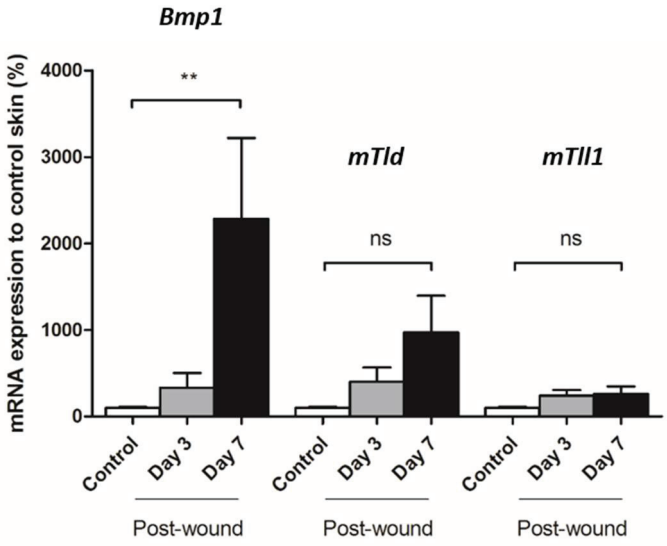

Figure 27: BTP mRNA expression during skin wound healing in mice

Relative mRNA expression of BMP-1/Tolloid like Proteinases (BTPs) analysed by qRT-PCR in skin wounds from C57BL/6 mice at different time points. Unwounded mice were used as control mice (100%); day 3 and day 7 correspond to wounded skin collected after 3 or 7 days. While *mTld* and *mTll1* mRNA levels did not lead to any significant change during the healing process, *Bmp1* was significantly increased 7 days after wounding. The values are means ± SEM (n = 6 in each group; Kruskal-Wallis test: **, p-value < 0.01; *ns, non-significant*).

As the detection of the BMP-1 protein is very challenging by Western blotting, the abundance of the BMP-1/mTLD protein was assessed by immunostaining in control and wounded skin (3 and 7 days post-wound). The antibody used for this experiment (rabbit anti-

BMP-1 antibody, Arnold et *al.* 2016) is specific for the two isoforms, BMP-1 and mTLD, and only recognizes the active forms of the proteins. Immunofluorescence staining showed an increase in BMP-1/mTLD expression during the proliferative phase of wound healing (day 7 post-wound), which correlates with the qRT-PCR data (***Figure 28***).

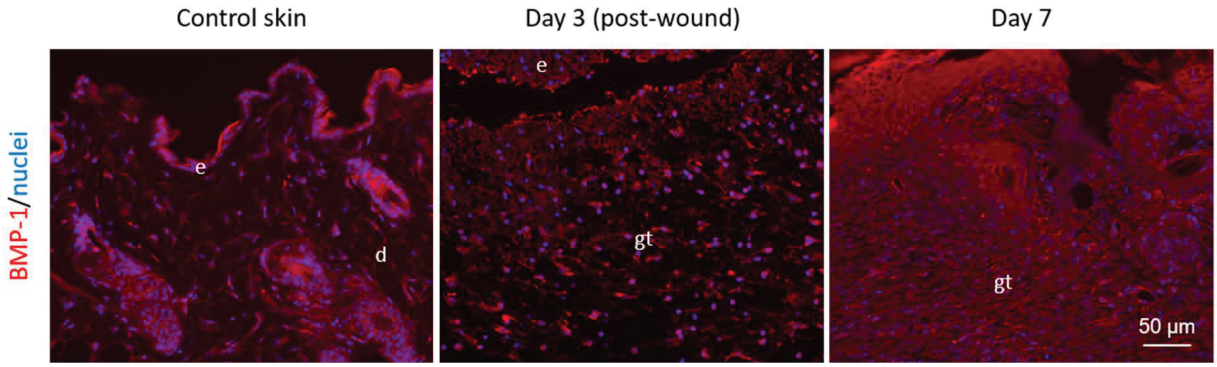

Figure 28: BMP-1/mTLD expression in mouse skin during wound healing

Immunostaining of BMP-1/mTLD (red) in paraffin sections using a polyclonal anti-BMP-1 antibody (Arnold et *al.* 2016, 1:200) with pepsin antigen retrieval (n = 3; only representative pictures are shown). Nuclei were stained using DAPI (blue). The BMP-1/mTLD protein was significantly increased 7 days after wounding compared to control skin and 3 day-wound. *e, epidermis; d, dermis; gt, granulation tissue.*

These results suggest that BTPs, and mainly BMP-1, are important enzymes during the proliferative phase of wound healing, a stage which is characterized by increased ECM synthesis and deposition, and especially increased collagen deposition.

2) PCPE expression patterns during skin wound healing

qRT-PCR analyses were performed to determine the expression levels of *Pcolce* and *Pcolce2* transcripts (encoding mouse PCPE-1 and PCPE-2 proteins respectively) in normal mouse skin and after wounding (at 3 and 7 days post-injury). Efficiency of the designed primers was also tested and validated; specific *Pcolce* and *Pcolce2* primers were considered as similarly efficient, with a reaction efficiency above 90%. Thus, we could compare the basal expression levels of *Pcolce* and *Pcolce2* in mouse skin and found *Pcolce* to be 2-4 times more expressed than *Pcolce2* (data not shown).

Then, *Pcolce* and *Pcolce2* mRNA expression was determined in wounded skin (3 and 7 days post-wound) by qRT-PCR and compared to control skin (***Figure 29***). As observed in the presented graph, a significant increase in *Pcolce* mRNA expression was detected 7 days after wounding, while no significant change was detected 3 days post-wound. In contrast, *Pcolce2* expression showed no significant changes during the whole wound healing process at the

mRNA level. These results suggest that PCPE-1 seems more co-regulated with BMP-1/mTLD expression during skin wound healing than PCPE-2.

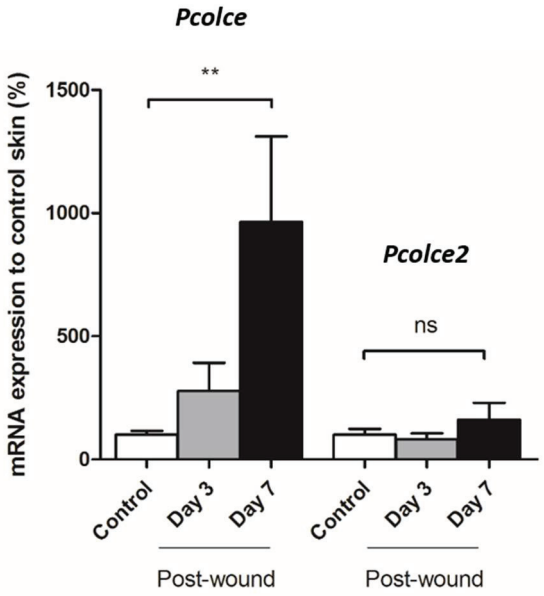

Figure 29: *Pcolce* and *Pcolce2* mRNA expression during skin wound healing in mice

Pcolce and *Pcolce2* mRNA quantitation by qRT-PCR in skin wounds of C57BL/6 mice at different time points (days 3 and 7 post-injury). Skin of unwounded mice was used as control (100%). While *Pcolce2* expression was unchanged during wound healing, *Pcolce* mRNA was significantly increased 7 days after wounding (day 7) compared to control skin. The values are means ± SEM (n = 6 in each group; Kruskal-Wallis test: **, p-value < 0.01; *ns, non-significant*).

To go further, the protein levels of PCPE-1 and PCPE-2 were evaluated by immunoblotting and/or immunostaining in mouse skin. Western blotting analyses were performed on wound lysates and PCPE-1 protein was detected using an antibody directed against mouse PCPE-1 (R&D, AF2239). The densities of the bands corresponding to PCPE-1 were measured by densitometry using the ImageJ software and normalized to GAPDH. Data for the control skin were assigned a value of 100% and all other time points were calculated as a percentage of this value. In line with the qRT-PCR results, PCPE-1 protein was significantly increased in the wounds after 7 days, as shown in the Western blot and the graph (***Figure 30A***). Another anti-PCPE-1 antibody (Moali et *al.* 2005) was used to detect PCPE-1 in cryosections by immunofluorescence because the one used for Western blotting was not working. Immunofluorescence analyses revealed a stronger staining in the granulation tissue of wounded skin sections at day 7 (***Figure 30B***). Together, these results showed that mRNA and protein levels of PCPE-1 followed the expression pattern of BMP-1 during the healing of mouse wounds. This suggests that PCPE-1 might also play a role during the proliferative phase of wound healing, probably by enhancing BMP-1-mediated procollagen processing.

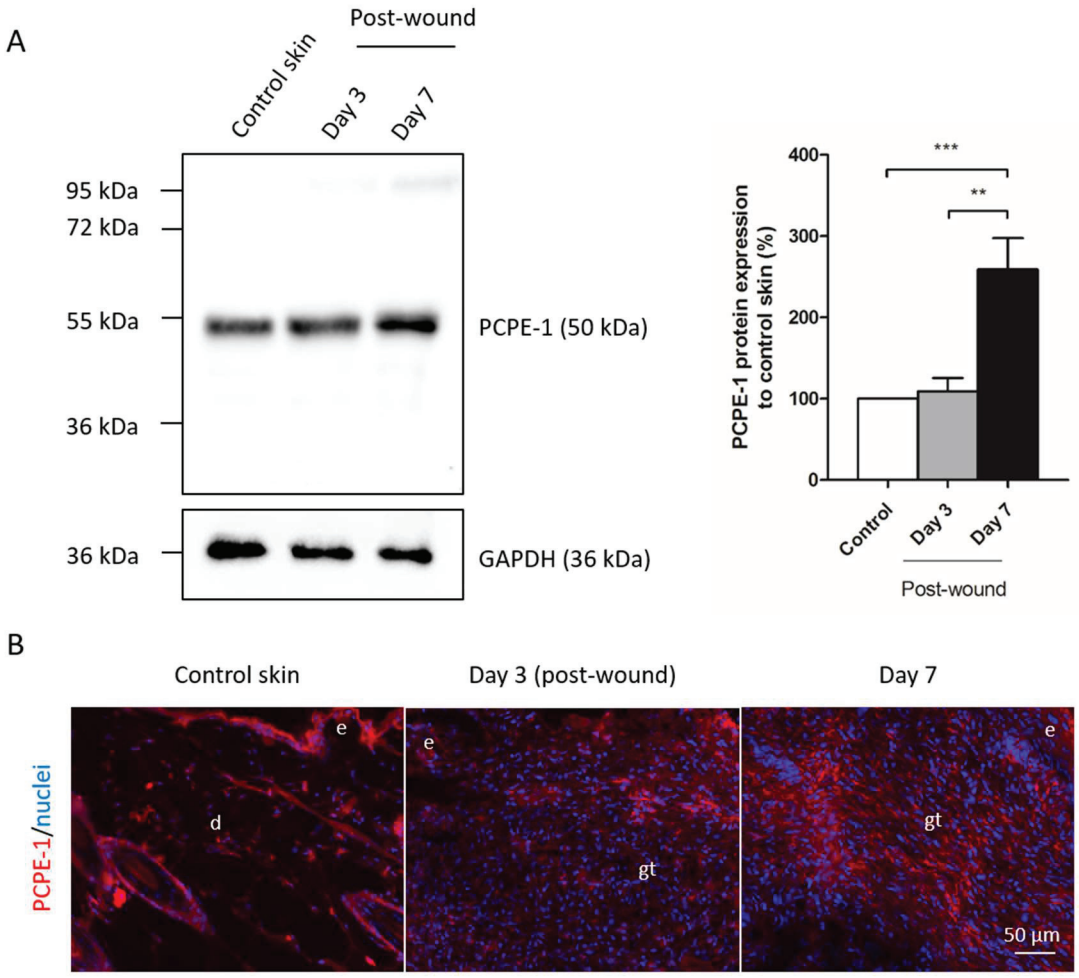

Figure 30: PCPE-1 expression during skin wound healing in mice

(A) Detection of PCPE-1 protein by Western blotting on wound lysates (3 and 7 days after injury) and quantification using ImageJ. The values represent means ± SEM (n = 6 in each group; ANOVA test with Dunnett multiple comparison: **, p-value < 0.01; ***, p-value < 0.001). **(B)** Immunostaining of PCPE-1 (red) in mouse skin cryosections using a polyclonal anti-PCPE-1 antibody (Moali et *al.* 2005, 1:100) with PFA fixation (n = 3; only representative pictures are shown). Nuclei were stained using DAPI (blue). By Western blotting and immunostaining, we found that the expression level of PCPE-1 was significantly increased 7 days after wounding compared to control skin and 3 day-wound. *e, epidermis; d, dermis; gt, granulation tissue.*

Then, the abundance of the PCPE-2 protein was determined during skin wound healing. Unfortunately, we were unable to detect PCPE-2 by Western blotting, neither in normal skin nor in wounds. We used sections of paraffin-embedded mouse skin to detect PCPE-2 by immunofluorescence. Three different polyclonal antibodies directed against a large sequence of the entire protein (> 200 amino acids) or a peptide (located in the CUB2-NTR linker) were used to detect PCPE-2 (***Table 22***): two commercial antibodies purchased from GeneTex (GTX103410) and Abcam (ab28345), and an antibody produced and described by Xu and colleagues (Xu et *al.* 2000).

Anti-PCPE-2 antibody	Name	Immunogenic sequence
GTX 103410 (GeneTex)	GTX	Sequence > 200 amino acids including the following sequence, the exact sequence is proprietary.
Ab28345 (Abcam)	Abcam	End of CUB2 and beginning of the CUB2-NTR linker; the exact sequence is proprietary.
Xu et *al.* 2000	Xu et *al.*	End of CUB2 and CUB2-NTR linker, following sequence: IGHYIFRPKKLPTTTEQPVTTTFPVTTG

Table 22: List of the anti-PCPE-2 antibodies used and their immunogenic sequence

All the three revealed similar staining patterns of PCPE-2 (***Figure 31***); the results obtained with the GTX antibody only will be shown in the following sections. PCPE-2 was barely detectable in unwounded mouse skin (control skin; ***Figure 32***). After injury, we observed a strong and punctate staining for PCPE-2 in the early stages of wound healing. This expression pattern was unexpected and completely different from what we observed for PCPE-1 (***Figure 30B***), so additional time points were added to go deeper with the analysis (days 1, 2 and 15 post-wound). PCPE-2 was found to be most highly abundant from days 1 to 3 after injury, corresponding to the inflammatory phase of wound healing. Then, its abundance significantly decreased 7 and 15 days post-wound, suggesting that PCPE-2 might play a role in the inflammatory stage rather than the proliferative stage of the healing process.

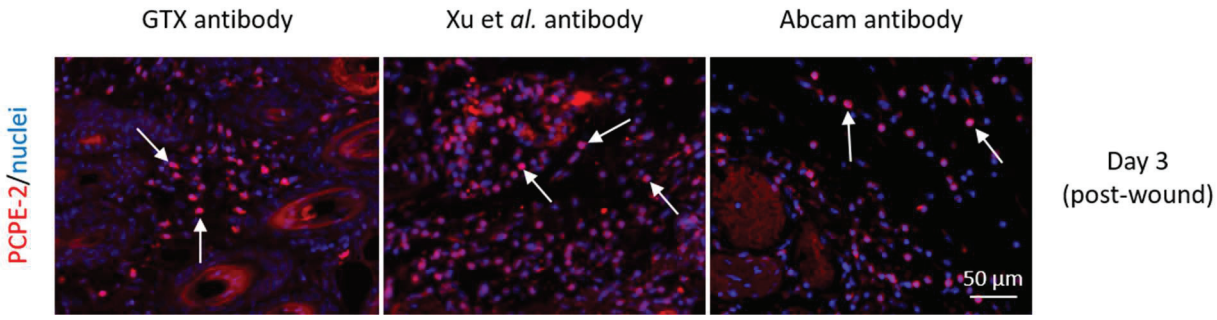

Figure 31: PCPE-2 pattern of expression using three different antibodies

Immunostaining of PCPE-2 (red) in sections of paraffin-embedded skin from C57BL/6 mouse wounds (at day 3) using three rabbit polyclonal anti-PCPE-2 antibodies (GTX, Xu et *al.* and Abcam, 1:100; representative images of n = 3). Nuclei were stained using DAPI (blue).

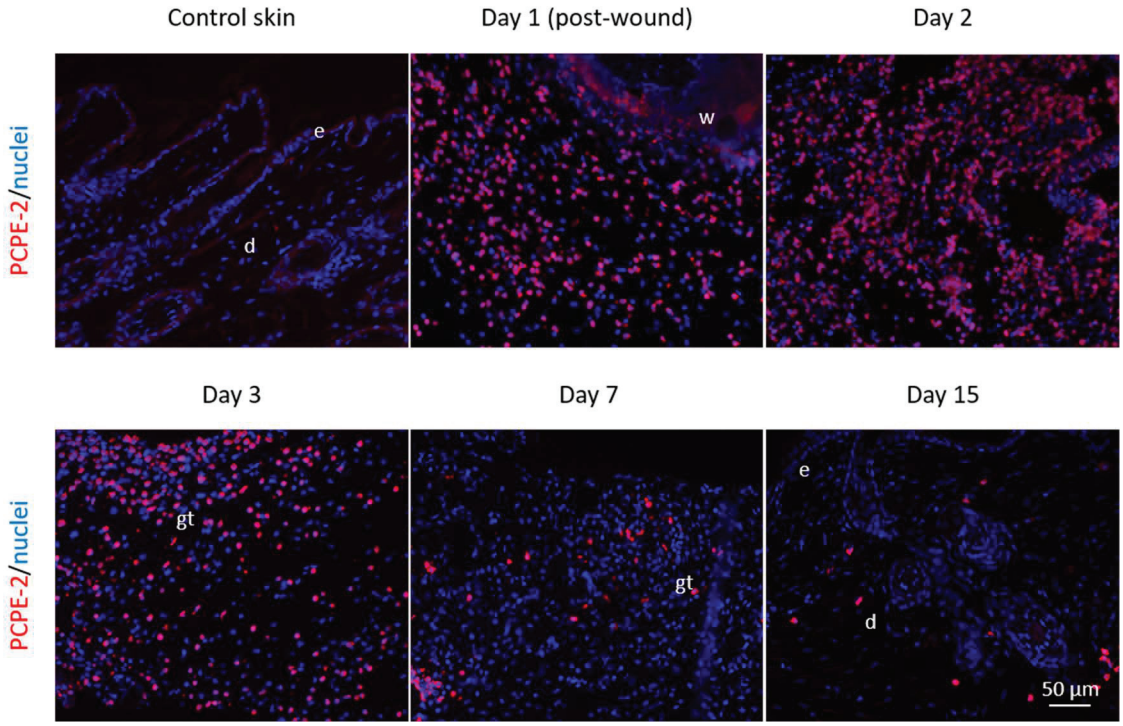

Figure 32: PCPE-2 expression during skin wound healing in mice

Immunostaining of PCPE-2 (red) in paraffin-embedded skin sections from C57BL/6 mouse wounds using a rabbit polyclonal anti-PCPE-2 antibody (GTX103410, 1:100; representative images of n = 3-4 in each group). Nuclei were stained using DAPI (blue). In mouse skin, the expression pattern of PCPE-2 is different from that of PCPE-1 with a strong and punctate staining during the early stages of wound healing. The PCPE-2 protein is highly abundant from 1 to 3 days after wounding and then its expression decreased at days 7 and 15. *e, epidermis; d, dermis; w, wound; gt, granulation tissue.*

To support this hypothesis, PCPE-2 abundance was then studied in a genetic mouse model of RDEB, which is known to involve chronic inflammation[185]. RDEB is an inherited skin-blistering disorder caused by mutations in the *COL7A1* gene, which encodes type VII collagen, a protein involved in the attachment of the epidermis to the underlying dermis (see "Chapter 1: Introduction"). Patients with RDEB exhibit non-healing wounds, fibrosis and scarring, and in the most severe cases, squamous cell carcinoma[186]. A RDEB mouse model hypomorphic for *Col7a1* expression was developed by the group of Pr. Bruckner-Tuderman[184]. These RDEB mice show greatly diminished type VII collagen levels at the DEJ and are, in the context of wound healing, characterized by skin inflammation and delayed wound closure[187]. Interestingly, PCPE-2 was found to be expressed in the dermis of unwounded RDEB mice, whereas the protein was not detected in the skin of WT mice (***Figure 33***), as previously mentioned. However, after wounding of the mice, levels of PCPE-2 were similar in control and RDEB skin along the healing process, as observed 3 days post-wound. Thus, the PCPE-2 protein might not be involved in the delayed wound healing observed in RDEB but might still be important for physiological wound healing.

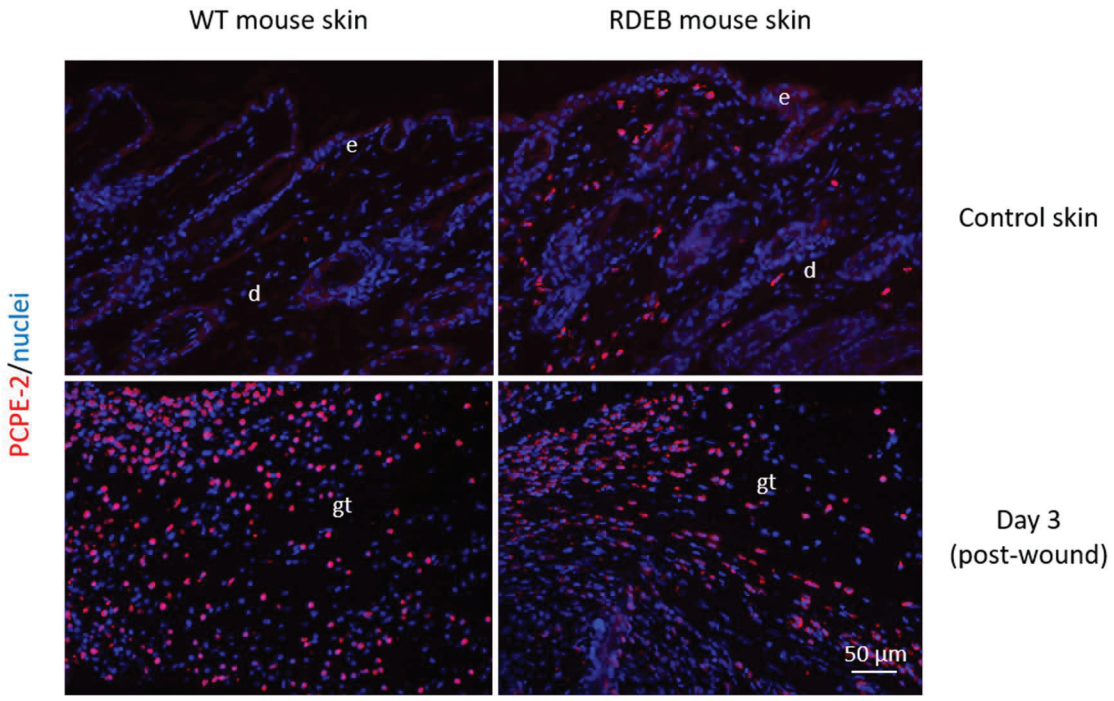

Figure 33: PCPE-2 expression during wound healing in WT and RDEB mouse skin

Immunostaining of PCPE-2 in paraffin-embedded skin sections from C57BL/6 WT and collagen VII-deficient (RDEB) mouse wounds using a rabbit polyclonal anti-PCPE-2 antibody (GTX103410, 1:100; representative images of n = 3 in each group). While PCPE-2 was barely detectable in the control skin of WT mice, the protein is much more expressed in RDEB skin, characterized by persistent inflammation. However, PCPE-2 expression is similar in wounds of WT and RDEB mice after 3 days. *WT, wild-type; RDEB, recessive dystrophic epidermolysis bullosa; e, epidermis; d, dermis; gt, granulation tissue.*

Altogether, PCPE-1 and PCPE-2 exhibit different patterns and kinetics of expression during murine wound healing suggesting that they might have different functions. PCPE-1, which is highly expressed during the proliferation phase, could be important for the collagen deposition and tissue repair as expected. In contrast, PCPE-2 seems to be stimulated during the inflammatory phase of tissue repair or in pathological conditions (as observed in RDEB mice). The importance of the contribution from the latter will be addressed in the next part, using pathological human wounds and in chapter 6 using a *Pcolce2* KO mouse model.

II. Pathological human wounds

To investigate the role of BTPs and PCPEs during wound healing, skin biopsies from healthy donors and patients with wound healing pathologies were collected by Dr. Dimitra Kiritsi at the Medical Center of the Freiburg University (Germany). The wound healing conditions included RDEB wounds, hypertrophic scars (HTS) and keloids. As previously described (see chapter 1), impaired healing leads to different types of pathological wounds such as non-healing wounds or abnormal scars (HTS and keloids). RDEB is a skin-blistering disease that manifests in delayed wound healing and scars. In contrast, HTS and keloids are two different forms of pathological scars resulting from excessive ECM deposition.

1) BMP-1/mTLD expression in pathological wounds

Firstly, we investigated the abundance of BMP-1/mTLD in normal human skin and RDEB skin by immunofluorescence analysis. In line with their role in the renewal of collagen matrix during skin homeostasis, BMP-1/mTLD was expressed in the dermis of normal human skin (***Figure 34***; left panels). Interestingly, a high increase in BMP-1/mTLD abundance was detected in the skin of RDEB patients. Dysregulation of the proteases involved in collagen maturation and deposition could therefore contribute to the development of fibrosis and scars in RDEB skin.

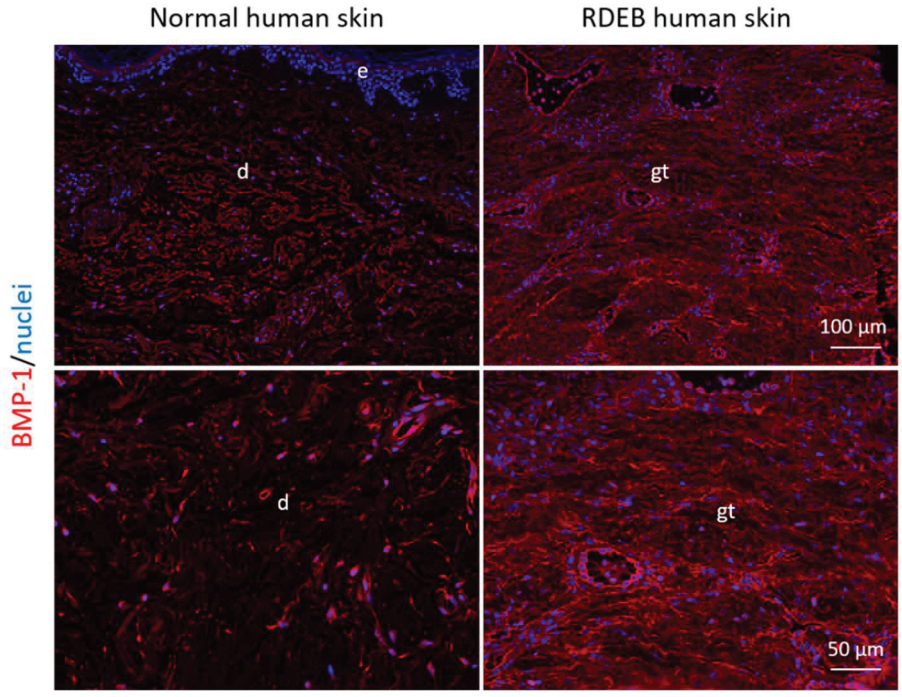

Figure 34: BMP-1/mTLD expression in normal and RDEB human skin

Immunostaining of BMP-1/mTLD in sections of paraffin-embedded normal and RDEB human skin using a rabbit polyclonal anti-BMP-1 antibody (Arnold et *al.* 2016, 1:100; n = 4 in each group). Upper and lower panels are respectively 10X (scale bar: 100 µm) and 20X (scale bar: 50 µm) magnification. BMP-1 is expressed in the dermis of normal human skin (left panels) and its expression is highly increased in the skin of RDEB patients (right panels). *e, epidermis; d, dermis; gt, granulation tissue.*

Then, we also looked at the BMP-1/mTLD abundance in two kinds of scars with known excessive collagen deposition, HTS and keloids but we did not detect any increase in BMP-1/mTLD abundance in any of the scar types, at least in the center of the scars (***Figure 35***). Rather, the levels of active BMP-1/mTLD seemed downregulated at these sites compared to normal human skin. The periphery of keloids, which may represent a region of actively progressing fibrosis, was not analysed.

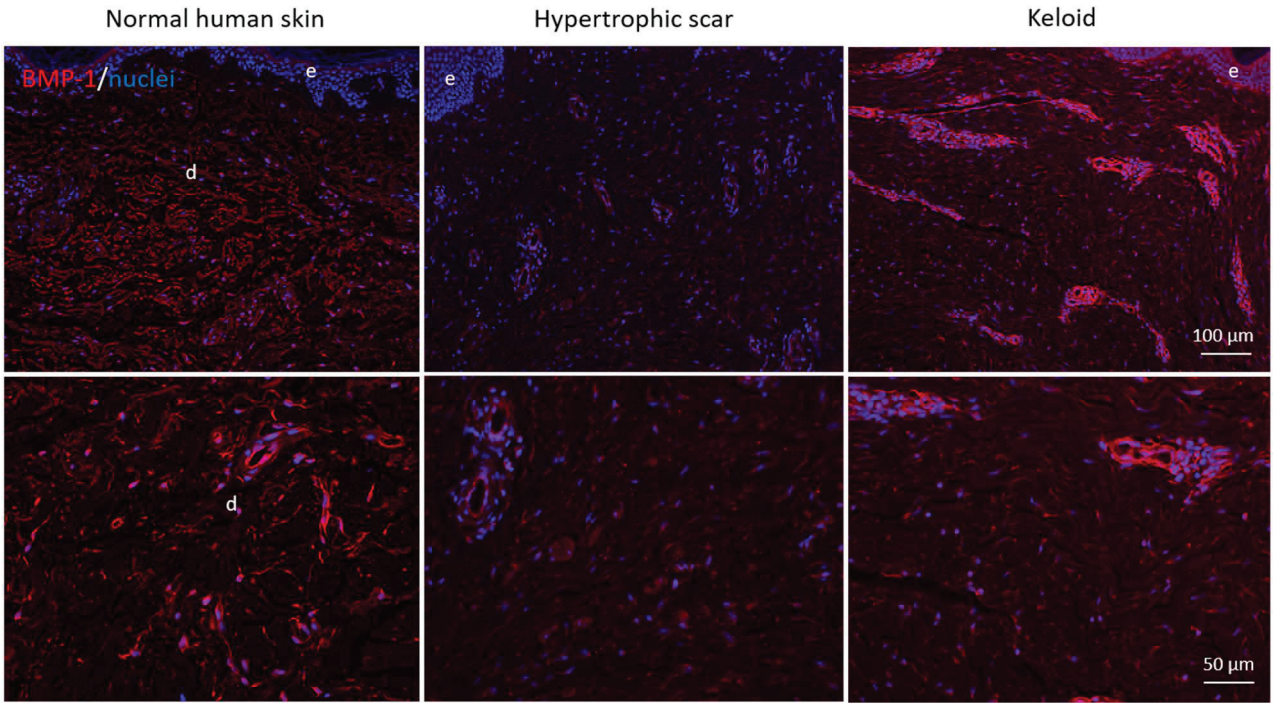

Figure 35: BMP-1/mTLD expression in normal human skin, hypertrophic scars and keloids
Immunostaining of BMP-1/mTLD using a rabbit polyclonal anti-BMP-1 antibody (Arnold et *al.* 2016, 1:100; representative pictures of n = 4 in each group) in sections of paraffin-embedded human normal skin, HTS and keloids. Upper and lower panels are respectively 10X (scale bar: 100 µm) and 20X (scale bar: 50 µm) magnification. BMP-1/mTLD is expressed in the dermis of normal human skin (left panels) as previously observed. In abnormal wounds such as hypertrophic scars (middle) and keloids (right), their expression is downregulated in comparison to normal skin.

These results showed for the first time that the BMP-1/mTLD proteases are not uniformly altered in conditions of dermal scarring or fibrosis. Instead, the abundance of BMP-1/mTLD appears to be indication dependent. It is important to note that RDEB skin, in contrast to HTS, display actively progressing fibrosis. This may suggest that BMP-1/mTLD activity is needed to perpetuate dermal fibrosis. Unfortunately, we could not confirm these results by qRT-PCR and Western blotting because of the limited availability of patient samples that can be used for such analyses. For the same reasons, we did not analyse the abundance of PCPE-1 in human sections. Indeed, human samples are usually collected and embedded in paraffin for diagnostic

(H&E staining) while the anti-human PCPE-1 antibody was only validated on cryosections for immunofluorescence.

2) Expression of PCPE-2 in human pathological wounds

Next, PCPE-2 abundance was evaluated in the same collection of biopsies taken from patients with wound healing pathologies as previously used. In normal human skin, PCPE-2 was detected in both the epidermis and the dermis, with a higher expression in the epidermal layer than in the dermal layer (***Figure 36***). In RDEB skin, the expression of PCPE-2 was strongly increased compared to normal human skin, with a much higher number of distinctly PCPE-2 positive-cells observed in the dermis. These results confirmed the higher abundance of PCPE-2 previously observed in the RDEB mouse model (***Figure 33***). As inflammation is a key feature of the RDEB disease, these results also suggested a potential link between PCPE-2 and inflammation.

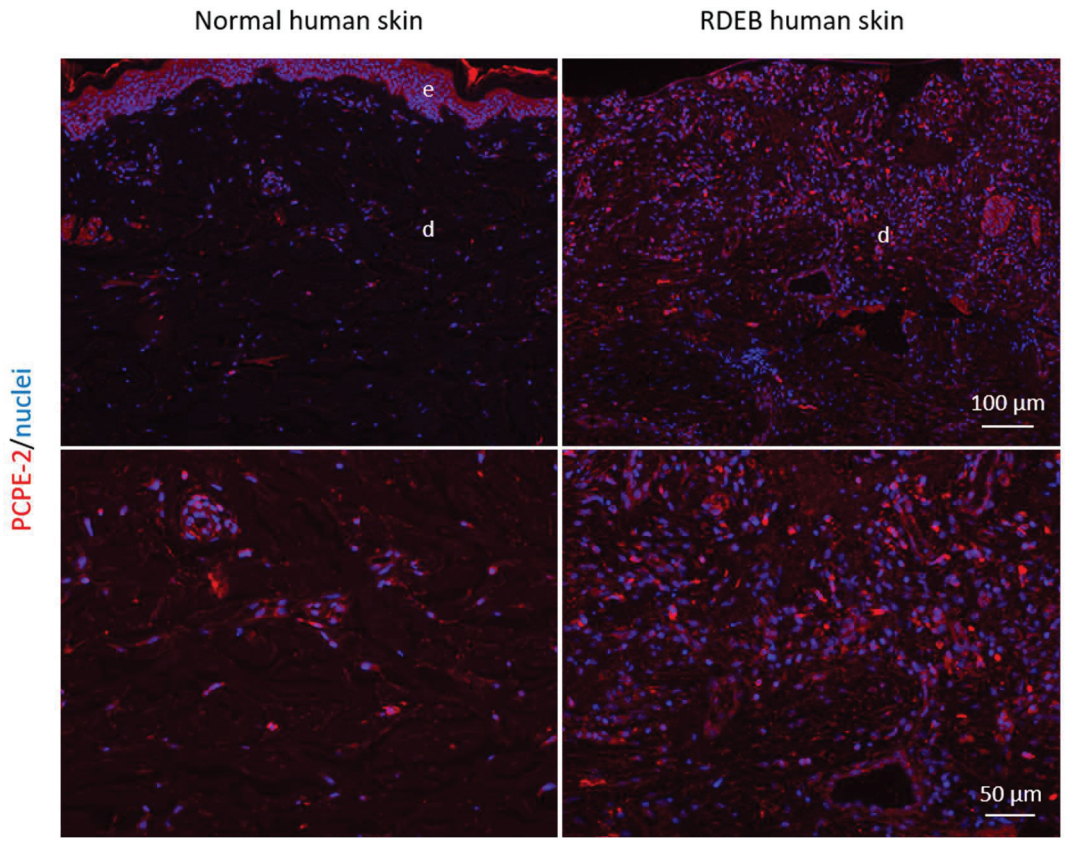

Figure 36: PCPE-2 expression in normal and RDEB human skin

Immunostaining of PCPE-2 in sections of paraffin-embedded human skin using a rabbit polyclonal anti-PCPE-2 antibody (GTX103410, 1:100; n = 4 in each group). Upper and lower panels are respectively 10X (scale bar: 100 µm) and 20X (scale bar: 50 µm) magnification. Expression levels of PCPE-2 were quite low in the dermis of normal human skin (red staining), but seemed to be higher in the epidermal layer. In contrast, dermal expression of PCPE-2 was highly increased in scars of RDEB human skin. *e, epidermis; d, dermis; gt, granulation tissue; s, scar.*

Moreover, we investigated the expression of PCPE-2 in scars. HTS showed slightly higher PCPE-2 abundance than normal human skin (***Figure 37***). In contrast, keloids displayed low levels of PCPE-2. No observable PCPE-2 was found in the epidermis of keloids, unlike the relatively strong epidermal staining that is observed in normal skin. In the keloid scar, only a few cells seemed to express PCPE-2. As keloids are made of a dense mass of ECM and are cell sparse, we looked at the expression of PCPE-2 in the peripheral region. Interestingly, we found many PCPE-2 positive-cells in the periphery, with a clear demarcation between the scar and the surrounding unaffected skin (***Figure 38***; white dotted lines). This result indicates that PCPE-2 is present in a specific cell subtype that could be involved in keloid progression.

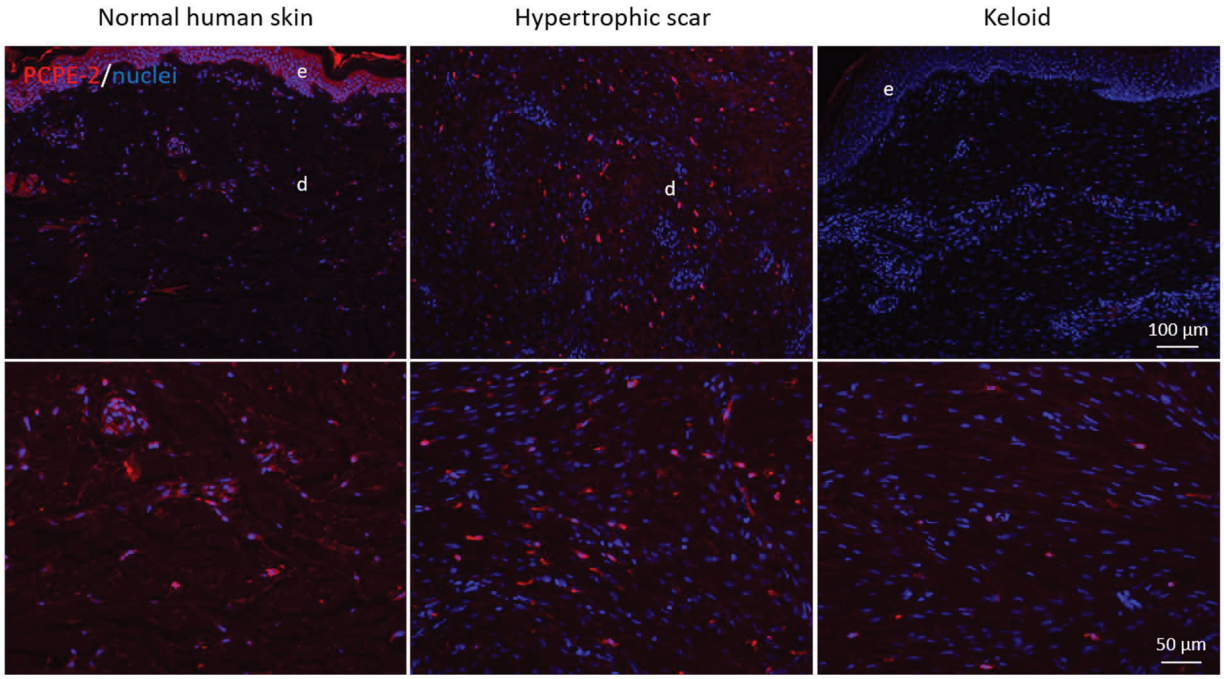

Figure 37: PCPE-2 expression in normal human skin and abnormal scars (HTS and keloids)

Immunostaining of PCPE-2 in sections of paraffin-embedded human skin using a rabbit polyclonal anti-PCPE-2 antibody (GTX103410, 1:100; n = 4 in each group). Upper and lower panels are respectively 10X (scale bar: 100 µm) and 20X (scale bar: 50 µm) magnification. In comparison to normal skin, PCPE-2 expression was slightly increased in hypertrophic scars (HTS), not in keloids. Moreover, PCPE-2, which is expressed in the epidermis of normal skin, is not detected in the epidermal layer of keloids.

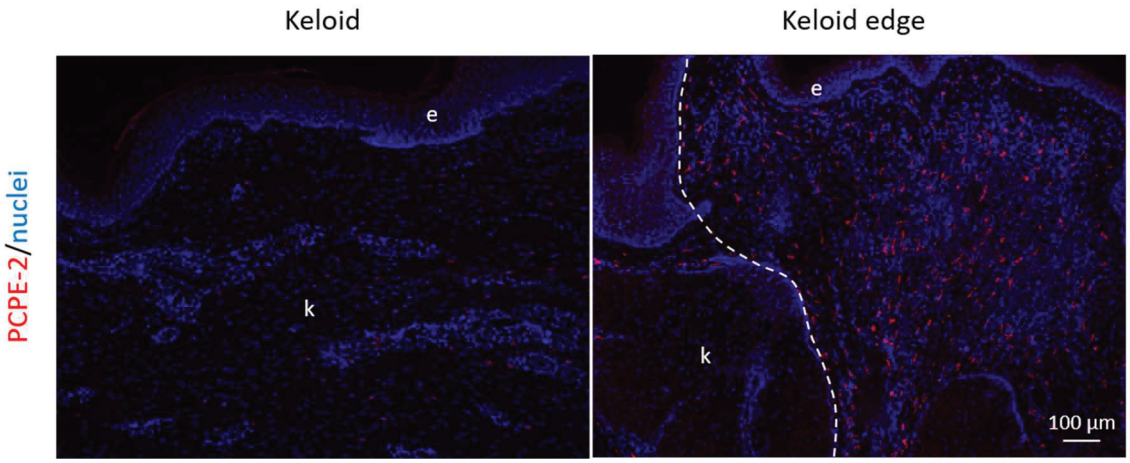

Figure 38: PCPE-2 expression in the keloid mass and at the keloid edges.
Immunostaining of PCPE-2 in sections of paraffin-embedded keloid using a rabbit polyclonal anti-PCPE-2 antibody (GTX103410, 1:100; n = 3). PCPE-2 expression in keloids was studied more carefully with particular attention on keloid edges. Indeed, whereas PCPE-2 was not found to be expressed into the keloid mass, it seemed to be highly expressed around keloids. *e, epidermis; k, keloid mass.*

All these results highlighted a differential expression of BTPs, PCPE-1 and PCPE-2 within the skin. BMP-1 and PCPE-1 were mainly found in the dermis and appeared to be highly abundant during the proliferation phase of wound healing. In contrast, PCPE-2 seemed to be mainly located within the epidermis and appeared in specific cells in the dermis in inflammatory conditions. Thus, we then analysed in more detail the distribution of each protein in different cell types found in the skin.

III. Expression of BTPs and PCPEs in skin cells

1) Keratinocytes and fibroblasts

a. BTPs

As already mentioned, the BTP family consist of four proteases: BMP-1, mTLD, mTLL-1 and -2 that can be differentially expressed within the organism. To determine their cellular distribution in the skin, we looked at their mRNA expression in the two main cell types of the skin, keratinocytes and fibroblasts from mice (***Figure 39A***) and humans (***Figure 39B***). *BMP1* and *mTLD* (*Bmp1* and *mTld* in mice) appeared to be the most expressed BTP isoforms in these dermal cells and were both more expressed in fibroblasts than keratinocytes. *mTll1* was very lowly expressed in normal mouse keratinocytes (NMK) and fibroblasts (NMF) and was undetectable in human cells. Also levels of *mTll2* were undetectable in murine cells and

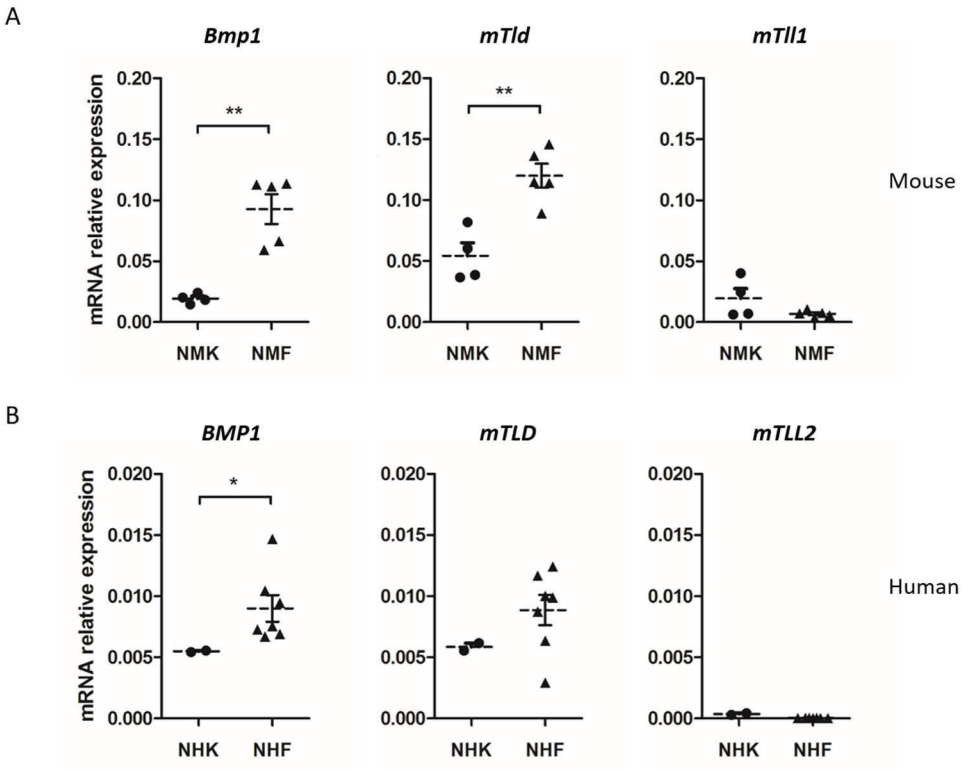

Figure 39: BTP expression in murine and human keratinocytes and fibroblasts

mRNA quantification of *BMP1*, *mTLD* and *mTLL1* or *mTLL2* expression by qRT-PCR in primary keratinocytes and fibroblasts isolated from mouse **(A)** and human skin **(B)**. We found *mTLL1* and *mTLL2* to be respectively lowly expressed in mouse and human cells (*mTLL2* was not detected in mouse skin, neither *mTLL1* in human cells). Both *BMP1* and *mTLD* were detected in keratinocytes and fibroblasts with a higher expression in mouse fibroblasts. *BMP-1* was also found to be more expressed in human fibroblasts while no significant difference was observed for *mTLD*. The values are means ± SEM (n = 2-4 for keratinocytes and n = 5-6 for fibroblasts; t-test: *, p-value < 0.05; **, p < 0.01). *NHK, normal human keratinocytes; NHF, normal human fibroblasts; NMK, normal murine keratinocytes; NMF, normal murine fibroblasts.*

relatively low in normal human keratinocytes (NHK) and fibroblasts (NHF). Unfortunately, we were unable to detect BMP-1/mTLD by Western blotting (data not shown) using two different and well-validated antibodies (Arnold et *al.* 2006 and MAB1927). This suggests that although the transcripts were readily detected, the protein level in normal fibroblasts and keratinocytes appears to be low.

b. PCPE-1

PCPE-1 is already known to be mainly expressed by fibroblasts in various organs. We confirmed by qRT-PCR and Western blotting that PCPE-1 is highly expressed by primary fibroblasts isolated from murine skin. Indeed, mRNA levels of *Pcolce*, encoding the PCPE-1 protein, were high in mouse fibroblasts (NMF; ***Figure 40A***). On the contrary, *Pcolce* expression is very low in mouse keratinocytes (NMK) and is about 100-fold lower than in fibroblasts. By Western blotting, the PCPE-1 protein was detected in the conditioned medium (***Figure 40B***, right panel) and the cell/matrix lysate (left panel) of fibroblasts, but not in keratinocytes. Thus, these results confirmed that PCPE-1 is mainly found in mouse fibroblasts and is not expressed or at a very low level by mouse keratinocytes. Then, PCPE-1 expression was analysed in primary keratinocytes and fibroblasts isolated from human skin. Again, human fibroblasts (NHF) exhibited high levels of *PCOLCE* mRNA while human keratinocytes (NHK) did not (***Figure 41A***). This was also true at the protein level as shown by Western blotting (***Figure 41B***).

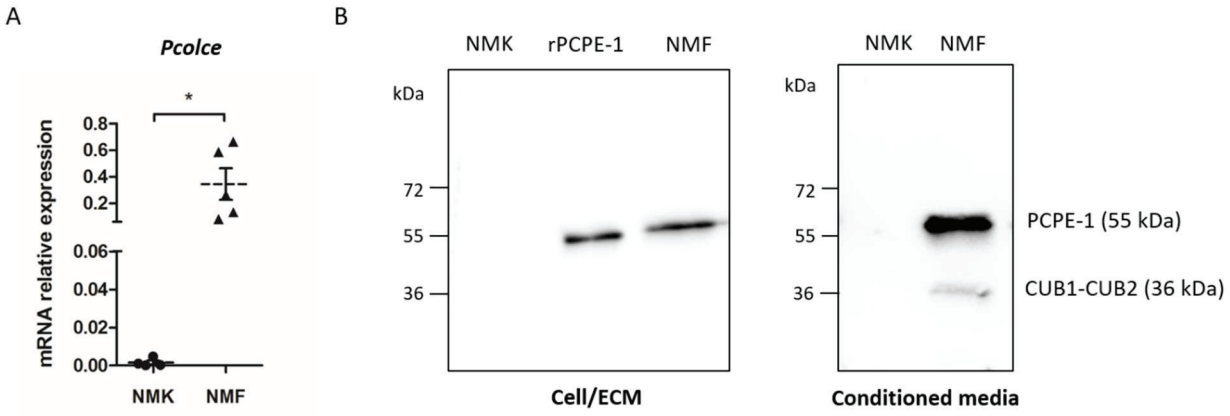

Figure 40: PCPE-1 expression in mouse keratinocytes and fibroblasts

(A) mRNA relative quantification of mouse *Pcolce* by qRT-PCR from primary keratinocytes and fibroblasts isolated from mouse skin. The values are means ± SEM (n = 4 for keratinocytes and n = 5 for fibroblasts; t-test: *, p-value < 0.05). **(B)** PCPE-1 detection by Western blotting (anti-mouse PCPE-1 antibody, R&D, AF2239) on cell/matrix lysates or conditioned media of mouse keratinocytes and fibroblasts cultured for 48 hours in serum-free medium (n = 3; 10% acrylamide gel, reducing conditions). Conditioned media were precipitated using ammonium sulfate while cells and extracellular matrix were lysed together in Np-40 buffer (see chapter 2). We found PCPE-1 to be highly expressed by skin fibroblasts, and not detected in keratinocytes. PCPE-1 protein is detected in both the cell/ECM lysate and the conditioned medium of fibroblasts. *rPCPE-1, recombinant PCPE-1.*

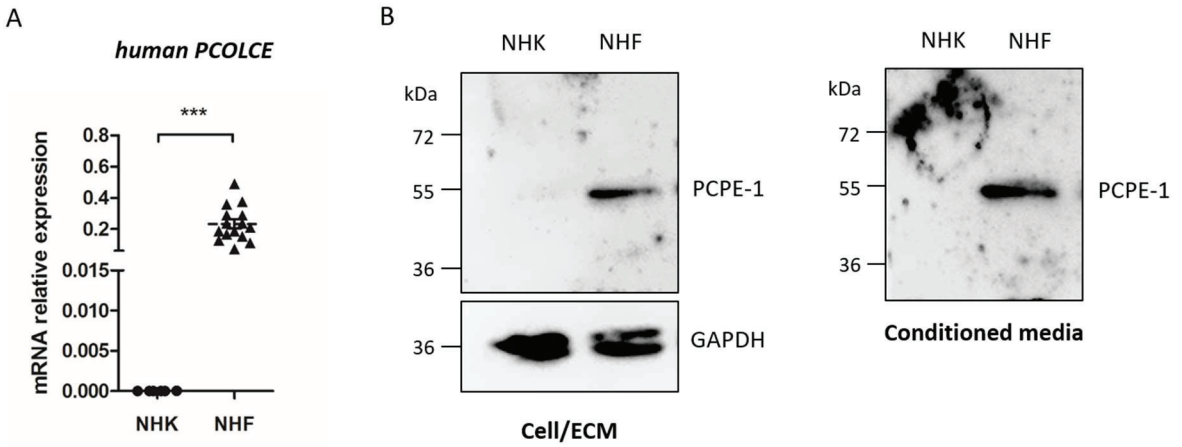

Figure 41: PCPE-1 expression in human keratinocytes and fibroblasts

(A) mRNA relative quantification of human *PCOLCE* by qRT-PCR in primary keratinocytes and fibroblasts isolated from human skin. The values are means ± SEM (n = 6 for each cell type; t-test: ***, p-value < 0.001). **(B)** PCPE-1 detection by Western blotting (anti-human PCPE-1 antibody, Moali et *al.* 2005) in cell/matrix lysates or conditioned media of human keratinocytes and fibroblasts cultured for 48 hours in serum-free medium (n = 6; 12% acrylamide gel, reducing conditions). Conditioned media were precipitated using ammonium sulfate while cells and ECM were lysed in Laemmli buffer (see chapter 2). PCPE-1 protein is abundant in the cell layer and the conditioned medium of skin fibroblasts, not in keratinocytes.

Moreover, we further analysed the localization of PCPE-1 in human fibroblasts by Western blotting. For this purpose, the conditioned medium (CM) was collected and the ECM was extracted alone (ECM) or together with the cells (cell/ECM lysate) using appropriate protocols (see chapter 2, §VI.1.a). In brief, an ammonium hydroxide solution (20 mM NH_4OH) was used to remove the cells and the ECM was collected in Laemmli buffer. As shown in Figure 42, PCPE-1 was mainly present in the conditioned medium, but also found in the cell/ECM lysate. However, PCPE-1 was almost not detected in the ECM alone, suggesting a limited deposition of PCPE-1 in the matrix during cell culture.

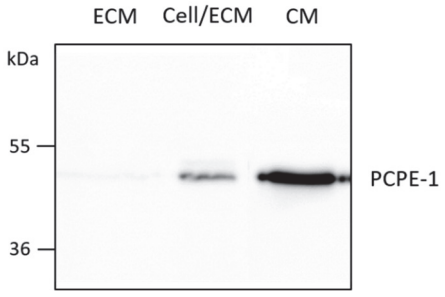

Figure 42: PCPE-1 distribution in human skin fibroblasts

PCPE-1 detection by Western blotting in the ECM, the cell/ECM lysate and the conditioned medium of human fibroblasts using the anti-human PCPE-1 antibody (Moali et *al.* 2005). The ECM was isolated from the cells using a NH_4OH solution (20 mM) and then lysed using Laemmli buffer in reducing conditions, as used for the cell/ECM lysate. Conditioned medium (CM) was collected and directly loaded onto a polyacrylamide gel (40 µL). While PCPE-1 was barely detected in the ECM, the protein was found in high amount in the conditioned medium and to a smaller extent, in the cell/ECM lysate.

c. PCPE-2

While PCPE-1 has been well studied, the expression of PCPE-2 has not been investigated so far in the skin. Firstly, we compared the expression levels of PCPE-1 and PCPE-2 in primary keratinocytes and fibroblasts from mouse and human skin. By qRT-PCR, we showed that *Pcolce2*, the gene encoding the mouse PCPE-2 protein, is significantly more expressed by normal mouse keratinocytes than *Pcolce* (NMK; ***Figure 43A***). However, its expression in mouse fibroblasts is very weak compared to *Pcolce*. Furthermore, the qPCR results were confirmed at the protein level. By Western blotting, we showed that PCPE-2 is highly abundant in mouse keratinocytes in cell/ECM lysates, but is undetectable in mouse fibroblasts (***Figure 43B***), confirming the qPCR analysis. Altogether, these results suggest that PCPE-2 is mainly expressed by keratinocytes while PCPE-1 is expressed by fibroblasts in mouse skin.

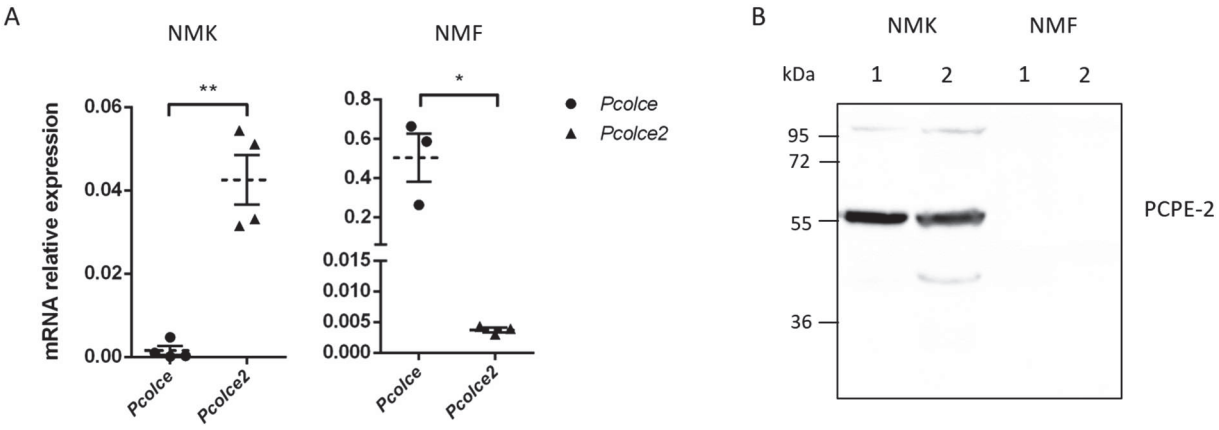

Figure 43: PCPE-2 expression in mouse primary keratinocytes and fibroblasts.

(A) Comparison of the mRNA expression levels of the *Pcolce* and *Pcolce2* genes by qRT-PCR in normal mouse keratinocytes and fibroblasts (NMK and NMF respectively). The qPCR results revealed that *Pcolce2* is significantly more expressed in keratinocytes than *Pcolce* while the latter is mainly detected in fibroblasts. The values are means ± SEM (n = 2 for keratinocytes and 3 for fibroblasts; t-test: *, p-value < 0.05; **, p-value < 0.01). **(B)** PCPE-2 protein detection by Western blotting in cell/ECM lysates (rabbit polyclonal anti-PCPE-2 antibody, GTX103410, n = 2; 12% acrylamide gel, non-reducing conditions) showing a high expression of PCPE-2 in keratinocytes, not in fibroblasts.

Then, we compared the mRNA levels of *PCOLCE* and *PCOLCE2* expression in human keratinocytes and fibroblasts isolated from healthy skin by qRT-PCR (***Figure 44A***). In accordance with mouse cells, the mRNA level of *PCOLCE2* is significantly higher in human keratinocytes than *PCOLCE*, which was almost undetectable. Also, *PCOLCE2* was lower expressed than *PCOLCE* in human fibroblasts. The expression of PCPE-2 in human keratinocytes was confirmed at the protein level by Western blotting (***Figure 44B***). PCPE-2 protein was highly detected in the cell layer of human keratinocytes and not detected in fibroblasts. To further analyse the localization of PCPE-2 in keratinocytes, we assessed its

expression in the conditioned medium, in the cells or in the surrounding ECM. We found PCPE-2 to be mainly expressed in the cell/ECM lysate, as well as in the ECM alone, suggesting that in contrast to PCPE-1, PCPE-2 remains attached to the cells, or interacts with ECM components (***Figure 44C***).

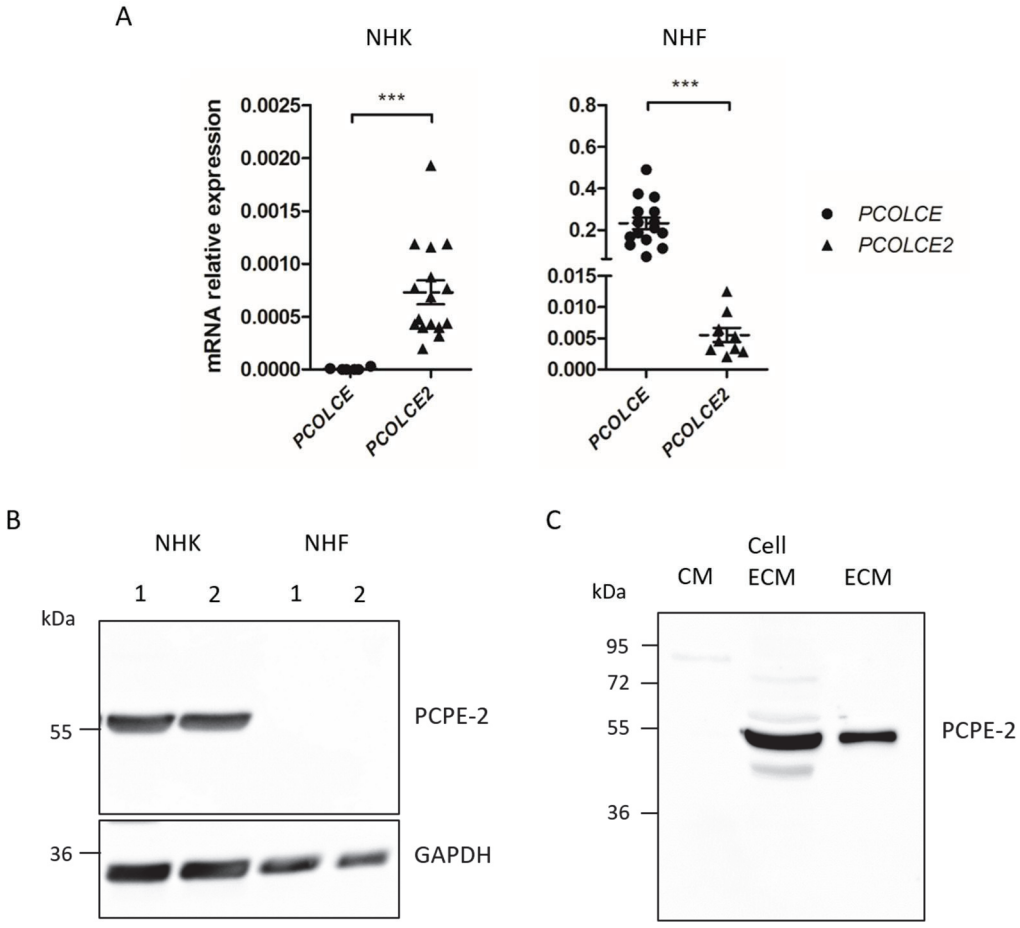

Figure 44: PCPE-2 expression in human primary keratinocytes and fibroblasts

(A) Comparison of the mRNA expression levels of the *PCOLCE* and *PCOLCE2* genes by qRT-PCR in normal human keratinocytes and fibroblasts (NHK and NHF respectively). The mRNA levels of *PCOLCE2* are higher in keratinocytes and lower in fibroblasts than the levels of *PCOLCE*. The values are the means ± SEM (n = 6; t-test: ***, p-value < 0.001). **(B)** PCPE-2 detection by Western blotting (rabbit polyclonal anti-PCPE-2 antibody, GTX103410) in the cell/ECM layers of normal human keratinocytes (NHK; n = 2) and fibroblasts (NHF; n = 4; 12% acrylamide gel, non-reducing conditions). PCPE-2 is well expressed in keratinocytes and is not detected in fibroblasts. **(C)** PCPE-2 detection by Western blotting in the conditioned medium (CM), the cell layer (cell/ECM) and the matrix (ECM) of keratinocytes. PCPE-2 is not detected in the conditioned medium of human keratinocytes but is found attached to the cells and the keratinocyte matrix (15% acrylamide gel, reducing conditions).

Then, we proceeded to investigate whether PCPE-2 was differentially expressed in the layers of human epidermis. A calcium gradient within the epidermis promotes differentiation of keratinocytes. At each stage of differentiation, keratinocytes have different functions and express various markers[7,8]. For instance, basal keratinocytes are proliferative and express keratin 5 and 14, while differentiated keratinocytes do not divide and express specific markers such as keratin 1, loricrin and involucrin.

Toward this end, human primary keratinocytes were cultured and differentiated for 5 days with 1.8 mM of calcium (Ca^{2+}). During the calcium treatment, keratinocytes underwent morphological changes with the development of cell-cell contacts. The microscopic observations were confirmed by qRT-PCR with the upregulation of specific differentiation markers: keratin-1 (*KRT1*), involucrin (*IVL*) and loricrin (*LOR*). The four donors responded differentially to the calcium treatment and the values were very variable with an increase in mRNA expression comprised between 4- and 1000-fold. Thus, it was not possible to pool these data sets and therefore data are shown by pair (two donors per graph). For all cases, we observed an increase in *KRT1*, *IVL* and *LOR* mRNA levels in Ca^{2+}-treated keratinocytes, compared to untreated cells (NT, ***Figure 45A***). Upregulation of the three genes confirmed the correct differentiation of Ca^{2+}-treated keratinocytes. In parallel, we found a decrease in the mRNA expression of *PCOLCE2* in these keratinocytes (fold change of 0.52), suggesting that PCPE-2 might be more expressed in basal keratinocytes than in differentiated corneocytes.

This was then confirmed by immunofluorescence in sections of paraffin-embedded human skin where the strongest PCPE-2 staining was detected in keratinocytes from the basal layer (***Figure 45B***).

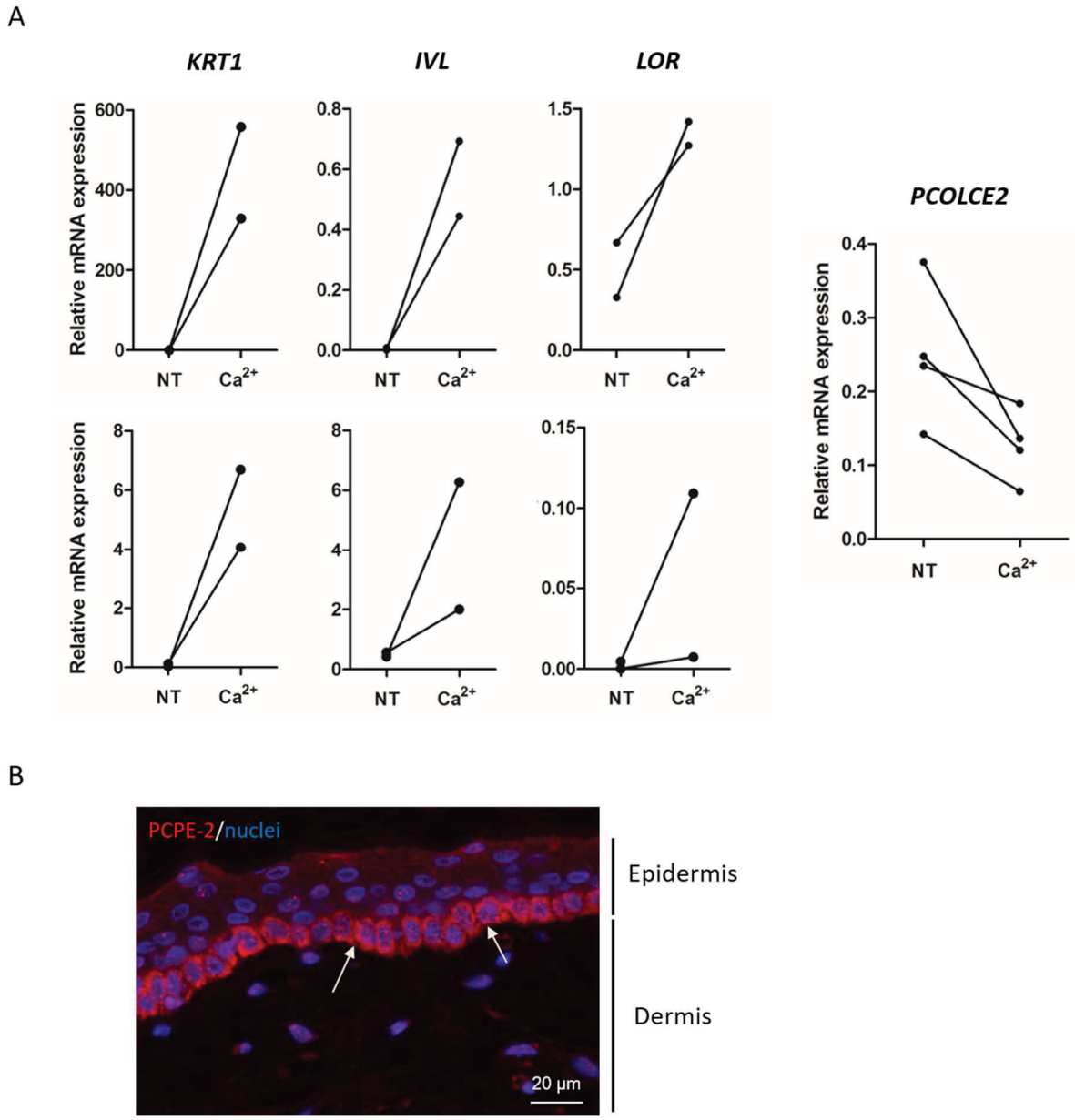

Figure 45: PCPE-2 is mainly expressed in basal keratinocytes

(A) Keratin 1 (*KRT1*), involucrin (*IVL*), loricrin (*LOR*) and *PCOLCE2* mRNA expression in human keratinocytes before or after differentiation with calcium chloride (1.8 mM for 5 days). The connected scatterplot is used to represent paired data (same donor, before and after differentiation). The differentiation markers, *KRT1*, *IVL* and *LOR* were upregulated in Ca^{2+}-treated keratinocytes compared to non-treated keratinocytes (NT) and *PCOLCE2* gene appeared to be downregulated (n = 4). **(B)** Immunostaining of PCPE-2 in paraffin-embedded human skin using a polyclonal rabbit PCPE-2 antibody (GTX103410; n = 3). By immunofluorescence, we observed that PCPE-2 is mainly expressed by basal keratinocytes in the epidermis of human skin.

2) Immune cells

a. PCPE-2 expression in mouse skin

As shown above, PCPE-2 was mainly expressed by keratinocytes in the skin and to a lesser extent by dermal fibroblasts. However, the previous immunostaining of PCPE-2 in mouse wounds displayed specific and punctate labeling in the dermis around the wound area (see §I.2; ***Figure 32***). This staining was stronger during the inflammatory stage of wound healing and seemed to be intracellular. We thus wondered if PCPE-2 could be expressed by other cell types during tissue repair and especially by immune cells that are attracted into the wounds in the first days following injury (from 1 to 5 days after wounding). To answer this question, we analysed co-localization of PCPE-2 with several immune cell markers (F4-80, GR-1 and Ly6G, primarily detecting macrophages, granulocytic cells and neutrophils respectively) in mouse skin by immunostaining (***Figure 46***). A time point where a strong PCPE-2 staining was observed was chosen for the co-localization experiments, i.e. 3 days post-wounding. As observed in Figure 46, in WT mouse skin PCPE-2 did not co-localize with F4-80, which is a common marker used for macrophages (top panel). This result was also confirmed in RDEB mouse skin (right panel).

However, we found PCPE-2 and GR-1 to perfectly co-localize in both WT and RDEB mouse skin, suggesting that PCPE-2 would be expressed by GR-1 positive-cells. The GR-1 marker is a granulocytic marker made of two components, Ly6C and Ly6G. It can be expressed by monocytes, neutrophils and eosinophils. Neutrophils are known to be strongly recruited and involved in the first stage of wound healing and express the Ly6G marker. Therefore, we used Ly6G as a neutrophil marker to determine whether PCPE-2 was expressed by these cells in the wounds. Interestingly, we found a clear co-localization of PCPE-2 and Ly6G in WT and RDEB mouse skin, suggesting that PCPE-2 is expressed by neutrophils.

To confirm these unexpected results, the co-localization experiments were repeated with two other anti-PCPE-2 antibodies (Abcam and Xu et *al.*) raised against different regions of PCPE-2 and similar results were obtained (data not shown). Altogether, these findings suggest that, during wound healing, PCPE-2 can also be expressed by immune cells infiltrating the wound and especially neutrophils in mouse skin. In order to translate these findings in humans, we then performed the co-localization studies in human skin biopsies.

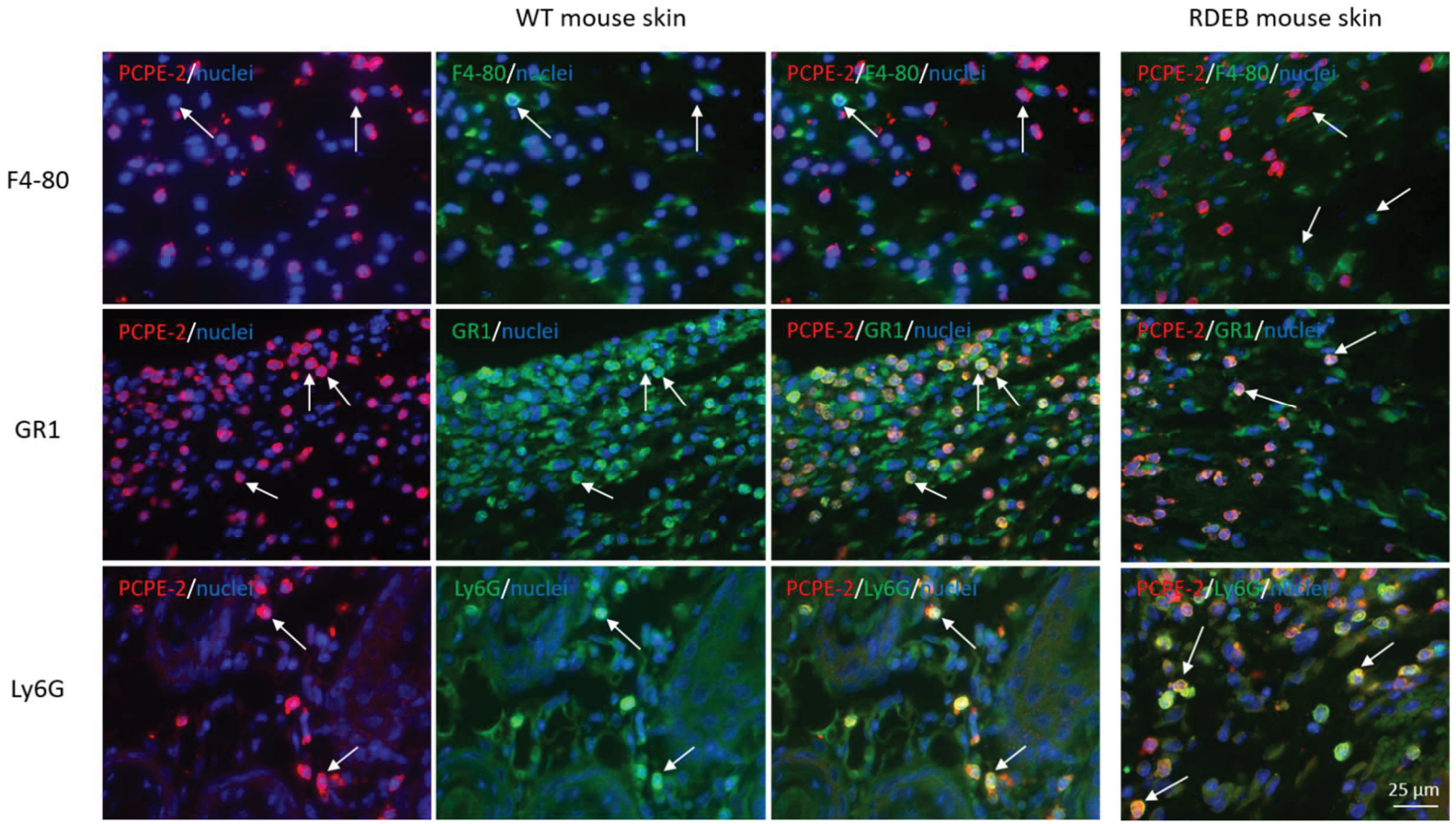

Figure 46: Co-localization of PCPE-2 with inflammatory markers in mouse skin

Immunostaining of PCPE-2 (red) with different inflammatory markers: F4-80, GR1 and Ly6G (green) in WT and RDEB mouse skin (3 days after wounding; representative images of n = 2-3). While PCPE-2 did not co-localize with F4-80, a marker of macrophages, it appeared to be expressed by $GR1^{+}$ and $Ly6G^{+}$ cells, i.e. neutrophils in WT and RDEB mouse skin. Nuclei were stained using DAPI (blue).

b. PCPE-2 expression in human skin

Sections of paraffin-embedded healthy human skin, RDEB skin, hypertrophic scars and keloids were used to stain PCPE-2 with inflammatory markers: CD68 for macrophages and elastase for neutrophils. The same polyclonal anti-PCPE-2 antibodies (GTX, Abcam, and Xu et *al.*) as used in mouse skin were tested in these experiments. Surprisingly, no co-localization of PCPE-2 with elastase was found in human skin (***Figure 47***). However, PCPE-2 appeared to be expressed by CD68-positive macrophages in humans. Thus, mouse and human seem to differ in the immune cell type specific expression of PCPE-2, with PCPE-2 being expressed by neutrophils in wounded mouse skin and macrophages in wounded human skin.

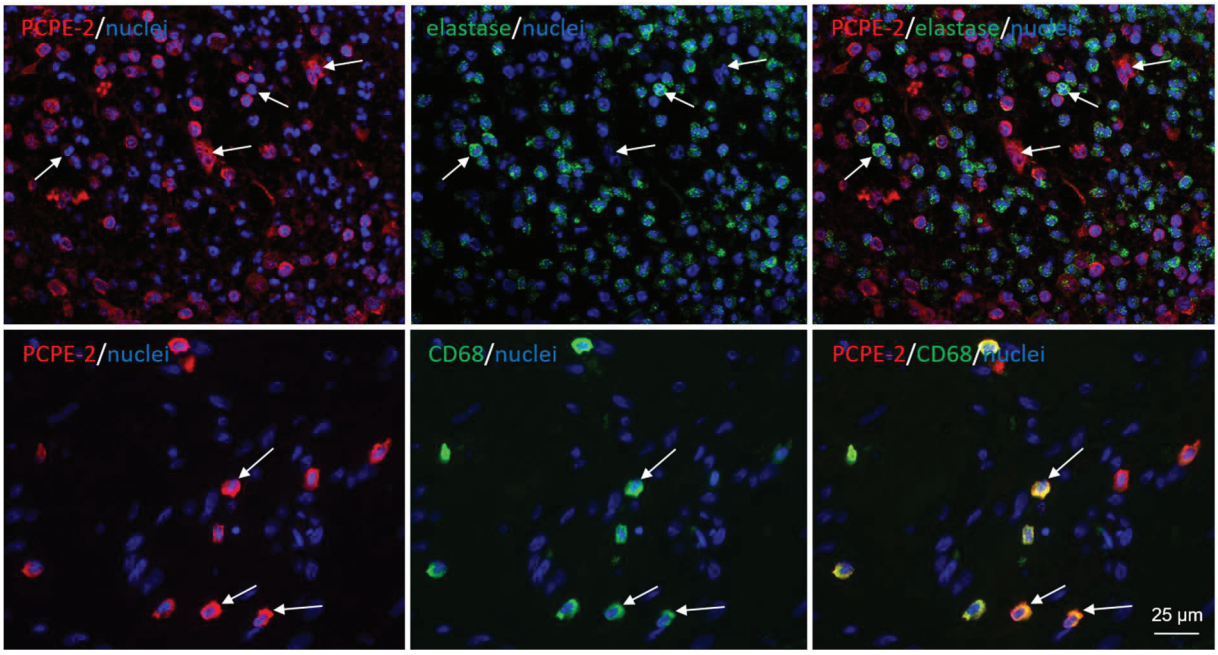

Figure 47: Co-localization of PCPE-2 with inflammatory markers in human skin
Immunostaining of PCPE-2 (red) with different inflammatory markers: elastase and CD68 (green) in human RDEB skin biopsies. PCPE-2 did not co-localize with elastase, a marker of human neutrophils but appeared to be expressed by $CD68^{+}$ cells, i.e. macrophages in humans (representative images of n = 3). Nuclei were stained using DAPI (blue).

c. PCPE-2 expression in cultured monocytes and macrophages

As neutrophils are challenging to culture *in vitro* and PCPE-2 appeared to be rather expressed by macrophages in humans, we cultured human monocytic cell lines in order to confirm the expression of PCPE-2 in these cells. We used the most common cell lines for monocyte studies, THP-1 and U937 cells. These cells are grown in suspension and can be differentiated into macrophages using PMA (phorbol 12-myristate 13-acetate). Once differentiated, morphological changes are easily observable as they become adherent. We

evaluated the expression of the *PCOLCE2* gene by qRT-PCR in monocytes and PMA-induced macrophages. Interestingly, we observed a high expression of PCPE-2 in these two cell types. Moreover, PCPE-2 was significantly increased in PMA-induced macrophages (***Figure 48A***). These results were confirmed by flow cytometry, with 74.3% of the THP-1 cells expressing the PCPE-2 protein (***Figure 48B***). Interestingly, *PCOLCE* was almost undetectable in monocytes and PMA-induced macrophages at the mRNA level; by flow cytometry, only 8.3% of THP-1 cells expressed PCPE-1. These results confirmed the expression of PCPE-2 by two different human macrophage cell lines.

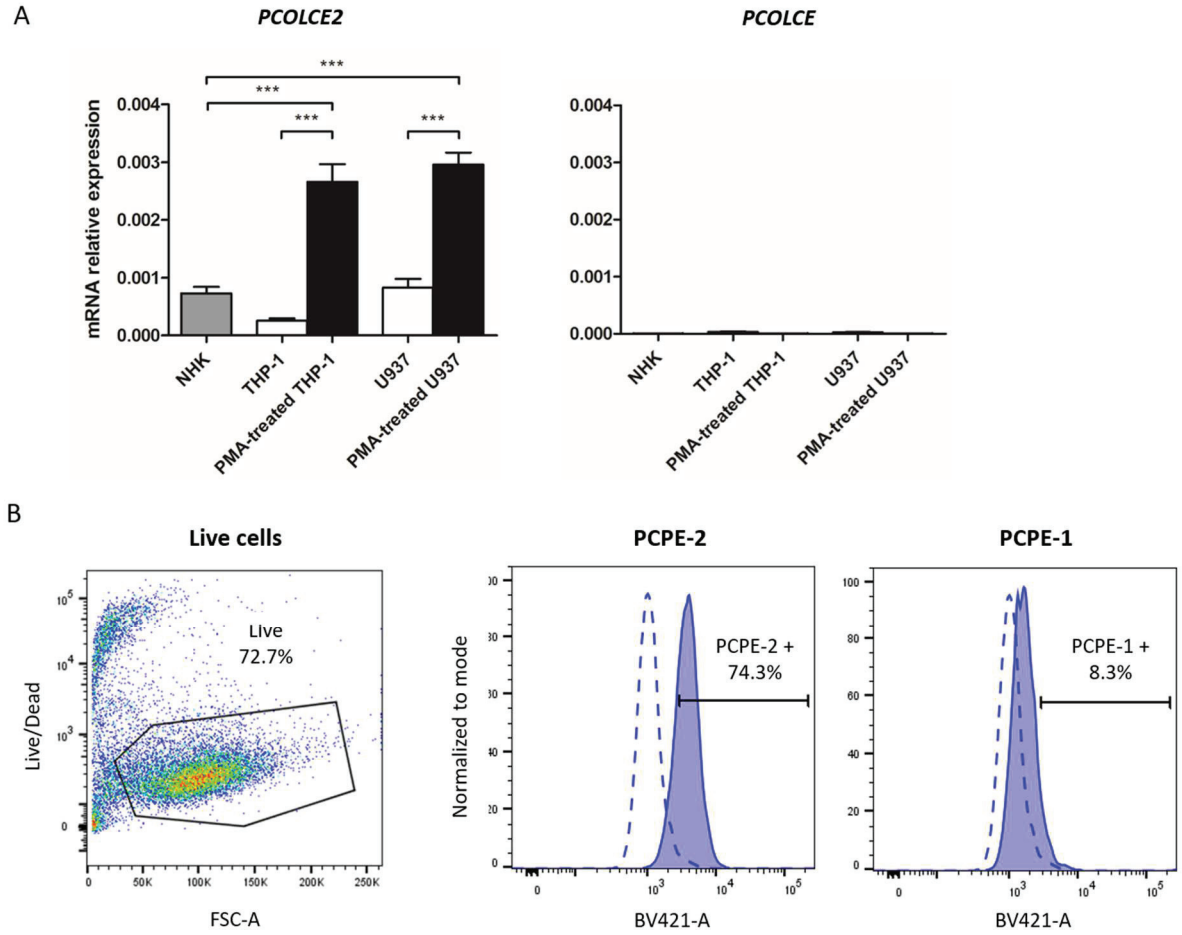

Figure 48: PCPE-2 mRNA and protein expression in THP-1 and U937 monocyte cell lines

(A) mRNA expression of *PCOLCE2* and *PCOLCE* by qRT-PCR in normal human keratinocytes (NHK), THP-1 and U937 monocytes cell lines and PMA-induced macrophages (n = 4; ANOVA test with Tukey post-test: ***, p-value < 0.001). *PCOLCE2* gene is significantly more expressed in macrophage-like cells than in keratinocytes and monocytes, while *PCOLCE* is almost undetectable in these cell types. **(B)** PCPE-2 and PCPE-1 protein expression in THP-1 monocytes by flow cytometry using anti-PCPE-2 (GTX) and PCPE-1 (Moali et *al.* 2005; 1:100) antibodies (representative graphs of n = 2).

Then, we wanted to address the question of whether PCPE-2 was more expressed by inflammatory "M1" macrophages or anti-inflammatory "M2" macrophages, two subpopulations that play different roles in skin. Based on a validated protocol[183], THP-1 monocytes were firstly differentiated into M0 macrophages using PMA for 24 hours. Then, M0 macrophages were incubated with LPS/IFNγ for 24 hours to obtain M1 macrophages or with IL-4/IL-13 for 72 hours for M2 macrophages. M1 polarization was assessed by measuring the mRNA expression levels of classical M1 markers: TNFα and IL1β, which are pro-inflammatory cytokines. A significant increase of *TNFA* and *IL1B* mRNA levels was observed by qRT-PCR in THP-1 cells treated with LPS and IFNγ (***Figure 49***). M2 polarization was evaluated by measuring the expression of M2 markers: MRC1 (*MRC1*) and fibronectin (*FN*). THP-1 cells treated with IL-4 and IL-13 exhibited higher mRNA levels of these two markers by qRT-PCR.

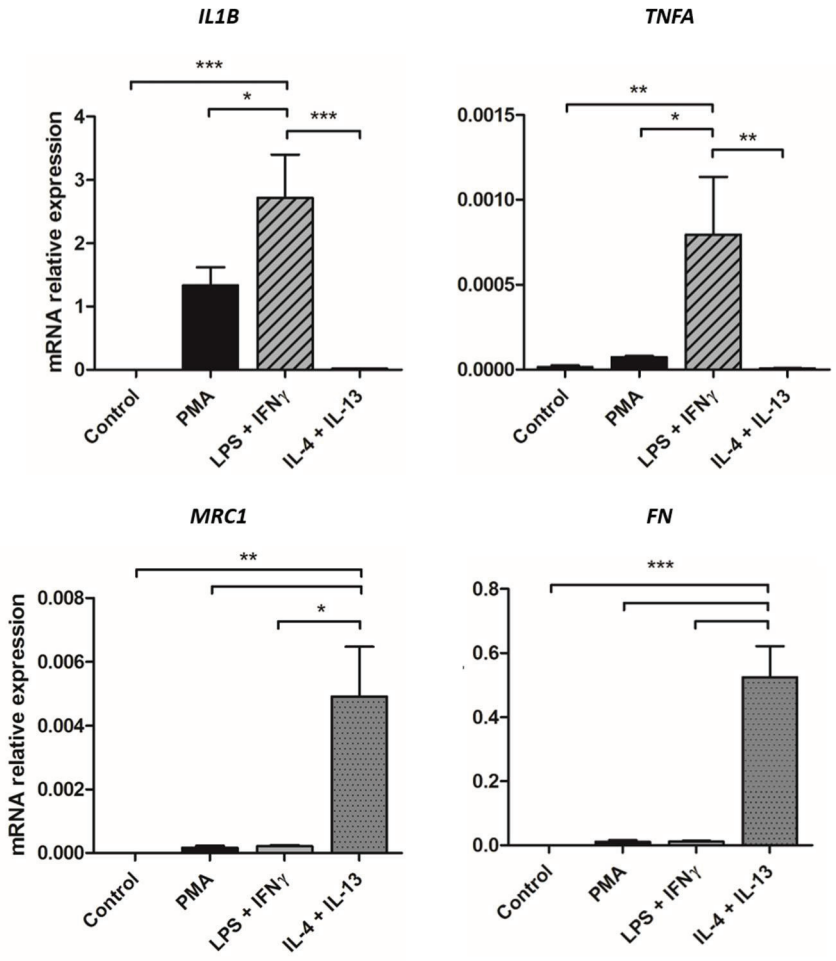

Figure 49: mRNA expression of M1 and M2 markers in polarized THP-1 cells
mRNA expression of *IL1B* and *TNFA* (M1 markers) and *MRC1* and *FN* (fibronectin; M2 markers) by qRT-PCR in THP-1 monocytes (control) or PMA-induced macrophages (PMA) treated with LPS/IFNγ for 24 hours or IL-4/IL-13 for 72 hours (n = 6; ANOVA test with Tukey post-test: *, p-value < 0.05; **, p < 0.01; ***, p < 0.001).

Once the M1 or M2 polarization of THP-1 cells was validated, we evaluated the expression of *PCOLCE2* mRNA in M1 and M2 polarized cells. Interestingly, we found *PCOLCE2* to be significantly more expressed in PMA-induced macrophages (M0) and IL-4/IL-13-treated cells (M2) than in monocytes (control) and LPS/IFNγ-treated cells (M1; ***Figure 50***). These results suggest that PCPE-2 is more expressed by M2 macrophages than M1 macrophages at the mRNA levels, although we could not confirm these data at the protein levels (data not shown). In contrast, *PCOLCE* was almost undetectable in these cells. Moreover, it is important to note that *BMP1* and *mTLD* were also found to be highly expressed in PMA-induced macrophages (M0, M1 and M2) without any difference in mRNA expression levels between the three macrophage subpopulations. *mTLL2* is very lowly expressed in THP-1 cells (no qPCR primers have been validated for mTLL-1 because of its very low expression in the human cells tested).

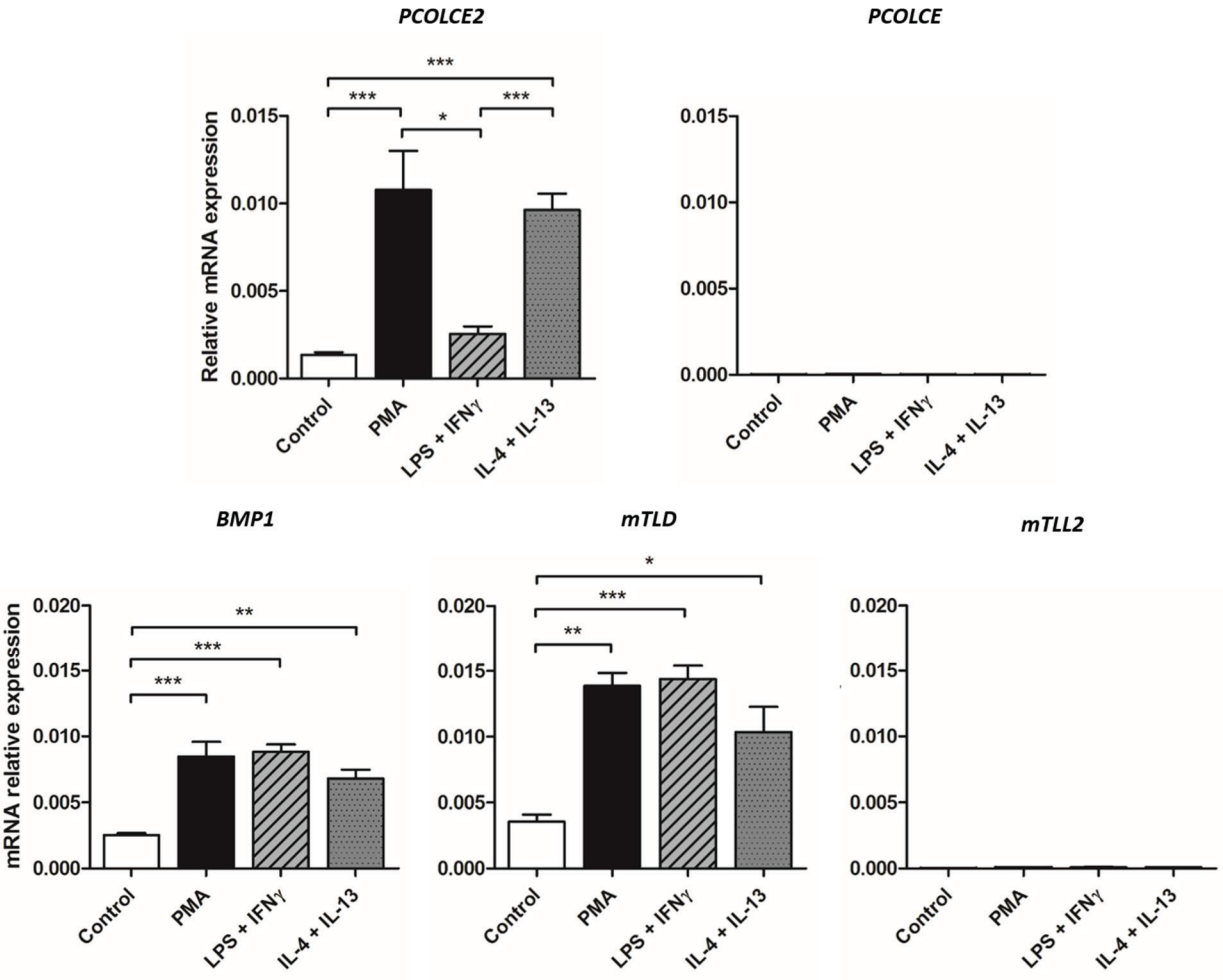

Figure 50: Expression of PCPEs and BTPs in M1 and M2 polarized THP-1 macrophages
mRNA expression of *PCOLCE2, PCOLCE, BMP1, mTLD and mTLL2* in THP-1 monocytes (control), in PMA-induced macrophages (PMA), in M1 (LPS/IFNγ) and M2 macrophages (IL-4/IL-13) by qRT-PCR (n = 3-6 experiments; ANOVA test with Tukey post-test: *, p-value < 0.05, ***, p-value < 0.001).

IV. Discussion

1) BTPs and PCPE-1 are upregulated during the proliferation phase of wound healing

In this chapter, we first studied the expression of BTPs (BMP-1, mTLD, mTLL-1 and -2) and PCPEs (PCPE-1 and -2) in the skin during wound healing using a mouse model. Full-thickness wounds were created on the back skin of the mice and the wound closure was followed over time. In normal mouse skin, BMP-1 and mTLD showed the highest level of expression compared to low mTLL-1 expression and undetectable levels of mTLL-2. After wounding, mRNA and protein levels of BMP-1 and mTLD increased at 7 days, corresponding to the proliferation phase of wound healing while mTLL-1 expression was unchanged.

Correlated to the increase in BMP-1 and mTLD expression, the expression of PCPE-1 was also significantly increased at the mRNA and protein levels 7 days after injury. Previous data from other groups already demonstrated an upregulation of BMP-1 and PCPE-1 when active collagen deposition occurs in tissue, mainly during tissue repair or fibrosis. In line with our wound healing assay, Malecaze et *al.* showed that PCPE-1, together with BMP-1, was upregulated during corneal scarring[136]. The *Bmp1* gene was also found to be upregulated in a mouse myocardial infarction model[122]. Increased levels of circulating mTLD are observed together with excessive collagen accumulation in renal fibrosis[140]; and systemic inhibition of mTLD seems to decrease the progression of the disease in a rat model[188]. Moreover, several studies describe PCPEs as key players in the development of fibrosis in various organs (heart, liver and muscle). Indeed, PCPE-1, which is barely detectable in normal liver, is highly expressed in the liver of rats or mice with carbon tetrachloride (CCl_4)-induced liver fibrosis[189,190]. Plasma concentrations of PCPE-1 correlate with the severity of the disease in mice, opening interesting perspectives to use PCPE-1 as a fibrosis marker. Supporting these data, Ippolito et *al.* recently identified the *Pcolce* gene as the most strongly correlated to toxic liver fibrosis in rats exposed to industrial chemicals (including CCl_4)[191]. Similar observations were found in a mouse model of Duchenne muscular dystrophy: PCPE-1 expression was highly increased in the diaphragms of these *mdx* mice, characterized by an excess of collagen deposition and muscle fibrosis[190]. All these results, together with our data, highlight the close correlation between PCPE-1 abundance and collagen accumulation.

In parallel, the expression of BTPs and PCPE-1 was analysed in the two main cell types of the skin: keratinocytes and dermal fibroblasts. BMP-1 and mTLD appeared to be both expressed in keratinocytes and fibroblasts from mouse and human skin, with a higher mRNA

expression in fibroblasts. These results were not confirmed at the protein level as the detection of these two proteins by Western blotting was really challenging. However, previous results from Lee et *al.* already showed that both keratinocytes and fibroblasts express BTPs and that only fibroblasts express the active form of BMP-1 and mTLD (with keratinocytes expressing only the proform of BTPs)[192]. mTLL-1 and -2 seemed to be expressed to a much lower extent in skin cells, with mTLL-1 detected only in mouse cells and mTLL-2 only in human cells. Thus, BMP-1 and mTLD appeared to be the most expressed BTPs in keratinocytes and dermal fibroblasts. Like BMP-1/mTLD, PCPE-1 is expressed and secreted by mouse and human fibroblasts, which is consistent with its role in fibrillar collagen biosynthesis. In contrast, the *PCOLCE* mRNA was undetectable in mouse and human keratinocytes, which confirms the results from the same previous study of Lee et *al.* where PCPE-1 protein was undetectable in human keratinocytes by Western blotting[192]. Our results show that this is also true for mouse keratinocytes.

Thus, once secreted by fibroblasts, active BTPs and PCPE-1 are likely to participate in collagen deposition during the proliferative and remodelling phases of wound healing. The proliferation phase includes migration and differentiation of fibroblasts, followed by secretion of high amounts of ECM components and especially collagens. The latter are secreted as procollagens that need to be processed to form proper fibrils into the new tissue. This is probably at this stage of the healing process that BTPs and PCPE-1 play a significant role. According to recent results from the Greenspan's group, the loss of BMP-1 in skin leads to reduced thickness of the dermis and delayed wound healing, confirming the importance of BMP-1 for proper healing[135]. The same group also recently showed a decrease in corneal wound healing in *Pcolce* KO mice, deficient in PCPE-1[193]. The mechanism by which PCPE-1 play an important role during wound healing remains unknown and PCPE-1 seems to be involved at different levels. First, PCPE-1 participates in the collagen processing and deposition within the wounds by enhancing the activity of BTPs. Massoudi et *al.* showed a decrease in procollagen processing in corneal fibroblasts isolated from *Pcolce* KO mice, although it was not confirmed *in vivo*. Supporting these data, fibroblasts isolated from HTS and keloids, scars characterized by excessive deposition of type I and III collagens exhibit increased transcriptional expression of PCPE-1 (as well as other enzymes involved in the 4-hydroxylation of procollagen α chain before trimerization and secretion, P4HA and PLOD)[194]. This upregulation of PCPE-1 was confirmed at the protein level in fibroblasts isolated from HTS by mass spectrometry and Western blotting[195].

Beside its role in enhancing procollagen processing, PCPE-1 could have other functions in ECM-rich tissues. Recently, several studies related the involvement of PCPE-1 in angiogenesis. PCPE-1, together with other fibroblast-derived proteins (collagen I, SPARC, IGFBP7 and βig-h3), was reported to participate in lumen formation during endothelial cell sprouting *in vitro*[196]. Later, Salza et *al.* reported that PCPE-1 can bind to the anti-angiogenic factor, endostatin via its NTR domain[164]. They also showed that PCPE-1 can inhibit angiogenesis using an *in vitro* tube formation assay, which is consistent with the recent report of Massoudi et *al.* showing an increase in corneal blood vessel formation in *Pcolce* KO mice[193]. Whether PCPE-1 has direct angiogenic or anti-angiogenic functions still needs to be clarified. PCPE-1 could also indirectly regulate angiogenesis through the regulation of ECM properties and organization. However, this function would remain consistent with its important role during wound healing, as the formation of new blood vessels is a critical step for granulation tissue formation.

Altogether, the close correlation between PCPE-1 expression and procollagen processing and deposition in wounds and fibrotic tissues clearly indicates the importance of PCPE-1 in the development of these tissue repair-derived pathologies. However, little is known about PCPE-2 and our study revealed important potential differences between PCPE-1 and -2 in the skin.

2) PCPE-2 might play a different role during the inflammatory phase

In mouse and human, the expression levels of PCPE-2 were relatively low in fibroblasts compared to PCPE-1. In contrast, PCPE-2 was well expressed in mouse and human keratinocytes and appeared to be more abundant in proliferative keratinocytes in the basal layer of the epidermis. Altogether, these results indicate that keratinocytes, as well as fibroblasts, express PCPE-2 in variable amounts while PCPE-1 is exclusively expressed by fibroblasts. The role played by PCPE-2 in keratinocytes is completely unknown and PCPE-2 might have a function different from enhancing procollagen processing in the epidermis. In agreement with a low expression in fibroblasts, PCPE-2 seemed to be lowly expressed in the dermis of normal skin; however, its expression was induced upon injury and under pathological conditions. Indeed, although the mRNA level of *Pcolce2* was unchanged during wound healing, a strong and punctate staining was observed during the early stages of wound healing, with the highest expression at days 1 and 2 post-injury. These data suggested that PCPE-2 was rather expressed during the inflammatory phase of wound healing while its homologous protein, PCPE-1 was increased during the proliferative phase. Similarly, PCPE-2 which was almost undetectable in human skin was strongly induced in RDEB skin, characterized by delayed wound closure and

excessive inflammation. Further investigations revealed that the cells positive for PCPE-2 during the inflammatory phase were neutrophils in mouse skin. However, macrophages, but not neutrophils, seemed to express PCPE-2 in humans. This could be explained by differences between species; indeed, it is known that the immune system is not identical in mice and humans[40]. Besides, both macrophages and neutrophils have the same myeloid origin.

To confirm these unexpected results, the expression of PCPE-2 was evaluated in two human monocyte cell lines, THP-1 and U937, before and after differentiation into macrophages. In these cellular models, we also found PCPE-2, but not PCPE-1, to be expressed at a higher level in differentiated macrophages. Interestingly, BMP-1 and mTLD were also well expressed in these cells. However, it would be interesting to determine if BTPs are secreted in the extracellular space, if they are present in an active form and what can be their function in these cells. Since recently, there is increasing evidence for a link between inflammation and fibrosis as the inflammatory phase of tissue repair strongly influences tissue remodelling[197–199]. A key component of the innate immunity system is the activation of complement proteins, triggered by interaction with self- or non-self molecules and resulting in the production of inflammatory mediators. The complement system includes defence collagens, C1q and Mannose-Binding Lectin (MBL), and their interacting partners, C1s/C1r and MBL-serine proteases (MASP) respectively, permitting complement activation through different pathways. Recently, the activation of the complement system was shown to be critical for the pathogenesis of pulmonary fibrosis[200]. Consistent with these results, I participated to a study from the groups of N. Thielens, C. Moali and L. Bruckner-Tuderman showing that BTPs can interact with defence collagens C1q and MBL without inhibiting complement activation[201] (Article 1). C1q and MBL are expressed by macrophages in response to tissue injury and promote M2 polarization and secretion of anti-inflammatory cytokines[202]. In this study, we showed that BTPs can interact with C1q and MBL and indeed co-localize with defence collagens *in vivo*, which might serve to resolve inflammation and promote tissue repair in a coordinated manner. This was the first proof of direct interaction between BTPs and defence collagens and, more interestingly, unpublished results from our group also support interaction of C1q and PCPE-1. Whether defence collagens can also bind to PCPE-2 remains unknown and will be investigated. However, these results suggest a link between innate immunity and PCPEs.

Our results also supported the fact that PCPE-2 can be expressed by different human macrophage subsets under certain conditions. Consistent with our results, Finkernagel et *al.* identified the *PCOLCE2* transcript by RNA sequencing, together with *BMP1,* in different macrophage subpopulations (monocyte-derived macrophages, resident peritoneal macrophages

and tumor-associated macrophages (TAMs) isolated from human ovarian carcinoma)[203]. More interestingly, *PCOLCE2* was upregulated with 29 other ECM remodelling genes (including *CO1A1*, *CO1A3*, *CO1A5*, etc.) in TAMs and the protein was well detected by ELISA. Moreover, *PCOLCE2* was also identified in the transcriptome of neutrophils and its expression was increased in neutrophils isolated from children with cystic fibrosis, compared to children with juvenile idiopathic arthritis[204]. These data provide further evidence for an expression of PCPE-2 by different inflammatory subpopulations under pathological conditions.

Although the role of PCPE-2 in immune cells is unknown, it might still be involved in ECM remodelling as macrophages express many ECM components. Initially, macrophages were thought to play only a proteolytic role during tissue repair, but now appear to play a much wider and more complicated role. They express almost all the human collagens, enzymes involved in procollagen processing (including *BMP1*)[205] and other ECM proteins such as fibronectin, syndecans, betaglycan[206] and glypican[207]. They can contribute to wound healing at various levels (wound closure, angiogenesis, granulation tissue formation). Furthermore, macrophages also express various scavenger receptors, including the scavenger receptor class B type I (SR-BI)[208,209]. Recently, M. Sorci-Thomas and colleagues showed that PCPE-2 may enhance SR-BI function by promoting its oligomerization at the cell surface (oral presentation, 51 Annual Scientific Meeting of the European Society for Clinical Investigation, 2017). In the absence of PCPE-2, SR-BI is found as an inactive form in adipocytes and lipid droplet formation is impaired. Interestingly, SR-BI is also expressed by keratinocytes, with a higher expression in the basal layer, and probably plays a role in the barrier function in the skin[210]. This pattern of expression correlates with the expression of PCPE-2 in proliferative keratinocytes and suggests that PCPE-2 could participate in the barrier function by regulating the activity of SR-BI.

At this point, PCPE-1 and PCPE-2 appeared to be expressed by different cell types with a strong expression of PCPE-1 by fibroblasts and a high expression of PCPE-2 by keratinocytes and immune cells, suggesting that these two proteins could have different functions in the skin. The role of PCPE-1 will be further analysed in dermal human fibroblasts, using Western blotting and proteomics, and described in the following chapter. Then, we will try to understand what could be the function(s) of PCPE-2 in keratinocytes and immune cells by *in vitro* and *in vivo* approaches (see chapters 5 and 6).

Chapter 4: Role of PCPE-1 in fibroblasts

I. Introduction

PCPE-1 is mainly expressed by fibroblasts in the skin and in other organs. Once secreted by fibroblasts into the extracellular space, PCPE-1 is supposed to enhance the processing of fibrillar collagens, as it does *in vitro*. Its enhancing effect is therefore likely to contribute to the accumulation of collagens during tissue repair processes, as PCPE-1 is upregulated during corneal and skin wound healing and fibrosis (see chapters 1 and 3). Thus, it would be interesting to understand how PCPE-1 expression is regulated in fibroblasts and whether PCPE-1 can respond to TGFβ, like many ECM proteins, including BTPs, do. TGFβ is known to increase ECM deposition and was previously shown to regulate BMP-1 and mTLD expression without affecting the expression of PCPE-1 in fibrogenic cells (including human dermal fibroblasts)[192]. However, upregulation of PCPE-1 by TGFβ1 has been demonstrated in liver stellate cells (LSCs)[189], smooth muscle cells (SMCs)[211], cardiac and dermal fibroblasts[212,213], which suggests differential effects of TGFβ on various cell types. Thus, the effect of TGFβ on PCPE-1 expression has been assessed in primary human dermal fibroblasts and the results will be described in the first part of this chapter.

Furthermore, we hypothesized that PCPE-1 could be a valuable target to prevent excessive collagen deposition in wound healing pathologies. However, for the development of this approach, it is imperative to understand whether PCPE-1 only functions to enhance procollagen processing or if it also has additional functions during tissue regeneration. Almost 20 years ago, some studies suggested that PCPE-1 could have other cellular functions. Firstly, Masuda et *al.*[214] demonstrated that the inactivation of the *Pcolce* gene in rat embryonic fibroblasts leads to uncontrolled and anchorage-independent cell growth, suggesting that PCPE-1 might play a role in controlling cell growth. Lately, Kanaki et *al.*[211] confirmed this hypothesis by showing a close correlation between PCPE-1 expression and cell quiescence in SMCs. Finally, Matsui and colleagues[215] showed that PCPE-1 might also be involved in protein synthesis by stabilizing RNA strands (through its RNA-binding domains) in hepatic stellate cells. To identify potential additional roles of PCPE-1 in fibroblasts, different strategies were tested to inhibit PCPE-1 expression and determine the consequences of this inhibition at the cellular and protein levels. These results will be described in the next parts of this chapter.

II. Effect of TGFβ on PCPE-1 expression

As previously shown, PCPE-1 is upregulated during the proliferation stage of wound healing (see chapter 3). TGFβ is a key player during the dermal wound healing process, notably by stimulating the differentiation of fibroblasts into myofibroblasts. These cells secrete high amount of ECM components, including collagens, and are responsible for wound contraction and granulation tissue formation during the proliferation phase. Thus, we asked if PCPE-1 could be more expressed in myofibroblasts and looked at the expression of PCPE-1 in response to TGFβ in fibroblasts, as this question is still controversial in the literature. Primary dermal fibroblasts from human donors grown on tissue culture plastic were differentiated into myofibroblasts with 10 ng/mL of TGFβ1 for 72 hours. Firstly, the differentiation of fibroblasts was confirmed by assessing the expression of α-SMA, a marker of myofibroblasts. In response to TGFβ, we observed α-SMA-positive stress fibers in the cytoplasm of fibroblasts by immunofluorescence (***Figure 51A***) and a significant increase in α-SMA expression in the cell layers by Western blotting (***Figure 51B***). Therefore, it was concluded that the differentiation of fibroblasts into myofibroblasts had been successful. Then, PCPE-1 expression was assessed in these cells by qRT-PCR and Western blotting (***Figure 51C***). No change in PCPE-1 expression was observed at the transcriptional and protein levels in response to TGFβ1, suggesting that, in our conditions, *in vitro* generated myofibroblasts do not express higher levels of PCPE-1 than

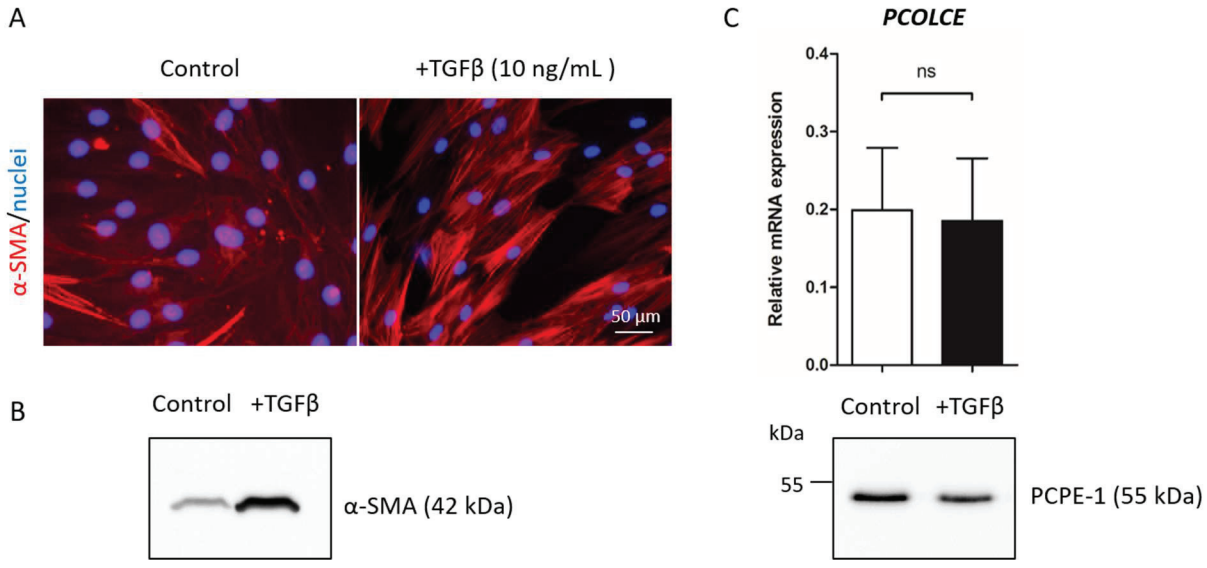

Figure 51: PCPE-1 expression in human dermal fibroblasts and myofibroblasts

(A) Immunostaining of α-smooth muscle actin (α-SMA) in primary human fibroblasts cultured with (+TGFβ) or without TGFβ (control) for 72 hours. **(B)** α-SMA detection by Western blotting in the cell layers. After a TGFβ treatment, an overexpression of α-SMA is observed by immunofluorescence and Western Blotting. **(C)** qRT-PCR and Western blotting showing no change in PCPE-1 mRNA and protein levels in response to TGFβ (n = 3; t-test: *ns, non-significant*).

normal fibroblasts, confirming the previous result from Lee et *al.* that PCPE-1 is not regulated by TGFβ in cultured dermal human fibroblasts.

III. Effects of PCPE-1 inhibition in fibroblasts

1) Inhibition of PCPE-1 and cell growth

PCPE-1 has been suggested to have additional functions than enhancing procollagen maturation, but limited information about them exists. We first decided to assess the importance of PCPE-1 in fibroblasts by evaluating the consequences of PCPE-1 inhibition. To inhibit PCPE-1 expression, the RNA (and protein) synthesis was downregulated using interference RNA strategies. Moreover, antagonist molecules named designed ankyrin repeat proteins (DARPins) and developed in the group of C. Moali in collaboration with the University of Zurich, were tested in parallel to inhibit the procollagen binding abilities of the PCPE-1 protein.

a. Small interfering RNA (siRNA)

The use of small interfering RNAs (siRNAs) directed against *PCOLCE* mRNA was tested as a first strategy to knockdown the gene encoding the PCPE-1 protein in primary human fibroblasts. Four different siRNA sequences were purchased in order to target various regions of the *PCOLCE* mRNA sequence; they were tested in parallel to determine the most efficient siRNA. Primary human fibroblasts were transfected with the siRNAs (numbered 1, 2, 3, or 4) using the HiPerfect transfection reagent (see chapter 2). A control siRNA, designed to not target any known human mRNA sequence, was used as negative control. After 16 hours of transfection, cells were switched in serum-free medium to allow Western blotting analysis of

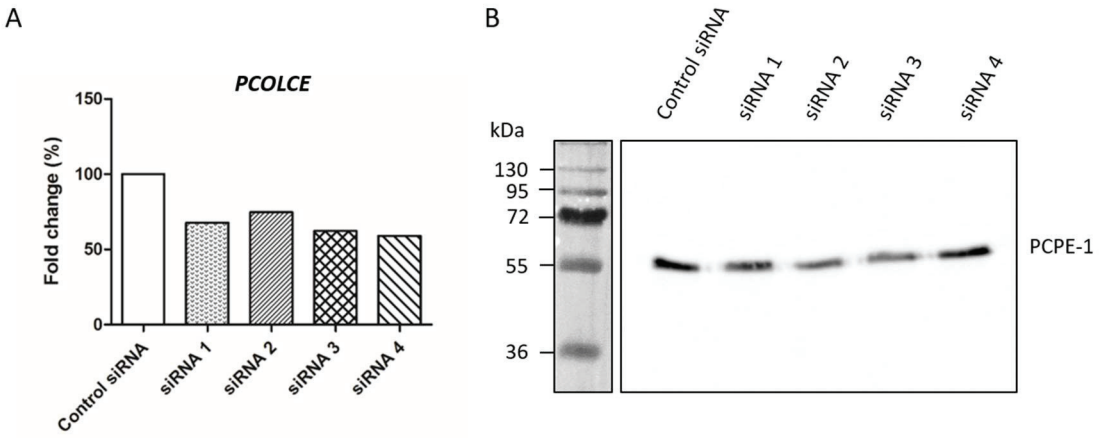

Figure 52: PCPE-1 knockdown in primary fibroblasts using PCPE-1 siRNAs
(A) *PCOLCE* mRNA expression by qRT-PCR in human primary fibroblasts transfected with four different siRNA (1, 2, 3 or 4), or a control siRNA. The values are shown as a percentage of the control siRNA (100%). **(B)** PCPE-1 protein expression detected by Western blotting (n = 3). Both PCPE-1 mRNA and protein were found to be only slightly downregulated (< 40% reduction) with siRNAs.

the conditioned medium. Media were collected 48 hours later and cells were harvested for RNA extraction. Firstly, *PCOLCE* mRNA levels were quantified by qRT-PCR in transfected fibroblasts and compared to cells transfected with the control siRNA. The values are shown as a percentage of the control siRNA (assigned to 100%). *PCOLCE* mRNA is slightly decreased in fibroblasts transfected with *PCOLCE* siRNAs compared to control siRNA (***Figure 52A***). However, the *PCOLCE* siRNA-transfected cells still expressed more than 60% of the basal *PCOLCE* level found in control siRNA-transfected cells. We found similar results at the protein level by Western blotting (***Figure 52B***). The PCPE-1 protein level was decreased after transfection with siRNA, but the inhibition was not sufficient (40% maximum) to observe a significant effect of the absence of PCPE-1 on fibroblasts; therefore another strategy was tested.

b. Short hairpin RNA (shRNA)

As it is well known that primary fibroblasts can be challenging to transfect with siRNAs, a strategy using shRNA sequences was assessed to silence the *PCOLCE* gene. Briefly, several shRNA sequences directed against the *PCOLCE* mRNA (A, B, C and D) were inserted into lentiviral particles and tested in cell culture, together with a non-effective scrambled shRNA used as a negative control. Primary human fibroblasts were infected with these lentiviruses with a multiplicity of infection of 50 and PCPE-1 levels were determined by qRT-PCR (data not shown) and Western blotting (***Figure 53A***). We observed that PCPE-1 expression was significantly reduced after infection with *PCOLCE* shRNA A, B and D whereas PCPE-1 level was similar to control with shRNA C. As the shRNA A and D seemed to be the two most efficient, they were combined to determine if a mixture of two shRNA could improve the inhibition of the *PCOLCE* gene. On the Western blot, the intensity of the band seemed to be weaker when fibroblasts were transduced by *PCOLCE* shRNA A+D, suggesting that combining two shRNAs could be more efficient (***Figure 53B***). Altogether, PCPE-1 silencing was efficient using the shRNA strategy and lentiviral delivery. No change in morphology or cell growth was noticed after shRNA infection and in the absence of PCPE-1 (***Figure 53C***). Thus, our results could not confirm a clear effect of PCPE-1 on fibroblast growth properties as previously reported[211,214]. The C-terminal processing of type I procollagen and the protein synthesis were analysed in shRNA infected-cells and the results will be presented below (see §III.2 and 3).

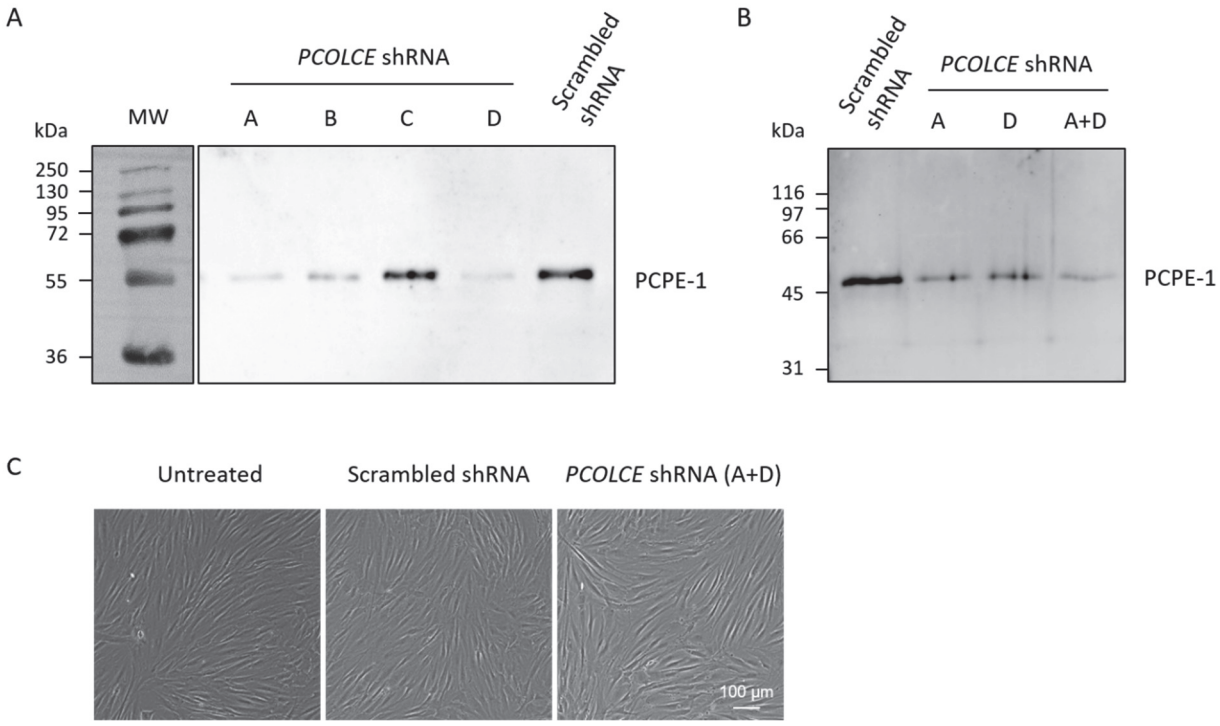

Figure 53: PCPE-1 knockdown in primary human fibroblasts using *PCOLCE* shRNA lentivirus

(A) PCPE-1 detection by Western blotting in the cell conditioned medium of human fibroblasts infected with *PCOLCE* shRNA lentiviral particles (A, B, C and D) or a scrambled shRNA used as a negative control (MOI of 50, 72 hours after infection). The shRNA lentiviruses A and D appeared to be the most efficient in inhibiting PCPE-1, while shRNA C did not have any effects. **(B)** PCPE-1 abundance in fibroblasts infected with a combination of shRNA A and D analysed by Western blotting. The combination of two shRNAs (A and D) seemed to be even more efficient to inhibit PCPE-1 at the protein level. **(C)** Microscopic observation of fibroblasts without shRNA infection (untreated) or after 72h of infection with scrambled or *PCOLCE* shRNA (A and D).

c. DARPins

In parallel, specific antagonists, named DARPins and directed against the human PCPE-1 protein were developed in collaboration with the group of A. Plückthun from the University of Zurich (HighThroughput Binder Selection Facility, Department of Biochemistry). Specific DARPins (DPs) were selected for their ability to interact with the PCPE-1 protein and inhibit its enhancing effect on procollagen processing. To validate these antagonists, two model substrates of procollagen III were used, Mini III and CPIII-long, containing the C-propeptide trimer of procollagen III (CPIII), the C-telopeptide and several triplets of the triple helix (33 and 3 respectively). Mini III and CPIII-long contain the cleavage site of BMP-1 and are efficiently processed by BTPs *in vitro*. PCPE-1 was shown to enhance the cleavage of these two model substrates through a strong and direct interaction, as for the full-length procollagen III[168]. As a negative control, a DP with no PCPE-1 binding property was used. While the control DP did not interact with PCPE-1, DP40 and DP56 were shown to specifically interact with

PCPE-1 and prevent its binding to Mini III by surface plasmon resonance (SPR; performed by Sandrine Vadon-Le Goff, ***Figure 54A***). Moreover, DP40 and DP56, by binding PCPE-1, inhibited its enhancing effect on CPIII-long processing (***Figure 54B***). DP40 or 56 treatment of fibroblasts did not affect their growth (data not shown). Therefore, DARPins efficiently antagonize the enhancing effect of PCPE-1 on collagen maturation *in vitro* without showing cellular toxicity or inhibiting cell proliferation.

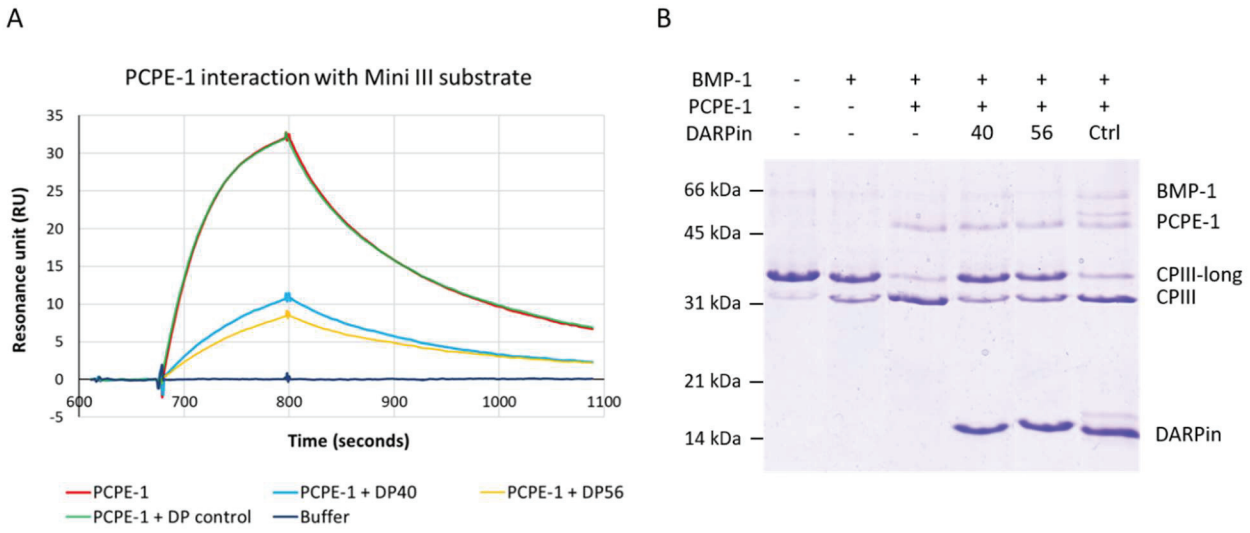

Figure 54: Inhibition of PCPE-1 binding and enhancing effect on procollagen III processing by DARPins (DP40 and DP56)

(A) Surface plasmon resonance experiments showing that DARPins 40 and 56 (DP40 and DP56) can prevent the binding of PCPE-1 to Mini III substrate while control DARPin has no effect on this interaction. 282 resonance units of Mini III were immobilized on a CM5 sensor chip and a mixture of 2.5 nM of PCPE-1 and 25 nM of DARPin were injected in 10 mM HEPES, 0.15M NaCl, 5 mM $CaCl_2$, P20 0.05% (50 µL/min). Association and dissociation of PCPE-1 with the substrate were monitored. The negative control corresponds to the injection of buffer alone (n = 3). **(B)** SDS-PAGE analysis (15% acrylamide gel, reducing conditions) and Coomassie Blue staining. CPIII-long substrate (340 nM) was incubated with BMP-1 (2.6 nM), PCPE-1 (80 nM) and DARPins (DP40, 56 or control; 1.6 µM) for 1h at 37°C (n = 4). DP40 and DP56 inhibit the enhancing activity of CPIII-long processing by PCPE-1.

2) C-terminal processing of type I procollagen

Both shRNA and DARPin strategies were used to inhibit PCPE-1 expression or activity respectively, and evaluate the effects of the absence of PCPE-1 on procollagen processing in cultured human fibroblasts.

Firstly, human skin fibroblasts were transfected with shRNA as previously described (see §III.1.b). *PCOLCE* shRNA transfected fibroblasts exhibit a 70% inhibition of PCPE-1 expression as observed on the Western blot (***Figure 55A***) and its quantification (***Figure 55B***, top panel). Then, the abundance of the procollagen I and the C-propeptide (CPI) was evaluated

using a CPI specific antibody (LF41). By Western blotting, levels of CPI seemed to be slightly decreased when PCPE-1 is downregulated. However, this did not lead to significant differences when the percentage of procollagen processing was quantified by comparing the amount of CPI to the total amount of procollagen I and CPI.

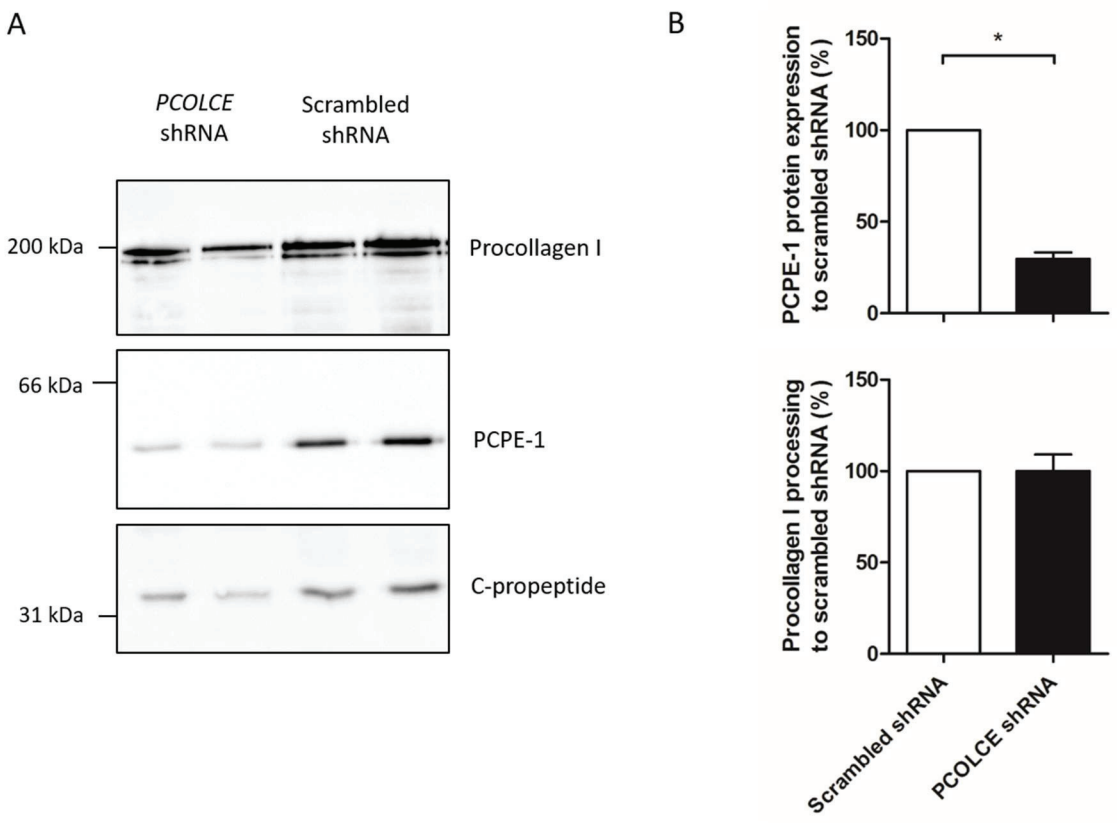

Figure 55: Procollagen I processing in *PCOLCE* knockdown fibroblasts

(A) Protein abundance of PCPE-1, type I procollagen and its C-propeptide by Western blotting (using the anti-PCPE-1 antibody (Moali et *al.* 2005) and the LF41 antibody raised against the C-terminal end of procollagen I) in the conditioned media of fibroblasts transfected with *PCOLCE* or scrambled shRNA (n = 5). **(B)** Quantification of PCPE-1 expression by densitometry using ImageJ (top panel) and calculation of the percentage of procollagen I processing by quantifying CPI amount compared to the total amount of procollagen I and CPI (bottom; t-test: * $p < 0.05$).

Then, we analysed procollagen processing in fibroblasts treated with DARPins, known to efficiently bind PCPE-1 and inhibit its collagen maturation enhancing effect *in vitro* (see §III.1.c) and we observed similar effects to those described with shRNA. In the first setting, human fibroblasts were cultured in the presence of recombinant PCPE-1 protein (5 µg/mL) and DARPins (DP40, 15 µg/mL) for 48 hours. Interestingly, the addition of exogenous PCPE-1 significantly increased the amount of C-propeptide released in the conditioned medium (***Figure 56A***) showing that BMP-1 and mTLD were active in our culture conditions. This enhancement was partially inhibited with the addition of DP40. Thus, DARPins can inhibit the procollagen processing induced by exogenous PCPE-1 in cell culture. In the second setting, procollagen

processing was assessed when DARPins alone were added in the fibroblast medium to evaluate the effects of DARPins on endogenous PCPE-1. However, DP40 and DP56 had no apparent effect on procollagen processing in these conditions. The amount of CPI was similar in all the conditions (***Figure 56B***). These results confirmed, by two different strategies, that the inhibition of endogenous PCPE-1 in cultured cells has little impact on procollagen I processing.

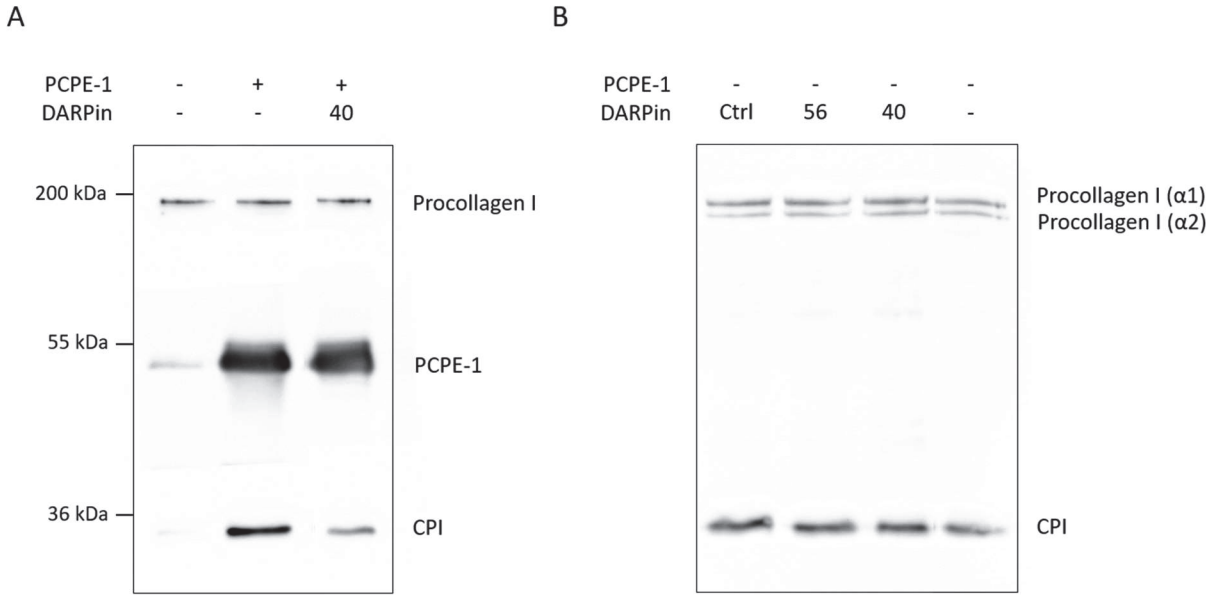

Figure 56: Procollagen I processing in fibroblasts treated with DARPins

(A) Immunodetection of PCPE-1, procollagen I and CPI by Western blotting in fibroblasts incubated with recombinant PCPE-1 protein (3.75 µg/mL) and DP40 (15 µg/mL). Addition of DP40 inhibits the enhancing effect induced by recombinant PCPE-1 on CPI cleavage. **(B)** Immunodetection of type I procollagen and its C-propeptide by Western blotting in fibroblasts incubated with control DP, DP56 or DP40 (15 µg/mL). No difference in procollagen processing was observed in DARPin treated-fibroblasts, compared to untreated fibroblasts.

Finally, to ensure that DARPins were able to access to the PCPE-1 protein in culture conditions, 293-EBNA cells stably expressing the Mini III substrate (293-EBNA-Mini III) were transfected with PCPE-1 or co-transfected with PCPE-1 and BMP-1. Then, these cells were treated with DP40 or control DP for 48 hours. The conditioned medium was then collected and analysed by Western blotting to evaluate the processing of Mini III in the presence of DARPins (***Figure 57***). When PCPE-1 only was overexpressed in 293-EBNA-Mini III, no significant change in Mini III processing was observed, in the presence or the absence of DARPins. However, when both BMP-1 and PCPE-1 were overexpressed, Mini III processing was significantly increased, as observed by the disappearance of the band corresponding to Mini III (40 kDa) and the appearance of the cleavage product, CPIII (30 kDa). Importantly, DP40 clearly prevented Mini III processing, while control DP did not, confirming once again that DP40 can

efficiently inhibit PCPE-1. Altogether, these results highlight that in basal conditions, the effect of PCPE-1 on procollagen processing is weak. When PCPE-1 is present in a higher amount, replicating fibroproliferative conditions, it significantly increases procollagen processing and can be efficiently inhibited using specific DARPins.

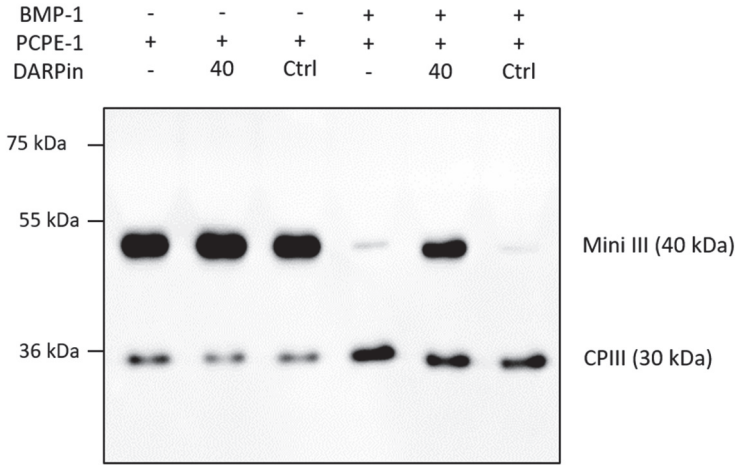

Figure 57: Mini III processing in 293-EBNA cells transfected with BMP-1 and PCPE-1 and treated with DARPins (40 and control)

293-EBNA cells stably expressing the Mini III substrate were transiently transfected with PCPE-1 and BMP-1 plasmids (4 µg of DNA). Cells were then treated with 15 µg/mL of DP40 or control DP for 48 hours to assess their accessibility to PCPE-1 produced by the cells. Mini III processing was then evaluated in the conditioned medium of 293-EBNA cells by Western blotting (12% gel, reducing conditions) using an anti-CPIII antibody (48B14).

3) Protein synthesis

Another potential role described for PCPE-1 is the regulation of protein synthesis. In order to explore this potential function in fibroblasts, we performed protein quantification by proteomics. Mass spectrometry (MS)-based proteomics are a powerful tool commonly used to quantify the abundance of proteins in biological samples[216]. Several methods can be used for the identification and relative quantification of proteins through MS, such as metabolic labelling (SILAC, stable isotope labelling by amino acids in cell culture), enzymatic or chemical labelling (ICAT, isotope-coded affinity tags; isobaric mass tags and others). Isobaric mass tags includes isobaric tags for relative and absolute quantification (iTRAQ) and tandem mass tags (TMT). These tags have identical overall mass and chemical structure but differ by the distribution of heavy isotopes among their structure. They consist of three functional groups: an amine-reactive group (N-hydroxysuccinimide-ester), an isotopic reporter group (N-methylpiperazine in TMT) and a balance group (carbonyl) which normalizes the total mass of the tags (***Figure 58***). These tags are amine-reactive and bind all the free amino groups of proteins and peptides, i.e. N-terminal extremities and lysines; however, labelling does not occur if the amino groups are modified (e.g. acetylation). In our experiments, TMT labelling was used to quantify the composition and abundance of proteins in the conditioned media of *PCOLCE* and scrambled shRNA-transduced fibroblasts.

a. Sample preparation and TMT labelling

Briefly, the conditioned medium of each condition was collected, mixed with protease inhibitors and concentrated by ultracentrifugation (10-kDa cut-off) to reach a sufficient protein concentration for TMT labeling (> 1 mg/mL). Protein concentration was measured using the Bradford assay and was comprised between 1.4 and 1.7 mg/mL. Importantly, the absence of PCPE-1 protein did not seem to affect the total amount of proteins, as protein concentrations of both conditions (scrambled shRNA/*PCOLCE* shRNA) were quite similar.

Once extracted, the proteins were denatured, reduced and alkylated before being digested into peptides by trypsin (***Figure 58***). Isobaric tags comprise a set of isotopic variants with different mass-to-charge ratio (*m/z*, from 126 to 131 for TMT tags). To distinguish the different conditions, peptides of each sample were labelled with a different isotopic variant of the TMT tags (TMT-127 and -129). Equal amounts of labelled samples were pooled before fractionation and clean-up. Then, TMT-labelled samples were simultaneously analysed by liquid chromatography – tandem mass spectrometry (LC-MS/MS) which is the combination of LC with tandem MS[217]. After the first MS, identical peptides belonging to different samples appear

as a single precursor ion. This precursor ion is selected and transferred into a collision cell to be fragmented into characteristic product ions, which allow peptide identification. In addition, the MS2 mode will yield distinct peaks for all the reporter ions (with distinct masses between *m/z* 126 and 131) and their intensities can be used to quantify the relative abundance of peptides in the samples.

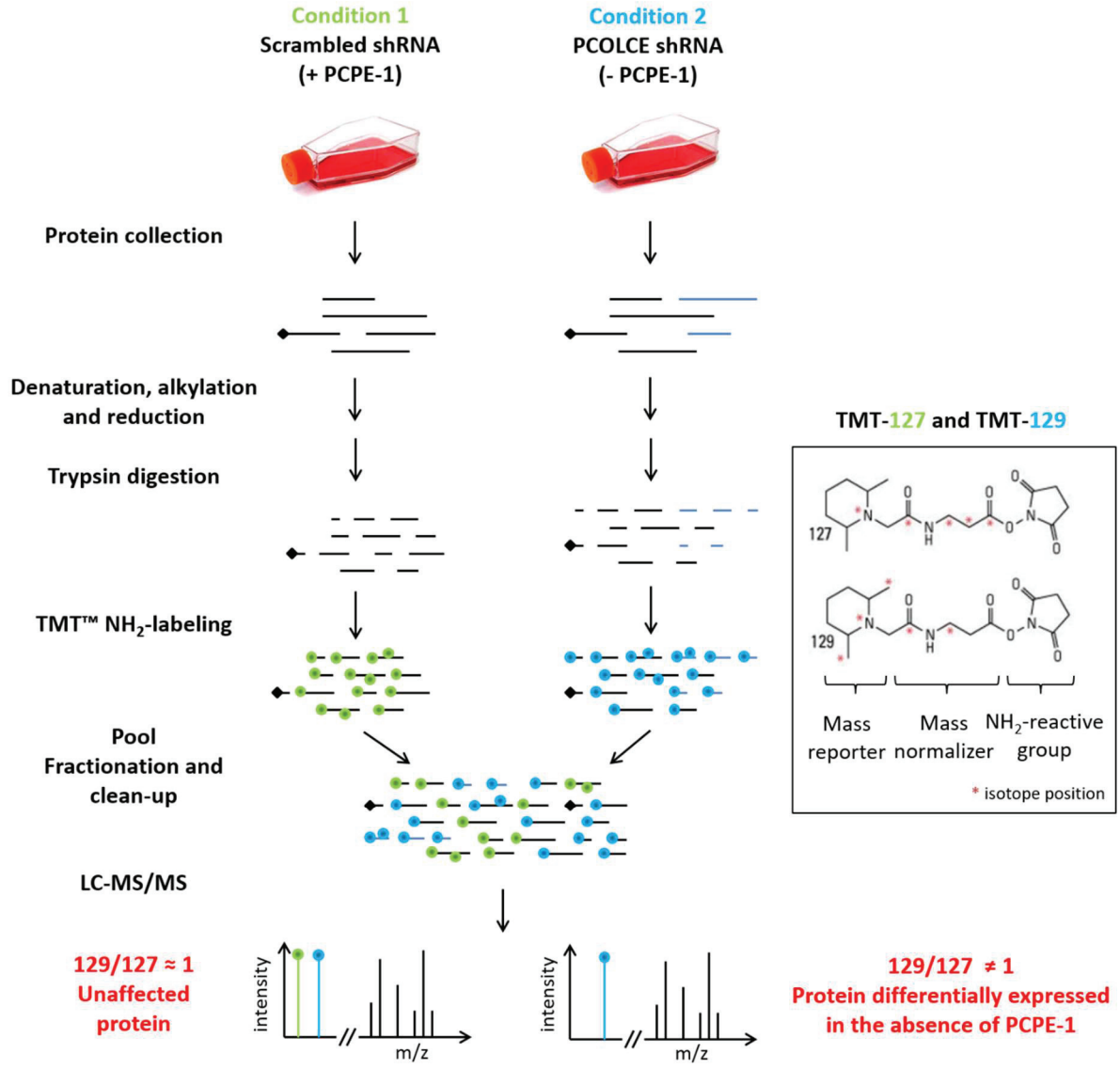

Figure 58: Workflow for TMT™ labeling experiments and LC-/MS-MS analysis
Conditioned media of fibroblasts infected with scrambled shRNA (+PCPE-1) or *PCOLCE* shRNA (-PCPE-1) are collected. After collection, proteins are denaturated, reduced and alkylated before being digested into peptides with trypsin. Then, peptides are labelled with a different TMT reagent, TMT-127 for scrambled shRNA and TMT-129 for *PCOLCE* shRNA (with a *m/z* of 127 and 129 Da respectively). Once mixed, peptides are analysed by LC-MS/MS, identified and quantified to determine if proteins are differentially expressed in the absence of PCPE-1 (n = 1). *TMT, tandem mass tag; LC, liquid chromatography; MS, mass spectrometry; m/z, mass-to-charge ratio.*

b. Protein identification and annotation

MS/MS data were searched against the human Swiss-Prot database using MASCOT allowing the identification of 492 proteins with high confidence (> 95%). Then, the list of proteins was analysed in detail using the Gene Ontology (GO) annotations (cellular location, expression, functions, etc.) to identify the relevant proteins. For our study, among the 492 identified proteins, 358 were associated to the GO terms "extracellular", "secreted" or "membrane", with 265 extracellular proteins (of which 62 can also be found at the cell membrane) and 93 membrane proteins. 19 nuclear proteins were also associated to the GO term "membrane" and were excluded from the list of relevant proteins. The presence of nuclear proteins in the conditioned medium can be explained by cell lysis. Indeed, the cells are infected with lentiviruses that penetrate the cells by endocytosis or membrane fusion; this infection could induce cell mortality. Also, cells are maintained in serum-free medium for 48 hours, which can sometimes lead to cell death and leakage of intracellular proteins. Out of the 358 membrane and extracellular proteins, 129 were associated to the "matrisome" term and can be divided into different categories (***Figure 59***). The matrisome has been defined as "all the proteins that can contribute to matrices in different situations" and contains the core matrisome with collagens, proteoglycans and glycoproteins and the matrisome-associated proteins including secreted factors, ECM-affiliated proteins and ECM regulators[218].

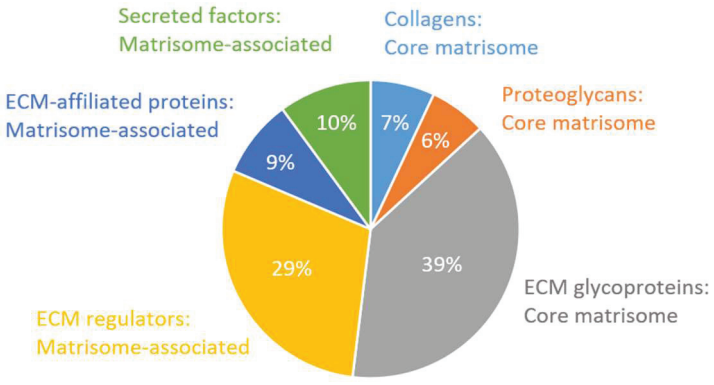

Figure 59: Matrisome annotation (129 proteins out of 358 secreted and membrane proteins)
Pie chart showing the distribution of the matrisome proteins identified in our samples. Among the 358 identified proteins, 129 are classified into the different categories of the matrisome.

Among them, we identified fibrillar collagens (I-III, V) and other collagens (IV, VI, XII, XIV, XV, XVI, XVIII, XXIII), enzymes involved in collagen processing (P3H, PLOD-1 and -3, LOXL2, ADAM-9, -10 and -12, BMP-1, PCPE-1), matrix metalloproteinases (MMP-1, -2 and -3) and their inhibitors (TIMP-1, -2 and -3). Components of the basement membrane such as fibulins and laminins (α2, α4, β1, β2 and γ1 subunits), proteins involved in the TGFβ pathway

(LTBP2, TSP-1) and proteins of the complement system (C1s and C1r, MASP-1) were also identified. All the annotated proteins are listed in the appendix according to their categories (***Appendix 2***).

c. Protein quantification

Once peptides have been identified and assigned to proteins, they can be quantified using the relative intensities of their TMT labels (ratio 129/127). The log_2 (129/127) value (corresponding to *PCOLCE* shRNA/control shRNA) was calculated and values were normalized, using the mean of the normal distribution (***Figure 60***). For this set of data, cut-offs were calculated to select the proteins significantly downregulated (μ-2σ, with μ the mean and σ the standard deviation) or upregulated (μ+2σ; with a p-value < 0.05). Among the relevant identified proteins, 4 proteins were upregulated (log_2 (129/127) >1.54) and 4 were downregulated (< 0.52; ***Table 23***) in PCPE-1-deficient cells.

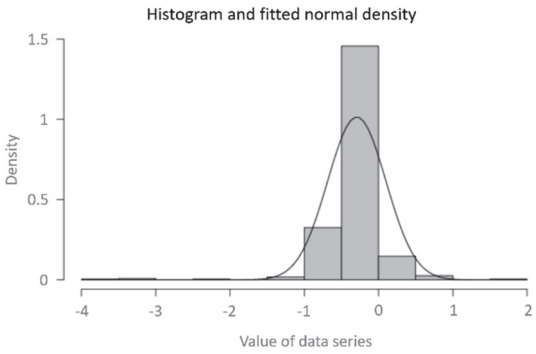

Figure 60: Gaussian distribution of the normalized log_2 (129/127) values

Accession number	Protein	Subcellular location (UniProt and GO annotations)	Log_2 (129/127)	+/-
Q03001	Dystonin (or BP230)	Cytoskeleton, cytosol, ER, extracellular region, nucleus, plasma membrane, etc.	1.78	+
P06703	S100-A6	Cytosol, ER, extracellular region, nucleus, plasma membrane, etc.	1.68	+
Q9NR96	Toll-like receptor 9	Lysosome, endosome, ER, extracellular space	1.63	+
P02647	Apolipoprotein A-I	Extracellular region	1.56	+
Q99584	S100-A13	Extracellular region, cytoplasm	0.49	-
Q9UBP4	Dickkopf-related protein 3	Extracellular region	0.47	-
P02458	Collagen alpha-1(II) chain	Extracellular region	0.45	-
Q9BXX0	EMILIN-2	Extracellular region	0.18	-

Table 23: Dysregulated proteins in fibroblast secretome in the absence of PCPE-1

Thus, the proteins found to be significantly upregulated in the absence of PCPE-1 are dystonin, the S100-A6 protein, the toll-like receptor 9 (TLR9) and the apolipoprotein A-I (ApoAI). Dystonin is a cytoskeletal linker protein and acts as an integrator of intermediate

filaments, actin and microtubule cytoskeleton networks[219]. The S100-A6 protein is a calcium sensor and modulator involved in the regulation of cellular functions[220]. TLR9 is a key component of the innate and adaptive immunity and is expressed by different cell populations in the skin, including fibroblasts[221]. Finally, ApoAI is the major component of HDL and mediates the reverse transport of cholesterol in adipocytes[222].

Among the downregulated proteins, we found the S100-A13 protein, involved in protein secretion[223] and angiogenesis[224,225]; dickkopf-related protein 3 (DKK3), an antagonist of the Wnt signalling pathway[226]; and EMILIN-2, a glycoprotein involved in the formation of elastic fibres[227]. Surprisingly, we detected the α1 chain of type II collagen, which is usually expressed by chondrocytes and not by fibroblasts[228]. It is even more surprising that this protein is significantly downregulated in the absence of PCPE-1.

If we go further in the analysis of the protein list, we find PCPE-1 very close to the cut-off (< 0.54) with a $\log_2$ (129/127) value of 0.57 and can be considered as downregulated by proteomics (its downregulation has already been confirmed by Western blotting; ***Figure 53B***). However, the abundance of other proteins known to be involved in the ECM deposition and degradation was not affected. Especially, fibrillar collagens (I, III and V) and other collagens (IV and VI) remain unchanged in the absence of PCPE-1 (***Table 24***). In conclusion, this proteomic experiment suggests that, in the absence of PCPE-1, expression of collagens and ECM-related proteins are not affected. With only 2.2% of dysregulated proteins in PCPE-1-deficient fibroblasts, the global effect of PCPE-1 on protein synthesis observed by Matsui et *al*[215]. was not confirmed by this proteomic approach.

Accession number	Protein	$\log_2$ (129/127)
P02452	Collagen alpha-1(I) chain	0.94
P08123	Collagen alpha-2(I) chain	0.90
P02461	Collagen alpha-1(III) chain	0.94
P02462	Collagen alpha-1(IV) chain	0.92
P20908	Collagen alpha-1(V) chain	0.98
P05997	Collagen alpha-2(V) chain	0.80
P25940	Collagen alpha-3(V) chain	0.85
P12109	Collagen alpha-1(VI) chain	0.96
P12110	Collagen alpha-2(VI) chain	0.83
P12111	Collagen alpha-3(VI) chain	0.90

Table 24: $\log_2$ (129/127) ratio of collagens detected in the secretome of fibroblasts

IV. Discussion

PCPE-1 is the most described and widely expressed protein of the PCPE family. It has been firstly discovered for its enhancing effect on the processing of fibrillar procollagen by BTPs[143,144]. As described in the introduction, PCPE-1 is mainly synthesized in collagen-rich tissues[145,148,152,169] and is involved in many tissue repair processes (bone repair, fibrosis, corneal wound healing, etc.). In the skin, PCPE-1 is mostly expressed in the dermis by fibroblasts and is upregulated during the wound healing process, especially during the proliferative phase when high amount of collagens are deposited (see chapter 3). Thus, we wondered how PCPE-1 was regulated in fibroblasts during tissue repair.

1) Effect of TGFβ on PCPE-1 expression

TGFβ is a key regulator during wound healing and participate, in many ways, to the deposition of a new ECM after injury. These include the inhibition of the production of MMPs and the induction of (i) MMP inhibitors, (ii) structural ECM components (i.e. procollagens, fibronectin, TSP-1) and (iii) LOX[229,230]. To contribute to ECM deposition, TGFβ also regulates the activity and expression of BMP-1 and mTLD in MG-63 osteosarcoma cells[192] and stimulates the secretion of the active form of ADAMTS-2, the main enzyme involved in the removal of the N-propeptide of fibrillar procollagens[231]. Moreover, TGFβ induces the differentiation of fibroblasts into myofibroblasts. Once differentiated, these cells have the ability to secrete higher amounts of ECM components and to contract the wound for a proper healing and tissue repair. In this context, we wondered whether PCPE-1 might be under the control of TGFβ in the skin and be more expressed in α-SMA-positive myofibroblasts than in dermal fibroblasts. However, no significant change in PCPE-1 expression was observed in dermal fibroblasts cultured in the presence of TGFβ1 (10 ng/mL). In these conditions, PCPE-1 expression was not affected by exogenous TGFβ1, while the differentiation of fibroblasts into myofibroblasts was confirmed by an increase in α-SMA expression. This confirmed the previous results from Lee and colleagues, showing that PCPE-1 was not regulated by TGFβ1 in MG-63 and fibrogenic cells (including human dermal fibroblasts)[192]. However, several publications reported the effect of TGFβ1 on PCPE-1 expression in different cell types (1.5-fold increase in the *PCOLCE* mRNA level in rat LSCs[189] and rat SMCs[211], 1.5- and 2-fold increase in the PCPE-1 protein level in human dermal fibroblasts[212] and rat heart fibroblasts[213] respectively). Finally, the group of R. Wordinger showed that TGFβ2, another member of the TGFβ family, decreased the expression of PCPE-1 in human optic nerve head cells (conference paper, ARVO 2015 Annual Meeting). Various cell types, duration of TGFβ treatment (24 or 48

hours) and concentrations (from 1 to 10 ng/mL) were used. All these apparently divergent results suggest that the regulation of PCPE-1 by TGFβ is cell- and tissue-specific and might depend on several factors (cell culture conditions, origin of the cells, etc.). In these conditions, it is difficult to extrapolate what will be the effect of TGFβ on PCPE-1 *in vivo* (e.g. in wound healing conditions). Many factors secreted during tissue repair might act together to stimulate the expression of PCPE-1 and a cellular model cannot mimic the wound environment. However, what is clear from our study is that TGFβ cannot be used to increase PCPE-1 expression in our fibroblast culture model. This could have been useful to screen modulators of PCPE-1 activity.

2) Specificity of PCPE-1 for procollagen processing

Besides its main effect on procollagen processing, other roles have been attributed to PCPE-1 and it is important to better characterize them for potential therapeutic applications. In order to understand the importance of PCPE-1 in human dermal fibroblasts, different strategies were developed to inhibit PCPE-1 expression. The siRNA strategy, which is one of the most frequently used gene silencing method, was not efficient in our case and we could not reach more than 40% inhibition of *PCOLCE* expression. Primary cells are considered challenging to transfect with siRNA and the transfection efficiency is often low. Indeed, they are not easily amenable to lipid-mediated transfection and it is recommend to use lentiviral delivery. In our experiments, we decided to use shRNA-containing lentiviruses to knockdown the *PCOLCE* gene because shRNA are renewable and known to deliver to most cells (including primary cells) while siRNAs are highly degradable. The shRNA strategy was much more efficient allowing a PCPE-1 knockdown of >70% at the protein level. No particular effect of the lentiviral infection, nor the absence of PCPE-1 was observed at the cellular level. The morphology of the cells, as well as the growth rate did not seem to be significantly affected by the absence of PCPE-1, which is in contradiction with the previous observation of Masuda and colleagues[214]. The authors showed that the inactivation of the *PCOLCE* gene using a retrovirus affected the cellular properties of a rat fibroblast cell line (RAT-2). Rat fibroblasts grew in an anchorage-independent manner without contact inhibition. In line with these results, Kanaki et *al.* demonstrated that proliferative rat SMCs showed decreased levels of PCPE-1 and that the expression of PCPE-1 was correlated with the expression of p21, a marker of cell growth inhibition and anti-correlated with proliferation marker (cyclin E) and cell number[211]. Again, these divergent results can reflect differences between rats and humans. Moreover, the studied cells being originated from different tissues (RAT-2 cells from embryos, SMCs from the aorta and NHFs from the skin), tissue-specific regulation of PCPE-1 can also explain such differences.

Following the results of Matsui et *al*. regarding the effect of PCPE-1 on protein synthesis, we also evaluated the total amount of secreted protein in the absence of PCPE-1. However, no difference in the protein synthesis was observed in cells infected with *PCOLCE* shRNA. Especially, we could not confirm the effect of PCPE-1 on collagenous and non-collagenous protein synthesis previously observed in HSCs derived from rat cirrhotic liver[215]. This study proposed that PCPE-1 binds and stabilizes RNA through its RNA-binding domain (NTR domain rich in positive charges). However, no clear demonstration of the relevance of an intracellular role for PCPE-1 was performed and we doubt that a protein containing seven disulfide bridges could be stable in the cell cytosol.

To further rule out the role of PCPE-1 in protein synthesis, we performed proteomic analyses on the conditioned media of fibroblasts in the presence or absence of PCPE-1. This experiment was performed only once but we observed that only very few proteins were dysregulated in the absence of PCPE-1. Among the 8 proteins which seem to be affected by PCPE-1 downregulation (dystonin, TLR9, ApoAI, S100-A6, S10-A13, DKK-3, α1 chain of type II collagen and EMILIN-2), one is a previously described substrate of BMP-1 (ApoAI) and two are extracellular matrix proteins (type II collagen and EMILIN-2). ApoAI, which is upregulated in the absence of PCPE-1, is the major protein component of the HDL. It is secreted as a proprotein and its N-propeptide is cleaved by BMP-1[232]. PCPE-2 was shown to enhance BMP-1 mediated-ApoAI processing *in vitro*[154], but this was not confirmed in other studies[173] and nothing is known about the effect of PCPE-1 on ApoAI expression or maturation. Importantly, none of the fibrillar collagens usually found in dermal fibroblasts were dysregulated in the absence of PCPE-1. However, it was very surprising to find the α1 chain of type II collagen downregulated in these conditions while type II collagen is usually found in chondrocytes and not in fibroblasts[228]. Interestingly, F. Ruggiero and J. Lafont have recently detected type XI collagen, which forms the core fibrillar network in cartilage with collagen II and IX[233], in human dermal fibroblasts and skin (personal communication). Here, the identification of collagen II was done with 11 peptides located all along the α1(II) protein sequence and 10.6% of the protein was covered, suggesting a high degree of confidence in the identification (***Appendix 3***; highlighted letters). Dermal fibroblasts mainly express types I, III and V collagens and are not thought to express type II collagen. One hypothesis could be that fibroblasts acquired a type II collagen secretory phenotype, as recently shown in stromal fibroblasts expressing higher levels of the initiation methionine transfer RNA ($tRNA_i^{Met}$)[234]. $tRNA_i^{Met}$ initiate the translation by directing the scanning ribosome to the start codon (AUG) on the mRNA sequence. In response to $tRNA_i^{Met}$, stromal fibroblasts switch to a chondrocyte-like phenotype and secrete type II collagen. Importantly, the authors of this study also found an

increase in PCPE-1 expression, correlated to the increase in collagen II by proteomics. Here, Western blotting analysis would be useful to confirm our proteomic result. Finally, the most downregulated protein in our proteomic data was EMILIN-2, an elastin microfibril interface-located protein[227]. EMILIN-2 is involved in the formation of elastic fibres and in the processes that regulate vessel assembly. This protein can trigger tumour cell death but also promote neo-angiogenesis. EMILIN-2 was recently shown to modulate the Wnt signalling pathway by interacting with Wnt1[235]. In the skin, EMILIN-2 is targeted to fibrillin microfibrils and is upregulated during wound healing with fibrillins and fibronectin[236]. However, it remains difficult to link EMILIN-2 to PCPE-1 without additional information, except that PCPE-1 was recently found to interact with another member of the elastic fibers, fibulin-4[80].

If confirmed, other dysregulated proteins could link PCPE-1 to the activation of innate immunity (TLR9)[237,238], the adhesion of epithelial cells to their basement membrane (dystonin)[239], cellular functions and secretory processes (S100-A6)[220], angiogenesis (S100-A13)[224,225] and collagen deposition through the Wnt/β-catenin[240] or the TGFβ1/Smad[241] signalling pathways (DKK-3). Nevertheless, our results are clearly too preliminary to draw any solid conclusion on these aspects and the most important point is that the downregulation of PCPE-1 does not affect the general protein synthesis as only eight extracellular proteins were dysregulated in PCPE-1-deficient fibroblasts, with ratios which are close to cut-offs. Moreover, no change in collagen abundance was observed, except for type II collagen. More studies will be required to understand the presence of collagen II in dermal fibroblasts and its downregulation in the absence of PCPE-1.

In this chapter, we showed that PCPE-1 can be efficiently downregulated by shRNAs or DARPins but this leads to a very minor effect on procollagen I processing, suggesting that endogenous levels of PCPE-1 are not required for this function, at least in cell culture. This also suggests that for therapeutic applications, side effects will be limited. Moreover, the loss of PCPE-1 does not seem to affect cell morphology or proliferation, and protein synthesis. Our proteomic data also indicate that the inhibition of PCPE-1 has no impact on the abundance of the major collagens of the skin, type I and III collagens, as well as other ECM-related proteins. These results suggest that PCPE-1 could be a valuable target to prevent procollagen processing in pathologies associated with excessive collagen deposition.

Chapter 5: Functional characterization of the PCPE-2 protein

I. Introduction

PCPE-1 and PCPE-2 were first characterized for their role in the enhancement of the procollagen processing mediated by BTPs. While PCPE-1 has been shown to enhance BTP activity related to the C-terminal processing of types I, II and III procollagens and to the N-terminal processing of type V procollagen, only few studies report the effects of its homologous protein, PCPE-2. Indeed, Steiglitz et *al.* have described that PCPE-2 is capable of enhancing the C-terminal processing of type II procollagen *in vitro*[148]. Lately, its enhancing effect was demonstrated on procollagen I in the conditioned medium of neonatal skin fibroblasts, without any comparison with the effect of PCPE-1[154]. Thus, the objectives of this work were to further understand and characterize the *in vitro* function(s) of PCPE-2. To achieve this, recombinant human PCPE-1 and PCPE-2 were produced in an eukaryotic system (mammalian cells). As PCPEs are secreted proteins, the culture medium of cells overexpressing PCPE-1 or PCPE-2 was collected and purified to isolate the protein of interest. For both PCPE-1 and PCPE-2, two constructs – non-tagged and histidine-tagged proteins – were produced and purified. PCPE-1 or PCPE-2 recombinant proteins were then tested on various BTP substrates to evaluate and compare their efficiency in the presence of recombinant BMP-1.

Among the wide repertoire of BTP substrates, fibrillar collagens are particularly interesting because of their role in skin integrity and wound healing and because they are supposedly the main targets of PCPE-1 and -2. Four different types of procollagens have therefore been tested but our study also include non-collagenous substrates.

II. Purification of recombinant proteins

1) PCPE-1 protein and its tagged-form, PCPE-1-8His

a. PCPE-1

The human PCPE-1 protein was produced in eukaryotic HEK 293-EBNA cells already transfected with a plasmid containing the human PCPE-1 sequence and available in the laboratory of C. Moali. Cells were cultivated for four weeks and the serum-free conditioned medium was collected every two or three days. As described previously by Moali et *al.*[151], PCPE-1 was purified by two steps of affinity chromatography – Affi-Gel blue and heparin – and then by size exclusion chromatography using a Superdex 200 column.

Affi-Gel blue gel provides a simple and efficient first step to remove residual serum proteins such as bovine serum albumin (BSA), which are essential for cell growth. PCPE-1 interacts with the Affi-Gel blue through hydrophobic and ionic interactions. After a wash with 2 M of sodium chloride (NaCl), PCPE-1 was eluted using 50% ethylene glycol. Fractions were analysed using SDS-PAGE under reducing conditions, followed by Coomassie Blue staining (***Figure 61***). The crude fraction (Cr) corresponds to the conditioned medium after the addition of protease inhibitors, pH adjustment and centrifugation. The flow-through (FT) is the fraction that did not bind to the Affi-Blue resin and the wash (W) is the fraction collected after the NaCl wash. Elution fractions, numbered from 1 to 22, were the fractions collected after the addition of ethylene glycol. This first step was efficient to remove many proteins contained in the culture medium, including BSA, and to purify PCPE-1. We obtained a main band corresponding to the PCPE-1 protein after electrophoresis analysis; however, some contaminants were still present in the elution fractions and the protein was not concentrated enough. Thus, the elution fractions (from numbers 12 to 22) were pooled and dialyzed. Because PCPE-1 has high affinity for heparin[147,162], the second step was the concentration and purification of the protein samples on a heparin sepharose column. Bound proteins can be eluted using a NaCl concentration gradient. High amounts of PCPE-1 were obtained between 0.3 M and 0.7 M of NaCl. The fractions containing PCPE-1 (6 to 11) were concentrated using a 10-kDa ultrafiltration device to obtain a smaller volume and a higher protein concentration. Finally, a gel filtration column based on protein separation by size, Superdex 200, was used to separate PCPE-1 from the last contaminants. The purified PCPE-1 protein was very pure, giving a yield of 6.8 mg of protein purified from 1.2 L of medium (i.e. 5.6 mg/L) and stored in 20 mM HEPES, 0.15 M NaCl, 5 mM $CaCl_2$ buffer.

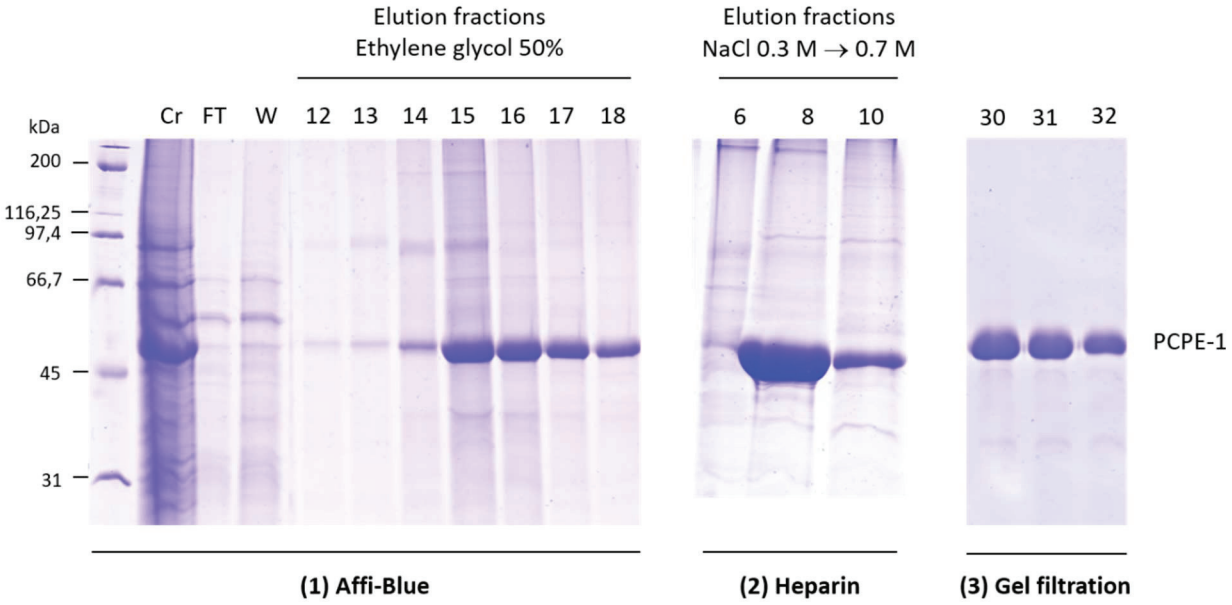

Figure 61: Electrophoresis analysis of each step of PCPE-1 purification (1) Affi-Blue, (2) heparin and (3) gel filtration. Three steps were performed to purify recombinant PCPE-1 protein from HEK 293-EBNA cell-conditioned medium. Elution fractions of the Affi-Gel Blue were collected, analysed by SDS-PAGE (10% acrylamide gel, non-reducing conditions) with Coomassie Blue staining and dialyzed. Then, the fractions were purified on a heparin column (10% acrylamide gel, non-reducing conditions). After concentration of the heparin elution fractions (6 to 11), the latter were injected into a Superdex 200 column to obtain a pure protein (10% acrylamide gel, non-reducing conditions). *Cr, crude sample; FT, flow-through; W, wash.*

b. PCPE-1-8His

For the histidine-tagged PCPE-1 protein, named PCPE-1-8His, the protocol was adapted from Blanc et *al.*[167]. As described previously, the protein was firstly purified on a nickel-charged affinity resin (Ni-NTA), commonly used to purify recombinant proteins with a histidine tag. Bound proteins can be eluted from the resin by competition with imidazole or histidine. In this protocol, PCPE-1-8His was eluted with a buffer containing 250 mM of imidazole. The elution fractions were pure and concentrated enough to be directly injected on a gel filtration column, the Superdex 200 (***Figure 62***). By exclusion chromatography, contaminants and imidazole were removed. From 0.75 L of conditioned medium, 3.1 mg of proteins were purified (i.e. 4.1 mg/L) and stored in 20 mM HEPES, 0.3M NaCl.

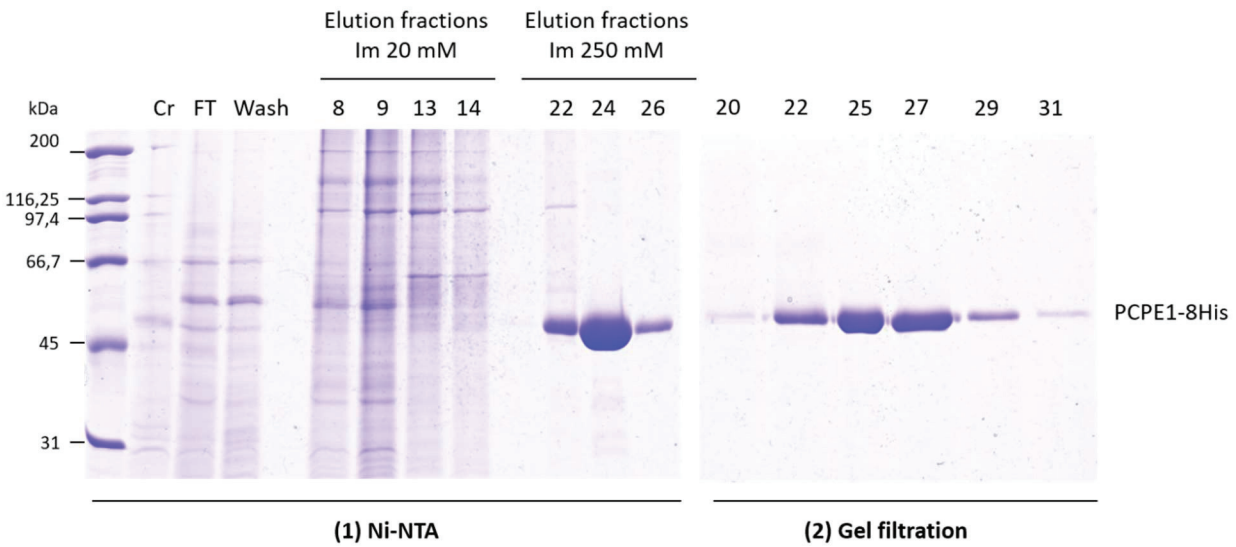

Figure 62: SDS-PAGE analysis of the His-tagged PCPE-1 purification steps (1) Ni-NTA and (2) gel filtration. A nickel-agarose resin (Ni-NTA) was used as a first step for PCPE-1-8His purification, the protein being eluted using 250 mM of imidazole. The peak fractions were then directly injected into a gel filtration column, the Superdex 200, to remove imidazole and residual contaminants from the purified protein. All the fractions were analysed using SDS-PAGE (10% acrylamide gel, non-reducing conditions) followed by Coomassie Blue staining. *Cr, crude sample; FT, flow-through; Im, imidazole.*

2) PCPE-2 proteins: PCPE-2, PCPE-2-8His and 6-His-PCPE-2

For PCPE-2 and the histidine constructs, the initial *PCOLCE2* sequence was not available in the laboratory, in contrast to PCPE-1, which has been intensively studied by Moali and colleagues in the last years. The human *PCOLCE2* sequence was obtained from a commercial pOTB7-PCPE-2 plasmid. Unfortunately, the sequence contained two important mutations (829G>T and 874C>A), the former resulting in the appearance of a stop codon and the latter leading to the replacement of a proline with an asparagine residue. Site-directed mutagenesis was performed to amplify and correct the *PCOLCE2* sequence by PCR before successive cloning into two plasmids (pJET and pCEP4). The final *PCOLCE2* sequence cloned into the pCEP4 plasmid was used to transfect eukaryotic cells.

a. PCPE-2

The human PCPE-2 recombinant protein was produced like PCPE-1, in mammalian cells for three weeks after stable transfection of HEK 293-EBNA cells with the pCEP4 plasmid containing the human *PCOLCE2* sequence. Although relatively low levels of PCPE-2 protein were detected (data not shown), conditioned media were collected every two or three days and purified on a Heparin Sepharose™ 6 Fast Flow column. Like PCPE-1, PCPE-2 can bind heparin with a strong affinity[146,148,152] and be eluted using a NaCl gradient. Two steps of elution were

performed with increasing concentrations of NaCl: the first one with 0.1 M to 0.6 M of NaCl, the second one with 0.6 to 2 M of NaCl. Both elution fractions were analysed on acrylamide gels by SDS-PAGE and Coomassie Blue staining (***Figure 63A***). A protein band was visible at the size of PCPE-2 (around 45 kDa; black arrow) in the first fractions (6 and 7); lower bands, which could be proteolytic forms of the protein were also detected in fractions 6 to 9 (red arrows). In the late fractions (15 and 16), contaminants or proteolytic fragments were observed above 31 kDa (red arrows). By Western blotting, we confirmed that fractions 6, 7 and 8 contained both the intact protein (***Figure 63B***, black arrow) and proteolytic fragments of PCPE-2 (red arrow). However, PCPE-2 was almost undetectable in the other elution fractions.

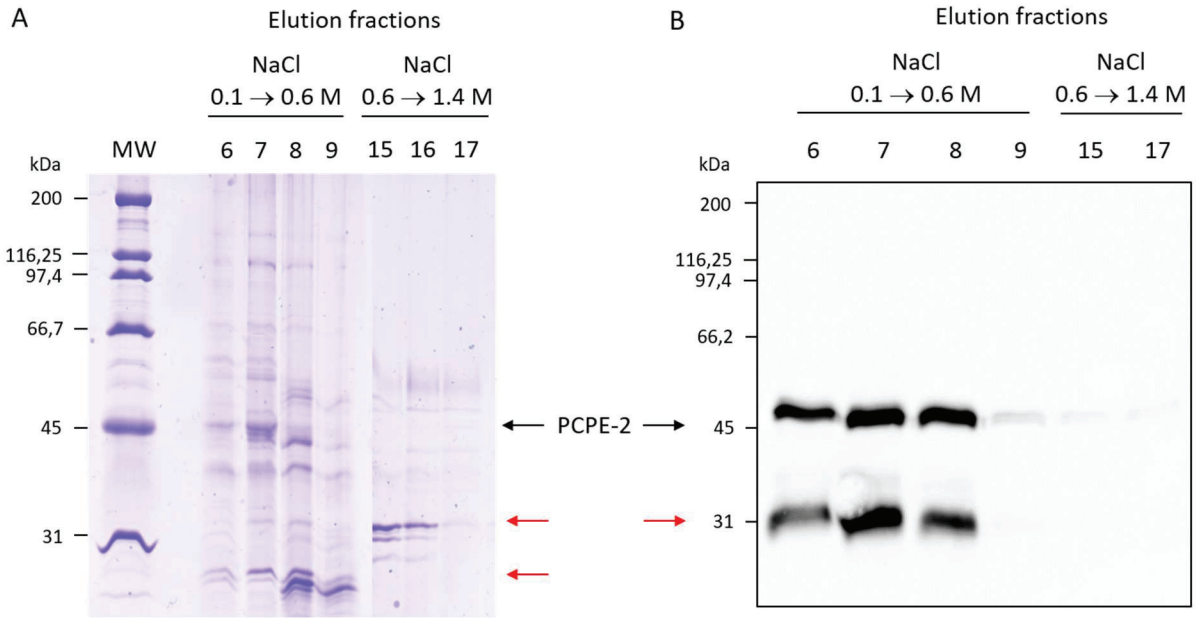

Figure 63: Heparin purification of PCPE-2

A heparin column was used to purify the PCPE-2 protein; two salt gradients were tested in order to elute the protein (0.1 to 0.6 M and 0.6 to 1.4 M of NaCl). SDS-PAGE analysis followed by Coomassie Blue staining (10% acrylamide gel, non-reducing conditions; **A**) and Western blotting analysis (10% acrylamide gel, reducing conditions, anti-PCPE-2 GTX antibody; **B**) of elution fractions.

Thus, the level of expression of the PCPE-2 protein appeared to be much lower than for PCPE-1. Moreover, these results suggested that the PCPE-2 protein was unstable and degraded during the production and/or the purification; we did not go further with this construct and focused on the His-tagged constructs.

b. PCPE-2-8His

The PCPE-2-8His construct corresponds to the PCPE-2 protein with an additional 8-His tag at the C-terminal end of the protein. This plasmid construct was designed in order to facilitate the purification, through the histidine tag. A similar protocol as the one developed for PCPE-1-8His was used for the purification of PCPE-2-8His. The first Ni-NTA purification step was quite efficient to purify the protein (***Figure 64***, (1) Ni-NTA). Then, the elution fractions containing PCPE-2-8His were injected onto a heparin column and the PCPE-2-8His protein was eluted using a salt gradient: 0.5 to 1 M of NaCl (***Figure 64***, (2) heparin). This step did not really improve the purity of the protein – a contaminant was still detectable around 97 kDa in the purified protein – but contributed to the removal of imidazole added in the samples during the nickel-agarose (Ni-NTA) purification step. The protein was then concentrated on a 10 kDa-ultracentrifugation device to reach a final protein concentration of 300 µg/mL. A final step of purification on a Superdex column would have been useful to get rid of this contaminant. However, the protein remained stuck into the column, so we could not use the gel filtration as a final step of purification, as we did for PCPE-1. In total, 1.4 L of medium was purified to obtain 1.65 mg of protein (1.2 mg/L), stored in 20 mM NaH_2PO_4/HEPES, 0.6 M NaCl, with 0.1% of octyl-β-D-glucopyranoside to avoid protein precipitation.

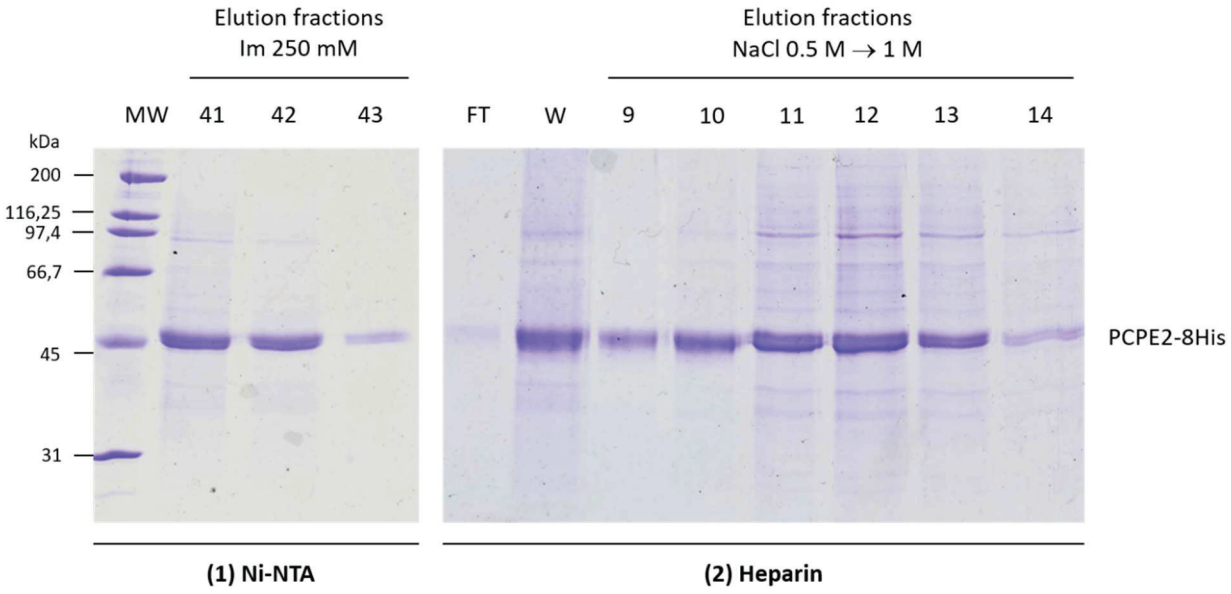

Figure 64 : Nickel-agarose (Ni-NTA) and heparin purification of PCPE-2-8His
Similarly as for PCPE-1-8-His, a nickel-agarose resin (Ni-NTA) was used as the first step of PCPE-2-8His purification. The protein was eluted using 250 mM of imidazole. The elutions fractions were quite pure but contained a high amount of imidazole which was removed by another purification step on a heparin sepharose column. *MW, molecular weight; FT, flow-through; W, wash; Im, imidazole.*

c. 6His-PCPE-2

The 6His-PCPE-2 construct is composed of the human *PCOLCE2* sequence with a 6-histidine tag at the N-terminal end of the protein. It was designed in order to prevent a potential negative effects of the C-terminal tag (in the PCPE-2-8His) on the stability, the conformation or the activity of the protein. After transient transfection and production in HEK 293T cells, the conditioned medium was purified on a heparin column. As observed by SDS-PAGE (***Figure 65***), the high amounts of BSA present in the conditioned medium before the purification (presence of 2% serum in the culture medium) were removed in the flow-through (FT) and the wash (W). Then, two elution gradients of NaCl were performed: the first one – from 0.15 to 0.5 M of NaCl – did not elute the protein but allowed the removal of contaminants, including residual BSA. Then, the 6His-PCPE-2 protein was eluted with NaCl gradient from 0.5 to 0.7 M of NaCl.

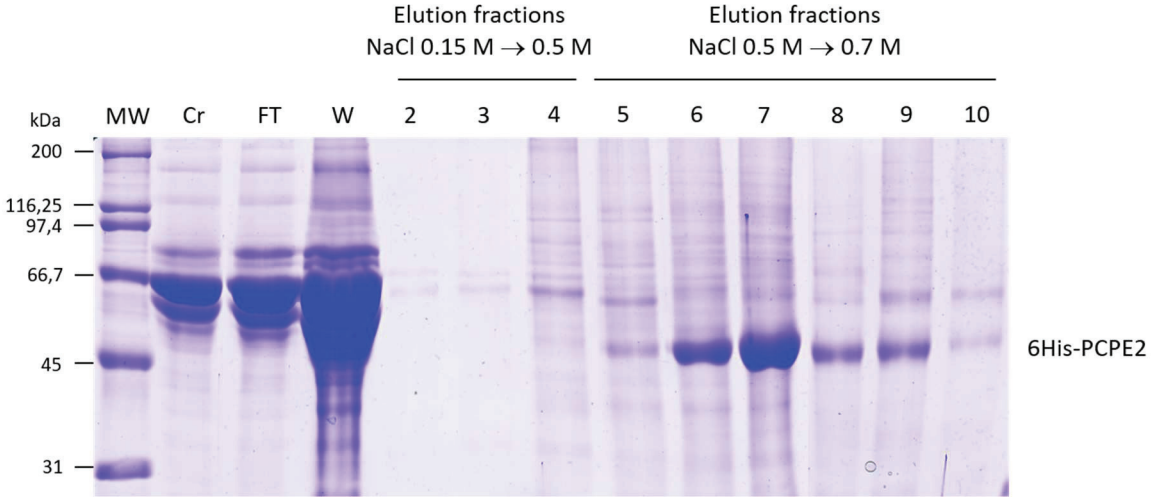

Figure 65 : Heparin purification of 6His-PCPE-2

The first step of purification of 6His-PCPE-2 was performed using a heparin sepharose column. The conditioned media was loaded onto the column and all the proteins with high affinity for heparin, especially PCPE-2 bound to the column. Using a salt gradient, proteins were progressively eluted. For 6His-PCPE-2, a gradient from 0.5 to 0.7 M of NaCl was necessary. The elution fractions containing the protein were selected for the next step. *Cr, crude; FT, flow-through; W, wash.*

The elution fractions containing the 6His-PCPE-2 protein were selected and purified on a nickel-agarose resin (Ni-NTA; ***Figure 66***). Proteins were eluted with an imidazole gradient (from 80 to 200 mM). After these two steps, the 6His-PCPE-2 protein was pure and concentrated enough to be used for the cleavage assays. However, an additional step of affinity chromatography was necessary to remove the imidazole. As the purified protein could not be dialyzed (problem of precipitation), a HiTRAP Heparin HP prepacked column (GE Healthcare) was used and the 6His-PCPE-2 protein was eluted with 0.6 M of NaCl (data not shown).

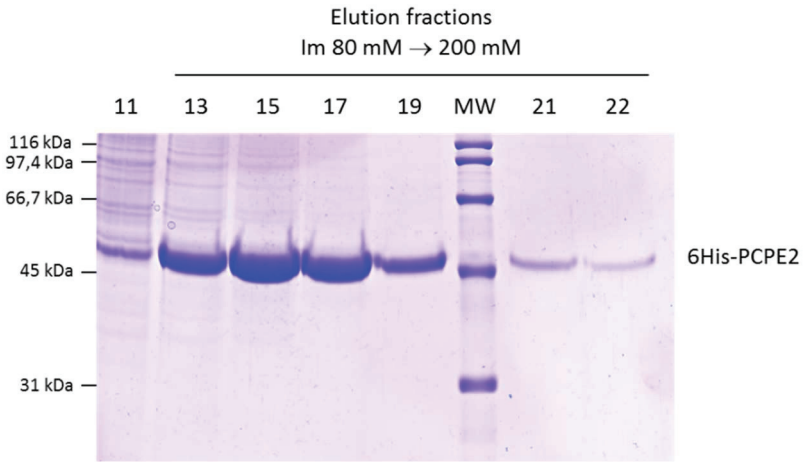

Figure 66 : Nickel-agarose (Ni-NTA) purification of 6His-PCPE-2

The second step of purification was a Nickel-agarose (Ni-NTA) purification to purify the histidine-tagged proteins with high affinity for nickel ions. 6His-PCPE-2 protein was efficiently purified with a gradient of imidazole (from 80 to 200 nM). *MW, molecular weight; Im, imidazole.*

Finally, 750 µg of protein were purified from 500 mL of medium (i.e. 1.5 mg/L) and stored in 20 mM HEPES, 0.6 M NaCl, 5 mM $CaCl_2$, with 0.1% of octyl-β-D-glucopyranoside, high amounts of NaCl and octyl-β-D-glucopyranoside being necessary to avoid precipitation of the protein. After analysis by SDS-PAGE under reducing conditions, the purified protein was very pure and visible around 45 kDa (***Figure 67***). Under non-reducing conditions, some aggregates were visible at the top of the gel (around 200 kDa). A last step of purification on a Superdex column would have been beneficial to get rid of these aggregates. However, as for PCPE-2-8His, the 6His-PCPE-2 protein remained stuck into the column, so we could not use the gel filtration as a final step of purification, as we did for PCPE-1. Thus, the purified 6His-PCPE-2 protein was used as it was for the cleavage assays of BTP substrates in order to characterize its effects *in vitro*.

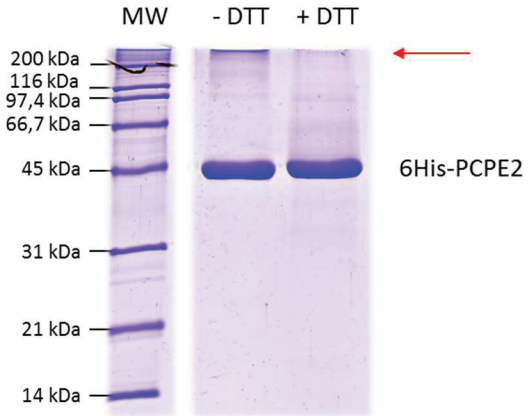

Figure 67: Analysis by SDS-PAGE of the purified 6His-PCPE-2 protein in reducing or non-reducing conditions (+/-DTT)

Seven µg of final protein were analysed by SDS-PAGE after reduction with dithiothreitol (+DTT, 12% acrylamide gel). As expected, the native 6His-PCPE-2 protein appears around 45 kDa. In non-reducing conditions (-DTT), the protein forms some aggregates which are visible as a molecular weight band around 200 kDa (red arrow).

Finally, immunodetection of PCPE-1 was performed on the purified PCPE-2-8His and 6His-PCPE-2 recombinant proteins to ensure that our proteins were not contaminated by residual endogenous PCPE-1, although HEK 293-T cells do not express PCPE-1 (or at very low levels; data not shown). We showed that both PCPE-2-8His and 6His-PCPE-2 proteins did not contain any residual PCPE-1 (***Figure 68***).

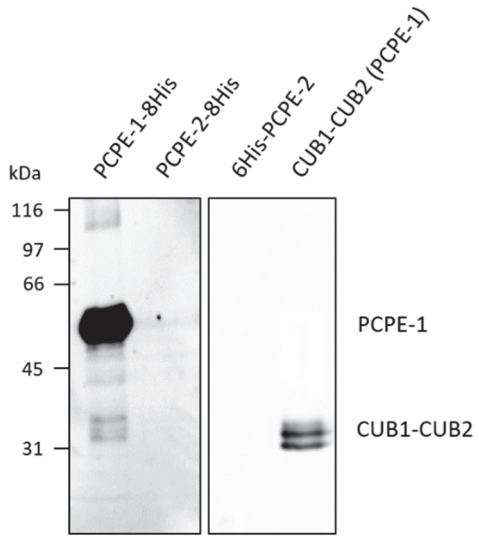

Figure 68: Immunodetection of PCPE-1 in the PCPE-2 recombinant proteins

Detection of PCPE-1 by Western blotting (anti-human PCPE-1, Moali et al. 2005) in the purified recombinant PCPE-2 proteins. PCPE-1-8His and CUB1-CUB2 (from PCPE-1) recombinant proteins were used as positive controls. 30 ng of recombinant PCPE-1 (and CUB1-CUB2) and 200 ng of recombinant PCPE-2 proteins were loaded onto a 10% acrylamide gel and analysed under reducing conditions (n = 1).

III. *In vitro* cleavage assays

To fully characterize PCPE-2, the purified recombinant proteins were tested *in vitro* to determine their ability to enhance the activity of BTPs. The principle of these *in vitro* assays is to incubate the substrate (as a recombinant protein or enriched in cell conditioned medium) at 37°C with the recombinant BMP-1 protease in the presence or absence of the enhancer, PCPE-1 or PCPE-2. Processing of the substrate is analysed either by Coomassie Blue (or SYPRO Ruby) staining, or by Western blotting (see chapter 2). As untagged recombinant PCPE-2 was not successfully purified, only the histidine-tagged forms of PCPE-2 (PCPE-2-8His and 6His-PCPE-2) were used for the *in vitro* assays. In order to have comparable experiments, the tagged form of PCPE-1 (PCPE-1-8His) was also used. A wide repertoire of substrates was tested and similar results were obtained with both His-tagged PCPE-2 variants, even if the stability of the 6His-PCPE-2 seemed better than that of PCPE-2-8His (which may be linked to the absence of calcium in the storage buffer of the latter). This suggested that the location of the tag (N-ter or C-ter) does not affect the function of the protein but may also have a role to control protein stability. The results for the 6His-PCPE-2 *in vitro* assays only will be presented below.

1) Fibrillar procollagens

As described in the introduction, fibrillar collagens constitute a subgroup of the collagen family which has the ability to form fibrils. Types I, II and III procollagens are the most abundant collagens in tissues and are usually called major collagens, whereas type V and XI are known as minor fibrillary collagens. Type I collagen is the main constituent of the dermis and forms heterotypic fibrils with type III and V collagens, where the latter regulates the diameter of the fibrils.

The enhancing effect of PCPE-1 on fibrillar procollagens (I-III, V) has been well described in the last years. The group of C. Moali has confirmed the effect of PCPE-1 *in vitro* using two recombinant proteins, PCPE-1 and the histidine tagged-form, PCPE-1-8His. Moreover, they showed that one molecule of PCPE-1 for one trimer of procollagen is both necessary and sufficient to have the maximum enhancing activity[168]. However, only few studies report the effect of PCPE-2. The following *in vitro* cleavage assays aim at studying more carefully the effect of PCPE-2 recombinant protein and at comparing its effect with that of recombinant PCPE-1.

a. Effect of PCPE-2 on type I procollagen

Firstly, PCPE-2 effect was tested on recombinant type I procollagen, which was produced in yeast and purified in our group by Aurore Berthier. Procollagen I (150 nM) was incubated with recombinant BMP-1 (23 nM) at 37°C for 2 hours, in the absence or the presence of PCPE-1-8His (150 nM) or 6His-PCPE-2 (150 and 300 nM). Processing of procollagen I was assessed using SDS-PAGE and SYPRO™ Ruby staining (***Figure 69A***). The intensity of the upper bands corresponding to the two procollagen I chains (α1 and 2) was reduced when BMP-1 was added. BMP-1 cleaved the procollagen resulting in two products for each chain, the pN-collagen, which is the procollagen lacking the C-propeptide (~130 kDa) and the C-propeptide around 30 kDa. In the presence of PCPE-1, the procollagen was completely processed in the

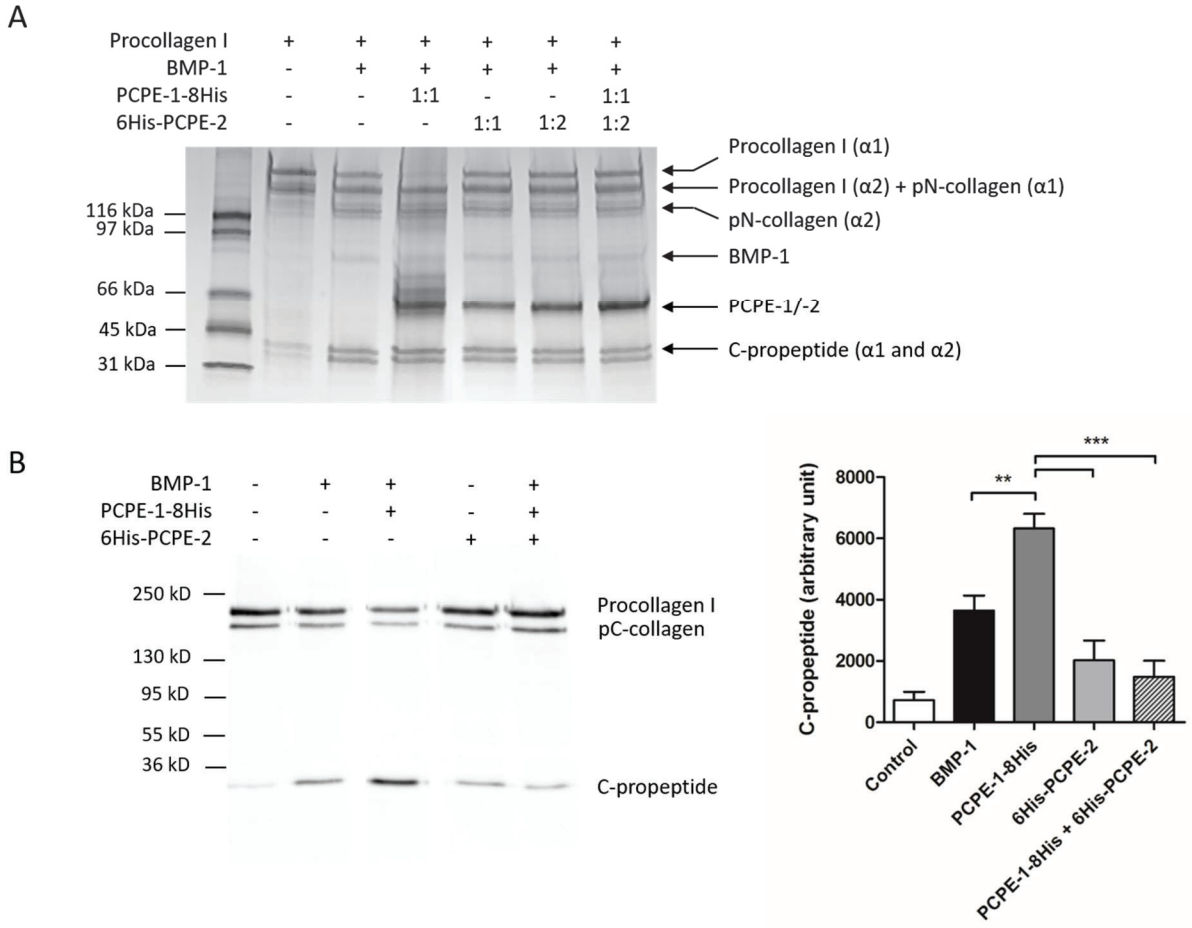

Figure 69: Procollagen I processing by BMP-1 with PCPE-1 or PCPE-2

(A) SDS-PAGE analysis (4-20% acrylamide gel, reducing conditions) and SYPRO™ Ruby protein staining. Recombinant procollagen I (150 nM) was incubated with various concentrations of PCPE-1-8His or 6His-PCPE-2 proteins: 150 nM (PCPE:procollagen 1:1) or 300 nM (1:2) for 5 minutes. Then, BMP-1 (23 nM) was added to the reaction mixture (total volume of 30 µL) for 1h30 at 37°C (n = 4).
(B) Western blotting using a specific antibody raised against the C-propeptide of procollagen I (LF41, which only recognizes the α1 chain) and quantification of the amount of C-propeptide. Fibroblast conditioned medium was incubated with 10 nM of BMP-1 and 750 nM of PCPE-1-8His and/or 6His-PCPE-2 for 2h at 37°C (n = 7).

pN form by BMP-1. Surprisingly, under the same conditions, PCPE-2 did not enhance the BMP-1-mediated cleavage and the procollagen was processed to the same extent as with BMP-1 alone. Moreover, and interestingly, when both PCPE-1 and PCPE-2 were added together, PCPE-2 seemed to prevent the enhancing effect of PCPE-1.

These results were confirmed using another system, the procollagen I-rich conditioned medium of human skin fibroblasts. The medium was directly incubated with recombinant BMP-1 (10 nM), in the presence or the absence of PCPE-1-8His or 6His-PCPE-2 (750 nM), for 2 hours at 37°C and procollagen I processing was analysed by Western blotting using an anti-C-propeptide I antibody (LF41; ***Figure 69B***). As observed with the recombinant protein, procollagen I processing was enhanced by PCPE-1, but not by PCPE-2. The cleavage of the C-propeptide in the presence of 6His-PCPE-2 was similar to the cleavage with BMP-1 alone. Again, PCPE-2 seemed to prevent the enhancing effect of PCPE-1 on procollagen I processing. These results were unexpected because they contradict the current dogma that PCPE-2 is a procollagen C-proteinase enhancer and the previous reports showing enhancing activity. Of note, only two publications have shown direct evidence of PCPE-2 enhancing activity, which makes it much less documented than for PCPE-1. To go further, the processing of other fibrillar collagens was tested *in vitro*.

b. Effect of PCPE-2 on type II procollagen

While type II collagen is not a constituent of the skin and is found in cartilage, its processing also involves BTPs and can be enhanced by PCPE-1 and -2 according to the work done by the group of D. Greenspan[148]. In order to understand the effect of PCPE-2, processing of type II procollagen was studied in the conditioned medium of primary articular chondrocytes given by the group of Frédéric Mallein-Gerin (LBTI, Lyon). Indeed, these cells, which are isolated from human cartilage, produce high amounts of type II procollagen homo-trimer. Conditioned medium was directly incubated with BMP-1 (10 nM), PCPE-1-8His and/or 6His-PCPE-2 (500 nM) at 37°C for 3 hours. Procollagen II processing was analysed by Western blotting using a monoclonal mouse antibody directed against human procollagen II (***Figure 70***). In the absence of BMP-1 and PCPE, a single band corresponding to the intact procollagen II (140 kDa) was observed. When BMP-1 was added, the procollagen II was cleaved, i.e. a second band, which probably corresponded to the pN-collagen II, appeared. The intensity of the procollagen II band was reduced whereas the one corresponding to the C-propeptide II (CPII, 28 kDa) was increased. This proteolytic cleavage was even more notable in the presence of PCPE-1, which stimulated the processing of procollagen II. However, 6His-PCPE-2 did not have any effect on procollagen II processing as the bands corresponding to the procollagen and

the C-propeptide seemed similar to the ones observed with BMP-1 alone (lane 6 compared to lane 2). These results confirmed the absence of enhancing effect of PCPE-2 on procollagen processing as previously observed on procollagen I.

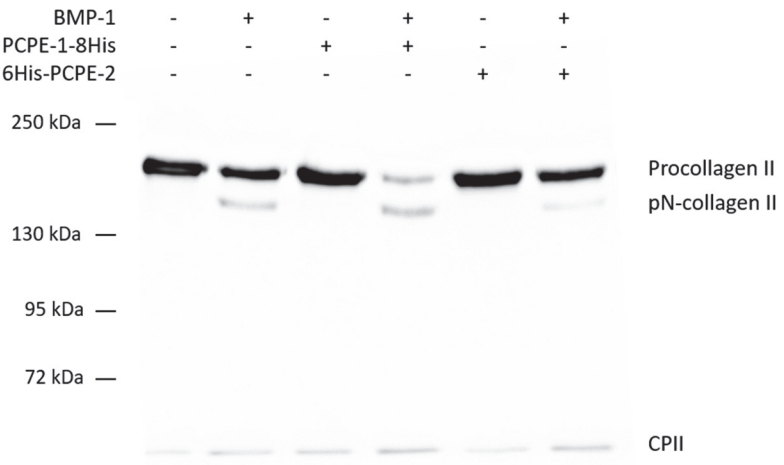

Figure 70: Procollagen II processing by BMP-1 in the presence or absence of PCPE-1 or -2
Western blot analysis (6% acrylamide gel, reducing conditions) using a specific antibody raised against procollagen II (gift from Jean-Baptiste Vincourt, Nancy). Articular chondrocyte conditioned medium was incubated with 10 nM of BMP-1 in the presence or absence of 500 nM of PCPE-1-8His or 6His-PCPE-2 for 3h at 37°C (representative experiment of n = 5).

c. Effect of PCPE-2 on type III procollagen

To study procollagen III processing, the two model substrates, Mini III and CPIII-long, already described in the previous chapter were used. Firstly, the cleavage of CPIII-long by BMP-1 was tested with or without the recombinant 6His-PCPE-2 protein (***Figure 71A***). For this experiment, various molar ratios of PCPE:substrate were tested: one equivalent of PCPE for two equivalents of substrate (molar ratio 1:2), one equivalent of PCPE for one equivalent of substrate (1:1) or three equivalents of PCPE for one equivalent of CPIII-long (3:1). Figure 71B shows that PCPE-1 enhanced the processing of CPIII-long by BMP-1 up to 4-fold. However, when similar concentrations of PCPE-2 were used, only a weak enhancement of CPIII-long processing was observed (activation up to 1.5-fold with molar ratios of 1:2 and 1:1). With higher amount of PCPE-2 (molar ratio with the substrate 3:1), this weak enhancing effect was lost and the processing of CPIII-long seemed to be similar to the processing with BMP-1 alone, suggesting that PCPE-2 has no effect on BMP-1 activity above the 1:1 ratio. Thus, for the first time in our assays, a very small effect of PCPE-2 on procollagen processing was observed; however, it remains much less efficient compared to PCPE-1 and depends on the enhancer:substrate molar ratio.

To determine why 6His-PCPE-2 was a weaker enhancer of BMP-1-mediated CPIII-long processing, we analysed the ability of the protein to interact with the substrate, as PCPE-1 does. SPR experiments were performed by Sandrine Vadon-Le Goff in our laboratory using another model substrate of procollagen III, Mini III. Both Mini III and CPIII-long have been well characterized by the group of C. Moali and were shown to interact similarly with PCPE-1 and to be cleaved by BMP-1. These experiments revealed that both PCPE-1 and PCPE-2 interact with Mini III with similar and high affinity (nanomolar range; ***Figure 71C***). Although PCPE-2 can bind the procollagen III, it does not efficiently enhance its processing as PCPE-1 does.

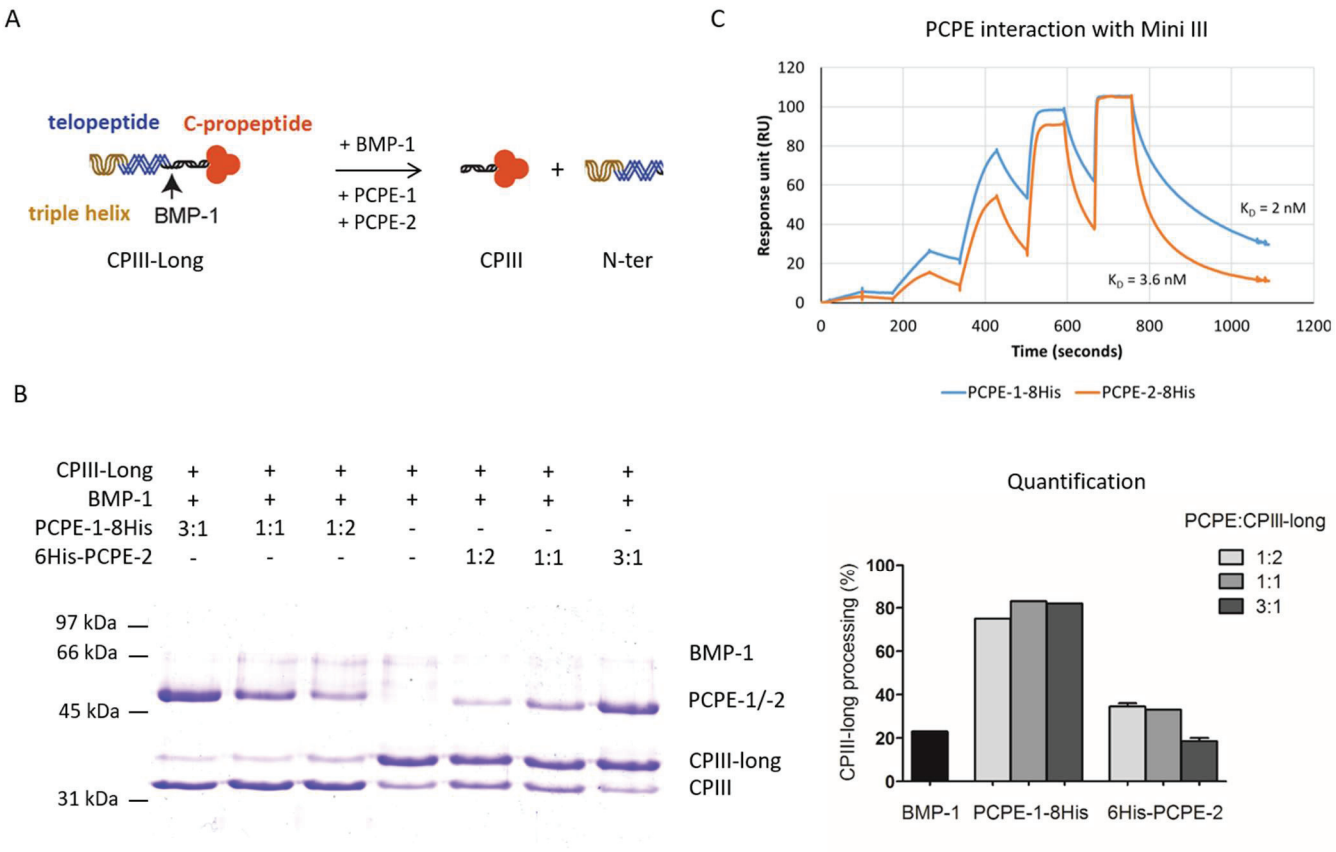

Figure 71: CPIII-long processing by BMP-1 in the presence or absence of PCPE-1 or -2

(A) Schematic representation of CPIII-long cleavage by BMP-1. CPIII-long is a model substrate of procollagen III containing the C-propeptide, the C-telopeptide and three triplets of the triple helix. The BMP-1 cleavage site is located at the junction between the telopeptide and the C-propeptide. BMP-1 efficiently cleaves CPIII-long resulting in two products called CPIII and N-ter. **(B)** SDS-PAGE analysis (15% acrylamide gel, reducing conditions) and Coomassie Blue staining. CPIII-long (320 nM) was incubated with various concentrations of PCPE-1-8His or 6His-PCPE-2 proteins: 160 nM (PCPE:CPIII-long 1:2), 320 nM (1:1) and 980 nM (3:1) for 5 minutes. Then, BMP-1 (2.4 nM) was added to the reaction mixture (total volume 30 µL) for 1h at 37°C (n = 10). Intensities of the bands were quantified by densitometry. **(C)** 384 resonance units of the Mini III substrate were immobilized on a CM5 sensor chip and increased concentrations (from 1 to 356 nM) of PCPE-1-8His or PCPE-2-8His were injected in 10 mM HEPES, 0.15M NaCl, 5 mM $CaCl_2$, P20 0.05% (50 µL/min). Association and dissociation of PCPE with the substrate were followed overtime (n = 2).

To get further insight into PCPE-2 function, we tested the effect of 6His-PCPE-2 when CPIII-long cleavage is mediated by another protease of the BTP family, mTLL-1 (produced and purified by members of my group). We already knew that the mTLL-1 protease is less efficient than BMP-1 in processing CPIII-long but PCPE-1 is still able to enhance its cleavage[242]. Various molar ratios of 6His-PCPE-2:CPIII-long were tested with 34 nM of mTLL-1 (1:2, 1:1, 3:1 and 5:1). With a 1:1 ratio, we observed that both PCPE-1 and PCPE-2 enhanced CPIII-long processing by about 3.5-fold (***Figure 72***). However, when higher amounts of PCPE-2 (3:1 and 5:1 ratios) were used, the effect of PCPE-2 on mTLL-1-mediated CPIII-long processing was reduced to a 2-fold enhancement. In conclusion, when equimolar amounts of enhancer and substrate are used, 6His-PCPE-2 is an enhancer of the processing of CPIII-long by mTLL-1, but this enhancement is inhibited at higher concentrations of PCPE-2. This suggests a dependence of PCPE-2 activity on the protease concentration as mTLL-1 is used here at a much higher concentration (>10-fold) than BMP-1 in previous experiments.

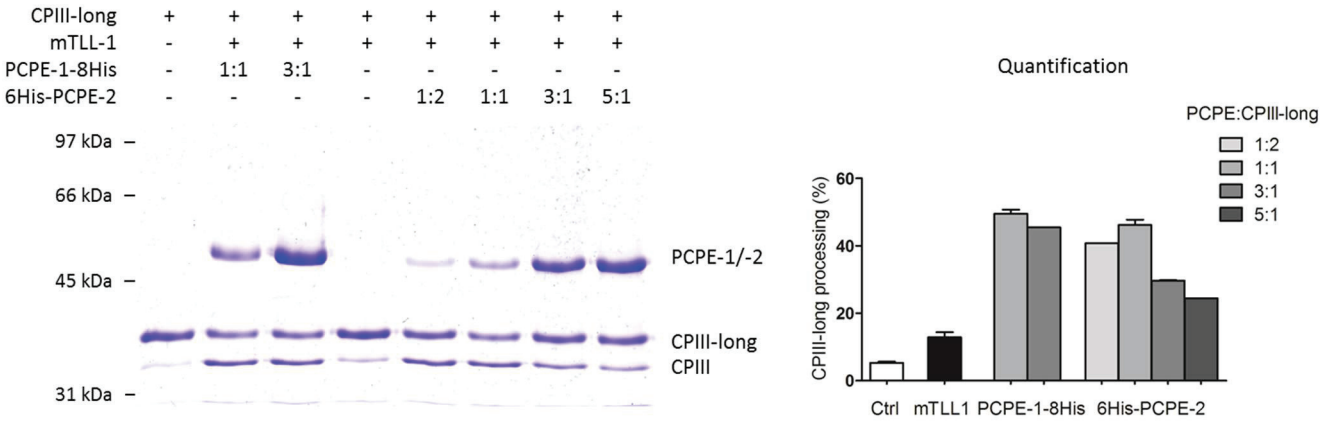

Figure 72: CPIII-long processing by mTLL-1 with PCPE-1 and -2

SDS-PAGE electrophoresis (15% acrylamide gel, reducing conditions) and Coomassie Blue staining. CPIII-long (320 nM) was incubated with various concentrations of PCPE-1-8His or 6His-PCPE-2 proteins: 160 nM (PCPE:CPIII-long 1:2), 320 nM (1:1) 980 nM (3:1) and 1.6 µM (5:1) for 5 minutes. Then, mTLL-1 (34 nM) was added to the reaction mixture (30 µL) for 4h at 37°C. Intensities of the bands were quantified by densitometry (n = 2).

d. Effect of PCPE-2 on type V procollagen

Then, the processing of type V procollagen was assayed *in vitro* using a recombinant model substrate of the procollagen V protein, named pNα1(V) and provided by Florence Ruggiero (Institut de Génomique Fonctionnelle de Lyon). This substrate encompasses the N-propeptide and 11 triplets of the COL1 triple-helical domain of human procollagen V (***Figure 73A***), including the N-terminal cleavage site. Whereas BMP-1 was previously associated to the C-terminal processing of fibrillar procollagens (I, II, III, V and XI), it has been shown that

BMP-1 also cleaves the N-terminal propeptide of type V procollagen[100] (cleavage site between the TSPN-1 and VAR domains: Ser^{254}-Gln^{255}) and that PCPE-1 enhances this N-terminal processing[150]. From the results presented in Figure 73B, we observe that the intact pNα1(V) substrate (97 kDa) is partially cleaved by BMP-1 in the conditions of the assay; the proteolytic fragment, TSPN-1 appears around 31 kDa. When sufficient amounts of PCPE-1 were added (at least half an equivalent of PCPE for one equivalent of substrate, i.e. 1:2 ratio), pNα1(V) processing increased by up to 2.2-fold, as shown on the quantification graph. Very surprisingly, when PCPE-2 was added, the processing of pNα1(V) by BMP-1 was completely abolished. Even the smallest amount of PCPE-2 (1:8 ratio) was sufficient to inhibit pNα1(V) processing. One more time, this result highlighted functional differences between recombinant PCPE-1 and -2 proteins and suggested that PCPE-2 could directly inhibit the protease, in addition to or independently of a direct effect on the substrate. To confirm this hypothesis, the processing of BMP-1 substrates, other than fibrillar collagens, was also tested.

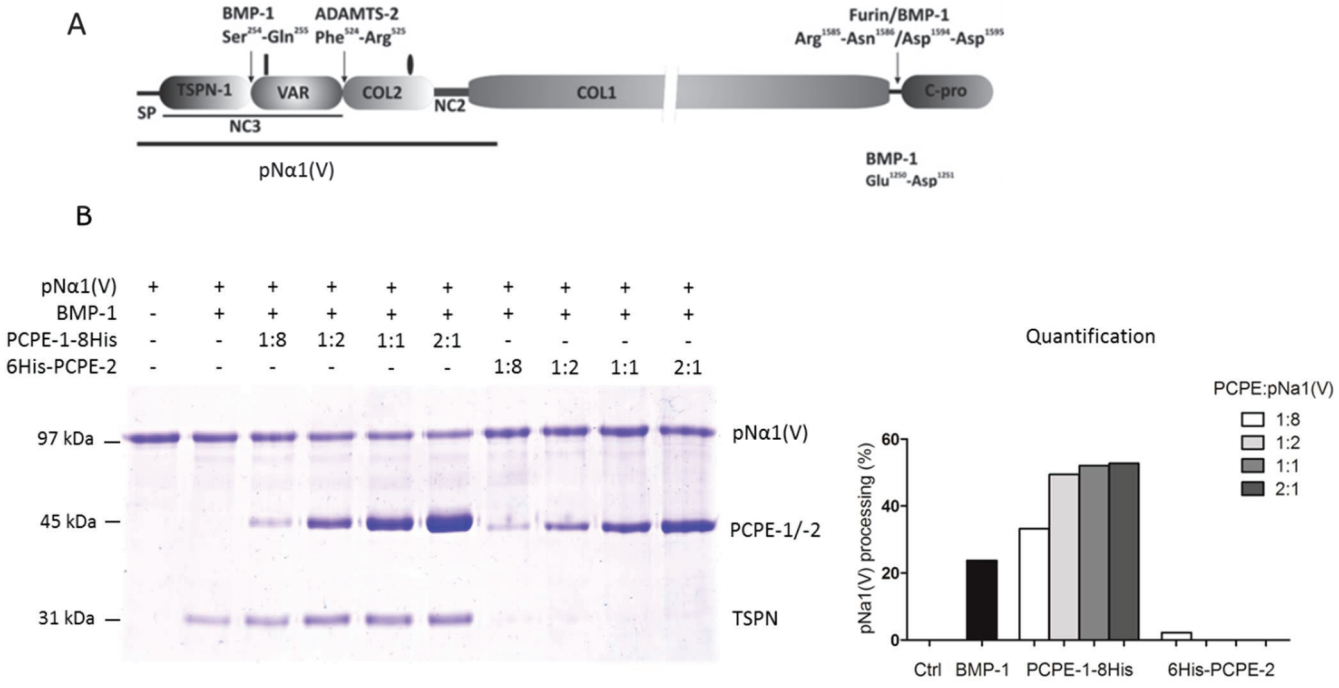

Figure 73: Procollagen V processing by BMP-1 in the presence or absence of PCPEs

(A) Structure of human procollagen V and the derived pN-collagen α1V model substrate used for the *in vitro* assay[149]. **(B)** SDS-PAGE (12% acrylamide gel, reducing conditions) and Coomassie Blue staining. pN-collagen α1V (800 nM) was incubated with various concentrations of PCPE-1-8His or 6His-PCPE-2 proteins: 100 nM (1:8), 400 nM (1:2), 800 nM (1:1) and 1.6 µM (2:1) for 5 minutes. Then, BMP-1 (30 nM) was added to the reaction mixture (40 µL total volume) for 2 hours at 37°C (n = 1). pN-collagen α1V processing was calculated as a percentage by quantifying the intact pNα1(V) protein and the released fragment by densitometry (ImageJ).

2) Non collagenous substrates of BMP-1

PCPE-1 is known to be substrate-specific and to affect only the processing of fibrillar collagens. In this study, following the unexpected results obtained above with these collagens, we wondered if 6His-PCPE-2 protein could stimulate BMP-1 processing of others substrates that are not affected by PCPE-1 such as thrombospondin-1, chordin, and betaglycan[151].

Thrombospondin-1 (TSP-1) is a multifunctional extracellular glycoprotein involved in cell adhesion, apoptosis and TGFβ activation, which exhibits pro- and anti-angiogenic properties. TSP-1 is expressed by many cell types including keratinocytes, fibroblasts and macrophage-like cells and has been involved in several tissue repair processes including skin and cornea wound healing[243]. TSP-1 is a multi-domain trimeric protein of 510-kDa and the group of C. Moali recently showed that TSP-1 can be physiologically cleaved by BMP-1, enlarging the substrate repertoire of the protease, work to which I contributed by showing that the cleavage of TSP-1 by BMP-1 induces myofibroblast differentiation (Article 2, Anastasi et *al.* submitted). This work also showed that PCPE-1 has no effect on the cleavage of TSP-1 by BMP-1. However, the effect of PCPE-2 has not been investigated yet. Thus, the processing of recombinant TSP-1 was assayed in the presence or absence of PCPE-1-8His or 6His-PCPE-2. 200 nM of human TSP-1 (purified from human platelets) were incubated with 30 nM of BMP-1 with or without PCPE-1 or PCPE-2 (200, 800 nM or 1 µM) for 4 hours at 4°C. We confirmed that PCPE-1 did not influence TSP-1 cleavage; TSP-1 is similarly cleaved by BMP-1 with or without PCPE-1 (***Figure 74A***) and the amount of processing is not significantly changed (around 25% of cleavage). Surprisingly, we found that 6His-PCPE-2 also inhibited TSP-1 processing mediated by BMP-1; the proteolytic fragment was not detected when PCPE-2 was added to the reaction. This result suggests that 6His-PCPE-2 can inhibit BMP-1 activity on TSP-1.

Chordin, a major antagonist of BMP-2 and BMP-4 during development is a well-known substrate of BMP-1[244]. Recombinant mouse chordin protein, purchased from R&D Systems and containing two protein products (116 and 90 kDa; corresponding to two splice variants according to the supplier) was used for the *in vitro* assay. 370 nM of chordin were incubated with two different concentrations of PCPEs: 370 nM (1:1 molar ratio) and 740 nM (2:1). Recombinant BMP-1 (20 or 40 nM) was added for 4 hours at 37°C. By SDS-PAGE analysis (***Figure 74B***), we showed that BMP-1 cleaves the two chordin forms resulting in a central proteolytic fragment (83 kDa) and the N- and C-terminal products (15 and 13 kDa respectively). While PCPE-1 had no effect on the processing of chordin, PCPE-2 partially inhibited its cleavage by BMP-1. The bands corresponding to the proteolytic fragment and the propeptides were still detectable by Coomassie Blue staining, but their intensity was much weaker.

Betaglycan, also known as TGFβ receptor III, is a proteoglycan co-receptor that binds TGFβ proteins with high affinity and thereby natively regulates TGFβ signalling. Cleavage of betaglycan by BTPs results in the release and prolonged activity of TGFβ1[117]. To see if PCPEs could have an effect on the cleavage of betaglycan, rat betaglycan without GAG chains (780 nM; provided by Fernando Lopez-Casillas, Universidad Nacional Autonoma de Mexico, Mexico City) was incubated with BMP-1 (50 nM) in the absence or presence of PCPE-1 or PCPE-2 (780 nM or 1 µM) for 4 hours at 4°C. SDS-PAGE analysis (***Figure 74C***) showed that the full-length betaglycan (100 kDa) was cleaved by BMP-1, resulting in two new fragments (60 and 40 kDa). As expected, PCPE-1 had no effect on this cleavage and the intensity of the bands corresponding to the two new fragments is similar to the condition with BMP-1 alone. In the presence of PCPE-2, this cleavage was inhibited as the two proteolytic fragments almost disappeared, suggesting one more time the inhibitory effect of the 6His-PCPE-2 recombinant protein on BMP-1 activity.

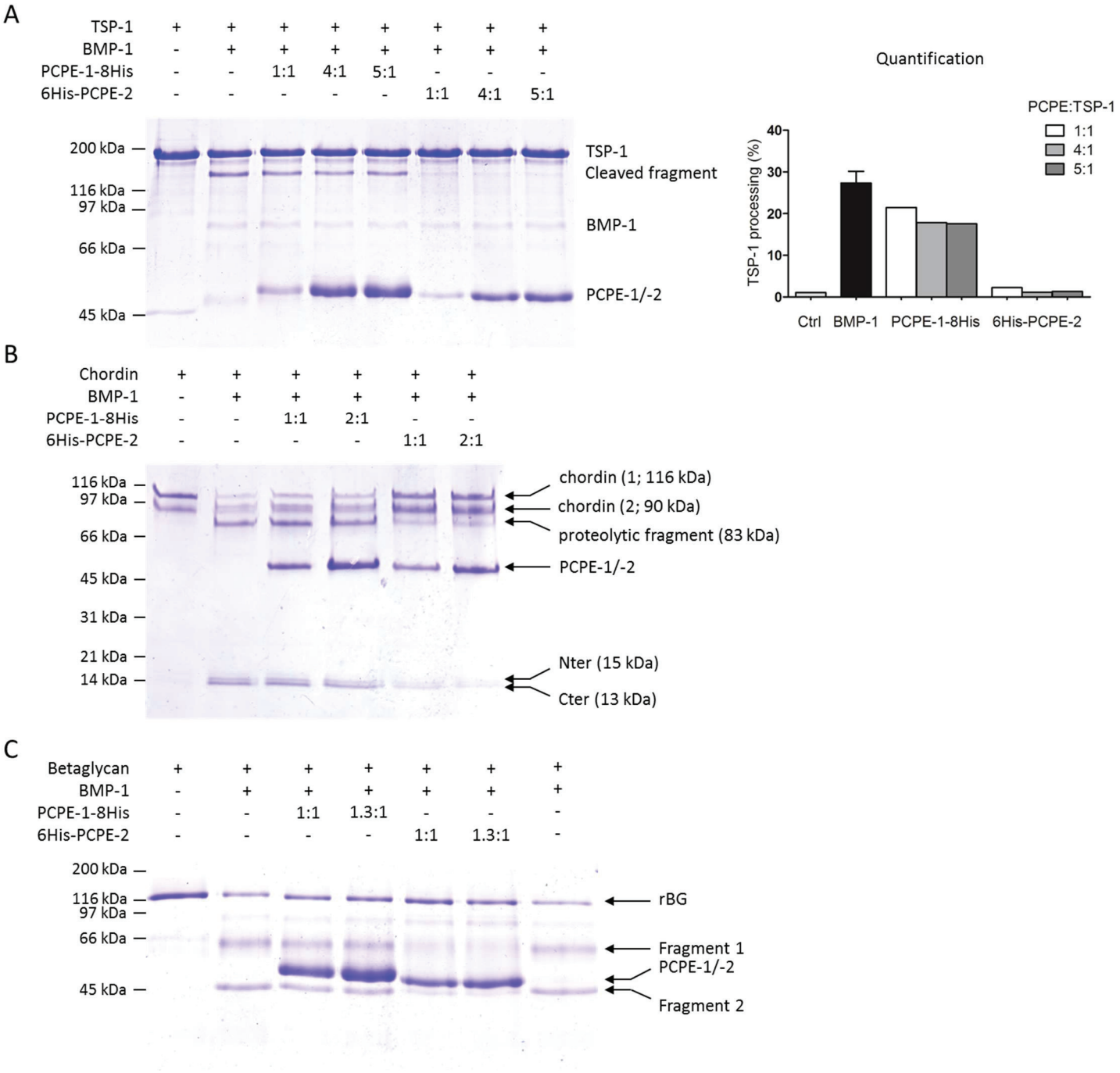

Figure 74: Processing of thrombospondin-1 (A) chordin (B) and betaglycan (C) by BMP-1

(A) 200 nM of thrombospondin-1 (TSP-1) were incubated with various concentrations of PCPE-1-8His or 6His-PCPE-2 proteins: 200 nM (1:1), 800 nM (4:1) or 1 µM (5:1). Then, 30 nM of BMP-1 were added to the reaction mixture (40 µL) and incubated for 4h at 37°C (n = 1). TSP-1 processing was analysed on a 8% acrylamide gel by Coomassie Blue staining and quantified (as a percentage) by densitometry using the Image J software. **(B)** 370 nM of chordin were incubated with 370 (1:1) or 740 nM (2:1) of PCPE and 20 nM of BMP-1 in a total volume of 40 µL for 4h at 37°C (n = 1). The reactions were analysed under reducing conditions on a 4-20% acrylamide gel. **(C)** 780 nM of betaglycan (rBG) were incubated with 0.78 (1:1) or 1 µM (1.3:1) of PCPE and 50 nM of BMP-1 in a total volume of 30 µL for 4h at 37°C (n = 3). Analyses were done on a 10% acrylamide gel under reducing conditions.

3) Direct effect of PCPE-2 on BMP-1 activity

The effect of the 6His-PCPE-2 recombinant protein on BMP-1 activity was also tested in our group by Sandrine Vadon-Le Goff using a fluorogenic peptide substrate, Mca-YVADAPK-Dnp (Enzo Life Sciences). This peptide contains a highly fluorescent 7-methoxycoumarin (Mca) group and is coupled to a quencher 2,4-dinitrophenyl (Dnp) group. BMP-1 is able to cleave the substrate at a specific site between the fluorescent and the quencher moieties, causing an increase in fluorescence.

The fluorescence measured in the presence of BMP-1 alone was considered as 100%. As a negative control, BMP-1 (6.7 nM) was incubated with the fluorogenic peptide (20 µM) and PCPE-1-8His; as expected, the latter did not affect the cleavage of the substrate (***Figure 75A***). When the 6His-PCPE-2 protein was added, the substrate was no longer efficiently cleaved by BMP-1 and the inhibition of BMP-1 activity was correlated to 6His-PCPE-2 concentrations (from 0.1 to 680 nM). Then, IC_{50} values were determined by plotting the ratio of the inhibited versus uninhibited enzyme activities against the inhibitor concentration. Non-linear regression analysis and calculations were performed using GraphPad Prism (n = 3; ***Figure 75B***). Although the inhibition of BMP-1 activity was not complete, these results showed that the 6His-PCPE-2 recombinant protein can directly inhibit BMP-1 (IC_{50} of 6.16 nM). Thus, PCPE-2 might prevent the processing of various BTP substrates (collagens and others) by a direct inhibition of BMP-1.

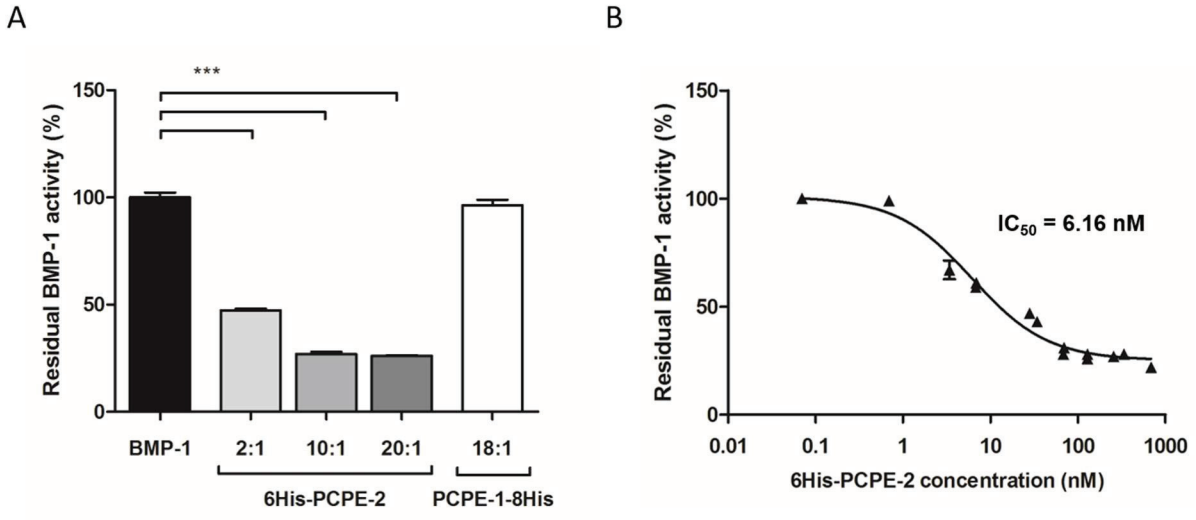

Figure 75: BMP-1 activity on a fluorogenic peptide in the presence or absence of 6His-PCPE-2

(A) BMP-1 activity on a fluorogenic peptide determined by measuring the fluorescence in the presence or absence of 6His-PCPE-2. BMP-1 (6.7 nM) was incubated alone with the fluorogenic peptide (20 µM), or with 6His-PCPE-2 (ratio 2:1, 10:1 or 20:1) or PCPE-1-8His (18:1) at 37°C. The fluorescence was monitored during 20 min using an Infinite M1000 Tecan reader (excitation wavelength: 320 nm; emission wavelength: 405 nm). **(B)** IC_{50} calculation for 6His-PCPE-2 using GraphPad Prism (n = 3).

IV. Discussion

In this chapter, several recombinant PCPE-2 proteins were produced in eukaryotic cells in order to characterize the functions of PCPE-2 *in vitro*: PCPE-2, PCPE-2-8His containing the human PCPE-2 sequence and an additional 8-histidine tag in C-terminal, and 6His-PCPE-2 with a 6-histidine tag at the N-terminus. Two his-tagged constructs were elaborated to ensure that the position of the tag would not affect the stability or the conformation of the protein. The amounts of PCPE-2-8His and 6His-PCPE-2 produced by the cells were very low compared to the production of PCPE-1-8His. It is known that the C-terminal NTR domain of PCPE-1 is involved in the interaction of the protein with heparin and HSPGs[147]. As the affinity of PCPE-2 for HSPGs seems to be even stronger, we hypothesized that its NTR domain might bind to the cells during the production. To investigate this aspect, 293-T cells were treated after transfection with heparin to compete with the PCPE-2 protein potentially bound to the cells. However, the yield of production did not improve in the presence of heparin. Only his-tagged proteins were efficiently purified and used for *in vitro* cleavage assays on various BTP substrates.

Interestingly, we showed that these two proteins were significantly less efficient than PCPE-1-8His in enhancing the processing of major fibrillar collagens (I-III; ***Table 25***). 6His-PCPE-2 did not have any enhancing effect on the processing of types I and II procollagens by BMP-1 in the conditions of the assay. These results were unexpected as two previous studies reported the enhancing effect of PCPE-2 on types I and II procollagens[148,154]. Steiglitz et *al.* showed that the human recombinant PCPE-2 protein enhanced the processing of recombinant procollagen II. While several steps of purification were necessary to purify PCPE-2 in our experiments, their protein was simply purified on a heparin-sepharose column and could contain residual amounts of endogenous PCPE-1. Importantly, the authors used 293-EBNA cells to produce recombinant PCPE-2, while these cells express high levels of endogenous PCPE-1 (data not shown). In the second study, the effect of PCPE-2 was shown on procollagen I-rich fibroblast medium and no information was given about the purification of the PCPE-2 protein.

Consistent with the results on procollagens I and II, we showed that the enhancing effect of PCPE-2 on procollagen III, was significantly less than for PCPE-1. It was even more surprising because both proteins were able to interact with the substrate with similar affinities. Moreover, we showed that PCPE-2 can prevent the enhancing effect of PCPE-1 on procollagen processing. These results suggest that PCPE-2 is a weak enhancer of the activity of BMP-1 on major fibrillar collagens and can compete with its homologous protein, PCPE-1.

Furthermore, PCPE-2 can inhibit the processing of other BMP-1 substrates. It prevents the N-terminal processing of procollagen V, which is usually enhanced by PCPE-1 and the maturation of non-collagenous substrates, that is not affected by PCPE-1 (TSP-1, chordin and betaglycan)[151]. Finally, using a fluorogenic peptide substrate, we demonstrated that the 6His-PCPE-2 recombinant protein can directly inhibit BMP-1 *in vitro*. This inhibitory effect on several different substrates shows that the direct interaction of PCPE-2 with BMP-1 is likely probable. The affinity between the two proteins will soon be investigated by SPR experiments. Interestingly, it was previously shown that PCPE-1 only has a moderate affinity for BMP-1 and that this is not the main driving mechanism in the activation mechanism.

Therefore, the PCPE-2 protein we have produced seems to have two co-existing effects: an enhancing effect on the processing of major fibrillar procollagens (III at least) and a strong inhibition of BMP-1 activity.

Substrates		Effect of PCPE-1		Effect of PCPE-2	
		BMP-1	mTLL-1	BMP-1	mTLL-1
Collagenous	Procollagen I (C-propeptide)	++	n.d.	0	n.d.
	Procollagen II (C-propeptide)	++	n.d.	0	n.d.
	Procollagen III (C-propeptide)	++	++	+/-	++
	Procollagen V (N-propeptide)	+	n.d.	-	n.d.
Non-collagenous	TSP-1	0	n.d.	-	n.d.
	Chordin	0	n.d.	-	n.d.
	Betaglycan	0	n.d.	-	n.d.
	Peptide	0	n.d.	-	n.d.

Table 25: Summary of the observed effects of PCPE-1 and PCPE-2 on the tested substrates
++, strong enhancing effect; +, enhancing effect; +/-, weak enhancing effect; 0, no effect; -, inhibition; n.d. no data.

In light of these unexpected results, we wondered whether the protein was properly folded and acted similarly to the *in vivo* protein. David Hulmes performed dynamic light scattering (DLS) experiments to determine the particle size and distribution and found that the 6His-PCPE-2 protein appears to be much bigger than expected (about 6 times bigger) and might be an oligomer, which could also explain why purification on Superdex 200 did not work. Whether this conformation is found *in vivo* or is an artefact of the production/purification remains

unknown and needs to be investigated. Importantly, the DLS experiment (n = 1) has not been performed on a freshly purified protein and we have shown by SPR that the quality of the protein was altered after freezing/thawing. Although its stability has been improved with our present optimized protocol, the PCPE-2 recombinant protein remains less stable than PCPE-1 and DLS should be replicated on a freshly purified protein. A large-scale production of 6His-PCPE-2 is currently in progress to repeat these experiments and perform additional analyses of the protein by analytical ultracentrifugation, SPR and mass spectrometry. Analytical ultracentrifugation is a versatile method for analysing and characterizing proteins in solution and will help us to determine if the purified protein is an oligomer or not.

In parallel, we also tried to produce another construct of PCPE-2, lacking the C-terminal NTR domain (CUB1-CUB2) to determine which domain would be important for the observed inhibitory effect of PCPE-2. Indeed, as the CUB1-CUB2 domains of PCPE-1 and -2 are very similar, it would be very interesting to evaluate whether these two domains alone act similarly *in vitro*. The differential effects of PCPE-2 on fibrillar collagens and non-collagenous substrates might be due to the less conserved NTR domain or the linker between CUB2 and NTR. Unfortunately, the purification of CUB1-CUB2 from PCPE-2 was unsuccessful because the protein was aggregated. One more time, the solubility of the protein seemed to be a major problem for the production and purification of PCPE-2. High amounts of octyl-β-D-glucopyranoside and salts were necessary to avoid protein precipitation and maintain the solubility of PCPE-2. Consistent with these *in vitro* observations, the PCPE-2 protein was always detected in the cell lysates of keratinocytes, monocytes and macrophages, but not in the conditioned-medium, as observed for PCPE-1 in fibroblasts. For this reason, we hypothesized that PCPE-2 might bind to HSPGs, integrins (through its RGD domain) or SR-BI at the cell surface. Macrophages were thus treated with either heparin, an RGD peptide, an anti-SRBI antibody or EDTA in order to prevent this interaction; these assays were unsuccessful and did not lead to the release of more PCPE-2 in the conditioned medium. Altogether, these results suggest that the PCPE-2 protein is not very stable in solution and might be found in another form *in vivo*, e.g. stabilized by an unknown partner at the cell surface.

Whether the purified protein is not correctly folded or the PCPE-2 protein acts differently because of a different *in vivo* function remains to be determined by additional analyses. As described in chapter 3, PCPE-2 appears to be differentially expressed in the skin compared to PCPE-1, so it would not be surprising that PCPE-1 and PCPE-2 actually have different functions. Moreover, interaction with procollagen III and enhancing activity on procollagen

substrates in some conditions clearly indicate that the PCPE-2 recombinant protein is not completely unfolded, but suggest again of inhibitory activity towards BMP-1.

In conclusion, PCPE-2 seems to have no effect or to slightly activate the processing of collagenous substrates. This effect is strongly dependent on the protease concentration, which is not observed for PCPE-1. PCPE-2 also has a clear inhibitory effect on the processing of non-collagenous substrates. Thus, PCPE-2 might bind to the procollagen substrates (yielding activation of the C-terminal processing) as well as the protease (yielding inhibition). The effects of PCPE-2 seem much more complex and can vary a lot depending on the relative concentration of the three partners.

To further understand the *in vivo* role of PCPE-2, the consequences of the absence of PCPE-2 were assessed in a mouse model lacking the PCPE-2 protein and this is the subject of the next chapter.

Chapter 6: *Pcolce2* knockout mice

I. Validation of the *Pcolce2* knockout

Pcolce2 knockout (KO) embryos were a kind gift of Dr. C. Bleul and C. Happe from the Max-Planck-Institute for Immunology and Epigenetics (Freiburg). In this mouse model, a large part of the exon 3 of the *Pcolce2* gene (corresponding to nucleotides 258 to 431 of the mRNA sequence) was replaced by a neocassette (IRES-lacZ/neomycin resistance cassette; ***Figure 76A***). Genotyping of the mice was done on genomic DNA from tail biopsies using the same primers as previously described by the group of C. Bleul[172]. Two primer pairs were used, one amplifying a fragment of 709 base pairs (bp) corresponding to the intron 2 and exon 3 in the WT allele, while the other primer pair amplifies the neocassette (584 bp) in the KO allele (***Figure 76B***).

To assure that the *Pcolce2* transcript was absent in this model, PCR was also performed on the RNA isolated from the heart, oesophagus and skin of these mice. PCR primers previously described[172] (CB648 and CB650) amplified a fragment comprising exons 2 to 5 of the gene, while new designed primers (6 and 7) amplified the exons 2 to 4, as shown in Figure 76A. In the heart, oesophagus and skin, no transcript was amplified in *Pcolce2* KO mice using the three pairs of primers, compared to WT mice. These results confirmed that the *Pcolce2* mRNA transcript is absent in these KO mice, or alternatively that the transcript is too long to be amplified by PCR (the length of the introduced neocassette being around 5 kb).

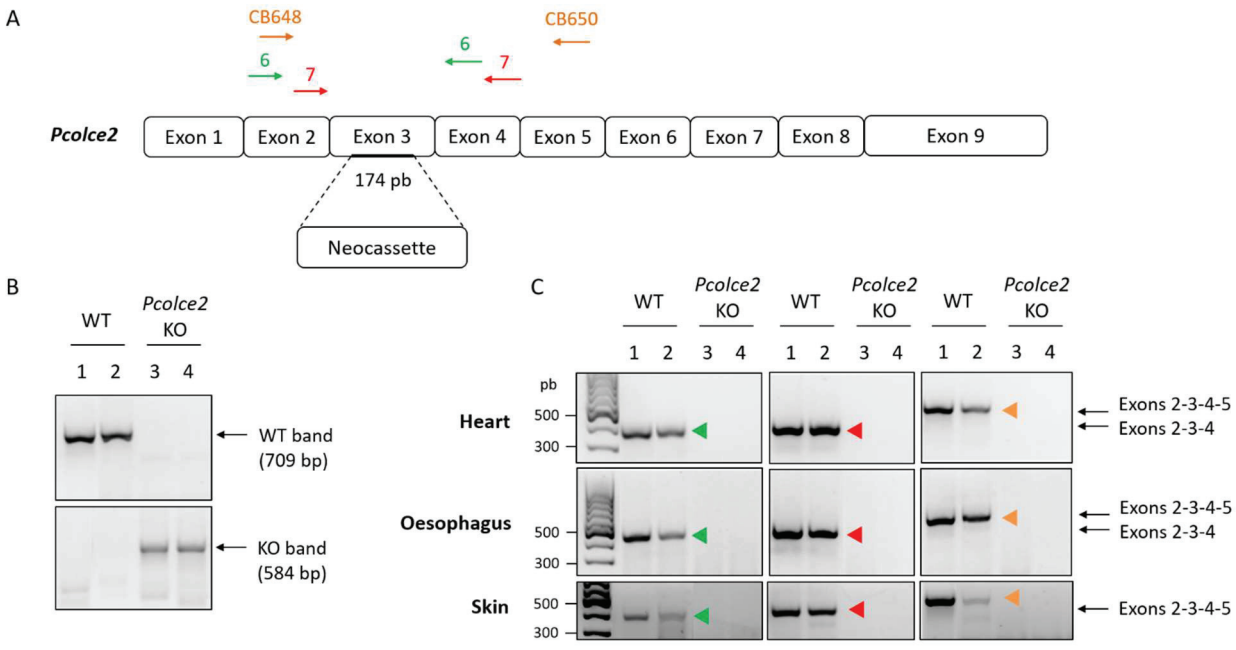

Figure 76: Validation of the absence of the exon 3 of *Pcolce2* by PCR

(A) Schematic representation of the *Pcolce2* gene and position of the PCR primers used. **(B)** Genotyping of WT and *Pcolce2* KO mice by PCR on genomic DNA from tail biopsies and migration on a 1.2% agarose gel. **(C)** Amplification of *Pcolce2* mRNA fragments in the heart, oesophagus and skin by PCR using different pairs of primers and migration on a 1.5% agarose gel.

Then, the protein levels of PCPE-2 were checked in the heart, oesophagus and skin by Western blotting and in the skin by immunofluorescence, using three different antibodies (from Abcam, Xu et *al.* and GTX). The human recombinant protein (55 kDa) was used as a positive control; because of the instability of the recombinant protein after multiple cycles of freezing/thawing, a degradation product of around 35 kDa was observed in some blots. As already observed during our early characterization of PCPE-2 expression in mouse skin (see chapter 3), the detection of PCPE-2 in skin by Western blotting was very challenging. A very faint band around 55 kDa, at the same size as the recombinant protein, was observed in skin (***Figure 77A***). It was also present in the oesophagus, but seemed shifted towards lower molecular weights in the heart. However, more unexpectedly, this band was detected similarly in the WT and *Pcolce2* KO mice and multiple unspecific bands were observed with all three antibodies (around 250 and 130 kDa).

Since the results described above confirmed the absence of the *Pcolce2* transcript (or at least, the absence of a large part of the transcript), this suggests that the 55 kDa-band is likely unspecific. Moreover, the staining previously observed for PCPE-2 in the wounds (at day 3) was still present in the *Pcolce2* KO mice as observed on the immunofluorescence images (***Figure 77B***), suggesting that either the protein was still present in the skin, or more likely and in accordance with the Western blot analyses that the three antibodies used were unspecific in immunofluorescence analysis. More specific anti-PCPE-2 antibodies would be needed to conclusively confirm the absence of PCPE-2 protein in *Pcolce2* KO mice.

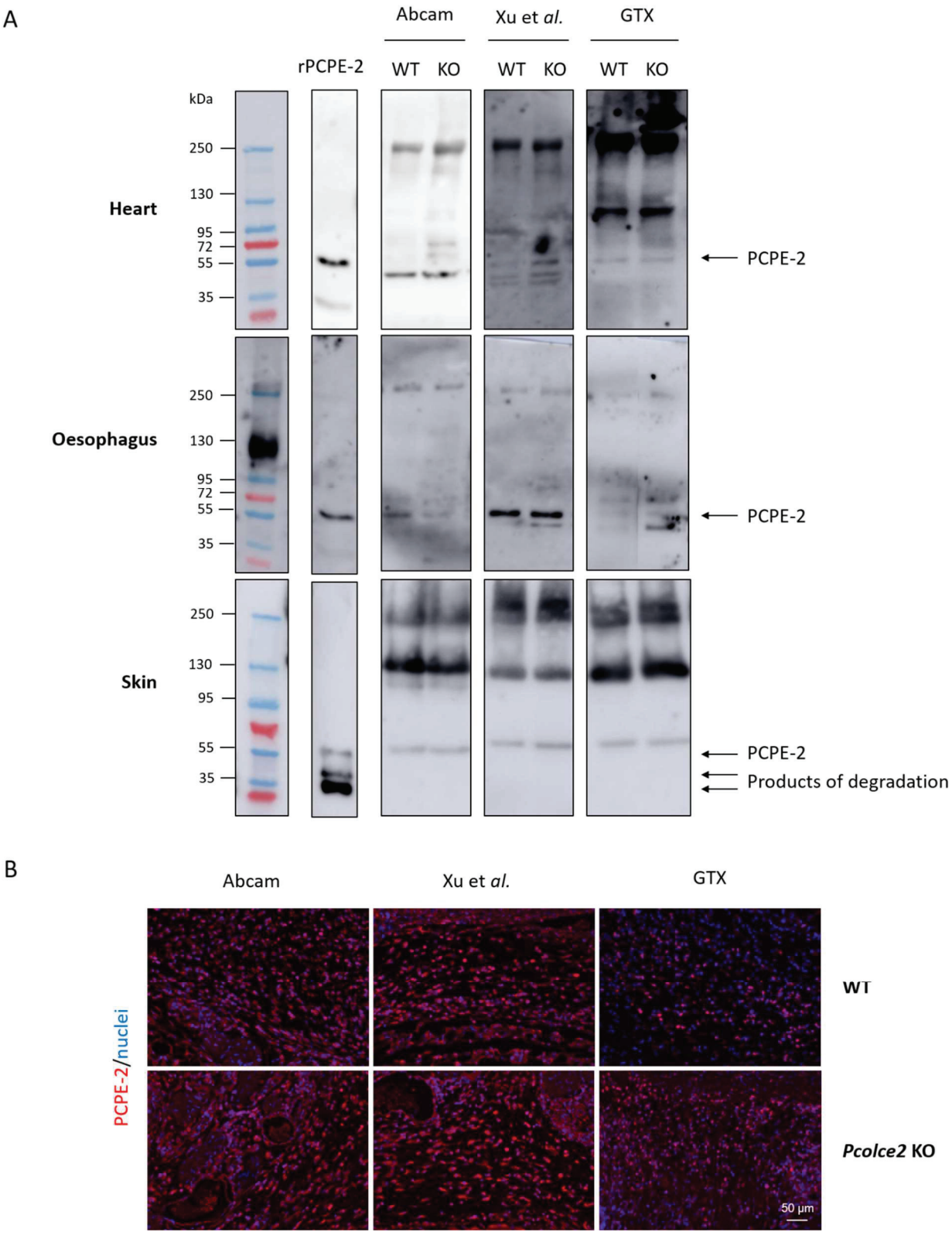

Figure 77: Detection of the PCPE-2 protein in *Pcolce2* KO mice

(A) Detection of the PCPE-2 protein by Western blotting in the heart, oesophagus and skin using three different antibodies (Abcam, Xu et *al.* and GTX; 4-15% acrylamide gel; n = 3). Unspecific bands are observed and especially, a protein similar to PCPE-2 in size is detected in WT and KO mice with the three antibodies. **(B)** Detection of the PCPE-2 protein by immunofluorescence in day 3 wounds of WT and *Pcolce2* KO mice using the same three different antibodies. The same staining is observed in WT and KO mice (representative images of n = 2).

II. Characterization of the *Pcolce2* KO skin

As already described, the *Pcolce2* KO mice were viable and fertile and did not show gross developmental abnormalities. No particular phenotype was observed in these mice and the morphology of the skin looked similar to control skin. Despite of the difficulties to confirm the absence of PCPE-2 in *Pcolce2* KO mice at the protein level, we trusted the genetic analyses and proceeded to characterize the *Pcolce2* KO model. First, we analysed the skin of these mice at the histological and molecular levels.

1) Structure of the skin

Hematoxylin and eosin (H&E) staining was done on paraffin skin sections from WT and *Pcolce2* KO mice. Histological examination of the back skin revealed no apparent differences between WT and *Pcolce2* KO mice (***Figure 78***; n = 2). The size of the epidermis and the dermis seemed similar and no aberrancy was observed in the global ECM organization using this technique.

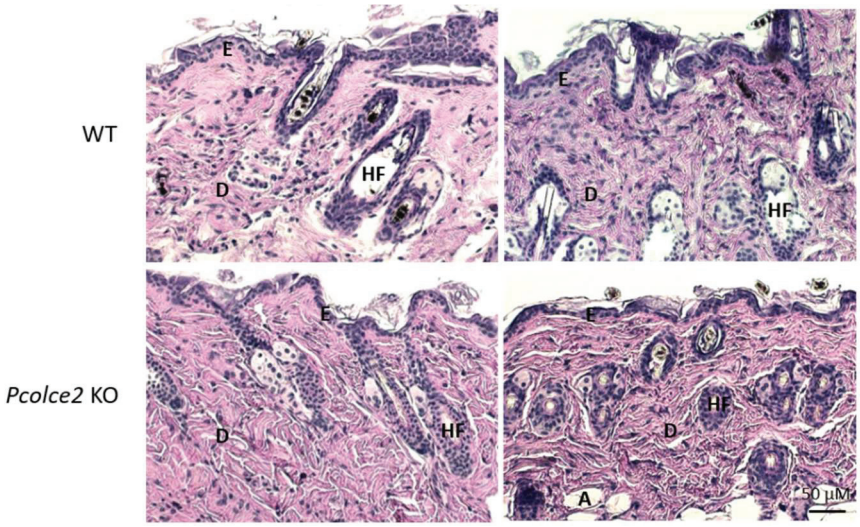

Figure 78: Structure of the *Pcolce2* KO skin by H&E staining

Hematoxylin and eosin (H&E) staining of WT and *Pcolce2* KO mouse back skin (n = 2) showing no apparent differences in the skin morphology. Scale bar: 50 µM. *E, epidermis; D, dermis; HF, hair follicle, A, adipocyte.*

2) Molecular changes

a. Expression of PCPE-1 and BTPs

We wondered if the absence of PCPE-2 could affect the expression of its homologous protein, PCPE-1 or BTPs. We analysed the expression of PCPE-1 by qRT-PCR and Western blotting, as well as the expression of BTPs by qRT-PCR (the detection of BMP/mTLD by

Western blotting being challenging with our antibodies). No significant difference in the PCPE-1 and BTP expression was observed in the absence of PCPE-2 (***Figure 79***; n = 6), suggesting that PCPE-1 does not compensate for the lack of PCPE-2 in this mouse model.

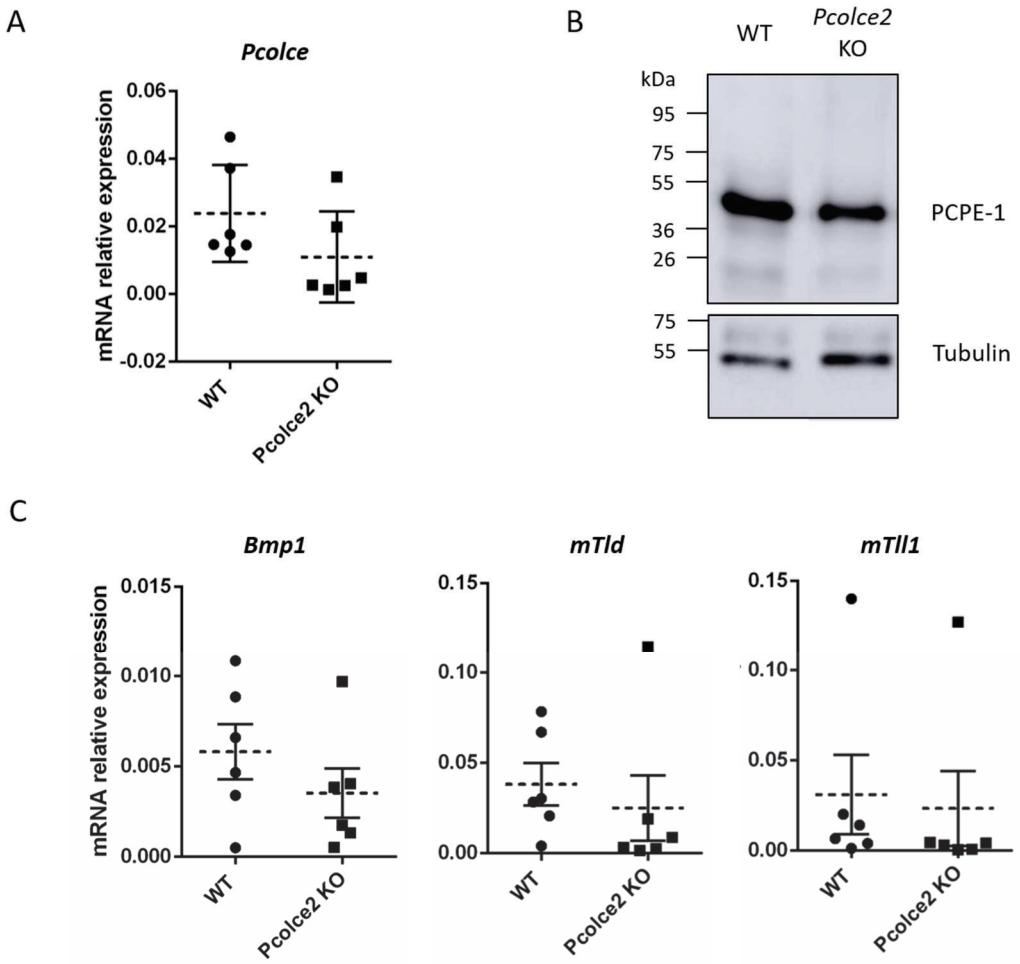

Figure 79: Expression of PCPE-1 and BTPs in *Pcolce2* KO mouse skin

(A) Relative mRNA quantification of *Pcolce* by qRT-PCR (n = 6; t-test). **(B)** Detection of PCPE-1 by Western blotting (R&D, AF2239) in skin lysates of WT and *Pcolce2* KO mice (4-15% acrylamide gel; n = 3). **(C)** Relative mRNA quantification of *Bmp1*, *mTld* and *mTll1* mRNA by qRT-PCR (n = 6; t-test).

b. Expression of other markers

We also analysed the expression of other proteins that are important for the structure of the skin, the ECM deposition or the repair process (collagen I, fibronectin, α-SMA, TSP-1, tenascin C). Among the proteins tested, we found α-SMA to be differentially expressed in the skin of *Pcolce2* KO mice. Interestingly, α-SMA protein was downregulated in the skin of *Pcolce2* KO mice compared to WT mice (***Figure 80***). By Western blotting, we observed that the intensity of the 42 kDa-band corresponding to α-SMA was significantly decreased in the skin of *Pcolce2* KO mice, compared to WT skin, while abundance of other proteins (here tenascin C or TSP-1) was unchanged. These results were confirmed by immunofluorescence in

sections of paraffin-embedded skin. In the skin of *Pcolce2* KO mice, α-SMA staining seemed to be of lower intensity and the α-SMA rich-structures corresponding to blood vessels appeared smaller than in WT skin, suggesting that PCPE-2 loss impacts skin vascularization. Quantification of α-SMA staining using ImageJ confirmed the decrease in α-SMA expression in the skin of *Pcolce2* KO mice. These findings suggest that PCPE-2 could be important for the organization of the ECM and the contractile property of the skin during wound healing, which are prime functions of α-SMA positive myofibroblasts.

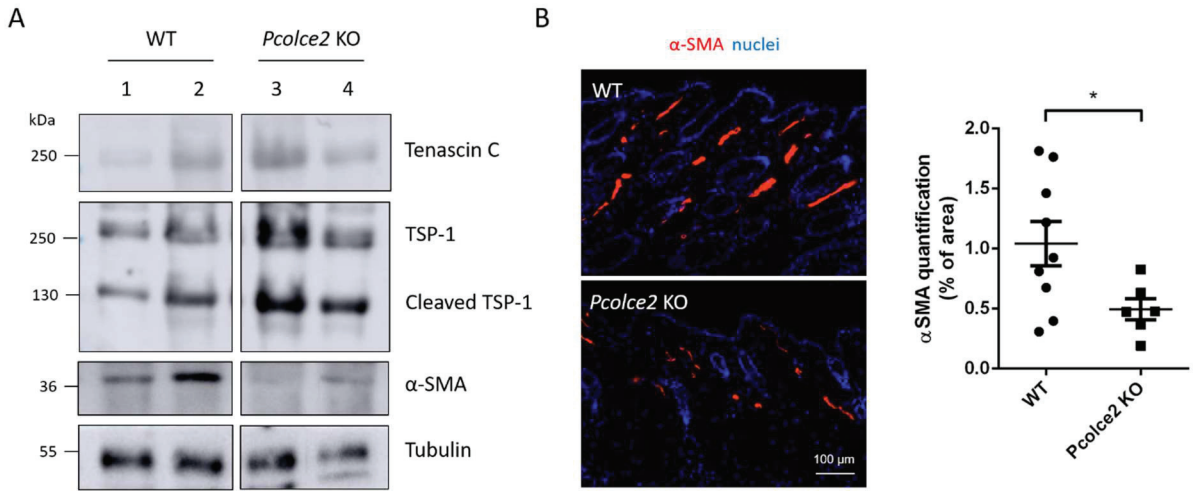

Figure 80: Expression of tenascin C, TSP-1 and α-SMA in *Pcolce2* KO mice

(A) Detection of tenascin C, TSP-1 and α-SMA in the skin of WT and *Pcolce2* KO mice by Western blotting showing a decrease in αSMA abundance in the absence of PCPE-2 (4-15% acrylamide gel; n = 3). Tubulin was used as a loading control. **(B)** Detection of α-SMA in paraffin-embedded skin from WT and *Pcolce2* KO mice by immunofluorescence using a Cy3 conjugate-antibody (Sigma, C6198). The abundance of αSMA was quantified using ImageJ (n = 2 mice, 3-6 pictures/mouse; t-test: * $p < 0.05$).

III. Wound healing assay

To investigate the role of PCPE-2 during wound healing, two full-thickness skin wounds per mouse were created on the back of WT and *Pcolce2* KO mice, as previously done (see chapter 3). The wounds were monitored and photographed at days 0, 1, 3, 5 and 7 after wounding to assess the gross wound closure (***Figure 81A***). Skin and wound samples were collected at different time points: before wounding (control skin), 3 days post-wounding (day 3) and 7 days post-wounding (day 7) for immunohistological and protein abundance analyses. The wound healing assay on *Pcolce2* KO mice was performed only once and will be replicated in the next months; preliminary results are presented in the next paragraphs.

1) Wound closure

To assess the gross wound closure in the absence of PCPE-2, the wound area was measured using ImageJ in WT and *Pcolce2* KO mice and expressed as a percentage of the total wound area, day 0 post-wound being considered as 100%. No statistically significant difference in the gross wound healing was observed between the two genotypes (***Figure 81B***; n = 12 for days 0, 1 and 3 post-wounding, n = 6 for days 5 and 7). However, there was a tendency to slower healing in the later stages (> 5 days), which must be confirmed with later time points and higher numbers of wounds. This suggests that loss of PCPE-2 does not have an obvious macroscopic effect on wound closure. However, detailed histological analyses are needed to assess potential effects on re-epithelialization, granulation tissue formation, ECM maturation, angiogenesis, inflammation and specific maturation of sub-tissues compartments.

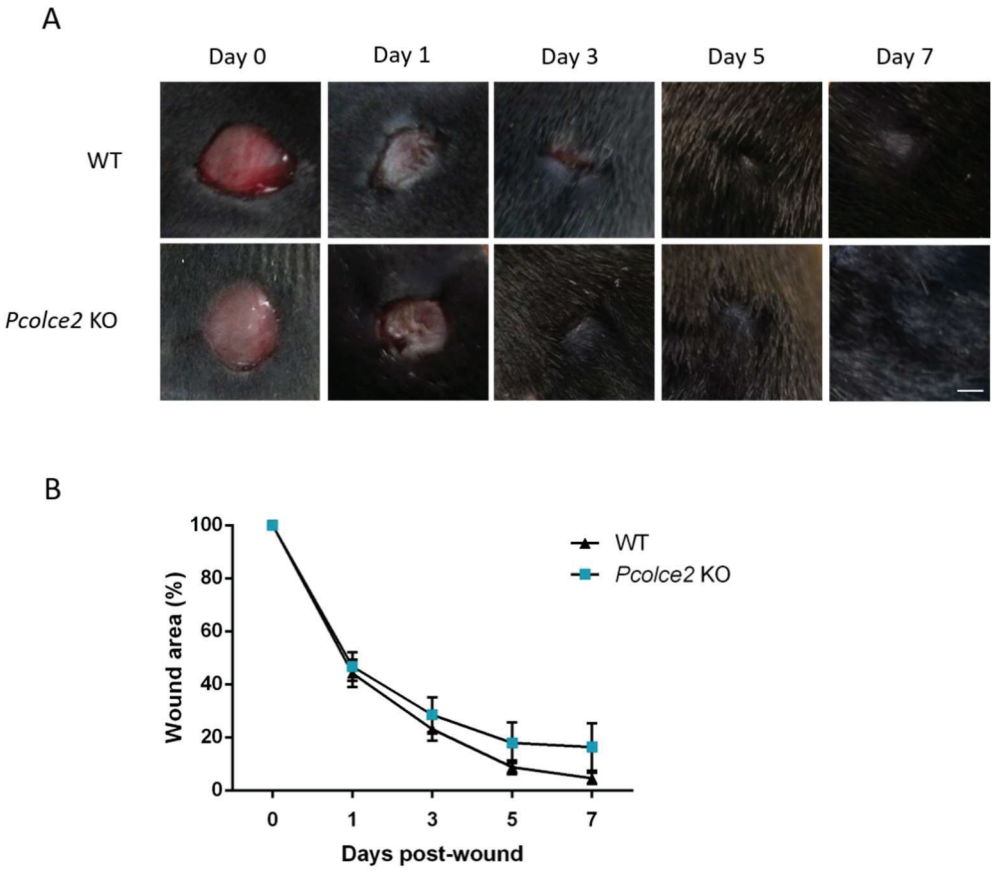

Figure 81: Wound closure in *Pcolce2* KO mice

(A) Closure of 6-mm punch biopsy wounds on the back skin of WT and Pcolce2 KO mice over time. Scale bar: 20 mm. **(B)** Quantification of the wound area using the ImageJ software (n = 12 wounds for days 0, 1 and 3 and n = 6 for days 5 and 7; ANOVA test).

2) Re-epithelialization

Re-epithelialization of the wound was analysed at day 3 post-injury in WT and *Pcolce2* KO mice. The epithelial tongue was visualized by H&E staining (***Figure 82A***) and measured using ImageJ. The length of the epithelial tongue (red arrows) was expressed as a percentage of the total wound area (black arrows). These are preliminary results as only two wounds have been used for the quantification (because of lack of time); however, these results indicated a tendency for the re-epithelialization to be decreased in the absence of PCPE-2 (***Figure 82B***), which would be in accordance with the tendency to protracted gross healing observed in 5 and 7 day-old *Pcolce2* KO wounds. To verify this observation, a larger sample size is needed. At day 7 post-injury, the analysed wounds of WT and *Pcolce2* KO mice were both completely re-epithelialized (***Figure 82C***); however, as only one WT wound and two *Pcolce2* KO wounds were investigated by H&E staining, the data are preliminary and a potential difference in granulation tissue formation cannot be excluded.

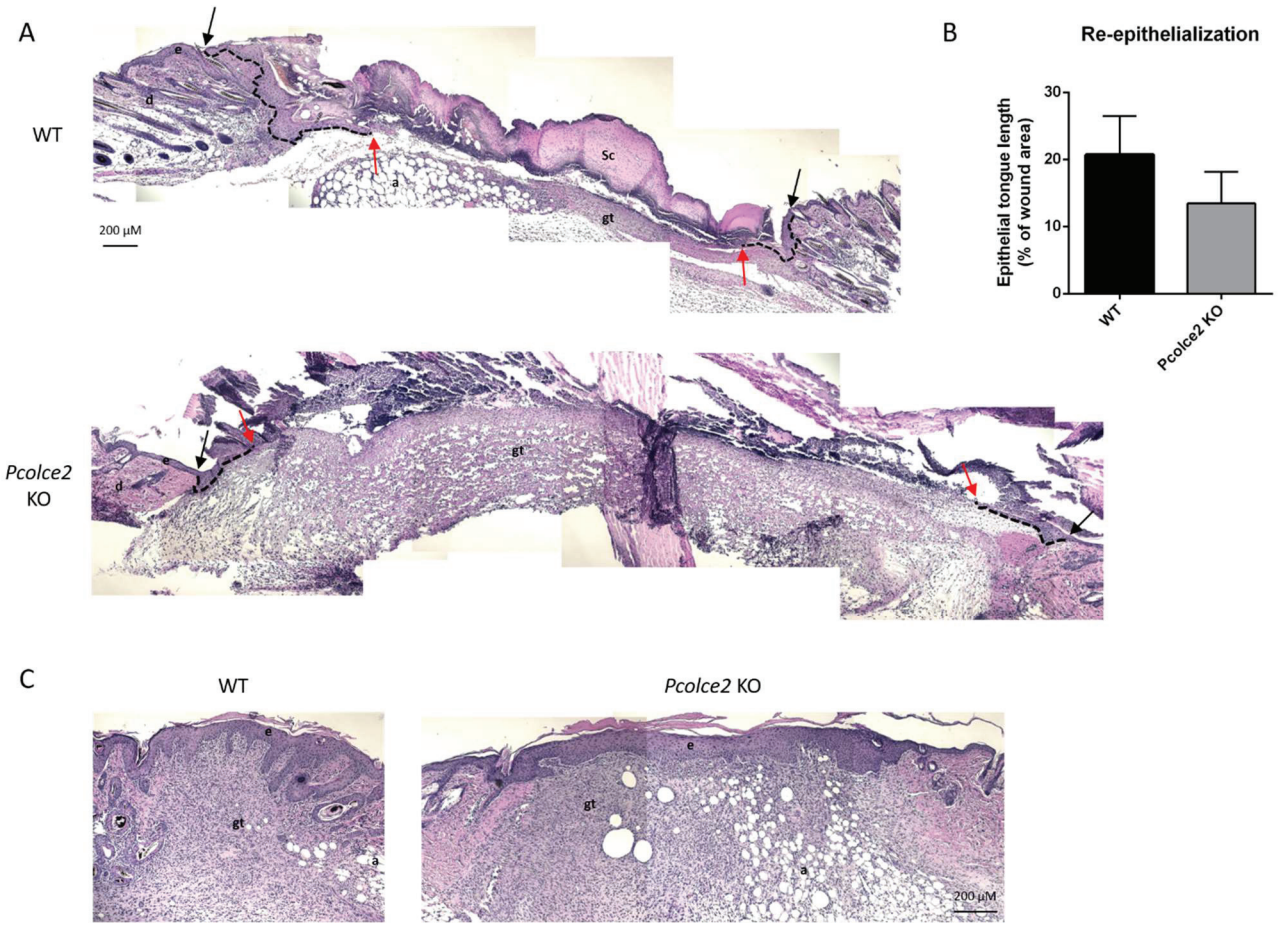

Figure 82: Re-epithelialization of the wounds days 3 and 7 post-injury

(A) H&E staining of the wounds at day 3 in WT and *Pcolce2* KO mice (black arrows delineate the initial wound borders and red arrows the epithelial front). **(B)** Quantification of percent re-epithelialization in WT and *Pcolce2* KO wounds (n = 2). **(C)** H&E staining of the wounds at day 7 in WT and *Pcolce2* KO mice (n = 1-2). *a, adipose tissue; sc, scab; d, dermis; e, epidermis; gt, granulation tissue.*

3) Infiltration of immune cells

As the inflammatory stage is a key step for a proper healing, we also analysed the infiltration of immune cells within the wounds at day 3 and day 7 post-injury. Normal skin and wounds were collected and prepared for flow cytometry analysis. Expression of various inflammatory markers was analysed: CD45 for leukocytes, CD11b for myeloid cells, Ly6G for neutrophils and F4/80 for macrophages. The amount of CD11b-positive ($CD11b^+$) cells was expressed as a percentage of the total population of $CD45^+$ leukocytes while the number of $Ly6G^+$ and $F4/80^+$ cells was expressed as a percentage of the $CD11b^+$ myeloid population (***Figure 83A***). No significant difference was observed in the number of $CD45^+$ leukocytes and $CD11b^+$ myeloid cells in the absence of PCPE-2 in normal and wounded skin. Among the myeloid subset, different subpopulations of cells were identified: $Ly6G^+$ $F4/80^-$ cells, i.e. neutrophils; $Ly6G^-$ $F4/80^+$ cells, i.e. macrophages; and another $Ly6G^{int}$ $F4/80^{int}$ population that expressed intermediate levels of Ly6G and F4/80. This later population seemed to be changed in unwounded skin in the absence of PCPE-2; *Pcolce2* KO mice showed higher levels of $Ly6G^{int}$ $F4/80^{int}$ cells than WT mice in normal skin. The markers used here are not sufficient to

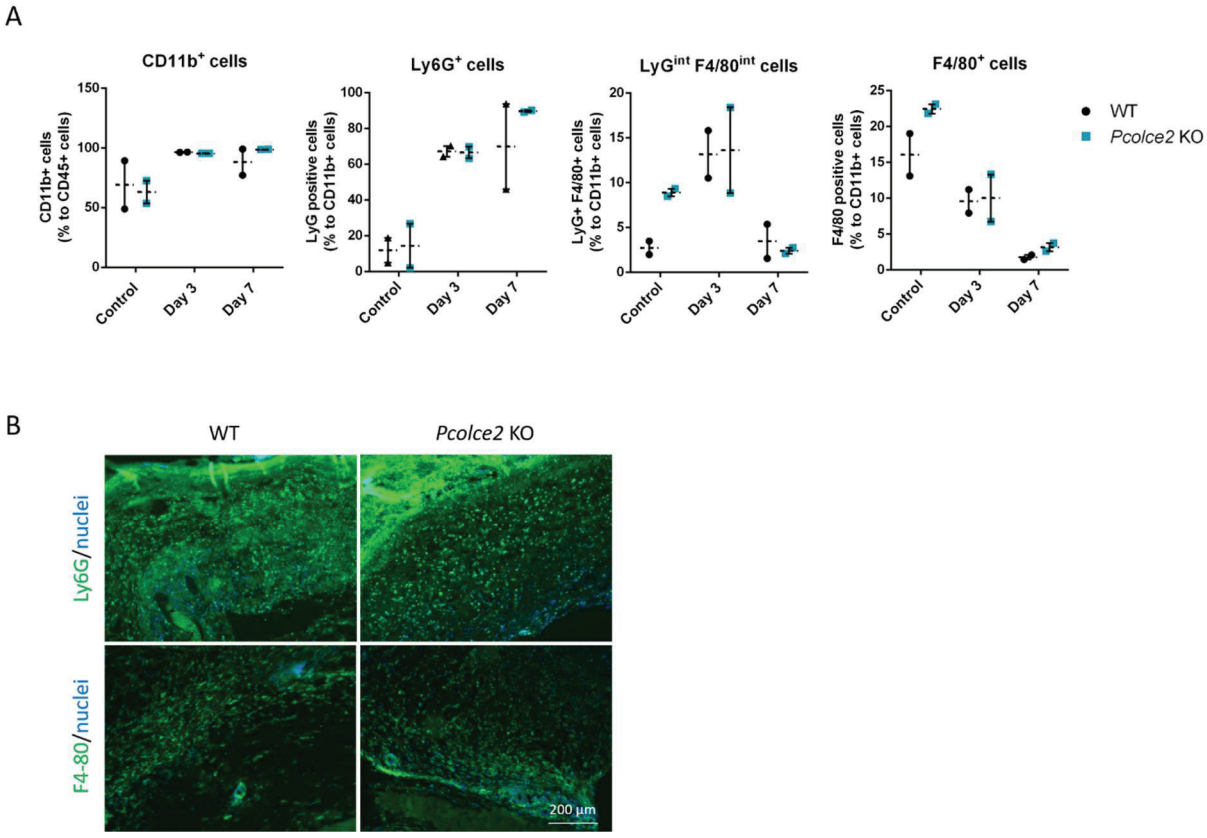

Figure 83: Recruitment of immune cells in the absence of PCPE-2

(A) Percentage of $CD11b^+$ (to $CD45^+$ cells), $Ly6G^+$ and $F4/80^+$ cells (to $CD11b^+$ cells) quantified by flow cytometry in normal and wounded skin of WT and *Pcolce2* KO mice (n = 2). **(B)** Detection of $Ly6G^+$ and $F4/80^+$ cells by immunofluorescence in day 3 wounds of WT and *Pcolce2* KO mice (n = 2).

clearly identify this Ly6G^{int} F4/80^{int} population. Based on the literature, these cells might be eosinophils, which are myeloid cells expressing both Ly6G and F4/80[245]. Further investigations will be necessary to identify this population. In addition, macrophages defined as Ly6G^{-} F4/80^{+} also appeared to be increased in unwounded *Pcolce2* KO skin. Again, no difference was seen in wounded skin. Neutrophils defined as Ly6G^{+} F4/80^{-} appeared unaltered in all conditions. Importantly, the low sample size (n = 2) limits the conclusions that can be drawn from these analyses and, in order to generate statistically meaningful data, analyses of additional samples are needed. Nevertheless, the indication that PCPE-2 deficiency did not grossly affect the ability to recruit neutrophils and macrophages to wounded skin was also supported by immunohistological analysis showing no overt differences of Ly6G^{+} and F4/80^{+} cells in 3-day WT and *Pcolce2* KO wounds (***Figure 83B***).

4) α-SMA expression

Based on the previous results in normal skin, the expression of α-SMA was analysed by Western blotting in the wounds of *Pcolce2* KO mice. As α-SMA-positive myofibroblasts start populating the wounds during the proliferative phase of wound healing, day 7 wounds were lysed for protein analysis. As previously observed in normal skin, we found αSMA to be downregulated in the wounds of *Pcolce2* KO mice by Western blotting (***Figure 84A***). Immunohistological analysis of WT and *Pcolce2* KO wounds showed that α-SMA-positive myofibroblasts were located at the edges of the wounds in *Pcolce2* KO skin and did not migrate within the wounds (***Figure 84B***). Compared to WT wounds, α-SMA staining seemed decreased in the granulation tissue of *Pcolce2* KO wounds. Again, these results are preliminary and additional analyses will be necessary to conclude about the consequences of the absence of PCPE-2. However, these first observations suggest that PCPE-2 might play a role in the formation of the granulation tissue, the consequences of which remain to be determined for the later stages of wound healing.

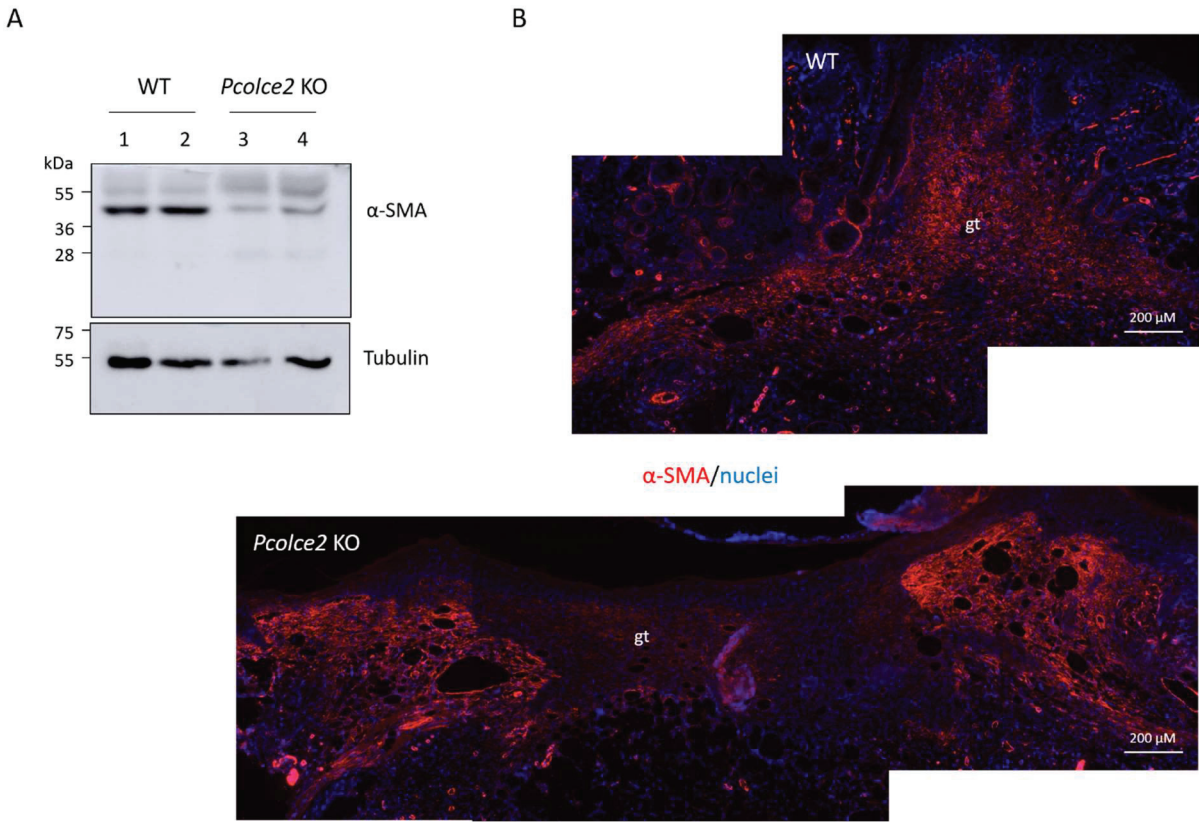

Figure 84: α-SMA expression in wounds of *Pcolce2* KO mice 7 days post-injury

(A) Detection of α-SMA in the wound lysates of WT and *Pcolce2* KO mice day 7 post-injury by Western blotting using a monoclonal mouse antibody (Sigma, A5528; 4-15% acrylamide gel; n = 2). Tubulin was used as a loading control. α-SMA is downregulated in *Pcolce2* KO mice in day 7 wounds. **(B)** Immunostaining of α-SMA (red; Sigma, C6198) in paraffin-embedded WT and *Pcolce2* KO wounds at day 7 post-injury (n = 1). *gt, granulation tissue.*

IV. Discussion

1) Technical issues encountered

In this last chapter, we analysed the role of PCPE-2 during skin wound healing using a *Pcolce2* KO mouse model. The *Pcolce2* KO line was developed by the group of C. Bleul (Max-Planck-Institute for Immunology and Epigenetics, Freiburg) and used in several studies during the last years[172,173,176,180]. Importantly, for this mouse model, PCPE-2 protein abundance has so far not been carefully analysed and none of these studies showed the absence of PCPE-2 in *Pcolce2* KO mouse tissues at the protein level. To validate the loss of the PCPE-2 protein, WT and *Pcolce2* KO mouse skin sections were stained with three different anti-PCPE-2 antibodies. To our surprise, the specific punctate staining observed in our previous studies (see chapter 3) was evidenced both in the skin of *Pcolce2* KO and WT mice. We then asked the question whether the antibodies used might give unspecific signal in mouse skin or whether the protein (or a part of the protein) might be still present. Indeed, although a large part of the exon 3 of the *Pcolce2* gene has been replaced by a neo cassette, the splice acceptor and donor of the exon are preserved making it potentially feasible that the neo cassette containing exon 3 is removed during splicing of the pre-mRNA. Unfortunately, lack of specific antibodies hampered such analysis and instead, we had to rely on a PCR-based approach. We could not detect the mRNA transcript of *Pcolce2* by PCR using three different pairs of primers located between the exons 2 and 5. Thus, these results confirmed the absence or low abundance of the *Pcolce2* transcript, which allowed us to conclude that the *Pcolce2* KO line is indeed deficient in PCPE-2.

As PCPE-2 is lowly expressed in the skin, it was challenging to detect the protein in this tissue by Western blotting and the specificity of these antibodies was tested on two other organs known to express higher levels of PCPE-2, the heart and oesophagus. Unfortunately, as discussed above, multiple cross-reacting bands were detected with the three antibodies. Although a band was detected around 55 kDa, its size was not always consistent with the size of the recombinant PCPE-2 and, above all, the signal was similar in WT and *Pcolce2* KO mice. Altogether, these findings suggest that the anti-PCPE-2 antibodies were unspecific in mouse tissues and question the reliability of the co-localization experiments previously performed (see chapter 3). Although these results were replicated in human monocyte cell lines, the mouse and human skin staining cannot be trusted and should be repeated with a highly specific anti-PCPE-2 antibody. Only few anti-PCPE-2 antibodies (that do not recognize PCPE-1) are commercially available, including the antibodies used here (Abcam and GTX). Surprisingly, Baicu and colleagues, who analysed PCPE-2 deficiency in a model of myocardial infarction, previously used the GTX antibody to detect PCPE-2 in the heart, with a strong and clear signal[180]. The

authors did not report any issue about the specificity of this antibody. In our experiments, PCPE-2 was well detected by Western blotting in primary keratinocytes and monocyte cell lines (THP-1 and U937). In these analyses, this antibody detected only one band (at the correct size) suggesting that the unspecific staining is limited to complex samples, i.e. tissues.

All these issues were encountered in the last weeks of my PhD, so we did not have time to solve the problem and to repeat the staining with reliable antibodies. However, to our knowledge, no confirmed antibodies are commercially available and this might explain the lack of data concerning the abundance of PCPE-2 in tissues. This did not preclude the preliminary investigation of the role of PCPE-2 in skin using the *Pcolce2* KO mice.

2) Consequences of the absence of PCPE-2 in skin

As previously described, the *Pcolce2* KO mice did not show any developmental abnormalities and their overall appearance was similar to WT mice. The general aspect of the skin looked comparable in WT and *Pcolce2* KO mice, but it is important to note that both PCPE-1 and PCPE-2 are expressed in skin. Potentially, PCPE-1 could compensate for the loss of PCPE-2 expression; however, its mRNA and protein expression remained unchanged in the skin in the absence of PCPE-2. This would suggest that no obvious compensation by PCPE-1 occurs in PCPE-2-deficient mice. Nevertheless, as PCPE-1 seems to be much more abundant in skin than PCPE-2, a relatively modest increase in PCPE-1 abundance could compensate for PCPE-2 loss and this would be challenging to detect by our analyses.

Wound healing experiments were then performed to evaluate the role of PCPE-2 during skin wound healing. No significant difference was observed in the general closure and the re-epithelialization of the wounds in the absence of PCPE-2, although a tendency to delayed re-epithelialization was noticed, demonstrating that PCPE-2 does not play a major role in the healing process.

To examine the general morphology of the skin, WT and *Pcolce2* KO skin were stained with hematoxylin/eosin. Both WT and *Pcolce2* KO skin morphology seemed grossly similar in uninjured skin and 7-day wounds. It is interesting to make a parallel with a recent report from Greenspan's group showing no major differences in the morphology of corneas of WT and *Pcolce* KO mice[193]. In contrast to BTPs that are essential to maintain the structure of the skin[135], the absence of PCPE-1 or PCPE-2 does not seem to affect the general morphology of ECM-rich tissues (skin, cornea).

PCPE-2, like PCPE-1, was previously reported to enhance the processing of procollagens I and II mediated by BTPs[148]. Consistent with this activity, *Pcolce2* KO mice exhibited reduced

myocardial collagen deposition in a model of pressure overload hypertrophy[180]. In our study, the extent of procollagen I processing was evaluated in normal skin and wounds of the same *Pcolce2* KO model. However, no clear evidence of decreased procollagen processing was found in the absence of PCPE-2 (data not shown). In line with our results, no change in procollagen I processing and collagen content was found in the cornea of *Pcolce* KO mice before and after injury[193]. While PCPE-1, and PCPE-2 to a lesser extent, significantly enhance the activity of BTPs *in vitro*, they seem to play a rather minor role *in vivo* (or undetectable at the analysed time points) and might be important for the proper formation of collagens fibrils and the general organization of the tissue (e.g. a role in angiogenesis for PCPE-1[193]).

Several studies have also demonstrated a specific role of PCPE-2 in lipid metabolism. Francone et *al.* showed that PCPE-2 was important for HDL maturation and functions[176]. Then, the group of M. Sorci-Thomas revealed that PCPE-2 can protect from diet-induced atherosclerosis by promoting the reverse cholesterol transport mediated by SR-BI[173]. As previously mentioned, unpublished results of the same group suggested that PCPE-2 can control adipocyte maturation by maintaining SR-BI conformation. By histological observations of the skin, we did not notice clear differences in the adipose tissue of the *Pcolce2* KO mice. Further analyses would however be necessary to investigate the role of PCPE-2 in adipose tissue formation.

Beside its role in lipid metabolism, we tried to understand the function(s) of PCPE-2 in the skin by looking at the abundance of several proteins known to play a role during wound healing. Among the proteins investigated, α-SMA was significantly downregulated in the absence of PCPE-2 in normal and wounded skin. The reduced α-SMA staining observed in normal skin might be due to reduced abundance of pericytes. A potential effect of PCPE-2 on angiogenesis should therefore be investigated. The decrease in α-SMA staining in *Pcolce2* KO wounds rather suggest that PCPE-2 might be important for the activation of fibroblasts and the quality of the granulation tissue. Preliminary immunofluorescence results suggested that the migration of myofibroblasts within the wound might be altered in the absence of PCPE-2. Noticeably, this is confirmed by Western blotting and suggests another function of PCPE-2 in the formation of the granulation tissue. However, this is too early to conclude at this stage and a higher number of wounds should be analysed to confirm this first observation. Interestingly, Massoudi and colleagues did not observe such a difference in the abundance of α-SMA in mature corneal wounds in the absence of PCPE-1[193], suggesting that this function could be specific to PCPE-2 or could be due to a transient delay in granulation tissue formation. It would

be interesting to analyse later time points to see if PCPE-2 loss has any major impact on the final scar which is formed at the end of the remodelling phase.

Finally, we found PCPE-2 to be expressed in human macrophage-like cells and wondered if the absence of PCPE-2 could affect the infiltration of neutrophils and macrophages in the wounds of *Pcolce2* KO mice. Although a controlled acute inflammatory response is necessary for proper wound healing, persistence of immune cells in the skin can be associated to skin pathologies (e.g. HTS, keloids, RDEB). Our results, though preliminary, showed that the recruitment of neutrophils and macrophages was not altered during wound healing in WT and *Pcolce2* KO mice. These experiments would need to be repeated but suggest that PCPE-2 is not necessary for the proper infiltration of immune cells within the wound.

Altogether, this study did not provide evidence for a clear role of PCPE-2 in mouse skin but points toward a role in dermal homeostasis and repair. The effects of the loss of PCPE-2 observed during wound healing are transient and rather modest and suggest that PCPE-2 does not play a major role in wound closure and the inflammatory response. Preliminary, but interesting results about α-SMA expression however suggest that PCPE-2 could be important for fibroblast activation during granulation tissue formation.

General discussion and conclusion

As “procollagen C-proteinase enhancers”, PCPE-1 and PCPE-2 are presently described as regulators of collagen fibrillogenesis. Elevated abundance of these two proteins, and mainly PCPE-1, has been extensively associated to physiological and pathological tissue repair processes (fibrosis, corneal and skin wound healing) that involve increased collagen deposition. In the last years, there was also increasing evidence that PCPE-1 can be a biomarker of fibrosis in various organs. In this context, the aims of my project were to extend our knowledge of PCPEs and to better describe their expression and role during skin wound healing.

First, using a mouse wound healing model, we showed that PCPE-1 was upregulated during the proliferative phase of wound healing and that its expression correlates with the pattern of expression and distribution of BMP-1 in the dermis (see chapter 3). Thus, this work provided the first time spatio-temporal analysis of PCPE-1 expression during skin wound healing. It suggests that PCPE-1 is an important player during the proliferation phase of skin wound healing when high amounts of collagen are being deposited to reconstitute the injured tissue. This confirms one more time the correlation between increased levels of PCPE-1 and collagen accumulation during tissue repair.

Then, based on the finding that fibroblasts are the main source of PCPE-1 in the skin (at least among the three tested cell types), we investigated the role of PCPE-1 in a PCPE-1-deficient cellular model. Expected functions included procollagen processing but also cell growth[214], protein synthesis[215] and angiogenesis[164,193,196]. Our data showed that loss of PCPE-1 does not affect the growth properties of human dermal fibroblasts, nor global protein synthesis. Expression of collagen (except type II collagen, which is usually found in cartilage) and ECM-related proteins remains largely unchanged. More surprising to us was the lack of significant effect of PCPE-1 deficiency on procollagen processing. It seems that the endogenous basal levels of PCPE-1, at least in culture conditions, only play a minor role in fibrillar collagen maturation. Interestingly however, when PCPE-1 concentration was increased by the addition of exogenous protein, the expected enhancement was clearly observed showing that PCPE-1 activity directly depends on the relative concentrations of the enhancer and its binding partners. It would thus be interesting and relevant to replicate these experiments in cells from fibroproliferative conditions (e.g. fibroblasts isolated from HTS or keloids) where PCPE-1 expression and activity are expected to be naturally increased. However, these results already lead to two important conclusions:

- PCPE-1 specificity for procollagen processing presently remains unchallenged in fibroblasts

- Decreasing PCPE-1 expression or inhibiting its activity in basal conditions has no major impact on procollagen processing.

This is actually interesting from a therapeutic perspective as specificity for a defined activity of the target and for diseased tissues (e.g. fibrotic organs where PCPE-1 is upregulated) should warrant limited side effects. In this context, the DARPins that we developed as the first antagonists of PCPE-1, in collaboration with the University of Zurich, represent very promising tools to inhibit PCPE-1 activity in various fibrotic disorders, including skin diseases. They were already used *in cellulo* in the course of my project and did not show any obvious toxicity, suggesting that these could also be used in animal models to selectively target PCPE-1 *in vivo*. DARPins (targeting VEGF and/or hepatocyte growth factor) are already in phase II and III clinical trials, for the treatment of cancer[246] and neovascular age-related macular degeneration[247] respectively. The use of DARPins targeting PCPE-1 *in vivo* is currently the subject of a new project in the group of C. Moali.

Despite these promising results, a lot of things remain to be done to fully characterize PCPE-1 functions in skin wound healing and determine if PCPE-1 is a valuable target to regulate fibrillogenesis in non-healing wounds or fibrotic scars. Especially, it will be important to functionally assess PCPE-1 in skin wound healing to see if it is indeed paramount for the regulation of collagen fibrillogenesis. This can be done through two main types of approaches: the use of transgenic mouse models (as done in chapter 6 for PCPE-2) and the development of pharmacological approaches to inhibit PCPE-1 (using DARPins or other tools). This would also offer the opportunity to have a closer look at the putative function of PCPE-1 in angiogenesis, which was not evaluated in the course of this work by lack of time. Pro-angiogenic properties would remain consistent with tissue repair and development of fibrosis as oxygen and nutrient supply is necessary for the formation of a new tissue.

Furthermore, although PCPE-1 was already found to be upregulated in fibroblasts isolated from HTS and keloids[194,195], a detailed understanding of PCPE-1 abundance in human wound healing-related pathologies (e.g. RDEB wounds, HTS and keloid scars) would be important. It would actually help us to determine the best indications to optimize a potential treatment based on the modulation of PCPE-1 activity.

The study of PCPE-2 was more challenging as some issues were encountered with the specificity of antibodies and the production of the recombinant proteins. We showed that PCPE-2 is scarcely expressed in skin, with a low expression in fibroblasts and a higher expression in keratinocytes (see chapter 3). This was the first evidence of distinct differences between PCPE-2 and PCPE-1, which is almost exclusively expressed in fibroblasts. Moreover, PCPE-2 appears to be expressed in myeloid cells, together with BTPs, while PCPE-1 is not. These differences in cellular distributions are consistent with the differential effects of PCPEs observed *in vitro* on procollagen processing (see chapter 5). Indeed, recombinant PCPE-2 seems to be a very weak enhancer of major fibrillar procollagens (I-III) processing. Strikingly, PCPE-2 seems to even compete with its homologous protein PCPE-1 in these assays, leading to an inhibition of its enhancing effect. In parallel, PCPE-2 appears to directly inhibit BMP-1 activity, preventing the processing of non-collagenous substrates and minor fibrillar collagens (***Figure 85***).

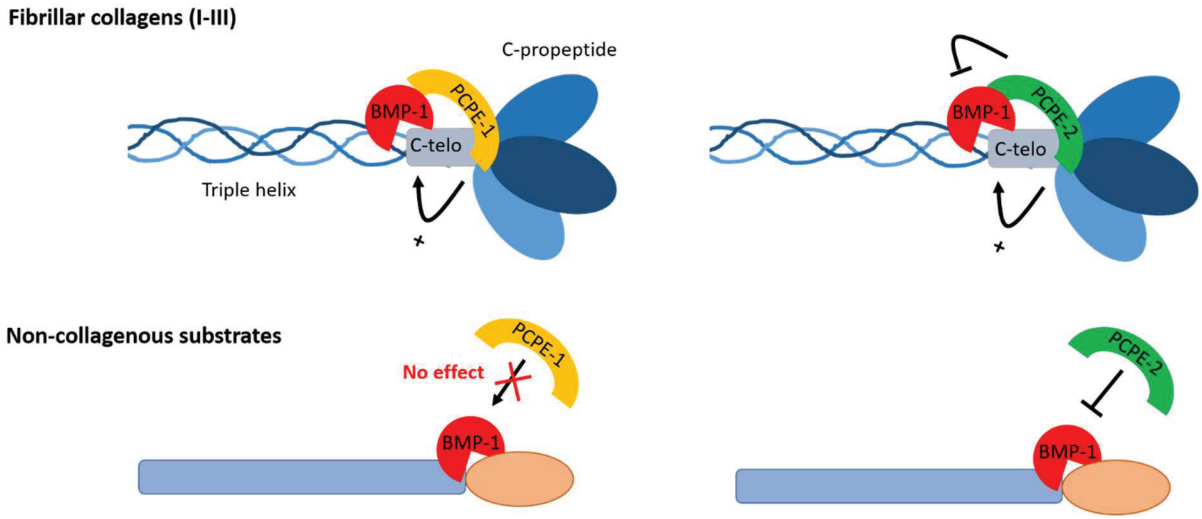

Figure 85: Possible model to explain *in vitro* functions of PCPE-2 on BMP-1 activity

Our present hypothesis to explain these apparently confusing results is that the way PCPE-2 interacts with the procollagen maturation complex is only partially conserved with PCPE-1. Exactly like PCPE-1, it can probably bind to the C-propeptide of collagens I-III through its CUB domains. This is actually supported by the recent resolution of the crystal structure of the complex between the CUB domains of PCPE-1 and the collagen III C-propeptide (Pulido-Gomez et *al.* submitted) which shows that all the major interaction sites involved in complex formation on the PCPE-1 side are also conserved in PCPE-2 (***Figure 19*** and ***Figure 86***). What differs between the two isoforms could be their interaction with the protease. Whereas PCPE-1 only develops weak interactions with BMP-1 (at least in the absence

of substrate[161]) with no obvious direct effect on non-collagenous substrates, it seems that PCPE-2 can directly bind the protease in a way that leads to direct protease inhibition. This is shown by the inhibition of a large panel of substrates including small peptides (see chapter 5). In the case of major fibrillar procollagens, these two combined interactions lead to complex effects on procollagen processing (such as bell-shaped curves for procollagen III) with a weak enhancement at low PCPE-2 concentrations (reflecting dominant enhancement through PCPE/procollagen interaction) and inhibition/no effect at higher concentrations (reflecting dominant inhibition of BMP-1 activity). This model has to be confirmed through the analysis of PCPE-2 interaction with BMP-1 by SPR. However, since previously identified BMP-1 inhibitors are either broad-spectrum (α2-macroglobulin), or controversial (BMP-4 and SFRPs), our results describe PCPE-2 as the first specific endogenous inhibitor of BMP-1 in humans.

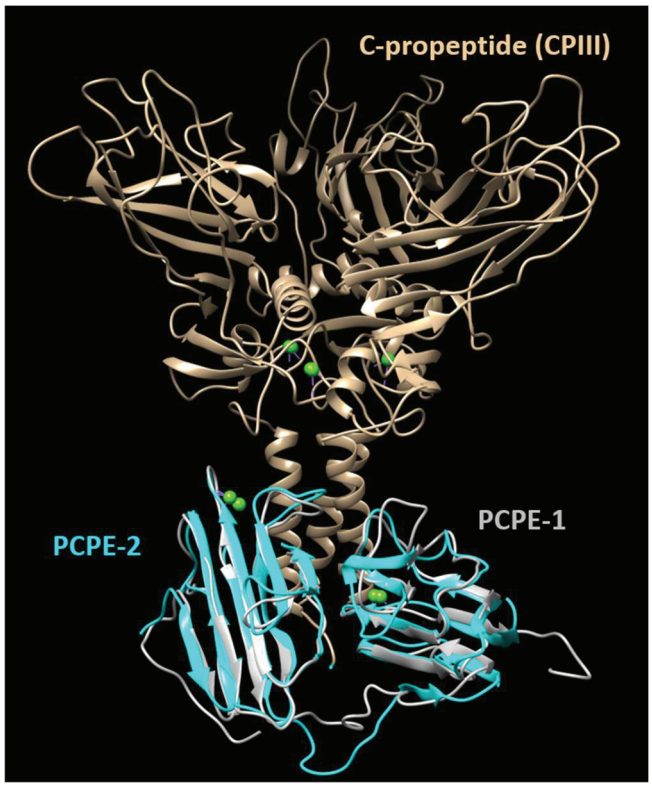

Figure 86: Superposition of CUB domains of PCPE-2 and the CPIII-PCPE-1 structure

The model of CUB1-CUB2 domains of PCPE-2 (blue) was performed by Emmanuel Bettler (IBCP, Lyon) and superimposed with the CPIII-PCPE-1 structure (grey; Pulido-Gomez et *al.* submitted). Similar complex between CPIII and PCPE-2 is likely to occur, as the structure and the sites important for the interactions are conserved between the CUB1-CUB2 domains of PCPE-1 and PCPE-2. Calcium ions are represented as green spheres.

Finally, the *in vivo* role of PCPE-2 was investigated using a murine KO model of *Pcolce2* (see chapter 6). Interestingly, the loss of PCPE-2 is not compensated by PCPE-1 in mice and does not strongly affect the morphology of unchallenged skin. However, a decrease in α-SMA expression was observed around vessel-like structures in normal *Pcolce2* KO skin suggesting that the abundance of pericytes might be reduced. Further investigations will be necessary to determine if PCPE-2 can play a role in vascular development and homeostasis, as PCPE-1 could also do, even if the mechanism is unknown.

Based on the expression studies of chapter 3 (PCPE-2 expressed by myeloid cells) and the functional exploration of chapter 5 (showing broad inhibition of BMP-1/PCPE-1 activities by PCPE-2), one possible role for PCPE-2 could have been to prevent premature formation of the granulation tissue by BMP-1 and PCPE-1 during the inflammatory phase. In addition to ECM deposition, BMP-1 also controls the activity of TGF-β[117,242] (Article 2, Anastasi et *al.* submitted) which is known to be a potent anti-inflammatory growth factor and should be kept silent during the early days of the wound healing process. However, this hypothesis could not be confirmed yet by our wound healing experiments. Expression of PCPE-2 remained unchanged at the mRNA level and the lack of specific anti-PCPE-2 antibodies hindered the analysis of the distribution of the protein in skin (see chapters 3 and 6). With the low number of replicates that could be analysed, no significant differences were observed in the wound healing experiments performed with the *Pcolce2* KO mice, although a tendency of a decreased re-epithelialization was noticed. Noteworthy however, preliminary results suggested that the migration of α-SMA-positive myofibroblasts might be altered in wounds of *Pcolce2* KO mice; whether this a direct consequence of the loss of PCPE-2 remains unknown and warrants further investigations. These data are preliminary and wound healing experiments will be replicated to better understand the function(s) of PCPE-2 in skin and its potential role during wound healing.

Altogether, these findings lead to new and unexpected perspectives about the role of PCPE-2 and strongly suggest that PCPE-1 and PCPE-2 might have different functions *in vivo*.

Bibliography

1. Ventrelli, L., Marsilio Strambini, L. & Barillaro, G. Microneedles for Transdermal Biosensing: Current Picture and Future Direction. *Adv. Healthc. Mater.* **4,** 2606–2640 (2015).
2. Wickett, R. R. & Visscher, M. O. Structure and function of the epidermal barrier. *Am. J. Infect. Control* **34,** S98–S110 (2006).
3. Lai-Cheong, J. E. & McGrath, J. A. Structure and function of skin, hair and nails. *Med. (United Kingdom)* **41,** 317–320 (2013).
4. Breitkreutz, D., Mirancea, N. & Nischt, R. Basement membranes in skin: Unique matrix structures with diverse functions? *Histochem. Cell Biol.* **132,** 1–10 (2009).
5. Blanpain, C. & Fuchs, E. Epidermal homeostasis: a balancing act of stem cells in the skin. *Nat. Rev. Mol. Cell Biol.* **10,** 207–217 (2009).
6. Wei, J. C. J. *et al.* Allometric scaling of skin thickness, elasticity, viscoelasticity to mass for micro-medical device translation: from mice, rats, rabbits, pigs to humans. *Sci. Rep.* **7,** 15885 (2017).
7. Eckert, R. L. & Rorke, E. A. Molecular biology of keratinocyte differentiation. *Environmental Health Perspectives* **80,** 109–116 (1989).
8. Eckhart, L., Lippens, S., Tschachler, E. & Declercq, W. Cell death by cornification. *Biochim. Biophys. Acta - Mol. Cell Res.* **1833,** 3471–3480 (2013).
9. Skobe, M. & Detmar, M. Structure, function, and molecular control of the skin lymphatic system. *J. Investig. Dermatol. Symp. Proc.* **5,** 14–9 (2000).
10. Schmidt, E. & Zillikens, D. Pemphigoid diseases. *Lancet* **381,** 320–332 (2013).
11. Borradori, L. & Sonnenberg, A. Structure and function of hemidesmosomes: more than cimple adhesion complexes. *J. Invest. Dermatol.* **112,** 411–418 (1999).
12. Bruckner-Tuderman, L. Hereditary skin diseases of anchoring fibrils. in *Journal of Dermatological Science* **20,** 122–133 (1999).
13. Aumailley, M., Has, C., Tunggal, L. & Bruckner-Tuderman, L. Molecular basis of inherited skin-blistering disorders, and therapeutic implications. *Expert Rev. Mol. Med.* **8,** 1–21 (2006).
14. Limbert, G. Mathematical and computational modelling of skin biophysics: a review. *Proc. R. Soc. A Math. Phys. Eng. Sci.* **473,** 20170257 (2017).
15. Lawlor, K. & Kaur, P. Dermal contributions to human interfollicular epidermal architecture and self-renewal. *Int. J. Mol. Sci.* **16,** 28098–28107 (2015).
16. Sorrell, J. M. Fibroblast heterogeneity: More than skin deep. *J. Cell Sci.* **117,** 667–675 (2004).
17. Baldock, C. *et al.* Shape of tropoelastin, the highly extensible protein that controls human tissue elasticity. *Proc. Natl. Acad. Sci.* **108,** 4322–4327 (2011).
18. Cooper, G. M. & Hausman, R. E. The cell: A molecular approach. 2nd Edition. *Sinauer Associates* 1–820 (2000).
19. Yanagishita, M. Function of proteoglycans in the extracellular matrix. *Acta Pathol. Jpn.* **43,** 283–293 (1993).
20. Iozzo, R. V. & Schaefer, L. Proteoglycan form and function: A comprehensive nomenclature of proteoglycans. *Matrix Biol.* **42,** 11–55 (2015).
21. Smith, M. M. & Melrose, J. Proteoglycans in normal and healing skin. *Adv. Wound Care* **4,** 152–173 (2015).
22. Nomura, Y. Structural change in decorin with skin aging. *Connect. Tissue Res.* **47,** 249–255 (2006).
23. Nastase, M. V., Young, M. F. & Schaefer, L. Biglycan. *J. Histochem. Cytochem.* **60,** 963–975 (2012).
24. Klingberg, F., Hinz, B. & White, E. S. The myofibroblast matrix: Implications for tissue repair and fibrosis. *J. Pathol.* **229,** 298–309 (2013).
25. Pasparakis, M., Haase, I. & Nestle, F. O. Mechanisms regulating skin immunity and inflammation. *Nat. Rev. Immunol.* **14,** 289–301 (2014).

26. Crowther, M., Brown, N. J., Bishop, E. T. & Lewis, C. E. Microenvironmental influence on macrophage regulation of angiogenesis in wounds and malignant tumors. *J. Leukoc. Biol.* **70,** 478–90 (2001).
27. Davies, L. C., Jenkins, S. J., Allen, J. E. & Taylor, P. R. Tissue-resident macrophages. *Nat. Immunol.* **14,** 986–995 (2013).
28. Rőszer, T. Understanding the mysterious M2 macrophage through activation markers and effector mechanisms. *Mediators Inflamm.* **2015,** 1–16 (2015).
29. Nestle, F. O., Di Meglio, P., Qin, J.-Z. & Nickoloff, B. J. Skin immune sentinels in health and disease. *Nat. Rev. Immunol.* **9,** 679–91 (2009).
30. Janssens, A. S. *et al.* Mast cell distribution in normal adult skin. *J. Clin. Pathol.* **58,** 285–9 (2005).
31. Harvima, I. T. & Nilsson, G. Mast cells as regulators of skin inflammation and immunity. *Acta Derm. Venereol.* **91,** 644–650 (2011).
32. Choe, S. S., Huh, J. Y., Hwang, I. J., Kim, J. I. & Kim, J. B. Adipose tissue remodeling: Its role in energy metabolism and metabolic disorders. *Front. Endocrinol. (Lausanne).* **7,** 1–16 (2016).
33. Boulais, N. & Misery, L. The epidermis: A sensory tissue. *Eur. J. Dermatol.* **18,** 119–27 (2008).
34. Schneider, M. R., Schmidt-Ullrich, R. & Paus, R. The hair follicle as a dynamic miniorgan. *Current Biology* **19,** (2009).
35. Balañá, M. E., Charreau, H. E. & Leirós, G. J. Epidermal stem cells and skin tissue engineering in hair follicle regeneration. *World J. Stem Cells* **7,** 711–27 (2015).
36. Khavari, P. A. Modelling cancer in human skin tissue. *Nat. Rev. Cancer* **6,** 270–80 (2006).
37. Gerber, P. A. *et al.* The top skin-associated genes: A comparative analysis of human and mouse skin transcriptomes. *Biol. Chem.* **395,** 577–591 (2014).
38. Naldaiz-Gastesi, N. *et al.* Identification and characterization of the dermal panniculus carnosus muscle stem cells. *Stem Cell Reports* **7,** 411–424 (2016).
39. Wojciechowicz, K., Gledhill, K., Ambler, C. A., Manning, C. B. & Jahoda, C. A. B. Development of the mouse dermal adipose layer occurs independently of subcutaneous adipose tissue and is marked by restricted early expression of FABP4. *PLoS One* **8,** 1–15 (2013).
40. Mestas, J. & Hughes, C. C. W. Of mice and not men: differences between mouse and human immunology. *J. Immunol.* **172,** 2731–2738 (2004).
41. Havran, W. L. & Jameson, J. M. Epidermal T cells and wound healing. *J. Immunol.* **184,** 5423–5428 (2010).
42. Macleod, A. S. *et al.* Dendritic epidermal T cells regulate skin antimicrobial barrier function. *J. Clin. Invest.* **123,** 4364–4374 (2013).
43. Zomer, H. D. & Trentin, A. G. Skin wound healing in humans and mice: Challenges in translational research. *J. Dermatol. Sci.* (2017). doi:10.1016/j.jdermsci.2017.12.009
44. Epstein, F. H., Singer, A. J. & Clark, R. A. F. Cutaneous Wound Healing. *N. Engl. J. Med.* **341,** 738–746 (1999).
45. Gurtner, G. C., Werner, S., Barrandon, Y. & Longaker, M. T. Wound repair and regeneration. *Nature* **453,** 314–321 (2008).
46. Guo, S. & DiPietro, L. A. Factors affecting wound healing. *J. Dent. Res.* **89,** 219–229 (2010).
47. Leoni, G., Neumann, P.-A., Sumagin, R., Denning, T. L. & Nusrat, A. Wound repair: role of immune–epithelial interactions. *Mucosal Immunol.* **8,** 959–968 (2015).
48. Koh, T. J. & DiPietro, L. A. Inflammation and wound healing: The role of the macrophage. *Expert Rev. Mol. Med.* **13,** e23 (2011).
49. Landén, N. X., Li, D. & Ståhle, M. Transition from inflammation to proliferation: A critical step during wound healing. *Cell. Mol. Life Sci.* **73,** 3861–3885 (2016).

50. Strbo, N., Yin, N. & Stojadinovic, O. Innate and adaptive immune responses in wound epithelialization. *Adv. wound care* **3,** 492–501 (2014).
51. Pastar, I. *et al.* Epithelialization in wound healing: A comprehensive review. *Adv. Wound Care* **3,** 445–464 (2014).
52. Hinz, B. Myofibroblasts. *Exp. Eye Res.* **142,** 56–70 (2016).
53. Brenmoehl, J. Transforming growth factor-beta 1 induces intestinal myofibroblast differentiation and modulates their migration. *World J. Gastroenterol.* **15,** 1431 (2009).
54. Midgley, A. C. *et al.* Transforming Growth Factor-Beta 1 (TGF-Beta 1)-stimulated Fibroblast to Myofibroblast Differentiation Is Mediated by Hyaluronan (HA)-facilitated Epidermal Growth Factor Receptor (EGFR) and CD44 Co-localization in Lipid Rafts. *J. Biol. Chem.* **288,** 14824–14838 (2013).
55. Ucuzian, A. A., Gassman, A. A., East, A. T. & Greisler, H. P. Molecular mediators of angiogenesis. *J. Burn Care Res.* **31,** 158–175 (2010).
56. Guest, J. F. *et al.* Health economic burden that wounds impose on the National Health Service in the UK. *BMJ Open* **5,** e009283 (2015).
57. Graves, N. & Zheng, H. Modelling the direct health care costs of chronic wounds in Australia. *Wound Pract. Res.* **22,** 20–33 (2014).
58. Demidova-Rice, T. N., Hamblin, M. R. & Herman, I. M. Acute and impaired wound healing. *Adv. Skin Wound Care* **25,** 304–314 (2012).
59. Nunan, R., Harding, K. G. & Martin, P. Clinical challenges of chronic wounds: searching for an optimal animal model to recapitulate their complexity. *Dis. Model. Mech.* **7,** 1205–13 (2014).
60. Ogawa, R. Keloid and hypertrophic scars are the result of chronic inflammation in the reticular dermis. *Int. J. Mol. Sci.* **18,** 606 (2017).
61. Wolfram, D., Tzankov, A., Pülzl, P. & Piza-Katzer, H. Hypertrophic scars and keloids - A review of their pathophysiology, risk factors, and therapeutic management. *Dermatologic Surg.* **35,** 171–181 (2009).
62. Rabello, F., Souza, C. & Farina Jr, J. Update on hypertrophic scar treatment. *Clinics* **69,** 565–573 (2014).
63. Akaishi, S., Ogawa, R. & Hyakusoku, H. Keloid and hypertrophic scar: Neurogenic inflammation hypotheses. *Med. Hypotheses* **71,** 32–38 (2008).
64. Huang, C., Murphy, G. F., Akaishi, S. & Ogawa, R. Keloids and hypertrophic scars. *Plast. Reconstr. Surg. Glob. Open* **1,** e25 (2013).
65. Dong, X., Zhang, C., Ma, S. & Wen, H. Mast cell chymase in keloid induces profibrotic response via transforming growth factor-β1/Smad activation in keloid fibroblasts. *Int. J. Clin. Exp. Pathol.* **7,** 3596–3607 (2014).
66. Exposito, J.-Y., Valcourt, U., Cluzel, C. & Lethias, C. The fibrillar collagen family. *Int. J. Mol. Sci.* **11,** 407–426 (2010).
67. Mouw, J. K., Ou, G. & Weaver, V. M. Extracellular matrix assembly: a multiscale deconstruction. *Nat. Rev. Mol. Cell Biol.* **15,** 771–785 (2014).
68. Chung, H. J. & Uitto, J. Type VII collagen: The anchoring fibril protein at fault in dystrophic epidermolysis bullosa. *Dermatol. Clin.* **28,** 93–105 (2010).
69. Ricard-Blum, S. The collagen family. *Cold Spring Harb. Perspect. Biol.* **3,** a004978–a004978 (2011).
70. Grässel, S., Unsöld, C., Schäcke, H., Bruckner-Tuderman, L. & Bruckner, P. Collagen XVI is expressed by human dermal fibroblasts and keratinocytes and is associated with the microfibrillar apparatus in the upper papillary dermis. *Matrix Biol.* **18,** 309–317 (1999).
71. Agarwal, P. *et al.* Collagen XII and XIV, new partners of cartilage oligomeric matrix protein in the skin extracellular matrix suprastructure. *J. Biol. Chem.* **287,** 22549–22559 (2012).
72. Myllyharju, J. Collagens, modifying enzymes and their mutations in humans, flies and

worms. *Trends Genet.* **20,** 33–43 (2004).
73. Kant, R., Bali, A., Singh, N. & Jaggi, A. S. Prolyl 4 hydroxylase: A critical target in the pathophysiology of diseases. *Korean Journal of Physiology and Pharmacology* **17,** 111–120 (2013).
74. Hosper, N. A., Bank, R. A. & van den Berg, P. P. Human amniotic fluid-derived mesenchymal cells from fetuses with a neural tube defect do not deposit collagen type I protein after TGF-β1 stimulation in vitro. *Stem Cells Dev.* **23,** 555–562 (2014).
75. Vadon-Le Goff, S., Hulmes, D. J. S. & Moali, C. BMP-1/tolloid-like proteinases synchronize matrix assembly with growth factor activation to promote morphogenesis and tissue remodeling. *Matrix Biol.* **44–46,** 14–23 (2015).
76. Broder, C. *et al.* Metalloproteases meprin α and meprin β are C- and N-procollagen proteinases important for collagen assembly and tensile strength. *Proc. Natl. Acad. Sci. U. S. A.* **110,** 14219–24 (2013).
77. Suzuki, N. *et al.* Failure of ventral body wall closure in mouse embryos lacking a procollagen C-proteinase encoded by Bmp1, a mammalian gene related to Drosophila tolloid. *Development* **122,** 3587–3595 (1996).
78. Pappano, W. N., Steiglitz, B. M., Scott, I. C., Keene, D. R. & Greenspan, D. S. Use of Bmp1/Tll1 doubly homozygous null mice and proteomics to identify and validate in vivo substrates of bone morphogenetic protein 1/tolloid-like metalloproteinases. *Mol. Cell. Biol.* **23,** 4428–38 (2003).
79. Bekhouche, M. & Colige, A. The procollagen N-proteinases ADAMTS2, 3 and 14 in pathophysiology. *Matrix Biol.* **44–46,** 46–53 (2015).
80. Papke, C. L. *et al.* Loss of fibulin-4 disrupts collagen synthesis and maturation: Implications for pathology resulting from EFEMP2 mutations. *Hum. Mol. Genet.* **24,** 5867–5879 (2015).
81. Chen, S. & Birk, D. E. The regulatory roles of small leucine-rich proteoglycans in extracellular matrix assembly. *FEBS J.* **280,** 2120–2137 (2013).
82. Kalamajski, S. *et al.* Increased C-telopeptide cross-linking of tendon type I collagen in fibromodulin-deficient mice. *J. Biol. Chem.* **289,** 18873–18879 (2014).
83. Birk, D. . Type V collagen: Heterotypic type I/V collagen interactions in the regulation of fibril assembly. *Micron* **32,** 223–237 (2001).
84. Liu, X., Wu, H., Byrne, M., Krane, S. & Jaenisch, R. Type III collagen is crucial for collagen I fibrillogenesis and for normal cardiovascular development. *Proc. Natl. Acad. Sci.* **94,** 1852–1856 (1997).
85. Eyre, D., Weis, M. & Wu, J.-J. Articular cartilage collagen: An irreplaceable framework? *Eur. Cells Mater.* **12,** 57–63 (2006).
86. Wu, J.-J., Weis, M. A., Kim, L. S., Carter, B. G. & Eyre, D. R. Differences in chain usage and cross-linking specificities of cartilage type V/XI collagen isoforms with age and tissue. *J. Biol. Chem.* **284,** 5539–5545 (2009).
87. Wozney, J. M. *et al.* Novel Regulators of Bone Formation : Molecular Clones and Activities Linked references are available on JSTOR for this article : Novel Regulators of Bone Formation : Molecular Clones and Activities. *Science (80-.).* **242,** 1528–1534 (1988).
88. Shimell, M. J., Ferguson, E. L., Childs, S. F. & Michael, B. O. The Drosophila Dorsal-Ventral Patterning Gene tolloid Is Related to Human Bone Morphogenetic Protein 1. *Cell* **67,** 469–481 (1991).
89. Takahara, K., Lyons, G. E. & Greenspan, D. S. Bone morphogenetic protein-1 and a mammalian tolloid homologue (mTld) are encoded by alternatively spliced transcripts which are differentially expressed in some tissues. *J. Biol. Chem.* **269,** 32572–32578 (1994).
90. Scott, I. C. *et al.* Mammalian BMP-1/tolloid-related metalloproteinases, including novel family member mammalian tolloid-like 2, have differential enzymatic activities and

distributions of expression relevant to patterning and skeletogenesis. *Dev. Biol.* **213,** 283–300 (1999).
91. Ge, G. & Greenspan, D. S. Developmental roles of the BMP1/TLD metalloproteinases. *Birth Defects Res. Part C Embryo Today Rev.* **78,** 47–68 (2006).
92. Clark, T. G. *et al.* The mammalian tolloid-like 1 gene, Tll1, is necessary for normal septation and positioning of the heart. *Development* **126,** 2631–42 (1999).
93. Kessler, E., Takahara, K., Biniaminov, L., Brusel, M. & Greenspan, D. S. Bone morphogenetic protein-1: The type I procollagen C-proteinase. *Science.* **271,** 360–362 (1996).
94. Hopkins, D. R., Keles, S. & Greenspan, D. S. The bone morphogenetic protein 1/Tolloid-like metalloproteinases. *Matrix Biol.* **26,** 508–523 (2007).
95. Yamada, Y., Mudryj, M. & de Crombrugghe, B. A uniquely conserved regulatory signal is found around the translation initiation site in three different collagen genes. *J. Biol. Chem.* **258,** 14914–9 (1983).
96. Kessler, E., Fichard, A., Chanut-Delalande, H., Brusel, M. & Ruggiero, F. Bone morphogenetic protein-1 (BMP-1) mediates C-terminal processing of procollagen V homotrimer. *J. Biol. Chem.* **276,** 27051–27057 (2001).
97. Gopalakrishnan, B., Wang, W.-M. & Greenspan, D. S. Biosynthetic processing of the pro-α1(V)pro-α2(V)pro-α3(V) procollagen heterotrimer. *J. Biol. Chem.* **279,** 30904–30912 (2004).
98. Bonod-Bidaud, C. *et al.* Enzymatic cleavage specificity of the proα1(V) chain processing analysed by site-directed mutagenesis. *Biochem. J.* **405,** 299–306 (2007).
99. Pappano, W. N., Steiglitz, B. M., Scott, I. C., Keene, D. R. & Greenspan, D. S. Use of Bmp1/Tll1 doubly homozygous null mice and proteomics to identify and validate in vivo substrates of bone morphogenetic protein 1/tolloid-like metalloproteinases. *Mol. Cell. Biol.* **23,** 4428–4438 (2003).
100. Unsöld, C., Pappano, W. N., Imamura, Y., Steiglitz, B. M. & Greenspan, D. S. Biosynthetic processing of the pro-α1(V)2 pro-α2(V) collagen heterotrimer by Bone Morphogenetic Protein-1 and furin-like proprotein convertases. *J. Biol. Chem.* **277,** 5596–5602 (2002).
101. Scott, I. C. *et al.* Bone morphogenetic protein-1 processes probiglycan. *J. Biol. Chem.* **275,** 30504–30511 (2000).
102. Ge, G. *et al.* Bone morphogenetic protein-1/tolloid-related metalloproteinases process osteoglycin and enhance its ability to regulate collagen fibrillogenesis. *J. Biol. Chem.* **279,** 41626–41633 (2004).
103. von Marschall, Z. & Fisher, L. W. Decorin is processed by three isoforms of bone morphogenetic protein-1 (BMP1). *Biochem. Biophys. Res. Commun.* **391,** 1374–1378 (2010).
104. Panchenko, M. V., Stetler-Stevenson, W. G., Trubetskoy, O. V., Gacheru, S. N. & Kagan, H. M. Metalloproteinase activity secreted by fibrogenic cells in the processing of prolysyl oxidase. *J. Biol. Chem.* **271,** 7113–7119 (1996).
105. Borel, A. *et al.* Lysyl oxidase-like protein from bovine aorta: Isolation and maturation to an active form by bone morphogenetic protein-1. *J. Biol. Chem.* **276,** 48944–48949 (2001).
106. Amano, S. *et al.* Bone morphogenetic protein 1 is an extracellular processing enzyme of the laminin 5 2 Chain. *J. Biol. Chem.* **275,** 22728–22735 (2000).
107. Bruckner-Tuderman, L. Can type VII collagen injections cure dystrophic epidermolysis bullosa? *Mol. Ther.* **17,** 6–7 (2009).
108. Chen, M., Keene, D. R., Costa, F. K., Tahk, S. H. & Woodley, D. T. The Carboxyl Terminus of Type VII Collagen Mediates Antiparallel Dimer Formation and Constitutes a New Antigenic Epitope for Epidermolysis Bullosa Acquisita Autoantibodies. *J. Biol. Chem.* **276,** 21649–21655 (2001).

109. Rattenholl, A. *et al.* Proteinases of the bone morphogenetic protein-1 family convert procollagen VII to mature anchoring fibril collagen. *J. Biol. Chem.* **277,** 26372–26378 (2002).
110. Veitch, D. P. *et al.* Mammalian tolloid metalloproteinase, and not matrix metalloprotease 2 or membrane type 1 metalloprotease, processes laminin-5 in keratinocytes and skin. *J. Biol. Chem.* **278,** 15661–15668 (2003).
111. Iorio, V., Troughton, L. D. & Hamill, K. J. Laminins: Roles and utility in wound repair. *Adv. Wound Care* **4,** 250–263 (2015).
112. Behrens, D. T. *et al.* The epidermal basement membrane is a composite of separate laminin- or collagen IV-containing networks connected by aggregated perlecan, but not by nidogens. *J. Biol. Chem.* **287,** 18700–18709 (2012).
113. Iozzo, R. V., Zoeller, J. J. & Nyström, A. Basement membrane proteoglycans: Modulators par excellence of cancer growth and angiogenesis. *Molecules and Cells* **27,** 503–513 (2009).
114. Gonzalez, E. M. *et al.* BMP-1/tolloid-like metalloproteases process endorepellin, the angiostatic C-terminal fragment of perlecan. *J. Biol. Chem.* **280,** 7080–7087 (2005).
115. Moali, C. & Hulmes, D. J. S. Roles and regulation of BMP1/tolloid-like proteinases: Collagen/matrix, assembly, growth factor activation, and beyond. *De Gruyter*. 539-561 (2012).
116. Ge, G. & Greenspan, D. S. BMP1 controls TGFβ1 activation via cleavage of latent TGFβ-binding protein. *J. Cell Biol.* **175,** 111–120 (2006).
117. Delolme, F. *et al.* Proteolytic control of TGF-β co-receptor activity by BMP-1/tolloid-like proteases revealed by quantitative iTRAQ proteomics. *Cell. Mol. Life Sci.* **72,** 1009–1027 (2015).
118. Wipff, P. & Hinz, B. Integrins and the activation of latent transforming growth factor β1 – An intimate relationship. *Eur. J. Cell Biol.* **87,** 601–615 (2008).
119. Zhang, Y., Ge, G. & Greenspan, D. S. Inhibition of bone morphogenetic protein 1 by native and altered forms of α2-macroglobulin. *J. Biol. Chem.* **281,** 39096–39104 (2006).
120. Lee, H. X., Mendes, F. A., Plouhinec, J. L. & De Robertis, E. M. Enzymatic regulation of pattern: BMP4 binds CUB domains of tolloids and inhibits proteinase activity. *Genes Dev.* **23,** 2551–2562 (2009).
121. Lee, H. X., Ambrosio, A. L., Reversade, B. & De Robertis, E. M. Embryonic dorsal-ventral signaling: Secreted Frizzled-related proteins as inhibitors of tolloid proteinases. *Cell* **124,** 147–159 (2006).
122. Kobayashi, K. *et al.* Secreted Frizzled-related protein 2 is a procollagen C proteinase enhancer with a role in fibrosis associated with myocardial infarction. *Nat. Cell Biol.* **11,** 46–55 (2009).
123. Bijakowski, C. *et al.* Sizzled is unique among secreted Frizzled-related proteins for its ability to specifically inhibit Bone Morphogenetic Protein-1 (BMP-1)/tolloid-like proteinases. *J. Biol. Chem.* **287,** 33581–33593 (2012).
124. Maruhashi, T., Kii, I., Saito, M. & Kudo, A. Interaction between periostin and BMP-1 promotes proteolytic activation of lysyl oxidase. *J. Biol. Chem.* **285,** 13294–13303 (2010).
125. Scott, I. C. *et al.* Homologues of Twisted gastrulation are extracellular cofactors in antagonism of BMP signalling. *Nature* **410,** 475–478 (2001).
126. Inomata, H., Haraguchi, T. & Sasai, Y. Robust stability of the embryonic axial pattern requires a secreted scaffold for chordin degradation. *Cell* **134,** 854–865 (2008).
127. Huang, G. *et al.* Fibronectin binds and enhances the activity of Bone Morphogenetic Protein-1. *J. Biol. Chem.* **284,** 25879–25888 (2009).
128. Martínez-Glez, V. *et al.* Identification of a mutation causing deficient BMP1/mTLD proteolytic activity in autosomal recessive osteogenesis imperfecta. *Hum. Mutat.* **33,** 343–350 (2012).

129. Asharani, P. V. *et al.* Attenuated BMP1 function compromises osteogenesis, leading to bone fragility in humans and zebrafish. *Am. J. Hum. Genet.* **90,** 661–674 (2012).
130. Fahiminiya, S. *et al.* A polyadenylation site variant causes transcript specific BMP1 deficiency and frequent fractures in children. *Hum. Mol. Genet.* **24,** 516–524 (2015).
131. Cho, S. Y. *et al.* Osteogenesis imperfecta type I caused by a novel mutation in the start codon of the COL1A1 gene in a Korean family. *Ann. Clin. Lab. Sci.* **45,** 100–5 (2015).
132. Syx, D. *et al.* Defective proteolytic processing of fibrillar procollagens and prodecorin due to biallelic BMP1 mutations results in a severe, progressive form of osteogenesis imperfecta. *J. Bone Miner. Res.* **30,** 1445–1456 (2015).
133. Clark, T. G. *et al.* The mammalian tolloid-like 1 gene, Tll1, is necessary for normal septation and positioning of the heart. *Development* **126,** 2631–42 (1999).
134. Muir, A. M. *et al.* Induced ablation of Bmp1 and Tll1 produces osteogenesis imperfecta in mice. *Hum. Mol. Genet.* **23,** 3085–3101 (2014).
135. Muir, A. M. *et al.* BMP1-like proteinases are essential to the structure and wound healing of skin. *Matrix Biol.* **56,** 114–131 (2016).
136. Malecaze, F. *et al.* Upregulation of bone morphogenetic protein-1/mammalian tolloid and procollagen C-proteinase enhancer-1 in corneal scarring. *Invest. Ophthalmol. Vis. Sci.* **55,** 6712–6721 (2014).
137. Wang, J. *et al.* BMP1 and TLL1 are required for maintaining periodontal homeostasis. *J. Dent. Res.* **96,** 578–585 (2017).
138. Wang, J. *et al.* Essential roles of bone morphogenetic protein-1 and mammalian tolloid-like 1 in postnatal root dentin formation. *J. Endod.* **43,** 109–115 (2017).
139. Zhang, H., Jani, P., Liang, T., Lu, Y. & Qin, C. Inactivation of bone morphogenetic protein 1 (Bmp1) and tolloid-like 1 (Tll1) in cells expressing type I collagen leads to dental and periodontal defects in mice. *J. Mol. Histol.* **48,** 83–98 (2017).
140. Grgurevic, L. *et al.* Circulating bone morphogenetic protein 1-3 isoform increases renal fibrosis. *J. Am. Soc. Nephrol.* **22,** 681–692 (2011).
141. López, B. *et al.* Identification of a potential cardiac antifibrotic mechanism of torasemide in patients with chronic heart failure. *J. Am. Coll. Cardiol.* **50,** 859–867 (2007).
142. Beaumont, J. *et al.* microRNA-122 down-regulation may play a role in severe myocardial fibrosis in human aortic stenosis through TGF-β1 up-regulation. *Clin. Sci. (Lond).* **126,** 497–506 (2014).
143. Adar, R., Kessler, E. & Goldberg, B. Evidence for a protein that enhances the activity of type I procollagen C-proteinase. *Coll. Relat. Res.* **6,** 267–277 (1986).
144. Kessler, E. & Adar, R. Type I procollagen C-proteinase from mouse fibroblasts. Purification and demonstration of a 55-kDa enhancer glycoprotein. *Eur. J. Biochem.* **186,** 115–121 (1989).
145. Takahara, K. *et al.* Type I procollagen COOH-terminal proteinase enhancer protein: Identification, primary structure, and chromosomal localization of the cognate human gene (PCOLCE). *J. Biol. Chem.* **269,** 26280–26285 (1994).
146. Xu, H., Acott, T. S. & Wirtz, M. K. Identification and expression of a novel type I procollagen C-proteinase enhancer protein gene from the glaucoma candidate region on 3q21-q24. *Genomics* **66,** 264–273 (2000).
147. Moschcovich, L. *et al.* Folding and activity of recombinant human procollagen C-proteinase enhancer. *Eur. J. Biochem.* **268,** 2991–2996 (2001).
148. Steiglitz, B. M., Keene, D. R. & Greenspan, D. S. PCOLCE2 encodes a functional procollagen C-proteinase enhancer (PCPE2) that is a collagen-binding protein differing in distribution of expression and post-translational modification from the previously described PCPE1. *J. Biol. Chem.* **277,** 49820–49830 (2002).
149. Vadon-Le Goff, S. *et al.* Procollagen C-Proteinase Enhancer stimulates procollagen processing by binding to the C-propeptide region only. *J. Biol. Chem.* **286,** 38932–38938 (2011).

150. Symoens, S. *et al.* Identification of binding partners interacting with the α1-N-propeptide of type V collagen. *Biochem. J.* **433,** 371–81 (2011).
151. Moali, C. *et al.* Substrate-specific modulation of a multisubstrate proteinase: C-terminal processing of fibrillar procollagens is the only BMP-1-dependent activity to be enhanced by PCPE-1. *J. Biol. Chem.* **280,** 24188–24194 (2005).
152. Steiglitz, B. M. *et al.* Procollagen C-proteinase enhancer 1 genes are important determinants of the mechanical properties and geometry of bone and the ultrastructure of connective tissues. *Mol. Cell. Biol.* **26,** 238–49 (2006).
153. Petropoulou, V., Garrigue-Antar, L. & Kadleri, K. E. Identification of the minimal domain structure of bone morphogenetic protein-1 (BMP-1) for chordinase activity: Chordinase activity is not enhanced by procollagen C-proteinase enhancer-1 (PCPE-1). *J. Biol. Chem.* **280,** 22616–22623 (2005).
154. Zhu, J. *et al.* Regulation of apoAI processing by procollagen C-proteinase enhancer-2 and bone morphogenetic protein-1. *J. Lipid Res.* **50,** 1330–1339 (2009).
155. Gaboriaud, C. *et al.* Structure and properties of the Ca2+-binding CUB domain, a widespread ligand-recognition unit involved in major biological functions. *Biochem. J.* **439,** 185–193 (2011).
156. Hulmes, D. J. S., Mould, A. P. & Kessler, E. The CUB domains of procollagen C-proteinase enhancer control collagen assembly solely by their effect on procollagen C-proteinase/bone morphogenetic protein-1. *Matrix Biol.* **16,** 41–45 (1997).
157. Kronenberg, D. *et al.* Strong cooperativity and loose geometry between CUB domains are the basis for procollagen C-proteinase enhancer activity. *J. Biol. Chem.* **284,** 33437–33446 (2009).
158. Bányai, L. & Patthy, L. The NTR module: Domains of netrins, secreted frizzled related proteins, and type I procollagen C-proteinase enhancer protein are homologous with tissue inhibitors of metalloproteases. *Protein Sci.* **8,** 1636–1642 (1999).
159. Liepinsh, E. *et al.* NMR structure of the netrin-like domain (NTR) of human type I procollagen C-proteinase enhancer defines structural consensus of NTR domains and assesses potential proteinase inhibitory activity and ligand binding. *J. Biol. Chem.* **278,** 25982–25989 (2003).
160. Mott, J. D. *et al.* Post-translational proteolytic processing of procollagen C-terminal proteinase enhancer releases a metalloproteinase inhibitor. *J. Biol. Chem.* **275,** 1384–1390 (2000).
161. Bekhouche, M. *et al.* Role of the netrin-like domain of procollagen C-proteinase enhancer-1 in the control of metalloproteinase activity. *J. Biol. Chem.* **285,** 15950–15959 (2010).
162. Weiss, T. *et al.* Binding of procollagen C-proteinase enhancer-1 (PCPE-1) to heparin/heparan sulfate: Properties and role in PCPE-1 interaction with cells. *J. Biol. Chem.* **285,** 33867–33874 (2010).
163. Weiss, T., Brusel, M., Rousselle, P. & Kessler, E. The NTR domain of Procollagen C-Proteinase Enhancer-1 (PCPE-1) mediates PCPE-1 binding to syndecans-1, -2 and -4 as well as fibronectin. *Int. J. Biochem. Cell Biol.* **57,** 45–53 (2014).
164. Salza, R. *et al.* Extended interaction network of Procollagen C-Proteinase Enhancer-1 in the extracellular matrix. *Biochem. J.* **457,** 137–49 (2014).
165. Morimoto, H. *et al.* Procollagen C-proteinase enhancer-1 (PCPE-1) interacts with beta2-microglobulin (beta2-m) and may help initiate beta2-m amyloid fibril formation in connective tissues. *Matrix Biol.* **27,** 211–219 (2008).
166. Mesilaty-Gross, S. *et al.* Different patterns of human serum procollagen C-proteinase enhancer 1 (PCPE1). *Clin. Chim. Acta* **403,** 76–80 (2009).
167. Blanc, G. *et al.* Insights into how CUB domains can exert specific functions while sharing a common fold: Conserved and specific features of the CUB1 domain contribute to the molecular basis of Procollagen C-Proteinase Enhancer-1 activity. *J. Biol. Chem.*

282, 16924–16933 (2007).
168. Bourhis, J.-M. *et al.* Procollagen C-proteinase enhancer grasps the stalk of the C-propeptide trimer to boost collagen precursor maturation. *Proc. Natl. Acad. Sci. U. S. A.* **110,** 6394–9 (2013).
169. Kessler, E., Mould, A. P. & Hulmes, D. J. S. Procollagen type I C-Proteinase Enhancer is a naturally occurring connective tissue glycoprotein. *Biochem. Biophys. Res. Commun.* **173,** 81–86 (1990).
170. Scott, I. C., Clark, T. G., Takahara, K., Hoffman, G. G. & Greenspan, D. S. Structural organization and expression patterns of the human and mouse genes for the type I procollagen COOH-terminal proteinase enhancer protein. *Genomics* **55,** 229–234 (1999).
171. Kumar, S. *et al.* Identification and initial characterization of 5000 expressed sequenced tags (ESTs) each from adult human normal and osteoarthritic cartilage cDNA libraries. *Osteoarthr. Cartil.* **9,** 641–653 (2001).
172. Heinzel, K. & Bleul, C. C. The Foxn1-dependent transcripts PCOLCE2 and mPPP1R16B are not required for normal thymopoiesis. *Eur. J. Immunol.* **37,** 2562–2571 (2007).
173. Pollard, R. D. *et al.* Procollagen C-endopeptidase enhancer protein 2 (PCPE2) reduces atherosclerosis in mice by enhancing scavenger receptor class B1 (SR-BI)-mediated high-density lipoprotein (HDL)-cholesteryl ester uptake. *J. Biol. Chem.* **290,** 15496–15511 (2015).
174. Grgurevic, L., Macek, B., Durdevic, D. & Vukicevic, S. Detection of bone and cartilage-related proteins in plasma of patients with a bone fracture using liquid chromatography–mass spectrometry. *Int. Orthop.* **31,** 743–751 (2007).
175. Hinds, D. A. *et al.* Application of pooled genotyping to scan candidate regions for association with HDL cholesterol levels. *Hum. Genomics* **1,** 421–34 (2004).
176. Francone, O. L. *et al.* Disruption of the murine procollagen C-proteinase enhancer 2 gene causes accumulation of pro-apoA-I and increased HDL levels. *J. Lipid Res.* **52,** 1974–83 (2011).
177. Kessler-Icekson, G., Schlesinger, H., Freimann, S. & Kessler, E. Expression of procollagen C-proteinase enhancer-1 in the remodeling rat heart is stimulated by aldosterone. *Int. J. Biochem. Cell Biol.* **38,** 358–365 (2006).
178. Reichert, K. *et al.* Atorvastatin improves ventricular remodeling after myocardial infarction by interfering with collagen metabolism. *PLoS One* **11,** 1–17 (2016).
179. Yu, L. *et al.* Genetic and pharmacological inhibition of galectin-3 prevents cardiac remodeling by interfering with myocardial fibrogenesis. *Circ. Hear. Fail.* **6,** 107–117 (2013).
180. Baicu, C. F. *et al.* Effects of the absence of procollagen C-endopeptidase enhancer-2 on myocardial collagen accumulation in chronic pressure overload. *Am. J. Physiol. Heart Circ. Physiol.* **303,** H234-40 (2012).
181. Raz, V. *et al.* Nuclear entrapment and extracellular depletion of PCOLCE is associated with muscle degeneration in oculopharyngeal muscular dystrophy. *BMC Neurol.* **13,** 70 (2013).
182. Achari, Y. *et al.* Molecular events surrounding collagen fibril assembly in the early healing rabbit medial collateral ligament--failure to recapitulate normal ligament development. *Connect. Tissue Res.* **52,** 301–12 (2011).
183. Genin, M., Clement, F., Fattaccioli, A., Raes, M. & Michiels, C. M1 and M2 macrophages derived from THP-1 cells differentially modulate the response of cancer cells to etoposide. *BMC Cancer* **15,** 577 (2015).
184. Fritsch, A. *et al.* A hypomorphic mouse model of dystrophic epidermolysis bullosa reveals mechanisms of disease and response to fibroblast therapy. *J. Clin. Invest.* **118,** 1669–1679 (2008).

185. Nyström, A. *et al.* Losartan ameliorates dystrophic epidermolysis bullosa and uncovers new disease mechanisms. *EMBO Mol Med* **7,** 1211–1228 (2015).
186. Mittapalli, V. R. *et al.* Injury-driven stiffening of the dermis expedites skin carcinoma progression. *Cancer Res.* **76,** 940–951 (2016).
187. Nyström, A. *et al.* Collagen VII plays a dual role in wound healing. *J. Clin. Invest.* **123,** 3498–3509 (2013).
188. Grgurevic, L. *et al.* Systemic inhibition of BMP1-3 decreases progression of CCl4-induced liver fibrosis in rats. *Growth Factors* **0,** 1–15 (2018).
189. Ogata, I. *et al.* Up-regulation of type I procollagen C-proteinase enhancer protein messenger RNA in rats with CCl4-induced liver fibrosis. *Hepatology* **26,** 611–617 (1997).
190. Hassoun, E., Safrin, M., Ziv, H., Pri-Chen, S. & Kessler, E. Procollagen C-proteinase enhancer 1 (PCPE-1) as a plasma marker of muscle and liver fibrosis in mice. *PLoS One* **11,** 1–17 (2016).
191. Ippolito, D. L. *et al.* Gene expression patterns associated with histopathology in toxic liver fibrosis. *Toxicol. Sci.* **149,** 67–88 (2016).
192. Lee, S., Solow-Cordero, D. E., Kessler, E., Takahara, K. & Greenspan, D. S. Transforming growth factor-beta regulation of bone morphogenetic protein-1/procollagen C-proteinase and related proteins in fibrogenic cells and keratinocytes. *J. Biol. Chem.* **272,** 19059–19066 (1997).
193. Massoudi, D., Germer, C. J., Glisch, J. M. & Greenspan, D. S. Procollagen C-proteinase enhancer-1 (PCPE-1) functions as an anti-angiogenic factor and enhances epithelial recovery in injured cornea. *Cell Tissue Res.* **370,** 461–476 (2017).
194. Wong, V. W., You, F., Januszyk, M., Gurtner, G. C. & Kuang, A. A. Transcriptional profiling of rapamycin-treated fibroblasts from hypertrophic and keloid scars. *Ann. Plast. Surg.* **72,** 711–719 (2014).
195. Ma, L. *et al.* Comparative proteomic analysis of extracellular matrix proteins secreted by hypertrophic scar with normal skin fibroblasts. *Burn. Trauma* **2,** 76 (2014).
196. Newman, a. C., Nakatsu, M. N., Chou, W., Gershon, P. D. & Hughes, C. C. W. The requirement for fibroblasts in angiogenesis: Fibroblast-derived matrix proteins are essential for endothelial cell lumen formation. *Mol. Biol. Cell* **22,** 3791–3800 (2011).
197. Knipper, J. A. *et al.* Interleukin-4 receptor α signaling in myeloid cells controls collagen fibril assembly in skin repair. *Immunity* **43,** 803–816 (2015).
198. Prabhu, S. D. & Frangogiannis, N. G. The biological basis for cardiac repair after myocardial infarction. *Circ. Res.* **119,** 91–112 (2016).
199. Vannella, K. M. & Wynn, T. A. Mechanisms of organ injury and repair by macrophages. *Annu. Rev. Physiol.* **79,** 593–617 (2017).
200. Gu, H. *et al.* Contribution of the anaphylatoxin receptors, C3aR and C5aR, to the pathogenesis of pulmonary fibrosis. *FASEB J.* **30,** 2336–2350 (2016).
201. Lacroix, M. *et al.* Interaction of complement defence collagens C1q and Mannose-Binding Lectin with BMP-1/Tolloid-like proteinases. *Sci. Rep.* **7,** 16958 (2017).
202. Bohlson, S. S., O'Conner, S. D., Hulsebus, H. J., Ho, M.-M. & Fraser, D. A. Complement, C1q, and C1q-related molecules regulate macrophage polarization. *Front. Immunol.* **5,** 402 (2014).
203. Finkernagel, F. *et al.* The transcriptional signature of human ovarian carcinoma macrophages is associated with extracellular matrix reorganization. *Oncotarget* (2016). doi:10.18632/oncotarget.12180
204. Jiang, K., Sun, X., Chen, Y., Shen, Y. & Jarvis, J. N. RNA sequencing from human neutrophils reveals distinct transcriptional differences associated with chronic inflammatory states. *BMC Med. Genomics* **8,** 55 (2015).
205. Schnoor, M. *et al.* Production of type VI collagen by human macrophages: A new dimension in macrophage functional heterogeneity. *J. Immunol.* **180,** 5707–5719 (2008).

206. Saphire, A. C. S., Bobardt, M. D., Zhang, Z., David, G. & Gallay, P. a. Syndecans serve as attachment receptors for human immunodeficiency virus type 1 on macrophages. *J. Virol.* **75,** 9187–9200 (2001).
207. Manakil, J. F., Sugerman, P. B., Li, H., Seymour, G. J. & Bartold, P. M. Cell-surface proteoglycan expression by lymphocytes from peripheral blood and gingiva in health and periodontal disease. *J. Dent. Res.* **80,** 1704–1710 (2001).
208. Hirano, K. *et al.* Expression of human scavenger receptor class B type I in cultured human monocyte-derived macrophages and atherosclerotic lesions. *Circ. Res.* **85,** 108–16 (1999).
209. Ji, A. *et al.* Scavenger receptor SR-BI in macrophage lipid metabolism. *Atherosclerosis* **217,** 106–112 (2011).
210. Tsuruoka, H. *et al.* Scavenger Receptor class B type I is expressed in cultured keratinocytes and epidermis. *J. Biol. Chem.* **277,** 2916–2922 (2002).
211. Kanaki, T. *et al.* The regulatory expression of procollagen COOH-terminal proteinase enhancer in the proliferation of vascular smooth muscle cells. *Biochem Biophys Res Commun* **270,** 1049–1054 (2000).
212. Parsons, M. Mechanical load enhances procollagen processing in dermal fibroblasts by regulating levels of procollagen C-proteinase. *Exp. Cell Res.* **252,** 319–331 (1999).
213. Shalitin, N., Schlesinger, H., Levy, M. J., Kessler, E. & Kessler-Icekson, G. Expression of procollagen C-proteinase enhancer in cultured rat heart fibroblasts: Evidence for co-regulation with type I collagen. *J. Cell. Biochem.* **90,** 397–407 (2003).
214. Masuda, M., Igarashi, H., Kano, M. & Yoshikura, H. Effects of Procollagen C-Proteinase Enhancer protein on the growth of cultured rat fibroblasts revealed by an excisable retroviral vector. *Cell Growth Differ.* **9,** 381–91 (1998).
215. Matsui, A. *et al.* Stabilization of RNA strands in protein synthesis by type I Procollagen C-Proteinase Enhancer protein, a potential RNA-binding protein, in hepatic stellate cells. *Biochem. Biophys. Res. Commun* **902,** 898–902 (2002).
216. Rauniyar, N. & Yates, J. R. Isobaric labeling-based relative quantification in shotgun proteomics. *J. Proteome Res.* **13,** 5293–5309 (2014).
217. Vogeser, M. & Parhofer, K. Liquid chromatography tandem-mass spectrometry (LC-MS/MS) - Technique and applications in endocrinology. *Exp. Clin. Endocrinol. Diabetes* **115,** 559–570 (2007).
218. Hynes, R. O. & Naba, A. Overview of the matrisome - An inventory of extracellular matrix constituents and functions. *Cold Spring Harb. Perspect. Biol.* **4,** a004903–a004903 (2012).
219. Künzli, K., Favre, B., Chofflon, M. & Borradori, L. One gene but different proteins and diseases: The complexity of dystonin and bullous pemphigoid antigen 1. *Exp. Dermatol.* **25,** 10–16 (2016).
220. Leśniak, W., Słomnicki, Ł. P. & Filipek, A. S100A6 - New facts and features. *Biochem. Biophys. Res. Commun.* **390,** 1087–1092 (2009).
221. Yao, C. *et al.* Toll-like receptor family members in skin fibroblasts are functional and have a higher expression compared to skin keratinocytes. *Int. J. Mol. Med.* **35,** 1443–1450 (2015).
222. Frank, P. G. & Marcel, Y. L. Apolipoprotein A-I: Structure-function relationships. *J. Lipid Res.* **41,** 853–72 (2000).
223. Landriscina, M. *et al.* S100A13 participates in the release of fibroblast growth factor 1 in response to heat shock in vitro. *J. Biol. Chem.* **276,** 22544–22552 (2001).
224. Landriscina, M. *et al.* S100A13, a new marker of angiogenesis in human astrocytic gliomas. *J. Neurooncol.* **80,** 251–259 (2006).
225. Massi, D. *et al.* S100A13 is a new angiogenic marker in human melanoma. *Mod. Pathol.* **23,** 804–813 (2010).
226. Xiang, T. *et al.* Epigenetic silencing of the WNT antagonist Dickkopf 3 disrupts normal

Wnt/β-catenin signalling and apoptosis regulation in breast cancer cells. *J. Cell. Mol. Med.* **17,** 1236–1246 (2013).
227. Doliana, R. *et al.* Isolation and characterization of EMILIN-2, a new component of the growing EMILINs family and a member of the EMI domain-containing superfamily. *J. Biol. Chem.* **276,** 12003–12011 (2001).
228. Hayashi, M. Differential localization of mRNAs of collagen types I and II in chick fibroblasts, chondrocytes, and corneal cells by in situ hybridization using cDNA probes. *J. Cell Biol.* **102,** 2302–2309 (1986).
229. Massague, J. The transforming growth factor-beta family. *Annu. Rev. Cell Biol.* **6,** 597–641 (1990).
230. Feres-Filho, E. J., Choi, Y. J., Han, X., Takala, T. E. S. & Trackman, P. C. Pre- and post-translational regulation of lysyl oxidase by transforming growth factor-β1 in osteoblastic MC3T3-E1 cells. *J. Biol. Chem.* **270,** 30797–30803 (1995).
231. Wang, W.-M. *et al.* Transforming growth factor-β induces secretion of activated ADAMTS-2. *J. Biol. Chem.* **278,** 19549–19557 (2003).
232. Chau, P., Fielding, P. E. & Fielding, C. J. Bone morphogenetic protein-1 (BMP-1) cleaves human proapolipoprotein A1 and regulates its activation for lipid binding. *Biochemistry* **46,** 8445–8450 (2007).
233. Eyre, D. Collagen of articular cartilage. *Arthritis Res.* **4,** 30–35 (2002).
234. Clarke, C. J. *et al.* The initiator methionine tRNA drives secretion of type II Collagen from stromal fibroblasts to promote tumor growth and angiogenesis. *Curr. Biol.* **26,** 755–765 (2016).
235. Marastoni, S. *et al.* EMILIN2 down-modulates the Wnt signalling pathway and suppresses breast cancer cell growth and migration. *J. Pathol.* **232,** 391–404 (2014).
236. Schiavinato, A. *et al.* Targeting of EMILIN-1 and EMILIN-2 to fibrillin microfibrils facilitates their incorporation into the extracellular matrix. *J. Invest. Dermatol.* **136,** 1150–1160 (2016).
237. Hemmi, H. *et al.* A Toll-like receptor recognizes bacterial DNA. *Nature* **408,** 740–5 (2000).
238. Ashkar, A. & Rosenthal, K. Toll-like receptor 9, CpG DNA and innate immunity. *Curr. Mol. Med.* **2,** 545–556 (2002).
239. Hopkinson, S. B. & Jones, J. C. R. The N terminus of the transmembrane protein BP180 interacts with the N-terminal domain of BP230, thereby mediating keratin cytoskeleton anchorage to the cell surface at the site of the hemidesmosome. *Mol. Biol. Cell* **11,** 277–286 (2000).
240. Zhang, Y. *et al.* Dickkopf-3 attenuates pressure overload-induced cardiac remodelling. *Cardiovasc. Res.* **102,** 35–45 (2014).
241. Li, Y. *et al.* DKK3 regulates cell proliferation, apoptosis and collagen synthesis in keloid fibroblasts via TGF-β1/Smad signaling pathway. *Biomed. Pharmacother.* **91,** 174–180 (2017).
242. Ge, G., Zhang, Y., Steiglitz, B. M. & Greenspan, D. S. Mammalian tolloid-like 1 binds procollagen C-proteinase enhancer protein 1 and differs from bone morphogenetic protein 1 in the functional roles of homologous protein domains. *J. Biol. Chem.* **281,** 10786–10798 (2006).
243. Kyriakides, T. R. & MacLauchlan, S. The role of thrombospondins in wound healing, ischemia, and the foreign body reaction. *J. Cell Commun. Signal.* **3,** 215–225 (2009).
244. Piccolo, S. *et al.* Cleavage of chordin by xolloid metalloprotease suggests a role for proteolytic processing in the regulation of Spemann organizer activity. *Cell* **91,** 407–16 (1997).
245. Lee, J. J. *et al.* Human versus mouse eosinophils: 'That which we call an eosinophil, by any other name would stain as red'. *J. Allergy Clin. Immunol.* **130,** 572–584 (2012).
246. Fiedler, U. *et al.* MP0250, a VEGF and HGF neutralizing DARPin molecule shows high

anti-tumor efficacy in mouse xenograft and patient-derived tumor models. *Oncotarget* **8,** 98371–98383 (2017).

247. Souied, E. H. *et al.* Treatment of exudative age-related macular degeneration with a designed ankyrin repeat protein that binds vascular endothelial growth factor: A phase I/II study. *Am. J. Ophthalmol.* **158,** 724–732.e2 (2014).

Appendixes

Appendix 1: The collagen family, their type, composition and distribution in human tissues

Collagen is composed of one or several α chains, which can form homo- or hetero-trimers. Subgroups of collagens can be distinguished by the supramolecular assemblies of these chains: fibrils and anchoring fibrils, beaded filaments, networks, fibril-associated collagens with interrupted triple helices (FACITs), multiplexins and membrane collagens. Collagens are mainly found in organs rich in connective tissues.

Collagen types	Number of α chains	Trimer composition	Molecular assembly	Location
Type I collagen	2	$[\alpha1(I)]_3$ $[\alpha1(I)]_2[\alpha2(I)]$	Fibrils	Dermis, bone, tendon, cornea
Type II collagen	1	$[\alpha1(II)]_3$	Fibrils	Cartilage
Type III collagen	1	$[\alpha1(III)]_3$	Fibrils	Dermis, blood vessels
Type IV collagen	6	$[\alpha1(IV)]_2[\alpha2(IV)]$ $[\alpha3(IV)][\alpha4(IV)][\alpha5(IV)]$ $[\alpha5(IV)]_2[\alpha6(IV)]$	Network	Basement membrane
Type V collagen	4	$[\alpha1(V)]_2[\alpha2(V)]$ $[\alpha1(V)][\alpha2(V)][\alpha3(V)]$ $[\alpha1(V)]_3$	Fibrils	Dermis, bone, cornea, placenta
Type VI collagen	4	$[\alpha1(VI)][\alpha2(VI)][\alpha3(VI)]$	Beaded filaments	Dermis, bone, muscle
Type VII collagen	1	$[\alpha1(VII)]_3$	Anchoring fibrils	Basement membrane (including dermal-epidermal junction)
Type VIII collagen	2	$[\alpha1(VIII)]_2[\alpha2(VIII)]$ $[\alpha1(VIII)]_3$ $[\alpha2(VIII)]_3$	Network	Cornea
Type IX collagen	3	$[\alpha1(IX)][\alpha2(IX)][\alpha3(IX)]$	FACIT	Cartilage
Type X collagen	1	$[\alpha1(X)]_3$	Network	Cartilage
Type XI collagen	3	$[\alpha1(XI)][\alpha2(XI)][\alpha3(XI)]$	Fibrils	Cartilage
Type XII collagen	1	$[\alpha1(XII)]_3$	FACIT	Dermis, tendon, ligament
Type XIII collagen	1	$[\alpha1(XIII)]_3$	Membrane	Neuromuscular junctions
Type XIV collagen	1	$[\alpha1(XIV)]_3$	FACIT	Dermis, bone, cartilage
Type XV collagen	1	$[\alpha1(XV)]_3$	Multiplexin	Basement membrane
Type XVI collagen	1	$[\alpha1(XVI)]_3$	FACIT	Dermis, kidney
Type XVII collagen	1	$[\alpha1(XVII)]_3$	Membrane	Hemidesmosomes

Type XVIII collagen	1	$[\alpha1(XVIII)]_3$	Multiplexin	Basement membrane, liver, retina
Type XIX collagen	1	$[\alpha1(XIX)]_3$	FACIT	Basement membrane
Type XX collagen	1	$[\alpha1(XX)]_3$	FACIT	Cornea
Type XXI collagen	1	$[\alpha1(XXI)]_3$	FACIT	Stomach, kidney
Type XXII collagen	1	$[\alpha1(XXII)]_3$	FACIT	Muscle-tendon junction
Type XXIII collagen	1	$[\alpha1(XXIII)]_3$	Membrane	Epidermis
Type XXIV collagen	1	$[\alpha1(XXIV)]_3$	Fibrils	Bone, cornea
Type XXV collagen	1	$[\alpha1(XXV)]_3$	Membrane	Brain
Type XXVI collagen	1	$[\alpha1(XXVI)]_3$	-	Testicle, ovary
Type XXVII collagen	1	$[\alpha1(XXVII)]_3$	Fibrils	Cartilage
Type XXVIII collagen	1	$[\alpha1(XXVIII)]_3$	-	Basement membrane

Appendix 2: Matrisome annotation

Categorie	Accession number	Protein
Collagens	P02452	Collagen alpha-1(I) chain
	P08123	Collagen alpha-2(I) chain
	P02458	Collagen alpha-1(II) chain
	P02461	Collagen alpha-1(III) chain
	P02462	Collagen alpha-1(IV) chain
	P20908	Collagen alpha-1(V) chain
	P05997	Collagen alpha-2(V) chain
	P25940	Collagen alpha-3(V) chain
	P12109	Collagen alpha-1(VI) chain
	P12110	Collagen alpha-2(VI) chain
	P12111	Collagen alpha-3(VI) chain
	Q99715	Collagen alpha-1(XII) chain
	Q05707	Collagen alpha-1(XIV) chain
	P39059	Collagen alpha-1(XV) chain
	Q07092	Collagen alpha-1(XVI) chain
	P39060	Collagen alpha-1(XVIII) chain
	Q86Y22	Collagen alpha-1(XXIII) chain
Proteoglycans	P21810	Biglycan
	P51888	Prolargin
	P51884	Lumican
	Q08629	Testican-1
	P07585	Decorin
	Q7Z5L7	Podocan
	P98160	Basement membrane-specific heparan sulfate proteoglycan core protein
	P13611	Versican core protein
Glycoproteins	Q12805	EGF-containing fibulin-like extracellular matrix protein 1
	O95967	EGF-containing fibulin-like extracellular matrix protein 2
	P24043	Laminin subunit alpha-2
	Q16363	Laminin subunit alpha-4
	P07942	Laminin subunit beta-1
	P55268	Laminin subunit beta-2
	P11047	Laminin subunit gamma-1
	P17936	Insulin-like growth factor-binding protein 3

Glycoproteins	P22692	Insulin-like growth factor-binding protein 4
	P24592	Insulin-like growth factor-binding protein 6
	Q16270	Insulin-like growth factor-binding protein 7
	Q14393	Growth arrest-specific protein 6
	Q8IUX7	Adipocyte enhancer-binding protein 1
	Q15113	Procollagen C-endopeptidase enhancer 1
	Q9BUD6	Spondin-2
	P49747	Cartilage oligomeric matrix protein
	P23142	Fibulin-1
	P98095	Fibulin-2
	Q9UBX5	Fibulin-5
	P35555	Fibrillin-1
	Q92626	Peroxidasin homolog
	P55001	Microfibrillar-associated protein 2
	Q13361	Microfibrillar-associated protein 5
	P48745	Protein NOV homolog
	P29279	Connective tissue growth factor
	Q96CG8	Collagen triple helix repeat-containing protein 1
	Q15582	Transforming growth factor-beta-induced protein ig-h3
	O76076	WNT1-inducible-signalling pathway protein 2
	Q16610	Extracellular matrix protein 1
	Q14766	Latent-transforming growth factor beta-binding protein 1
	Q14767	Latent-transforming growth factor beta-binding protein 2
	Q9Y6C2	Emilin-1
	Q9BXX0	Emilin-2
	P02751	Fibronectin
	O00622	Protein CYR61
	Q15063	Periostin
	Q07507	Dermatopontin
	Q96RW7	Hemicentin-1
	P09486	SPARC
	P07996	Thrombospondin-1
	P35442	Thrombospondin-2
	P04004	Vitronectin
	P14543	Nidogen-1
	P24821	Tenascin
	P22105	Tenascin-X

Glycoproteins	Q08431	Lactadherin
	Q7Z7G0	Target of Nesh-SH3
	O00468	Agrin
	Q6UXI7	Vitrin
	Q9NR99	Matrix-remodelling-associated protein 5
ECM regulators	P20742	Pregnancy zone protein
	P01023	Alpha-2-macroglobulin
	P00742	Coagulation factor X
	P48740	Mannan-binding lectin serine protease 1
	Q13219	Pappalysin-1
	P07858	Cathepsin B
	P07339	Cathepsin D
	P43235	Cathepsin K
	Q9UBR2	Cathepsin Z
	P05155	Plasma protease C1 inhibitor
	Q6YHK3	CD109 antigen
	Q13443	Disintegrin and metalloproteinase domain-containing protein 9
	O14672	Disintegrin and metalloproteinase domain-containing protein 10
	O43184	Disintegrin and metalloproteinase domain-containing protein 12
	Q8N6G6	ADAMTS-like protein 1
	P03956	Interstitial collagenase (or MMP-1)
	P08253	72 kDa type IV collagenase (or MMP-2)
	P08254	Stromelysin-1 (or MMP-3)
	P28300	Protein-lysine 6-oxidase
	P13497	Bone morphogenetic protein 1 (BMP-1)
	P01033	Metalloproteinase inhibitor 1 (TIMP-1)
	P16035	Metalloproteinase inhibitor 2 (TIMP-2)
	P35625	Metalloproteinase inhibitor 3 (TIMP-3)
	P01034	Cystatin-C
	P36955	Pigment epithelium-derived factor
	Q6UXH9	Inactive serine protease PAMR1
	Q8IWU6	Extracellular sulfatase Sulf-1
	P10619	Lysosomal protective protein
	P53634	Dipeptidyl peptidase 1
	Q32P28	Prolyl 3-hydroxylase 1 (P3H)
	Q9Y4K0	Lysyl oxidase homolog 2 (LOXL2)
	P30740	Leukocyte elastase inhibitor

ECM regulators	Q02809	Procollagen-lysine,2-oxoglutarate 5-dioxygenase 1 (PLOD1)
	O60568	Procollagen-lysine,2-oxoglutarate 5-dioxygenase 3 (PLOD3)
	Q92743	Serine protease HTRA1
	P01042	Kininogen-1
	P07093	Glia-derived nexin
	P05121	Plasminogen activator inhibitor 1
ECM-affiliated proteins	P05452	Tetranectin
	P04083	Annexin A1
	P07355	Annexin A2
	P08758	Annexin A5
	Q9Y240	C-type lectin domain family 11 member A
	P35052	Glypican-1
	P09382	Galectin-1
	P17931	Galectin-3
	O75326	Semaphorin-7A
	Q5KU26	Collectin-12
	O15031	Plexin-B2
Secreted factors	P19883	Follistatin
	Q9GZP0	Platelet-derived growth factor D
	Q12841	Follistatin-related protein 1
	P48061	Stromal cell-derived factor 1
	P26447	Protein S100-A4
	P06703	Protein S100-A6
	P31949	Protein S100-A11
	Q99584	Protein S100-A13
	Q96FQ6	Protein S100-A16
	Q9BY76	Angiopoietin-related protein 4
	Q8IX30	Signal peptide, CUB and EGF-like domain-containing protein 3
	P09603	Macrophage colony-stimulating factor 1
	Q96HF1	Secreted frizzled-related protein 2

Appendix 3: Position of the 11 peptides used to identify the α1 chain of human collagen II in dermal fibroblasts by proteomics

>sp|P02458|CO2A1_HUMAN Collagen alpha-1(II) chain OS=Homo sapiens GN=COL2A1 PE=1 SV=3

MIRLGAPQTLVLLTLLVAAVLRCQGQDVQEAGSCVQDGQRYNDKDVWKPEPCRICVCDTG
TVLCDDIICEDVKDCLSPEIPFGECCPICPTDLATASGQPGPKGQKGEPGDIKDIVGPKG
PPGPQGPAGEQGPRGDRGDKGEKGAPGPRGRDGEPGTPGNPGPPGPPGPPGPPGLGGNFA
AQMAGGFDEKAGGAQLGVMQGPMGPMGPRGPPGPAGAPGPQGFQGNPGEPGEPGVSGPMG
PRGPPGPPGKPGDDGEAGKPGKAGERGPPGPQGARGFPGTPGLPGVKGHRGYPGLDGAKG
EAGAPGVKGESGSPGENGSPGPMGPRGLPGERGRTGPAGAAGARGNDGQPGPAGPPGPVG
PAGGPGFPGAPGAKGEAGPTGARGPEGAQGPRGEPGTPGSPGPAGASGNPGTDGIPGAKG
SAGAPGIAGAPGFPGPRGPPGPQGATGPLGPKGQTGEPGIAGFKGEQGPKGEPGPAGPQG
APGPAGEEGKRGARGEPGGVGPIGPPGERGAPGNRGFPGQDGLAGPKGAPGERGPSGLAG
PKGANGDPGRPGEPGLPGARGLTGRPGDAGPQGKVGPSGAPGEDGRPGPPGPQGARGQPG
VMGFPGPKGANGEPGKAGEKGLPGAPGLRGLPGKDGETGAAGPPGPAGPAGERGEQGAPG
PSGFQGLPGPPGPPGEGGKPGDQGVPGEAGAPGLVGPRGERGFPGERGSPGAQGLQGPRG
LPGTPGTDGPKGASGPAGPPGAQGPPGLQGMPGERGAAGIAGPKGDRGDVGEKGPEGAPG
KDGGRGLTGPIGPPGPAGANGEKGEVGPPGPAGSAGARGAPGERGETGPPGPAGFAGPPG
ADGQPGAKGEQGEAGQKGDAGAPGPQGPSGAPGPQGPTGVTGPKGARGAQGPPGATGFPG
AAGRVGPPGSNGNPGPPGPPGPSGKDGPKGARGDSGPPGRAGEPGLQGPAGPPGEKGEPG
DDGPSGAEGPPGPQGLAGQRGIVGLPGQRGERGFPGLPGPSGEPGKQGAPGASGDRGPPG
PVGPPGLTGPAGEPGREGSPGADGPPGRDGAAGVKGDRGETGAVGAPGAPGPPGSPGPAG
PTGKQGDRGEAGAQGPMGPSGPAGARGIQGPQGPRGDKGEAGEPGERGLKGHRGFTGLQG
LPGPPGPSGDQGASGPAGPSGPRGPPGPVGPSGKDGANGIPGPIGPPGPRGRSGETGPAG
PPGNPGPPGPPGPPGPGIDMSAFAGLGPREKGPDPLQYMRADQAAGGLRQHDAEVDATLK
SLNNQIESIRSPEGSRKNPARTCRDLKLCHPEWKSGDYWIDPNQGCTLDAMKVFCNMETG
ETCVYPNPANVPKKNWWSSKSKEKKHIWFGETINGGFHFSYGDDNLAPNTANVQMTFLRL
LSTEGSQNITYHCKNSIAYLDEAAGNLKKALLIQGSNDVEIRAEGNSRFTYTALKDGCTK
HTGKWGKTVIEYRSQKTSRLPIIDIAPMDIGGPEQEFGVDIGPVCFL

Communication & Training

List of publications

Article 1: Lacroix M.*, Tessier A.*, Dumestre-Pérard C., Vadon-Le Goff S., Gout E., Bruckner-Tuderman L., Nyström A., Ricard-Blum S., Moali C., Hulmes D. and Thielens NM. (2017) **Interaction of Complement Defense Collagens C1q and Mannose-Binding Lectin with BMP-1/Tolloid-like Proteinases.** Scientific Reports, 7, 16958. *: equal contribution

Article 2: Anastasi C.*, Rousselle P.*, Talantikite M., Tessier A., Bachmann A., Alcaraz L., Fortin L., Delolme F., Armengaud J., Auxenfans C., Fournié P., Vadon-Le Goff S., Valcourt U., and Moali C. **Bone Morphogenetic Protein-1 promotes cell motility and TGF-β activation through the cleavage of the matricellular protein TSP-1.** *: equal contribution (submitted)

Abstract : Tessier A., Vadon-Le Goff S., Bruckner-Tuderman L., Nyström A., and Moali C. (2016) **Fonctions divergentes des "Procollagen C-Proteinase Enhancers", PCPE-1 et -2, dans la cicatrisation cutanée.** Annales de Dermatologie et de Vénérologie, 143, S430-1.

Book chapter: Tessier A. et Moali C. (2017) Synthèse et dégradation des collagènes du derme. **Biologie Cutanée, CoBIP 2017**, 102-116, Editions Matrix, Ed. Marek Haftek.

Article 1: Lacroix, Tessier et *al.* 2017, *Scientific Reports*

www.nature.com/scientificreports

SCIENTIFIC REPORTS

OPEN

Interaction of Complement Defence Collagens C1q and Mannose-Binding Lectin with BMP-1/Tolloid-like Proteinases

Received: 8 September 2017
Accepted: 19 November 2017
Published online: 05 December 2017

Monique Lacroix[1], Agnès Tessier[2], Chantal Dumestre-Pérard[3,4], Sandrine Vadon-Le Goff[2], Evelyne Gout[1], Leena Bruckner-Tuderman[5], Dimitra Kiritsi[5], Alexander Nyström[5], Sylvie Ricard-Blum[6], Catherine Moali[2], David J. S. Hulmes[2] & Nicole M. Thielens[1]

The defence collagens C1q and mannose-binding lectin (MBL) are immune recognition proteins that associate with the serine proteinases C1r/C1s and MBL-associated serine proteases (MASPs) to trigger activation of complement, a major innate immune system. Bone morphogenetic protein-1 (BMP-1)/tolloid-like proteinases (BTPs) are metalloproteinases with major roles in extracellular matrix assembly and growth factor signalling. Despite their different functions, C1r/C1s/MASPs and BTPs share structural similarities, including a specific CUB-EGF-CUB domain arrangement found only in these enzymes that mediates interactions with collagen-like proteins, suggesting a possible functional relationship. Here we investigated the potential interactions between the defence collagens C1q and MBL and the BTPs BMP-1 and mammalian tolloid-like-1 (mTLL-1). C1q and MBL bound to immobilized BMP-1 and mTLL-1 with nanomolar affinities. These interactions involved the collagen-like regions of the defence collagens and were inhibited by pre-incubation of C1q or MBL with their cognate complement proteinases. Soluble BMP-1 and mTLL-1 did not inhibit complement activation and the defence collagens were neither substrates nor inhibitors of BMP-1. Finally, C1q co-localized with BMP-1 in skin biopsies following melanoma excision and from patients with recessive dystrophic epidermolysis bullosa. The observed interactions provide support for a functional link between complement and BTPs during inflammation and tissue repair.

The complement system is a complex extracellular protein cascade that, when triggered by interactions with self or non-self molecules, results in the production of inflammatory mediators and a membrane attack complex that helps destroy invading cells (for recent reviews see[1,2]). It comprises several proteins, including proteases and their substrates/interaction partners, permitting complement activation by one of three pathways (classical, lectin, alternative), all of which converge in the activation of component C3. The classical pathway is triggered by interactions of targets with component C1 which consists of three proteins C1r, C1s and C1q. C1r and C1s are multi-domain serine proteases where two copies of each form a tetramer that associates with C1q, a hexameric recognition protein of the defence collagens family resembling a bouquet of flowers[3]. The lectin pathway is initiated by similar complexes, consisting of other defence collagens, including collectins (mannose-binding lectin (MBL), collectin-10 or collectin-11) and ficolins, bound to MBL-associated serine proteases (MASP-1 and MASP-2)[4]. Binding of the initiating complexes to appropriate targets through the globular recognition domains

[1]Univ. Grenoble Alpes, CNRS, CEA, IBS, F-38000, Grenoble, France. [2]Univ. Lyon, Université Claude Bernard Lyon 1, CNRS, Tissue Biology and Therapeutic Engineering Unit, LBTI, UMR 5305, F-69367, Lyon, France. [3]Laboratoire d'Immunologie, Pôle de Biologie, CHU Grenoble Alpes, 38700, La Tronche, France. [4]BNI group, TIMC-IMAG UMR5525 Université Grenoble Alpes, 38706, La Tronche, France. [5]Department of Dermatology, Medical Center – University of Freiburg, Faculty of Medicine, University of Freiburg, Freiburg, Germany. [6]Univ. Lyon, University Claude Bernard Lyon 1, INSA Lyon, CPE, Institute of Molecular and Supramolecular Chemistry and Biochemistry (ICBMS), UMR 5246, F-69622, Villeurbanne, France. Monique Lacroix and Agnès Tessier contributed equally to this work. Correspondence and requests for materials should be addressed to D.J.S.H. (email: david.hulmes@ibcp.fr) or N.M.T. (email: nicole.thielens@ibs.fr)

N.B. Contributions to the work: Protein purification and immunofluorescence.

of the defence collagens triggers sequential activation of the C1r and C1s or MASP-1 and MASP-2 proteases that are bound to the collagen-like stalks of the recognition proteins. A third homologous protease, MASP-3, is found in association with the recognition proteins of the lectin pathway, but it is not involved in triggering activation of the lectin pathway. Activated C1s and MASP-2 are both able to cleave the complement components C4 and C2, which results in the formation of the C3 convertase C4bC2a. The alternative pathway begins with direct activation of component C3 by a C3 convertase assembled from spontaneously hydrolysed C3 and factors B and D on target surfaces[5]. The involvement of MASP-3 in activation of pro-factor D has recently been established[6].

Bone morphogenetic protein-1 (BMP-1)/tolloid-like proteinases, otherwise known as BTPs, are extracellular zinc-dependent metalloproteinases whose main roles are in extracellular matrix assembly and growth factor signalling[7]. For example, they control collagen assembly by cleavage of propeptides from precursor forms of collagens, lysyl oxidases and small leucine rich proteoglycans, and they activate growth factors by maturation of latent forms or cleavage of growth factor antagonists. They are also involved in angiogenesis and biomineralization[7]. BTP family members in humans include bone morphogenetic protein-1 (BMP-1), mammalian Tolloid (mTLD), and mammalian Tolloid-like-1 (mTLL-1) and -2 (mTLL-2).They have been shown to control many aspects of development, growth and tissue repair, and are involved in diseases such as cancer and fibrosis[7].

Despite their different roles, proteins of the complement and BTP systems share many similarities. In particular, though complement proteases are serine proteases and BTPs are metalloproteinases, the non-catalytic domains of C1r, C1s, MASP-1 and MASP-2 and the BTPs include both CUB (complement C1r/C1s, Uegf, Bmp1) and EGF (epidermal growth factor) domains[8,9] (Fig. 1A). Furthermore, the trimodular CUB-EGF-CUB motif is found in all these proteinases, but nowhere else in mammalian protein databases. This motif plays key roles in the binding of complement proteases to defence collagens, and in the recognition of procollagen substrates by BTPs[7,10,11]. In addition, there is increasing evidence for a link between complement and BTPs during inflammation and tissue repair, as found for example in myocardial infarction[12] and pulmonary fibrosis[13]. Despite this, to date there have been no studies on possible interactions between BTPs and defence collagens. Here we describe interactions between C1q and MBL and the BTPs BMP-1 and mTLL-1 that provide further support for such a functional connection.

Results

The defence collagens C1q and MBL interact with BMP-1 and mTLL-1. The possible interaction of the defence collagens C1q and MBL with BTPs was investigated by surface plasmon resonance spectroscopy (SPR), as previously described to study the interactions between C1q and MBL and their associated complement proteases[10,14,15]. BMP-1 and mTLL-1 were immobilized on the surface of a sensor chip and the defence collagens injected over the immobilized proteinases in the presence of Ca^{2+} ions. Both C1q and MBL bound dose-dependently to immobilized BMP-1 (Fig. 2A,B) and mTLL-1 (Fig. 2C,D). Binding was Ca^{2+}-dependent since all interactions were abolished in the presence of EDTA (Supplementary Fig. S1). The kinetic parameters of the interactions were determined by global fitting of the curves using a 1:1 binding model (Fig. 2A–D). BMP-1 interacted with C1q and MBL with high affinity, as reflected by affinity constants (K_D) in the nM range (0.48 and 1.3 nM, respectively), the C1q/BMP-1 complex being slightly more stable than the MBL/BMP-1 complex, as indicated by a 4-fold lower dissociation rate constant (Table 1). The mTLL-1 proteinase also bound to C1q and MBL with kinetic and dissociation constants in the same range as those measured for BMP-1 (Table 1). The k_a value for the C1q-mTLL1 interaction was slightly lower than that for the C1q-BMP-1 complex and slightly higher in the case of MBL (Table 1). Despite these minor differences, these data indicate a high affinity binding of C1q or MBL to both BMP-1 and mTLL-1.

Immobilization of C1q and MBL on the surface of a sensor chip and injection of soluble BMP-1 (50 nM) and mTLL-1 (150 nM) did not result in any detectable interaction in the case of C1q and only weak binding in the case of MBL (Supplementary Fig. S2), indicating that the SPR configuration with immobilized BTPs is required for stable interaction with the defence collagens. This is in contrast to published observations on the binding of complement proteases to immobilized defence collagens which showed affinity constants in the nanomolar range: C1s-C1r-C1r-C1s tetramer on C1q (1.5–2.7 nM)[10,11], MASP-3 dimer on C1q (1.35 nM)[16], MASP-1, MASP-2 and MASP-3 dimers on MBL (3.2 nM, 2.6 nM and 2.6 nM, respectively)[17]. To check for the effects of immobilization, we also measured binding of C1q and MBL to immobilized MASP-2 (Supplementary Fig. S3). By kinetic analysis (Supplementary Fig. S4), a corresponding affinity constant of 1.7 nM was obtained (Table 1), similar to that found for the reverse configuration.

We next pre-incubated C1q and MBL with soluble BMP-1 or mTLL-1 (molar excess of these proteinases to the defence collagens of 6-fold) before injection over immobilized BMP-1 and mTLL-1. No or very limited inhibition of the interactions was observed, as illustrated in the case of C1q and MBL pre-incubated with soluble mTLL-1 and injected over immobilized mTLL-1 (Fig. 2E,F) or of MBL pre-incubated with soluble BMP-1 and injected over immobilized BMP-1 (Supplementary Fig. S5). These results strongly suggest that stable complexes with BTPs did not form in solution, which is consistent with the observed absence or weakness of interactions between soluble BMP-1 or mTLL-1 and the immobilized defence collagens.

BMP-1 and mTLL-1 interact with the collagen-like stalks of C1q and with MBL at the complement protease binding site. It has been shown previously that analogous interactions occur between the collagen-like regions of C1q or MBL and the interaction region (CUB1-EGF-CUB2) of C1r and C1s or MASPs, allowing cross-interaction between the subcomponents of the classical and lectin complement pathways[10,11,16]. To investigate whether BMP-1 and mTLL-1 bind to homologous regions within C1q and MBL, we investigated the capacity of the C1s-C1r-C1r-C1s tetramer and the MASP-2 dimer to compete for binding of C1q and MBL to the BTPs. C1q was pre-incubated with C1s-C1r-C1r-C1s or MASP-2 and MBL with MASP-2 and the mixtures were injected over immobilized BMP-1 and mTLL-1. Pre-assembly of the C1 or of the C1q-MASP-2 complex strongly

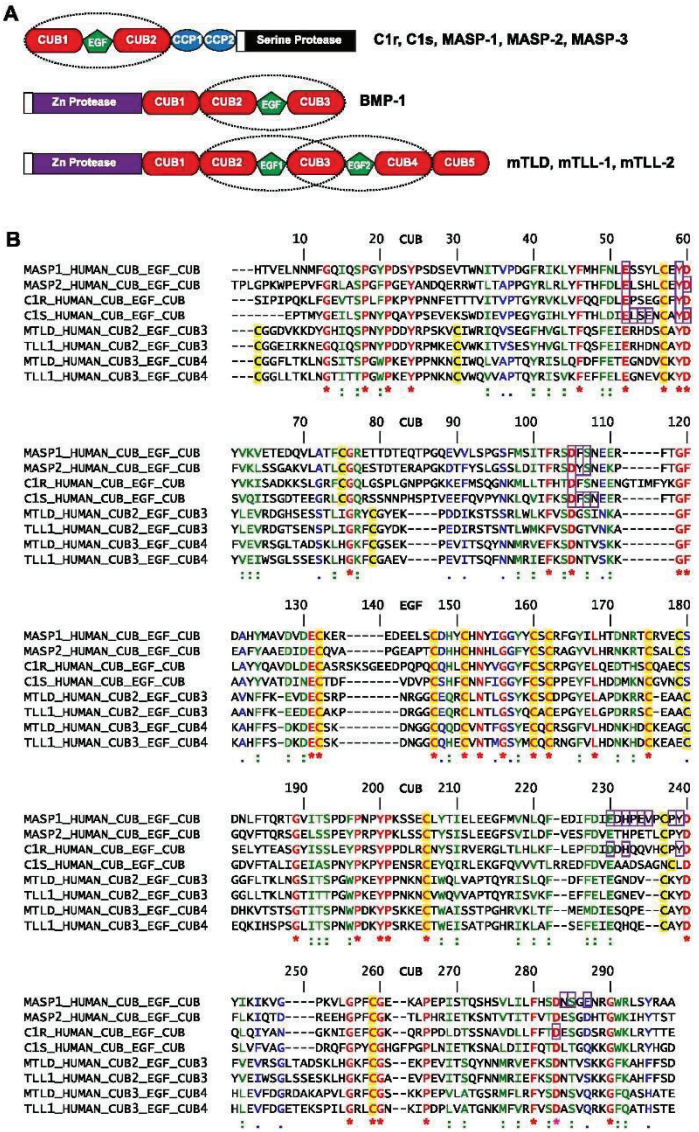

Figure 1. C1r/C1s/MASPs and BTPs are modular proteinases with CUB-EGF-CUB motifs. **(A)** These proteins consist of a protease domain linked to an N-terminal (C1r, C1s, MASPs) or C-terminal (BTPs) non-catalytic region that contains one or two trimodular CUB-EGF-CUB motif(s). CUB: complement C1r/C1s, Uegf, Bmp1; EGF: epidermal growth factor; CCP: complement control protein. Note that BMP-1 and mTLD are products of alternative splicing from the same gene, as is also the case for MASP-1 and MASP-3. The amino acid sequences of BMP-1 and mTLD are identical up to the end of the CUB3 domain, while those of MASP-1 and MASP-3 are identical up to the end of the CCP2 domain. **(B)** Sequence alignment of CUB-EGF-CUB motifs in complement proteases and BTPs. Identical residues are in red (*), strongly similar residues are in green (:) and similar residues are in blue (.). Cysteines are highlighted in yellow. Residues involved in Ca^{2+} binding are in bold. Regions involved in binding to MBL or C1q are boxed[10,15,40,54].

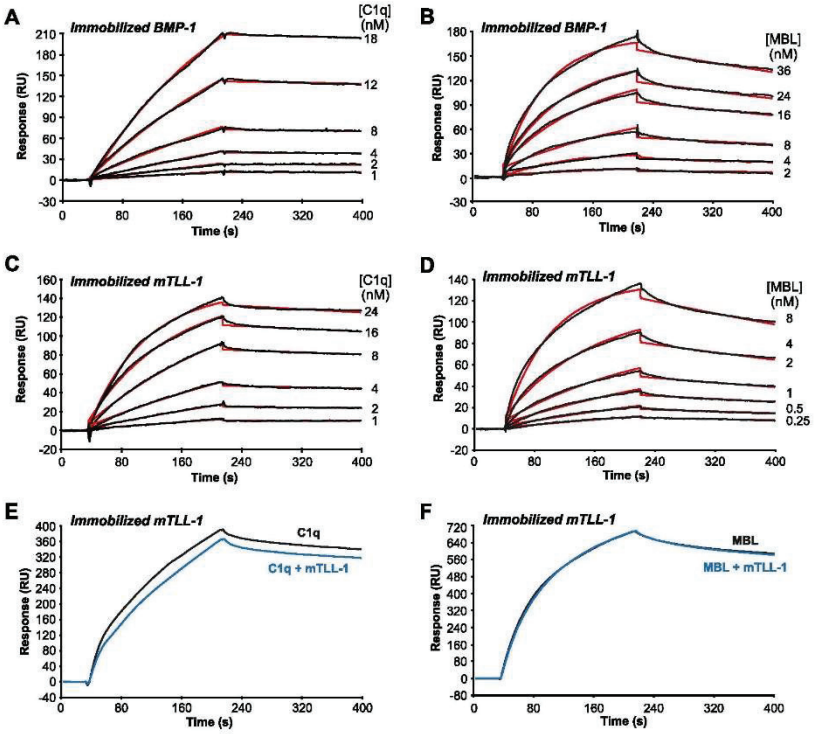

Figure 2. Kinetic analyses of the interaction of C1q or MBL with immobilized BMP-1 or mTLL-1 and competition with soluble mTLL-1 for C1q or MBL binding to immobilized mTLL-1. (**A**,**B**) Sixty µl of C1q and MBL were injected at the indicated concentrations over immobilized BMP-1 (740 and 850 RU, respectively) in 50 mM triethanolamine-HCl, 145 mM NaCl, 2 mM $CaCl_2$, 0.005% surfactant P20, pH 7.4. (**C**,**D**) C1q and MBL were injected over immobilized mTLL-1 (310 and 720 RU) under the same conditions as in (**A**,**B**). Fits shown as red lines were obtained by global fitting of the data using a 1:1 Langmuir binding model. Chi2 values were between 0.6 and 3.6. Each kinetic analysis shown is representative of three (**B**,**C**) and four (**A**,**D**) independent experiments performed on separate sensor chips. (**E**,**F**) C1q and MBL (10 nM) were incubated for 15 min at room temperature in the presence of mTLL-1 (60 nM) before injection over immobilized mTLL-1 (3,400 RU) in 50 mM triethanolamine-HCl, 145 mM NaCl, 2 mM $CaCl_2$, 0.005% surfactant P20, pH 7.4. One representative experiment out of two is shown.

Immobilized ligand	Soluble analyte	k_a (M^{-1} s^{-1})	k_d (s^{-1})	K_D (M)	n[a]
BMP-1	C1q	$4.4 \pm 0.5 \times 10^5$	$2.1 \pm 0.7 \times 10^{-4}$	$4.8 \pm 1.9 \times 10^{-10}$	5
BMP-1	MBL	$7.4 \pm 1.4 \times 10^5$	$8.7 \pm 1.7 \times 10^{-4}$	$1.3 \pm 0.5 \times 10^{-9}$	4
mTLL-1	C1q	$3.6 \pm 0.9 \times 10^5$	$3.0 \pm 0.9 \times 10^{-4}$	$8.9 \pm 0.9 \times 10^{-10}$	4
mTLL-1	MBL	$1.4 \pm 0.2 \times 10^6$	$8.2 \pm 2.6 \times 10^{-4}$	$5.8 \pm 1.7 \times 10^{-10}$	5
MASP-2	MBL	$2.8 \pm 0.4 \times 10^5$	$4.7 \pm 1.5 \times 10^{-4}$	$1.7 \pm 0.3 \times 10^{-9}$	2

Table 1. Kinetic and equilibrium dissociation constants for binding of C1q and MBL to immobilized BMP-1 and mTLL-1. [a]Number of separate experiments on different sensor chips. Values are expressed as mean ± standard error.

inhibited subsequent interaction with BMP-1 (Fig. 3A) and mTLL-1 (Fig. 3B). Similarly, pre-incubation of MBL with MASP-2 prevented MBL binding to BMP-1 (Fig. 3C) and mTLL-1 (Fig. 3D), suggesting a steric hindrance effect or direct competition of the complement proteases with the BTPs for a common binding site on the collagen stalks of C1q and MBL.

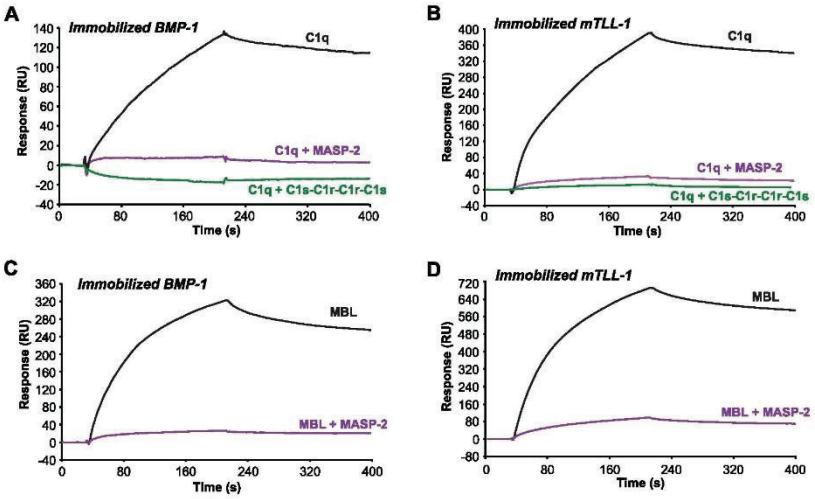

Figure 3. Competition by soluble proteases for binding of C1q and MBL to immobilized BMP-1 or mTLL-1. (**A**,**B**) C1q (10 nM) was incubated 15 min at room temperature in the presence or absence of the C1s-C1r-C1r-C1s tetramer (10 nM) or MASP-2 (60 nM) before injection over immobilized BMP-1 (2,300 RU) and mTLL-1 (3,400 RU) in 50 mM triethanolamine-HCl, 145 mM NaCl, 2 mM $CaCl_2$, 0.005% surfactant P20, pH 7.4. (**C**,**D**) MBL (10 nM) was incubated in the presence or absence of MASP-2 (60 nM) before injection over immobilized BMP-1 and mTLL-1 under the same conditions as in (**A**,**B**). (**A**–**D**) One representative experiment out of two is shown.

To further locate the BTP binding site on C1q, we used the two functional regions of C1q, *i.e.* its globular regions (GRs) involved in target recognition and its collagen-like regions (CLRs) involved in interaction with C1r and C1s. The CLRs (~190 kDa) comprise six collagen-like triple helices, held together through their N-terminal parts and the GRs (~48 kDa) correspond to the C-terminal trimeric globular regions of the helices. The CLRs bound to immobilized BMP-1 and mTLL-1 whereas no or very weak binding was observed for the GRs (Fig. 4A,B). Similarly, no interaction was detected for the recombinant trimeric carbohydrate recognition domain of MBL (CRD) (Fig. 4A,B).

We have previously generated MBL mutants devoid of MASP-binding ability after mutation of the Lys55 residue of the collagen-like regions[18]. The capacity of the MBL K55A and K55E mutants to interact with immobilized BTPs was compared to that of wild-type MBL. As shown in Fig. 4C,D, both mutations strongly inhibited the interaction, indicating that Lys55 of MBL is essential for the interaction with both BMP-1 and mTLL-1.

Soluble BMP-1 and mTLL-1 do not inhibit complement activation. The fact that BMP-1 and mTLL-1 interact with C1q and MBL at the complement protease binding site raised the question of a possible inhibition of complement activation by BTPs. MBL-dependent activation of the lectin complement pathway was measured in mannan-coated microwells by C4b deposition ELISA[19] using human MBL-deficient serum reconstituted with 2 µg/ml MBL. Pre-incubation of MBL with BMP-1 (Fig. 5A) or mTLL-1 (Fig. 5B) up to a BMP-1/mTLL-1:MBL molar ratio of 30/36:1 yielded no evidence for inhibition of complement activation.

The possible inhibition of the classical complement pathway was also investigated using a C1 activation assay, based on measurement of the self-activation of the C1 complex reconstituted from its isolated purified subcomponents, C1q and the proenzyme C1s-C1r-C1r-C1s tetramer, in the absence of C1-Inhibitor. Incubation of the C1 complex at 30 or 37 °C results in C1r self-activation, followed by C1s activation by activated C1r. Pre-incubation of C1q with BMP-1 (molar BMP-1 excess over C1q up to 3.2-fold) or mTLL-1 (molar excess up to 4-fold) before addition of the proenzyme C1s-C1r-C1r-C1s tetramer and incubation of the resulting complex at 30 °C had no effect on C1 spontaneous activation, determined from the amounts of A and B chains of activated C1s generated (Fig. 5C,D).

These data provided no evidence for an effect of BTPs in solution on complement activation, which is consistent with the observed absence of formation of stable complexes in solution between C1q/MBL and BMP-1/mTLL-1 in the competition experiments.

Defence collagens are neither substrates nor inhibitors of soluble BMP-1. To look for possible proteolytic cleavage of the defence collagens by BMP-1, we incubated C1q or MBL with human BMP-1, in conditions known to cleave a standard BMP-1 substrate derived from procollagen III (CPIII-long) which is cleaved between the large C-propeptide trimer (3 x ~30 kDa) and the region (3 x ~3 kDa) comprising the three

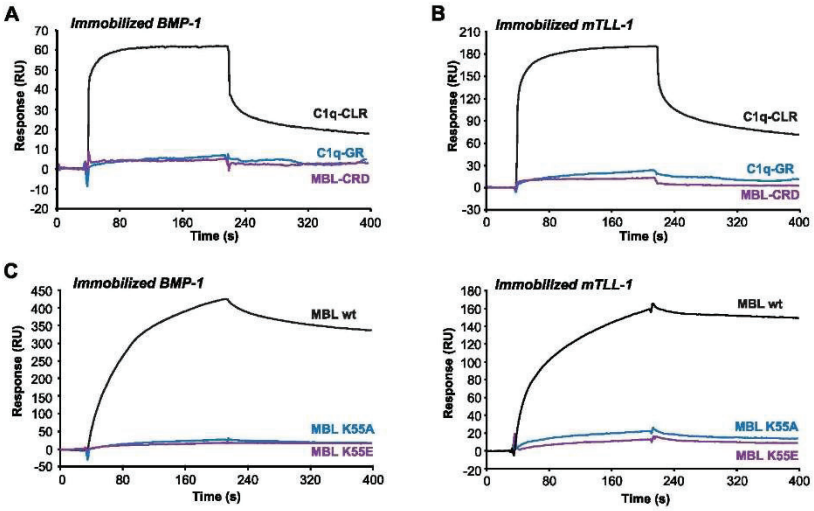

Figure 4. The BMP-1 and mTLL-1 binding site is located in the collagen-like regions of C1q and Lys55 of MBL is essential for the interaction. The collagen-like regions of C1q (CLR), the globular regions of C1q (GR) and the trimeric carbohydrate recognition domain of MBL (CRD) were injected at a concentration of 500 nM over (**A**) immobilized BMP-1 (2,300 RU) and (**B**) mTLL-1 (1,120 RU) in 50 mM triethanolamine-HCl, 145 mM NaCl, 2 mM $CaCl_2$, 0.005% surfactant P20, pH 7.4. Wild-type (wt) MBL and its K55A and K55E mutants (16 nM) were injected over (**C**) immobilized BMP-1 (2,300 RU) and (**D**) mTLL-1 (310 RU) under the same conditions as in (**A**). (**A–D**) One representative experiment out of three is shown.

C-terminal Gly-X-Y triplets of the collagen triple-helix and the C-telopeptide[20]. As shown in Fig. 6A, there was no evidence of BMP-1 cleavage of C1q or MBL in these conditions. We also checked whether pre-incubation with defence collagens might inhibit cleavage of CPIII-long by BMP-1. As shown in Fig. 6B, we found no evidence of inhibition at molar ratios of C1q or MBL to substrate of up to 5:1. These results indicate therefore that the defence collagens are neither substrates nor inhibitors of BMP-1 activity in solution, at least on a standard procollagen III-like substrate.

BMP-1/C1q co-localization in tissue inflammation. To test the possibility of an interaction of C1q with BMP-1 in physiological conditions, we investigated the expression of these two proteins in human skin sections by immunofluorescence. Skin biopsies from clinically non-inflamed regions adjacent to sites of melanoma excision or from patients with recessive dystrophic epidermolysis bullosa (RDEB) were used. RDEB is an inherited skin-blistering disorder caused by mutations in the *COL7A1* gene which encodes type VII collagen, an extracellular matrix (ECM) protein that forms the anchoring fibrils involved in the attachment of the epidermis to the underlying dermis. Skin of RDEB patients exhibits impaired wound healing and scarring and is characterized by strong inflammation[21,22], as found by the presence of high levels of C1q[23]. As shown in Fig. 7, C1q protein was expressed in biopsies from clinically non-inflamed skin from sites adjacent to melanoma excision and also from RDEB patient skin, as well as BMP-1. Evidence for co-localization of BMP-1 and C1q was found in all cases (Fig. 7). Co-localization of C1q and BMP-1 was further corroborated, using several images (n = 10), by calculation of the Pearson correlation coefficient between C1q and BMP-1 staining. This revealed a moderate to strong co-localization of C1q and BMP-1 staining, as indicated by a correlation coefficient ranging from 0.475 to 0.695 (Supplementary Fig. S7).

Discussion

In recent years, it has become increasingly clear that the roles of the ECM and innate immunity are closely intertwined[12,24–28]. The defence collagens C1q and MBL play pivotal roles, either as part of the C1 and MBL-MASP complexes where they promote inflammation via the complement cascade, or when, free of such complexes, they contribute locally to the resolution of inflammation prior to tissue repair. C1q and MBL bind to several ECM constituents, including the small leucine-rich repeat proteoglycans (SLRPs) decorin and biglycan[29,30] and cartilage oligomeric matrix protein (COMP)[31], with various outcomes in terms of complement activation. Decorin and biglycan bind to both C1q CLRs and GRs and prevent activation of the classical complement pathway; they also bind MBL, but only biglycan inhibits the lectin pathway[30]. Similarly, COMP prevents activation of both pathways by binding to the CLRs of C1q or MBL[31]. In contrast, other SLRPs such as fibromodulin and osteoadherin and the metalloproteinase MT1-MMP have been found to trigger complement activation by binding to the GRs of C1q[29,32]. The ECM proteins fibronectin[33] and laminin[34] also bind to C1q, likely through its CLRs, but with

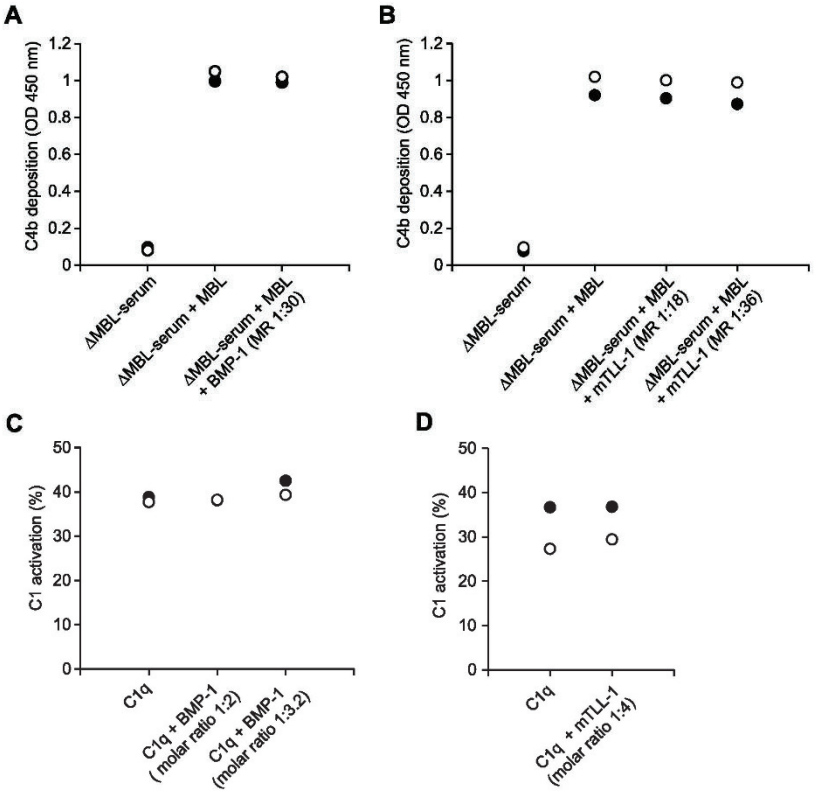

Figure 5. Soluble BMP-1 and mTLL-1 inhibit neither activation of the lectin pathway of human serum complement nor activation of the reconstituted C1 complex. (**A**,**B**) MBL-deficient (Δ-MBL) serum reconstituted with 2 μg/ml MBL, preincubated or not with BMP-1 or mTLL-1 at the indicated molar ratios (MR), was added to mannan-coated microtiter wells. The resulting MASP-2 cleaving activity was measured by a C4b deposition assay. Two independent experiments were performed and each data point is the mean of duplicate (**A**) and quadruplicate measurements (**B**). (**C**,**D**) Complexes (0.25 μM) reconstituted from C1q, pre-incubated or not with BMP-1 or mTLL-1 at the indicated MR, and proenzyme C1s-C1r-C1r-C1s were incubated for 30 min at 30 °C. The extent of C1 self-activation was measured by SDS-PAGE, followed by Western blot analysis using an anti-C1s antibody. The values obtained in two independent experiments are plotted as white and black circles, respectively.

unknown effects on complement activation. Finally, MBL and C1q interact with the collagen receptors integrin α2β1[35] and LAIR-1[36]. The C1q-α2β1 interaction is thought to play a role in mast cell activation and cytokine secretion[35] whereas C1q binding to LAIR-1 leads to differentiation arrest of dendritic cells (DC) and suppression of DC-derived pro-inflammatory cytokine production[36].

In addition to interacting with ECM proteins and related receptors, C1q and MBL act as opsonins to facilitate the clearance of apoptotic cells by tissue macrophages and DCs[37,38] which themselves are major producers of these defence collagens. Macrophages also produce many cytokines, which, depending on macrophage polarization, can be either pro-inflammatory (M1 macrophages) or anti-inflammatory (M2 macrophages). C1q has been shown to regulate the switch to the M2 phenotype[39], resulting in the production of anti-inflammatory cytokines such as TGF-β which is crucial for ECM homeostasis and tissue repair. As an example of this continuity between innate immunity and ECM, M2 macrophage activation via the IL-4 receptor has recently been shown to enhance tissue repair, including vascularisation and collagen assembly, in a skin wound-healing model[27]. Using a similar model, C1q has also been shown to enhance wound repair by stimulating angiogenesis via interactions with endothelial cell receptors[24]. Finally, the periodontal form of Ehlers-Danlos syndrome (pEDS), characterised by periodontitis and gingival recessions but also skin abnormalities such as easy bruising, fragility and abnormal

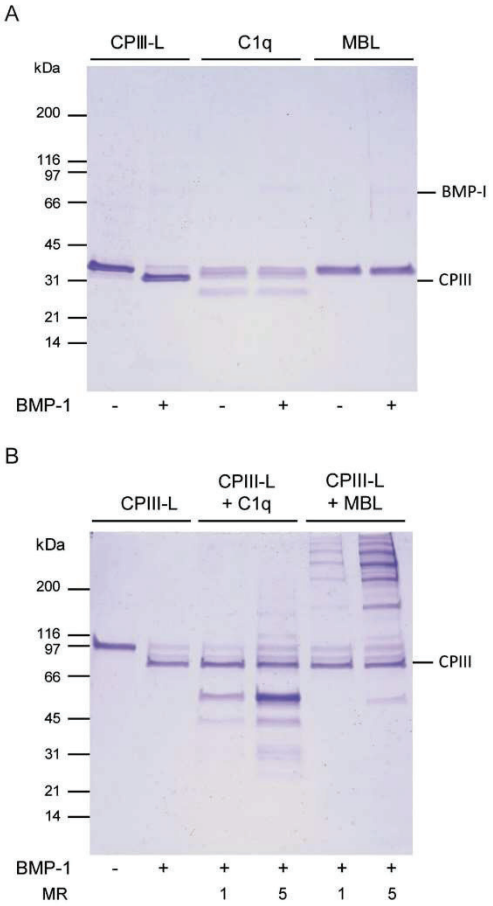

Figure 6. Defence collagens are neither substrates nor inhibitors of BMP-1 in solution. (**A**) CPIII-long (CPIII-L) or defence collagens C1q and MBL (all at 400 nM) were incubated with BMP-1 (20 nM) for 2 h then analyzed by SDS-PAGE (reducing conditions) on a 4–20% acrylamide gradient gel. The band at approximately 30 kDa in lane 2 corresponds to the released C-propeptide (CPIII). Bands for C1q and MBL are unchanged after incubation with BMP-1. (**B**) BMP-1 cleavage of CPIII-long in the absence or presence of defence collagens. Conditions were as in (**A**), except that SDS-PAGE was done in non-reducing conditions. CPIII indicates the released C-propeptide trimer from CPIII-long, the amount of which is unaffected by the presence of C1q or MBL. The molar ratios (MR) of C1q or MBL to CPIII-long are indicated. Whereas C1q analysis under reducing conditions yields a double band containing the A and B chains (31 and 30 kDa, respectively), and the C chain at 26 kDa, analysis under non-reducing conditions yields characteristic A-B and C-C dimers (53 and 48 kDa, respectively). Recombinant MBL migrates as a single band of 30 kDa under reducing conditions and yields a typical ladder-like pattern corresponding to different oligomers under non-reducing conditions. Each gel is representative of three separate experiments. Images are cropped for clarity and conciseness. Full-size gels (including markers) are presented in Supplementary Fig. S6.

collagen fibrils, was recently shown to be caused by mutations in the complement proteases C1r and C1s, though the underlying molecular mechanisms are unknown[25].

In view of these links between innate immunity and the extracellular matrix, as well as the presence of CUB-EGF-CUB motifs in both complement proteases (C1r, C1s, MASPs) and BTPs, we sought to determine whether BMP-1 and mTLL-1 might interact with the complement proteins C1q and MBL. We found that both C1q and MBL were able to bind to immobilized BMP-1 and mTLL-1, with affinities in the nanomolar range. As also found for their cognate binding partners, binding of BMP-1/mTLL-1 to C1q/MBL was Ca^{2+}-dependent

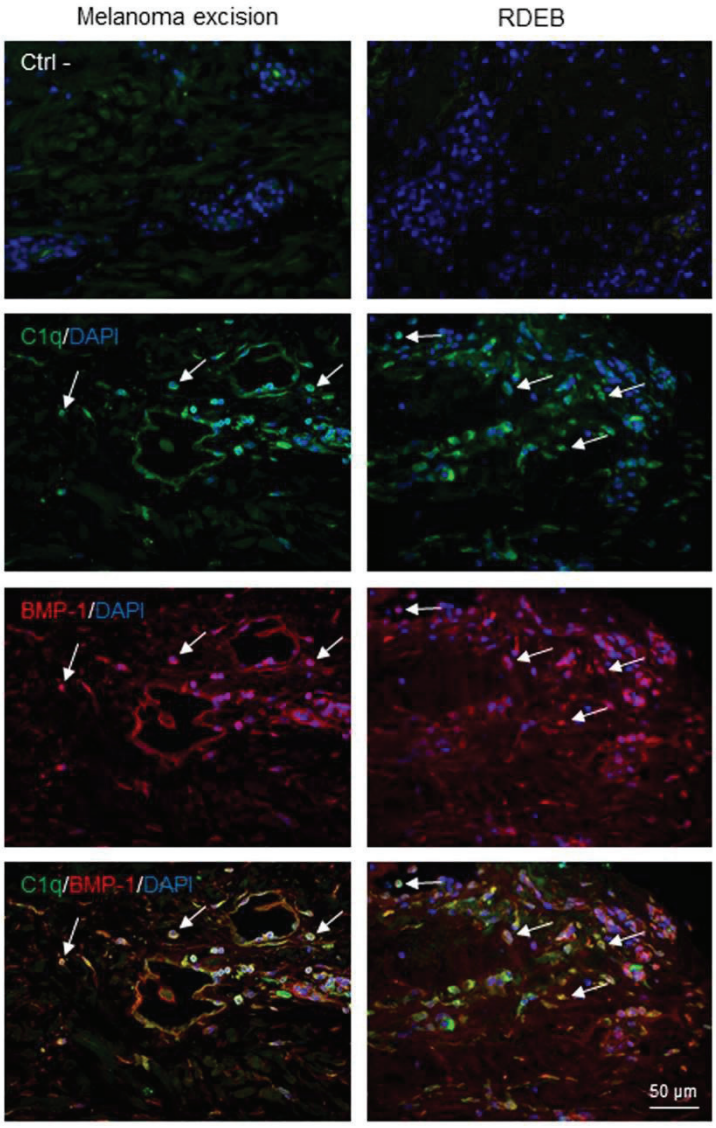

Figure 7. C1q protein colocalizes with BMP-1 in skin biopsies from patients following melanoma excision or with recessive dystrophic epidermolysis bullosa (RDEB). Paraffin-embedded human skin sections were stained with antibodies to C1q (green) and BMP-1 (red). Nuclei were counterstained with DAPI (blue). Images were acquired with a 40X objective (scale bar = 50 µm). Tissue sections were also stained without primary antibody (secondary antibodies only) as negative controls (Ctrl −). Arrows indicate regions positive for C1q and BMP-1 that are co-localized in the lower panels.

and to the collagen-like region. Experimental evidence for this was provided by competition experiments using complement proteases, for C1q using separated globular and collagen-like domains and finally for MBL using site-directed Lys55 mutants in the region of the known MASP binding site[18]. Residues analogous to Lys55 have

been shown to play similar roles in C1q binding to C1s-C1r-C1r-C1s[16,40]. These observations suggest that BMP-1/mTLL-1 binding to C1q and MBL involve similar interactions to those between these defence collagens and their cognate binding partners, mostly likely involving CUB domains. Comparison of sequences for the trimodular CUB-EGF-CUB motifs found in complement proteases and BTPs (Fig. 1B) shows conservation in BTPs of residues known to be important for complement protease binding to C1q/MBL, particularly the acidic residues that are also involved in Ca^{2+} binding. In contrast, there is less conservation of interacting residues adjacent to these sites.

BTP binding affinities on defence collagens were similar to those previously obtained for complement proteases[10,11,17], albeit that in the latter case the defence collagens were in the immobilized phase. Control experiments performed here showed that the binding affinities for C1q/MBL on immobilized MASP-2 were similar to those found for the reverse configuration. In contrast, when BMP-1 or mTTL-1 was in the mobile phase, little or no binding was found to immobilized C1q or MBL, despite the fact that mTLL-1, unlike BMP-1, appears to be a dimer in solution[41]. This is reminiscent of previous studies where binding of MBL to the complement receptor CR1, which involves the same protease binding site, was only observed when CR1 was in the immobilized phase[42]. These observations suggest that, unlike for their cognate binding partners, binding of C1q/MBL to BMP-1/mTLL-1 either requires a conformational change induced by immobilization or is a cooperative phenomenon involving multiple BMP-1/mTLL-1 monomers immobilized in close proximity on the sensor chip. Both interpretations are consistent with the observation that soluble BMP-1/mTLL-1 could not compete for C1q/MBL binding to the immobilized BTPs, in contrast to soluble C1s-C1r-C1r-C1s/MASP-2 which strongly inhibited BTP binding to C1q/MBL in either configuration.

Soluble BMP-1 and mTLL-1 did not inhibit activation of the classical and lectin complement pathways and the defence collagens were neither substrates nor inhibitors of BMP-1 in solution, suggesting that the functional consequences of the observed molecular crosstalk are limited to situations where BMP-1 is bound to the matrix. In this regard, the immunofluorescence data showed clear evidence of co-localization of C1q and BMP-1 in biopsies from clinically non-inflamed skin, adjacent to melanoma excision sites and from patients suffering from RDEB. The presence of C1q in the former is expected since C1q has been found to be associated with stromal elements at the invasion edge of several tumours, including melanoma[43]. In an RDEB mouse model, increased expression of C1q has been documented by mass spectrometry and biochemical analysis[23]. The observed co-localization of C1q and BMP-1 suggests that these proteins might interact *in vivo*. Since the *in vitro* data show that binding of defence collagens to BTPs requires the latter to be immobilized on a solid support, this suggests that there may be a similar requirement *in vivo*. As it has been shown that BMP-1 binds to the fibronectin matrix produced by culture human neonatal fibroblasts[44], one such candidate is fibronectin, which also binds C1q[33]. Thus interactions analogous to the observed *in vitro* interaction between free C1q/MBL and immobilized BTPs might serve to co-localize these proteins *in vivo*, so as to coordinate resolution of inflammation and tissue repair.

Methods

Proteins. C1q and the proenzyme form of the C1s-C1r-C1r-C1s tetramer were purified from human serum and quantified as described previously[45,46]. The collagen-like regions (CLRs) and the globular regions (GRs) of C1q were prepared by limited pepsin and collagenase digestion of C1q, respectively, and purified and quantified as described previously[46,47]. Recombinant human mannose-binding lectin (MBL) and its K55A and K55E variants were produced in Freestyle 293-F cells (Thermofisher Scientific) and purified by affinity chromatography on N-acetylglucosamine-agarose (Sigma-Aldrich) as described previously[18]. The molar concentration of MBL was estimated using a molecular weight of 305 kDa, assuming a majority of tetrameric species present in the samples. The recombinant trimeric carbohydrate recognition domain of MBL was produced in a baculovirus-insect cells system and purified as described by Gjelstrup *et al.*[48]. Recombinant human MASP-2 (stabilized in a proenzyme form by mutation of the active site Ser 618 into Ala[17]) was produced in *Drosophila* S2 cells as described for human ficolin-1[49,50]. Briefly, the cDNA encoding MASP-2 was cloned into the pMT/BiP/V5-His A *Drosophila* expression vector (Thermofisher Scientific) and used for stable transfection of S2 *Drosophila* cells. Stable transfectants were expanded in Schneider's *Drosophila* medium (Thermofisher Scientific) supplemented with 10% (v/v) heat-inactivated foetal calf serum and 500 µg/ml G418. Production of recombinant MASP-2 was induced by adding 750 µM $CuSO_4$ to the culture medium without added serum, and the culture supernatants were harvested after 72 h incubation. Recombinant MASP-2 was purified by affinity chromatography on a C1q-Sepharose column, as described for purification of recombinant MASP-3[42], and its molar concentration estimated using a MW value of 74,160 and an absorption coefficient (A1%, 1 cm) at 280 nm of 15.7.

Recombinant human BMP-1 with a C-terminal FLAG tag and mTLL-1 with a C-terminal 6x-His tag were produced in HEK 293-EBNA cells as described[41,51,52]. The BTP substrate CPIII-long (derived from human procollagen III) was produced in HEK 293'T' cells[20]. SDS-PAGE analysis of all purified proteins used is provided in Supplementary Fig. S8.

Surface plasmon resonance spectroscopy. All experiments were performed on a BIAcore 3000 instrument (GE Healthcare) at 25 °C. Ligands were covalently immobilized on CM5 sensor chips in 10 mM HEPES, 150 mM NaCl, 3 mM EDTA, pH 7.4 containing 0.005% surfactant P20 using amine coupling chemistry according to the manufacturer's instructions (GE Healthcare). Protein ligands were diluted in 10 mM sodium acetate at the following concentrations and pH values for injection over the activated dextran surface: BMP-1, mTLL-1 and MBL: 5–10, 1.8–7.4 and 25 µg/ml (pH 4.0); C1q: 35 µg/ml (pH 5.0); MASP-2: 17 µg/ml (pH 3.5). Binding was measured at a flow rate of 20 µl/min in 50 mM triethanolamine-HCl, 145 mM NaCl, pH 7.4, containing 0.005% surfactant P20 and 2 mM $CaCl_2$ or 3 mM EDTA. Sixty microliters of each soluble analyte at the desired concentrations were injected over the immobilized ligands, and the surfaces were regenerated by 10 µl injections of 10 mM Tris-HCl, 1 M NaCl, 10 mM EDTA, pH 7.4 and, if needed, 10 µl of running buffer containing 3 M $MgCl_2$.

A control flow cell submitted to all coupling steps without immobilized protein was used as a reference, and the specific binding signal was obtained by subtracting the background signal over the reference surface. For competition assays, C1q and MBL were incubated for 15 min at room temperature with MASP-2, BMP-1 or mTLL-1 before injection over the immobilized proteinases.

Data were analyzed by global fitting to a 1:1 Langmuir binding model of both the association and dissociation phases for at least six analyte concentrations simultaneously, using the BIAevaluation 3.2 software (GE Healthcare). Buffer blanks were subtracted from the datasets used for kinetic analysis (double referencing). The apparent equilibrium dissociation constants (K_D) were calculated from the ratio of the dissociation and association rate constants (k_d/k_a). Chi2 values were below 7 in all cases.

Complement activation assays. A C4 cleavage ELISA was used to measure human serum complement activation via the MBL-dependent lectin pathway. Activation was measured as described by Dumestre-Pérard *et al.*[19], using mannan-coated plates and human MBL-deficient serum reconstituted with 2 µg/ml recombinant human MBL (pre-incubated or not with BMP-1 for 30 min at room temperature), except that plates were developed with tetramethylbenzidine (Sigma), the reaction was stopped by 1 N H_2SO_4 and absorbance was read at 450 nm.

For the C1 complex activation assay, C1 (0.25 µM) was first reconstituted from purified serum C1q and the proenzyme C1s-C1r-C1r-C1s tetramer[46]. Self-activation was measured by incubating the resulting complexes at 30 °C for 30 min in 50 mM triethanolamine-HCl, 145 mM NaCl, 2.5 mM $CaCl_2$, pH 7.4. The extent of C1 activation was determined from the amounts of the A and B chains of activated C1s generated, following Western blot analysis using an anti-C1s antibody and alkaline phosphatase immunodetection[46]. Image acquisition and densitometric analysis were performed using the ChemiDoc MP imager with Image Lab software (Bio-Rad). Pre-incubation of C1q with BMP-1 or mTLL-1 prior to C1 reconstitution was performed at room temperature for 20 min.

BMP-1 cleavage activity. For BMP-1 cleavage assays, aliquots of purified plasma-derived human C1q (1 mg/ml) and recombinant human MBL (1 mg/ml) were first dialyzed against assay buffer (50 mM Hepes pH 7.4, 150 mM NaCl, 5 mM $CaCl_2$). CPIII-long[20], in the same buffer, was used as a positive control. Reactions (30 µl volume) were set up, in LoBind Eppendorf tubes, using 400 nM substrate (C1q, MBL) and 20 nM recombinant human BMP-1, followed by incubation for 2 h at 37 °C. Reactions were stopped by transfer to ice and addition of 7.5 µl of 5x Laemmli sample buffer (containing dithiothreitol to a final concentration of 50 mM), followed by heating to 100 °C for 3 min. Samples were analyzed by SDS-PAGE using 4–20% gradient gels (BioRad) and staining with Commassie Blue. To look for possible inhibition of BMP-1 cleavage, mini-procollagen III assays were set up as before, but in the absence or presence of C1q or MBL (400 nM or 2 µM for each). Samples for SDS-PAGE were prepared as before, except in non-reducing conditions, and analyzed using 4–20% gradient gels.

Immunofluorescence analysis of human skin biopsies. Human skin biopsies were obtained using experimental protocols approved by the Ethics Committee of the University of Freiburg (approval number 45/03–110631) in accordance with the declaration of Helsinki and with written informed consent from all participants and/or their legal guardians. Samples were obtained from four patients following melanoma excision (clinically non-inflamed regions adjacent to the sites of excision, to at least ensure safety margins) and from four patients with recessive dystrophic epidermolysis bullosa (RDEB). For immunofluorescence analysis, samples were first fixed in formalin and embedded in paraffin. Sections (4 µm) were then cut, de-paraffinized and re-suspended in xylene and ethanol. Antigens were retrieved by pronase digestion (0.05% solution in PBS, Roche). Sections were blocked in 3% bovine serum albumin (Chem Cruz) diluted in TBS-0.05% Tween 20 and stained with primary and secondary antibodies diluted in blocking solution. Primary antibodies used were mouse monoclonal anti-C1q (Abcam, clone 9A7, ab71089) and rabbit polyclonal anti-BMP-1 directed against active proteinase[53] (it should be noted that this antibody recognizes both BMP-1 and mTLD as the antigen used is in the catalytic domain which is identical in both proteinases). Secondary antibodies used were, respectively, AlexaFluor 488-conjugated goat anti-mouse IgG and AlexaFluor 594-conjugated goat anti-rabbit IgG (ThermoFisher Scientific) antibodies. Finally, sections were counterstained with 4′,6-diamidino-2-phenylindole (DAPI) and mounted in Fluorescence Mounting Medium (Dako). Stained sections were analyzed with an Axioplan2 fluorescence microscope (Zeiss), capturing images using a black and white camera followed by analysis with ImageJ.

References

1. Merle, N. S., Church, S. E., Fremeaux-Bacchi, V. & Roumenina, L. T. Complement System Part I - Molecular Mechanisms of Activation and Regulation. *Front Immunol* **6**, 262, https://doi.org/10.3389/fimmu.2015.00262 (2015).
2. Ricklin, D., Hajishengallis, G., Yang, K. & Lambris, J. D. Complement: a key system for immune surveillance and homeostasis. *Nat Immunol* **11**, 785–797 (2010).
3. Gaboriaud, C., Ling, W. L., Thielens, N. M., Bally, I. & Rossi, V. Deciphering the fine details of c1 assembly and activation mechanisms: "mission impossible"? *Front Immunol* **5**, 565, https://doi.org/10.3389/fimmu.2014.00565 (2014).
4. Garred, P. *et al.* A journey through the lectin pathway of complement-MBL and beyond. *Immunol Rev* **274**, 74–97 (2016).
5. Meri, S. Self-nonself discrimination by the complement system. *FEBS Lett* **590**, 2418–2434 (2016).
6. Dobo, J. *et al.* MASP-3 is the exclusive pro-factor D activator in resting blood: the lectin and the alternative complement pathways are fundamentally linked. *Sci Rep* **6**, 31877, https://doi.org/10.1038/srep31877 (2016).
7. Vadon-Le Goff, S., Hulmes, D. J. & Moali, C. BMP-1/tolloid-like proteinases synchronize matrix assembly with growth factor activation to promote morphogenesis and tissue remodeling. *Matrix Biol* **44-46**, 14–23 (2015).
8. Bork, P. & Beckmann, G. The CUB domain. A widespread module in developmentally regulated proteins. *J Mol Biol* **231**, 539–545 (1993).
9. Gaboriaud, C. *et al.* Structure and properties of the Ca(2+)-binding CUB domain, a widespread ligand-recognition unit involved in major biological functions. *Biochem J* **439**, 185–193 (2011).

10. Bally, I. *et al.* Identification of the C1q-binding Sites of Human C1r and C1s: a refined three-dimensional model of the C1 complex of complement. *J Biol Chem* **284**, 19340–19348 (2009).
11. Phillips, A. E. *et al.* Analogous interactions in initiating complexes of the classical and lectin pathways of complement. *J Immunol* **182**, 7708–7717 (2009).
12. Prabhu, S. D. & Frangogiannis, N. G. The Biological Basis for Cardiac Repair After Myocardial Infarction: From Inflammation to Fibrosis. *Circ Res* **119**, 91–112 (2016).
13. Gu, H. *et al.* Contribution of the anaphylatoxin receptors, C3aR and C5aR, to the pathogenesis of pulmonary fibrosis. *FASEB J* **30**, 2336–2350 (2016).
14. Cseh, S. *et al.* Characterization of the interaction between L-ficolin/p35 and mannan-binding lectin-associated serine proteases-1 and -2. *J Immunol* **169**, 5735–5743 (2002).
15. Teillet, F. *et al.* Crystal structure of the CUB1-EGF-CUB2 domain of human MASP-1/3 and identification of its interaction sites with mannan-binding lectin and ficolins. *J Biol Chem* **283**, 25715–25724 (2008).
16. Bally, I. *et al.* Expression of recombinant human complement C1q allows identification of the C1r/C1s-binding sites. *Proc Natl Acad Sci USA* **110**, 8650–8655 (2013).
17. Zundel, S. *et al.* Characterization of recombinant mannan-binding lectin-associated serine protease (MASP)-3 suggests an activation mechanism different from that of MASP-1 and MASP-2. *J Immunol* **172**, 4342–4350 (2004).
18. Teillet, F. *et al.* Identification of the site of human mannan-binding lectin involved in the interaction with its partner serine proteases: the essential role of Lys55. *J Immunol* **178**, 5710–5716 (2007).
19. Dumestre-Perard, C. *et al.* Evaluation and clinical interest of mannan binding lectin function in human plasma. *Mol Immunol* **39**, 465–473 (2002).
20. Bourhis, J. M. *et al.* Procollagen C-proteinase enhancer grasps the stalk of the C-propeptide trimer to boost collagen precursor maturation. *Proc Natl Acad Sci USA* **110**, 6394–6399 (2013).
21. Fritsch, A. *et al.* A hypomorphic mouse model of dystrophic epidermolysis bullosa reveals mechanisms of disease and response to fibroblast therapy. *J Clin Invest* **118**, 1669–1679 (2008).
22. Nystrom, A. *et al.* Collagen VII plays a dual role in wound healing. *J Clin Invest* **123**, 3498–3509 (2013).
23. Nystrom, A. *et al.* Losartan ameliorates dystrophic epidermolysis bullosa and uncovers new disease mechanisms. *EMBO Mol Med* **7**, 1211–1228 (2015).
24. Bossi, F. *et al.* C1q as a unique player in angiogenesis with therapeutic implication in wound healing. *Proc Natl Acad Sci USA* **111**, 4209–4214 (2014).
25. Kapferer-Seebacher, I. *et al.* Periodontal Ehlers-Danlos Syndrome Is Caused by Mutations in C1R and C1S, which Encode Subcomponents C1r and C1s of Complement. *Am J Hum Genet* **99**, 1005–1014 (2016).
26. Kelsh, R. M. & McKeown-Longo, P. J. Topographical changes in extracellular matrix: Activation of TLR4 signaling and solid tumor progression. *Trends Cancer Res* **9**, 1–13 (2013).
27. Knipper, J. A. *et al.* Interleukin-4 Receptor alpha Signaling in Myeloid Cells Controls Collagen Fibril Assembly in Skin Repair. *Immunity* **43**, 803–816 (2015).
28. Kouser, L. *et al.* Emerging and Novel Functions of Complement Protein C1q. *Front Immunol* **6**, 317, https://doi.org/10.3389/fimmu.2015.00317 (2015).
29. Sjoberg, A. P. *et al.* Short leucine-rich glycoproteins of the extracellular matrix display diverse patterns of complement interaction and activation. *Mol Immunol* **46**, 830–839 (2009).
30. Groeneveld, T. W. *et al.* Interactions of the extracellular matrix proteoglycans decorin and biglycan with C1q and collectins. *J Immunol* **175**, 4715–4723 (2005).
31. Happonen, K. E. *et al.* Regulation of complement by cartilage oligomeric matrix protein allows for a novel molecular diagnostic principle in rheumatoid arthritis. *Arthritis Rheum* **62**, 3574–3583 (2010).
32. Rozanov, D. V. *et al.* Non-proteolytic, receptor/ligand interactions associate cellular membrane type-1 matrix metalloproteinase with the complement component C1q. *J Biol Chem* **279**, 50321–50328 (2004).
33. Bing, D. H., Almeda, S., Isliker, H., Lahav, J. & Hynes, R. O. Fibronectin binds to the C1q component of complement. *Proc Natl Acad Sci USA* **79**, 4198–4201 (1982).
34. Bohnsack, J. F. *et al.* The C1q subunit of the first component of complement binds to laminin: a mechanism for the deposition and retention of immune complexes in basement membrane. *Proc Natl Acad Sci USA* **82**, 3824–3828 (1985).
35. Edelson, B. T. *et al.* Novel collectin/C1q receptor mediates mast cell activation and innate immunity. *Blood* **107**, 143–150 (2006).
36. Son, M., Santiago-Schwarz, F., Al-Abed, Y. & Diamond, B. C1q limits dendritic cell differentiation and activation by engaging LAIR-1. *Proc Natl Acad Sci USA* **109**, E3160–3167 (2012).
37. Bohlson, S. S., O'Conner, S. D., Hulsebus, H. J., Ho, M. M. & Fraser, D. A. Complement, c1q, and c1q-related molecules regulate macrophage polarization. *Front Immunol* **5**, 402, https://doi.org/10.3389/fimmu.2014.00402 (2014).
38. Fraser, D. A. & Tenner, A. J. Directing an appropriate immune response: the role of defense collagens and other soluble pattern recognition molecules. *Curr Drug Targets* **9**, 113–122 (2008).
39. Benoit, M. E., Clarke, E. V., Morgado, P., Fraser, D. A. & Tenner, A. J. Complement protein C1q directs macrophage polarization and limits inflammasome activity during the uptake of apoptotic cells. *J Immunol* **188**, 5682–5693 (2012).
40. Venkatraman Girija, U. *et al.* Structural basis of the C1q/C1s interaction and its central role in assembly of the C1 complex of complement activation. *Proc Natl Acad Sci USA* **110**, 13916–13920 (2013).
41. Berry, R., Jowitt, T. A., Garrigue-Antar, L., Kadler, K. E. & Baldock, C. Structural and functional evidence for a substrate exclusion mechanism in mammalian tolloid like-1 (TLL-1) proteinase. *FEBS Lett* **584**, 657–661 (2010).
42. Jacquet, M. *et al.* Deciphering complement receptor type 1 interactions with recognition proteins of the lectin complement pathway. *J Immunol* **190**, 3721–3731 (2013).
43. Bulla, R. *et al.* C1q acts in the tumour microenvironment as a cancer-promoting factor independently of complement activation. *Nat Commun* **7**, 10346, https://doi.org/10.1038/ncomms10346 (2016).
44. Huang, G. *et al.* Fibronectin binds and enhances the activity of bone morphogenetic protein 1. *J Biol Chem* **284**, 25879–25888 (2009).
45. Arlaud, G. J., Sim, R. B., Duplaa, A. M. & Colomb, M. G. Differential elution of Clq, Clr and Cls from human Cl bound to immune aggregates. Use in the rapid purification of Cl subcomponents. *Mol Immunol* **16**, 445–450 (1979).
46. Tacnet-Delorme, P., Chevallier, S. & Arlaud, G. J. Beta-amyloid fibrils activate the C1 complex of complement under physiological conditions: evidence for a binding site for A beta on the C1q globular regions. *J Immunol* **167**, 6374–6381 (2001).
47. Moreau, C. *et al.* Structural and Functional Characterization of a Single-Chain Form of the Recognition Domain of Complement Protein C1q. *Front Immunol* **7**, 79, https://doi.org/10.3389/fimmu.2016.00079 (2016).
48. Gjelstrup, L. C. *et al.* The role of nanometer-scaled ligand patterns in polyvalent binding by large mannan-binding lectin oligomers. *J Immunol* **188**, 1292–1306 (2012).
49. Gout, E. *et al.* Carbohydrate recognition properties of human ficolins: glycan array screening reveals the sialic acid binding specificity of M-ficolin. *J Biol Chem* **285**, 6612–6622 (2010).
50. Liu, Y. *et al.* Human M-ficolin is a secretory protein that activates the lectin complement pathway. *J Immunol* **175**, 3150–3156 (2005).
51. Bijakowski, C. *et al.* Sizzled is unique among secreted frizzled-related proteins for its ability to specifically inhibit bone morphogenetic protein-1 (BMP-1)/tolloid-like proteinases. *J Biol Chem* **287**, 33581–33593 (2012).

Article 2: Anastasi et *al.* Submitted

Bone morphogenetic protein-1 regulates cell adhesion and TGF-β activation through the cleavage of the matricellular protein TSP-1

Cyril Anastasi[1,¥], Patricia Rousselle[1,¥], Maya Talantikite[1], Agnès Tessier[1], Alice Bachmann[1], Lindsay B. Alcaraz[2], Laetitia Fortin[1], Frédéric Delolme[1,3], Jean Armengaud[4], Céline Auxenfans[1,5], Pierre Fournié[6,7], Ulrich Valcourt[1,2], Sandrine Vadon-Le Goff[1], Catherine Moali[1,*]

[1]UMR 5305, Tissue Biology and Therapeutic Engineering Laboratory Laboratory (LBTI), University of Lyon, CNRS, 69367, Lyon, France.
[2]INSERM U1052, CNRS UMR 5286, Cancer Research Center of Lyon (CRCL), University of Lyon, Centre Léon Bérard, 69373 Lyon, France.
[3]SFR Biosciences, ENS de Lyon, INSERM US8, CNRS UMS3444, University of Lyon, 69366 Lyon, France
[4]Innovative Technologies for Detection and Diagnostics Laboratory (DRF/Joliot/DMTS/SPI/Li2D), CEA Marcoule, 30200 Bagnols-sur-Cèze, France
[5]Tissue and Cell Bank, Hospices Civils de Lyon, 69437 Lyon, France
[6]Ophthalmology Department, Purpan University Hospital, 31059 Toulouse, France
[7]UMR 1056, Epidermis Differentiation and Rheumatoid Autoimmunity Unit (UDEAR), University of Toulouse, CNRS, INSERM, 31059 Toulouse, France

[¥]C.A and P.R. contributed equally to the work

[*] To whom correspondence should be addressed: e-mail: c.moali@ibcp.fr

KEYWORDS: cell adhesion, TGF-β, myofibroblast, thrombospondin-1, extracellular matrix, metalloproteinase

ONE SENTENCE SUMMARY: Here we explain how the metalloproteinase BMP-1, a known regulator of morphogenesis and tissue repair, controls cell adhesion/motility and TGF-β-driven cell differentiation, in a context-dependent manner, through the cleavage of the matricellular protein thrombospondin-1 (TSP-1).

N.B. Contributions to the work: Cell culture and immunofluorescence.

ABSTRACT

Bone Morphogenetic Protein-1 (BMP-1) has recently emerged as an important metalloproteinase that synchronizes growth factor activation with extracellular matrix assembly during morphogenesis and tissue repair. However, the mechanisms involved are highly context-dependent and remain elusive. Starting from the unexplained observation that BMP-1 overexpression induced marked phenotypic changes in two model cell lines, we here describe a new mechanism by which BMP-1 simultaneously impacts cell-matrix interactions and growth factor activity. In HT1080 and 293-EBNA cells, increasing BMP-1 expression led to a loss of cell adhesion and a concomitant stimulation of cell migration which could be linked to the matricellular glycoprotein thrombospondin-1 (TSP-1). TSP-1 was cleaved by BMP-1 between the VWFC/procollagen-like domain and the type 1 repeats which mediate several key TSP-1 functions. This cleavage induced TSP-1 release from the extracellular matrix and abolished its previously described multi-site cooperative interactions with HT1080 cell receptors. In addition, BMP-1-dependent proteolysis was found to enhance the ability of TSP-1 to activate latent TGF-β, leading to increased TGF-β signaling through the canonical Smad pathway. In primary stromal cells from cornea (keratocytes), TSP-1 was also cleaved at low basal BMP-1 levels but this cleavage had no major consequence on cell adhesion. In contrast, processed TSP-1 promoted the differentiation of keratocytes into myofibroblasts through α-SMA production, in agreement with the detection of the TSP-1 processed form in human corneal scars. Our results indicate that BMP-1 can both trigger cell motility and stimulate TGF-β signaling in TSP-1-rich microenvironments, with important potential consequences for tumor progression and wound healing.

INTRODUCTION

Bone morphogenetic protein-1 (BMP-1) and related proteinases belonging to the BTP (BMP-1/tolloid-like proteinases) family are now recognized as key regulators of several developmental and physiological processes. Their crucial role in development was first established in *Drosophila* and *Xenopus* embryos where they directly control dorso-ventral patterning (*1, 2*). This was further supported by knock-out studies in mice showing that deletion of the *Bmp1* or *Tll1* (tolloid-like 1) gene leads to early lethality and is associated with developmental defects such as gut herniation (*3*) and abnormal septation and positioning of the heart (*4*). Mutations of the *BMP1* gene in humans were also found to cause osteogenesis imperfecta (*5*), a bone disorder characterized by brittle bones which are prone to fracture. A similar phenotype is observed in adult mice upon *Bmp1* conditional ablation with further features of periodontal disease and skin fragility (*6-8*). In addition, BTPs are known to be involved in the control of muscle growth and homeostasis (*9*) and in wound healing/tissue repair (*6, 10*). Finally, several pathological conditions seem to involve increased BMP-1 expression including osteoarthritis (*11*), heart fibrosis (*12, 13*), corneal scarring (*10*), keloids (*14*) and type 1 diabetes (*15*) and BMP-1 was recently found to belong to a group of signature extracellular matrix (ECM) proteins associated with the high metastatic potential of breast tumors (*16*).

BMP-1 is a member of the astacin subgroup of metzincin metalloproteinases (*17*). The latent proform of the proteinase is processed in the secretory pathway to the mature enzyme which is composed of a catalytic domain followed by three CUB (complement, uEGF, BMP-1) domains and one EGF (epidermal growth factor) domain. The non-catalytic domains also play a major role by regulating substrate access to the active site and processing (*18, 19*). Around thirty BMP-1 substrates have been identified and characterized biochemically, as reviewed in (*20, 21*). An important group of substrates consists of ECM precursor proteins which acquire the ability to form three-dimensional networks upon proteolytic maturation. Well-known examples are procollagens I-III which can form fibers after C-terminal propeptide removal by BTPs to provide the principal scaffolding component of most connective tissues. Other prominent BMP-1 substrates belonging to this group are minor fibrillar procollagens (V and XI), small leucine-rich proteoglycans (decorin, osteoglycin and biglycan), basement membrane components (laminin 332 and collagen VII) and mineralization factors (dentin matrix protein 1 and dentin sialophosphoprotein).

The second major group of substrates consists of latent forms or antagonists of growth factors which, upon cleavage, result in increased signaling activities. The first substrate to be evidenced in this group was chordin, a major antagonist of BMP-2 and BMP-4 during development (*2, 22*). Also, the latent forms of BMP-11 and GDF-8/myostatin (an inhibitor of muscle growth, (*9*)) as well as IGFBP3 (which can bind and sequester IGF-I and II, (*23*)) can be cleaved by BMP-1 to release the active growth factors. A natural ligand of myostatin (WFIKKN1) was also found to behave as both a substrate of BMP-1 and a positive regulator of BMP-1-dependent myostatin activation (*24*). Finally, three proteins involved in the control of TGF-β activity (latent TGF-β binding protein-1, betaglycan and CD109) have been shown to be under the proteolytic control of BMP-1 (*25, 26*).

Additionally, several potential BMP-1 substrates awaiting validation were recently identified in a proteomic screen (*25*) suggesting that the substrate repertoire of the proteinase is still not fully characterized and that numerous new functions remain to be discovered. However, linking the

phenotype of *Bmp1*-deficient animals and disease mechanisms to this large panel of substrates remains challenging as most BMP-1 activities are strongly contextual and interconnected. In the present study, we investigated the striking phenotype induced by BMP-1 overexpression in two human cell lines and revealed that this is mainly due to the cleavage of thrombospondin-1, an ECM protein classified as "matricellular" for its ability to dynamically co-regulate cell-matrix interactions and TGF-β signaling.

RESULTS

BMP-1 disrupts cell adhesion in 293-EBNA and HT1080 cells.

293-EBNA cells derived from human embryonic kidney and transfected with a plasmid encoding human BMP-1 have been widely used to produce recombinant BMP-1 (*27-29*). However, when these cells are grown to high density, they massively detach from culture plates in the form of cell-cell adherent sheets (Fig. 1A). This can be avoided using plates coated with poly-D-lysine (*28*) but the mechanism underlying this observation has until now remained unclear. As a first step, we added a specific synthetic BMP-1 inhibitor in the culture medium (*25*) and observed that the BMP-1-transfected cells could be efficiently maintained in the adherent state (Fig. 1A). This result was the first indication that the loss of adhesion involved the catalytic activity of BMP-1. We also observed that the secreted form of BMP-1 was present both in the cell supernatant and the ECM (Fig. 1B).

In order to determine if the loss of cell adhesion was a general property of BMP-1-transfected cells, a construct encoding the BMP-1 protein was also stably transfected in the human fibrosarcoma cell line HT1080 to produce HT1080-BMP-1 cells (*25*). Control cells transfected with a construct encoding the inactive E94A mutant of BMP-1 (HT1080-E94A; (*25*)) were used in parallel. The adhesion of HT1080 cells also seemed very dependent on the presence of active BMP-1 since HT1080-BMP-1 cells, but not HT1080-E94A cells, lost their ability to adhere when grown to high cell densities. In contrast to 293-EBNA cells however, the loss of adhesion in HT1080 cells was preceded by striking modifications in cell morphology (Fig. 1C; Supplemental Movies S1 and S2) which became more pronounced when the cell density increased. None of these modifications were observed in HT1080-E94A cells which behaved very much like parental HT1080 cells (HT1080; Fig. 1C). Finally, the exogenous specific inhibitor of BMP-1 activity from *Xenopus* called sizzled (*30, 31*) was added to the HT1080-BMP-1 cells and found to inhibit both morphological changes and cell detachment (Fig. 1C). We can therefore conclude that in two different cell lines, HT1080 and 293-EBNA cells, BMP-1 induces a loss of cell adhesion which involves the catalytic activity of the proteinase.

The next step was to evaluate the effect of BMP-1 expression on cell migration. In a time-lapse experiment performed with cells at low confluency (around 20 %), HT1080-BMP-1 cells were found to migrate more than 43 % faster than control HT1080 and HT1080-E94A cells (Fig. 1D). The directionality of the migration however did not seem to be affected (Fig. 1E). Finally, we used flow cytometry and annexin V labeling to determine if cell detachment could be a consequence of cell apoptosis. At the two cell densities that were analyzed (20 % and 50 %), we found that apoptotic cells represented less than 3 % of the total cell population and that cell viability was superior to 94 % for

all three HT1080 cell types (Supplemental Fig. S1). These results clearly show that apoptosis is not a major determinant of the observed changes in cell adhesion and migration.

The adhesion phenotype observed in HT1080-BMP-1 cells is due to changes in the ECM.

In order to determine if the loss of cell adhesion observed with HT1080-BMP-1 cells was triggered by a modification of cell surface receptors or a modification of the underlying ECM, we compared the adhesion of control HT1080 cells (chemically detached with EDTA) or HT1080-BMP-1 cells (chemically or spontaneously detached) on the ECMs previously deposited by these cells. While both cell types could adhere normally on the ECM deposited by control cells, their adhesion to the ECM of HT1080-BMP-1 cells was severely impaired (Fig. 2A). When observed under a microscope, cells plated on the ECM conditioned by HT1080-BMP-1 cells were round in shape and most were floating in the medium; in contrast, they could spread and firmly adhere to the ECM conditioned by control cells (Fig. 2B). These results led to the conclusion that the most important changes induced by the activity of BMP-1 occurred in the ECM while the cell surface was not significantly altered.

Thrombospondin-1 is cleaved by BMP-1 and released from the matrix.

Our next aim was to identify the ECM substrate(s) processed by BMP-1. Based on our knowledge of the repertoire of proteins secreted by HT1080 cells characterized in a previous study (*25*), we screened the most prominent ECM components produced by these cells using western blotting and identified thrombospondin-1 (TSP-1) as a promising candidate substrate. A fragment of TSP-1 was found to accumulate in the conditioned medium of HT1080-BMP-1 cells, while this was not detected in the medium of untransfected cells (Fig. 3A). In vitro, the same fragment migrating at around 120 kDa, as determined by SDS-PAGE, was released when TSP-1 (purified from human platelets) was incubated with recombinant BMP-1 (Fig. 3A). The fragment was also found to be present in the medium of 293-EBNA cells and was significantly more abundant in BMP-1-transfected cells compared to cells transfected with an empty vector (Fig. 3B). The latter result suggested that this specific TSP-1 cleavage was common to the two cell lines which had a similar adhesion phenotype. Finally, we observed that full-length TSP-1 was present in the ECM deposited by the control cells but almost completely absent from the ECM of BMP-1-transfected cells (Fig. 3B). Since the TSP-1 fragment was never detected in the ECM of these two cell types, it seems that BMP-1 cleaves the matrix-embedded TSP-1 and thereby triggers its release from the ECM.

In order to get more insight into the biochemical features of the proteolytic processing involved, we performed in vitro cleavage assays with varying proteinase concentrations and incubation times. The resulting products were analyzed by SDS-PAGE in reducing and non-reducing conditions (Fig. 3C). As expected, the cleavage products increased when the protease:substrate ratio or the incubation time was increased. However, the cleavage pattern was very dependent on the presence of reducing agents. While two main cleavage products were observed at around 120 and 50 kDa in reducing conditions, four products, two above 200 kDa, one around 120 kDa and one around 100 kDa, were detected in non-reducing conditions. This apparent discrepancy can be explained by the trimeric nature of TSP-1 where molecules are held together by inter-chain disulfide bonds involving two cysteines in their N-terminal half (Fig. 3D); this results in intermediate species when only one or two

chain(s) are cleaved, as observed in non-reducing conditions. We then analyzed the upper fragment (fragment 1) observed in reducing conditions by N-terminal Edman sequencing and could unambiguously localize the BMP-1 cleavage site between serine 375 and aspartate 376 (N-terminal sequence: DSADX), in perfect agreement with the known specificity of BMP-1 (*20*). Moreover, cleavage site identification using a mass-spectrometry-based approach involving isotopic labeling of neo-peptides (ATOMS; (*25, 32*)) confirmed that the peptide starting with Asp376 and ending with Arg402 was much more abundant in the presence of BMP-1 than in its absence (proteinase:control ratio = 47 based on 5 identifications). Furthermore, two unusual post-translational modifications on W385 (C-mannosylation) and S394 (disaccharide Glc-Fuc-O) were unambiguously detected on this peptide (Fig. S2), confirming the findings of a previous study (*33*).

Finally, the effect of various known BMP-1 regulators was assessed to determine if they could modulate TSP-1 cleavage as was previously described for other BMP-1 substrates (*21*). Direct interaction of TSP-1 with several of these regulators (procollagen C-proteinase enhancer-1 PCPE-1 and secreted frizzled related proteins sFRP-1 and sFRP-2) has been reported (*34, 35*). However, while the *Xenopus* protein sizzled was found to efficiently inhibit the cleavage, its human homologs sFRP-1 and -2 only had a weak inhibitory effect when used at high concentrations (10-fold excess relative to BMP-1) and PCPE-1 was without effect (Fig. 3E-F). The complete inhibition of TSP-1 processing by sizzled is coherent with the reversion of the adhesion phenotype observed in HT1080 cells in the presence of this protein (Fig. 1C).

TSP-1 cleavage abolishes its ability to promote cell adhesion.

The cleavage site identified above is localized in the short linker between the VWFC domain and the TSP type 1 repeats (TSRs; Fig. 3D) which were previously shown to support several TSP-1 functions. TSRs can interact with (i) several β1 integrins (*36*), thereby controlling cell adhesion and migration, (ii) CD36, another important receptor mediating cell adhesion and TSP-1 anti-angiogenic properties (*37*) and (iii) latent TGF-β leading to the release of the active growth factor (*38*). In relation to the striking adhesion phenotype described above, we performed functional assays to determine if the cleavage of TSP-1 by BMP-1 affected its ability to promote cell adhesion. Using siRNAs directed against human TSP-1, we first demonstrated that TSP-1 was critical for the adhesion of HT1080 cells. When TSP-1 expression was decreased (by more than 70 % as determined by western blotting, Fig. 4A), the cells changed their morphology, became rounded and seemed to be more loosely attached to the plates, with several of them being completely detached (Fig. 4A). In a second series of experiments, we analyzed whether cleaved TSP-1 was still capable of promoting HT1080 adhesion. TSP-1 was first submitted to BMP-1 proteolytic activity for 4 h, then incubated overnight in a 96-well plate and adhesion of HT1080 cells to the cleaved and intact proteins was measured. We observed that processing by BMP-1 completely abolished the ability of TSP-1 to promote adhesion (Fig. 4B, condition 4). The loss of TSP-1 adhesive properties was clearly due to proteolysis as incubation with the BMP-1 inactive mutant did not lead to the same effect (Fig. 4B, condition 3). Control experiments were also performed to exclude (i) protein unfolding after prolonged incubation at 37°C (the intact protein incubated in the same conditions was even slightly more active than the protein incubated at

4°C, conditions 1 and 2) or (ii) differential coating efficiency of 96-well plates by intact and cleaved TSP-1 (Supplemental Fig. S3).

TSP-1 cleavage enhances its ability to activate TGF-β.

Another major function of TSRs is to release the active form of TGF-β which, after secretion, remains bound to its propeptide (latency associated peptide LAP) and is kept in the latent form. When TSP-1 was added to HT1080 cells, the canonical TGF-β pathway was indeed found to be activated, as evidenced by the detection of the phosphorylated form of Smad2 60 min after TSP-1 addition (Fig. 5A, conditions 1 and 2). We also analyzed the ability of cleaved TSP-1 (prepared as above) to trigger TGF-β signaling and found that it was even more efficient than the intact protein to perform this function (Fig. 5A, condition 3). After quantitation and normalization with the level of α-actin or total Smad2, the enhancement ratio was calculated to be around 2.7 (Fig. 5B). The increased TGF-β activation capacity of cleaved TSP-1 was confirmed using a luciferase reporter assay (*25*). At the two concentrations of TSP-1 that were tested (14 and 41 nM), luciferase activity was more than 2-fold higher after incubation with active BMP-1 than with inactive BMP-1 or buffer alone (Fig. 5C). This demonstrates the higher TGF-β activation capacity of cleaved TSP-1 compared to the full-length form.

TSP-1 is physiologically cleaved in human primary keratocytes and induces myofibroblast differentiation

To get further insight into the effect of the type of ECM proteins synthesized by cells on the BMP-1-dependent adhesion phenotype, we assessed the effect of increasing the amount of BMP-1 in the culture medium of a cell type known to secrete a collagen-rich ECM. These cells are human primary keratocytes (corneal stromal cells) which were previously demonstrated to be a suitable model to study BMP-1 proteolytic activities (*25*). As illustrated in Fig. 6A, we found no change in the adhesion profile of keratocytes in BMP-1-supplemented culture medium conditions where HT1080 cell adhesion was largely hindered. However, when we sought to detect TSP-1 in their conditioned medium, we observed that TSP-1 was present in two forms corresponding to full-length TSP-1 and to a cleaved product similar in size to the fragment identified in HT1080 and 293-EBNA cells (Fig. 6B). This fragment disappeared in the presence of two different BMP-1 inhibitors, showing the direct involvement of the proteinase. These results indicated that (i) the endogenous levels of BMP-1 expressed by human keratocytes (Fig. 6C) were sufficient to cleave TSP-1 to a significant extent but (ii) unlike in HT1080 cells, TSP-1 did not appear to be a major adhesion molecule for keratocytes.

We also analyzed the ability of cleaved TSP-1 to trigger TGF-β signaling in primary keratocytes. Similarly to what was noted for HT1080 cells, an increase in the level of Smad2 phosphorylation was observed in the presence of cleaved TSP-1 (Fig. 7A-B). In addition, cleaved TSP-1 was significantly more efficient than intact TSP-1 in inducing the expression of TGF-β target genes such as α-smooth muscle actin (α-SMA; Fig. 7C-D). This further shows that the cleavage of TSP-1 by BMP-1 can promote the differentiation of keratocytes into myofibroblasts. Since both BMP-1 and TSP-1 have previously been proposed to play a role in the development of corneal scarring (*10, 39*), we analyzed 4 human corneas from patients presenting with permanent corneal scars and collected at the time of corneal

transplantation. Scars were caused by perforating traumas or corneal ulcers which occurred between 6 and 26 months before surgery. In the lysates of all 4 corneas, a TSP1 product migrating at the same size as the BMP-1-dependent fragment identified in keratocyte supernatant was detected (Fig. 8). This result suggests that BMP-1-dependent processing of TSP-1 also occurs in vivo and could contribute to the development of corneal scars.

DISCUSSION

Cell growth, survival and differentiation result from the integration of numerous mechanical and molecular cues present in the external environment of cells. One prominent source of these signals is the ECM which surrounds cells and provides a large diversity of components with various abilities to promote cell adhesion through specific interactions with cellular receptors. These cell-matrix interactions can also trigger signaling and regulate other aspects of cell behavior including migration, proliferation and differentiation. Here, we show for the first time that, by directly modifying the ECM, BMP-1 strongly alters the ability of two cell types to adhere and migrate. In contrast, cell survival was not affected excluding the possibility that the de-adhesive effect of BMP-1 was the direct result of cell death induction.

Several metalloproteinases have previously been shown to induce a similar disruption of cell-matrix contacts. For example, transfection of MT1-MMP (also known as MMP-14) in the ovarian cancer cell line OVCA433 was found to induce the spontaneous detachment of cell-cell adherent multi-cellular aggregates (*40*), in a way that resembles the effect of BMP-1 on 293-EBNA cells. In this case, the decreased adhesive strength was attributed to ectodomain shedding of the integrin α3 chain by MT1-MMP. In another example (*41*), addition of recombinant ADAMTS-2 to cultures of endothelial cells led to cell retraction and rounding and to the formation of cell clusters, as observed with HT1080-BMP-1 cells at high cell density. However, important differences between our results and the latter study were the concomitant induction of apoptosis and the fact that the observed effects were not mediated by the catalytic activity of the proteinase. These examples illustrate the diversity of mechanisms by which proteases can regulate cell-matrix interactions, both through proteolytic and non-proteolytic activities.

As for MT1-MMP, the drastic alterations of cell properties induced by BMP-1 in HT1080 and 293-EBNA cells were clearly dependent on its catalytic activity and we could link the loss of adhesion to the cleavage of thrombospondin-1. Several interaction sites with cellular receptors have been identified in TSP-1 (*36, 42*), especially with β1 integrins (TSPN domain, type 1-3 repeats; Fig. 3D), β3 integrins (type 3 repeats), heparan sulfate proteoglycans (TSPN domain, type 1 repeats), CD36 (type 1 repeats) and CD47/IAP (C-terminal domain). As a result, the adhesive and chemotactic properties of TSP-1 will depend on several parameters such as the cell type, the TSP-1 region and concentration and the soluble or matrix-bound presentation of the protein. A previous study has shown that HT1080 cells attach and spread on coated TSP-1 (*43*) through a multi-site cooperative attachment process involving both the interaction of the N-terminal TSPN domain with heparan-sulfate proteoglycans and the interaction of type 1 repeats with CD36. HT1080 cells could still attach but not spread on a 140 kDa C-terminal fragment of TSP-1, generated after thrombin cleavage (Fig. 3D) and

lacking the heparin-binding TSPN domain. In contrast, they could neither attach nor spread on the TSPN domain alone (*43*).

By cleaving TSP-1 at a different location, between the procollagen-like/VWFC domain and the type 1 repeats (TSR; Fig. 3D), BMP-1 had an even more dramatic effect on the adhesion of HT1080 cells on coated TSP-1. Even the C-terminal 120 kDa fragment bearing the CD36 interaction site lost its ability to promote cell attachment. Since processing occurs just before the known CD36 interaction site located within the second type 1 repeat (*36*), it is most likely that the cleavage by BMP-1 induces a major conformational rearrangement of this region, at the level of each polypeptide chain and of the quaternary structure (through the loss of the trimeric organization), thereby leading to disruption of the CD36 interaction site. In addition, we observed that the BMP-1-dependent cleavage of TSP-1 triggers the release of the TSR-bearing fragment from the matrix, probably through the disruption of interactions with matrix components such as fibronectin. A similar mechanism of transfer from the matrix to the soluble phase has been previously observed upon cleavage of TSP-1 by ADAMTS-1 (*44*), at a third upstream site located just before the VWFC domain (Fig. 3D) which also leads to monomeric C-terminal fragments. The observed loss of adhesion in cultures of HT1080 cells could therefore arise from the combined effects of (i) a conformational change disrupting CD36 binding site, (ii) a decreased amount of the TSR-containing portion of the protein in the extracellular matrix and (iii) the competition between insoluble and soluble forms of TSP-1 to bind cells. Finally, disruption of the CD36 binding site is likely to affect adhesion and migration of other cell types, especially endothelial cells where it is known to play a major role (*37*), and suggests novel hypotheses to link BMP-1 expression and biological processes involving neovascularization (*10, 15, 16*).

Binding of cell receptors to TSRs being a common feature of many TSP-1-dependent adhesion processes, BMP-1 has the potential to regulate several of these. However, this will not always lead to the disruption of cell-matrix interactions, as illustrated here in the case of keratocytes which are not affected by cleaved TSP-1 despite relatively high endogenous levels of processing. Integration of signals coming from pro- and anti-adhesive molecules at the cellular level clearly depends on the cell type (and the presence of specific receptors at the cell surface) and on the molecular composition of its surrounding ECM. In this regard, an important difference between keratocytes and other cell lines studied is that HT1080 and 293-EBNA cells do not produce any fibrillar collagens while the latter are known to represent the main anchoring molecules for keratocytes in the corneal environment.

To our knowledge, this is also the first time that proteolytic regulation of TGF-β activation by TSP-1 has been evidenced. The mechanism by which TSP-1 turns cell-secreted latent TGF-β into active TGF-β has been largely documented (*45*). This involves the disruption of specific non covalent interactions between the mature TGF-β growth factor and its LAP propeptide through competing interactions between the type 1 repeats in TSP-1 and both parts of the TGF-β latent complex. Especially, the KRFK sequence located at the beginning of the second TSR can efficiently replace the RKPK sequence in TGF-β to interact with the LSKL sequence in LAP, thereby leading to the exposure of TGF-β which otherwise remains buried within the complex (*45, 46*). Our results showing that this activation mechanism is enhanced after cleavage of TSP-1 by BMP-1 suggest a better accessibility or more favorable conformation of the TSR to efficiently interact with the latent complex when the

protein is in the form of monomeric C-terminal fragments than in intact trimeric form. Alternatively, the TGF-β growth factor bound to the TSP-1 fragment could find easier access to its receptors through a better presentation or increased solubility. In all cases, this represents another mechanism by which BMP-1 enhances TGF-β signaling, to be added to the previously reported cleavages of LTBP1, betaglycan and CD109 (*21*). These mechanisms can all synergize to increase the pool and bio-availability of active TGF-β and we can expect major consequences for the control of tumor progression, immunity and wound healing.

The potentiation of TGF-β signaling by cleaved TSP-1 is common to HT1080 cells and keratocytes and our results indicate that it could play a role in the differentiation of the latter into myofibroblasts. This is of great significance in the context of corneal wound healing where it was previously reported that TSP-1 expression precedes α-SMA induction and could regulate myofibroblast recruitment into the wound (*39*). After wound closure, stromal remodeling remains active until myofibroblasts disappear from the wound, a process which can take several years and lead to scarring. The control of myofibroblast differentiation is therefore a major issue to prevent the formation of irreversible scars. Here, we demonstrate that TSP-1 has the capacity to induce the differentiation of keratocytes into myofibroblasts and that this effect is significantly enhanced after cleavage by BMP-1. This adds another important role for this proteinase in corneal wounds and scars where its expression is known to be strongly increased and to be co-localized with α-SMA (*10*). Our present results show that a BMP-1-dependent processed form of TSP-1 is also found in human corneal scars which provides a mechanistic hypothesis to explain how BMP-1 can drive pathological healing through TSP-1 regulated proteolysis. Beyond corneal scarring, this mechanism could also apply to other repair processes where BMP-1 and myofibroblasts are already known to co-exist (e.g. skin wound healing, cardiac fibrosis).

The importance of regulated proteolysis, in contrast to degradation, to finely tune the properties and activities of ECM proteins has been demonstrated in several pathophysiological remodeling processes, including development, wound healing, fibrosis and cancer. This is again nicely illustrated in our study as the unique location of the BMP-1 cleavage site in TSP-1, just before the type 1 repeats which support a large number of its activities, identifies an important regulatory mechanism to control cell motility and TGF-β signaling in a concerted manner. This also confirms that proteolysis is an important aspect of TSP-1 regulation and definitely establishes BMP-1 as a key molecular hub to coordinate the crosstalk between ECM-derived cues and growth factor signaling.

MATERIALS AND METHODS

Cell cultures and human corneas – HT1080 cells (ATCC CCL-121) were grown in Dulbecco's modified Eagle's medium (DMEM) with 10 % fetal calf serum (FCS) and 50 µg/ml gentamycin. HT1080 cells, stably transfected with a piRESneo2 vector encoding human BMP-1 fused with a 6His tag at the C-terminus or the same construct with the E94A mutation, were obtained and grown in DMEM with 10 % FCS and 250 µg/ml G418 sulfate, as described previously (*25*). 293-EBNA cells overexpressing human native BMP-1 were also available from a previous study (*28*). A control 293-EBNA cell line transfected with the empty pCEP4 vector was produced using the same protocol. Primary

keratocytes from human corneas were isolated as previously described (*25*), in accordance with ethical regulations, and grown in DMEM/Ham's F12 (1:1), 10 % iron-supplemented calf serum, 5 ng/mL bFGF and 1 % antibiotic/antimycotic solution. All cells were verified for the absence of mycoplasma with the MycoAlert detection kit (Ozyme).

For conditioned medium analysis by western blotting, the cells were extensively washed with PBS and maintained between 8 and 48 h in serum-free medium. The medium was then collected, centrifuged at 200 g for 5 min, supplemented with protease inhibitors (Complete, Roche) and stored at -80°C. The extracellular matrix from the same cultures was also collected after solubilization in 0.325 M Tris-HCl pH 6.9, 25 % glycerol and 10 % SDS. Prior to this step, cells were removed by adding 20 mM NH_4OH for 5 min and the matrix was washed several times with water. Equal amounts of total proteins (medium, determined by Bradford assay) or equal volumes (ECM) were loaded onto the gels for western-blot analyses.

Four corneal samples from patients presenting permanent stromal scars were collected, according to the tenets of the declaration of Helsinki, at the time of corneal transplantation. Patient 1 (male, age 25) had his cornea perforated by broken glass 17 months prior to surgery. Patient 2 (male, age 66) had a handiwork accident 6 months before surgery. Patient 3 (male, age 68) suffered from a corneal ulcer since 2 years. Patient 4 (male, age 50) was injured by a perforating metal foreign body more than 2 years before. Corneas were frozen at -80°C after surgery before being processed for immuno-blotting. In brief, frozen corneas were ground in a mortar, homogenized in Laemmli buffer and boiled at 100°C for 10 min. After centrifugation at 15,000 g for 15 min, the supernatant was collected and analyzed.

Proteins, antibodies and inhibitors – Recombinant human BMP-1, PCPE-1, sFRP-1, sFRP-2 and Xenopus sizzled were produced and purified, as previously described (*30, 47, 48*). Thrombospondin-1 was purified from human platelets, provided by the Etablissement Français du Sang (Lyon Gerland) in agreement with French regulations, according to the protocol developed by Lawler and co-workers (*49*) with minor modifications. In brief, after 3 washes in Baezinger A buffer (0.102 M NaCl, 3.9 mM K_2HPO_4, 3.9 mM Na_2HPO_4, 22 mM NaH_2PO_4, 5.5 mM glucose pH 6.3), the platelet pellet was resuspended in Baezinger B buffer (15 mM Tris, 0.14 M NaCl, 5 mM glucose pH 7.6) with 2 mM $CaCl_2$ (50 mL of buffer for approximately 3 mL of pellet). Fifty mL of resuspended platelets were then gently mixed for 2 min at room temperature with 50 u thrombin (GE Healthcare) and kept on ice for 5-10 min until complete aggregation. After centrifugation at 1,400 g for 5 min, 1 mM Pefabloc was added to block thrombin activity. The supernatant was further centrifuged at 35,000 g for 20 min at 4°C, stored at 4°C for one night and centrifuged again at 1,400 g for 20 min. This was followed by heparin Sepharose chromatography (6 Fast Flow, GE Healthcare) using a 0.15 M NaCl to 2 M NaCl gradient in 15 mM Tris pH 7.6, 2 mM $CaCl_2$. TSP-1-containing fractions were then pooled, concentrated in an Amicon Ultra (cut-off 100 kDa, Millipore) and injected on a Superdex S200 16/600 column equilibrated in 20 mM Tris pH 11, 0.15 M NaCl, 2 mM $CaCl_2$. The pH of the major peak fractions was then rapidly decreased to 7.5-8.0 and the protein was concentrated, dialyzed against 20 mM HEPES pH 7.4, 0.5 M NaCl, 2.5 mM $CaCl_2$ and flash frozen in liquid nitrogen before storage at -80°C in LoBind microtubes (Eppendorf).

Mouse monoclonal anti-human TSP-1 (MAB3074) and rat monoclonal anti-human BMP-1 (MAB1927) antibodies were from R&D Systems, rabbit polyclonal anti-human collagen VI antibody (20611) was from Novotec, rabbit polyclonal anti-Smad2/3 (3102) and anti-Phospho-Smad2 (Ser465/467; 3108) from Cell Signaling Technology, mouse monoclonal anti-actin (A3854) from Sigma-Aldrich and rabbit polyclonal anti-α-SMA (ab5694) from Abcam. HRP-coupled secondary antibodies were purchased from Cell Signaling Technology and goat anti-rabbit Alexa Fluor 594-coupled secondary antibody (A-11037) from Thermo Scientific.

The BMP-1 hydroxamate inhibitor used in cell cultures was the N-substituted aryl sulfonamide hydroxamate 90 described in (*50*), which was prepared as reported (*25*). It was dissolved in DMSO before addition to the culture medium.

Microscopy - Phase contrast images were taken with a Nikon TE300 inverted microscope. For time-lapse experiments, 40,000 cells/well of each cell type were seeded in a 6-well plate and grown for 24 h in DMEM containing 10 % FCS. Then, cell migration was monitored at 37°C in a humidified atmosphere with 5 % CO_2 using an Axiovert 100M Zeiss microscope equipped with a CCD camera (one picture every 5 min for 4 h). In three independent experiments, movements of 10 cells in 3 fields (30 in total/cell type/experiment) were analyzed using ImageJ software. The velocity was calculated for each individual cell and values for the 3 cell populations were compared using one-way ANOVA and Tukey post-ANOVA test.

Flow cytometry – 150,000 or 500,000 cells were seeded in 100 mm culture dishes and grown for 48 h to obtain around 20 and 50 % confluency. Cells were then detached with accutase (Sigma-Aldrich), washed with PBS and with the binding buffer provided in the Annexin V-FITC Apoptosis detection kit (BioVision). 500,000 cells were resuspended in 500 µl binding buffer, incubated for 5 min with 5 µl of Annexin V-FITC and 5 µl of propidium iodide in the dark and analyzed with a FACS LSR II apparatus (Becton Dickinson) equipped with the FACSDiva software.

RNA interference – TSP-1 expression in HT1080 cells was decreased using validated siRNAs directed against human TSP-1 from Qiagen (Hs_THBS1_5 with target sequence 5'-TACGAATGTAGAGATCCCTAA and Hs_THBS1_7 with target sequence 5'-CGGCGTGAAGTGTACTAGCTA). A control siRNA against the decoy sequence 5'-AATTCTCCGAACGTGTCACGT was also used. 300,000 HT1080 cells/well were seeded in 6-well plates with DMEM containing 10 % FCS. Thirty min after seeding, transfection mixes containing siRNA, DMEM and HiPerFect Transfection Reagent (Qiagen), prepared as recommended by the manufacturer, were added to the cells (25 nM final siRNA concentration). Pictures were taken every 24 h for 3 days and the medium was collected at day 3 after 48 h of serum starvation for western blot analysis.

In vitro cleavage assays and N-terminal sequencing - All activity assays were performed at 37°C in 40-200 µl of 50 mM HEPES pH 7.4, 0.15 M NaCl, 5 mM $CaCl_2$, 0.02 % n-octyl-β-D-glucopyranoside (buffer A). Incubation time and protease:substrate ratios were varied as indicated. Cleavage

monitoring was performed by SDS-PAGE and detection was with Coomassie Blue or Sypro Ruby (Sigma-Aldrich). Sypro Ruby-stained gels were analyzed on a Typhoon FLA 9500 gel scanner (GE Healthcare) and band intensities quantified using ImageQuant TL (GE Healthcare). For Edman N-terminal sequencing, 10 µg of TSP-1 were incubated with and without 4 µg BMP-1 in 200 µl buffer A for 4 h. The two samples were then processed for Edman sequencing on PVDF membranes and analyzed with an Applied Biosystems 473 protein sequencer.

For ATOMS experiments, half the amounts of BMP-1 and TSP-1 (keeping concentrations constant) were used. Samples were processed as described in (*25*) and peptides were analyzed with a Q-Exactive HF tandem mass spectrometer (Thermo Scientific) coupled to an Ultimate 3000 nanoLC system (Dionex) (*51*). Briefly, peptides were first desalted on line on a reverse phase Acclaim PepMap100 C18 precolumn (5 µm, 100 Å, 300 µm id x 5 mm) for 5 min at 2 % CH_3CN at a flow rate of 10 µl/min, and then resolved at a flow rate of 0.300 µl/min with a 180 min gradient of CH_3CN, 0.1 % formic acid applied onto the reverse phase Acclaim PepMap100 C18 column (3 µm, 100 Å, 75 µm id x 500 mm) from 4 to 40 % CH_3CN. The Q-Exactive HF instrument was operated according to a Top20 data-dependent method consisting in a scan cycle initiated with a full scan of peptide ions in the ultra-high-field Orbitrap analyzer, followed by selection of the precursor with a fixed first mass parameter set at 80 m/z, high energy collisional dissociation with a normalized energy collision fixed at 33 eV and MS/MS scans on the 20 most abundant precursor ions. Full scan mass spectra were acquired from m/z 350 to 1 800 with an Automatic Gain Control (AGC) target set at $3x10^6$ ions and a resolution of 60,000. MS/MS scans were initiated at a resolution of 15,000 when the ACG target reached 10^5 ions with a threshold intensity of 10^5 and potential charge states of 2+ and 3+ after ion selection performed with a dynamic exclusion of 10 s.

Adhesion assays - Conditioned ECMs were prepared from subconfluent plates. Cells were washed with PBS, detached using 20 mM NH_4OH and discarded. The remaining ECM layer was washed with PBS, incubated with 1 % BSA in PBS and washed again. Prior to adhesion assays, cells from additional plates were detached with 5 mM EDTA in PBS (HT1080 and HT1080-BMP-1) or collected after spontaneous detachment (HT1080-BMP-1) and 60,000 cells/well were plated on conditioned ECM in 96-well plates. Adhesion assays were then performed as previously described *(52)*. Alternatively, cells could be seeded in larger wells for phase contrast imaging. To assess adhesion of HT1080 cells on intact and cleaved TSP-1, wells were coated with protein solutions overnight at 4°C and saturated with 1 % BSA in PBS. HT1080 cells were prepared and detached from the plates as described above. Absorbance measurements at 570 nm shows the extent of cell adhesion after fixation and staining with 0.1% crystal violet.

ELISA assay – 96-well Costar culture-treated microtiter plates (also used for adhesion assays) were coated overnight at 4°C with 50 µl of each protein solution diluted in TBS (10 mM Tris-HCl pH 8, 0.15 M NaCl) + 5 mM $CaCl_2$. Wells were then blocked with 5 % (w/v) milk in TBS and incubated successively with anti-human TSP-1 antibody and horse anti-mouse antibody coupled to HRP. 2,2'-azino-bis(3-ethylbenzthiazoline-6-sulfonic acid) ammonium salt was used as HRP substrate and color

development was measured at 405 nm after 15 min in a microtiter plate reader (Tecan Infinite M1000).

Detection of TGF-β activity – TGF-β activity was monitored first through the immuno-detection of phosphorylated Smad 2 (P-Smad2). 100,000 HT1080 cells or 30,000 keratocytes were grown in 12-well plates with 1 mL complete medium for 48 h. Solutions containing thrombospondin-1 (incubated or not with active or inactive BMP-1) and control conditions (in 100 µl) were then added to the cells for 30 min (keratocytes) or 1 h (HT1080 cells). The cell supernatant was then discarded, cells were washed with PBS and cell lysates were collected in RIPA buffer (50 mM Tris pH 8, 0.15 M NaCl, 1 % NP-40, 0.5 % sodium deoxycholate and 0.1 % SDS) containing protease (Complete, Roche) and phosphatase (PhosSTOP, Roche) inhibitors. 20 µg of total protein/lane (Bradford assay) were loaded on gels for immuno-detection of P-Smad2, Smad2 or actin.

TGF-β activity was also assessed through a reporter gene assay. In this experiment, 50,000 HT1080 cells were seeded in 24-well plates with DMEM + 10 % FCS. After 24 h, they were co-transfected with (i) the pGL3-basic reporter plasmid (Promega) encoding firefly luciferase under the control of 9 repeats of a SMAD-binding element ($(CAGA)_9$-Luc) and (ii) the phRLCMV vector (Promega) encoding Renilla luciferase under the control of the cytomegalovirus ubiquitous promoter, in order to determine the transfection efficiency and to normalize luciferase values. The following day, samples containing thrombospondin-1 (incubated or not with active or inactive BMP-1) and control conditions were added for 24 h. Proteins were extracted from HT1080 cells in Passive Lysis Buffer (Promega) and transcriptional responses were measured with the Dual-Luciferase Reporter Assay System (Promega).

Immunofluorescence – Human keratocytes (50,000 cells/well in 6-well plates) were seeded in their complete growth medium. After one day, cells were washed with PBS and treated for 72 h with 10 ng/mL TGF-β, intact TSP-1, cleaved TSP-1 or vehicle solutions in serum-free medium. Then, cells were fixed and permeabilized with cold methanol. Immuno-detection was carried out with anti-α-SMA and anti-rabbit Alexa Fluor 594 secondary antibodies. Nuclei were stained with DAPI. Fluorescence images were taken using a Zeiss Axioplan 2 microscope and α-SMA positive cells (with clear organized fibers) were counted using ImageJ in 20 different fields/condition (10 fields/replicate). Values for the 5 conditions tested were compared using one-way ANOVA and Tukey post-ANOVA test.

SUPPLEMENTARY MATERIALS

Figure S1: Effect of BMP-1 on apoptosis.

Figure S2: Mass spectrum and attribution of b and y ions for peptide 376-402 of human platelet TSP-1 defining BMP-1 cleavage site.

Figure S3: Coating of 96-well plates is equally efficient with intact and cleaved TSP-1.

Movie S1: Time lapse recording (one image every 15 min for 17 h) of subconfluent HT1080 cells.

Movie S2: Time lapse recording (one image every 15 min for 17 h) of the morphological changes preceding cell detachment in subconfluent HT1080-BMP-1 cells.

REFERENCES

1. S. A. Goodman, R. Albano, F. C. Wardle, G. Matthews, D. Tannahill, L. Dale, BMP1-related metalloproteinases promote the development of ventral mesoderm in early Xenopus embryos. *Dev. Biol.* **195**, 144-157 (1998).
2. G. Marques, M. Musacchio, M. J. Shimell, K. Wunnenberg-Stapleton, K. W. Cho, M. B. O'Connor, Production of a DPP activity gradient in the early Drosophila embryo through the opposing actions of the SOG and TLD proteins. *Cell* **91**, 417-426 (1997).
3. N. Suzuki, P. A. Labosky, Y. Furuta, L. Hargett, R. Dunn, A. B. Fogo, K. Takahara, D. M. Peters, D. S. Greenspan, B. L. Hogan, Failure of ventral body wall closure in mouse embryos lacking a procollagen C-proteinase encoded by Bmp1, a mammalian gene related to Drosophila tolloid. *Development* **122**, 3587-3595 (1996).
4. T. G. Clark, S. J. Conway, I. C. Scott, P. A. Labosky, G. Winnier, J. Bundy, B. L. Hogan, D. S. Greenspan, The mammalian Tolloid-like 1 gene, Tll1, is necessary for normal septation and positioning of the heart. *Development* **126**, 2631-2642 (1999).
5. D. Syx, B. Guillemyn, S. Symoens, A. B. Sousa, A. Medeira, M. Whiteford, T. Hermanns-Le, P. J. Coucke, A. De Paepe, F. Malfait, Defective proteolytic processing of fibrillar procollagens and prodecorin due to biallelic BMP1 mutations results in a severe, progressive form of Osteogenesis Imperfecta. *J. Bone Miner. Res.* **30**, 1445-1456 (2015).
6. A. M. Muir, D. Massoudi, N. Nguyen, D. R. Keene, S. J. Lee, D. E. Birk, J. M. Davidson, M. P. Marinkovich, D. S. Greenspan, BMP1-like proteinases are essential to the structure and wound healing of skin. *Matrix Biol.* **56**, 114-131 (2016).
7. A. M. Muir, Y. Ren, D. H. Butz, N. A. Davis, R. D. Blank, D. E. Birk, S. J. Lee, D. Rowe, J. Q. Feng, D. S. Greenspan, Induced ablation of Bmp1 and Tll1 produces osteogenesis imperfecta in mice. *Hum. Mol. Genet.* **23**, 3085-3101 (2014).
8. J. Wang, D. Massoudi, Y. Ren, A. M. Muir, S. E. Harris, D. S. Greenspan, J. Q. Feng, BMP1 and TLL1 are required for maintaining periodontal homeostasis. *J. Dent. Res.* **96**, 578-585 (2017).
9. N. M. Wolfman, A. C. McPherron, W. N. Pappano, M. V. Davies, K. Song, K. N. Tomkinson, J. F. Wright, L. Zhao, S. M. Sebald, D. S. Greenspan, S. J. Lee, Activation of latent myostatin by the BMP-1/tolloid family of metalloproteinases. *Proc. Natl. Acad. Sci. U.S.A* **100**, 15842-15846 (2003).
10. F. Malecaze, D. Massoudi, P. Fournie, C. Tricoire, M. Cassagne, M. Malbouyres, D. J. Hulmes, C. Moali, S. D. Galiacy, Upregulation of bone morphogenetic protein-1/mammalian tolloid and procollagen C-proteinase enhancer-1 in corneal scarring. *Invest. Ophthalmol. Vis. Sci.* **55**, 6712-6721 (2014).
11. E. Sanchez-Sabate, L. Alvarez, E. Gil-Garay, L. Munuera, N. Vilaboa, Identification of differentially expressed genes in trabecular bone from the iliac crest of osteoarthritic patients. *Osteoarthritis Cartilage* **17**, 1106-1114 (2009).
12. J. Beaumont, B. Lopez, N. Hermida, B. Schroen, G. San Jose, S. Heymans, F. Valencia, J. J. Gomez-Doblas, E. De Teresa, J. Diez, A. Gonzalez, microRNA-122 down-regulation may play a role in severe myocardial fibrosis in human aortic stenosis through TGF-beta1 up-regulation. *Clin. Sci.* **126**, 497-506 (2014).
13. B. Lopez, A. Gonzalez, J. Beaumont, R. Querejeta, M. Larman, J. Diez, Identification of a potential cardiac antifibrotic mechanism of torasemide in patients with chronic heart failure. *J. Am. Coll. Cardiol.* **50**, 859-867 (2007).
14. J. Fuentes-Duculan, K. M. Bonifacio, M. Suarez-Farinas, N. Kunjravia, S. Garcet, T. Cruz, C. Q. Wang, H. Xu, P. Gilleadeau, M. Sullivan-Whalen, M. H. Tirgan, J. G. Krueger, Aberrant connective tissue differentiation towards cartilage and bone underlies human keloids in African Americans. *Exp. Dermatol.*, (2016).

15. P. Perimenis, T. Bouckenooghe, J. Delplanque, E. Moitrot, E. Eury, S. Lobbens, P. Gosset, L. Devisme, B. Duvillie, A. Abderrahmani, L. Storme, P. Fontaine, P. Froguel, A. Vambergue, Placental antiangiogenic prolactin fragments are increased in human and rat maternal diabetes. *Biochim. Biophys. Acta* **1842**, 1783-1793 (2014).
16. A. Naba, K. R. Clauser, J. M. Lamar, S. A. Carr, R. O. Hynes, Extracellular matrix signatures of human mammary carcinoma identify novel metastasis promoters. *Elife.* **3**, e01308 (2014).
17. J. S. Bond, R. J. Beynon, The astacin family of metalloendopeptidases. *Protein Sci.* **4**, 1247-1261 (1995).
18. R. Berry, T. A. Jowitt, J. Ferrand, M. Roessle, J. G. Grossmann, E. G. Canty-Laird, R. A. Kammerer, K. E. Kadler, C. Baldock, Role of dimerization and substrate exclusion in the regulation of bone morphogenetic protein-1 and mammalian tolloid. *Proc. Natl. Acad. Sci. U.S.A* **106**, 8561-8566 (2009).
19. C. Wermter, M. Howel, V. Hintze, B. Bombosch, K. Aufenvenne, I. Yiallouros, W. Stocker, The protease domain of procollagen C-proteinase (BMP1) lacks substrate selectivity, which is conferred by non-proteolytic domains. *Biol. Chem.* **388**, 513-521 (2007).
20. C. Moali, D. J. Hulmes, in *Extracellular Matrix : Pathobiology and Signaling,* M. Karamanos, Ed. (De Gruyter, Berlin, 2012), pp. 539-561.
21. S. Vadon-Le Goff, D. J. Hulmes, C. Moali, BMP-1/tolloid-like proteinases synchronize matrix assembly with growth factor activation to promote morphogenesis and tissue remodeling. *Matrix Biol.* **44-46C**, 14-23 (2015).
22. P. Blader, S. Rastegar, N. Fischer, U. Strahle, Cleavage of the BMP-4 antagonist chordin by zebrafish tolloid. *Science* **278**, 1937-1940 (1997).
23. B. Kim, G. Huang, W. B. Ho, D. S. Greenspan, Bone Morphogenetic Protein-1 Processes Insulin-like Growth Factor-binding Protein 3. *J. Biol. Chem.* **286**, 29014-29025 (2011).
24. G. Szlama, V. Vasarhelyi, M. Trexler, L. Patthy, Influence of WFIKKN1 on BMP1-mediated activation of latent myostatin. *FEBS J.* **283**, 4515-4527 (2016).
25. F. Delolme, C. Anastasi, L. B. Alcaraz, V. Mendoza, S. Vadon-Le Goff, M. Talantikite, R. Capomaccio, J. Mevaere, L. Fortin, D. Mazzocut, O. Damour, I. Zanella-Cleon, D. J. Hulmes, C. M. Overall, U. Valcourt, F. Lopez-Casillas, C. Moali, Proteolytic control of TGF-beta co-receptor activity by BMP-1/tolloid-like proteases revealed by quantitative iTRAQ proteomics. *Cell. Mol. Life Sci.* **72**, 1009-1027 (2015).
26. G. Ge, D. S. Greenspan, BMP1 controls TGFbeta1 activation via cleavage of latent TGFbeta-binding protein. *J.Cell Biol.* **175**, 111-120 (2006).
27. L. Garrigue-Antar, N. Hartigan, K. E. Kadler, Post-translational modification of bone morphogenetic protein-1 is required for secretion and stability of the protein. *J. Biol. Chem.* **277**, 43327-43334 (2002).
28. C. Moali, B. Font, F. Ruggiero, D. Eichenberger, P. Rousselle, V. Francois, A. Oldberg, L. Bruckner-Tuderman, D. J. Hulmes, Substrate-specific modulation of a multisubstrate proteinase. C-terminal processing of fibrillar procollagens is the only BMP-1-dependent activity to be enhanced by PCPE-1. *J. Biol. Chem.* **280**, 24188-24194 (2005).
29. I. C. Scott, I. L. Blitz, W. N. Pappano, Y. Imamura, T. G. Clark, B. M. Steiglitz, C. L. Thomas, S. A. Maas, K. Takahara, K. W. Cho, D. S. Greenspan, Mammalian BMP-1/Tolloid-related metalloproteinases, including novel family member mammalian Tolloid-like 2, have differential enzymatic activities and distributions of expression relevant to patterning and skeletogenesis. *Dev. Biol.* **213**, 283-300 (1999).
30. C. Bijakowski, S. Vadon-Le Goff, F. Delolme, J. M. Bourhis, P. Lecorche, F. Ruggiero, C. Becker-Pauly, I. Yiallouros, W. Stocker, V. Dive, D. J. Hulmes, C. Moali, Sizzled is unique among secreted frizzled-related proteins for its ability to specifically inhibit bone morphogenetic protein-1 (BMP-1)/tolloid-like proteinases. *J. Biol. Chem.* **287**, 33581-33593 (2012).
31. H. X. Lee, A. L. Ambrosio, B. Reversade, E. M. De Robertis, Embryonic dorsal-ventral signaling: secreted frizzled-related proteins as inhibitors of tolloid proteinases. *Cell* **124**, 147-159 (2006).

32. A. Doucet, C. M. Overall, Broad coverage identification of multiple proteolytic cleavage site sequences in complex high molecular weight proteins using quantitative proteomics as a complement to edman sequencing. *Mol. Cell Proteomics.* **10**, M110.003533 (2011).
33. J. Hofsteenge, K. G. Huwiler, B. Macek, D. Hess, J. Lawler, D. F. Mosher, J. Peter-Katalinic, C-mannosylation and O-fucosylation of the thrombospondin type 1 module. *J. Biol. Chem.* **276**, 6485-6498 (2001).
34. G. Martin-Manso, M. J. Calzada, Y. Chuman, J. M. Sipes, C. P. Xavier, V. Wolf, S. A. Kuznetsova, J. S. Rubin, D. D. Roberts, sFRP-1 binds via its netrin-related motif to the N-module of thrombospondin-1 and blocks thrombospondin-1 stimulation of MDA-MB-231 breast carcinoma cell adhesion and migration. *Arch. Biochem. Biophys.* **509**, 147-156 (2011).
35. R. Salza, F. Peysselon, E. Chautard, C. Faye, L. Moschcovich, T. Weiss, L. Perrin-Cocon, V. Lotteau, E. Kessler, S. Ricard-Blum, Extended interaction network of procollagen C-proteinase enhancer-1 in the extracellular matrix. *Biochem. J.* **457**, 137-149 (2014).
36. H. Chen, M. E. Herndon, J. Lawler, The cell biology of thrombospondin-1. *Matrix Biol.* **19**, 597-614 (2000).
37. P. R. Lawler, J. Lawler, Molecular basis for the regulation of angiogenesis by thrombospondin-1 and -2. *Cold Spring Harb. Perspect. Med.* **2**, a006627 (2012).
38. M. T. Sweetwyne, J. E. Murphy-Ullrich, Thrombospondin1 in tissue repair and fibrosis: TGF-beta-dependent and independent mechanisms. *Matrix Biol.* **31**, 178-186 (2012).
39. M. Matsuba, A. E. Hutcheon, J. D. Zieske, Localization of thrombospondin-1 and myofibroblasts during corneal wound repair. *Exp. Eye Res.* **93**, 534-540 (2011).
40. N. M. Moss, M. V. Barbolina, Y. Liu, L. Sun, H. G. Munshi, M. S. Stack, Ovarian cancer cell detachment and multicellular aggregate formation are regulated by membrane type 1 matrix metalloproteinase: a potential role in I.p. metastatic dissemination. *Cancer Res.* **69**, 7121-7129 (2009).
41. J. Dubail, F. Kesteloot, C. Deroanne, P. Motte, V. Lambert, J. M. Rakic, C. Lapiere, B. Nusgens, A. Colige, ADAMTS-2 functions as anti-angiogenic and anti-tumoral molecule independently of its catalytic activity. *Cell. Mol. Life Sci.* **67**, 4213-4232 (2010).
42. M. J. Calzada, D. S. Annis, B. Zeng, C. Marcinkiewicz, B. Banas, J. Lawler, D. F. Mosher, D. D. Roberts, Identification of novel beta1 integrin binding sites in the type 1 and type 2 repeats of thrombospondin-1. *J. Biol. Chem.* **279**, 41734-41743 (2004).
43. A. S. Asch, J. Tepler, S. Silbiger, R. L. Nachman, Cellular attachment to thrombospondin. Cooperative interactions between receptor systems. *J. Biol. Chem.* **266**, 1740-1745 (1991).
44. N. V. Lee, M. Sato, D. S. Annis, J. A. Loo, L. Wu, D. F. Mosher, M. L. Iruela-Arispe, ADAMTS1 mediates the release of antiangiogenic polypeptides from TSP1 and 2. *EMBO J.* **25**, 5270-5283 (2006).
45. J. E. Murphy-Ullrich, M. J. Suto, Thrombospondin-1 regulation of latent TGF-beta activation: A therapeutic target for fibrotic disease. *Matrix Biol.* (in press).
46. M. Shi, J. Zhu, R. Wang, X. Chen, L. Mi, T. Walz, T. A. Springer, Latent TGF-beta structure and activation. *Nature* **474**, 343-349 (2011).
47. G. Blanc, B. Font, D. Eichenberger, C. Moreau, S. Ricard-Blum, D. J. Hulmes, C. Moali, Insights into how CUB domains can exert specific functions while sharing a common fold: Conserved and specific features of the CUB1 domain contribute to the molecular basis of procollagen C-proteinase enhancer-1 activity. *J. Biol. Chem.* **282**, 16924-16933 (2007).
48. C. W. Hung, T. Koudelka, C. Anastasi, A. Becker, C. Moali, A. Tholey, Characterization of post-translational modifications in full-length human BMP-1 confirms the presence of a rare vicinal disulfide linkage in the catalytic domain and highlights novel features of the EGF domain. *J. Proteomics* **138**, 136-145 (2016).
49. K. O. Yee, M. Duquette, A. Ludlow, J. Lawler, Purification and analysis of thrombospondin-1. *Curr. Protoc. Cell Biol.* **Chapter 10**, Unit 10.10 (2003).

50. E. Turtle, N. Chow, C. Yang, S. Sosa, U. Bauer, M. Brenner, D. Solow-Cordero, W. B. Ho, Design and synthesis of procollagen C-proteinase inhibitors. *Bioorg. Med. Chem. Lett.* **22**, 7397-7401 (2012).
51. G. Klein, C. Mathe, M. Biola-Clier, S. Devineau, E. Drouineau, E. Hatem, L. Marichal, B. Alonso, J. C. Gaillard, G. Lagniel, J. Armengaud, M. Carriere, S. Chedin, Y. Boulard, S. Pin, J. P. Renault, J. C. Aude, J. Labarre, RNA-binding proteins are a major target of silica nanoparticles in cell extracts. *Nanotoxicology* **10**, 1555-1564 (2016).
52. S. Bachy, F. Letourneur, P. Rousselle, Syndecan-1 interaction with the LG4/5 domain in laminin-332 is essential for keratinocyte migration. *J. Cell. Physiol.* **214**, 238-249 (2008).

Acknowledgements: We are grateful to Joanne Murphy-Ullrich (UAB, Birmingham) for very useful tips on how to handle thrombospondin-1, to Claire Lethias (LBTI, Lyon) for providing most of the antibodies used in the preliminary screening of candidate substrates and to David Hulmes (LBTI, Lyon) for critical reading of the manuscript. We also thank Thibault Andrieu, Christophe Chamot and Dominique Mazzocut from the SFR Biosciences (UMS 3444, Lyon) for their help in performing flow cytometry, time lapse experiments and automated Edman Sequencing respectively. **Funding:** This work was supported by the CNRS, the University of Lyon, the Région Auvergne Rhône-Alpes (ARC 2013 to M.T. and C.M.), the ANR-07-PHYSIO-022-01 to C.M., the ANR-13-RPIB-0003-01 grant to P.R., the Ligue Nationale contre le Cancer (to L.B.A and P.R.) and the Ligue contre le Cancer-Comité du Rhône (to U.V.). **Author contributions:** C.M. and P.R. designed the project. C. Anastasi, P.R., M.T., A.T., A.B., L.B.A., L.F., F.D., J.A., S.V.L.G and C.M. performed experiments. C. Auxenfans and P.F. collected and provided human primary cells and corneas. C.M., P.R., C. Anastasi, S.V.L.G, F.D. and U.V. analyzed the data. C.M. wrote the manuscript. **Competing interests:** The authors declare that they have no competing interests.

ABBREVIATIONS

α-SMA: α-smooth muscle actin; BMP: bone morphogenetic protein; BSA: bovine serum albumin; BTP: BMP-1/tolloid-like proteinase; CUB: complement, uEGF, BMP-1; DMEM: Dulbecco's modified Eagle's medium; ECM: extracellular matrix; EGF: epidermal growth factor; FCS: fetal calf serum; LAP: latency associated peptide; PCPE: procollagen C-proteinase enhancer; PBS: phosphate buffer saline; sFRP: secreted frizzled related protein; TGF-β: transforming growth factor β; TLL: Tolloid-like; TSP-1: thrombospondin-1; TSR: thrombospondin repeat; VWFC: Von Willebrand factor C.

FIGURE LEGENDS

Figure 1: Changes in cell adhesion and migration induced by BMP-1 activity. (A) Phase contrast pictures of subconfluent 293 EBNA cells stably transfected with the empty pCEP4 vector or a pCEP4 construct encoding BMP-1, in the absence or presence of a synthetic BMP-1 hydroxamate inhibitor (Hxt, 10 µM). Bar = 150 µm. **(B)** Immunoblot showing the expression of BMP-1 in the medium and ECM of 293 EBNA cells. **(C)** Phase contrast images of HT1080-E94A and HT1080-BMP-1 cells, at three different growth states, showing the morphological changes preceding the loss of cell adhesion. For comparison, parental HT1080 cells and HT1080-BMP-1 cells grown in the presence of 25 µg/ml of the sizzled (Szl) inhibitor are also shown. Bar = 50 µm **(D)** Migration velocity of HT1080, HT1080-BMP-1 and HT1080-E94A cells calculated using videomicroscopy images taken over a period of 4 h (means ± 95 % confidence interval). ***: *p*-value < 10^{-5}. **(E)** Cell tracking of 30 individual cells for HT1080, HT1080-BMP-1 and HT1080-E94A cells.

Figure 2: BMP-1 alters cell adhesion through ECM modification. (A) Adhesion of HT1080 and HT1080-BMP-1 cells on the ECM deposited by the same cells. Prior to the assay, the HT1080 cells to be tested were detached from culture plates with EDTA while the HT1080-BMP-1 cells were either detached with EDTA (w EDTA) or collected after spontaneous detachment (w/o EDTA). ECM was prepared by removing cells with 20 mM NH_4OH. Means ± SD (n=3). **(B)** Phase contrast images of HT1080 cells seeded on the conditioned ECM of HT1080, HT1080-E94A and HT1080-BMP-1 cells in the absence of FCS (3 h 30 after seeding). Bar = 50 µm.

Figure 3: TSP-1 is cleaved by BMP-1. (A) Immuno-detection of TSP-1 and its proteolytic product in the conditioned medium of HT1080 (-) and HT1080-BMP-1 (+) cells at different time points after serum starvation (non-reducing conditions; 6 % acrylamide). A similar product is observed when purified human TSP-1 is incubated with recombinant BMP-1 (in vitro). **(B)** Immuno-detection of TSP-1 and its proteolytic product in the conditioned medium and ECM of 293-EBNA cells transfected with an empty vector (-) or a vector encoding BMP-1 (+) (non-reducing conditions; 6 % acrylamide). **(C)** Analysis of TSP-1 cleavage at increasing BMP-1:TSP-1 ratios and after different incubation times (left: reducing conditions; right: non-reducing conditions; 8 % acrylamide). # indicates the position of BMP-1. Note that, in non-reducing conditions, fragment 2 remains trimeric after cleavage while fragment 1 is released as a monomer. Additional bands at the top of the gel correspond to processing intermediates. **(D)** Domain structure of TSP-1 and positions of cleavage sites for BMP-1, thrombin, cathepsin G and ADAMTS-1. TSPN = Thrombospondin N-terminal; VWFC = Von Willebrand Factor type C; TSR = Thrombospondin type 1 repeats; EGF = Epidermal growth factor; C-ter = Thrombospondin C-terminal domain. **(E)** SDS-PAGE analysis of the cleavage of TSP-1 (210 nM) in the absence and presence of PCPE-1 (420 nM), Sizzled (1050 nM), sFRP-1 (1050 nM) and sFRP-2 (1050 nM). Incubation was for 4 h at 37°C with 105 nM BMP-1 (when present). BSA (1050 nM) was used as a negative control. Detection was with Coomassie Blue (8% acrylamide, reducing conditions). Note that PCPE-1 co-migrates with TSP-1 cleavage product 2 while sizzled, sFRP-1 and sFRP-2 migrate with or close to the dye front. **(F)** Fluorescence quantitation of TSP-1 cleavage performed on the same experiments analyzed using Sypro Ruby-stained gels (means ± SD, n=4).

Figure 4: Intact but not cleaved TSP-1 promotes the adhesion of HT1080 cells. (A) Phase-contrast images of HT1080 cells transfected with two siRNAs targeting TSP-1 or with a control siRNA (72 h after transfection; bar = 200 µm). Extinction efficiency was assessed through the immuno-detection of TSP-1 in the cell medium (loading control: collagen VI). **(B)** Adhesion of HT1080 cells on intact and cleaved TSP-1. TSP-1 was incubated for 4 h with (+) or without (-) BMP-1 or its inactive E94A mutant (*), at 4°C or 37°C prior to the assay (conditions 1-4). Control conditions with BMP-1 alone or buffer are also shown (conditions 5-6). Means ± SD from 3 independent experiments.

Figure 5: TSP-1 cleavage enhances TGF-β activation in HT1080 cells. (A) Immuno-detection of phosphorylated Smad2 (P-Smad2), Smad2/3 and actin in lysates of HT1080 cells treated for 60 min with solutions 1-7 (final TSP-1 concentration in culture medium: 16.4 nM). **(B)** Quantitation of phosphorylated Smad2 (P-Smad2) in the same conditions. Intensity was normalized relative to total Smad2 or actin. Means ± SD from 4 independent experiments. **(C)** Quantitation of luminescence in lysates of HT1080 cells transfected with the TGF-β reporter vector pGL3(CAGA)$_9$-Luc for 24 h and then treated with the same solutions 1-7 as in (A) (final TSP1 concentrations : 14 or 41 nM) or with 10 ng/ml TGF-β for another 24 h. Means ± SD from 3 independent experiments.

Figure 6: Effect of TSP-1 cleavage on the adhesion of keratocytes. (A) Adhesion of keratocytes is not affected by exogenous BMP-1. HT1080 cells were used as controls and seeded in the (serum-free) conditioned medium of HT1080 (a) or HT1080-BMP-1 (b) cells. Images were taken 24 h after seeding. Keratocytes were seeded in the freshly-collected (serum-free) conditioned medium of keratocytes in the absence of any additive (c) or after incubation at 37°C for 2 h with 185 nM (13 µg/ml) recombinant BMP-1 (d) or vehicle (e) or in the presence of 185 nM recombinant BMP-1 (f) or vehicle (g) or in the (serum-free) conditioned medium of keratocytes cultivated with 5 µM of the hydroxamate BMP-1 inhibitor (h). Images were taken 6 h after seeding. Bar = 50 µm. **(B)** Immuno-detection of TSP-1 and its proteolytic product in the conditioned medium of keratocytes cultured in serum-free conditions in the absence or presence of 5 µM of an hydroxamate inhibitor (Hxt) or 300 nM Sizzled (Szl). **(C)** Immuno-detection of endogenous BMP-1 in the conditioned medium of human primary keratocytes. Medium was collected after 48 h and concentrated using ultrafiltration. Sixty µg of total protein were loaded on a 10 % acrylamide gel (reducing conditions) with recombinant purified human BMP-1 as a control (50 ng, recBMP-1).

Figure 7: TSP-1 cleavage potentiates keratocyte differentiation into myofibroblasts. (A) Immuno-detection of P-Smad2, Smad2 and actin in cell lysates of keratocytes treated for 30 min with intact and cleaved TSP-1 (41 nM final concentration) or 10 ng/ml TGF-β. **(B)** Quantitation of phosphorylated Smad2 in the same conditions. Intensity was normalized relative to total Smad2 and actin. Means ± SD from 3 independent experiments. **(C)** Staining of α-SMA in primary keratocytes maintained for 72 h in serum-free medium containing intact TSP-1 (same condition 1 as in (A), 41 nM TSP-1), cleaved TSP-1 (condition 2), BMP-1 (condition 3), buffer (condition 4) or 10 ng/ml TGF-β. Bar = 100 µm. **(D)** Quantitation of cells with α-SMA fibers. All conditions were found to differ significantly from one

another (*p*-value < 0.001) except conditions 3 and 4 (n=20 images/condition; means ± 95 % confidence interval).

Figure 8: Detection of TSP-1 fragment 1 in human corneal scars. Immuno-detection of TSP-1 in 4 corneas from patients presenting permanent corneal scars. Various amounts of keratocyte supernatant (SN) corresponding to 0.2-1.5 µg total protein were also loaded on the gel (6 % acrylamide gel; non-reducing conditions). Before detection, the membrane was split into 2 parts and two different exposure times were used to reveal intact TSP-1 and fragment 1.

Figure 1

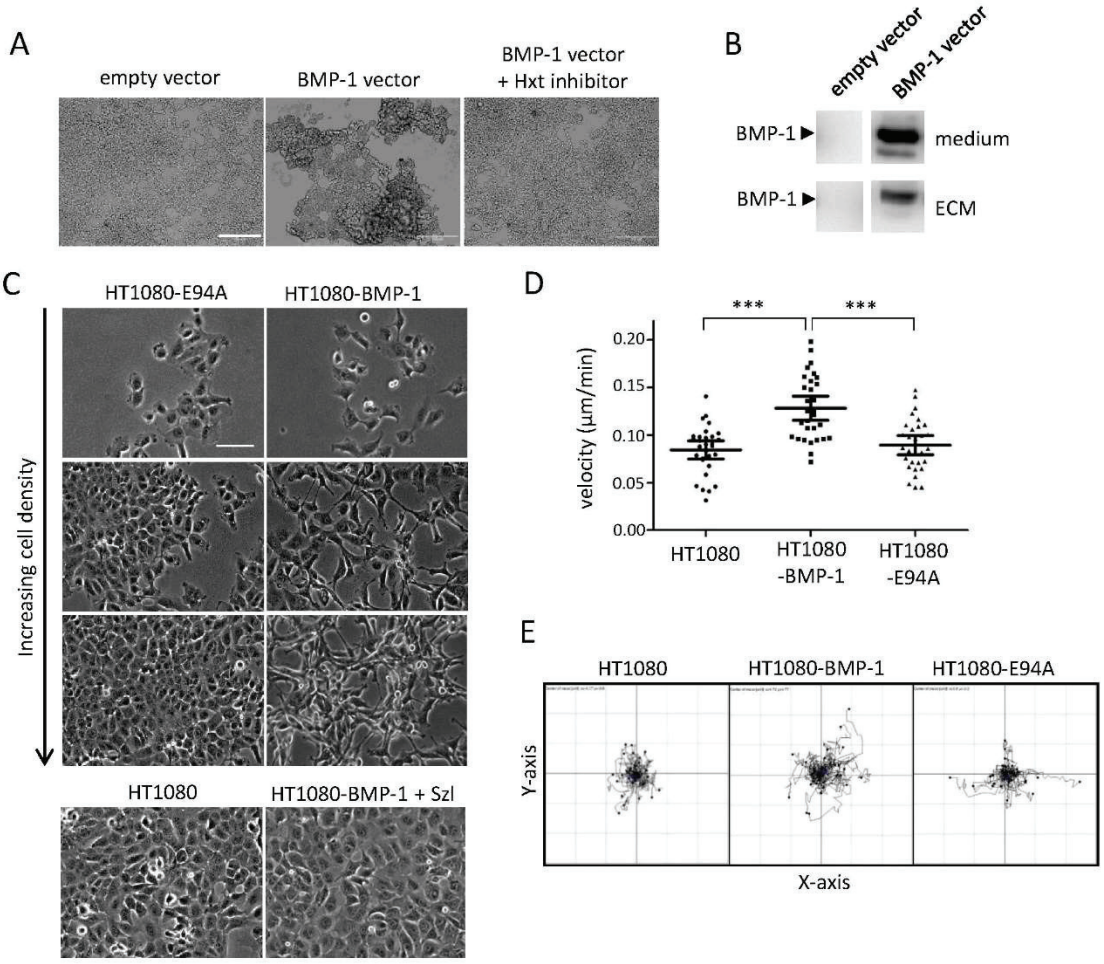
A
empty vector
BMP-1 vector
BMP-1 vector
+ Hxt inhibitor
B
empty vector
BMP-1 vector
BMP-1
medium
BMP-1
ECM
C
HT1080-E94A
HT1080-BMP-1
Increasing cell density
HT1080
HT1080-BMP-1 + Szl
D
***
***
velocity (µm/min)
0.20
0.15
0.10
0.05
0.00
HT1080
HT1080
-BMP-1
HT1080
-E94A
E
HT1080
HT1080-BMP-1
HT1080-E94A
Y-axis
X-axis

Figure 2

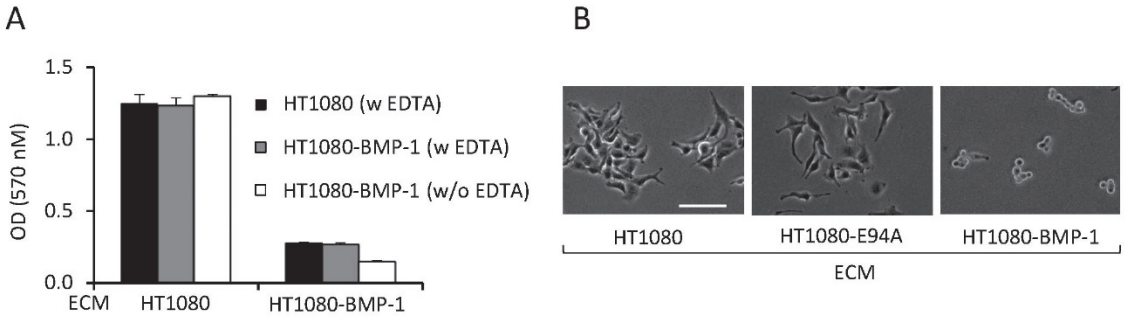
A
1.5
1.0
0.5
0.0
OD (570 nM)
HT1080 (w EDTA)
HT1080-BMP-1 (w EDTA)
HT1080-BMP-1 (w/o EDTA)
ECM
HT1080
HT1080-BMP-1
B
HT1080
HT1080-E94A
HT1080-BMP-1
ECM

Figure 3

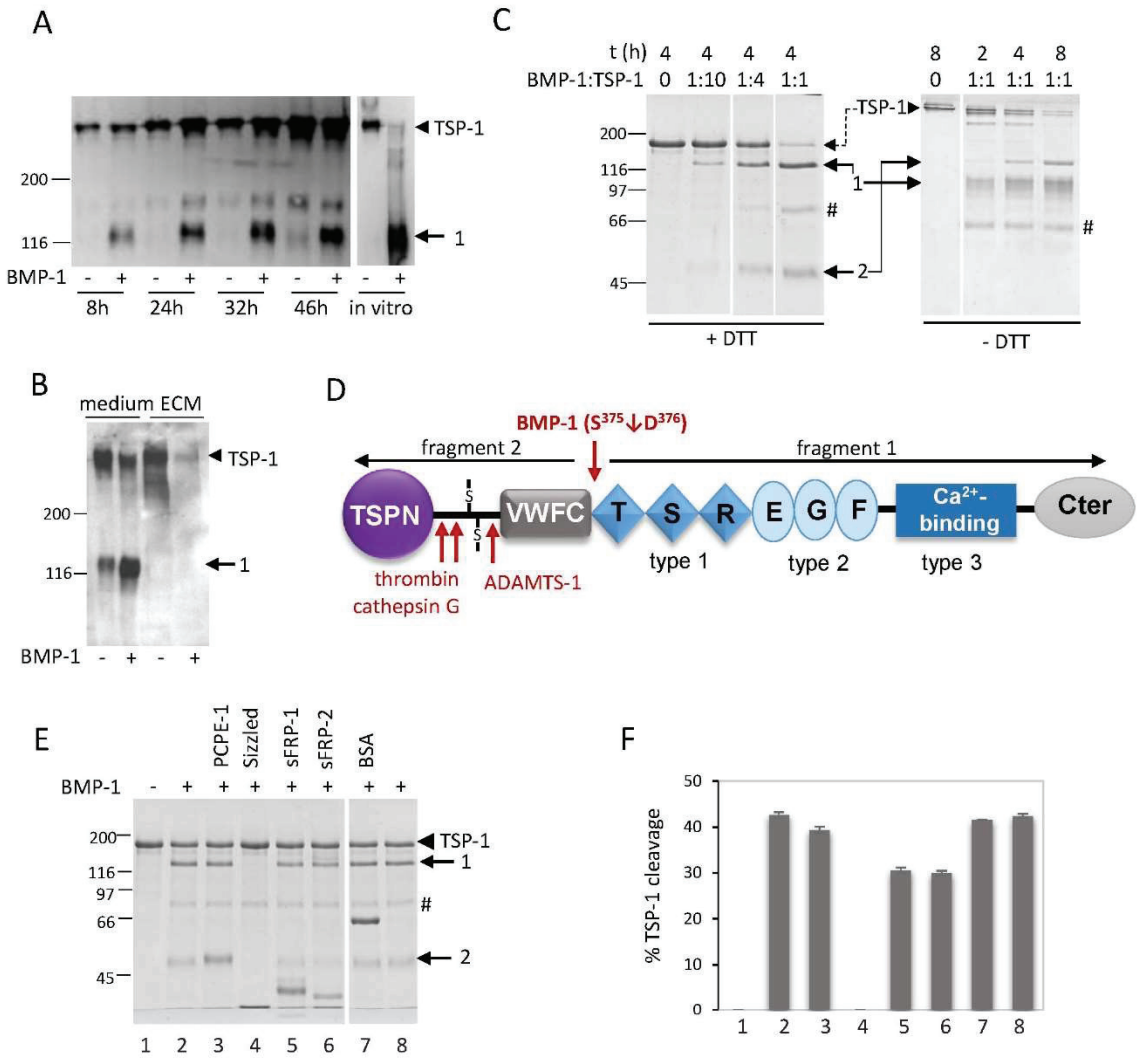
A
TSP-1
1
200
116
BMP-1 - + - + - + - + - +
8h 24h 32h 46h in vitro
C
t (h) 4 4 4 4 8 2 4 8
BMP-1:TSP-1 0 1:10 1:4 1:1 0 1:1 1:1 1:1
TSP-1
200
116
97
66
45
1
2
#
+ DTT
- DTT
B
medium ECM
TSP-1
1
200
116
BMP-1 - + - +
D
BMP-1 (S375↓D376)
fragment 2
fragment 1
TSPN
VWFC
T
S
R
E
G
F
Ca2+-binding
Cter
type 1
type 2
type 3
thrombin
cathepsin G
ADAMTS-1
E
PCPE-1
Sizzled
sFRP-1
sFRP-2
BSA
BMP-1 - + + + + + + +
TSP-1
1
2
#
200
116
97
66
45
1 2 3 4 5 6 7 8
F
% TSP-1 cleavage
50
40
30
20
10
0
1 2 3 4 5 6 7 8

Figure 4

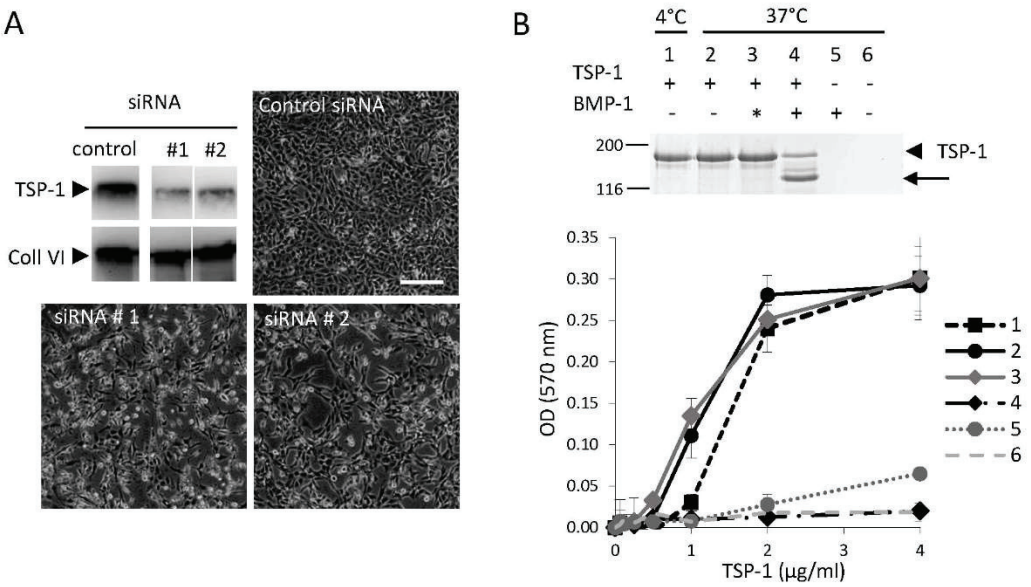
A
siRNA
control
#1
#2
TSP-1
Coll VI
Control siRNA
siRNA # 1
siRNA # 2
B
4°C
37°C
1 2 3 4 5 6
TSP-1 + + + + - -
BMP-1 - - * + + -
200
116
TSP-1
OD (570 nm)
0.35
0.30
0.25
0.20
0.15
0.10
0.05
0.00
0 1 2 3 4
TSP-1 (µg/ml)
1
2
3
4
5
6

Figure 5

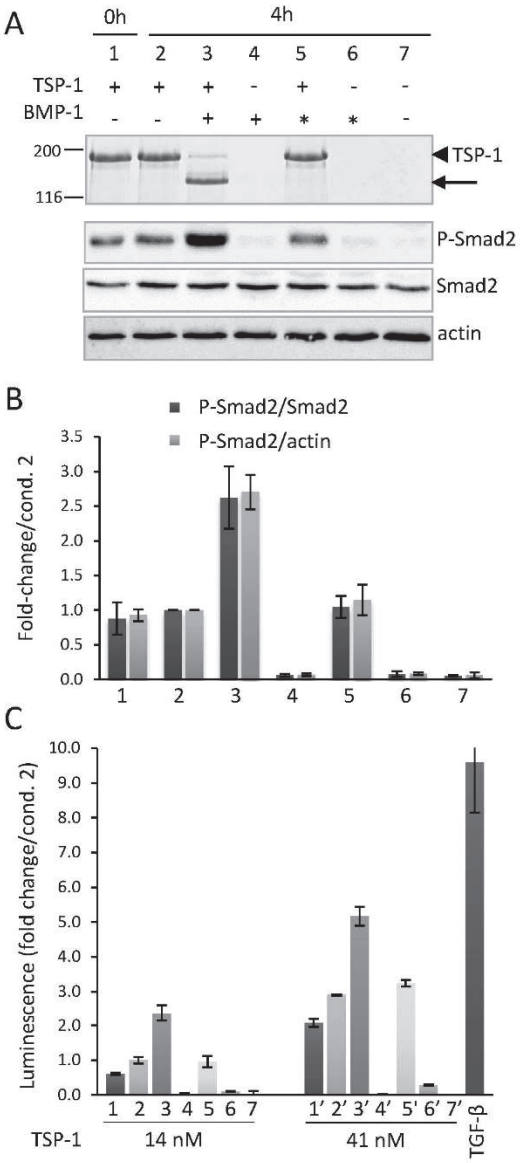
A
0h
4h
1 2 3 4 5 6 7
TSP-1 + + + - + - -
BMP-1 - - + + * * -
200
116
TSP-1
P-Smad2
Smad2
actin
B
P-Smad2/Smad2
P-Smad2/actin
Fold-change/cond. 2
3.5
3.0
2.5
2.0
1.5
1.0
0.5
0.0
1 2 3 4 5 6 7
C
Luminescence (fold change/cond. 2)
10.0
9.0
8.0
7.0
6.0
5.0
4.0
3.0
2.0
1.0
0.0
1 2 3 4 5 6 7
1' 2' 3' 4' 5' 6' 7'
TSP-1
14 nM
41 nM
TGF-β

Figure 6

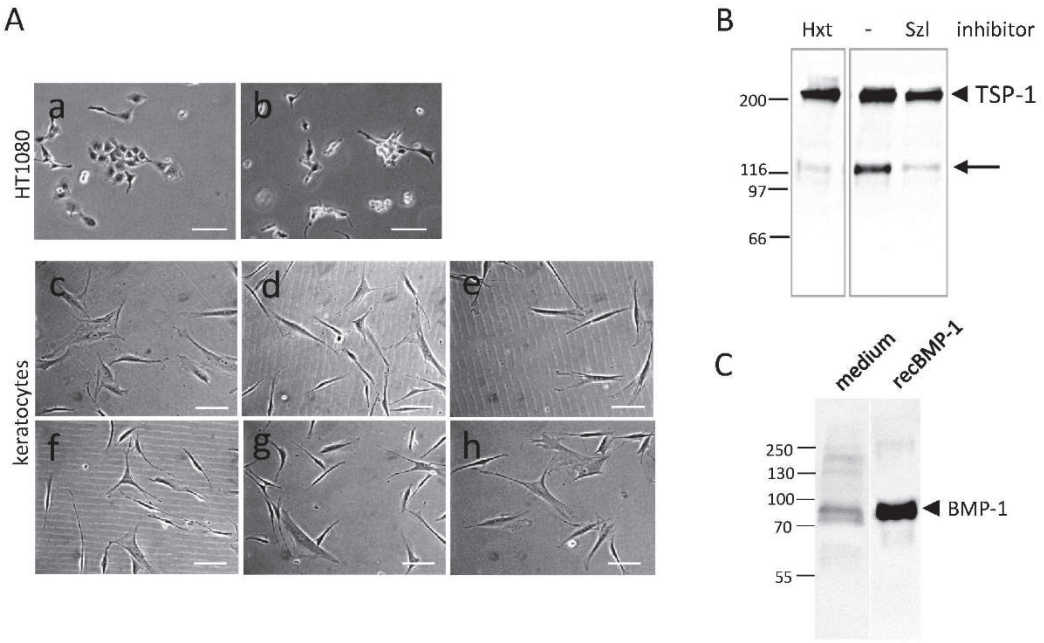
A
HT1080
keratocytes
a
b
c
d
e
f
g
h
B
Hxt
-
Szl
inhibitor
200
116
97
66
TSP-1
C
medium
recBMP-1
250
130
100
70
55
BMP-1

Figure 7

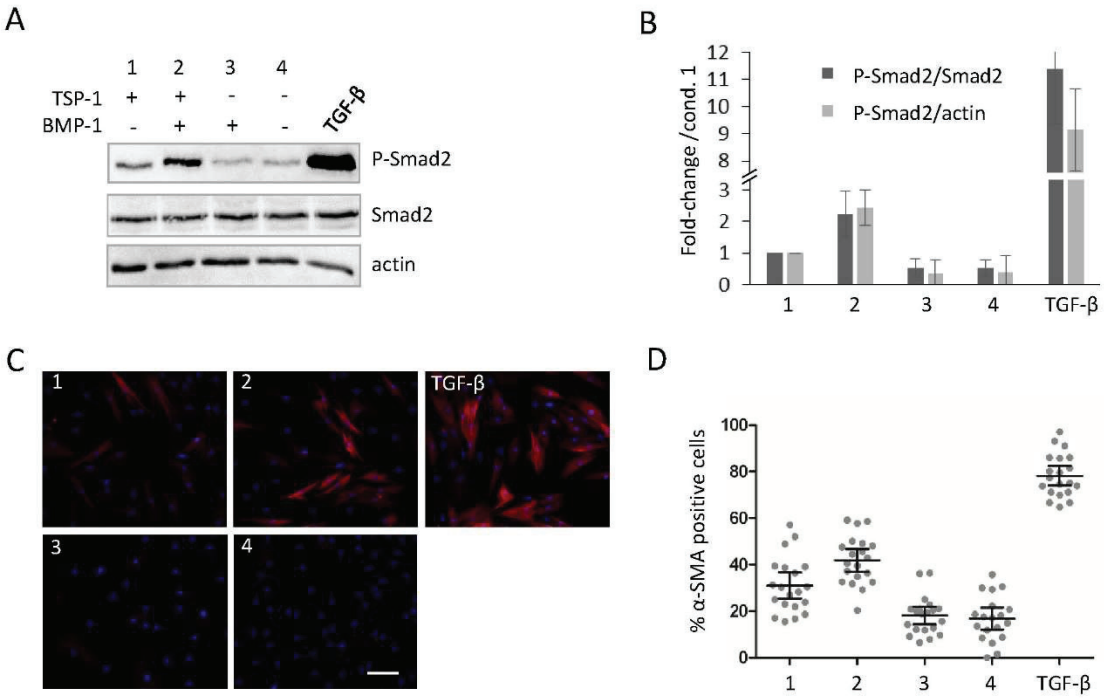
A
1 2 3 4
TSP-1 + + - -
BMP-1 - + + -
TGF-β
P-Smad2
Smad2
actin
B
Fold-change /cond. 1
P-Smad2/Smad2
P-Smad2/actin
1 2 3 4 TGF-β
C
1
2
TGF-β
3
4
D
% α-SMA positive cells
1 2 3 4 TGF-β

Figure 8

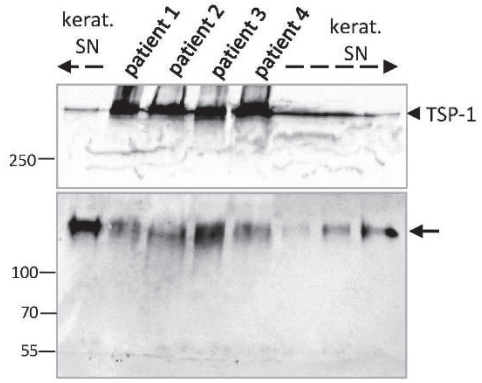
kerat. SN
patient 1
patient 2
patient 3
patient 4
kerat. SN
TSP-1
250
100
70
55

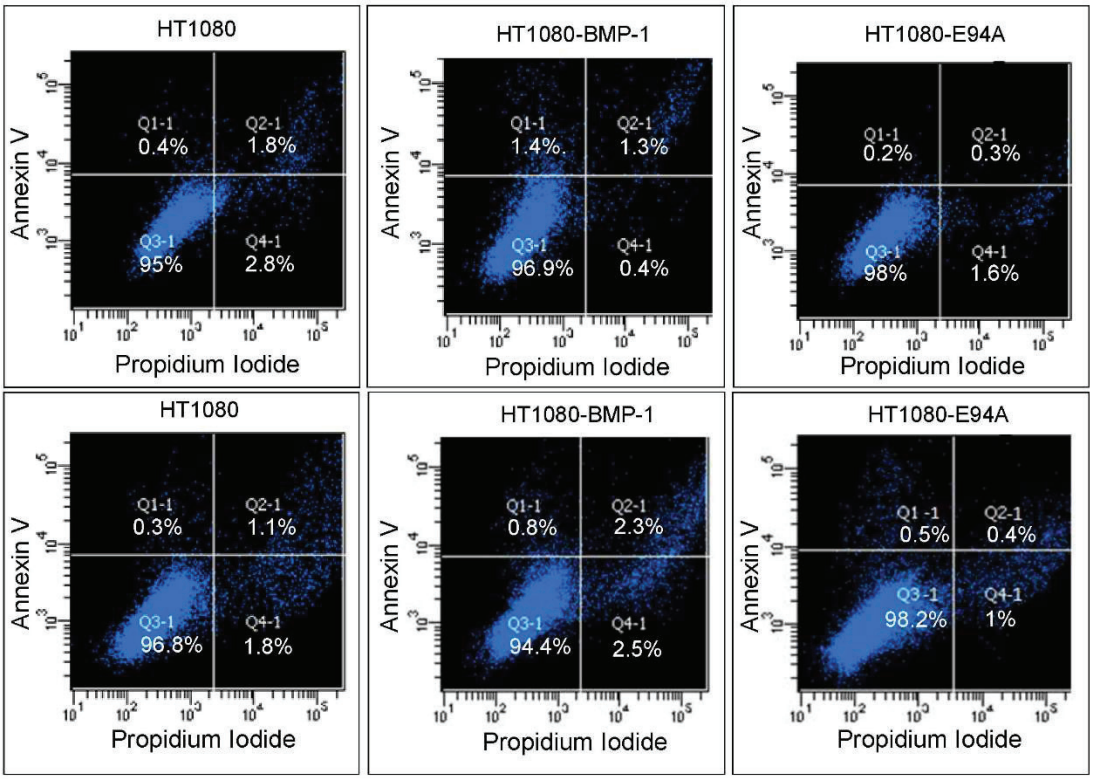

Figure S1: Effect of BMP-1 on apoptosis. Quantitation of cell apoptosis and necrosis using flow cytometry at low (around 20 %; top) and high (around 50%; bottom) cell density. Viable cells are found in the Q3-1 quarter and represent more than 94 % of the total cells.

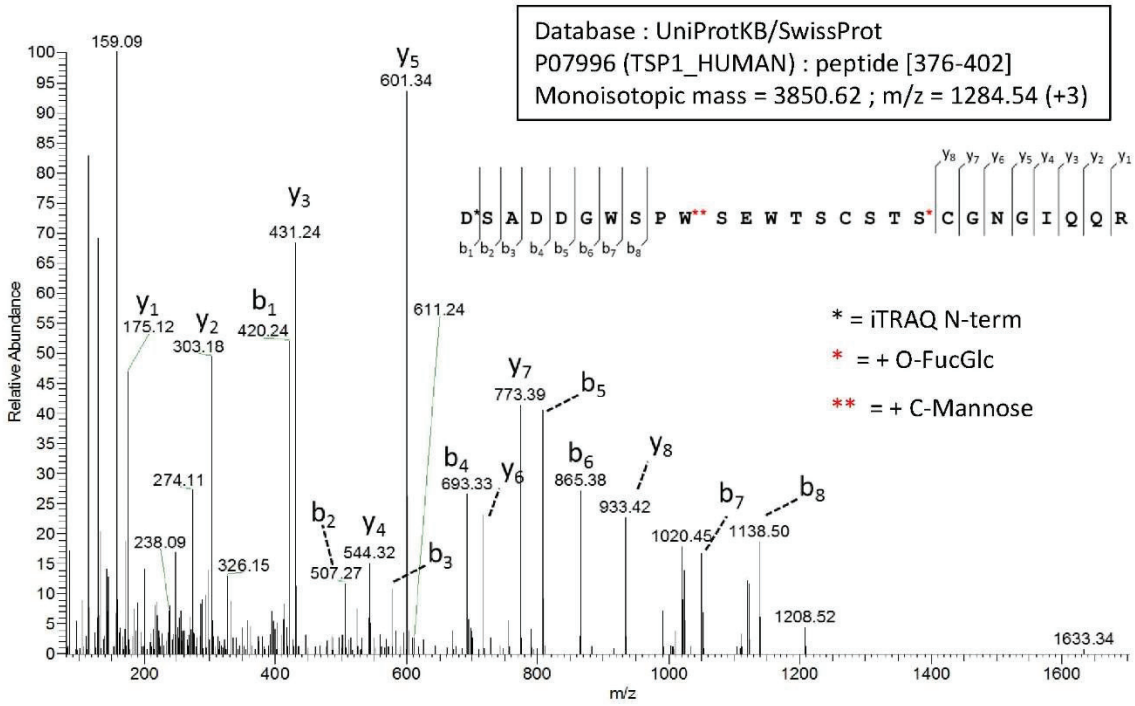

Figure S2: Mass spectrum and attribution of b and y ions for peptide 376-402 of human platelet TSP-1 defining BMP-1 cleavage site. Positions of peptide modifications are indicated by black and red asterisks.

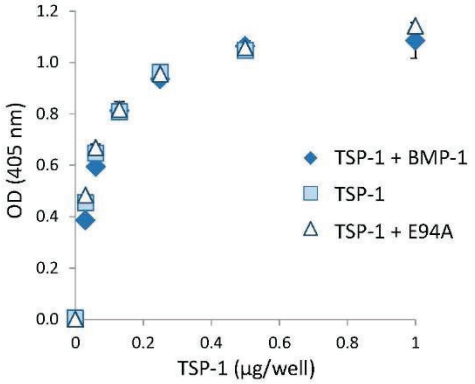

Figure S3: Coating of 96-well plates is equally efficient with intact and cleaved TSP-1. Prior to the assay, TSP-1 was incubated in the absence or presence of BMP-1 or its inactive mutant (E94A) in the conditions of Fig. 4B. Coating was performed overnight and its efficiency was measured using ELISA and the anti-TSP-1 antibody. Means ± SD (n=4).

Abstract: Tessier et *al.* 2016, *Annales de Dermatologie et Vénérologie*

Congrès Annuel de Recherche Dermatologique 2016
PARIS 6 et 7 décembre 2016

SRD

Société de Recherche Dermatologique

JDP2016/CARD-2931

Fonctions divergentes des "Procollagen C-Proteinase Enhancers", PCPE-1 et -2, dans la cicatrisation cutanée

Agnès Tessier[*1,2], Sandrine Vadon-Le Goff[1], Leena Bruckner-Tuderman[2], Alexander Nyström[2], Catherine Moali[1]
[1]Laboratoire de Biologie Tissulaire et Ingénierie Thérapeutique, CNRS - Université Claude Bernard Lyon 1, Lyon, France,
[2]Department of Dermatology, Medical Center, Albert-Ludwigs-Universität Freiburg, Freiburg, Allemagne

Introduction: Au cours de la cicatrisation cutanée, la balance entre synthèse et dégradation des collagènes joue un rôle crucial dans la restauration et le maintien de l'intégrité structurale et mécanique de la peau. De fait, diverses pathologies cutanées (plaies chroniques, cicatrices hypertrophiques et chéloides) affectant la santé et la qualité de vie des patients sont causées par des défauts de fibrillogenèse. Les collagènes sont synthétisés et sécrétés sous forme de précurseurs solubles par les fibroblastes. Dans l'espace extracellulaire, leur extrémité C-terminale est alors clivée par des protéases, de la famille BMP-1/Tolloid-like (BTPs), ce qui permet la formation de fibres de collagène. Ce clivage protéolytique est stimulé d'un facteur dix par une glycoprotéine, "Procollagen C-Proteinase Enhancer-1" (PCPE-1), connue pour être impliquée dans différents contextes de réparation tissulaire. Récemment, une deuxième isoforme de PCPE a été décrite : PCPE-2 serait capable de stimuler la maturation des procollagènes *in vitro* et jouerait un rôle essentiel dans la synthèse du collagène chez la souris dans un modèle d'hypertrophie cardiaque. Ainsi, l'objectif de ce travail est d'étudier les rôles de PCPE-1 et -2 dans la cicatrisation de la peau.
Matériel et Méthodes: Pour comprendre le rôle de PCPE-1 et -2 dans la cicatrisation, l'expression et la distribution des PCPEs et des BTPs ont été étudiées par qRT-PCR, western blot et immunofluorescence dans des modèles cellulaire (fibroblastes et kératinocytes) et tissulaire (modèle murin de cicatrisation). En parallèle, un système d'expression de PCPE-2 a été mis en place afin de produire la protéine humaine recombinante dans le but d'évaluer son activité sur les procollagènes.
Résultats: Les BTPs sont exprimées à la fois par les fibroblastes et les kératinocytes ; leur expression augmente pendant la cicatrisation dans la peau de souris. De façon intéressante, les deux isoformes de PCPEs ne sont pas exprimées par le même type cellulaire dans la peau : PCPE-1 est fortement exprimée par les fibroblastes et son expression augmente de façon significative après une lésion cutanée. A l'inverse, PCPE-2 n'est pas retrouvée dans la peau non lésée, mais est fortement exprimée par les neutrophiles dans les premières phases de cicatrisation chez la souris. Les premiers tests d'activité réalisés semblent démontrer que la protéine PCPE-2 purifiée a beaucoup moins d'effet que PCPE-1 sur la maturation des collagènes.
Discussion: Ces travaux suggèrent que PCPE-1 et -2 auraient des rôles distincts dans la cicatrisation cutanée. Alors que PCPE-1 est un acteur majeur de la fibrillogenèse dans la peau et pendant la cicatrisation, l'expression de PCPE-2 par des cellules immunitaires suggère une fonction alternative de cette isoforme. Notre objectif est désormais de comprendre le rôle de PCPE-2 exprimée par les neutrophiles pendant la cicatrisation.

Conflits d'intérêts: Aucun conflit à déclarer

Mots-clés: Cicatrisation cutanée, collagène, Procollagen C-Proteinase Enhancer (PCPE)

Book chapter: Moali et Tessier, *Biologie Cutanée CoBIP 2017*

1
Synthèse et dégradation des collagènes du derme

Agnès Tessier et Catherine Moali*

Laboratoire de Biologie Tissulaire et Ingénierie Thérapeutique – CNRS UMR5305, Université de Lyon
*Auteur pour la correspondance : catherine.moali@ibcp.fr

I – Introduction

Le derme est composé principalement de collagènes qui représentent 70 % de son poids sec. Les collagènes forment des réseaux tridimensionnels complexes, en interaction avec de nombreuses autres protéines de la matrice extracellulaire et avec les cellules résidentes qui sont responsables de leur synthèse (principalement les fibroblastes). Toute altération dans la composition et l'architecture des collagènes peut avoir d'énormes répercussions sur la fonctionnalité du derme tant au niveau mécanique et esthétique qu'au niveau de sa capacité à se réparer après une lésion ou à servir de réservoir pour les nombreuses molécules impliquées dans le maintien de l'homéostasie cutanée. Ainsi, le syndrome d'Ehlers-Danlos, souvent causé par des mutations dans les gènes codant pour les collagènes fibrillaires ou les protéines impliquées dans leur biosynthèse, se manifeste par une peau fragile et hyper extensible, formant des cicatrices atrophiques après lésion (Malfait and De Paepe, 2014). De la même façon, les cicatrices pathologiques (chéloïdes, cicatrices hypertrophiques, plaies chroniques) sont caractérisées par un excès ou par un déficit en collagènes qui peut être à l'origine de l'altération des propriétés mécaniques de la peau à l'endroit de la lésion, de douleurs plus ou moins intenses, d'un risque accru d'infections et/ou d'un handicap esthétique très invalidant (Mari et al., 2015; Menke et al., 2007; Wells et al., 2016; Zhu et al., 2016).

II – Les collagènes du derme

Les collagènes partagent la caractéristique commune de posséder au moins

un domaine en triple hélice avec des répétitions de la séquence $(GXY)_n$ où X et Y peuvent représenter n'importe quel résidu mais sont majoritairement des prolines (X) ou des hydroxyprolines (Y). Ils possèdent aussi la capacité de former ou de participer à des assemblages supra-moléculaires. Parmi les 28 types de collagènes répertoriés chez l'homme (Ricard-Blum, 2011), seuls les collagènes I, III, V, VI, VII, XII, XIV et XVI sont présents dans le derme en quantité détectable (Ruggiero et al., 2005).

La catégorie la plus connue de collagènes est celle des collagènes fibrillaires qui ont la capacité de s'agréger sous formes de fibres, facilement identifiées en microscopie électronique par leur périodicité (D = 64-67 nm) et une alternance de bandes claires et sombres. Cette striation caractéristique est définie par l'espacement régulier entre les molécules de collagène à l'intérieur des fibres. Les diamètres des fibres sont généralement compris entre 12 et 500 nm (Kadler et al., 2007) et ils sont très variables dans la peau où de grosses fibres peuvent co-exister avec des fibres beaucoup plus petites. On observe aussi que les faisceaux de fibres de la peau s'alignent suivant une orientation locale mais que cette orientation ne s'étend pas au-delà de quelques dizaines de microns et diffère d'un faisceau à l'autre. Le résultat est un réseau tridimensionnel complexe qui a l'aspect d'un tissage constitué de fibres entrecroisées et capables de résister à des pressions/torsions/étirements exercés dans toutes les directions. Les collagènes de la peau entrant dans la catégorie des collagènes fibrillaires sont les collagènes I, III et V qui sont synthétisés principalement sous forme d'hétérotrimères composés de deux chaînes différentes pour le type I et le type V ($[\alpha1]_2\alpha2$) et d'homotrimères pour le type III ($[\alpha1]_3$). Ils forment des fibres hétérotypiques où les trois types de collagènes s'auto-assemblent en différentes proportions (Birk, 2001; Henkel and Glanville, 1982). Les chiffres les plus répandus font état de 80 % de collagène I, 15 % de collagène III et 5 % de collagène V dans le derme (Chung and Uitto, 2010). Ils sont présents dans toute l'épaisseur du derme, même si le collagène V semble un peu plus présent au niveau du derme superficiel ou derme « papillaire » (Ruggiero et al., 2005), et lui confèrent rigidité et résistance.

Les collagènes VI et VII ne font pas partie des collagènes fibrillaires car ils ne forment pas des fibres striées mais d'autres types d'assemblage connus sous le nom de microfibrilles ou de fibres d'ancrage. Les régions en triple hélice occupent une proportion moins importante dans leur séquence que dans le cas des collagènes fibrillaires et peuvent comporter des

interruptions. Les microfibrilles de collagène VI s'assemblent latéralement à partir de modules tétramériques, eux-mêmes composés de 4 molécules hétérotrimériques α1(VI)α2(VI)α3(VI), pour former ce qu'on appelle couramment des « colliers de perle » ou des « filaments perlés » (Cescon et al., 2015). Le réseau de collagène VI s'intercale dans le réseau des collagènes fibrillaires et semble avoir pour fonction principale de permettre l'ancrage d'autres protéines matricielles ou des cellules et de maintenir l'intégrité des tissus. Les fibres d'ancrage formées par le collagène VII sont quant à elles situées à l'interface entre la jonction dermo-épidermique et le derme et assurent la cohésion entre le derme et l'épiderme (Chung and Uitto, 2010). Les homotrimères de collagène VII ($[\alpha1(VII)]_3$) s'associent en dimères anti-parallèles qui entourent les fibres de collagènes tout en interagissant à leurs extrémités avec les protéines de la lame basale. Cette organisation permet l'ancrage stable de la lame basale aux fibres de collagène du derme.

Les derniers types de collagène présents dans le derme sont les FACITs (fibril-associated collagens with interrupted triple helices) représentés ici par les collagènes XII, XIV et XVI. Comme leur nom l'indique, ils sont associés aux fibres de collagène mais ils n'ont pas la capacité de former par eux-mêmes des assemblages supra-moléculaires. On trouve les collagènes XII et XIV à la surface des fibres de collagène (Chiquet et al., 2014; Ruggiero et al., 2005) alors que le collagène XVI est localisé sur les microfibrilles de fibrilline au niveau du derme papillaire (Grassel and Bauer, 2013). Les collagènes FACITs sont généralement décrits comme des connecteurs participant à l'organisation de la matrice extracellulaire et à la régulation de ses propriétés mécaniques mais aussi comme des « lubrifiants » contrôlant les propriétés de surface des fibres (Bella and Hulmes, 2017).

Malgré la diversité des assemblages et des chaînes de collagène décrite ci-dessus, les fibroblastes et autres cellules résidentes de la peau sont capables de synthétiser tous les collagènes avec la bonne composition et stœchiométrie. Les paragraphes suivants décrivent les mécanismes d'assemblage et de dégradation des collagènes du derme qui permettent leur synthèse et leur renouvellement en situation d'homéostasie mais aussi au cours du développement et de la réparation tissulaire. Nous donnerons l'exemple particulier des collagènes fibrillaires qui sont à la fois les plus abondants et les mieux connus.

III – L'assemblage intracellulaire des collagènes fibrillaires

Les chaînes polypeptidiques de collagène sont synthétisées au niveau du réticulum endoplasmique (RE) où elles vont aussi commencer à être « décorées » par plusieurs types de modifications post-traductionnelles (hydroxylation de certaines prolines et lysines ; O- et N-glycosylations ; formation de ponts disulfures). L'hydroxylation des prolines semble jouer un rôle particulièrement critique car elle permettra ultérieurement d'assurer la stabilité de la triple hélice à 37°C. Les chaînes polypeptidiques ainsi obtenues sont appelées chaînes de procollagène (Fig. 1). L'étape suivante consiste à former des homo- ou hétéro-trimères possédant les bonnes compositions et stœchiométries à partir des 12 chaînes de procollagène qui sont potentiellement synthétisées simultanément par les cellules dermiques. Toute erreur dans ce processus conduirait à former des chimères non fonctionnelles entraînant leur dégradation par le protéasome ou une réponse de type « stress du RE » pouvant conduire à l'apoptose de la cellule.

Il est connu depuis de nombreuses années que la reconnaissance des chaînes de collagènes fibrillaires implique leur domaine globulaire C-terminal, appelé C-propeptide, mais jusque récemment, les mécanismes exacts de cette reconnaissance n'étaient pas compris. En 1997, l'équipe de N. Bulleid avait déjà observé que les C-propeptides des collagènes fibrillaires sont relativement bien conservés sauf au niveau de deux séquences centrales de 12 et 3 résidus très variables (Lees et al., 1997). Elle avait aussi confirmé que ces séquences jouent un rôle important dans la trimérisation car l'insertion des séquences variables de la chaîne α1 du collagène III dans la séquence de la chaîne α2 du collagène I (α2(I)), normalement incapable de trimériser en absence de la chaîne α1(I), conduit à la formation de trimères $[\alpha2(I)]_3$. Ces séquences ont par la suite été appelées « chain recognition sequences » (CRS) mais il a fallu attendre 2012 et la résolution de la première structure cristallographique d'un C-propeptide de collagène fibrillaire pour découvrir la nature des interactions mises en jeu. Cette structure a été obtenue pour le collagène III (Bourhis et al., 2012) et montre que la séquence variable de 12 résidus d'une chaîne interagit de façon spécifique avec la séquence de 3 résidus d'une autre chaîne pour former trois pont salins très stables. Par ailleurs, la formation des trimères est stabilisée par des ponts disulfures inter-chaînes. Dernièrement, la structure

du C-propeptide de l'homotrimère de collagène I, peu représenté *in vivo* sauf pendant le développement et dans certaines situations pathologiques, a également été résolue (Sharma et al., 2017). Elle a permis de modéliser la forme hétérotrimérique du C-propeptide I et d'en déduire les interactions spécifiques qui gouvernent l'assemblage du collagène le plus abondant dans le derme, le collagène I (Fig. 1). Notons que dans ce cas, trois interfaces différentes sont formées entre les monomères impliquant à la fois des résidus des CRS et des résidus situés ailleurs dans la séquence, notamment l'arginine 42 de la chaîne α1 et l'arginine 45 ainsi que le résidu C-terminal lysine 247 de la chaîne α2.

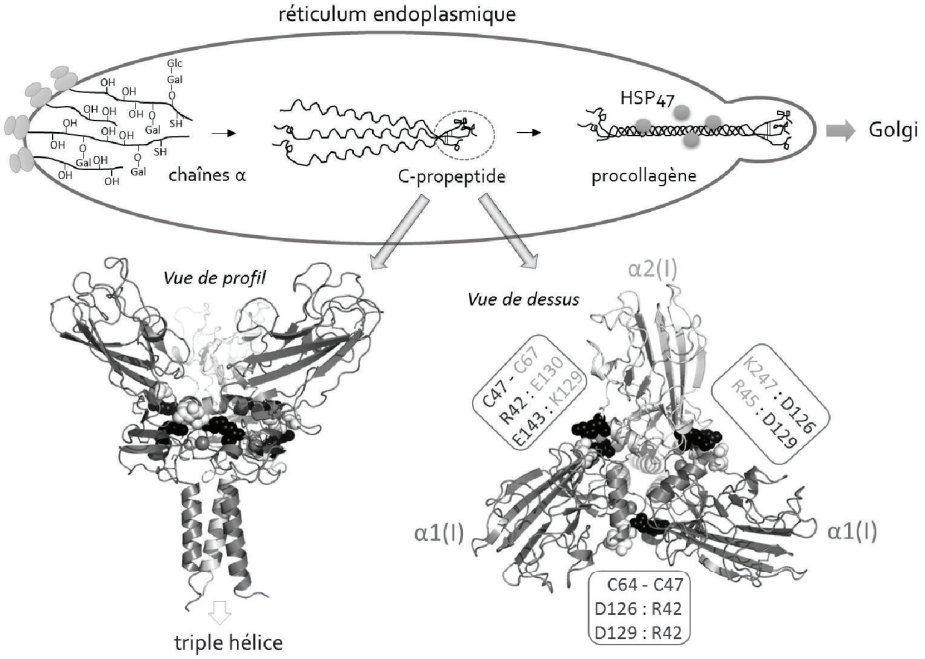

Figure 1 : Schéma simplifié de la synthèse des procollagènes fibrillaires dans le réticulum endoplasmique et rôle du C-propeptide dans l'initiation de l'assemblage intracellulaire des collagènes fibrillaires. Le modèle du C-propeptide hétérotrimérique de collagène I ($[\alpha1(I)]_2\alpha2(I)$) a été obtenu à partir de la structure cristallographique de l'homotrimère $[\alpha1(I)]_3$ (Sharma et al., 2017). Les interactions permettant la reconnaissance specifique des chaînes α1(I) et α2(I) sont détaillées sur la vue de dessus.

Une fois que les chaînes se sont associées grâce aux interactions que nous venons de décrire, la triple hélice se forme en progressant du côté C-

terminal vers le côté N-terminal. Ce processus est régulé par des chaperones dont certaines sont spécifiques des collagènes comme HSP47 (Ito and Nagata, 2017) et empêchent le mauvais repliement des triples hélices et la formation d'agrégats. La protéine HSP47 accompagne les procollagènes jusqu'au réseau cis-Golgi où elle se dissocie de son partenaire, sous l'effet d'une diminution du pH, pour être recyclée. Le transport entre le RE et l'appareil de Golgi nécessite par ailleurs des vésicules de plus grande taille que les vésicules COPII classiques (diamètre 60-80 nm) mais les mécanismes permettant leur croissance pour intégrer les grandes molécules de procollagènes fibrillaires peu flexibles (> 300 nm) sont encore largement méconnus (Gorur et al., 2017).

Enfin, les molécules de procollagènes sont sécrétées dans l'espace extracellulaire où elles vont subir des maturations supplémentaires qui aboutiront à la formation de fibres de collagènes.

IV – L'assemblage extracellulaire des fibres de collagène

Les molécules de procollagènes sécrétées n'ont pas la capacité de former des fibres car leurs extrémités N- et C-terminales (N- et C-propeptides) les maintiennent sous une forme soluble. Des étapes de maturation protéolytique vont donc être nécessaires pour éliminer les propeptides et diminuer la solubilité des molécules de collagène (Fig. 2). Ces étapes font intervenir des protéases spécifiques appelées « procollagen N-proteinases » (PNPs) et « procollagen C-proteinases » (PCPs) qui font partie de la famille des métalloprotéases regroupées sous le nom de metzincines. Cette famille est définie par une séquence consensus de liaison du zinc impliqué dans la catalyse et par une méthionine conservée. Les principales PNPs sont les isoformes 2 et 14 des ADAMTSs (« A Disintegrin And Metalloproteinase with ThromboSpondin motifs ») (Bekhouche and Colige, 2015) qui peuvent maturer l'extrémité N-terminale des collagènes I et III et les principales PCPs sont les protéases de la famille « BMP-1/tolloid-like » (BTPs) qui sont quant à elles responsables de la maturation C-terminale des collagènes I et III (Vadon-Le Goff et al., 2015).

Cette distinction ne s'applique pas au cas du collagène V qui peut faire intervenir plusieurs enzymes sur les différentes chaînes qui le composent et à des positions différentes. Ainsi, côté N-terminal, les BTPs et ADAMTS-2

peuvent cliver la chaîne α1(V) en deux positions différentes ce qui, pour les BTPs, conduit à la rétention partielle du N-propeptide (Colige et al., 2005; Imamura et al., 1998). Le produit de clivage qui en résulte confère au collagène V la propriété de pouvoir contrôler la croissance latérale des fibres grâce au N-propeptide résiduel qui projette à la surface des fibres (Fig. 2). Côté C-terminal, la furine a été impliquée dans la maturation de la chaîne α1(V), qui intervient probablement pendant le transit de la molécule dans le Golgi, tandis que les BTPs sont responsables du clivage de la chaîne α2(V).

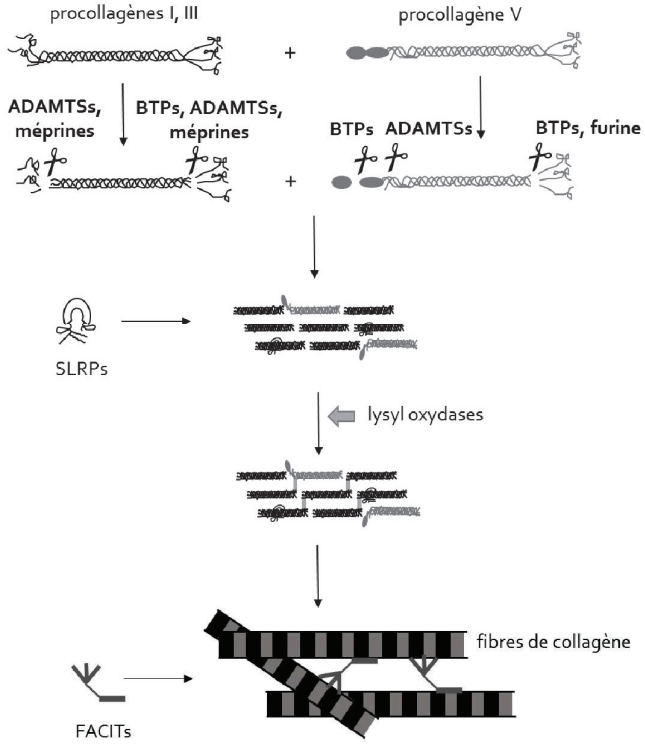

Figure 2 : Etapes extracellulaires de la formation des fibres de collagène. Différentes métalloprotéases clivent les extrémités N- et C-terminales des collagènes I, III et V pour induire la formation des fibres. Les SLRPs et les FACITs s'associent aux fibres en cours de nucléation ou assemblées pour réguler leurs propriétés (diamètre, espacement). Les fibres sont également réticulées sous l'action des lysyl oxydases, ce qui permet de stabiliser les molécules à l'intérieur des fibres.

Enfin, des études récentes ont mis en évidence que les protéases méprines α et β pouvaient aussi maturer les collagènes I et III et, dans ce cas, elles clivent simultanément le C-propeptide et le N-propeptide, permettant la formation de fibres en une seule étape (Broder et al., 2013; Kronenberg et al., 2010). Tous ces processus de maturation protéolytique semblent co-

exister dans la peau car les souris dépourvues d'au moins un type de PNP ou PCP présentent un phénotype marqué au niveau des fibres de collagène du derme : fibres peu nombreuses avec des projections à leur surface (« barbelés ») et incapacité à reconstituer le derme après une lésion dans le cas de l'inactivation des protéases BTPs (Muir et al., 2016; Suzuki et al., 1996); fibres également très anormales (« hiéroglyphes ») conduisant à une peau fragile comme dans le syndrome d'Ehlers-Danlos en absence d'ADAMTS-2 (Bekhouche and Colige, 2015); fibres moins denses et derme moins épais et résistant dans les souris knock-out (KO) méprines (Broder et al., 2013).

Une fois que les propeptides ont été clivés, les fibres peuvent se former de façon spontanée par agrégation. Le processus de fibrillogenèse conduit à une organisation très régulière des monomères de collagène dans la fibre qui sont tous orientés dans la même direction avec un espacement constant entre monomères adjacents (Bella and Hulmes, 2017). Cette organisation est à l'origine de la striation observée en microscopie électronique. Cependant, *in vivo*, la formation des fibres est fortement régulée et nécessite un très grand nombre de partenaires. En premier lieu, il a été montré que la présence de collagène V était indispensable à l'initiation de l'assemblage des fibres de collagène I du derme (Wenstrup et al., 2004). Par ailleurs, la fibrillogenèse dépend de nombreuses molécules non-collagéniques et ne peut se dérouler correctement en leur absence (Kadler et al., 2008). Parmi ces molécules on peut citer les petits protéoglycanes riches en leucine (SLRPs) tels que la décorine, le biglycan ou la fibromoduline qui interagissent avec les molécules de collagène pour réguler le diamètre des fibres et leur espacement (Chen and Birk, 2013) (Fig. 2). D'autres protéines très importantes sont les glycoprotéines SPARC (Rentz et al., 2007), fibronectine (Kadler et al., 2008) et thrombospondines 1 (Kim et al., 2015) et 2 (Calabro et al., 2014) mais aussi les récepteurs intégrines présents à la surface cellulaire (Kadler et al., 2008). Enfin, nous avons déjà mentionné le rôle de connecteur/espaceur joué par les collagènes FACITs (XII, XIV et XVI).

Après la fibrillogenèse (ou plus probablement simultanément avec le processus de fibrillogenèse), les fibres sont stabilisées par la formation de liaisons covalentes entre monomères de collagènes. Cette activité de réticulation des fibres est sous le contrôle des lysyl oxydases LOX et LOXL qui initient leur formation en modifiant des lysines ou hydroxy-lysines

spécifiques présentes dans les petites extrémités non hélicoïdales qui restent après les maturations protéolytiques (N- et C-télopeptides). Ces résidus modifiés et porteurs d'une fonction aldéhyde vont ensuite pouvoir réagir avec d'autres (hydroxy-)lysines présentes dans les triples hélices (Robins, 2007) pour former des ponts covalents entre monomères et apporter la résistance aux tissus.

V – Dégradation des monomères et des fibres de collagène

La dégradation du collagène est nécessaire dans de nombreux contextes physiologiques et pathologiques. En conditions d'homéostasie, elle permet le renouvellement de la matrice extracellulaire dermique. Une demi-vie de 15 ans a pu être calculée pour les collagènes du derme à partir du taux de racémisation des résidus aspartate (Verzijl et al., 2000), ce qui montre que leur vitesse de renouvellement est faible en conditions normales. Le renouvellement augmente cependant de façon significative dans les processus de remodelage tissulaire pour permettre le remplacement d'un tissu lésé ou la migration cellulaire. Ceci a été bien décrit par exemple dans le cas de la cicatrisation (Moali and Hulmes, 2009) ou de la progression tumorale (Friedl and Wolf, 2009).

A cause de la nature très compacte des triples hélices de collagène, seules quelques protéases sont capables de dégrader la forme native des collagènes et possèdent l'activité « collagénase ». Chez l'homme, ces protéases appartiennent principalement à la famille des MMPs (« matrix metalloproteases »), également membres des metzincines comme les PNPs et PCPs impliquées dans la maturation des procollagènes décrites plus haut. Les collagénases humaines sont les MMP-1, -8, -13 et -14 et ont la capacité de cliver la triple hélice des collagènes I et III au niveau d'un site spécifique localisé environ aux trois-quarts de la triple hélice en partant de son extrémité N-terminale (Manka et al., 2012) (Fig. 3). Ce clivage génère deux fragments de taille trois quart (fragment N-terminal) et un quart (fragment C-terminal) qui seront moins stables que la triple hélice entière et donc plus accessibles à la protéolyse dans les zones partiellement dénaturées. D'autres protéases peuvent alors entrer en jeu, telles que les gélatinases MMP-2 et MMP-9 qui ont une préférence pour le collagène dénaturé, et générer des fragments de plus petite taille pour une dégradation complète. Un autre mécanisme d'élimination des fragments issus de l'activité collagénase est

l'endocytose par le récepteur des collagènes uPARAP/Endo180 (Madsen et al., 2007).

Un mécanisme par lequel les collagénases humaines pourraient exercer leur propriété unique de cliver les collagènes fibrillaires a été proposé en 2012 par le groupe d'H. Nagase (Manka et al., 2012). Cette activé implique l'interaction de la MMP avec une séquence longue de 15-18 résidus répartis sur les trois chaînes de la triple hélice. Elle nécessite aussi la présence du domaine non catalytique des MMPs, appelé domaine hémopexine, qui interagit notamment avec un exosite situé à une distance de 10 résidus du site de clivage. Cette interaction permet le « débobinage » local de la triple hélice et l'accès de la protéase à son site de clivage sur une chaîne distincte de la chaîne tirée par le domaine hémopexine.

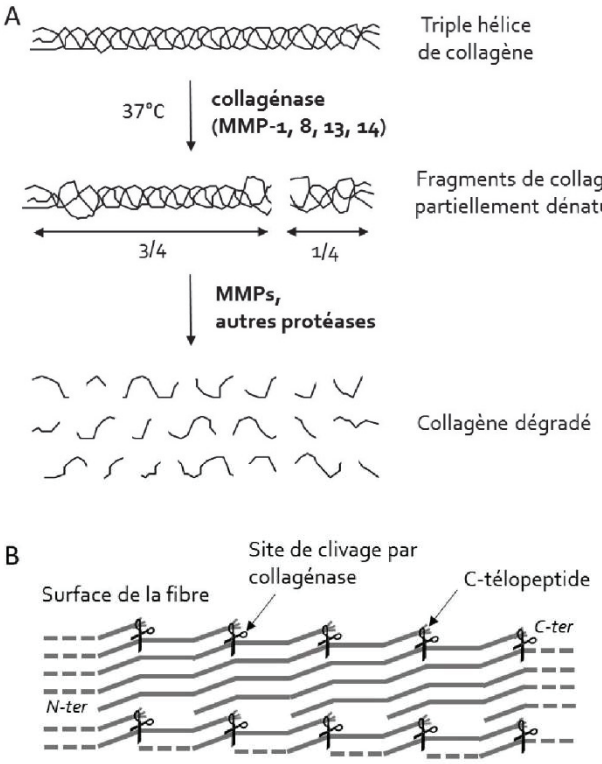

Figure 3 : Rôle des MMPs dans la dégradation des monomères (A) et des fibres de collagène (B). (A) La première étape de la dégradation des collagènes est réalisée par les MMPs possédant une activité collagénase et génère deux fragments qui seront moins stables et plus sensibles à la protéolyse que les molécules initiales. (B) Dans la fibre, les sites de clivage des collagénases sont en plus masqués par les C-télopeptides adjacents ou enfouis à l'intérieur de la fibre. D'après (Bella and Hulmes, 2017).

Malgré sa sophistication, ce mécanisme de clivage des monomères de

collagène ne rend pas compte de la situation rencontrée le plus fréquemment *in vivo* où les collagénases doivent s'attaquer à des sites enfouis au sein de fibres de collagène denses. Même à proximité de la surface des fibres, le site de clivage des collagénases est obstrué par le C-télopeptide du monomère de collagène adjacent. Plusieurs hypothèses ont donc été avancées pour expliquer le clivage à l'intérieur des fibres. La première est que les C-télopeptides doivent être préalablement dégradés mais la protéase responsable de cette activité n'a pas été décrite. La seconde est qu'il existe des zones de « respiration » dans les fibres qui permettent un accès plus aisé au site de clivage (Sarkar et al., 2012), favorisées par le fait que les molécules ne sont pas alignées sur toute leur longueur mais changent d'orientation dans les zones sans interruption (zones claires en microscopie électronique) pour former un angle de 5° par rapport à la direction de la fibre (Fig. 3) (Orgel et al., 2006). Les respirations pourraient également être induites par l'interaction des fibres avec leurs nombreux partenaires, en particulier les intégrines. Notons que le clivage d'un premier site à la surface de la fibre démasque le site de clivage suivant et induit la progression directionnelle de la MMP, guidée par la libération successive des sites de clivage (Sarkar et al., 2012).

La collagénase la plus efficace *in vivo* et la plus importante au niveau du derme semble être la MMP-14. A l'inverse de l'inactivation des BTPs qui conduit à une diminution de l'épaisseur du derme (Muir et al., 2016), l'inactivation de la MMP-14 conduit à son épaississement et à un processus de fibrose caractérisé par l'augmentation de la quantité de collagène I dans le derme des souris KO (Zigrino et al., 2016). Ceci démontre la spécialisation stricte de ces deux catégories de protéases entre biosynthèse et dégradation des fibres de collagènes.

VI – Conclusion

Malgré l'importance des collagènes dans de nombreux tissus et en particulier dans le derme, la recherche sur les collagènes est souvent considérée comme vieillotte et peu attractive. L'abondance de résultats récents sur la structure des fibres, les mécanismes d'assemblage intracellulaire et de sécrétion des trimères de collagène, les nombreux événements de protéolyse qu'ils subissent pour former ou renouveler les fibres ainsi que la diversité des partenaires auxquels ils sont associés *in vivo*

montrent que les questions qui restent à résoudre sont au contraire innombrables et très stimulantes. Elles ont des conséquences importantes en biologie cellulaire et tissulaire et sont également porteuses d'un fort potentiel translationnel, en particulier dans le contexte de la prise en charge des plaies et de la dermo-cosmétique.

Bibliographie

Bekhouche, M., and A. Colige. 2015. The procollagen N-proteinases ADAMTS2, 3 and 14 in pathophysiology. *Matrix Biol.* 44-46:46-53.

Bella, J., and D.J. Hulmes. 2017. Fibrillar Collagens. *Subcell. Biochem.* 82:457-490.

Birk, D.E. 2001. Type V collagen: heterotypic type I/V collagen interactions in the regulation of fibril assembly. *Micron*. 32:223-237.

Bourhis, J.M., N. Mariano, Y. Zhao, K. Harlos, J.Y. Exposito, E.Y. Jones, C. Moali, N. Aghajari, and D.J. Hulmes. 2012. Structural basis of fibrillar collagen trimerization and related genetic disorders. *Nat. Struct. Mol. Biol.* 19:1031-1036.

Broder, C., P. Arnold, S. Vadon-Le Goff, M.A. Konerding, K. Bahr, S. Muller, C.M. Overall, J.S. Bond, T. Koudelka, A. Tholey, D.J. Hulmes, C. Moali, and C. Becker-Pauly. 2013. Metalloproteases meprin alpha and meprin beta are C- and N-procollagen proteinases important for collagen assembly and tensile strength. *Proc. Natl. Acad. Sci. U.S.A.* 110:14219-14224.

Calabro, N.E., N.J. Kristofik, and T.R. Kyriakides. 2014. Thrombospondin-2 and extracellular matrix assembly. *Biochim. Biophys. Acta* 1840:2396-2402.

Cescon, M., F. Gattazzo, P. Chen, and P. Bonaldo. 2015. Collagen VI at a glance. *J. Cell. Sci.* 128:3525-3531.

Chen, S., and D.E. Birk. 2013. The regulatory roles of small leucine-rich proteoglycans in extracellular matrix assembly. *FEBS J.* 280:2120-2137.

Chiquet, M., D.E. Birk, C.G. Bonnemann, and M. Koch. 2014. Collagen XII: Protecting bone and muscle integrity by organizing collagen fibrils. *Int. J. Biochem. Cell Biol.* 53:51-54.

Chung, H.J., and J. Uitto. 2010. Type VII collagen: the anchoring fibril protein at fault in dystrophic epidermolysis bullosa. *Dermatol. Clin.* 28:93-105.

Colige, A., F. Ruggiero, I. Vandenberghe, J. Dubail, F. Kesteloot, J. Van Beeumen, A. Beschin, L. Brys, C.M. Lapiere, and B. Nusgens. 2005. Domains and maturation processes that regulate the activity of ADAMTS-2, a metalloproteinase cleaving the aminopropeptide of fibrillar procollagens types

I-III and V. *J. Biol. Chem.* 280:34397-34408.

Friedl, P., and K. Wolf. 2009. Proteolytic interstitial cell migration: a five-step process. *Cancer Metastasis Rev.* . 28:129-135.

Gorur, A., L. Yuan, S.J. Kenny, S. Baba, K. Xu, and R. Schekman. 2017. COPII-coated membranes function as transport carriers of intracellular procollagen I. *J. Cell. Biol.* 216:1745-1759.

Grassel, S., and R.J. Bauer. 2013. Collagen XVI in health and disease. *Matrix Biol.* 32:64-73.

Henkel, W., and R.W. Glanville. 1982. Covalent crosslinking between molecules of type I and type III collagen. The involvement of the N-terminal, nonhelical regions of the alpha 1 (I) and alpha 1 (III) chains in the formation of intermolecular crosslinks. *Eur. J. Biochem.* 122:205-213.

Imamura, Y., B.M. Steiglitz, and D.S. Greenspan. 1998. Bone morphogenetic protein-1 processes the NH2-terminal propeptide, and a furin-like proprotein convertase processes the COOH-terminal propeptide of pro-alpha1(V) collagen. *J. Biol. Chem.* 273:27511-27517.

Ito, S., and K. Nagata. 2017. Biology of Hsp47 (Serpin H1), a collagen-specific molecular chaperone. *Semin. Cell Dev. Biol.* 62:142-151.

Kadler, K.E., C. Baldock, J. Bella, and R.P. Boot-Handford. 2007. Collagens at a glance. *J. Cell. Sci.* 120:1955-1958.

Kadler, K.E., A. Hill, and E.G. Canty-Laird. 2008. Collagen fibrillogenesis: fibronectin, integrins, and minor collagens as organizers and nucleators. *Curr. Opin. Cell Biol.* 20:495-501.

Kim, D.J., E.D. Christofidou, D.R. Keene, M. Hassan Milde, and J.C. Adams. 2015. Intermolecular interactions of thrombospondins drive their accumulation in extracellular matrix. *Mol. Biol. Cell.* 26:2640-2654.

Kronenberg, D., B.C. Bruns, C. Moali, S. Vadon-Le Goff, E.E. Sterchi, H. Traupe, M. Bohm, D.J. Hulmes, W. Stocker, and C. Becker-Pauly. 2010. Processing of procollagen III by meprins: new players in extracellular matrix assembly? *J. Invest. Dermatol.* 130:2727-2735.

Lees, J.F., M. Tasab, and N.J. Bulleid. 1997. Identification of the molecular recognition sequence which determines the type-specific assembly of procollagen. *EMBO J.* 16:908-916.

Madsen, D.H., L.H. Engelholm, S. Ingvarsen, T. Hillig, R.A. Wagenaar-Miller, L. Kjoller, H. Gardsvoll, G. Hoyer-Hansen, K. Holmbeck, T.H. Bugge, and N. Behrendt. 2007. Extracellular collagenases and the endocytic receptor, urokinase plasminogen activator receptor-associated protein/Endo180, cooperate in fibroblast-mediated collagen degradation. *J. Biol. Chem.* 282:27037-27045.

Malfait, F., and A. De Paepe. 2014. The Ehlers-Danlos syndrome. *Adv. Exp. Med. Biol.* 802:129-143.

Manka, S.W., F. Carafoli, R. Visse, D. Bihan, N. Raynal, R.W. Farndale, G. Murphy, J.J. Enghild, E. Hohenester, and H. Nagase. 2012. Structural insights into triple-helical collagen cleavage by matrix metalloproteinase 1. *Proc. Natl. Acad. Sci. U.S.A.* 109:12461-12466.

Mari, W., S.G. Alsabri, N. Tabal, S. Younes, A. Sherif, and R. Simman. 2015. Novel Insights on Understanding of Keloid Scar: Article Review. *J. Am. Coll. Clin. Wound Spec.* 7:1-7.

Menke, N.B., K.R. Ward, T.M. Witten, D.G. Bonchev, and R.F. Diegelmann. 2007. Impaired wound healing. *Clin. Dermatol.* 25:19-25.

Moali, C., and D.J. Hulmes. 2009. Extracellular and cell surface proteases in wound healing: new players are still emerging. *Eur. J. Dermatol.* 19:552-564.

Muir, A.M., D. Massoudi, N. Nguyen, D.R. Keene, S.J. Lee, D.E. Birk, J.M. Davidson, M.P. Marinkovich, and D.S. Greenspan. 2016. BMP1-like proteinases are essential to the structure and wound healing of skin. *Matrix Biol.* 56:114-131.

Orgel, J.P., T.C. Irving, A. Miller, and T.J. Wess. 2006. Microfibrillar structure of type I collagen in situ. *Proc. Natl. Acad. Sci. U S A* 103:9001-9005.

Rentz, T.J., F. Poobalarahi, P. Bornstein, E.H. Sage, and A.D. Bradshaw. 2007. SPARC regulates processing of procollagen I and collagen fibrillogenesis in dermal fibroblasts. *J. Biol. Chem.* 282:22062-22071.

Ricard-Blum, S. 2011. The collagen family. *Cold Spring Harb. Perspect. Biol.* 3:a004978.

Robins, S.P. 2007. Biochemistry and functional significance of collagen cross-linking. *Biochem. Soc. Trans.* 35:849-852.

Ruggiero, F., M. Roulet, and C. Bonod-Bidaud. 2005. [Dermis collagens: beyond their structural properties]. *J. Soc. Biol.* 199:301-311.

Sarkar, S.K., B. Marmer, G. Goldberg, and K.C. Neuman. 2012. Single-molecule tracking of collagenase on native type I collagen fibrils reveals degradation mechanism. *Curr. Biol.* 22:1047-1056.

Sharma, U., L. Carrique, S. Vadon-Le Goff, N. Mariano, R.N. Georges, F. Delolme, P. Koivunen, J. Myllyharju, C. Moali, N. Aghajari, and D.J. Hulmes. 2017. Structural basis of homo- and heterotrimerization of collagen I. *Nat. Commun.* 8:14671.

Suzuki, N., P.A. Labosky, Y. Furuta, L. Hargett, R. Dunn, A.B. Fogo, K. Takahara, D.M. Peters, D.S. Greenspan, and B.L. Hogan. 1996. Failure of ventral body wall closure in mouse embryos lacking a procollagen C-proteinase encoded by Bmp1, a mammalian gene related to Drosophila tolloid. *Development.*

122:3587-3595.

Vadon-Le Goff, S., D.J. Hulmes, and C. Moali. 2015. BMP-1/tolloid-like proteinases synchronize matrix assembly with growth factor activation to promote morphogenesis and tissue remodeling. *Matrix Biol.* 44-46C:14-23.

Verzijl, N., J. DeGroot, S.R. Thorpe, R.A. Bank, J.N. Shaw, T.J. Lyons, J.W. Bijlsma, F.P. Lafeber, J.W. Baynes, and J.M. TeKoppele. 2000. Effect of collagen turnover on the accumulation of advanced glycation end products. *J. Biol. Chem.* 275:39027-39031.

Wells, A., A. Nuschke, and C.C. Yates. 2016. Skin tissue repair: Matrix microenvironmental influences. *Matrix Biol.* 49:25-36.

Wenstrup, R.J., J.B. Florer, E.W. Brunskill, S.M. Bell, I. Chervoneva, and D.E. Birk. 2004. Type V collagen controls the initiation of collagen fibril assembly. *J. Biol. Chem.* 279:53331-53337.

Zhu, Z., J. Ding, and E.E. Tredget. 2016. The molecular basis of hypertrophic scars. *Burns Trauma*. 4:2.

Zigrino, P., J. Brinckmann, A. Niehoff, Y. Lu, N. Giebeler, B. Eckes, K.E. Kadler, and C. Mauch. 2016. Fibroblast-Derived MMP-14 Regulates Collagen Homeostasis in Adult Skin. *J. Invest. Dermatol.* 136:1575-1583.

Oral communications

Evaluation of PCPE-1 and PCPE-2 as new therapeutic targets in skin wound healing

Summer school of the European Tissue Repair Society (London, United Kingdom, June 29-30th 2016)

Divergent functions of Procollagen C-Proteinase Enhancers, PCPE-1 and PCPE-2 in skin wound healing

21st Scientific Day of the EDISS doctoral school (Lyon, France, October 12th 2016)

Fonctions divergentes des Procollagen C-Proteinase Enhancers (PCPE) -1 et -2 dans la cicatrisation cutanée

Congrès Annuel de Recherche Dermatologique (Paris, France, December 6-7th 2016)

Procollagen C-Proteinase Enhancers, PCPE-1 and PCPE-2: divergent functions during skin wound healing?

David's Day (Lyon, France, November 9th 2017)

Procollagen C-Proteinase Enhancers, PCPE-1 and PCPE-2: divergent functions during skin wound healing?

ScarCon - European Tissue Repair Society congress (Amsterdam, Netherlands, May 31st-June 2th 2018)

Posters

Are Procollagen C-Proteinase Enhancers -1 and -2 playing identical roles in skin wound healing? Agnès Tessier, Sandrine Vadon-Le Goff, Naïma El Kholti, Leena Bruckner-Tuderman, Alexander Nyström, Catherine Moali.

Joint Meeting of the German (DGMB) and the French (SFBMec) Matrix Biology Societies (Freiburg, Germany, March 3-5th 2016)

Regulation of tumor-promoting ECM assembly in dystrophic epidermolysis bullosa. Agnès Tessier, Daniel Kruppa, Karina Zeyer, Florian Peters, Leena Bruckner-Tuderman, Christophe Becker-Pauly, Catherine Moali, Alexander Nyström.

3rd International Symposium – Control of cell motility in development and cancer (Freiburg, Germany, March 22-24th 2017)

Are Procollagen C-Proteinase Enhancers -1 and -2 playing similar roles in skin wound healing? Agnès Tessier, Sandrine Vadon-Le Goff, Leena Bruckner-Tuderman, Alexander Nyström, Catherine Moali.

Gordon Research Seminar and Conference – The multifaceted nature of collagens in development, disease and tissue repair (New London, USA, July 15-21st 2017)

Interaction of complement defence collagens C1q and MBL with BMP-1/tolloid-like proteinases. Monique Lacroix, Agnès Tessier, Chantal Dumestre-Pérard, Sandrine Vadon-Le Goff, Evelyne Gout, Leena Bruckner-Tuderman, Alexander Nyström, Sylvie Ricard-Blum, Catherine Moali, David J.S. Hulmes, Nicole M. Thielens.

16th European Meeting of Complement in Human Disease (Copenhagen, Denmark, September 8-12th 2017)

Joint Meeting of the German (DGMB) and the French (SFBMec) Matrix Biology Societies
(Freiburg, Germany, March 3-5th 2016)

Are Procollagen C-Proteinase Enhancers -1 and -2 playing similar roles in skin wound healing ?

Agnès Tessier[1,2], Sandrine Vadon Le Goff[1], Naïma El Kholti[1], Leena Bruckner-Tuderman[2], Alexander Nyström[2], Catherine Moali[1]

[1]Laboratoire de Biologie Tissulaire et Ingénierie Thérapeutique, UMR 5305, CNRS – University of Lyon, Lyon, France
[2]Department of Dermatology, Medical Center – University of Freiburg, Freiburg, Germany

Introduction

The imbalance between collagen assembly and degradation during skin wound healing is a major factor contributing to wound healing pathologies (e.g. chronic wounds, keloids, hypertrophic scars) affecting millions of individuals around the world. This highlights the crucial role played by collagen fibrillogenesis during wound healing to restore the structural and mechanical integrity of the skin. Fibrillar collagen precursors are synthesized by fibroblasts and processed in the extracellular space by zinc-dependent proteases, belonging to the BMP-1/Tolloid-like (BTP), meprin and ADAMTS families, to form collagen fibrils. The BTP-mediated proteolytic maturation of fibrillar procollagens is stimulated 10-fold by Procollagen C-Proteinase Enhancer-1 (PCPE-1), a glycoprotein known to be involved in several tissue repair processes but which has never been studied in the context of skin wound healing. Another PCPE isoform (PCPE-2) has also been described more recently and seems to enhance procollagen maturation *in vitro* and to be required for efficient collagen processing in a mouse model of cardiac hypertrophy. The main goal of our study is to analyze the possible redundant and specific roles of the two PCPE isoforms in skin wound healing.

Methods

To understand the roles of PCPE-1 and -2 in skin wound healing, we analyzed the expression and distribution of PCPEs and BTPs in primary keratinocytes and dermal fibroblasts and in wounded skin by qRT-PCR, western blotting and immunofluorescence. In parallel, we developed an expression system to produce recombinant PCPE-2 and evaluate its role on BMP-1 mediated-procollagen cleavage *in vitro*.

Results

BMP-1/mTLD expression is increased during wound healing.

BTPs (mainly the BMP-1 and mTLD isoforms) are expressed by primary keratinocytes and dermal fibroblasts. In mouse skin, the mRNA level of BMP-1 and mTLD is increased 7 days after wounding, suggesting that these two proteases play a role during the proliferative phase of the wound healing process.

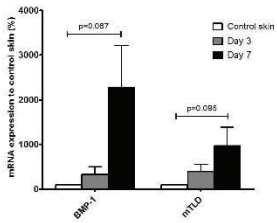

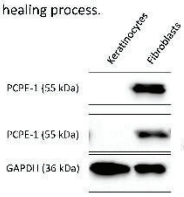

PCPE-1 is expressed by fibroblasts in the skin, but not by keratinocytes. PCPE-2 is expressed by none of these cell types (data not shown).

As observed for BMP-1/mTLD, PCPE-1 expression increases during the wound healing process. qRT-PCR, western blotting and immunofluorescence results show that the mRNA and protein levels of PCPE-1 follow the expression pattern of BMP-1 and mTLD in mouse skin: PCPE-1 is overexpressed 7 days after wounding, during the proliferative phase of wound healing.

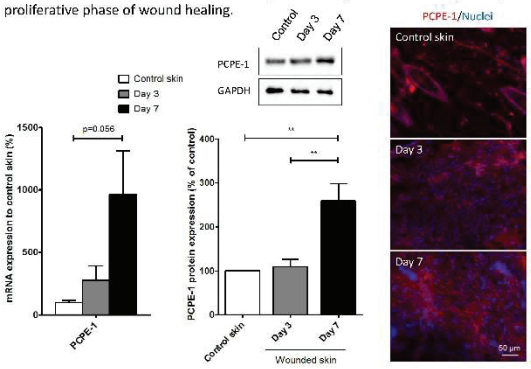

PCPE-2 is not expressed in intact skin, but is highly expressed during the wound healing process. In mouse skin, PCPE-2 is mainly expressed during the early phases of the healing process (day 3), suggesting a potential role during the inflammatory phase.

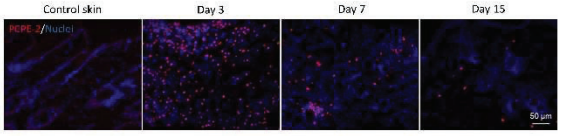

PCPE-2 is expressed by neutrophils in the wounded skin only. During wound healing, PCPE-2 is expressed by inflammatory cells characterized by the expression of the Ly6G marker, i.e neutrophils.

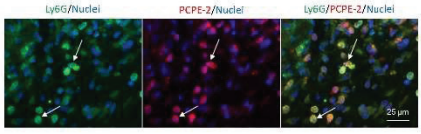

The PCPE-2 protein is not an efficient enhancer of BMP-1 mediated-type III procollagen processing *in vitro*.

Cleavage of CPIII-Long (short *version* of type III procollagen) by BMP-1 in the presence of purified PCPE-1 or PCPE-2 proteins.

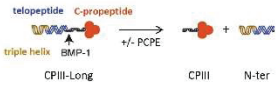

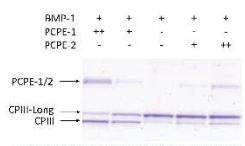

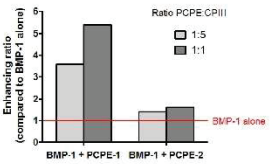

PCPE-1 protein is able to enhance the proteolytic cleavage of CPIII-Long by BMP-1 by up to 5-fold whereas PCPE-2 only has a weak effect on CPIII-Long processing (1.5-fold enhancement) *in vitro*.

Discussion

This work suggests that PCPE-1 and -2 both play roles during skin wound healing, but have distinct functions in this process. Like BMP-1 and mTLD, PCPE-1 expression is increased in mouse skin during the proliferative phase of wound healing, suggesting that all three partners collaborate to efficiently produce collagen fibrils during skin wound healing. In contrast, the specific expression pattern of PCPE-2 and its weak BMP-1-enhancing effect suggests that PCPE-2 could play a distinct role which remains to be elucidated. Interestingly, the possibility for alternative functions of PCPE-2 is also supported by reports from the literature showing that PCPE-2 is involved in HDL cholesterol transport. Thus, our next objective will be to better understand the function of PCPE-2 expressed in neutrophils during skin wound healing.

3rd International Symposium – Control of cell mobility in development and cancer
(Freiburg, Germany, March 22-24th 2017)

Regulation of tumor-promoting ECM assembly in dystrophic epidermolysis bullosa

Agnès Tessier[1,2], Daniel Kruppa[1], Karina Zeyer[1], Florian Peters[3], Leena Bruckner-Tuderman[1], Christoph Becker-Pauly[3], Catherine Moali[2], Alexander Nyström[1]

[1]Department of Dermatology, University Freiburg Medical Center, Freiburg, Germany
[2]University of Lyon-CNRS
[3]University of Kiel

Introduction

In dystrophic epidermolysis bullosa (DEB), patients show a great predisposition to develop cutaneous squamous cell carcinomas (cSCCs) due to tumor-promoting changes in the composition of their extracellular matrix (ECM). These changes could be due to altered activity of ECM maturing proteases like astacin like proteases (ALPs). ALPs are a group of metalloproteases that comprise BMP-1/tolloid-like proteases (BTPs) and meprins. Of these two groups, BTPs (BMP-1, mTLD, mTLL-1 and mTLL-2) are already well known as collagen maturing proteases that are also able to release and alter the bioavailability of TGF-β. The functions of meprins (meprin α and β) however remain more elusive. In the past few years that catalogue of known meprin substrates has been greatly expanded. Today it is known, that they are able to mature fibrillar collagens and cleave matrix proteins like laminins, nidogen-1 and fibronectin as well as enhance the attraction of neutrophils and leucocytes under fibrotic conditions.

In this poster we show, that the injury- and inflammation-induced changes in the skin of DEB patients alter the expression of ALPs in unaffected tissue as well as in healing wounds.

DEB mouse-model

Viable hypomorphic mouse-model:
- approx. 10% of the normal collagen VII is expressed
- development of mitten deformities and fibrosis on unprotected skin areas like the forepaws.

6-week-old mice

G: comparison of wild-type and DEB mice.

Human DEB

DEB resembled in mice

A-C: human mitten deformities over time in an 2 to 7 year old child.
D-F: DEB mouse paws, resembling the human disease progression.

Frisch A, Loeckermann S, Kern JS, et al. J Clin Invest. 2008;118(3):1059-1070.

Fibrosis

A-B: detachment of epidermis and dermis in the skin of a DEB mouse

C-F: significantly increased TGF-β and tenascin-C abundances, indicating a state of fibrosis in the injured skin areas of the DEB mouse

G-H: increased stiffness of the dermis due to bigger collagen fiber diameters

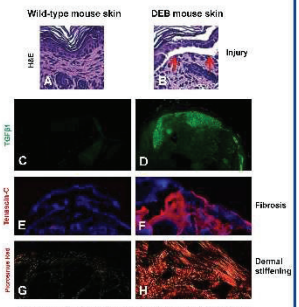

Picrosirius red staining, highlights the thickness of collagen fibres within the tissue. Green indicates thin fibres and red indicates thick ones

Nyström A, Thriene K, Mittapalli V, et al. EMBO Mol Med. 2015;7(9):1211-1228.

ALP expression in human cells

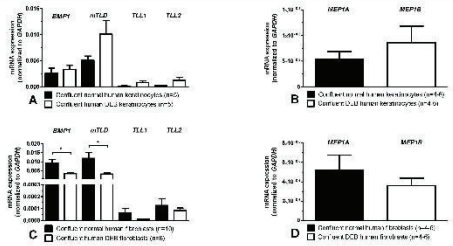

A: DEB keratinocytes show a altered BTP expression compared to normal human keratinocytes.
C: DEB fibroblasts show a lower abundance of all BTPs in comparison to normal human fibroblasts.

B+D: meprin mRNA expressions are not significantly altered in DEB keratinocytes and fibroblasts compared to their wild-type counter parts.

BMP-1 expression during wound healing

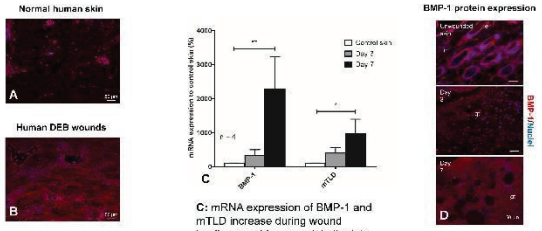

A-B: BMP-1 protein abundance in the dermis of human DEB wound is highly elevated compared to normal human skin

C: mRNA expression of BMP-1 and mTLD increase during wound healing, reaching a peak in the late proliferative phase at day seven after injury.

D: protein abundance of BMP-1 in the granulation tissue increase during the wound healing compared to unwounded skin

BTP expression in tissue

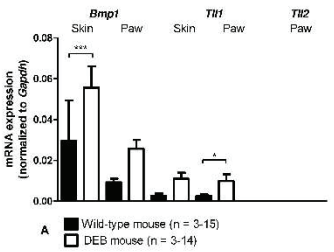

A: BTP mRNA expression in back-skin and paws of normal and DEB mice. All BTPs show a higher expression level in the DEB mouse model than in the wild-type mice, independent of sample localization

Conclusion

These results indicate, that inflammatory cells and/or wounding signals in the skin of DEB patients significantly contribute to the regulation of astacin-like proteases expression. Resulting in an altered tumor growth promoting ECM assembly. Due to this, invasion of cSCCs gets more frequently, resulting in a drastically lower survival rate for DEB patients, with tumors compared to patients without tumors.

Meprin expression in tissue

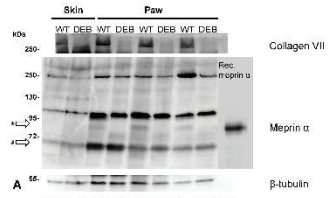

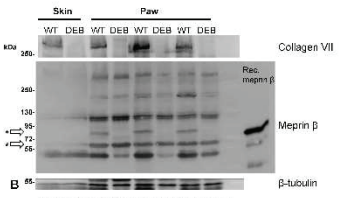

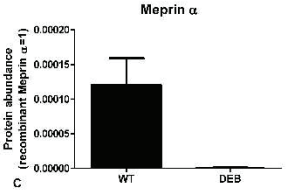

A: Meprin α abundance in skin and paws of wild-type and DEB mice. Lower abundance of full-length meprin α (~84kDa) can be seen in paws of DEB mice compared to wild-type mice. (Forepaws and skin from age-matched wild-type and fibrotic DEB mice.)
C: Quantification of bands with a molecular weight of ~84kDa, showing an strongly altered amount of full-length protein.

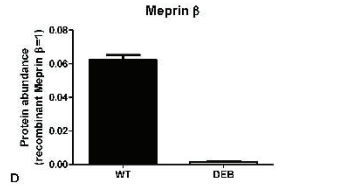

B: Meprin β abundance in skin and paws of wild-type and DEB mice. Lower abundance of full-length meprin β (~80kDa) can be seen in paws of DEB mice compared to wild-type mice. (Forepaws and skin from age-matched wild-type and fibrotic DEB mice.)
D: Quantification of bands wit ha molecular weight ~80kDa, showing an strongly altered amount of full-length protein.

Gordon Research Seminar and Conference – The multifaceted nature of collagens in development, disease and tissue repair (New London, USA, July 15-21st 2017)

Are Procollagen C-Proteinase Enhancers -1 and -2 (PCPEs) playing similar roles in skin wound healing ?

Agnès Tessier[1,2], Sandrine Vadon-Le Goff[1], Leena Bruckner-Tuderman[2], Alexander Nyström[2], Catherine Moali[1]

[1]Laboratoire de Biologie Tissulaire et Ingénierie Thérapeutique, UMR 5305, CNRS – University of Lyon, Lyon, France
[2]Department of Dermatology, Medical Center – University of Freiburg, Freiburg, Germany

Introduction

The imbalance between collagen assembly and degradation during skin wound healing is a major factor contributing to wound healing pathologies affecting millions of individuals around the world. This highlights the crucial role played by collagen fibrillogenesis during wound healing to restore the structural and mechanical integrity of the skin. Fibrillar collagen precursors are synthesized by fibroblasts and processed in the extracellular space by zinc-dependent proteases to form collagen fibrils. The BMP-1/Tolloid-like Proteases (BTPs) including BMP-1, mTLD, mTLL-1 and -2, are the main proteases responsible for the C-terminal processing of fibrillar procollagens. This proteolytic activity is stimulated up to 15-fold by Procollagen C-Proteinase Enhancer-1 (PCPE-1), a glycoprotein known to be involved in several tissue repair processes but which has never been studied in the context of skin wound healing. Another PCPE isoform (PCPE-2) has also been described more recently and seems to enhance procollagen maturation *in vitro* and to be required for efficient collagen processing in a mouse model of cardiac hypertrophy. The main goal of our study is to analyze the possible redundant and specific roles of the two PCPE isoforms in skin wound healing.

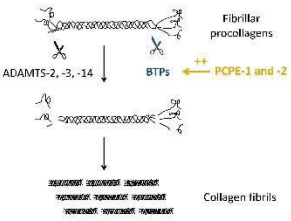

Results

I PCPE-1 and -2 have different expression patterns during wound healing.

PCPE-1 is induced during the proliferation phase of wound healing in mouse skin, together with BMP-1 (qPCR, Western blotting and immunofluorescence; n=6).

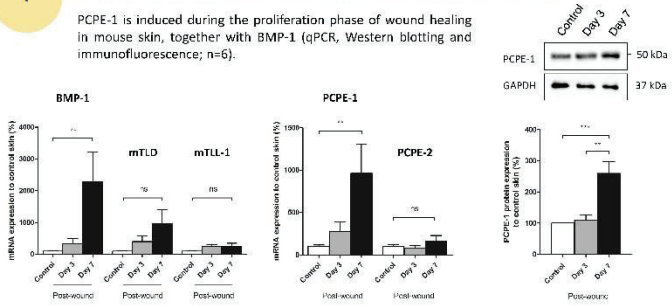

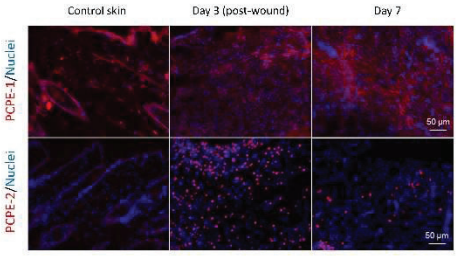

Though no significant change is observed for PCPE-2 at the RNA level, the PCPE-2 protein is transiently induced during the inflammatory phase of murine wound healing (immunofluorescence; n=6).

II PCPE-1 and -2 are differentially expressed in human cells.

While PCPE-1 is expressed by dermal fibroblasts only, PCPE-2 is found in fibroblasts (lower levels than PCPE-1), keratinocytes, monocytes (U937 and THP-1 human cell lines) and macrophages (PMA-treated monocytes).

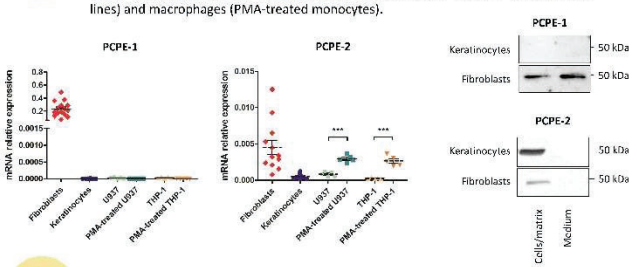

PCPE-2 is expressed by immune cells.

PCPE-2 is expressed by Ly6G+ cells, i.e. neutrophils in mouse skin during wound healing and by CD68+ cells, i.e. macrophages in human keloids.

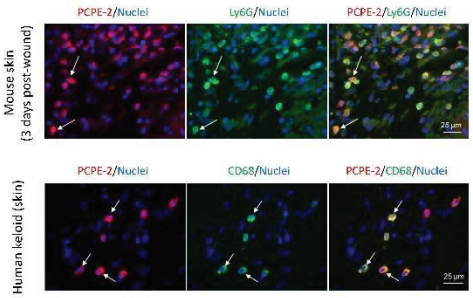

III PCPE-1 and PCPE-2 interact with procollagen substrates but are not equally efficient to enhance their maturation.

Enhancement of CPIII-long processing by up to 15-fold for PCPE-1; 1.5-fold at best for PCPE-2.

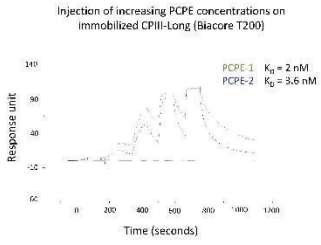

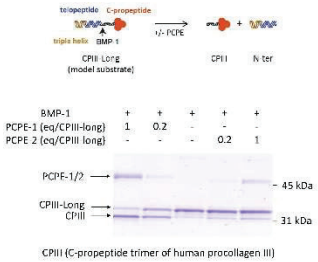

CPIII (C-propeptide trimer of human procollagen III)

Discussion

This work suggests that PCPE-1 and -2 both play roles during skin wound healing, but have distinct functions in this process. PCPE-1 and BMP-1 are increased in mouse skin during the proliferative phase of wound healing, suggesting that the two partners collaborate to efficiently produce collagen fibrils. In contrast, the wide expression pattern of PCPE-2 by numerous cell types found in the skin (especially immune cells during wound healing) and its weak BMP-1-enhancing effect suggest that PCPE-2 could play a distinct role which remains to be elucidated.

** p-value (p) < 0.05, ** p < 0.01, *** p < 0.001*

16th European Meeting of Complement in Human Disease
(Copenhagen, Denmark, September 8-12th 2017)

Interaction of complement defence collagens C1q and MBL with BMP-1/tolloid-like proteinases

Monique Lacroix[1], Agnès Tessier[2], Chantal Dumestre-Pérard[3], Sandrine Vadon-Le Goff[2], Evelyne Gout[1], Leena Bruckner-Tuderman[4], Alexander Nyström[4], Sylvie Ricard-Blum[5], Catherine Moali[2], David J.S. Hulmes[2], Nicole M. Thielens[1*]

[1]Institut de Biologie Structurale (IBS), Université Grenoble Alpes, CEA, CNRS, France; [2]Tissue Biology and Therapeutic Engineering Unit, UMR 5305 CNRS-University of Lyon 1, France; [3]Laboratoire d'Immunologie, Pôle de Biologie, CHU Grenoble Alpes, France; [4]Department of Dermatology, Medical Center, University of Freiburg, Germany; [5]Institute of Molecular and Supramolecular Chemistry and Biochemistry, UMR 5246 CNRS-University of Lyon 1, France

Background and objectives

Bone morphogenetic protein-1 (BMP-1)/tolloid-like proteinases (BTPs) are metalloproteinases with major roles in extracellular matrix assembly and growth factor signalling. They share many structural similarities with complement proteinases C1r/C1s/MASPs, despite their different functions. Indeed, their non-catalytic domains include both CUB (complement C1r/C1s, Uegf, Bmp1) and EGF (epidermal growth factor) domains.

C1r/C1s/MASPs and BPTs: modular proteases with CUB-EGF-CUB motifs

Furthermore, the **tridomain CUB-EGF-CUB motif** which is exclusively found in all these proteinases mediates interaction with collagen-like sequences. Thus, the association of C1r-C1s-MASPs with the defence collagens triggers complement activation while similar interactions likely control C-terminal processing of collagen precursors by BTPs.

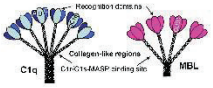

Assembly of the complement initiating complexes

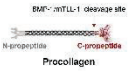

C-terminal processing of procollagen by BTPs
(Sharma et al. (2017) Nature Comm 8:14671)

Our aim was to investigate the potential interactions between proteins from both systems, namely the defence collagens C1q and MBL and the BTPs BMP-1 and mTLL-1.

The interactions between C1q or MBL and BMP-1 or mTLL-1 purified human proteins were analyzed by surface plasmon resonance spectroscopy. The possibility of an interaction of C1q with BMP-1 in pathophysiological conditions was further analyzed by immunofluorescence in human skin biopsies from patients following melanoma exclusion and with recessive dystrophic epidermolysis bullosa (RDEB).

Results

Soluble C1q and MBL interact strongly with immobilized BMP-1 and mTLL-1

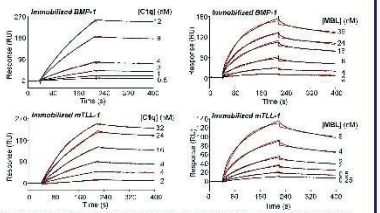

Binding of purified serum-derived human C1q or recombinant human MBL at the indicated concentrations was measured over immobilized BMP-1 (850-2300 RU) or mTLL-1 (720-1,900 RU) in 50 mM triethanolamine-HCl, 145 mM NaCl, 2 mM $CaCl_2$, 0.005% surfactant P20, pH 7.4 at a flow rate of 20 µl/min. Fits are shown as red lines and were obtained by global fitting of the data using a 1:1 Langmuir binding model (A + B ↔ AB, Evaluation 3.1). No binding was observed in the absence of EDTA in the running buffer.

Kinetic constants

Immobilized ligand	Soluble analyte	k_a (M^{-1} s^{-1})	k_d (s^{-1})	K_D (M)	n
BMP-1	C1q	4.6 – 9.6 x 10^4	2.3 – 3.6 x 10^{-4}	5.2 – 2.1 x 10^{-9}	4
BMP-1	MBL	0.8 – 1.4 x 10^5	9.6 – 1.2 x 10^{-4}	1.6 – 0.8 x 10^{-9}	3
mTLL-1	C1q	2.9 – 3.4 x 10^4	2.9 – 3.9 x 10^{-4}	1.1 – 0.4 x 10^{-8}	3
mTLL-1	MBL	1.4 – 3.3 x 10^5	8.6 – 2.9 x 10^{-4}	6.0 – 1.8 x 10^{-9}	4
MASP-2	MBL	2.8 – 3.4 x 10^4	4.7 – 1.5 x 10^{-4}	1.7 – 0.3 x 10^{-8}	2

The association (k_a) and dissociation (k_d) rate constants were determined by global fitting of the binding curves shown above. The apparent equilibrium dissociation constants K_D were determined from the k_d / k_a ratios.
*Number of separate experiments on different sensorchips. Values are expressed as mean ± SE.

Soluble BMP-1 and mTLL-1 interact poorly with immobilized C1q and MBL

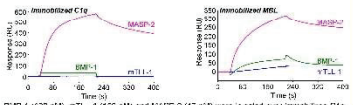

RMP-1 (133 nM), mTLL-1 (150 nM) and MASP-2 (47 nM) were injected over immobilized C1q (18,600 RU) or MBL (10,600 RU) in 50 mM triethanolamine-HCl, 145 mM NaCl, 2 mM $CaCl_2$, 0.005% surfactant P20, pH 7.4.

Soluble complement proteases compete for binding of C1q and MBL to immobilized mTLL-1

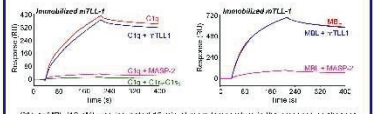

C1q or MBL (10 nM) was incubated 15 min at room temperature in the presence or absence of mTLL-1 (60 nM), the C1s-C1r-C1s tetramer (10 nM) or MASP-2 (60 nM) before injection over immobilized mTLL-1 (3,400 RU) in 50 mM triethanolamine-HCl, 145 mM NaCl, 2 mM $CaCl_2$, 0.005% surfactant P20, pH 7.4.

The BMP-1 and mTLL-1 binding site is located in the collagen-like regions of C1q

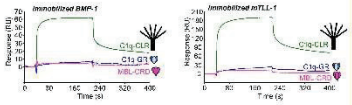

The collagen-like regions of C1q (CLR), the globular regions of C1q (GR) and the trimeric carbohydrate recognition domain of MBL (CRD) were injected at a concentration of 500 nM over immobilized BMP-1 (2 300 RU) and mTLL-1 (1,120 RU) in 50 mM triethanolamine-HCl 145 mM NaCl, 2 mM $CaCl_2$, 0.005% surfactant P20, pH 7.4.

Lysine 55 of the MASP binding site of MBL is essential for the interaction with BMP-1 and mTLL-1

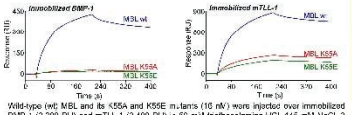

Wild-type (wt) MBL and its K55A and K55E mutants (16 nM) were injected over immobilized BMP-1 (2,300 RU) and mTLL-1 (3,400 RU) in 50 mM triethanolamine-HCl, 145 mM NaCl, 2 mM $CaCl_2$, 0.005% surfactant P20, pH 7.4.

Soluble BMP-1 and mTLL-1 do not inhibit complement activation

Activation of the lectin pathway of human serum complement

MBL-deficient (ΔMBL) serum reconstituted with 2 µg/ml MBL, pre-incubated or not with BMP-1 or mTLL-1 at the indicated molar ratios (MR), was added to mannan-coated wells. The resulting MASP-2 cleaving activity was measured by a C4b deposition assay.

Activation of the reconstituted C1 complex of the classical pathway

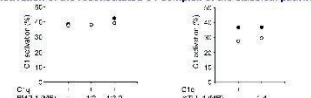

Complexes (0.25 µM) reconstituted from C1q, pre-incubated or not with BMP-1 or mTLL-1 at the indicated molar ratios (MR), and proenzyme C1s-C1r-C1s were incubated for 30 min at 30 °C. C1 activation was measured by SDS-PAGE and Western blot analysis using an anti-C1s antibody.

C1q and MBL are neither substrates of BMP-1 nor inhibitors of BMP-1 cleavage of a procollagen III-like substrate

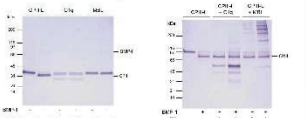

A BMP-1 substrate derived from human procollagen III (CPIII-L) or C1q and MBL (400 nM) were incubated with BMP-1 (20 nM) for 2 h, then analyzed by SDS-PAGE (reducing conditions). CPIII released C-propeptide. Bands for C1q and MBL are unchanged after incubation with BMP-1.

BMP-1 cleavage of CPIII-L in the absence or presence of C1q or MBL at the indicated molar ratios (MR) was analyzed by SDS-PAGE (non-reducing conditions). The amount of released C-propeptide (CPIII) is not affected by the presence of C1q or MBL.

C1q colocalizes with BMP-1 in skin biopsies from patients following melanoma excision or with recessive dystrophic epidermolysis bullosa (RDEB)

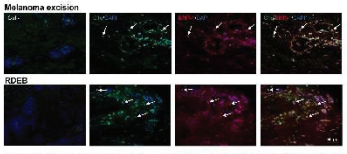

Paraffin-embedded human skin sections (prepared by Dr Dimitra Kritsi, University of Freiburg) were stained with antibodies to C1q (green) and BMP-1 (red). Nuclei were counterstained with DAPI (blue). Images were acquired with a 40X objective (scale bar = 50 µm). Ctrl: tissue sections stained without primary antibody (secondary antibodies only) as negative controls. Arrows indicate regions positive for C1q and BMP-1 that are co-localized.

Conclusions

- C1q and MBL bound to immobilized BMP-1 and mTLL-1 with affinities in the nM range. Soluble BTPs did not interact significantly with immobilized C1q and MBL.
- These interactions involved the collagen-like regions of the defence collagens and were abolished by pre-incubation of C1q or MBL with their cognate complement proteases.
- Soluble BMP-1 and mTLL-1 did not inhibit activation of the classical and lectin complement pathways and the defence collagens were neither substrates nor inhibitors of BMP-1 cleavage of a procollagen III-like substrate, suggesting that more complex mechanisms possibly underlie the molecular crosstalk.
- Co-localization of C1q and BMP-1 was observed in skin biopsies from inflamed regions adjacent to melanoma excision sites and from patients suffering from RDEB.
- In conclusion, **the observed interactions between MBL/C1q and BMP-1/mTLL-1 suggest a common mechanism mediated by the CUB-EGF-CUB motif of the BTPs and complement proteases. They provide further support for a functional link between complement and BTPs during inflammation and tissue repair.**

*Contact: nicole.thielens@ibs.fr

Funding and grants

Mobility funding (Explora Doc) from the **Rhône Alpes region** (6 months, 2014)

Short-term mobility grant from the **DAAD** (Deutscher Akademischer Austauschdienst, 4 months, 2014-2015)

Travel grant from the **SRD** (Société de Recherche Dermatologique, December 2016)

Travel grant from the **International Society of Matrix Biology** (ISMB) to attend the Gordon Collagen Seminar and Conference (August 2017)

Travel grant from the **Gordon Collagen Research** committee (September 2017)

Research fellowship for international mobility from the **René Touraine Foundation** (6 months, 2017-2018)

Training

Course in **company management**: regulatory affairs, business, marketing, risk management (University Claude Bernard Lyon 1, France; May 2015, 40 hours)

Cours de **Biologie de la Peau** (CoBIP, organized by Dr. Marek Haftek, Lyon, France; March 2016 and 2017, 3 days)

Courses in **statistics** (by Arkesys compagny, Lyon, France; April 19-20th 2017, 2 days)

Course in **animal experimentation**, level 1 (University Claude Bernard Lyon 1/Ecole Normal Supérieur; June 12-23rd 2017, 2 weeks)